EXAMINATION OF CATALYST AND REACTANT ELECTRONIC EFFECTS IN ENANTIOSELECTIVE REACTIONS

by

Katrina Helen Jensen

A dissertation submitted to the faculty of
The University of Utah
in partial fulfillment of the requirements for the degree of

Doctor of Philosophy

Department of Chemistry

The University of Utah

December 2010

The University of Utah Graduate School

STATEMENT OF DISSERTATION APPROVAL

The dissertation of **Katrina Helen Jensen**

has been approved by the following supervisory committee members:

Matthew S. Sigman	, Chair	**5/13/2010** Date Approved
C. Dale Poulter	, Member	**5/13/2010** Date Approved
Jon D. Rainier	, Member	**5/13/2010** Date Approved
Thomas G. Richmond	, Member	**5/13/2010** Date Approved
David P. Goldenberg	, Member	**5/13/2010** Date Approved

and by **Henry S. White**, Chair of the Department of **Chemistry**

and by Charles A. Wight, Dean of The Graduate School.

ABSTRACT

Given the potential for opposite enantiomers of a chiral molecule to have different biological effects, access to a single enantiomer of a compound is desirable. Asymmetric catalysis is a powerful method for the synthesis of enantiomerically enriched chiral building blocks, and a mechanistic understanding of the relationship between catalyst structure and selectivity has the potential to advance the field. Additionally, mechanistic investigation provides insight about the nature of reactive intermediates, which allows one to imagine new ways to obtain or intercept such intermediates in the pursuit of new reaction development. Herein are described studies of two catalytic systems with a focus on mechanistic understanding.

In the first system, a modular catalyst structure was used to systematically evaluate the effects of catalyst acidity in a hydrogen bond-catalyzed hetero Diels-Alder reaction. Linear free energy relationships between catalyst acidity and both rate and enantioselectivity were observed, where greater catalyst acidity leads to increased activity and selectivity. A relationship between reactant electronic nature and rate was also observed, although there is no such correlation to enantioselectivity, indicating the system is under catalyst control.

In the second study, a unique approach to alkene difunctionalization was taken based on a mechanistic hypothesis of a quinone methide intermediate in a related reaction. Substrates containing an alkene adjacent to an *ortho*-phenol and a tethered nucleophile were prepared, allowing for the regioselective addition of two distinct

nucleophiles. A key improvement to the catalytic system was achieved using a ligated copper cocatalyst, leading to improved reactivity without a detrimental effect on enantioselectivity. The reaction was applied to the dioxygenation and aminooxygenation of alkenes, resulting in the enantioselective formation of heterocyclic compounds bearing two adjacent chiral centers.

The mechanism of the alkene difunctionalization reaction was studied using physical organic chemistry techniques. The proposed quinone methide intermediate was trapped in a Diels Alder reaction. Kinetic analysis provided evidence of rate limiting attack of this intermediate and for copper involvement in more than solely catalyst turnover. Through examination of substrate electronic effects a Jaffé relationship was observed correlating rate to electronic perturbation at two positions of the phenol. Ligand effects were evaluated to provide evidence of rapid ligand exchange and a direct correlation between ligand electronic nature and enantioselectivity.

For my parents.

TABLE OF CONTENTS

LIST OF FIGURES

LIST OF TABLES

LIST OF ABBREVIATIONS

3 Å MS	three angstrom molecular sieves
Ac	acetyl
AcCl	acetyl chloride
Ac_2O	acetic anhydride
AcOH	acetic acid
*t*AmylOH	*tert*-Amyl alcohol
aq.	aqueous
atm	atmosphere
BHT	2,6-di-*tert*-butyl-4-methylphenol
Bn	benzyl
bs	broad singlet
Bu	butyl
*i*Bu	*iso*-butyl
*i*BuOCOCl	*iso*-butyl chloroformate
*t*Bu	*tert*-butyl
°C	degrees Celsius
ca.	circa
calcd	calculated
Cbz	carbobenzyloxy

CH_2Cl_2	dichloromethane
$CHCl_3$	chloroform
cm	centimeter
d	doublet
Δ	heat
DAST	diethylaminosulfurtrifluoride
DCC	*N,N'*-dicyclohexylcarbodiimide
DCE	1,2-dichloroethane
dd	doublet of doublets
ddd	doublet of doublet of doublets
DMAP	4-dimethylaminopyridine
DMF	dimethylformamide
DMSO	dimethyl sulfoxide
dr	diastereomeric ratio
EDCI	1-Ethyl-3-(3-dimethylaminopropyl)carbodiimide
ee	enantiomeric excess
equiv.	equivalents
er	enantiomeric ratio
ESI	electrospray ionization
Et	ethyl
Et_3N	triethylamine
Et_2O	diethyl ether

EtOAc	ethyl acetate
FTIR	fourier transform infrared spectroscopy
g	gram
GC	gas chromatography
h	hour
hν	ultraviolet light
HOBt	Hydroxybenzotriazole
HPLC	high pressure liquid chromatography
HRMS	high resolution mass spectrometry
Hz	Hertz
IR	infrared spectroscopy
KO*t*Bu	potassium *tert*-butoxide
L	liter
LFER	linear free energy relationship
$LiAlH_4$	lithium aluminum hydride
m	multiplet
M	molar
m	*meta*
Me	methyl
MeCN	acetonitrile
MeOCOCl	methyl chloroformate
MeOH	methanol

mg	milligram
MHz	megaHertz
min	minute
mL	milliliter
μL	microliter
mmol	millimole
μmol	micromole
mol	mole
mp	melting point
MS	mass spectrometry
NMM	*N*-methylmorpholine
NMR	nuclear magnetic resonance
Nu	nucleophile
o	*ortho*
OAc	acetate
obsvd.	observed
OTf	trifluoromethylsulfonate
p	*para*
Ph	phenyl
ppm	parts per million
*i*Pr	*iso*-propyl
*i*PrOH	*iso*-propyl alcohol

pyrox	pyridine oxazoline
q	quartet
quinox	quinoline oxazoline
RDS	rate determining step
Red-Al	sodium bis(2-methoxyethoxy)aluminum hydride
R_f	retention factor
rt	room temperature
s	singlet or second
SFC	supercritical fluid chromatography
STD DEV	standard deviation
sub	substrate
t	triplet
TBAF	tetrabutylammonium fluoride
TBS	*tert*-butyldimethylsilyl
TEMPO	2,2,6,6-Tetramethylpiperidine-*N*-oxyl
THF	tetrahydrofuran
TLC	thin layer chromatography
tol	toluene
TsCl	*para*-toluenesulfonyl chloride
UV	ultraviolet
vs.	versus

ACKNOWLEDGMENTS

I would not have been able to get to obtain my PhD without the help of numerous others, to whom I am extremely grateful. First, I would like to thank my advisor Matt Sigman for his mentorship. I appreciate the breadth of what he has taught me, including how to think like a scientist, scientific writing skills, how to prepare a presentation, and how to be a mentor myself. I am thankful for his patience with me as I struggled to find the confidence in myself that he continually had. Furthermore, I value the high standard to which he holds his research group.

I am incredibly thankful to past and present members of the Sigman research group for their support and friendship. Specifically, I would like to thank Sridhar Rajaram for his patience in teaching me practical organic chemistry. I would like to thank Jeremie Miller for being willing to stop everything, either to help me or to argue with me, both of which taught me a great deal. I would like to thank Candace Cornell for her strength and he sense of humor, Sarah Cummings for her confidence, advice, and friendship, and Susi Podhajsky for her friendship and her intellectual rigor. I am grateful to Brian Michel and Erik Werner for friendship and support.

Finally, I would like to thank my family. My parents, Cliff and Lonnie, have made me believe that I can accomplish anything to which I commit myself. They have always encouraged my curiosity about the world around me and how it works. For these reasons, they are most directly responsible for my success. I am grateful to my sister,

Kira, for encouraging and supporting my academic pursuits, but always reminding me of the important things outside of chemistry that make life wonderful. Most importantly, I would like to thank my husband Nick for his support, commitment, and friendship. He has been willing to move to new places with me, lift me up when I am feeling down, and always make me smile.

CHAPTER 1

SYSTEMATIC EVALUATION OF CATALYST ACIDITY IN A HYDROGEN BOND-CATALYZED REACTION

Introduction

Hydrogen bonding is of utmost importance to biology, and one crucial function is transition state stabilization during enzyme catalysis. For synthetic chemists, despite the fact that the use of chiral Lewis acids in asymmetric catalysis has been well established, the use of the proton, the smallest Lewis acid, in small chiral molecules imparting facial selectivity during catalysis has only been explored relatively recently.[1-3] Completely organic catalysts have the potential to avoid some disadvantages associated with metal catalysts, such as cost and removal of trace metals from products.[1] Despite early reports of enantioselective reactions catalyzed by proline[4,5] and cinchona alkaloids[6-9] in the 1970s and 1980s, hydrogen bonding in enantioselective catalysis has seen a surge of research activity only in the past decade. A plethora of catalyst structures have been found to be effective in imparting enantioselectivity in a number of reactions (Figure 1.1).[1,2,4,10-16] In addition to structural diversity, many different functional groups capable of hydrogen bond donation with a wide range of catalyst acidity have been found to be capable of activating substrates for catalysis. Catalyst structures with either single or multiple hydrogen bond donors have been successfully developed. While this area of

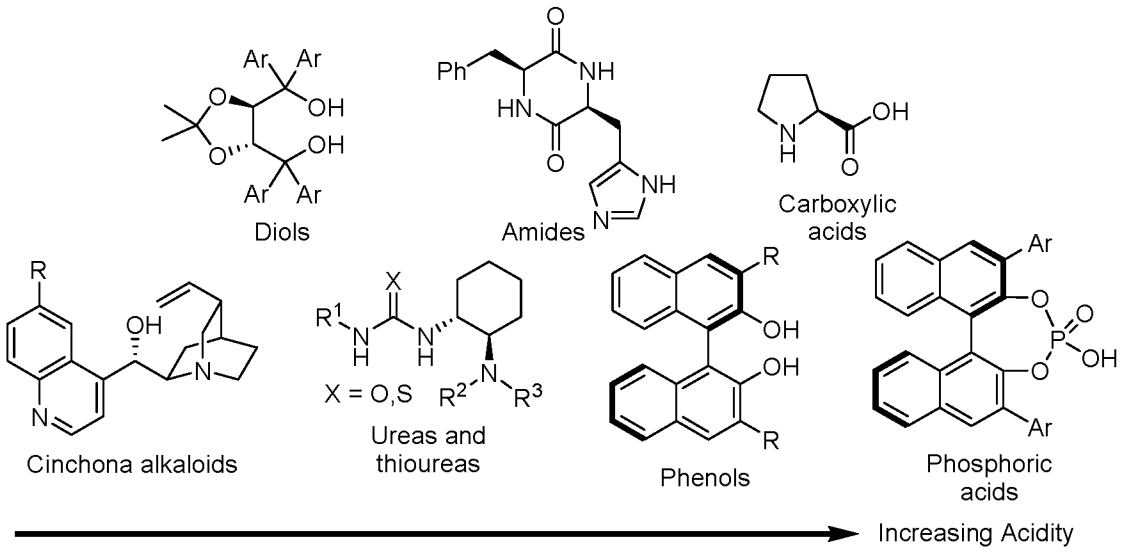

Figure 1.1. Small-molecule organic catalysts with hydrogen bond donors.

asymmetric catalysis is rapidly growing, mechanistic understanding of how subtle changes to catalyst structure affect selectivity is still scarce.[17-20]

Despite the development of successful catalysts with significant differences in acidity, covering a range of approximately 20 pK_a units, the influence of catalyst acidity upon reaction outcome, both in terms of rate and enantioselectivity, remains poorly understood. This lack of understanding is likely due to the fact that significant structural differences make the direct comparison of catalysts with different acidity uninformative. Occasionally, chiral organic catalysts are divided into two classifications: hydrogen bond catalysts and chiral Brønsted acid catalysts.[2] However, one may argue that a similar action is occurring in all cases, that is the formation of a hydrogen bond between the catalyst and the transition state structure leading to product; thus for the sake of simplicity they will be discussed herein without distinction except to point out differences in hydrogen bond donor acidity.

Background

Potential Effects of Catalyst Acidity

At the outset of our investigation, very few mechanistic studies had been performed on hydrogen bond catalyzed reactions.[17] Since then, Jacobsen and coworkers have reported significant mechanistic investigation into a number of reactions catalyzed by urea and thiourea hydrogen bond catalysts.[18-20] However, the effect of catalyst acidity in enantioselective hydrogen bond catalysis is still relatively unexplored mechanistically.[21] Although significant differences in both reactivity and selectivity with changes in catalyst acidity have been observed, most of these changes in catalyst acidity are accompanied with significant changes in catalyst structure. For example, in the enantioselective aldol reaction, differences in yield and enantioselectivity are seen between proline **1** and proline derivatives **2** and **3** (Figure 1.2).[22-24] Both acylsulfonamide **2** and tetrazole **2** have more acidic hydrogen bond donors than proline itself, suggesting that improvement of catalytic activity may be the result of increased hydrogen bond donor acidity. However, significant structural differences make ruling out other explanations impossible.

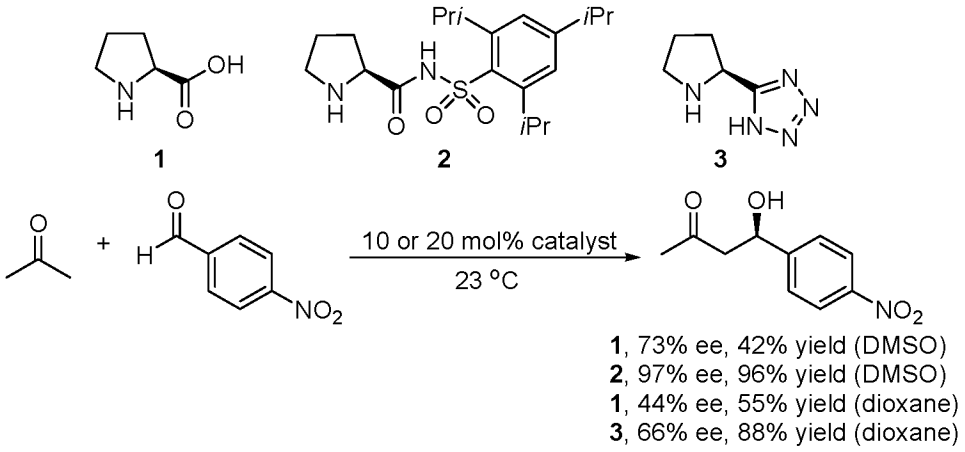

Figure 1.2. Proline and proline-derivatives as catalysts for the aldol reaction.

Systematic Evaluation of Acidity of an Achiral Hydrogen Bond Catalyst

Given the possibility for catalyst acidity to affect both activity and selectivity, it would be beneficial to probe such potential in a systematic manner. The insight that can be gained from such a detailed investigation is exemplified by the study performed by Hine and coworkers on the phenol (**4**) or biphenylenediol (**5**) catalyzed epoxide opening reaction (Figure 1.3).[25,26] To evaluate the role of hydrogen bond donors in catalysis, reaction rates were compared to catalyst pK_as. A Brønsted plot of phenol catalysts indicates a linear free energy relationship (LFER) between catalyst acidity and reaction rate. Interestingly, a discrepancy was discovered when biphenylenediol was included in the same plot. This catalyst is significantly more active than predicted by the LFER. This break indicates an effect other than acidity alone, interpreted as double hydrogen bonding during catalysis, where both hydrogen bond donors on biphenylenediol act in concert to activate the electrophile. Overall, this study shows the benefit of a systematic evaluation of a catalytic system in order to increase understanding of interactions in the transition state.

Despite this demonstration of the significant effect of catalyst acidity in a hydrogen bond catalyzed reaction, such a systematic study in an enantioselective reaction, where catalyst acidity has the potential to affect selectivity as well as activity, had not been performed prior to our entry into this area of research. A probable reason for this deficiency is the potentially difficult synthetic endeavour required to incorporate pK_a changes into certain catalysts without dramatic structural changes.

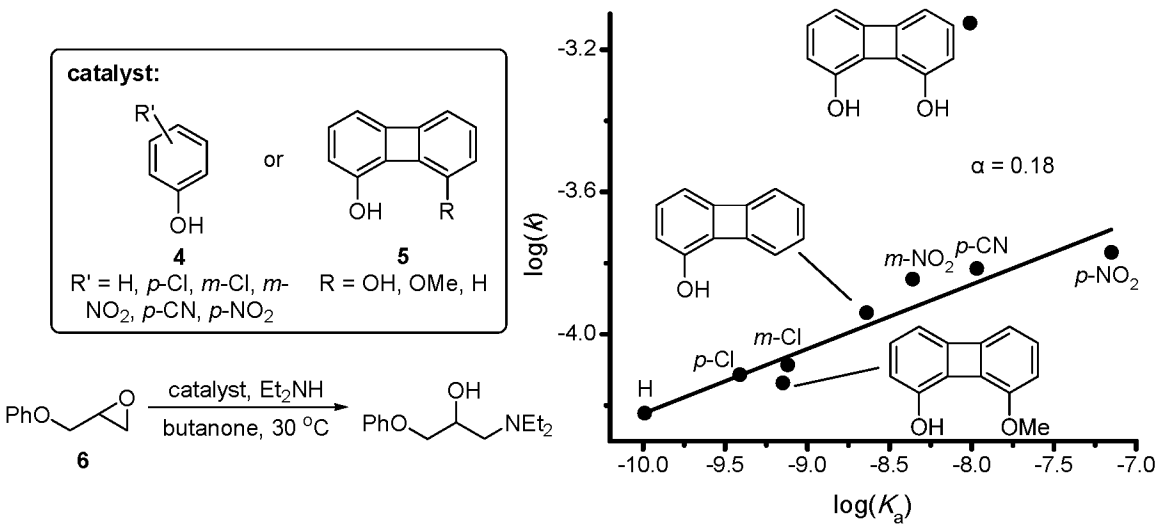

Figure 1.3. Hine's study of catalyst acidity effects and evidence for dual hydrogen bonding in a hydrogen bond-catalyzed epoxide opening reaction.

Development of a Modular Hydrogen Bond Catalyst

A hydrogen bond catalyst design developed in the Sigman laboratory consists of an oxazoline core and two pendant arms with sites capable of hydrogen bond donation (Figure 1.4).[27] This catalyst employs amino acid derivatives as the chiral building blocks, allowing for the incorporation of a variety of substituents into the catalyst structure. A key advantage of the design is its modularity, facilitating optimization of catalyst structure for a given reaction, as well as allowing systematic changes to be incorporated to advance understanding of the relationship between structure and selectivity.[28,29]

In order to evaluate the viability of this general motif as a hydrogen bond catalyst, a model reaction was chosen. One early example of a reaction catalyzed by a hydrogen bond catalyst with high enantioselectivity was the discovery by Rawal and coworkers of the hetero-Diels-Alder reaction[30] of the activated diene **7** with aldehydes catalyzed by the chiral diol TADDOL, **8** (Figure 1.5).[11] Further improvements in enantioselectivity and

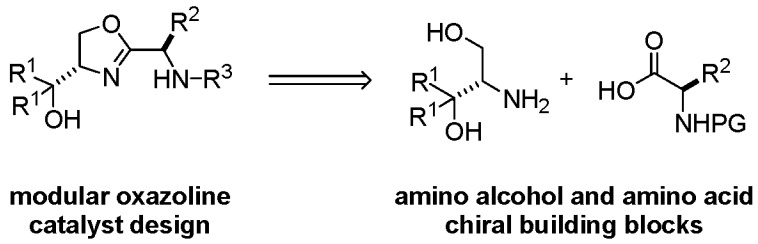

Figure 1.4. Modular hydrogen bond catalyst design.

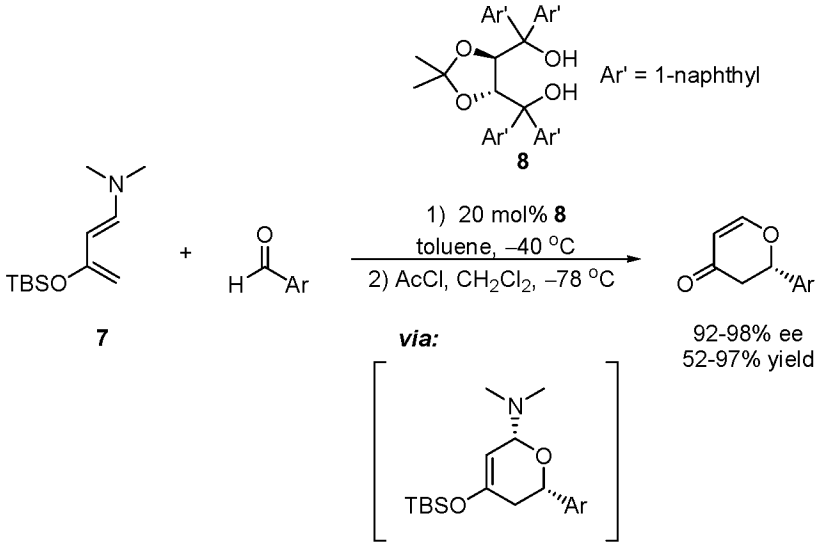

Figure 1.5. Rawal's hydrogen bond-catalyzed hetero Diels-Alder reaction.

substrate scope have since been made with an alternative chiral diol catalyst.[31]

The pioneering work developing a modular hydrogen bond catalyst in the Sigman laboratory was performed by Dr. Sridhar Rajaram.[27] He developed an effective synthesis of oxazoline-based catalysts and demonstrated the viability of the catalyst design by showing that it could be employed in the hetero-Diels-Alder reaction of Rawal's diene[32,33] with aromatic aldehydes. The modular nature of the catalyst design allowed for the evaluation of a variety of catalyst structures, with **9** as the optimal catalyst, providing dihydropyranone products in high enantiomeric excess (Figure 1.6).

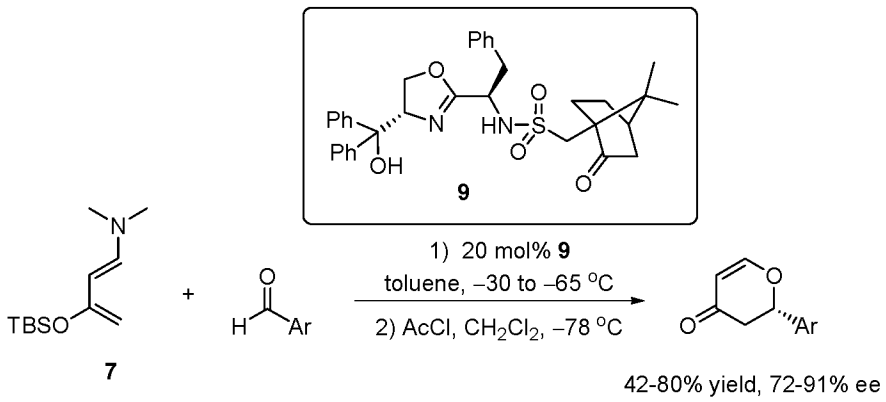

Figure 1.6. Modular oxazoline catalyst in the enantioselective hetero Diels-Alder reaction.

Effects of Catalyst Acidity in a Hydrogen Bond-Catalyzed Enantioselective Reaction

Following validation of the efficacy of the oxazoline-based catalyst design, the focus of the project turned to utilizing the catalyst's modularity to contribute to the mechanistic understanding of enantioselective hydrogen bond catalysis. Specifically, we hoped to systematically evaluate the importance of catalyst acidity.[21] We hypothesized that a more acidic catalyst may lead to a stronger hydrogen bond between catalyst and aldehyde, and consequently greater substrate activation, ultimately leading to a more active catalyst. Our catalyst was seen as an ideal template with which to test this hypothesis, as its modularity allows for systematic changes to one portion of the catalyst, while keeping the remainder of the catalyst unchanged. A series of halogenated acetamide derivative catalysts were chosen, as they provide a significant range of N–H acidity (approximately 5 pK_a units as measured in DMSO)[34,35] and all could be synthesized from a common precursor (Figure 1.7).

The synthesis of the catalysts was analogous to the route established by Dr. Sridhar Rajaram (Figure 1.7).[21,27] Amino diol **11** was synthesized via a Grignard reaction

of phenyl magnesium bromide with serine methyl ester hydrochloride **10**.[36] This amino diol was then coupled with *R*-*N*-Cbz-phenylalanine **12** using Anderson's coupling procedure with *iso*-butylchloroformate to activate the carboxylic acid prior to addition of the amine coupling partner.[37] The resulting peptide **13** was cyclized to oxazoline **14** using *p*-toluenesulfonyl chloride with DMAP and triethylamine as base.[38] Amine deprotection[39] followed by immediate acylation with the respective acetic anhydride resulted in the desired catalysts **15-17**, **19**. For the synthesis of **18**, fluoroacetic acid was used under Anderson's conditions to append this substituent to the catalyst.

The series of catalysts was then evaluated in the hetero-Diels-Alder reaction between Rawal's diene **7** and benzaldehyde **20** (Table 1.1). Isolated yields of the dihydropyranone product **21** were taken as the first indication that catalyst acidity may indeed affect catalytic activity, as more acidic catalysts generally gave higher product yields (Table 1.1). Interestingly, a trend in enantioselectivity was also observed, with the most acidic catalyst leading to the highest enantiomeric excess. This result was initially unexpected, as it was assumed that substituent size had the most significant effect on facial selectivity, and our assumption was that halogen substitution would have a minor effect upon the steric nature of the catalyst.

Because **15** was discovered to catalyze the hetero-Diels-Alder reaction with high enantioselectivity, the scope of the hetero-Diels-Alder reaction with this catalyst was examined (Table 1.2). In general, high enantioselectivity was obtained with aromatic aldehyde substrates (entries 1-5), highlighted by a 96% ee for 1-naphthaldehyde. An α,β-unsaturated aldehyde, cinnamaldehyde, also gives the product in high enantiomeric

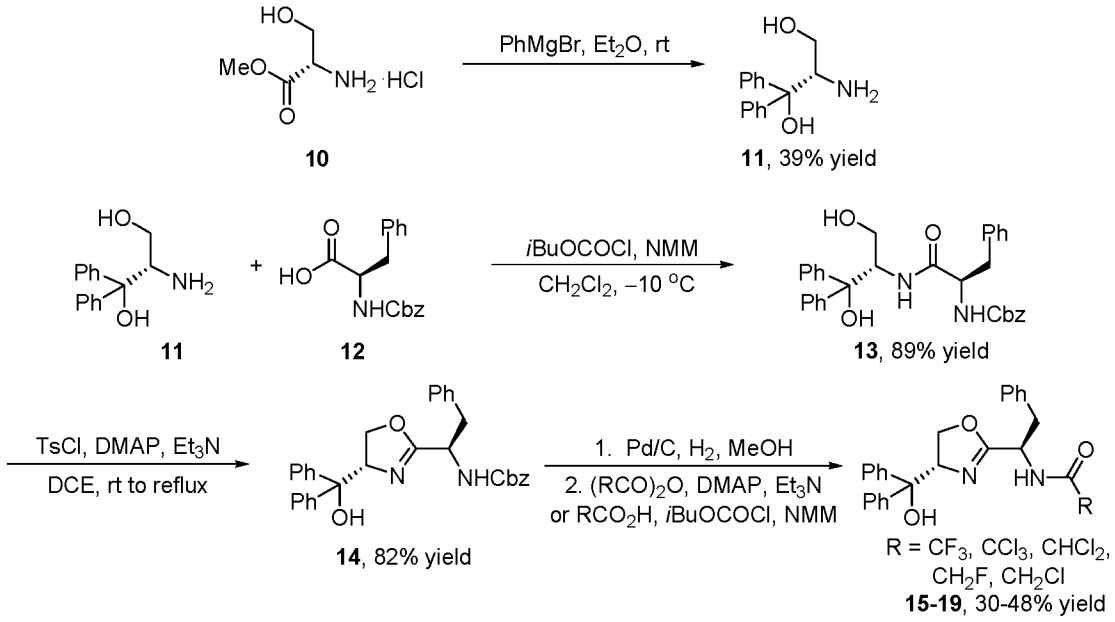

Figure 1.7. Catalyst synthesis.

Table 1.1. Oxazoline-amide catalyzed hetero Diels-Alder reaction.

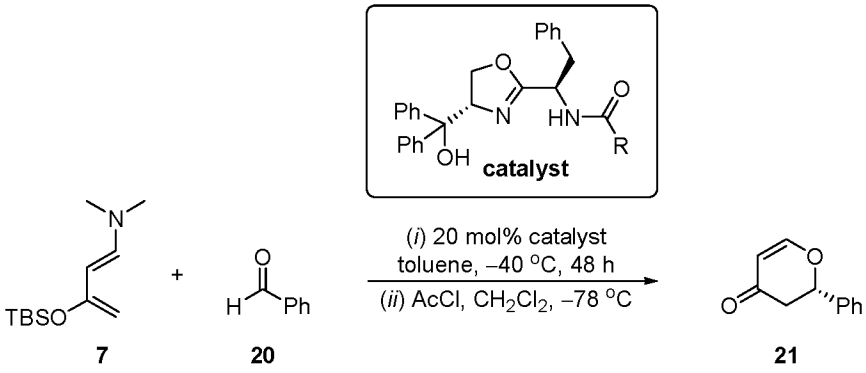

entry	catalyst	R	% yield	% ee	er
1	**15**	CF_3	67	91	95.3:4.7
2	**16**	CCl_3	61	81	90.6:9.4
3	**17**	$CHCl_2$	53	75	87.5:12.5
4	**18**	CH_2F	17	62	81.1:18.9
5	**19**	CH_2Cl	32	52	75.8:24.2

Table 1.2. Scope of enantioselective hetero Diels-Alder reaction catalyzed by **15**.

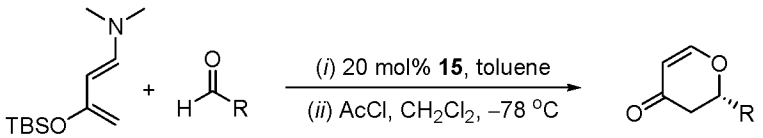

7

Entry	R	Time (h)	Temp (°C)	Yield (%)	ee (%)	er
1	Ph	60	-65	72	93	96:4
2	4-$O_2NC_6H_4$	48	-65	70	81	90:10
3	1-naphthyl	48	-55	74	96	98:2
4	4-ClC_6H_4	48	-55	74	83	92:8
5	4-$MeOC_6H_4$	72	-40	59	88	94:6
6	PhCH=CH	48	-65	65	90	95:5
7	$PhCH_2CH_2$	72	-40	43	47	73:27
8	$CH_3(CH_2)_4$	48	-40	32	30	65:35

excess (entry 6). Enantioselectivity is diminished for hydrocinnamaldehyde and hexanaldehyde (entries 7&8), but this marks an improvement as prior experimentation had shown catalyst **9** to be ineffective in the catalysis of the hetero Diels-Alder reaction with aliphatic aldehydes. Thus, while the series of catalysts was initially developed as a mechanistic probe, **15** was found to be a viable catalyst. This is encouraging because **15** is significantly simpler, having fewer stereocenters and a lower molecular weight, than the camphor sulfonamide catalyst **9**.

In order to gain a better understanding of how the observed trends in yield and enantioselectivity based on catalyst acidity may reflect the mechanism of the reaction, kinetic measurements were acquired using in situ IR spectroscopy, and the reaction rate dependence on each reaction component was determined (Figure 1.8). A first order dependence on [catalyst] provides evidence against a dimer or higher order species as the active catalyst (Figure 1.8 A). Initially, kinetic measurements were performed at room temperature for practicality, but based on the observation of a non-zero intercept, indicating a background reaction, all further measurements were performed at reduced temperature (either 0 or –45 °C). Saturation in [aldehyde] was observed (Figure 1.8 B), as well as a first order dependence on [diene] at high [aldehyde] (Figure 1.8 C). These results led to the proposal of the mechanism shown in Figure 1.9, where the catalyst and aldehyde bind reversibly to form an activated complex **C:A**, which reacts with diene in the rate limiting step to form the product.

Based upon the proposed mechanism, rate law derivation was performed following the Michaelis-Menton kinetic model. Assuming the second step is the rate

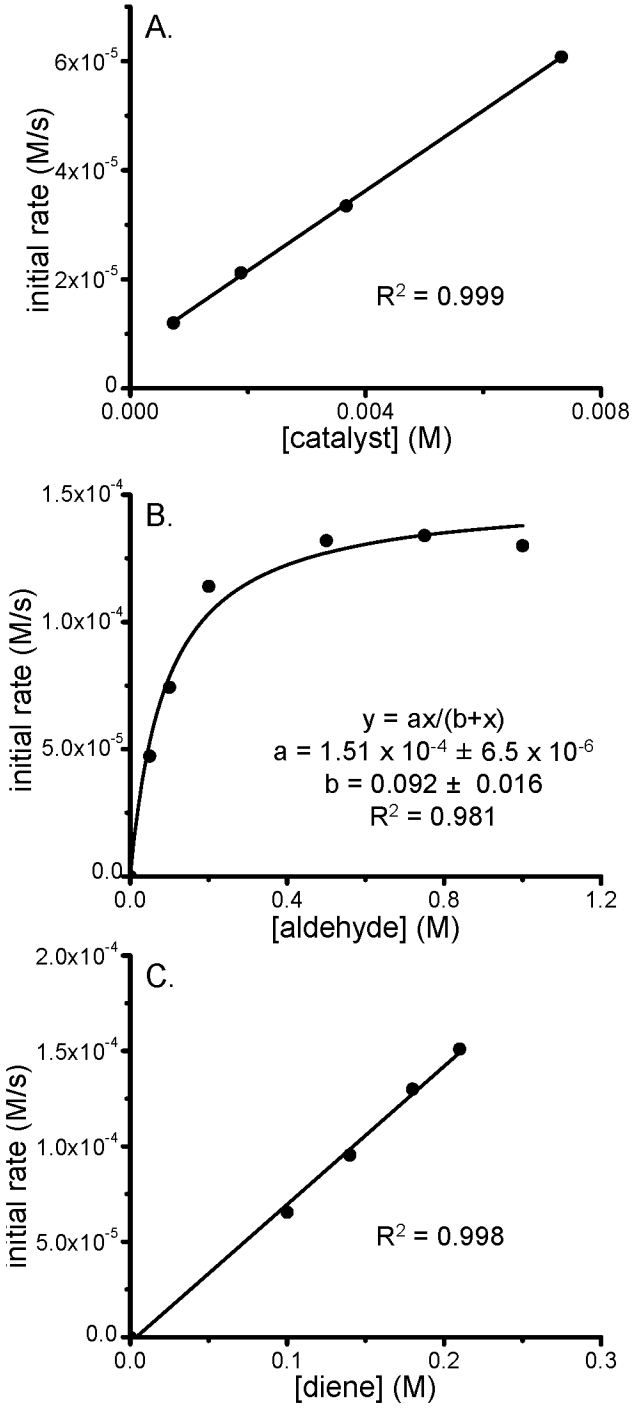

Figure 1.8. Reaction component dependencies measured by in situ IR spectroscopy. A. First order dependence on [catalyst], conditions: [**20**] = 0.37 M, [7] = 0.18 M, rt. B. Saturation in [aldehyde], conditions: [**15**] = 0.018 M, [7] = 0.18 M, 0 °C. C. First order dependence on [diene], conditions: [**15**] = 0.018 M, [**20**] = 1.0 M, 0 °C.

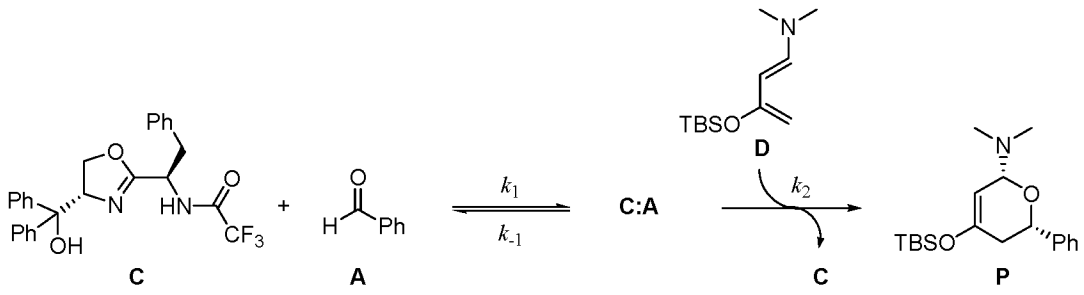

Figure 1.9. Proposed mechanism for the hetero Diels-Alder reaction catalyzed by **15**.

determining step, the rate of product formation is proportional to the product of the concentration of the two intermediates involved in this step, where **C:A** is the activated catalyst:aldehyde complex (equation 1).

$$\frac{d[P]}{dt} = k_2[C{:}A][D] \qquad \text{(eq. 1)}$$

As the catalyst exists in two different states in this mechanism, we define $[C]_T$ as the total catalyst concentration (equation 2).

$$[C] = [C_T] - [C{:}A] \qquad \text{(eq. 2)}$$

Using the steady state approximation (equation 3) allows us to solve for [C:A] (equation 4).

$$\frac{d[C{:}A]}{dt} = k_1([C_T] - [C{:}A])[A] - k_{-1}[C{:}A] - k_2[C{:}A][D] = 0 \qquad \text{(eq. 3)}$$

$$[C{:}A] = \frac{k_1[C_T][A]}{k_1[A] + k_{-1} + k_2[D]} \qquad \text{(eq. 4)}$$

Substitution into equation 1 results in the derived rate law (equation 5).

$$\frac{d[P]}{dt} = \frac{k_1 k_2 [C_T][A][D]}{k_1[A] + k_{-1} + k_2[D]} \quad \text{(eq. 5)}$$

Importantly, the derived rate law is consistent with the empirical observations. Specifically, when [aldehyde] is low the rate law can be simplified to

$$\frac{d[P]}{dt} = \frac{k_1 k_2 [C_T][A][D]}{k_{-1} + k_2[D]} \quad \text{(eq. 6)}$$

consistent with a first order dependence of rate on [aldehyde], and when [aldehyde] is high the rate law can be simplified to

$$\frac{d[P]}{dt} = k_2[C_T][D] \quad \text{(eq. 7)}$$

which is consistent with zero order dependence of rate on [aldehyde], and first order dependence on [catalyst] and [diene].

In light of the proposed mechanism, the question remained whether catalyst acidity is affecting binding equilibria of catalyst with substrate (k_1/k_{-1}), the rate of reaction of the activated aldehyde **C:A** with diene (k_2), or both. To determine the influence upon the second step, the reaction rate was measured for the complete series of catalysts **15-19** under saturation conditions. A clear trend was observed, with the most acidic catalyst leading to the highest rate (Figure 1.10 and Table 1.3).

In order to determine whether this trend in reaction could be directly correlated to the electronic nature of the catalyst, a Brønsted-type plot was constructed. The Brønsted equation (equation 8)[40] relates the rate of an acid-catalyzed reaction to the pK_a of the corresponding acid. The resulting linear free energy relationship is similar to the more

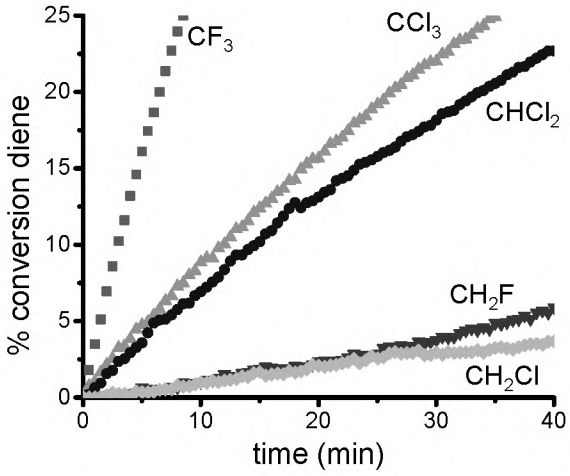

Figure 1.10. Conversion of diene vs. time for hydrogen bond catalyst **15-19**.

Table 1.3. Rate data and pK_a of corresponding acetic acids for catalyst series **15-19**.

R	pK_a of RCO_2H	average rate (M/s)	log(rate)
CF_3	–0.25	8.46×10^{-5}	–4.08
CCl_3	0.65	2.48×10^{-5}	–4.62
$CHCl_2$	1.29	1.98×10^{-5}	–4.72
CH_2F	2.66	3.61×10^{-6}	–5.44
CH_2Cl	2.86	2.81×10^{-6}	–5.56

$$\log(k) = -\alpha(pK_a) + C \qquad \text{(eq. 8)}$$

common Hammett relationship, where pK_as of benzoic acids are used as the reference measurement for the effect of electronic perturbations on rate or equilibrium. In our case, we chose to use the pK_a values of acetic acid derivatives measured in water the as reference, with the key assumption being that the electron-withdrawing ability of the R substituent affects the acidity of our catalyst and the acidity of the corresponding acetic acid derivative similarly.

A Brønsted-type plot was constructed by plotting log(rate) vs. pK_a of the corresponding acetic acid derivative (Figure 1.11). A linear free energy relationship was observed, indicating that the rate of the reaction under aldehyde saturation conditions can be directly correlated to the electronic nature of the catalyst.

To evaluate the effect of catalyst acidity upon substrate binding, the saturation curves for the most and least acidic catalysts, **15** and **19**, respectively, were examined (Figure 1.12, note y-axis scales are different). Comparing the curvature of these two plots, saturation is reached at much lower of [aldehyde] for the more acidic catalyst **15** (Figure 1.12, A) than for the least acidic catalyst **19** (Figure 1.12, B), indicating that binding equilibrium is also perturbed by catalyst acidity.

With the understanding that catalyst acidity has a direct effect on both substrate binding and rate of reaction with diene, we were interested in whether the observed trends in enantioselectivity could also be directly correlated to catalyst acidity. Considering that enantiomeric ratio is a measurement of the relative rate of formation of each enantiomer (er = k_S/k_R), a Brønsted-type plot was constructed by plotting log(er) vs. pK_a (Figure 1.13). A linear free energy relationship was observed between enantioselectivity and acidity, the first example of such a direct correlation in a hydrogen bond catalyzed reaction. This indicates that selectivity can be directly perturbed by hydrogen bond donating ability.

Substrate Electronic Effects

In an attempt to further understand the subtleties of the system, we chose to evaluate the influence of substrate electronic perturbations. We hypothesized that the electronic

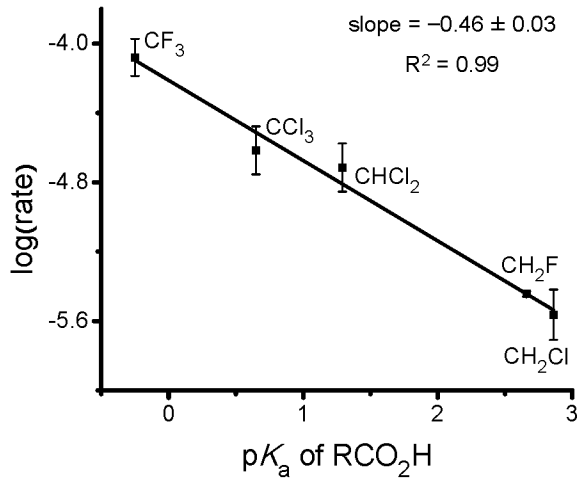

Figure 1.11. Linear free energy relationship between rate and pK_a of the corresponding acetic acid derivative.

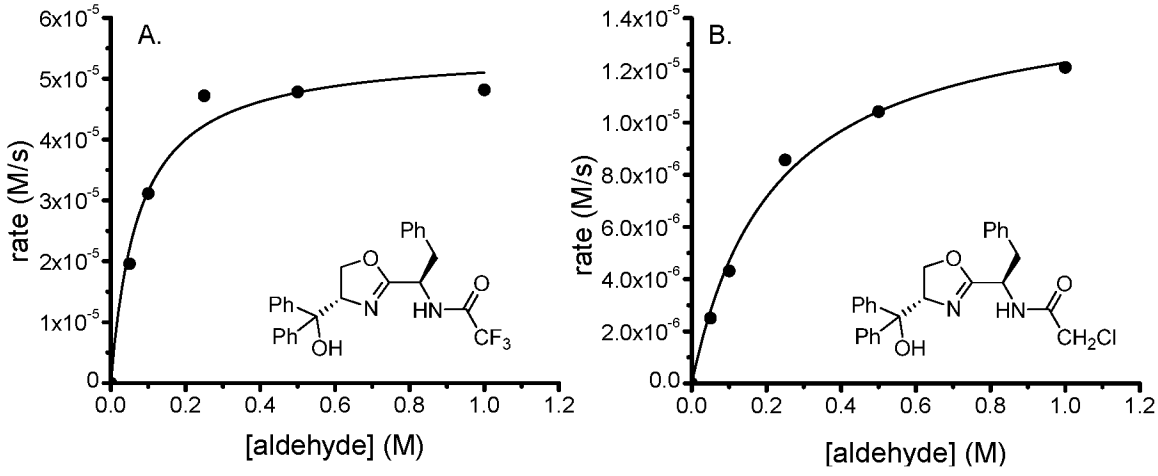

Figure 1.12. Comparison of saturation in [aldehyde] for catalysts **15** and **19**.
Conditions: [diene] = 0.075 M, [catalyst] = 0.018 M, –45 °C. Fit to y = ax/(b+x)
A. a = 5.47 x 10^{-5} ± 3.1 x 10^{-6}, b = 0.074 ± 0.017, R^2 = 0.97;
B. a = 1.45 x 10^{-5} ± 6.4 x 10^{-7}, b = 0.209 ± 0.029, R^2 = 0.99.

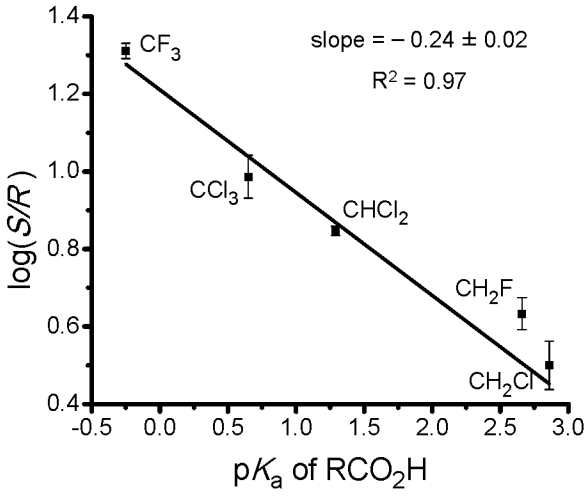

Figure 1.13. Linear free energy relationship between enantiomeric ratio and pK_a of the corresponding acetic acid derivative.

nature of the substrate could potentially affect both the rate at which the aldehyde reacts with the diene, as well as the Lewis basicity and thus the binding of substrate to catalyst. Therefore, a series of benzaldehyde derivatives with either electron-donating or electron-withdrawing substituents in the *para* position were examined. In situ IR was used to monitor the rate of the reaction. We first examined the two most electronically disparate cases within the series, *p*-anisaldehyde **22** and *p*-trifluromethylbenzaldehyde **23**. Initial reaction rates were measured over a range of [aldehyde]. Similar rates were observed at low [aldehyde], however, significant differences can be observed in the saturation curves for the two substrates. *p*-Anisaldehyde reaches saturation at a lower [aldehyde] (Figure 1.14 A), as would be expected with a more electron rich aldehyde which is a stronger Brønsted base and thus binds to the catalyst more effectively. On the other hand, *p*-trifluoromethylbenzaldehyde achieves a much higher rate of reaction at saturation (Figure 1.14 B), which is consistent with this being the more electron-poor, and thus more electrophilic aldehyde.

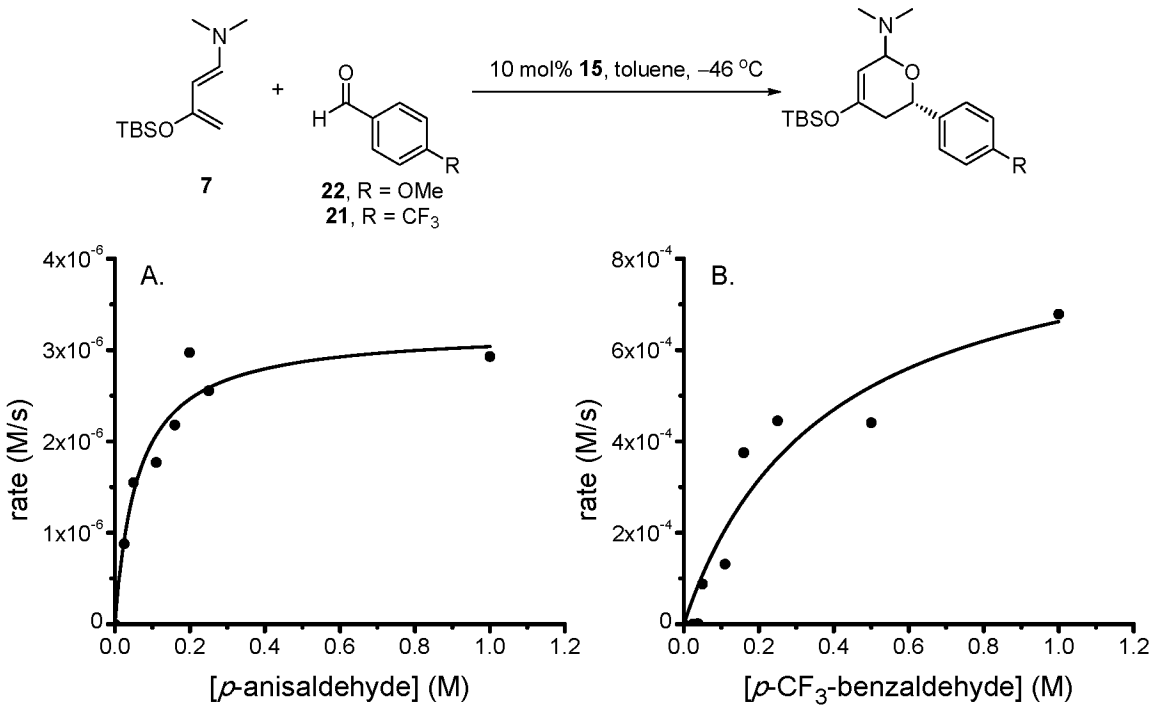

Figure 1.14. [aldehyde] saturation curves for benzaldehyde derivitives bearing an electron-donating group (A) and an electron-with drawing group (B). Conditions: [catalyst] = 0.016 M, [diene] = 0.16 M, –46 °C.

The rate of the hydrogen bond-catalyzed hetero-Diels-Alder reaction was measured at both high and low [aldehyde] with a series of benzaldehyde derivatives bearing electron-donating or electron-withdrawing substituents (Table 1.4). A Hammett plot was constructed by plotting the log of the rate vs. σ^+ (Figure 1.15). When [aldehyde] = 1.0 M (conditions where saturation is assumed) a linear free energy correlation is observed, with $\rho = 1.61 \pm 0.16$ (Figure 1.15 A). A positive ρ value indicates that there is a build up of negative charge, or diminution of positive charge, during the transition state. Additionally, the better fit obtained with σ^+ than with σ indicates significant resonance contribution from electron donating groups. This is consistent with the proposed mechanism in which a hydrogen bond is formed between aldehyde and catalyst, which

Table 1.4. Rate of hetero Diels-Alder reaction catalyzed by **15**. Conditions: [catalyst] = 0.016 M, [diene] = 0.16 M, –46 °C.

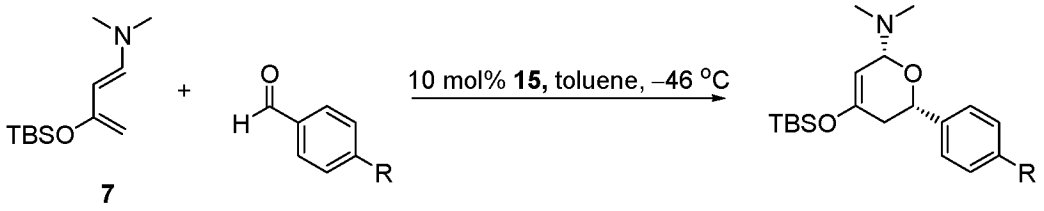

7

		[aldehyde] = 1.0 M		[aldehyde] = 0.025 M	
R	σ^+	average rate (M/s)	log(rate)	average rate (M/s)	log(rate)
CF_3	0.53	6.78×10^{-4}	–3.17	6.35×10^{-7}	–6.20
H	0	4.64×10^{-5}	–4.43	6.03×10^{-6}	–5.22
F	–0.07	2.93×10^{-5}	–4.53	6.51×10^{-6}	–5.19
Me	–0.31	2.61×10^{-5}	–4.58	2.90×10^{-6}	–5.54
OMe	–0.78	2.93×10^{-6}	–5.53	8.21×10^{-7}	–6.09

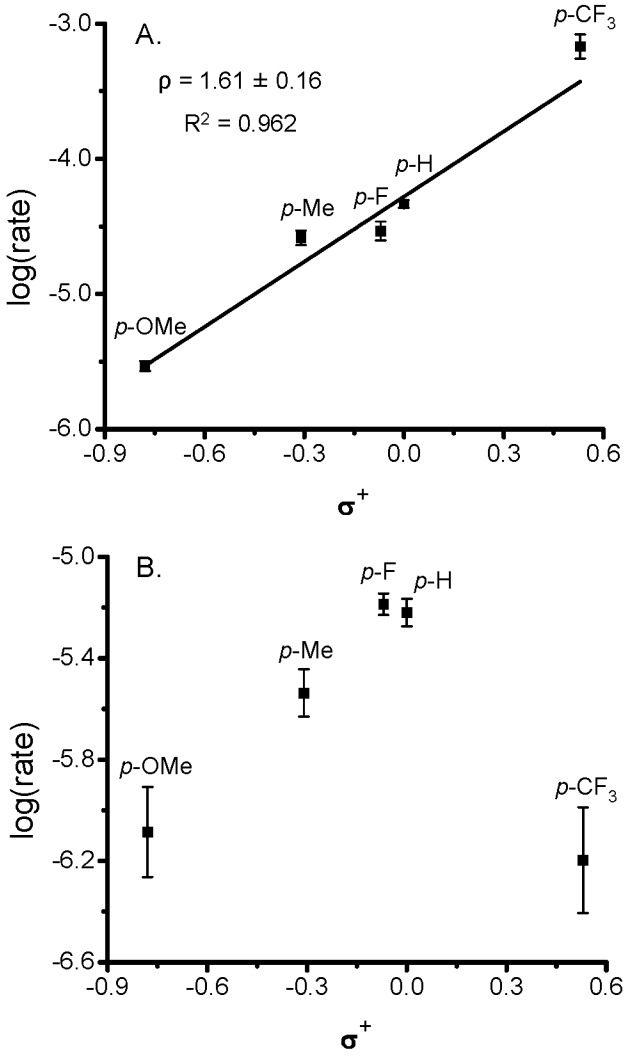

Figure 1.15. Hammett plots relating aldehyde electronic nature and reaction rate. Conditions: [catalyst] = 0.016 M, [diene] = 0.16 M, –46 °C, A. [aldehyde] = 1.0 M, B. [aldehyde] = 0.025 M.

would lead to a build up of positive charge on the carbonyl carbon of the aldehyde. Stabilization of this positive charge by electron donation would lead to a lower energy **C:A** intermediate, as demonstrated by the difference in saturation curves in Figure 1.14. A lower energy for the **C:A** intermediate would contribute to a higher activation energy for electron rich benzaldehyde derivatives, as evidenced by the decrease in k_2.

When [aldehyde] = 0.025 M, there appears to be a break in the Hammett plot (Figure 1.15 B). On the left hand side, ρ is positive as the substrates are electron rich enough to be in a situation where k_2 is rate limiting. In contrast, on the right hand side, ρ is negative, as electron withdrawing substituents decrease the rate of reaction, consistent with a situation where k_1 is rate limiting.

The observed Hammett correlation under saturation conditions is consistent with previous LFERs observed for other Diels-Alder reactions.[41-49] In general positive ρ values are observed with respect to electronic perturbations to the dienophile, whereas negative ρ values are observed when derivatives of the diene are examined. This is in agreement with the generally accepted view of a polar, asynchronous [4+2] cycloaddition pathway in which the diene and the dienophile can be considered the nucleophile and the electrophile, respectively.

Inspection of the enantiomeric excess of the products formed following workup with acetyl chloride shows no effect of the electronic nature of the aldehyde upon enantioselectivity (Table 1.5). Plotting log(er) vs. either σ or σ^+ shows no LFER (Figure 1.16). This indicates that the enantioselectivity of the reaction is solely under catalyst control (vide infra).

Table 1.5. Enantiomeric excess of hetero Diels-Alder adducts with benzaldehyde derivatives.

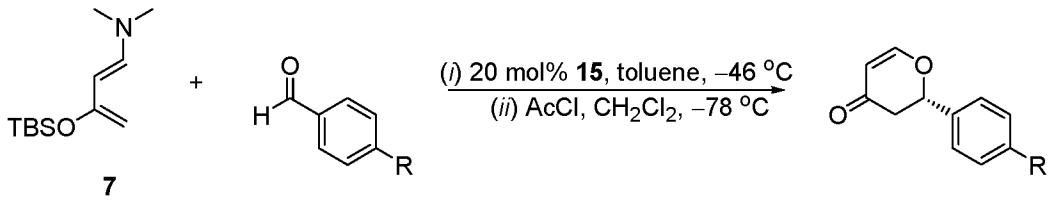

entry	R	% ee	er
1	CF_3	91	95:5
2	Cl	86	93:7
3	F	84	92:8
4	H	91	96:4
5	Me	83	92:8
6	OMe	90	95:5

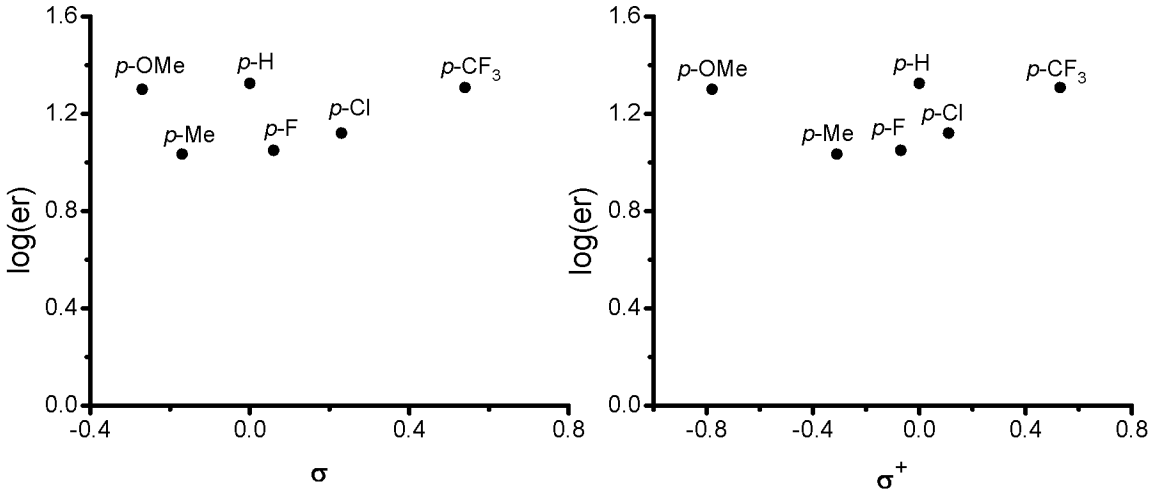

Figure 1.16. Hammett plots show no linear free energy relationship for enantioselectivity.

Origin of Catalyst Acidity Effect on Enantioselectivity

The observation of such direct effects of catalyst acidity on both rate and enantioselectivity should prove beneficial in the future design of hydrogen bond catalysts for asymmetric catalysis. While the effect upon rate was expected, the direct effect on enantioselectivity was not. Several explanations to account for such an effect can be proposed.

One explanation might be that a background, or uncatalyzed reaction, is occurring concurrent to the catalyzed reaction. This uncatalyzed reaction would result in racemic product, and thus the overall enantiomeric excess of product would be diminished. As k_{cat} decreases, the effect of a background reaction would certainly be more significant. In the case of our system, however, the background reaction at −45 °C is not significant. Furthermore, this explanation is inconsistent with the lack of a correlation between substrate electronic nature and enantioselectivity.

An attractive explanation is that a stronger hydrogen bond between the catalyst and the transition state is formed with the more acidic catalyst, leading to increased rigidity in the transition state. It has been reported that if the pK_a of the hydrogen bond donor and that of the protonated hydrogen bond acceptor are closely matched, a shorter and stronger hydrogen bond is formed.[50-52] While the pK_a difference between catalyst and protonated substrate is substantial, they are more closely matched with a more acidic catalyst. Furthermore, this disparity likely decreases in the transition state, as negative charge builds on the carbonyl oxygen. The formation of a stronger hydrogen bond in the transition state may lead to greater rigidity, and thus account for the higher enantioselectivity observed with more acidic catalysts. In contrast, there is a lack of

correlation between substrate electronic nature and enantioselectivity (Table 1.5). When considering a possible transition state structure, the substrate portion of the transition state structure, with negative charge on the oxygen atom stabilized by hydrogen bond formation to the catalyst, is analogous to the conjugate base of benzyl alcohol (Figure 1.17). The pK_a range of *para*-substituted benzylic alcohols is quite small (approximately 0.6 pK_a units, a 4-fold difference in K_a),[53] and thus has less of an impact on the strength of hydrogen bond formed in the transition state than the catalyst, where the range is significant (approximately 5 pK_a units, a 10^5-fold difference in K_a).[34,35]

Recent Examples of Acidity Effects in Hydrogen Bond Catalysis

Recently, Cheng and coworkers have reported the observation of LFERs between catalyst acidity with both rate and enantioselectivity within three different sets of thiourea

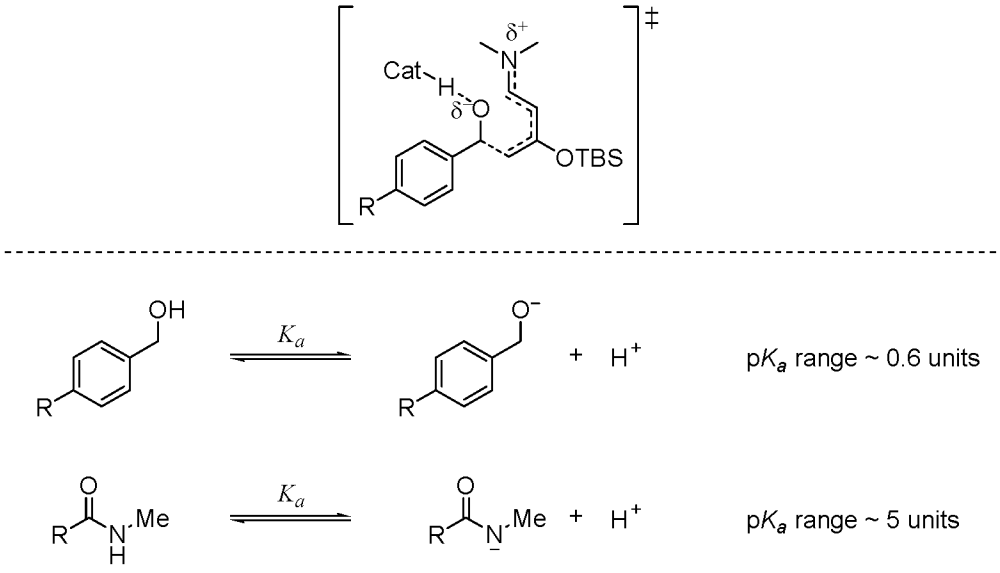

Figure 1.17. Effect of substituents on acidity of hydrogen bond donor and acceptor in proposed transition state.

catalysts in a Michael addition reaction between **24** and **25** (Figure 1.18, only one set of catalysts shown).[54] This provides support for the possibility that catalyst acidity effects may be widespread, and points to the potential for subtle changes to hydrogen bond catalyst structure to lead to significant improvements in reactivity and selectivity.

Another example of such an effect has been reported by Xu and coworkers in an aldol reaction catalyzed by proline derivatives **26-29** (Figure 1.19).[55] In this study, for three of the catalysts examined (**26-28**), enantiomeric ratio increases as the electron-withdrawing ability of the substituent on the phenol portion of the catalyst increases. However, in the case of catalyst **29** (R = NO_2), the enantioselectivity decreases relative to

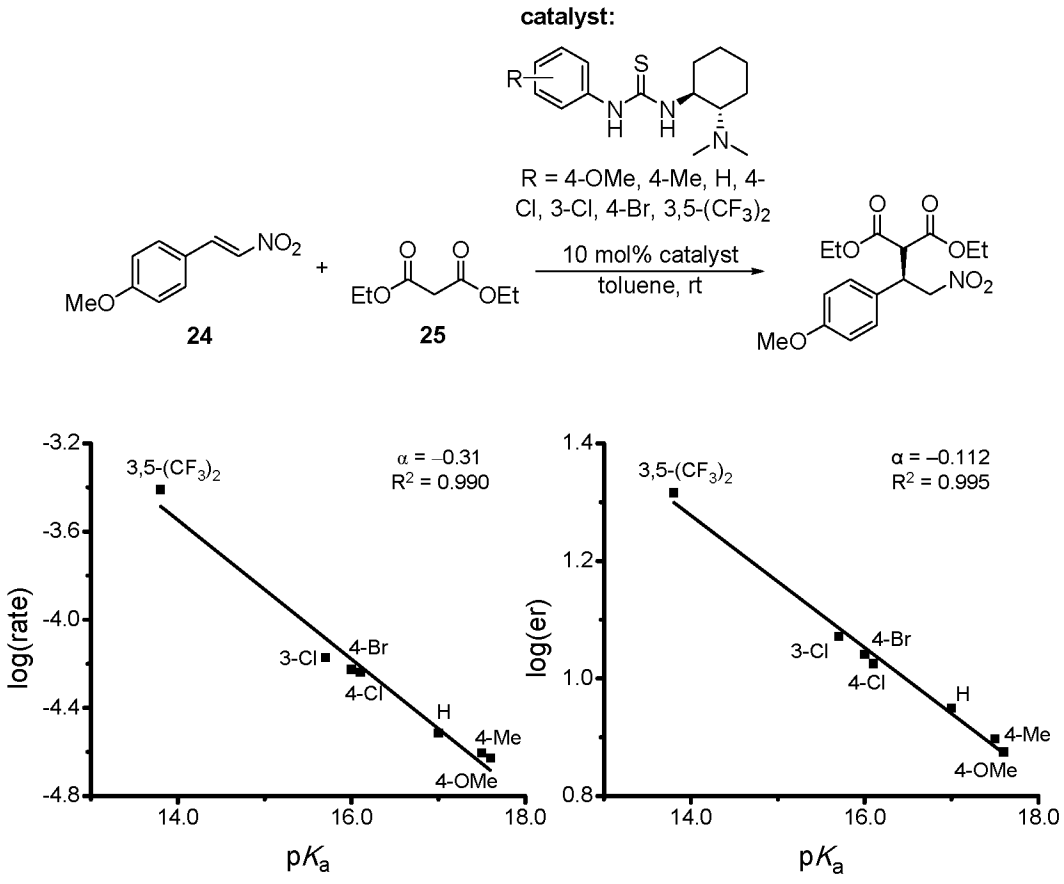

Figure 1.18. Effect of catalyst acidity on rate and enantioselectivity in thiourea-catalyzed Micheal reaction observed by Cheng and coworkers.

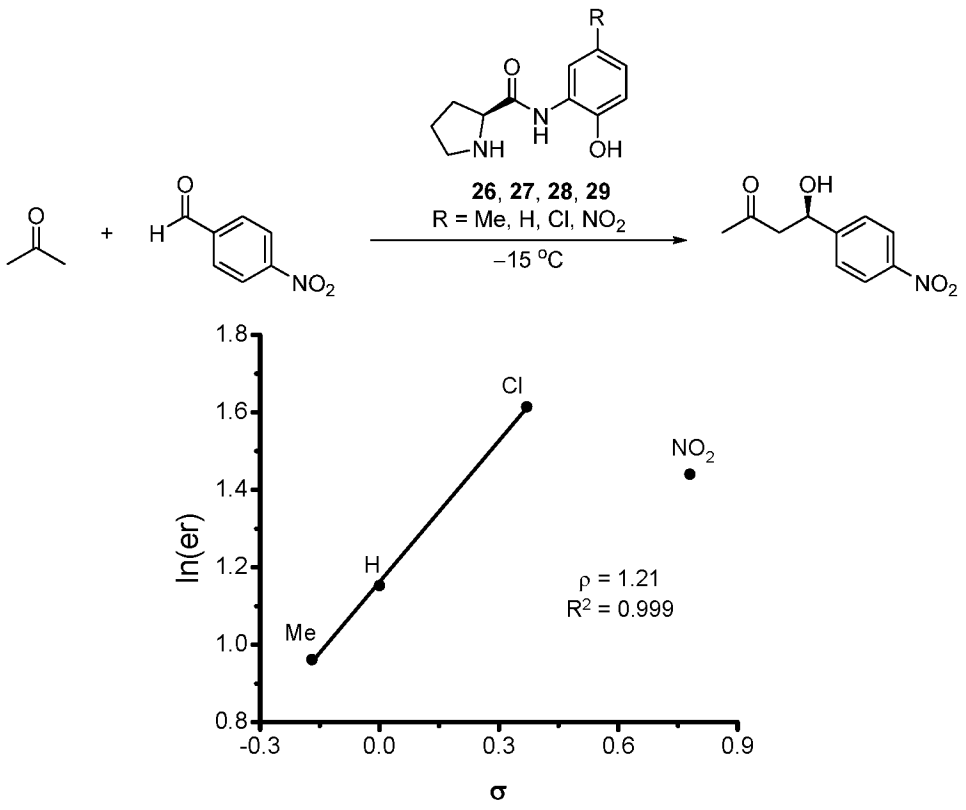

Figure 1.19. Xu and coworkers' report of electronic tuning of a proline-derived catalyst.

catalyst **28** (R = Cl). Catalyst **29** is treated as an outlier in the Hammett analysis, because it has low solubility. A linear free energy relationship was observed in plotting ln(er) vs. σ, although the strength of this analysis with only three data points can be questioned.

Interestingly, the opposite effect was recently reported by Johnston and coworkers for the Aza-Henry reaction, where a less acidic pyrolidine substituted chiral Brønsted acid **32** gave higher ee and yield of the product than more acidic **30** and **31** (Figure 1.20).[56] While it is difficult to determine if this represents a linear free energy relationship in a set of only three catalysts, it does demonstrate a trend opposite to what is seen in our system and others mentioned above. This demonstrates the capricious nature

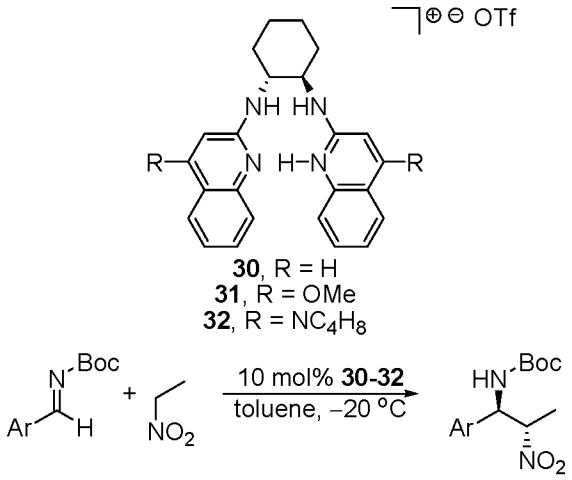

catalyst	R	% yield	% ee
30	H	29	87
31	OMe	52	73
32	NC_4H_8	78	90

Figure 1.20. Johnston and coworkers' observation of increased reactivity with decreased catalyst acidity in a hydrogen bond-catalyzed Aza-Henry reaction.

of enantioselective hydrogen bond catalysis, where it is paramount to remember that the key to improved catalysis is greater stabilization of the transition state *relative* to the ground state. Thus, it may not always hold, as this case demonstrates, that a more acidic catalyst is better. That is, if a more acidic catalyst lowers the energy of the substrate:catalyst complex more than that of the transition state, then this will reduce catalytic activity.

Conclusion

We have presented a detailed examination of the effect of catalyst acidity in an enantioselective hydrogen bond-catalyzed reaction. To the best of our knowledge, this is the first example of a systematic study wherein effects of electronic perturbations to both the catalyst and substrate are examined. A system where catalyst acidity controls

enantioselectivity is revealed. Ideal catalyst acidity is likely to differ depending on the specific reaction of interest, as the role of the catalyst is to stabilize the transition state more than the bound substrate intermediate, therefore it shouldn't be assumed that a more acidic catalyst will always lead to improved enantioselectivity. Optimal matching of the pK_as of catalyst and transition state structure should lead to improved catalyst performance in other systems as well, and the understanding gained in this study may aid in future catalyst design.

Experimental

General Considerations

Unless otherwise noted all reactions were performed under a nitrogen atmosphere with stirring. Glassware for all reactions was oven-dried at 110 °C and cooled in a dry atmosphere prior to use. CH_2Cl_2 was dried by filtration through alumina or distilled from CaH_2. MeOH was distilled from magnesium methoxide. Et_3N was distilled from CaH_2. DMAP was recrystallized from toluene. Toluene was dried by filtration through alumina. Liquid benzaldehyde derivatives were washed with saturated $NaHCO_3$ and brine, dried over $MgSO_4$, and distilled prior to use. Solid benzaldehyde derivatives were sublimed under reduced pressure prior to use. Acetyl chloride was distilled prior to use. All other reagents were purchased from commercial sources and used without further purification. Flash chromatography was performed using EM Reagent silica 60 (230-400 mesh). Analytical thin layer chromatography was performed with Whatman K6F Silica 60 Å plates. In situ IR was monitored using an ASI React IR 1000 with a diamond tipped probe, or with a Metler Toledo React IR ic10. IR spectra were recorded using a Mattson Satellite FTIR instrument. Nuclear magnetic resonance spectra were acquired recorded

in CD_2Cl_2 at 300 MHz for ^1H, and 75 MHz for ^{13}C. Chemical shifts for proton nuclear magnetic resonance (^1H NMR) spectra are reported in parts per million downfield relative to the center line of $CHDCl_2$ triplet at 5.34 ppm. Chemical shifts for carbon nuclear magnetic resonance (^{13}C NMR) spectra are reported in parts per million downfield relative to the center-line of the CD_2Cl_2 quintet at 54.0 ppm. The abbreviations s, d, t, dd, td, ddd, and m stand for the resonance multiplicities singlet, doublet, triplet, doublet of doublets, triplet of doublets, doublet of doublets of doublets, and multiplet, respectively. GC (gas chromatography) analysis was performed using a Hewlett Packard HP 6890 Series GC system fitted with a HP-Chiral permethylated β-cyclodextrin column. HPLC (high pressure liquid chromatography) analysis was performed using a Hewlett Packard Series 1100 instrument fitted with a chiral stationary phase (as indicated). Optical rotations were obtained (Na D line) using a Perkin Elmer Model 343 Polarimeter fitted with a micro cell with a 1 dm path length; concentrations are reported in g/100 mL. HRMS (high resolution mass spectrometry) analysis was performed using Waters LCP Premier XE. All melting points are uncorrected and recorded on Thomas Hoover Unimelt capillary melting point apparatus. ^1H NMR spectra of known compounds were compared to literature reports. Synthetic intermediates **11-14** were prepared by the method reported previously.[27] 1-Amino-3-siloxy-1,3-butadiene **7** was prepared and purified according to literature procedure.[57] The pyranone products have been reported previously.[31,58,59]

General Procedure for the Preparation of Catalysts 15-17, and 19

A 100 mL round bottom flask was charged with 44 mg of 10% Pd/C and the flask was flushed with nitrogen. In a separate 100 mL flask, 442.3 mg of oxazoline **14** (0.873

mmol) were dissolved in 6 mL of dry MeOH, and this solution was transferred via cannula into the flask containing Pd/C (on occasions when this is difficult, gentle warming or addition of excess MeOH is helpful and has no discernible effect on overall yield). A further 4 mL of MeOH (2 x 2 mL) were used for rinsing. The flask was then evacuated under water aspirator pressure and filled with H_2 from a balloon. The cycle was repeated thrice more, and the reaction mixture was stirred under a H_2 balloon atmosphere. On completion of reaction (7-8 h, by disappearance of oxazoline **14** on TLC, R_f = 0.6 with 1:1 EtOAc:hexanes), the reaction mixture was filtered through a pad of celite®. The filtrate was concentrated under reduced pressure, and the resulting residue was dissolved in benzene and concentrated under reduced pressure to remove exogenous water (2 x 30 mL benzene), then dried overnight under high vacuum and used without further purification. The residue from deprotection was dissolved in 5 mL of dry CH_2Cl_2 under nitrogen along with 10.7 mg of DMAP (0.087 mmol, 0.10 equiv.). To this solution, 490 μL of freshly distilled Et_3N (3.49 mmol, 4 equiv.) were added. The reaction mixture was cooled to 0 ^oC in an ice bath. In a separate flask, 123 μL of trifluoroacetic anhydride (95% pure, 0.873 mmol, 1 equiv.) were dissolved in 3 mL of CH_2Cl_2. This solution was transferred via cannula into the reaction flask. An additional 2 mL of CH_2Cl_2 were used for rinsing. The reaction mixture was stirred for 4 h, and then diluted with 30 mL of CH_2Cl_2 and washed with 30 mL of saturated aqueous $NaHCO_3$ followed by 30 mL of brine. The organic phase was dried over Na_2SO_4, filtered, and concentrated. The crude mixture in a minimum amount of CH_2Cl_2 was purified by flash silica-gel column chromatography with 20% to 25% to 30% Et_2O/hexanes as the solvent to give 178.8 mg of **15** (yield: 43%). R_f = 0.7 with 1:1 EtOAc:hexanes; white solid; mp: 50-52

°C; $[\alpha]_D^{20}$ = -20.4 (c = 0.28, $CHCl_3$); ^1H NMR (300, MHz CD_2Cl_2) δ = 2.50 (s, 1 H), 3.10 (dd, *J* = 6.6, 14.0 Hz, 1 H), 3.23 (dd, *J* = 6.0, 14.0 Hz, 1 H), 4.26 (d, *J* = 8.9 Hz, 1 H), 4.27 (d, *J* = 8.9 Hz, 1 H), 4.81 (ddd, *J* = 6.0, 6.5, 6.5 Hz, 1 H), 5.25 (dd, *J* = 8.9, 8.9 Hz, 1 H), 6.79 (br d, *J* = 6.0 Hz, 1 H), 7.13-7.37 (m, 11 H), 7.41-7.46 (m, 4 H). ^{13}C NMR (75 MHz, CD_2Cl_2) δ = 37.5, 50.0, 70.8, 73.2, 78.6, 115.8 (q, *J* = 288 Hz), 126.0, 126.5, 127.3, 127.5, 127.8, 128.4, 128.7, 129.1, 129.6, 135.3, 144.2, 145.9, 157.0 (q, *J* = 38 Hz), 167.1. IR: (KBr) 3482, 3393, 3062, 3030, 2360, 2343, 1721, 1668, 1543, 1496, 1449, 1210, 1173, 749, 700 cm^{-1}. HRMS $C_{26}H_{23}F_3N_2O_3$ m/z $(M+Na)^+$ calcd. 491.1558, obsvd. 491.1557.

Catalyst 16

Synthesized following the general procedure described above for the synthesis of catalyst **15** using trichloroacetic anhydride. Column chromatography: 20% to 25% to 30% Et_2O/hexanes. Yield: 37%; R_f = 0.7 with 1:1 EtOAc:hexanes; white solid; mp: 58-61 °C; $[\alpha]_D^{20}$ = -32.0 (c = 0.30, $CHCl_3$); ^1H NMR (300 MHz, CD_2Cl_2) δ = 2.66 (s, 1 H), 3.11 (dd, *J* = 7.0, 14.0 Hz, 1 H), 3.27 (dd, *J* = 5.6, 14.0 Hz, 1 H), 4.27 (d, *J* = 8.4 Hz, 1 H), 4.29 (d, *J* = 8.4 Hz, 1 H), 4.69 (ddd, *J* = 6.5, 6.5 Hz, 1 H), 5.26 (dd, *J* = 8.6, 8.6 Hz, 1 H), 7.13-7.37 (m, 12 H), 7.43-7.48 (m, 4 H). ^{13}C NMR (75 MHz, CD_2Cl_2) δ = 37.4, 51.2, 70.8, 73.0, 78.7, 126.1, 126.7, 127.2, 127.4, 127.8, 128.3, 128.7, 129.1, 129.7, 135.5, 144.2, 146.1, 161.8, 167.5. IR: (KBr) 3474, 3412, 3060, 3029, 2962, 2935, 2362, 2344, 1711, 1666, 1510, 1448, 1388, 1209, 1031, 984, 823, 751, 700 cm^{-1}. HRMS $C_{26}H_{23}Cl_3N_2O_3$ m/z $(M+Na)^+$ calcd. 539.0672, obsvd. 539.0682.

Catalyst 17

Synthesized following the general procedure described above for the synthesis of catalyst **15** using dichloroacetic anhydride. Column chromatography: 20% to 30% to 40% Et_2O/hexanes. Yield: 30%; R_f = 0.6 with 1:1 EtOAc:hexanes; white solid; mp: 52-54 °C; $[\alpha]_D^{20}$ = -25.7 (c = 0.30, $CHCl_3$); ^1H NMR (300 MHz, CD_2Cl_2) δ = 2.74 (s, 1 H), 3.08 (dd, *J* = 7.3, 13.9, 1 H), 3.23 (dd, *J* = 5.7, 14.0 Hz, 1 H), 4.25 (d, *J* = 8.5, 1 H), 4.25 (d, *J* = 8.5, 1 H), 4.69 (ddd, *J* = 6.7, 6.7, 6.7 Hz, 1 H), 5.25 (dd, *J* = 8.5, 8.5 Hz, 1 H), 5.80 (s, 1 H), 6.90 (br d, *J* = 6.4 Hz, 1 H), 7.15-7.37 (m, 11 H), 7.43-7.49 (m, 4 H). ^{13}C NMR (75 MHz, CD_2Cl_2) δ = 37.6, 50.4, 66.5, 70.6, 73.1, 78.7, 126.0, 126.6, 127.2, 127.3, 127.7, 128.3, 128.7, 129.1, 129.7, 135.7, 144.2, 146.2, 164.2, 167.8. IR: (KBr) 3407, 3060, 3028, 2966, 2933, 1664, 1525, 1495, 1448, 1195, 985, 810, 749, 700, 636 cm^{-1}. HRMS $C_{26}H_{24}Cl_2N_2O_3$ m/z $(M+Na)^+$ calcd. 505.1062, obsvd. 505.1069.

Catalyst 19

Synthesized following the general procedure described above for the synthesis of catalyst **15** using chloroacetic anhydride. Column chromatography: 30% to 40% to 50% to 60% Et_2O/hexanes. Yield: 32%; R_f = 0.5 with 1:1 EtOAc:hexanes; white solid; mp: 61-64 °C; $[\alpha]_D^{20}$ = 25.5 (c = 0.20, $CHCl_3$); ^1H NMR (300 MHz, CD_2Cl_2) δ = 3.06 (dd, *J* = 7.3, 13.9 Hz, 1 H), 3.11 (s, 1 H), 3.19 (dd, *J* = 5.9, 13.9 Hz, 1 H), 3.74 (d, *J* = 15.1 Hz, 1 H), 3.86 (d, *J* = 15.1 Hz, 1 H), 4.23 (d, *J* = 9.5 Hz, 1 H), 4.25 (d, *J* = 7.3 Hz, 1 H), 4.66 (ddd, *J* = 6.3, 6.7, 6.7 Hz, 1 H), 5.25 (dd, *J* = 7.3, 9.3 Hz, 1 H), 6.84 (br d, *J* = 6.1 Hz, 1 H), 7.16-7.46 (m, 11 H), 7.43-7.49 (m, 4 H). ^{13}C NMR (75 MHz, CD_2Cl_2) δ = 37.6, 42.8, 50.2, 70.5, 73.2, 78.8, 126.1, 126.5, 127.1, 127.3, 127.6, 128.3, 128.7, 129.1, 129.6, 136.1, 144.4, 146.5, 166.8. 168.1. IR: (KBr) 3403, 3060, 3028, 2960, 2936, 1657, 1529,

1495, 1448, 1390, 1184, 984, 749, 701 cm^{-1}. HRMS $C_{26}H_{25}ClN_2O_3$ m/z $(M+Na)^+$ calcd. 471.1451, obsvd. 471.1453.

Preparation of Catalyst 18

In a round bottom flask, 81.0 mg of sodium fluoroacetate (0.770 mmol, 1.3 equiv.) were dissolved in 3 mL of dry CH_2Cl_2 under nitrogen. To this solution, 103 μL of *N*-methylmorpholine (99% pure, 0.924 mmol, 1.56 equiv.) were added. The reaction mixture was cooled to -15 °C using a NaCl/ice cooling bath, and 120 μL of *iso*-butylchloroformate (97% pure, 0.89 mmol, 1.5 equiv.) were added dropwise. The contents are stirred at -15 °C for 45 min, after which a solution of the residue from Cbz deprotection (0.592 mmol, 1 equiv.) in 1 mL of dry CH_2Cl_2 along with 128 μL of *N*-Methylmorpholine (1.15 mmol, 1.95 equiv.) was added via cannula. An additional 1 mL of CH_2Cl_2 was used for rinsing. The reaction mixture was allowed to warm to room temperature, stirred for 8 h, and then diluted with 10 mL of CH_2Cl_2. The mixture was washed with 10 mL of water followed by 10 mL of brine. The organic layer was dried over Na_2SO_4 and concentrated. The resulting residue was dissolved in a minimal amount of CH_2Cl_2 and purified by flash silica-gel column chromatography with 30% to 40% to 50% Et_2O/hexanes as the solvent to give 78.2 mg of **18.** Yield: 31%, R_f = 0.4 with 1:1 EtOAc:hexanes, white solid; mp: 69-72 °C; $[\alpha]_D^{20}$ = 26.0 (c = 0.32, $CHCl_3$); ^1H NMR (300 MHz, CD_2Cl_2) δ = 3.06 (dd, *J* = 7.5, 14.0 Hz, 1 H), 3.17 (s, 1 H), 3.20 (dd, *J* = 5.9, 14.0 Hz, 1 H), 4.22 (d, *J* = 9.5 Hz, 1 H), 4.24 (d, *J* = 7.2 Hz, 1 H), 4.45 (dd, *J* = 14.4, 42.6 Hz, 1 H), 4.61 (dd, *J* = 14.4, 42.8 Hz, 1 H), 4.73 (ddd, *J* = 6.6, 6.6, 6.6 Hz, 1 H), 5.26 (dd, *J* = 7.3, 9.5 Hz, 1 H), 6.62 (br d, *J* = 4.6 Hz, 1 H), 7.16-7.36 (m, 11 H), 7.43-7.50 (m, 4 H). ^{13}C NMR (75 MHz, CD_2Cl_2) δ = 37.9, 49.4, 70.4, 73.2, 78.7, 80.5 (d, *J* = 173 Hz),

126.0, 126.5, 127.1, 127.2, 127.6, 128.3, 128.7, 129.0, 129.6, 136.1, 144.4, 146.6, 168.1, 168.4 (d, J = 18 Hz). IR: (KBr) 3413, 3060, 3029, 2959, 1662, 1533, 1495, 1448, 1185, 1043, 749, 701 cm^{-1}. HRMS $C_{26}H_{25}FN_2O_3$ m/z $(M+Na)^+$ calcd. 455.1747, obsvd. 455.1754.

Standard Procedure for the Hetero Diels-Alder Reaction

All pyranone products were prepared according to the following representative procedure: to an oven-dried 4 mL vial with a septum cap containing 20.6 mg of **15** (0.0440 mmol, 0.200 equiv.) under nitrogen, 500 μL of dry toluene were added followed by 45 μL of benzaldehyde (0.440 mmol, 2 equiv.). The vial was cooled to –40 °C and 50 mg of diene **7** (0.220 mmol, 1 equiv.) dissolved in 500 μL of toluene were transferred via cannula into the reaction vial. An additional 200 μL of toluene were used for rinsing. After stirring for 48 h at -40 °C, the reaction mixture was cooled to –78 °C, diluted with 2 mL of CH_2Cl_2, and 31 μL of acetyl chloride (0.440 mmol, 2 equiv.) were added. After stirring for 30 min the contents were directly transferred to a silica column for purification using 5% to 15% EtOAc/hexanes as eluent to give 26.1 mg of **21**. Yield; 67%; yellow oil.

Standard in situ FTIR Procedure:

The ASI React IR 1000 or the Metler Toledo React IR ic10 was used to analyze reaction progress in situ. For each reaction, the probe was cleaned and a background spectrum was taken. Disappearance of diene **7** was observed by recording the absorbance at maximum peak height (1648.2 cm^{-1} for ASI React IR 1000 or 1649.6 cm^{-1} Metler Toledo React IR ic10). The absorbance measurements were converted to concentration

units dividing by the constant (ε = 1.0885 or ε = 0.769) relating absorbance to concentration determined by constructing calibration curves of the starting materials (Beer's Law). The apparatus used was a 50 mL Schlenk flask with a side arm and a 24/40 ground glass joint for probe insertion. An ice water bath was used for reactions performed at 0 °C. A dry ice/MeCN bath was used for reactions performed at –45 °C. Standard solutions of catalyst, aldehyde, and diene were used and were prepared as follows: for catalyst: to a 10 mL Schlenk tube, 107.5 mg of **15** (0.229 mmol) were added. The tube was flushed with nitrogen, and 3 mL of toluene were added. For aldehyde: to a 25 mL volumetric flask fitted with a septum, 6.35 mL of benzaldehyde (62.5 mmol) were added under a nitrogen atmosphere. Toluene was added to the 25 mL mark. The solution was stirred and transferred via cannula into a Schlenk flask. For diene: to a 10 mL volumetric flask 2.5015 g of diene **7** (11.000 mmol) were added, the flask was fitted with a septum and the flask was purged with nitrogen. Toluene was added to the 10 mL mark. The solution was stirred and transferred via cannula into a Schlenk flask.

Each kinetic experiment was conducted similar to this example procedure: the probe was equipped with a 50 mL Schlenk flask fitted with a stirbar, and the flask was flushed with nitrogen. To the apparatus were added 241 μL of 0.076 M solution of **15** (0.018 mmol), 400 μL of 2.50 M solution of benzaldehyde (1.00 mmol), and 192 μL of toluene. The reaction flask was placed in an ice bath and allowed to stir for approximately 20 min. The IR instrument was programmed to collect spectra every 15 or 30 s. Following commencement of data collection, 167 μL of 1.10 M solution of diene **7**

(0.183 mmol) were added and data collection was continued for 1-6 h. Initial rates were determined after 5% conversion of diene.

Rate Data

The kinetic data for Figures 1.8, 1.11, 1.12, 1.14, and 1.15 are tabulated in Tables 1.6, 1.7, 1.8, 1.9, 1.10, 1.11, 1.12, 1.13, and 1.15.

Table 1.6. [catalyst] dependence data. Data for Figure 1.8 A.

[diene] = 0.18 M, [aldehyde] = 0.37 M, rt

[**15**] (M)	initial rate (M/s)
7.33E-4	1.20E-5
1.88E-3	2.12E-5
3.67E-3	3.35E-5
7.33E-3	6.08E-5

Table 1.7. [aldehyde] dependence data. Data for Figure 1.8 B.

[diene] = 0.18 M, [**15**] = 0.018 M, 0 ^{o}C

[aldehyde] (M)	initial rate (M/s)
0.05	4.73E-5
0.10	7.43E-5
0.20	1.14E-4
0.50	1.32E-4
0.75	1.34E-4
1.0	1.30E-4

Table 1.8. [diene] dependence data. Data for Figure 1.8 C.

[benzaldehyde] = 1.00 M, [**15**] = 0.0183 M, 0 °C

[diene] (M)	initial rate (M/s)
0.10	6.54E-5
0.14	9.54E-5
0.18	1.30E-4
0.21	1.51E-4

Table 1.9. Rate data for catalysts **15-19**. Data for Figure 1.11.

[diene] = 0.183 M, [aldehyde] = 0.780 M [catalyst] = 0.036 M, –46 °C

catalyst	pK_a of RCO_2H	rate (M/s) (1st run)	rate (M/s) (2nd run)	average rate (M/s)	log(rate)	error
15	-0.25	9.94E-5	6.98E-5	8.46E-5	–4.08	0.11
16	0.65	3.04E-5	1.92E-5	2.48E-5	–4.62	0.14
17	1.29	2.43E-5	1.53E-5	1.98E-5	–4.72	0.14
18	2.66	3.69E-6	3.52E-6	3.61E-6	–5.44	0.02
19	2.86	2.15E-6	3.47E-6	2.81E-6	–5.56	0.14

Table 1.10. [aldehyde] saturation with catalyst **15**. Data for Figure 1.12 A.

[diene] = 0.075 M, [**15**] = 0.0183 M, 0 °C

[benzaldehyde] (M)	initial rate (M/s)
0.05	1.96E-5
0.10	3.11E-5
0.25	4.72E-5
0.50	4.78E-5
1.00	4.91E-5
1.00	4.72E-5

Table 1.11. [aldehyde] saturation with catalyst **19**.
Data for Figure 1.12 B.

[diene] = 0.075 M, [**19**] = 0.0183 M, 0 °C

[benzaldehyde] (M)	initial rate (M/s)
0.05	2.51E-6
0.10	4.31E-6
0.25	8.57E-6
0.50	1.04E-5
0.75	1.09E-5
1.00	1.21E-5

Table 1.12. [*p*-anisaldehyde] saturation.
Data for Figure 1.14 A.

[diene] = 0.16 M, [**15**] = 0.016 M, –46 °C

[*p*-anisaldehyde] (M)	initial rate (M/s)
0.025	8.79E-7
0.050	1.55e-6
0.11	1.77E-6
0.16	2.18E-6
0.20	2.97E-6
0.25	2.56E-6
1.0	2.93E-6

Table 1.13. [*p*-CF_3-benzaldehyde] saturation. Data for Figure 1.14B.

[diene] = 0.16 M, [**15**] = 0.016 M, –46 °C

[*p*-CF_3benzaldehyde] (M)	initial rate (M/s)
0.025	6.35E-7
0.038	7.22E-7
0.050	8.78E-5
0.11	1.31E-4
0.16	3.75E-4
0.25	4.45E-4
0.50	4.41E-4
1.0	6.78E-4

Table 1.14. Rate data for Hammett plots. Data for Figure 1.15.

[diene] = 0.16 M, [**15**] = 0.016 M, –46 °C

R	[aldehyde] = 1.0 M average rate (M/s)	[aldehyde] = 0.025 M average rate (M/s)
CF_3	6.78×10^{-4}	6.35×10^{-7}
H	4.64×10^{-5}	6.03×10^{-6}
F	2.93×10^{-5}	6.51×10^{-6}
Me	2.61×10^{-5}	2.90×10^{-6}
OMe	2.93×10^{-6}	8.21×10^{-7}

HPLC or GC analysis using a chiral stationary phase was performed to determine the enantiomeric ratio of Diels Alder products. The methods used, retention times, and enantiomeric ratios are tabulated in Table 1.15.

Table 1.15. Chiral separation methods.

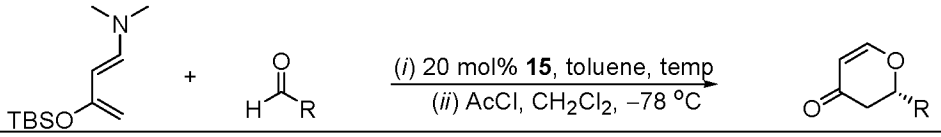

entry	R	Separation method	ret. time$_{major}$	ret. time$_{minor}$	% ee	er
1	$C_6H_4CF_3$	GC β-cyclodex column 130 °C for 20 min + 0.5 °C/min to 160 °C, hold 8 min + 10 °C/min to 200 °C, hold 8 min	27.6 min	28.8 min	91	95:5
2	C_6H_4Cl	GC β-cyclodex column 120 °C for 20 min + 0.4 °C/min to 140 °C, hold 2 min + 10 °C/min to 200 °C, hold 12 min	75.8 min	76.1 min	86	93:7
3	C_6H_4F	GC β-cyclodex column 120 °C for 90 min	50.1 min	54.1 min	84	92:8
4	C_6H_5	GC β-cyclodex column 120 °C for 90 min	45.2 min	48.7 min	91	96:4
5	C_6H_4Me	GC β-cyclodex column 120 °C for 90 min	74.8 min	80.0 min	83	92:8
6	C_6H_4OMe	GC β-cyclodex column 130 °C for 20 min + 0.5 °C/min to 160 °C, hold 8 min + 10 °C/min to 200 °C, hold 8 min	67.9 min	69.2 min	90	95:5
7	$C_6H_4NO_2$	HPLC Chiralcel-OD column 10:90 IPA:hexanes 1 mL/min	38.1 min	57.9 min	81	91:9
8	1-naphthyl	HPLC Chiralpack-AS 20:80 IPA:hexanes 1 mL/min	14.2 min	22.4 min	96	98:2
9	CH=CHPh	HPLC Chiralcel-OD column 10:90 IPA:hexanes 1 mL/min	21.5 min	47.5 min	90	95:5
10	CH_2CH_2Ph	HPLC Chiralcel-OD column 10:90 IPA:hexanes 1 mL/min	22.6 min	41.2 min	47	73:27
11	$(CH_2)_4CH_3$	HPLC Chiralcel-OD column 2.5:97.5 IPA:hexanes 0.5 mL/min	18.8 min	20.5 min	30	65:35

References

(1) Doyle, A. G.; Jacobsen, E. N. *Chem. Rev.* **2007**, *107*, 5713.

(2) Akiyama, T. *Chem. Rev.* **2007**, *107*, 5744.

(3) Taylor, M. S.; Jacobsen, E. N. *Angew. Chem., Int. Ed.* **2006**, *45*, 1520.

(4) Eder, U.; Sauer, G.; Wiechert, R. *Angew. Chem., Int. Ed. Engl.* **1971**, *10*, 496.

(5) Hajos, Z. G.; Parrish, D. R. *J. Org. Chem.* **1974**, *39*, 1615.

(6) Hiemstra, H.; Wynberg, H. *J. Am. Chem. Soc.* **1981**, *103*, 417.

(7) Dolling, U. H.; Davis, P.; Grabowski, E. J. J. *J. Am. Chem. Soc.* **1984**, *106*, 446.

(8) Conn, R. S. E.; Lovell, A. V.; Karady, S.; Weinstock, L. M. *J. Org. Chem.* **1986**, *51*, 4710.

(9) Wynberg, H. *Top. Stereochem.* **1986**, *16*, 87.

(10) Gaunt, M. J.; Johansson, C. C. C. *Chem. Rev.* **2007**, *107*, 5596.

(11) Huang, Y.; Unni, A. K.; Thadani, A. N.; Rawal, V. H. *Nature* **2003**, *424*, 146.

(12) Sigman, M. S.; Jacobsen, E. N. *J. Am. Chem. Soc.* **1998**, *120*, 4901.

(13) Miyabe, H.; Takemoto, Y. *Bull. Chem. Soc. Jpn.* **2008**, *81*, 785.

(14) Oku, J.; Inoue, S. *J. Chem. Soc., Chem. Commun.* **1981**, 229.

(15) McDougal, N. T.; Schaus, S. E. *J. Am. Chem. Soc.* **2003**, *125*, 12094.

(16) Mukherjee, S.; Yang, J. W.; Hoffmann, S.; List, B. *Chem. Rev.* **2007**, *107*, 5471.

(17) Vachal, P.; Jacobsen, E. N. *J. Am. Chem. Soc.* **2002**, *124*, 10012.

(18) Zuend, S. J.; Jacobsen, E. N. *J. Am. Chem. Soc.* **2007**, *129*, 15872.

(19) Zuend, S. J.; Jacobsen, E. N. *J. Am. Chem. Soc.* **2009**, *131*, 15358.

(20) Xu, H.; Zuend, S. J.; Woll, M. G.; Tao, Y.; Jacobsen, E. N. *Science* **2010**, *327*, 986.

(21) Jensen, K. H.; Sigman, M. S. *Angew. Chem., Int. Ed.* **2007**, *46*, 4748.

(22) Berkessel, A.; Koch, B.; Lex, J. *Advanced Synthesis & Catalysis* **2004**, *346*, 1141.

(23) Hartikka, A.; Arvidsson, P. I. *Tetrahedron: Asymmetry* **2004**, *15*, 1831.

(24) Hartikka, A.; Arvidsson, P. I. *Eur. J. Org. Chem.* **2005**, 4287.

(25) Hine, J.; Linden, S. M.; Kanagasabapathy, V. M. *J. Am. Chem. Soc.* **1985**, *107*, 1082.

(26) Hine, J.; Linden, S. M.; Kanagasabapathy, V. M. *J. Org. Chem.* **1985**, *50*, 5096.

(27) Rajaram, S.; Sigman, M. S. *Org. Lett.* **2005**, *7*, 5473.

(28) Miller, J. J.; Sigman, M. S. *Angew. Chem., Int. Ed.* **2008**, *47*, 771.

(29) Sigman, M. S.; Miller, J. J. *J. Org. Chem.* **2009**, *74*, 7633.

(30) Pellissier, H. *Tetrahedron* **2009**, *65*, 2839.

(31) Unni, A. K.; Takenaka, N.; Yamamoto, H.; Rawal, V. H. *J. Am. Chem. Soc.* **2005**, *127*, 1336.

(32) Huang, Y.; Rawal, V. H. *Org. Lett.* **2000**, *2*, 3321.

(33) Huang, Y.; Rawal, V. H. *J. Am. Chem. Soc.* **2002**, *124*, 9662.

(34) Bordwell, F. G. *Acc. Chem. Res.* **1988**, *21*, 456.

(35) Bordwell, F. G.; Fried, H. E.; Hughes, D. L.; Lynch, T. Y.; Satish, A. V.; Whang, Y. E. *J. Org. Chem.* **1990**, *55*, 3330.

(36) Sibi, M. P.; Chen, J.-X.; Cook, G. R. *Tetrahedron Lett.* **1999**, *40*, 3301.

(37) Anderson, G. W.; Zimmerman, J. E.; Callahan, F. M. *J. Am. Chem. Soc.* **1967**, *89*, 5012.

(38) Evans, D. A.; Peterson, G. S.; Johnson, J. S.; Barnes, D. M.; Campos, K. R.; Woerpel, K. A. *J. Org. Chem.* **1998**, *63*, 4541.

(39) Downing, S. V.; Aguilar, E.; Meyers, A. I. *J. Org. Chem.* **1999**, *64*, 826.

(40) Anslyn, E. V.; Dougherty, D. A. Modern Physical Organic Chemistry, University Science Books, 2006, p 466.

(41) Doyle, M. P.; Valenzuela, M.; Huang, P. *Proc. Natl. Acad. Sci. U. S. A.* **2004**, *101*, 5391.

(42) Benghait, I.; Becker, E. I. *J. Org. Chem.* **1958**, *23*, 885.

(43) Lotfi, M.; Roberts, R. M. G. *Tetrahedron* **1979**, *35*, 2131.

(44) Okamoto, Y.; Brown, H. C. *J. Org. Chem.* **1957**, *22*, 485.

(45) DeWitt, E. J.; Lester, C. T.; Ropp, G. A. *J. Am. Chem. Soc.* **1956**, *78*, 2101.

(46) Inukai, T.; Kojima, T. *J. Chem. Soc. D* **1969**, 1334.

(47) Salakhov, M. S.; Musaeva, N. F.; Suleimanov, S. N. *Org. React. (Tartu)* **1979**, *16*, 54.

(48) Domingo, L. R.; Saez, J. A. *Org. Biomol. Chem* **2009**, *7*, 3576.

(49) Charton, M. *J. Org. Chem.* **1966**, *31*, 3745.

(50) Perrin, C. L. *Science* **1994**, *266*, 1665.

(51) Cleland, W. W.; Kreevoy, M. M. *Science* **1994**, *264*, 1887.

(52) Schwartz, B.; Drueckhammer, D. G.; Usher, K. C.; Remington, S. J. *Biochemistry* **1995**, *34*, 15459.

(53) Based on calculated pKa values reported on Scifinder (Calculated using Advanced Chemistry Development Software V8.14).

(54) Li, X.; Deng, H.; Zhang, B.; Li, J.; Zhang, L.; Luo, S.; Cheng, J.-P. *Chem. Eur. J.* **2010**, *16*, 450.

(55) Du, J.; Li, Z.; Du, D.-M.; Xu, J. *ARKIVOC (Gainesville, FL, U. S.)* **2008**, 145.

(56) Davis, T. A.; Wilt, J. C.; Johnston, J. N. *J. Am. Chem. Soc.* **2010**, *132*, 2880.

(57) Kozmin, S. A.; He, S.; Rawal, V. H. *Organic Syntheses* **2002**, *78*, 152.

(58) Ji, B.; Yuan, Y.; Ding, K.; Meng, J. *Chem. Eur. J.* **2003**, *9*, 5989.

(59) Schaus, S. E.; Brånalt, J.; Jacobsen, E. N. *J. Org. Chem.* **1998**, *63*, 403.

CHAPTER 2

THE DEVELOPMENT OF AN ENANTIOSELECTIVE PALLADIUM-CATALYZED ALKENE DIFUNCTIONALIZATION REACTION

Introduction

The installation of two new functional groups across a double bond is a process with great potential synthetic utility (Figure 2.1). However, the development of a reaction that forms two new bonds in one step presents significant challenges. For these reactions to be useful, they must be selective. This includes diastereoselectivity, as two new stereocenters can be set (if $R^1 \neq H$, $R^2 \neq H$), regioselectivity, if the two new functional groups are different ($X \neq Y$), and enantioselectivity, if a chiral catalyst is used to control the absolute stereochemistry. Furthermore, chemoselectivity is also a concern, as catalysts used to perform these reactions may have a propensity to form other products. These reactions, termed alkene difunctionalization reactions, have been the focus of a significant amount of research within the field of catalysis. Considerable advancements have taken place, yet there is still incredible potential for the development of novel alkene difunctionalization reactions.

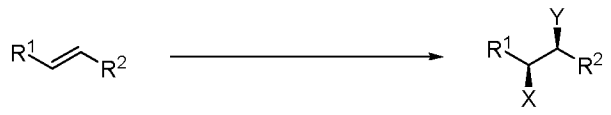

Figure 2.1. Alkene difunctionalization reactions.

The Sigman research group has become interested in alkene difunctionalization reactions as a part of a research program focused on developing new palladium-catalyzed alkene oxidations. This chapter examines the progress within this field and strategies for overcoming selectivity challenges and discusses the recent contributions we have made.

Background

Osmium-Catalyzed Alkene Difunctionalization Reactions

The exemplary alkene difunctionalization reaction is the Sharpless asymmetric dihydroxylation (Figure 2.2).[1,2] The process provides *syn*-diols in high enantioselectivity for a broad range of alkene substrates. Either enantiomer of the diol product can usually be obtained with the correct choice of chiral ligand, either $(DHQ)_2PHAL$ or $(DHDQ)_2PHAL$. The details of the reaction have been studied extensively, and the reaction is widely used in synthetic applications.

This methodology has been expanded to enantioselective aminohydroxylation, using an *N*-halogenated reagent (PGN-XNa) as the nitrogen source and oxidant (Figure 2.3).[3-12] When an unsymmetrical alkene is employed, regioselectivity in these reactions requires the use of electronically biased substrates, such as styrenes and α,β-unsaturated carbonyls.

An intramolecular variant of this reaction involving the in situ oxidation of an amide linked to the alkene in the substrate has been reported by Donohoe and

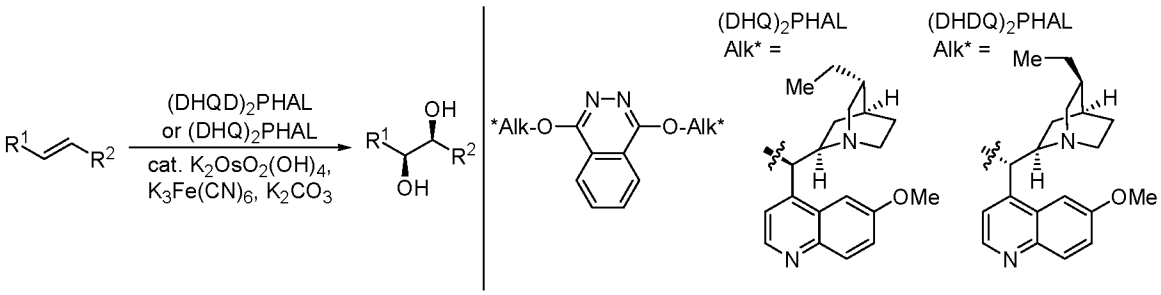

Figure 2.2. Sharpless osmium-catalyzed asymmetric dihydroxylation.

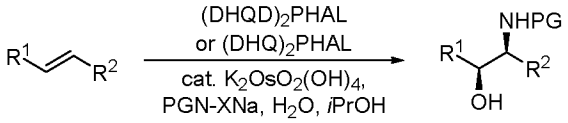

Figure 2.3. Sharpless enantioselective osmium-catalyzed alkene aminohydroxylation.

coworkers,[13-15] where regioselectivity is presumably influenced by the favorable formation of a five-member ring in the product (Figure 2.4). Unfortunately, the use of chiral ligands such as $(DHQ)_2PHAL$ or $(DHDQ)_2PHAL$ has failed to provide stereochemical induction to obtain enantiomerically enriched products.[13,14]

Given the considerable synthetic interest in the ability to form enantiomerically enriched heterocylic compounds in a catalytic fashion, approaches to alkene difunctionalization using metals in addition to osmium have become the focus of recent efforts in alkene difunctionalization.

Copper-Catalyzed Alkene Difunctionalization Reactions

Recent advancements in metal-catalyzed alkene difunctionalization reactions have been accomplished with the use of copper. Chemler and coworkers have reported an enantioselective copper-catalyzed intramolecular aminoarylation of alkenes using Ph-bisoxazoline ligand **1** (Figure 2.5).[16-18] The reaction is proposed to proceed through a

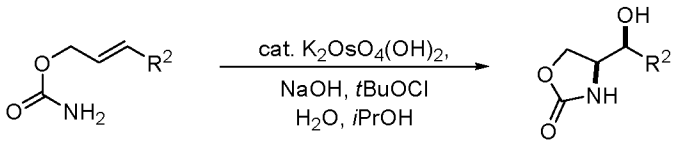

Figure 2.4. Osmium-catalyzed intramolecular amino-hydroxylation developed by Donohoe.

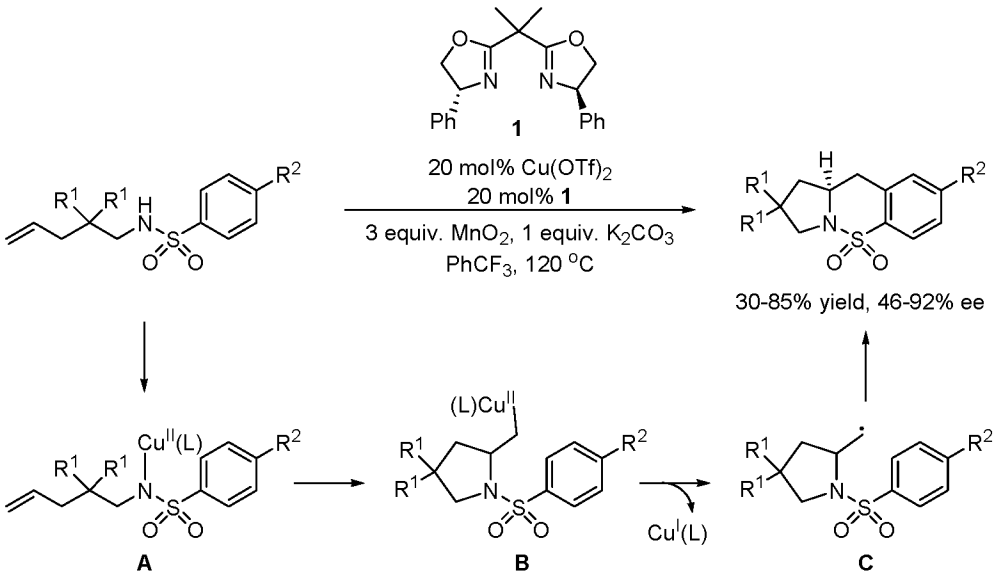

Figure 2.5. Chemler's copper-catalyzed enantioselective intramolecular carboamination.

syn-aminocupration of the alkene, to give intermediate **A**, followed by homolytic carbon-Cu bond cleavage and trapping of the subsequent radical intermediate **C** with the aromatic ring.

The same research group used a similar catalyst to accomplish copper-catalyzed aminooxygenation, by using TEMPO (**2**) as an oxidant, which reacts to form a new carbon oxygen bond in the product (Figure 2.6).[19] Up to 92% ee was obtained using bisoxazoline ligand **3**.

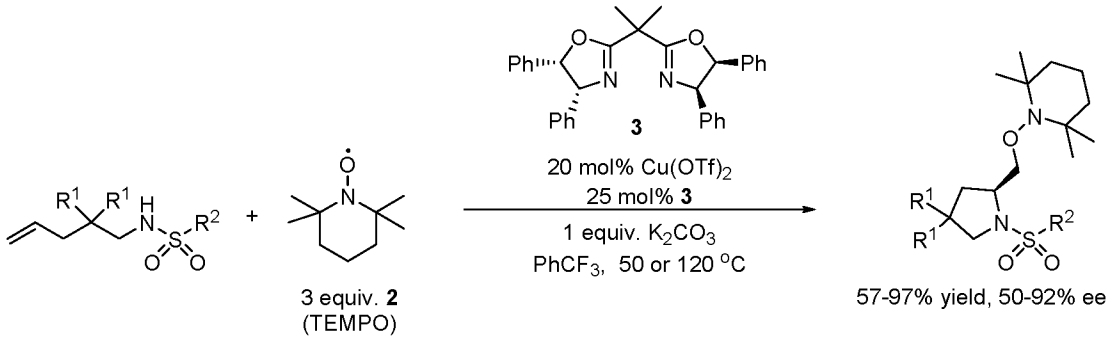

Figure 2.6. Copper-catalyzed enantioselective intramolecular alkene aminooxygenation developed by Chemler.

Yoon and coworkers have reported a copper-catalyzed alkene aminohydroxylation using an oxaziridine as the oxidant as well as the source of both oxygen and nitrogen atoms (Figure 2.7).[20-22] This reaction is proposed to proceed via initial activation of the oxaziridine **4** by binding to copper, followed by homolytic reaction with the alkene to give a transient Cu^{III} intermediate **B**, which reacts with the benzylic radical to give the product.[22] A diastereomeric mixture of products results when using racemic oxaziridine **4**.

These examples of copper-catalyzed alkene difunctionalization reactions are likely to inspire a number of new reactions of this type. However, the proposed radical intermediates may limit the types of functional groups that are compatible with these reactions.

Palladium-Catalyzed Alkene Difunctionalization Reactions

The majority of recent research on alkene difunctionalization has been with the use of palladium catalysts. A reason for this is the ease with which Pd(II) facilitates the

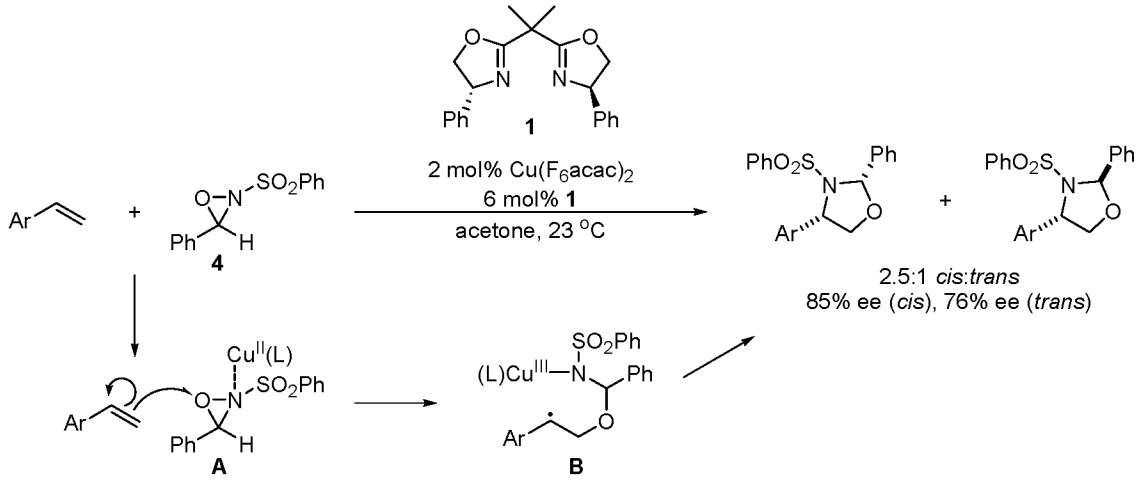

Figure 2.7. Yoon's copper-catalyzed enantioselective intermolecular alkene aminooxygenation.

addition of nucleophiles to alkenes.[23] However, an issue arises following formation of the resultant Pd-alkyl intermediate **B**, since these intermediates have the potential to undergo β-hydride elimination to yield Wacker-type products **5** (Figure 2.8).[24] While processes of this type are clearly useful, they generally only lead to functionalization at one of the two alkene carbons. Furthermore, any stereochemical information parlayed from a chiral catalyst in the initial nucleopalladation step is lost if β-hydride elimination occurs with the hydrogen at the stereocenter. Therefore, in order to achieve alkene difunctionalization, it is necessary to develop a system where the rate of the second functionalization step is greater than that of β-hydride elimination. Approaches to this problem can be divided into two general categories: (1) incorporation of a functional group in the substrate which coordinates to the Pd-alkyl intermediate to decrease the rate of β-hydride elimination, or (2) rapid reaction of the Pd^{II}-alkyl species.[25]

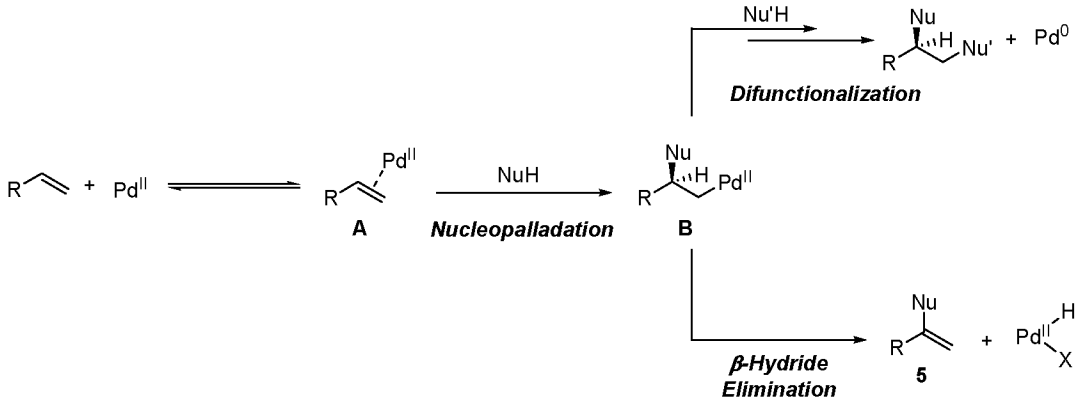

Figure 2.8. Palladium-catalyzed alkene difunctionalization and competing β-hydride elimination reactions.

π-Allyl Intermediates to Prevent β-Hydride Elimination

One of the most common types of substrates used in alkene difunctionalization is dienes. In this case, the second olefin coordinates to palladium, forming a π-allyl intermediate to prevent β-hydride elimination. Pioneering reaction development and mechanistic investigation of palladium-catalyzed diene difunctionalization was performed by Bäckvall and coworkers in the 1980s and 1990s.[23,26-32] Palladium-catalyzed diene diacetoxylation (Figure 2.9) is proposed to occur via coordination to Pd^{II} followed by *anti*-oxypalladation, resulting in formation of a palladium-π-allyl intermediate **B**. Nucleophilic attack of **B** by a second equivalent of acetate results in product formation and palladium reduction. Benzoquinone is present as an oxidant to regenerate Pd^{II}. Either the *cis* or *trans* product can be obtained, depending on the conditions. High [Cl^-] prevents acetate coordination, and the intermolecular attack by acetate on this species occurs on the face opposite palladium, leading to *cis*-**6**. Alternatively, with low [Cl^-], intramolecular attack by a coordinated acetate occurs to form the *trans*-**6**.[26]

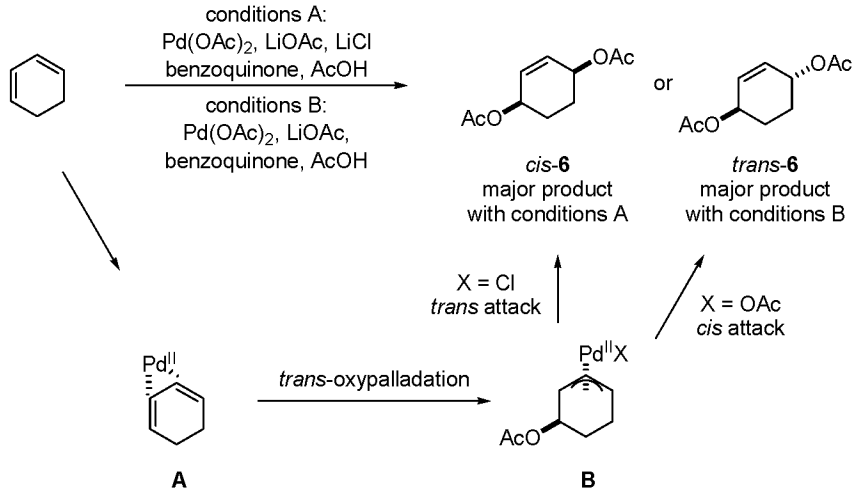

Figure 2.9. Bäckvall's palladium-catalyzed dioxygenation of dienes.

Bäckvall and coworkers also have reported intramolecular diene functionalization reactions, including dioxygenation, aminoacetoxylation, and aminochlorination reactions, demonstrating the diversity of potential products that can be formed with palladium-catalyzed alkene difunctionalization reactions (Figure 2.10). [31]

Recently, a palladium-catalyzed diene diamination has been reported by Lloyd-Jones and Booker-Milburn (Figure 2.11).[33] Utilization of *N,N'*-diethyl urea **7** as a nitrogen nucleophile results in diamination of the terminal alkene, likely proceeding through palladium-π-allyl intermediate **A**, and subsequent intramolecular attack by the now tethered second nucleophile.

A complimentary diene diamination reaction resulting in diamination at the terminal position has been reported by Shi and coworkers (Figure 2.12).[34-36] This reaction differs mechanistically, as it is proposed to be initiated by oxidative addition of di-*tert*-butyldiaziridinone **8** to Pd^0. The resulting palladacycle **A** undergoes alkene insertion to deliver palladium-π-allyl intermediate **B**, from which the mechanism

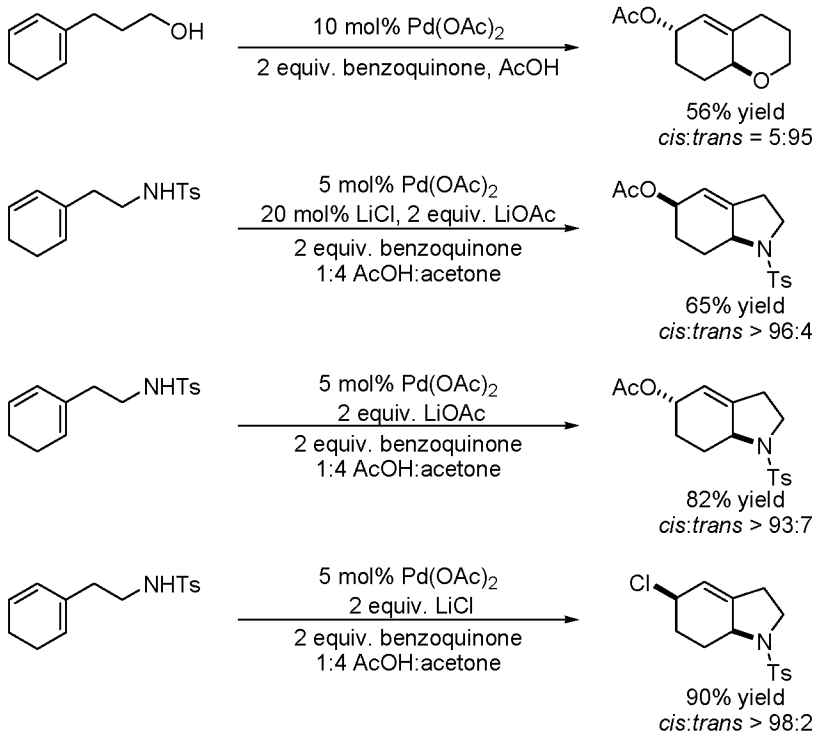

Figure 2.10. Palladium-catalyzed intramolecular diene alkoxyacetoxylation, aminoacetoxylation, and aminochlorination reactions developed by Bäckvall.

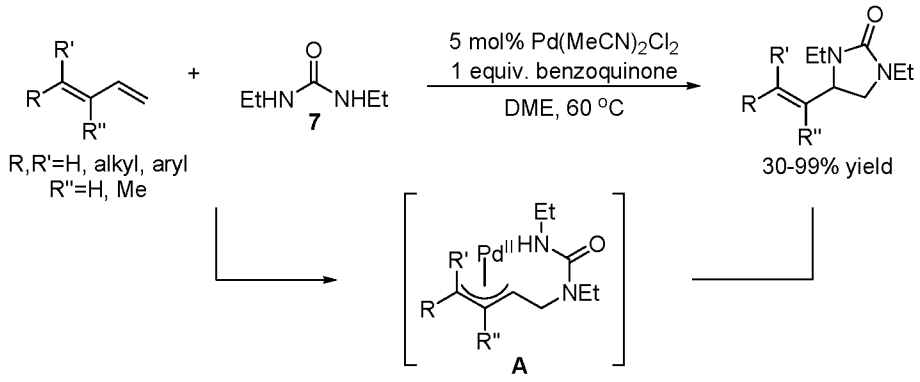

Figure 2.11. Palladium-catalyzed diamination of dienes developed by Lloyd-Jones and Booker-Milburn.

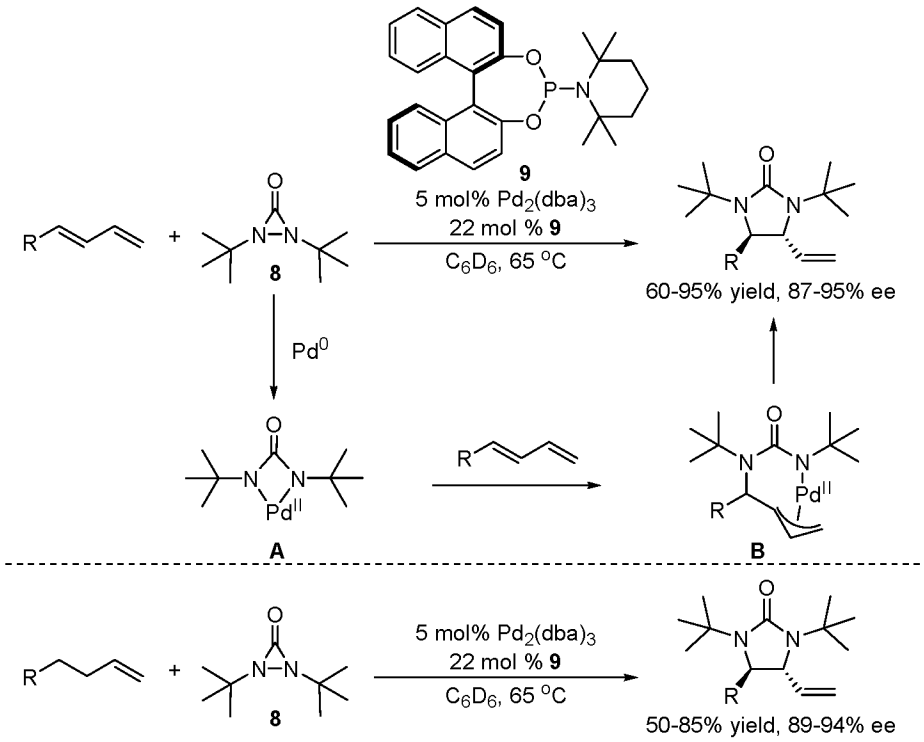

Figure 2.12. Shi's palladium-catalyzed diamination of dienes at the internal position.

proceeds similarly to other diene difunctionalization reactions. The use of phosphoramidite ligand **9** resulted in high levels of stereoinduction. Additionally, the authors demonstrated that this system could be applied to terminal alkenes capable of in situ diene formation.[37,38]

Trapping Pd-alkyl Intermediates via Insertion

In addition to the use of substrates containing conjugated dienes in palladium-catalyzed difunctionalization reactions, substrates containing an unconjugated second alkene have also been used (Figure 2.13). The result is an overall oxygen/carbon or nitrogen/carbon alkene difunctionalization. These reactions follow a general mechanism involving nucleopalladation of the first alkene to form intermediate **A**, followed by insertion of the second alkene forming **B**, and finally, β-hydride elimination.

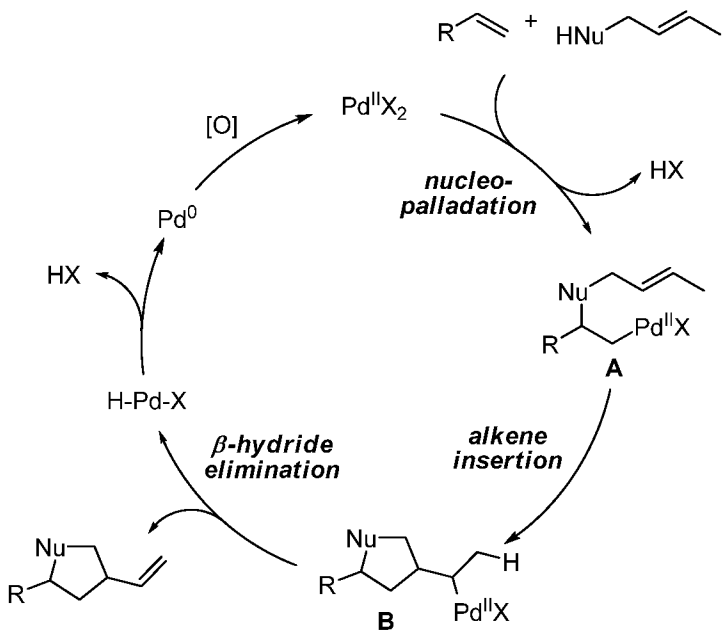

Figure 2.13. General mechanism for palladium-catalyzed difunctionalization reactions involving alkene insertion.

These reactions proceed by a mechanism similar to that proposed for palladium-catalyzed alkene alkoxycarbonylation reaction, pioneered by Semmelhack and coworkers in the 1980s and 1990s (Figure 2.14). This reaction proceeds through insertion of carbon monoxide into the Pd-alkyl bond of **B** and methanolysis of the resulting Pd-carbonyl species **C**.[39,40] This work undoubtedly has had significant influence on current research in this area.

Sasai and coworkers reported an enantioselective alkene difunctionalization reaction of this type with substrate **10** which contains an alcohol nucleophile and two alkenes (Figure 2.15).[41] Interestingly, selective intramolecular oxypalladation of one alkene sets the stereochemistry of the prochiral quaternary center, using bis(isoxazoline) **11** as the chiral ligand to form bicyclic product **12** in high enantiomeric excess.

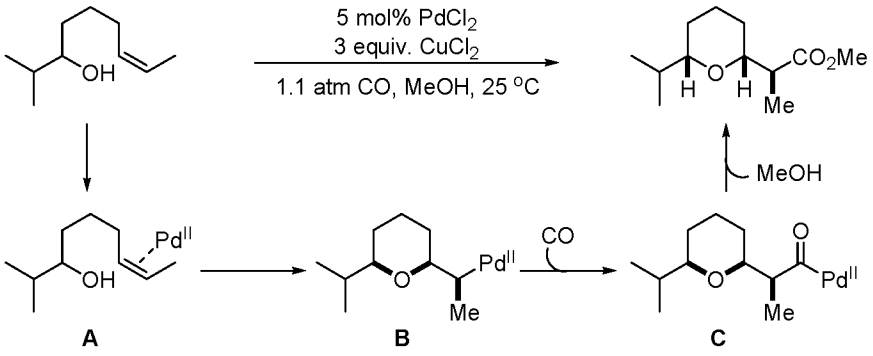

Figure 2.14. Semmelhack's palladium-catalyzed intramolecular alkoxycarbonylation.

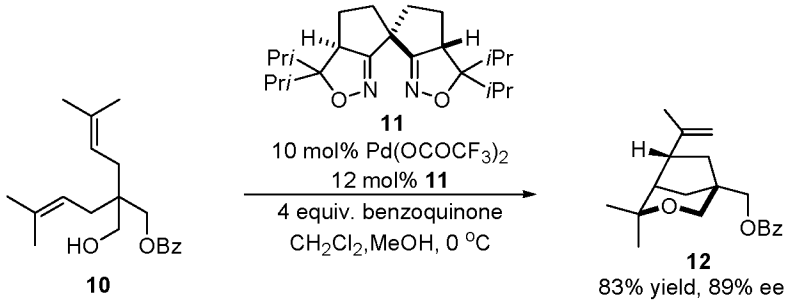

Figure 2.15. Sasai's enantioselective palladium-catalyzed oxypalladation/alkene insertion.

An intermolecular alkene difunctionalization reaction was reported by Hosokawa and coworkers, where enol ether **13** is proposed to undergo oxypalladation/alkene insertion, and the alcohol and alkene nucleophiles are linked in **14** (Figure 2.16).[42,43]

Analogous reactions involving an aminopalladation alkene insertion sequence have been reported. Yang and coworkers have developed an enantioselective intramolecular alkene difunctionalization reaction, where the nitrogen nucleophile and both alkenes are in the substrate (**15**, Figure 2.17).[44,45] Using (–)sparteine[44] **17** or (*S*)-quinox-*t*Bu[45] **18** the tricyclic products **16** can be obtained in high enantioselectivity.

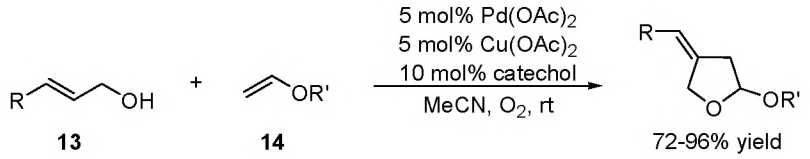

Figure 2.16. Hosokawa's palladium-catalyzed oxypalladation/alkene insertion of enol ethers.

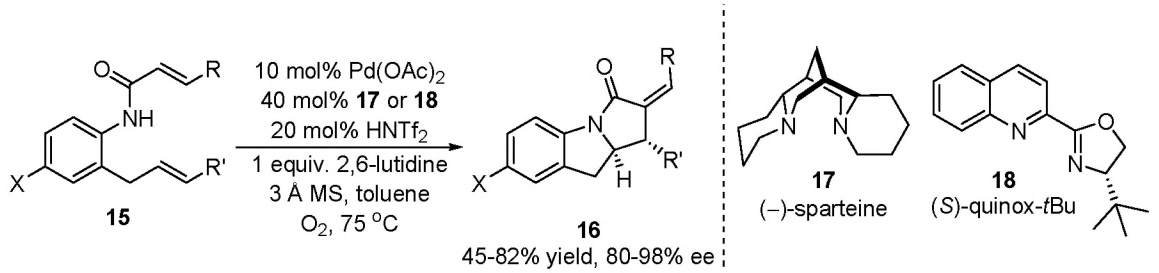

Figure 2.17. Enantioselective palladium-catalyzed aminopalladation/alkene insertion developed by Yang.

An intermolecular palladium-catalyzed carboamination of vinyl ethers **20** and styrenes **21** using allylic *p*-toluenesulfonamides **19** as the source of nitrogen and carbon nucleophiles was reported by Stahl and coworkers. (Figure 2.18).[46] Diastereoselectivity is modest, ranging from 1.3 to 2.4:1. To date, there are no examples of intermolecular reactions of this type that are enantioselective.

Palladium-Catalyzed Alkene Difunctionalization Involving Pd^{II} to Pd^{IV} Oxidation

Oxidation of a Pd^{II}-alkyl intermediate to Pd^{IV} is a strategy for palladium-catalyzed alkene difunctionalization with momentous recent developments.[47] Such a transformation increases the electrophilicity of the intermediate, thus making a second functionalization more facile (Figure 2.19). As with most of the Pd^{II}-Pd^{0}-catalyzed reactions discussed above, these reactions are hypothesized to begin by alkene

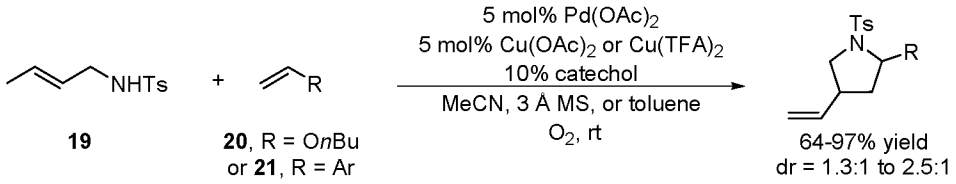

Figure 2.18. Stahl's intermolecular palladium-catalyzed carboamination of alkenes. Note: catechol was not used with styrenes (when R = Ar).

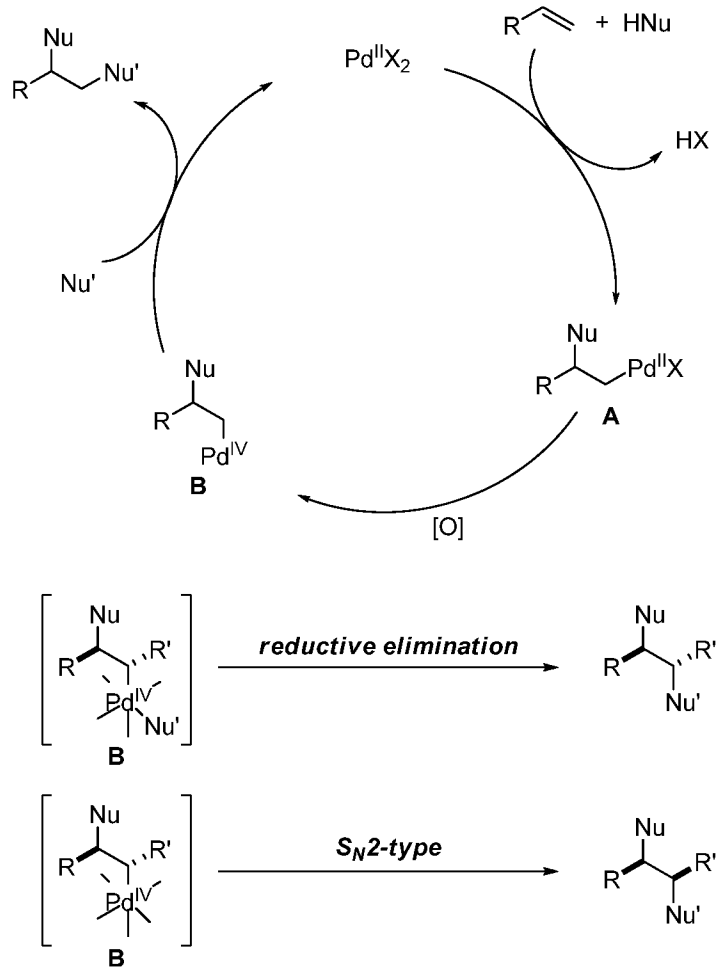

Figure 2.19. Proposed mechanism for palladium-catalyzed reaction invoking a Pd^{IV} intermediate.

coordination and nucleopalladation to form the first bond. Pd^{II}-alkyl intermediate **A** is subsequently oxidized to Pd^{IV} intermediate **B**. The second bond-forming step is hypothesized to proceed via two possible pathways: (1) reductive elimination of C-Nu from Pd^{IV}, resulting in retention of stereochemistry, or (2) nucleophilic attack of an external nucleophile, with Pd^{II} as the leaving group, resulting in inversion of stereochemistry. The two pathways can be distinguished, in cases where the stereochemical outcome of the nucleopalladation step is predictable.

The earliest examples of Pd-catalyzed reactions where a Pd^{IV} intermediate allows for alkene difunctionalization were reported by Sorenson and coworkers (Figure 2.20 A),[48] and shortly after, by Muñiz and coworkers (Figure 2.20 B)[49-51] in 2005. Both reactions use $PhI(OAc)_2$ as an oxidant and utilize substrates **22** or **23** containing nitrogen nucleophiles to undergo intramolecular nucleopalladation. Further advances include Stahl and coworkers' (Figure 2.20 C)[52] and Sanford and coworkers' (Figure 2.20 D)[53] reports of aminooxygenation reactions using phthalamide **24** as an intermolecular nucleophile.

Pd^{II}-Pd^{IV} catalytic cycles have been proposed recently for alkene diacetoxylation reactions. Song and Dong reported the reaction using $PhI(OAc)_2$ to provide dioxygenated products **25** in good yield and diastereoselectivity (Figure 2.21 A).[54] Subsequently, Jiang and coworkers reported a diacetoxylation reaction using O_2 as the sole oxidant (Figure 2.21, B).[55] This is the first alkene difunctionalization reaction where direct oxidation of Pd^{II} to Pd^{IV} by O_2 is proposed.

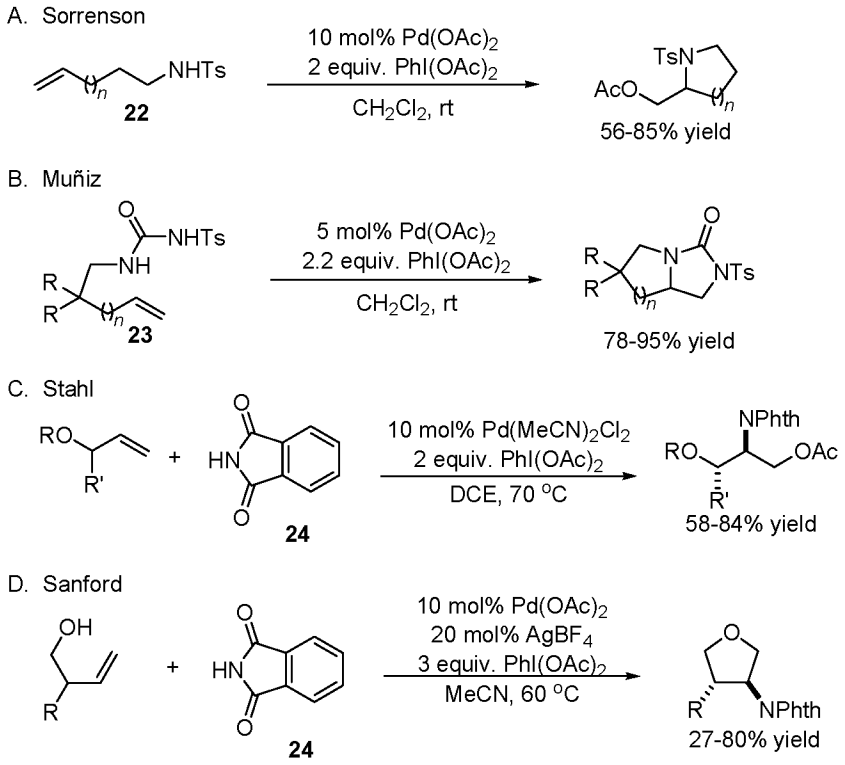

Figure 2.20. Early examples of Pd^{IV} in alkene difunctionalization reactions.

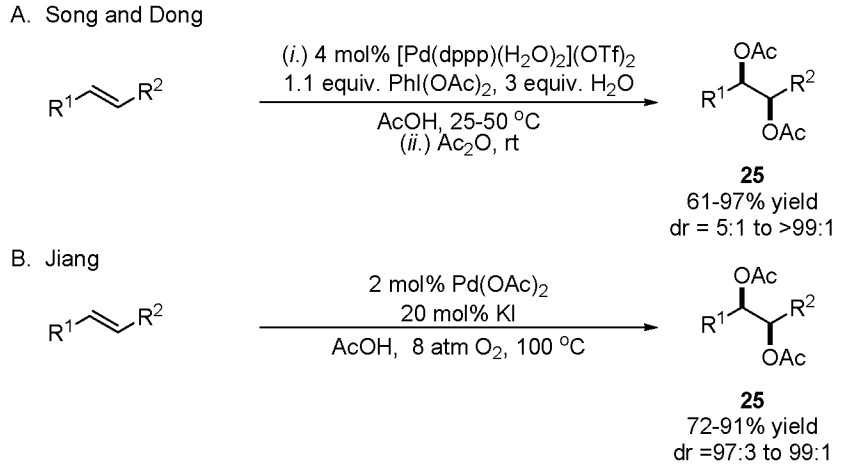

Figure 2.21. Palladium-catalyzed alkene diacetoxylation reactions.

Michael and coworkers have recently reported the use of an alternative oxidant, *N*-fluorobenzenesulfonimide **26** to access Pd^{IV} intermediates with alkene substrates **27** containing a linked nitrogen nucleophile.[56,57] In addition to being the oxidant, **26** is also the nitrogen source in the alkene diamination reaction (Figure 2.22, A).[56] However, when aromatic solvents are used, the predominant pathway is aminoarylation (Figure 2.22, B.),[57] presumably via aromatic attack upon the electrophilic Pd^{IV}-species in an electrophilic aromatic substitution mechanism.

Dioxygenation Reactions of Alkenes with an *o*-Phenol

Le Bras, Muzart, and coworkers reported the palladium-catalyzed dioxygenation of *ortho*-vinyl phenol **28** using ligand **29** (Figure 2.23).[58,59] A mixture of alkoxyhydroxylation (**30**) and dihydroxylation (**31**) products is obtained. The proposed mechanism involves a palladium-catalyzed alkene epoxidation with H_2O_2, followed by attack of intermediate **A** at the benzylic position with MeOH or water. Observation by mass spectrometry of a palladium-ligand-epoxide complex provides evidence in support of this mechanism. Additionally the authors submitted a benzyl-protected analogue **32** of

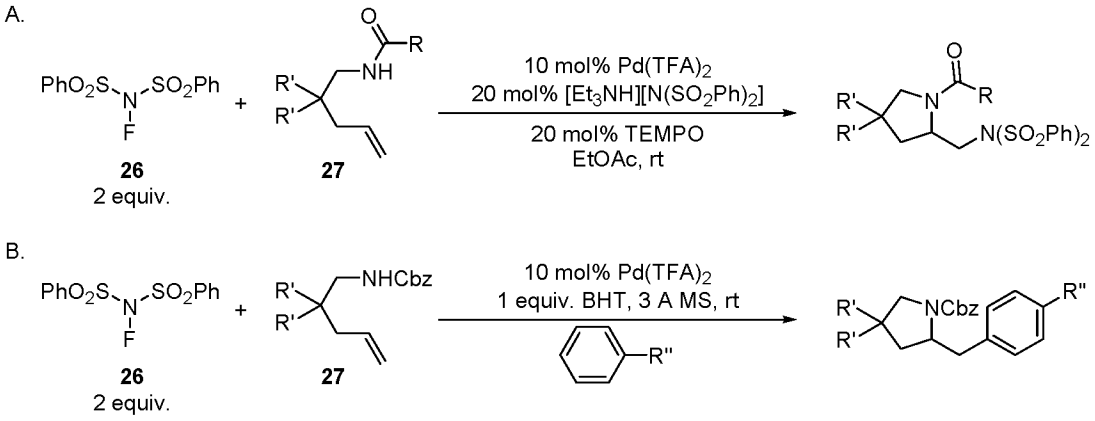

Figure 2.22. Michael's alkene diamination and aminoarylation reactions.

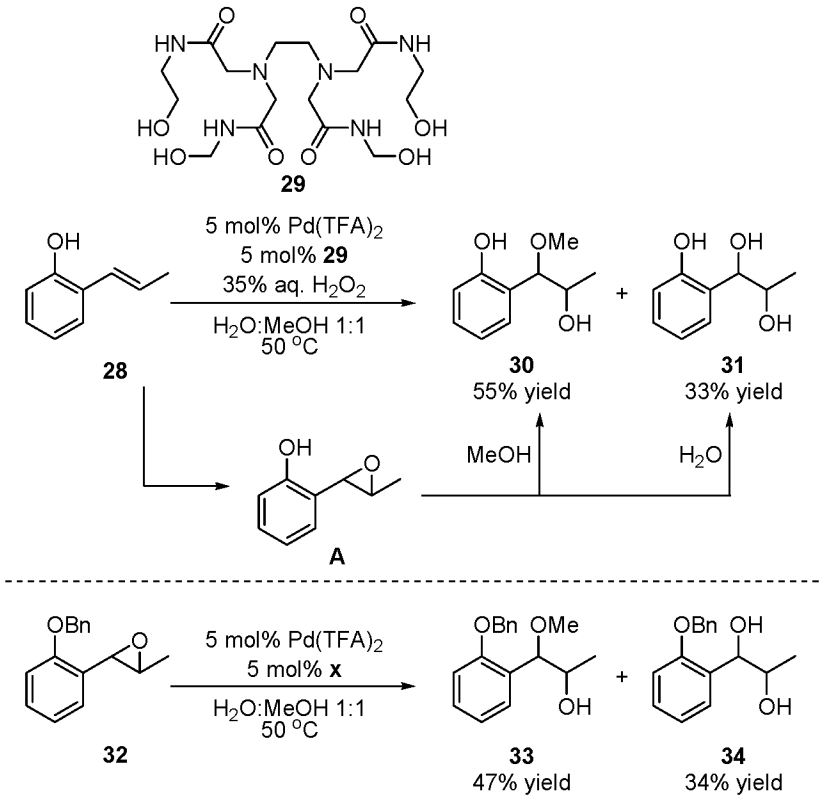

Figure 2.23. Palladium-catalyzed dioxygenation of propenyl phenol and proposed epoxide intermediate reported by Le Bras and Muzart.

the proposed epoxide intermediate to the reaction conditions and obtained a similar ratio of products **33** and **34**.

Shortly after this report, our group reported a similar reaction: a palladium-catalyzed dialkoxylation of propenylphenols, developed by Dr. Mitch Schultz (Figure 2.24).[60] The mechanism proposed for this reaction involves initial oxypalladation of the alkene resulting in a palladium-alkyl **A**. This intermediate is capable of forming a quinone methide intermediate **B** with simultaneous reduction to Pd^0. This key step prevents β-hydride elimination and allows the electrophilic quinone methide to be attacked by a second equivalent of alcohol. Support of this mechanism includes the

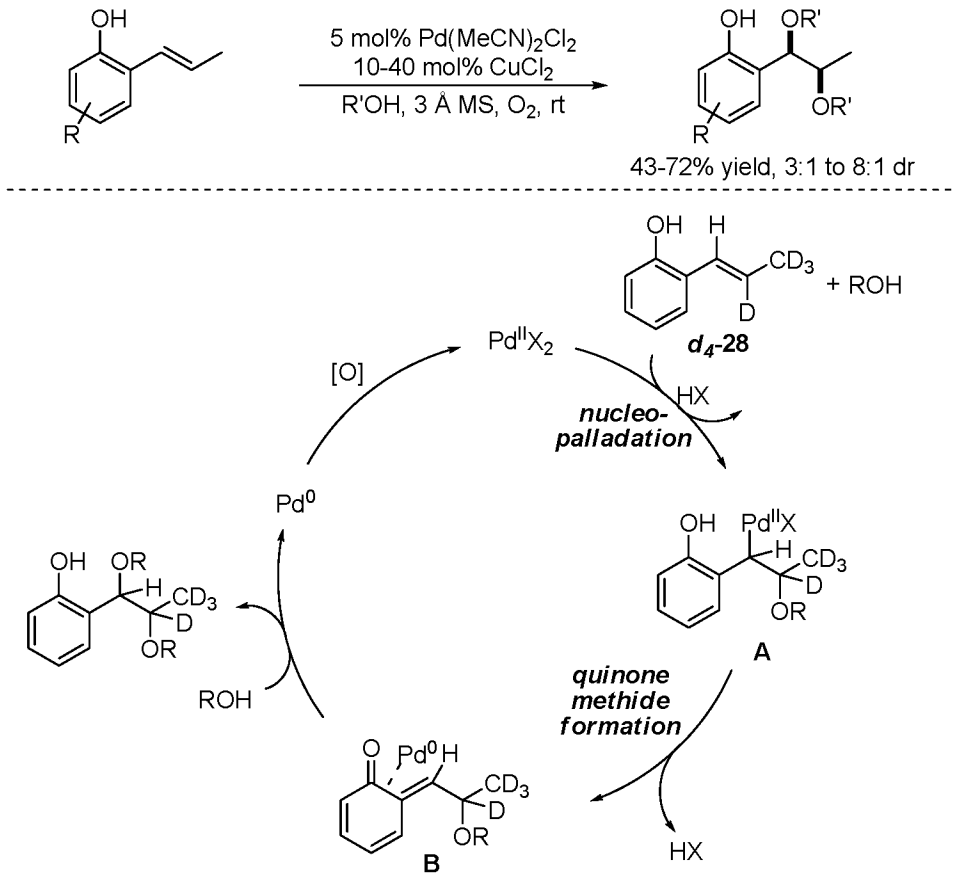

Figure 2.24. Palladium-catalyzed alkene dialkoxylation reaction and mechanistic proposal.

requirement of a free *ortho*-phenol. Additionally, when a deuterated substrate d_4-**28** is submitted to the reaction no washing of the deuterium labels is observed, indicating that β-hydride elimination from **A** does not occur.

An enantioselective version of this reaction was developed in our laboratory by Dr. Yang Zhang (Figure 2.25).[61] The use of chiral quinoline oxazoline ligands **35** and **36** provided the dioxygenated products in high enantioselectivity. Interestingly, a significant detrimental effect of added copper on enantioselectivity was observed. Therefore, despite slightly diminished yields, the reaction was performed in the absence of copper.

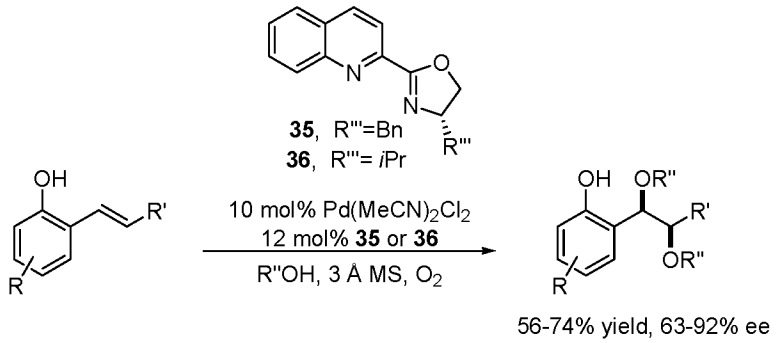

Figure 2.25. Enantioselective palladium-catalyzed dialkoxylation of alkenes capable of quinone methide formation.

Clearly, significant advancements have taken place in the field of palladium-catalyzed alkene difunctionalization reactions. However, the challenges of controlling regioselectivity and diastereoselectivity are still present. Furthermore, the development of enantioselective reactions has immense potential for advancement. The development of new alkene difunctionalization reactions that are regioselective, diastereoselective, and enantioselective remains a promising and exciting area of research.

Quinone Methide Approach to Alkene Difunctionalization

In light of the recent developments and present challenges in palladium-catalyzed alkene difunctionalization reactions, the possibility of expanding the asymmetric alkene dialkoxylation reaction (Figure 2.26 A) to a more synthetically applicable process wherein two distinct nucleophiles are added was highly attractive. Our approach was to develop a reaction wherein the initial nucleopalladation step would occur intramolecularly, followed by quinone methide formation and a second, intermolecular, nucleophilic attack, thus allowing for the distinction of the two addition steps (Figure 2.26 B).[62] This distinction would be made possible by the design of substrates which

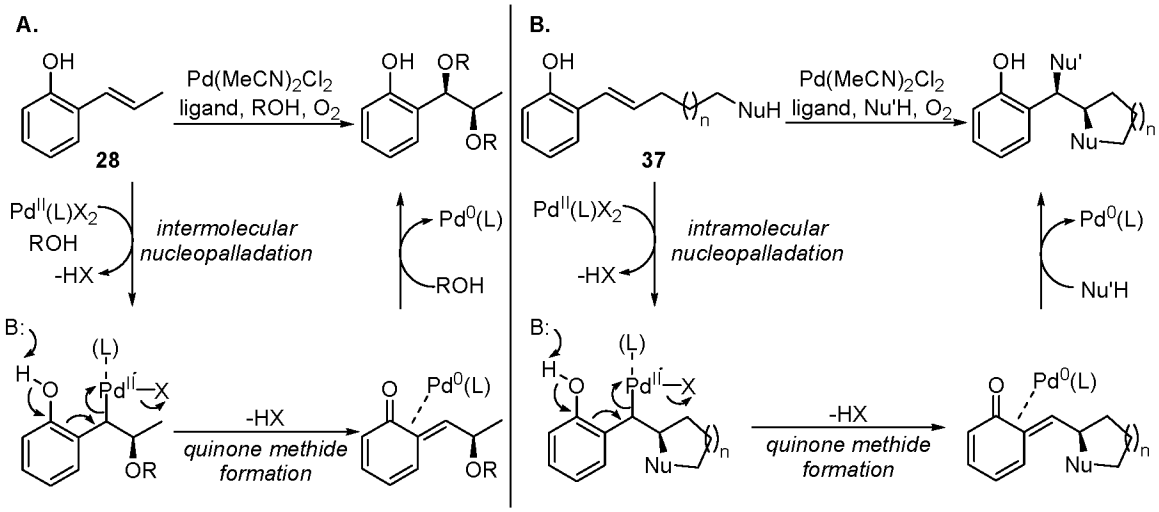

Figure 2.26. Quinone methide approach to alkene difunctionalization. A. Proposed quinone methide intermediate in alkene dialkoxylation reaction. B. Mechanistic proposal for regioselective palladium-catalyzed alkene difunctionalization reaction.

contain a nucleophile tethered to the alkene, such as in **37**. Given the high reactivity of quinone methide intermediates, this reaction seemed to have great potential for the addition of a variety of distinct nucleophiles. Furthermore, the potential to form quinone methide intermediates enantioselectively allows for the construction of complex chiral building blocks from relatively simple starting materials.

Initial Reaction Development and Optimization

To evaluate the viability of the proposed alkene difunctionalization reaction substrate **41**, containing an *o*-phenol with an adjacent alkene linked to a tertiary alcohol, was targeted for preparation (Figure 2.27). The substrate was synthesized via Wittig olefination of salicylaldehyde **39** with **38**, followed by addition of methyl Grignard to ester **40** in high overall yield.

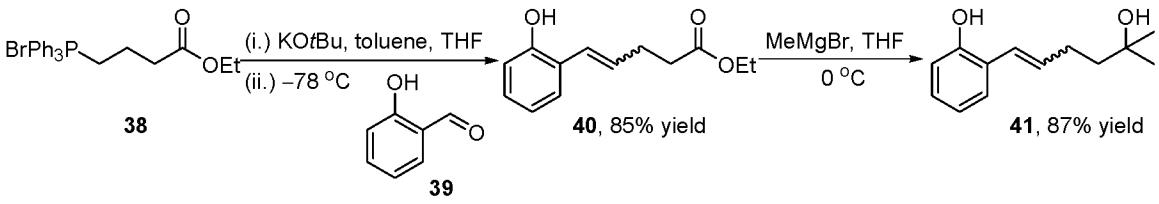

Figure 2.27. Synthesis of substrate **41**.

After submitting substrate **41** to the reaction conditions used for the palladium-catalyzed intermolecular alkene dialkoxylation reaction, it was found that a catalytic amount of base significantly improved the yield of the reaction (1% GC yield without added base vs. 10% GC yield with 25 mol% KO*t*Bu, Figure 2.28). Despite the low product yield, observation of the desired product **42** validated our proposal, and thus further development of the reaction was pursued. Note that a mixture of *E*- and *Z*-alkene isomers of the substrate **41** was used. However, based on the observation that alkene isomerization is rapid with propenyl phenol under the standard Pd-catalyzed alkene dialkoxylation reaction conditions,[60] this was not of concern. We later obtained and tested isomerically pure alkene, with no difference in results. It should also be noted that all yields reported in this section are GC yields, calculated based on an internal standard.

We evaluated a number of ligands early in the optimization of reaction conditions because of the potentially significant differences in trajectory of the incoming intramolecular nucleophile in this reaction, as compared to that of an exogenous nucleophile in the intermolecular alkene dialkoxylation reaction. The pyridine oxazoline ligand class (Figure 2.29) was chosen for evaluation based on the successful application of this ligand to the palladium-catalyzed intermolecular dialkoxylation reaction.[61] This ligand class is highly modular, as the substituents on both the pyridine and oxazoline

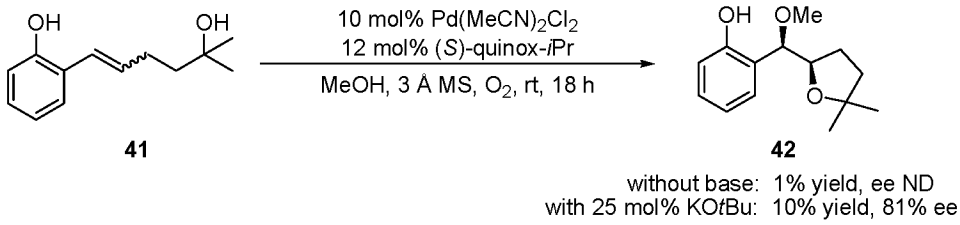

Figure 2.28. Observation of desired difunctionalized product.

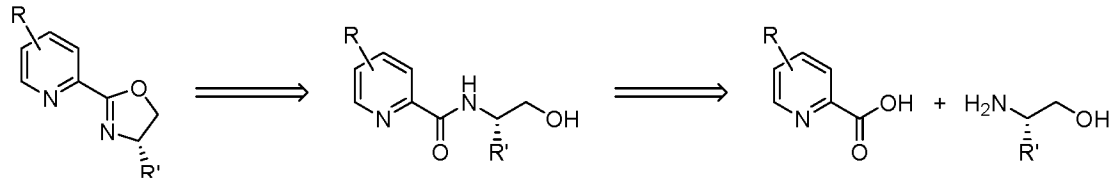

Figure 2.29. Pyridine oxazoline ligand class.

rings can be tuned independently of one another.[63,64] Most of these ligands can be synthesized in two steps from a picolinic acid derivative and an amino alcohol.[65,66]

Pyridine, 6-substituted-pyridine, and quinoline were evaluated in combination with a several oxazoline substituents (Figure 2.30). Pyridine oxazoline ligands **43-50**, both with and without additional substitution on the pyridine module, gave generally poor enantioselectivity. In contrast, most of the quinoline oxazolines **18**, **35**, **36**, and **51** led to improved enantioselectivity, as well as slightly higher yields. Quinox-*i*Pr **36** provided the highest enantiomeric excess of the product, and thus was chosen for further optimization of the reaction conditions.

Amount of base, concentration, and the addition of various additives to the reaction mixture were evaluated, with no significant gains in reaction outcome. Reflecting on the significant effects of copper on both chemoselectivity and enantioselectivity observed in the intermolecular dialkoxylation reaction of **28**, where

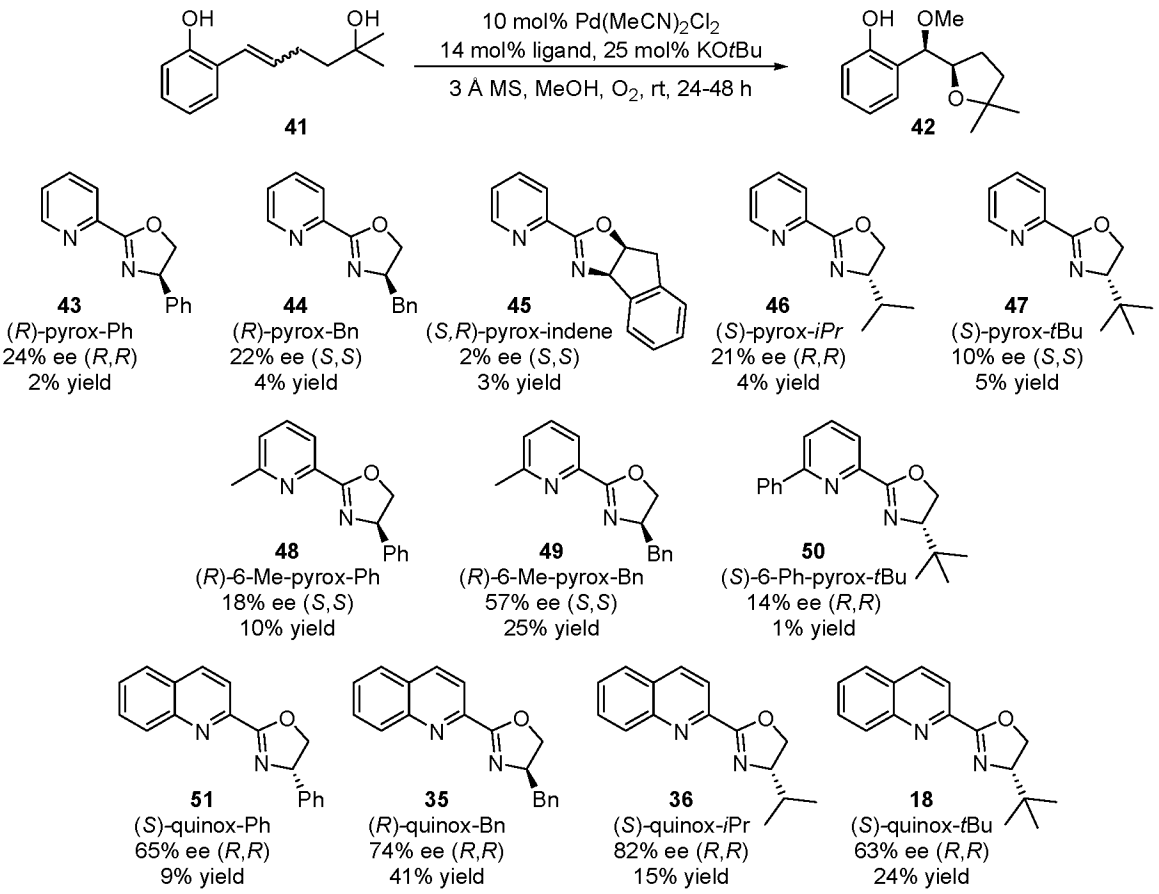

Figure 2.30. Evaluation of pyridine-oxazoline and quinoline-oxazoline ligands.

added copper increases product yield but decreases enantiomeric ratio (Table 2.1),[61] the use of copper as a cocatalyst was reexamined. We hypothesized that the reason for the detrimental effect of copper on enantioselectivity was that copper was confiscating the chiral ligand from palladium, thus leaving an achiral palladium species to catalyze the reaction, leading to nearly racemic product. In order to prevent this from occurring, preformed copper and palladium complexes with (*S*)-quinox-*i*Pr were prepared, making any ligand exchange inconsequential. Using 10 mol% Pd[(*S*)-quinox-*i*Pr]Cl_2 and 20 mol% Cu[(*S*)-quinox-*i*Pr]Cl_2, the product was obtained with no decrease in enantioselectivity, but in substantially higher yield in shorter reaction times (Table 2.2 entry 1 vs. entry 2). It was found that molecular sieves could be removed, palladium and copper loadings could be reduced, and use of weaker bicarbonate bases improved product yield (entries 3-5).

It was deemed desirable to develop conditions that allow for the use of intermolecular nucleophiles other than MeOH for the second addition step. Thus, a number of cosolvents were evaluated with 50 equivalents of MeOH (Table 2.3). The initial focus of this solvent screen was solvent influence on enantioselectivity, and an increase in enantioselectivity was observed with a number of solvents, while others resulted in decreased selectivity. Ethereal and aromatic solvents generally provided enhanced enantioselectivity. While we expected a potential decrease in rate with the use of cosolvents, it was observed that use of certain solvents resulted in significant decreases in chemoselectivity. As a crude measure of this selectivity, the area of product peak by GC compared to the area of all other peaks (besides starting material) is reported.

Table 2.1. Detrimental effect of copper on enantioselectivity in the palladium-catalyzed alkene dialkoxylation reaction.

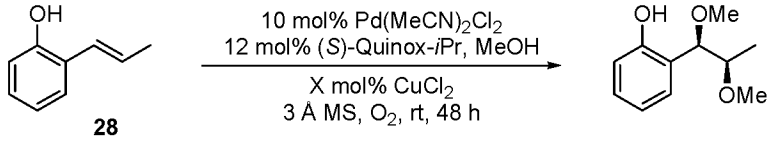

28

mol% $CuCl_2$	% GC yield	% ee	er
0	67	82	91:9
2.5	80	72	86:14
5	78	59	80:20
10	81	26	63:37
20	88	10	55:45

Table 2.2 Initial optimization.

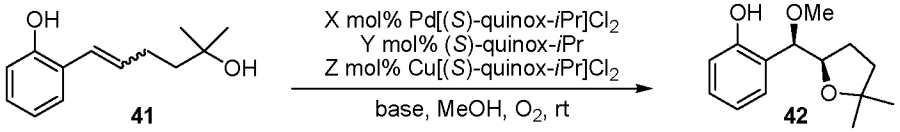

41 **42**

entry	X	Y	Z	base	additive	time	%conv[a]	%yield[a]	ee[b]
1	10	2	--	25 mo% KO*t*Bu	3 Å MS	18 h	89	10	80%
2	10	2	20	25 mo% KO*t*Bu	3 Å MS	0.5 h	100	81	79%
3	5	3	15	25 mo% KO*t*Bu	3 Å MS	0.5 h	99	20	82%
4	5	3	15	25 mo% KO*t*Bu	--	0.5 h	99	76	80%
5	2	1	8	10 mol% $NaHCO_3$	--	0.5 h	100	83	85%

Reactions run on 0.1 mmol scale with [**41**] = 0.1 M. [a]Determined by GC analysis using an internal standard. [b]Determined by GC with a column equipped with a chiral stationary phase.

Table 2.3. Cosolvent assessment.

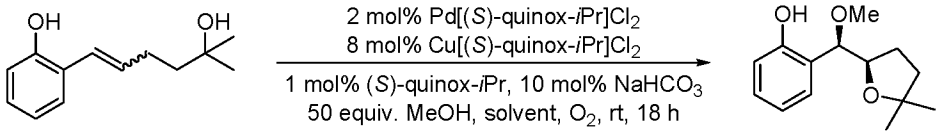

entry	solvent	ee	selectivity[a]
1	*t*BuOH	85%	0.1:1
2	*t*AmylOH	92%	0.4:1
3	toluene	94%	3.8:1
4	THF	93%	4:1
5	DCE	86%	1.6:1
6	CH_2Cl_2	73%	3:1
7	DMA	61%	5:1
8	DMF	60%	3.5:1
9	trifluorotoluene	76%	2:1
10	xylenes	91%	1.4:1
11	benzene	89%	3.2
12	dioxane	95%	2:1[b]
13	DME	95%	2:1
14	TBME	83%	5:1

[a]This is a ratio of area of product peaks: area of all other byproduct peaks observed by GC analysis [b]41 h

Toluene and THF as solvents provided the best overall results, in terms of ee, reaction time, and apparent chemoselectivity, and therefore these solvents were chosen for further pursuits.

Indeed, both THF and toluene, or a 1:1 mixture of the two solvents allowed for product formation with high enantioselectivity, short reaction times, and good yield (Table 2.4, entries 1-3). Further, it was found that in these solvents similar results could be obtained by in situ complex formation as with preformed complexes. Employment of Cu(I) in place of Cu(II) resulted in shorter reactions times, likely due to an effect of overall [Cl^-] (entry 4).[67,68]

Several ligands were reevaluated under the optimized reaction conditions with copper as a cocatalyst (Figure 2.31). While (*S*)-quinox-*i*Pr **36** still provides the highest enantioselectivity, it is interesting to note significant differences with the copper free conditions (Figure 2.30). It appears that 6-Me-pyridine and quinoline give nearly identical selectivity when the oxazoline substituent is kept constant. For example, both (*R*)-6-Me-pyrox-Bn **49** and (*R*)-quinox-Bn **35** give 78% ee (of the (*S*,*S*)-product) and (*S*)-6-Me-pyrox-*i*Pr **52** and (*S*)-quinox-*i*Pr **36** give 94% ee and 95% ee, respectively (of the (*R*,*R*)-product). It is interesting that (*S*)-pyrox-*t*Bu **47** gives relatively high ee (80%) as compared to previously observed (10%), while (*S*)-quinox-*t*Bu **18** gives low ee and yield.

Following the discovery of optimized reaction conditions (4 mol% $Pd(MeCN)_2Cl_2$, 8 mol% CuCl, 14 mol% (*S*)-quinox-*i*Pr, 40 mol% $KHCO_3$) we were interested in evaluating what other types of products could be formed. A plethora of potential substrates containing intramolecular nucleophilic functional groups were envisioned, and thus substrate synthesis was undertaken.

Table 2.4. Final optimization.

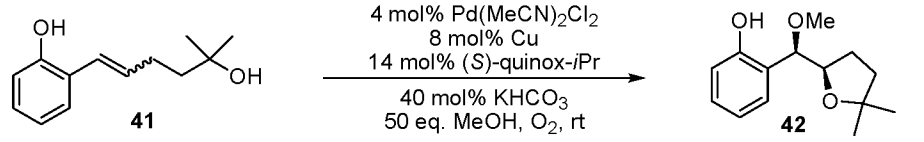

entry	solvent	Cu	time	%conv[a]	%yield[a]	ee[b]	er[b]	dr[b]
1	THF	$CuCl_2$	2 h	79	54	96%	98:2	7.8:1
2	toluene	$CuCl_2$	2 h	96	68	94%	97:3	5.1:1
3	1:1 THF:toluene	$CuCl_2$	5 h	100	67	94%	97:3	6.7:1
4	1:1 THF:toluene	CuCl	2 h	99	80	95%	98:2	8.9:1

Reactions run on 0.1 mmol scale with [**41**] = 0.1 M. [a]Determined by GC analysis using an internal standard. [b]Determined by GC with a column equipped with a chiral stationary phase.

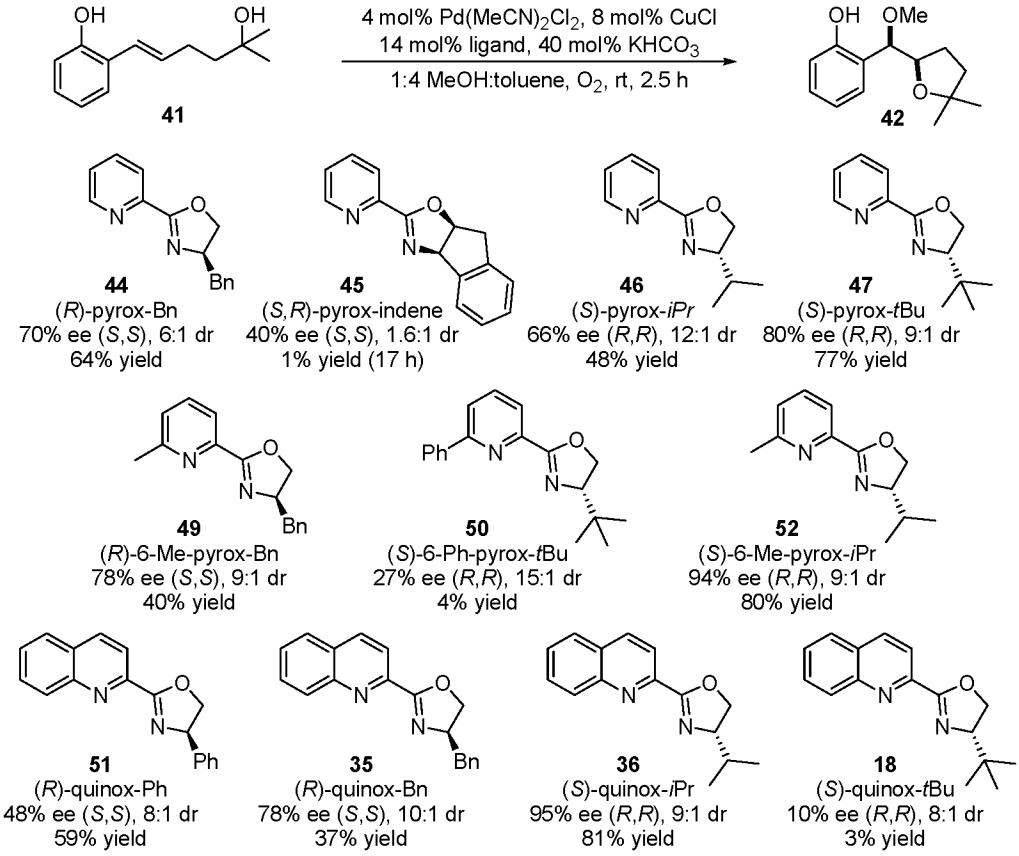

Figure 2.31. Ligand reevaluation under optimized reaction conditions.

Substrate Synthesis

In the pursuit determining what other ring systems could be obtained using this methodology, several substrates were synthesized. We were interested in evaluating what size of heterocycles could be formed as well as what types of intramolecular nucleophiles were compatible with the palladium-catalyzed difunctionalization reaction. This section details the successful synthesis of some of these substrates, as well as some of the synthetic challenges encountered during this process.

Substrates Containing Intramolecular Oxygen Nucleophiles

To evaluate the potential formation of other five-membered oxygen containing rings, the primary alcohol substrate **53** and the carboxylic acid substrate **54** were synthesized from a common intermediate **40** used in the synthesis of **41** (Figure 2.32). The primary alcohol **53** was formed via reduction with $LiAlH_4$ in 60% yield. The carboxylic acid substrate **54** was obtained in 84% yield via ester hydrolysis.

A similar Wittig olefination approach was attempted for the synthesis of substrates containing longer linkers, which would form 6- or 7-membered rings during cyclization. Unfortunately, the major product of the Wittig reaction was not the desired ester **55** or **56**, but rather the cyclic products **57** and **58** (Figure 2.33, A), proposed to arise from intramolecular nucleophilic addition of the olefin to the ester (Figure 2.33, B). This byproduct was not observed in the synthesis of **40** because it would have resulted in the formation of a highly strained four-membered ring. It was hypothesized that the ability of the phenoxide (formed under the basic Wittig conditions) to conjugate with the alkene, and thus contribute to its nucleophilicity, was responsible for the undesired reactivity.

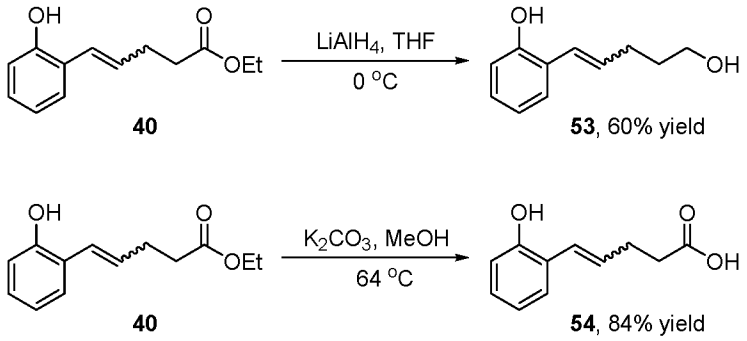

Figure 2.32. Synthesis of primary alcohol and carboxylic acid substrates.

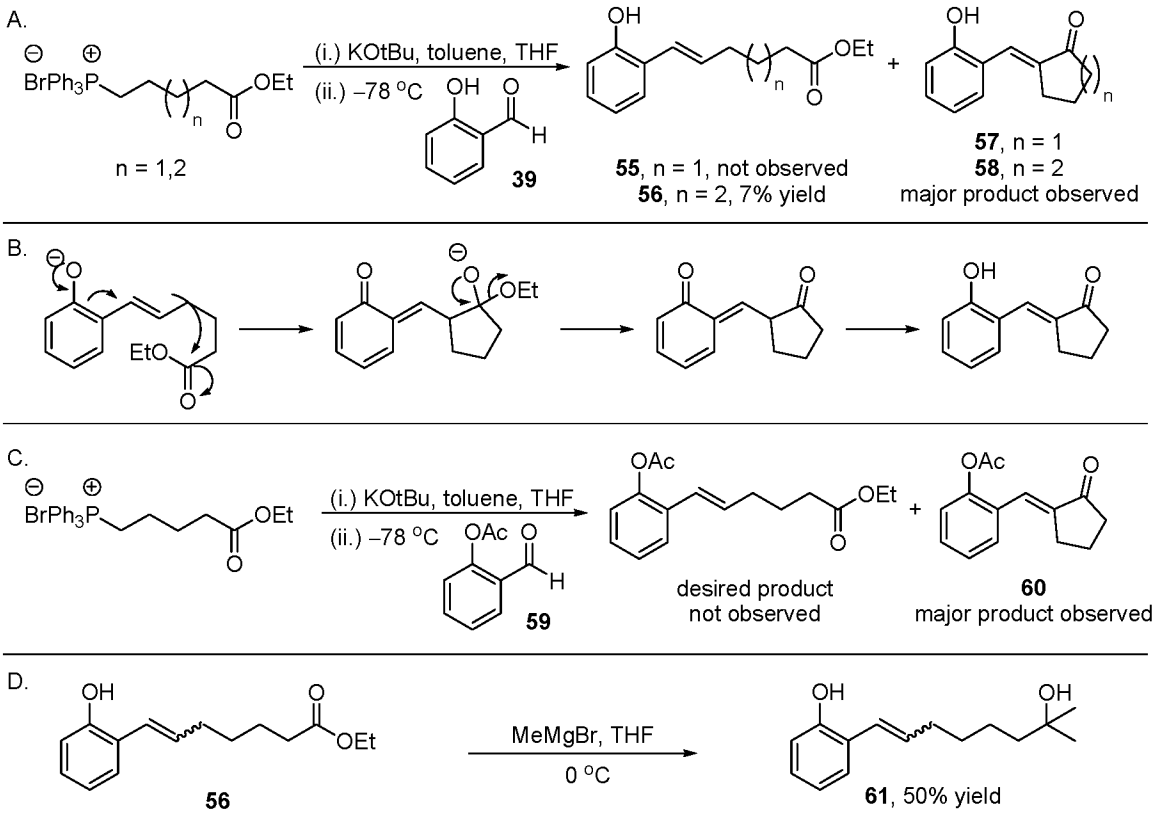

Figure 2.33. Attempted synthesis of substrates containing longer tethers between alkene and oxygen nucleophile.

Thus the Wittig reaction was attempted using acetate protected salicylaldehyde **59** (Figure 2.33, C). Unfortunately, the cycled α,β-unsaturated ketone **60** was again the major product of the reaction. The small amount of ester **56** that was isolated from the Wittig reaction was used to make the tertiary alcohol **61** via a Grignard reaction (Figure 2.33, D).

In light of the undesired products obtained from the Wittig reaction, a new approach to substrate synthesis was taken. Palladium-catalyzed Sonagashira coupling of iodide **62** and alkyne **63** gave intermediate **64** in high yield (Figure 2.34).[69] Alkyne hydrogenation using a poisoned catalyst followed by global deprotection gave the desired substrate **66**.

A similar Sonagashira cross coupling approach was taken for the synthesis of substrates containing an ether linkage between the alkene and the oxygen nucleophile (Figure 2.35). Substrate **70** was designed to form a 7-membered ring in the catalytic difunctionalization reaction with the gem-dimethyl substituents incorporated to provide a potential Thorpe-Ingold effect.[70] Alkyne **67** was synthesized via Williamson ether synthesis, and coupled with iodide **68** in a Sonagashira cross coupling reaction, providing **69**. TBS-ether deprotection followed by an alkyne reduction, believed to be directed by the adjacent phenol, provided the desired substrate **70**, albeit in poor overall yield.

We hypothesized that a reason for the poor yield of **70** was due to the instability of the free phenol alkyne, which was observed to decompose. Therefore, for the

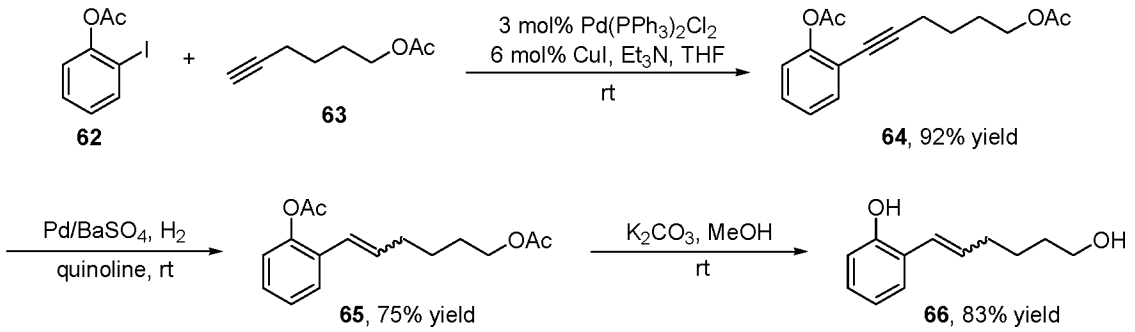

Figure 2.34. Sonagashira cross-coupling approach to substrate synthesis.

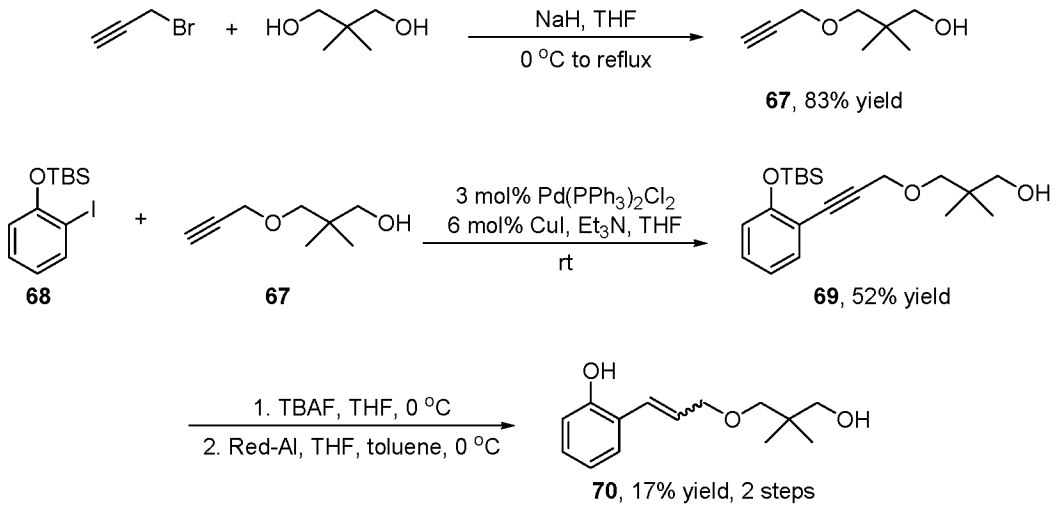

Figure 2.35. Synthesis of substrate **70**.

synthesis of an analogous substrate, **73**, Sonagashira cross coupling was performed with acetate protected iodophenol **62** and alkyne **71**[71] to give intermediate **72** (Figure 2.36). This then allowed for a one-pot phenol deprotection and alkyne reduction using Red-Al at 0 °C to give **73** in good yield.

For the synthesis of analogous substrates containing nitrogen linkage, a reductive amination approach was chosen (Figure 2.37). Aldehyde **74**[72] was submitted to reductive amination with amine **75**,[73] followed by protection of the amine with *p*-toluenesulfonyl chloride, and subsequent alcohol and phenol deprotection to give substrate **76**.

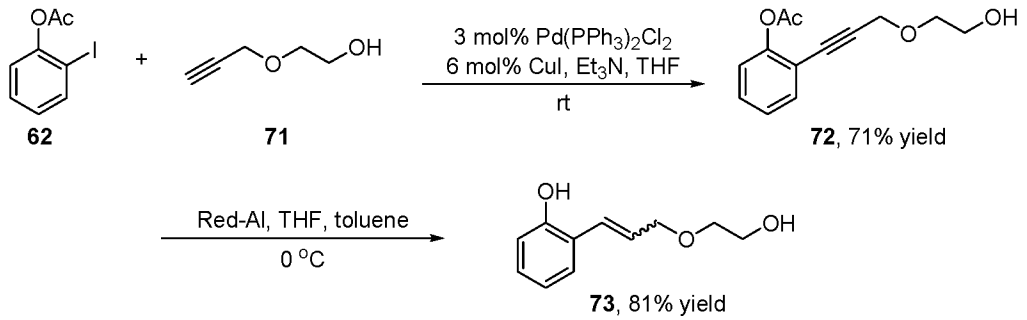

Figure 2.36. Synthesis of substrate **73**.

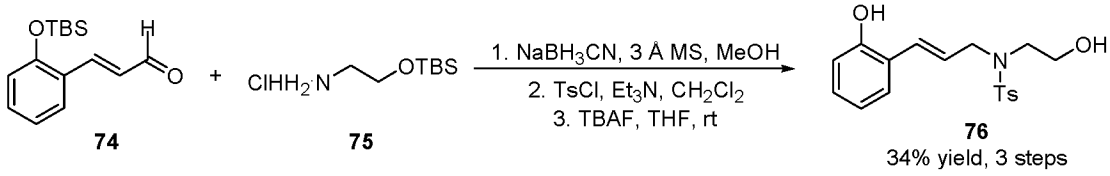

Figure 2.37. Reductive amination synthesis of nitrogen-linked substrates.

Substrates Containing Intramolecular Nitrogen Nucleophiles

In addition to the substrates discussed above which have oxygen nucleophiles linked to the alkene, a number of substrates were synthesized containing intramolecular nitrogen nucleophiles. A discussion of their synthesis is detailed below.

Synthesis of a tosyl protected carbamate substrate **79** was attempted by addition of alcohol **77** to tosyl isocyanate **78** (Figure 2.38, A). Proton NMR of the crude reaction material was consistent with the desired product. However, the substrate was observed to decompose on silica. It was hypothesized that the inherent instability of the substrate was due to the fact that the electron rich phenol is in conjugation with the alkene, allowing for facile and irreversible cleavage of the carbon oxygen bond, with loss of carbon dioxide and tosylamine. Based on this assumption, the substrate containing an additional methylene between the alkene to the carbamate was synthesized (Figure 2.38, B). Sonagashira cross coupling was employed to couple phenyl iodoacetate **62** with alkyne[74] **80**, albeit in low yield. Alkyne hydrogenation followed by phenol deprotection resulted in substrate **82**.

Methyl carbamate substrate **85** was synthesized using Sonagashira cross coupling of **62** with alkyne **83** to give intermediate **84** followed by hydrogenation, phthalamide deprotection, and carbamate formation (Figure 2.39). During this synthesis, it was found that hydrazine deprotected both the phthalamide and the acetate protected phenol. Subsequent addition of methyl chloroformate resulted in protection of both amine and phenol; however, selective deprotection of the phenol was accomplished to obtain substrate **85**.

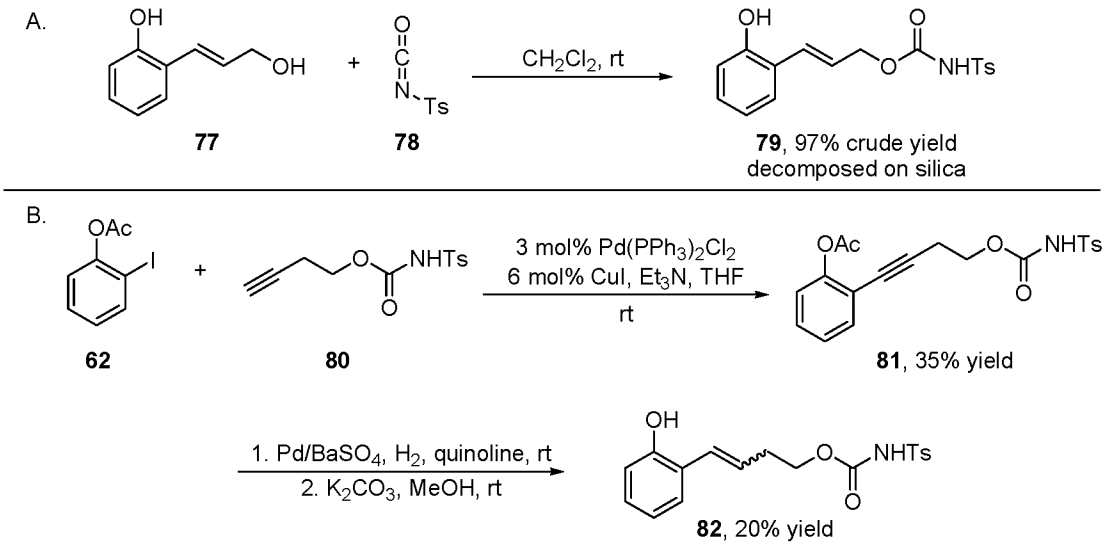

Figure 2.38. Synthesis of carbamate substrates.

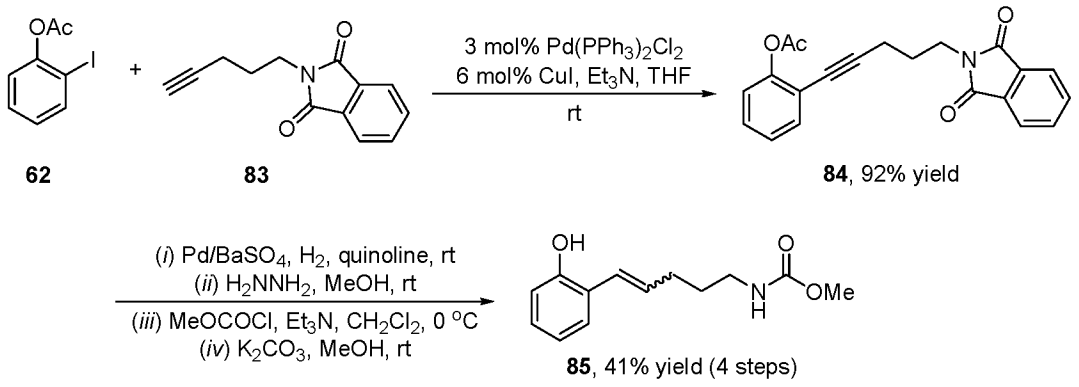

Figure 2.39 Synthesis of substrate **85**.

Evaluation of Substrate Scope

To evaluate the possible difunctionalized products that could be formed using this methodology, a number of intermolecular nucleophiles were examined, along with the aforementioned substrates.

Intermolecular Nucleophiles

The discovery of successful conditions using a cosolvent allowed for the evaluation of nucleophiles other than methanol. A fellow graduate student in our laboratory, Mr. Tejas Pathak, who was a collaborator on this project, evaluated the scope of intermolecular nucleophiles that could be used in this reaction. Since both THF and toluene were found to result in high enantioselectivity, both solvents, or a 1:1 toluene:THF mixture were evaluated for the addition of other exogenous nucleophiles.

In addition to methanol, several alcohols were found to be compatible with the reaction, leading to the difunctionalized products **86-92** (Table 2.5). The viability of simple primary alcohols as nucleophiles was demonstrated using *n*-butanol to form **86**. This is significant because of the fact that primary alcohols are known to undergo palladium-catalyzed alcohol oxidation much more readily than methanol and thus it was important to confirm that they can be used as exogenous nucleophiles under these conditions. In this case, the use of toluene as solvent was found to give slightly improved yields. Alcohols containing a functional group are also well tolerated, including 3-butenol, 2-methoxyethanol, and 2-chloroethanol, forming **87**, **88**, and **89**, respectively. It was also possible to form ethers **90** and **91** with the potential for deprotection to the free secondary alcohol at a later stage using benzyl alcohol and trimethylsilylethanol.

Table 2.5. Scope of exogenous alcohol nucleophiles.

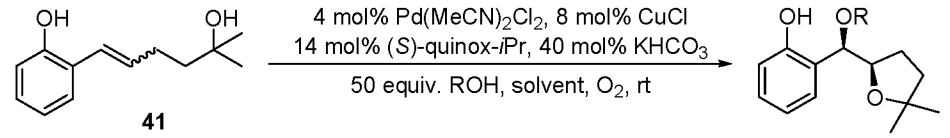

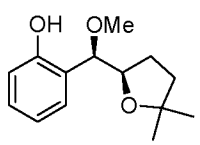

42
72% yield
1:1 THF:toluene, 3 h
97:3 er; 10:1 dr

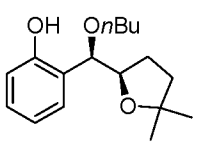

86
63% yield
toluene, 12 h
96:4 er; 5:1 dr

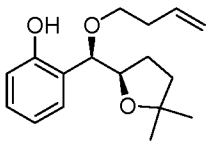

87
57% yield
toluene, 12 h
96:4 er; 4:1 dr

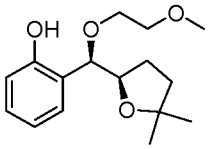

88
53% yield
1:1 THF:toluene,12 h
97:3 er; 9:1 dr

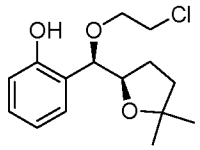

89
60% yield
toluene, 12 h
94:6 er; 5:1 dr

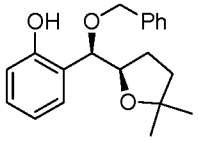

90
51% yield
1:1 THF:toluene, 16 h
97:3 er; 6:1 dr

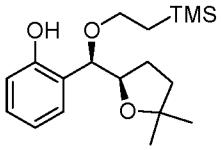

91
64% yield[a]
toluene, 16 h
99:1 er; 6:1 dr

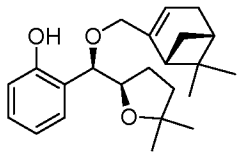

92
55% yield[a]
toluene, 12 h
10:1 dr

Isolated yield on 0.50 mmol scale. er for major diastereomer. [a]25 eq. of NuH.

In the evaluation of more polar nucleophiles, it was found that *tert*-amylalcohol was the preferable solvent for improved miscibility of the nucleophile (Table 2.6). Using water as exogenous nucleophile, the free secondary alcohol **93** was obtained in excellent enantiomeric ratio. *tert*-Amylalcohol was found to be preferred for other polar nucleophiles, such as ethylene glycol. While exploring what other types of nucleophiles could be used, we were excited to find that sodium azide is an effective nucleophile, demonstrating that an exogenous nitrogen nucleophile is viable. While low diastereoselectivity is observed, the diastereomers of **95** are readily separated. Currently, Mr. Tejas Pathak is exploring other viable nucleophile classes, and has found success using indole and pyrrole derivatives.[75]

Table 2.6. Continued scope of exogenous nucleophiles.

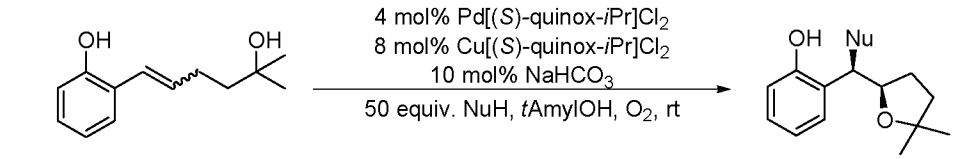

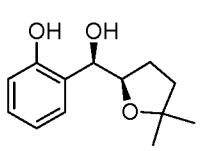

93
63% yield
24 h
98:2 er; 5:1 dr

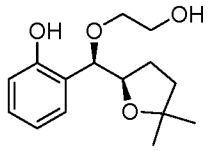

94
59% yield
24 h
95:5 er; 9:1 dr

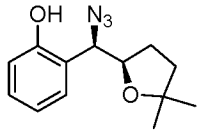

95
51% yield[a]
48 h
92:8 er; 1.4:1 dr

Isolated yield on 0.50 mmol scale. er for major diastereomer [a]2 equiv. of NaN_3, 30 °C.

Intramolecular Oxygen Nucleophiles

In evaluation of the scope of the palladium-catalyzed difunctionalization reaction, it was found that five and six membered rings could be successfully formed with tethered alcohol nucleophiles (Table 2.7). In addition to the tertiary alcohol substrate used for optimization and in the evaluation of the scope of exogenous nucleophiles, the analogous primary alcohol substrate **53** cyclized to the tetrahydrofuran product **96** in high enantio- and diastereoselectivity. Primary alcohol substrate **66** formed the six membered ring product **97** under the catalytic conditions, in high enantioselectivity, but decreased yield. A 1,4-dioxane ring **98** was formed from substrate **73**, in low yield but good enantioselectivity.

In evaluating the carboxylic acid substrate **54**, the 5-membered lactone product **99** was obtained in high yield. Unfortunately the enantiomeric ratio of the product was very low (Figure 2.40). One mechanistic hypothesis to account for this observation is a reversible nucleopalladation step, as a carboxylate is a better leaving group than an

Table 2.7. Scope of alcohol based nucleophile substrates.

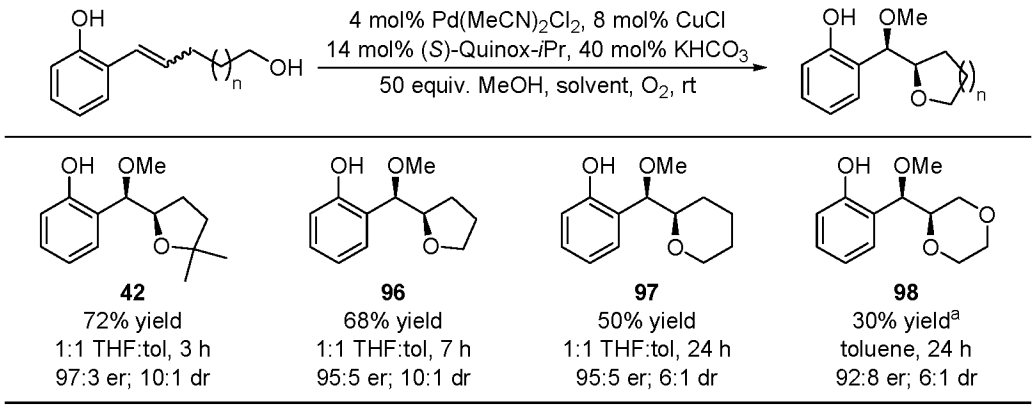

Isolated yield on 0.50 mmol scale. er for major diastereomer. [a]1 eq. $NaHCO_3$

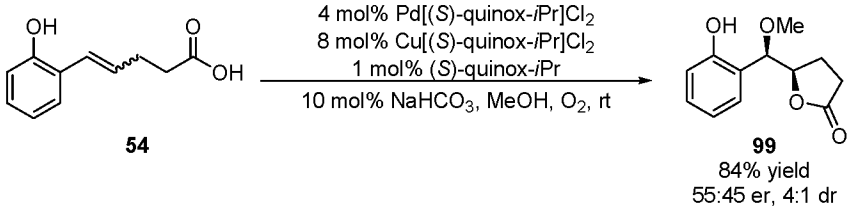

Figure 2.40. Evaluation of carboxylic acid substrate **54**.

alkoxide, which would lead to an erosion in enantioselectivity (Figure 2.41). Alternatively, the significant change in nucleophile pK_a may lead to a change in mechanism. The nucleopalladation step of palladium-catalyzed alkene functionalization reactions has been proposed to go through either a *trans*-nucleopalladation, where the nucleophile approaches the alkene from the face opposite palladium, or a *cis*-nucleopalladation, where the nucleophile coordinates palladium, followed by alkene insertion (Figure 2.41). The mechanism of nucleopalladation has been demonstrated to differ depending on the type of nucleophile and the reaction conditions.[76,77] The simultaneous occurrence of both pathways is likely to lead to a decrease in enantioselectivity.

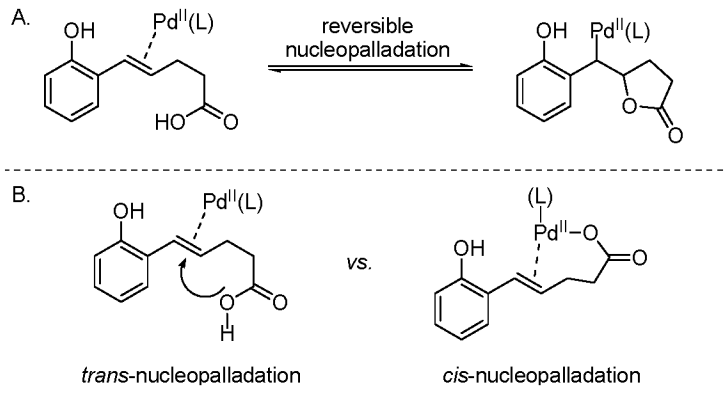

Figure 2.41. Mechanistic explanations for observed low enantiomeric excess.

Unfortunately, during attempts to form larger heterocycles using a longer tether between the nucleophile and the alkene, as in substrates **61** and **70**, the desired product was not observed in the crude reaction mixture, indicating that 7-membered ring formation is not feasible using the current conditions (Figure 2.42).

During the evaluation of a substrate **76** containing an alcohol linked to the alkene via a nitrogen linkage, proton NMR showed evidence of formation of the morpholine product **100** (Figure 2.43), however the product was difficult to separate from the ligand. Furthermore, the ratio of product to ligand indicated low yield, and the product was found to have low enantiomeric excess (62%). The low enantioselectivity may be due to the relatively bulky linker, which could have detrimental steric interactions with the chiral ligand during the enantiodetermining step. Given the poor results, further optimization and product characterization was not pursued for this substrate.

Intramolecular Nitrogen Nucleophiles

In an attempt to form heterocycles with nitrogen based nucleophiles, carbamate **82** was submitted to the standard reaction conditions, but unfortunately, no product

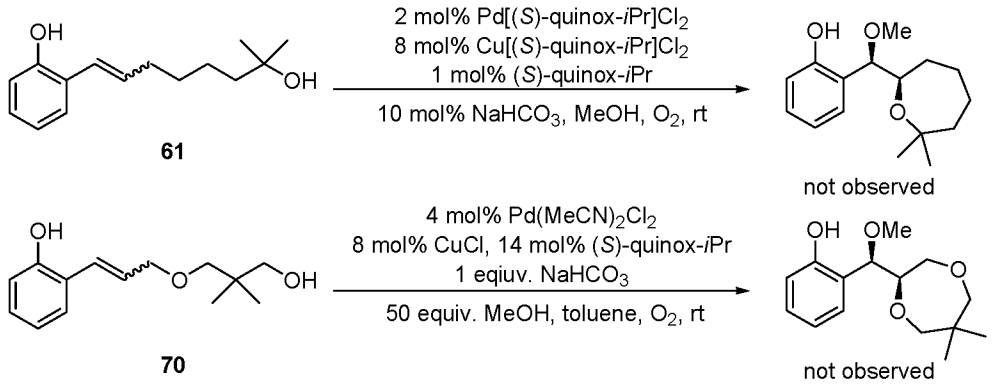

Figure 2.42. Attempted cyclization to form 7-membered ring systems.

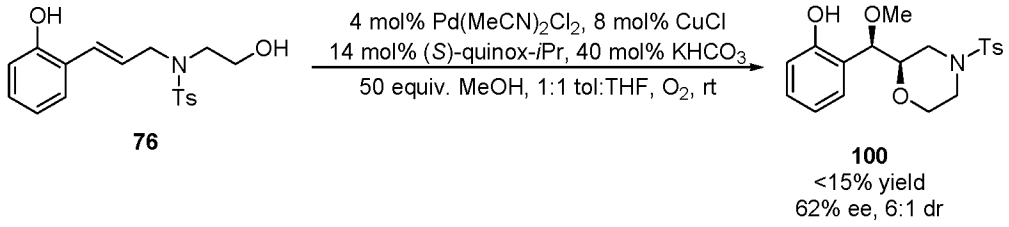

Figure 2.43. Formation of a morpholine derivative.

formation was observed (Figure 2.44 A). The carbamate protected substrate **85** was submitted to the alkene difunctionalization reaction conditions. The pyrrolidine containing product **101** was obtained, albeit in low yield and moderate enantioselectivity (Figure 2.44 B.).

The lack of successful alkene difunctionalization with substrates containing nitrogen nucleophiles under the current reaction conditions is unfortunate. One potential explanation may be that these substrates coordinate to palladium in such a way as to prevent reaction. It seems reasonable that the active species that under goes nucleopalladation is a bidentate phenoxide alkene-Pd complex (Figure 2.45 A, see

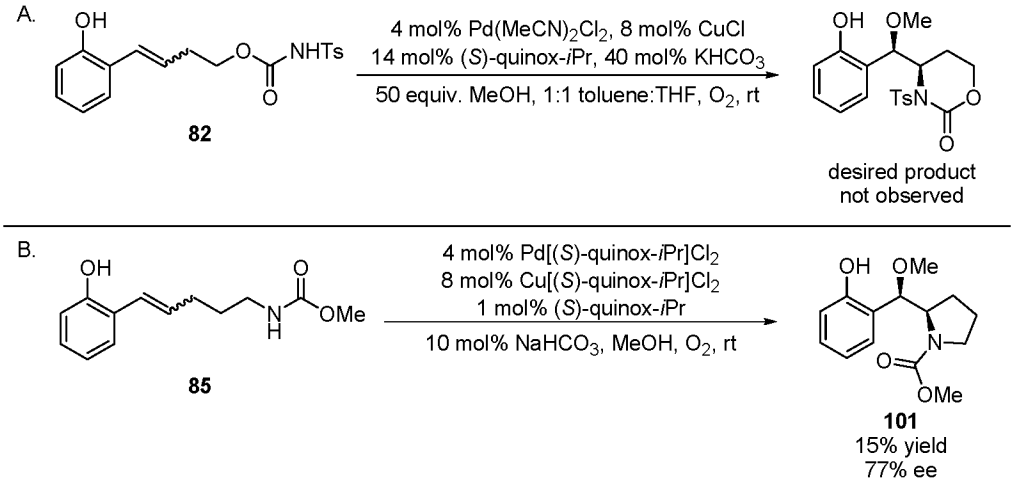

Figure 2.44. Nitrogen heterocycles.

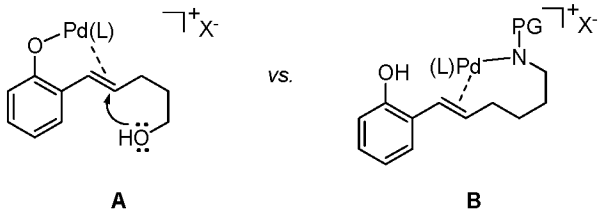

Figure 2.45. Potential reaction inhibition through substrate binding to palladium.

chapter for a more detailed explanation). If so, then a substrate which contains a more coordinating functional group may preferentially form a bidentate complex of type **B**, and thus inhibit or change the mechanism of the nucleopalladation process. This may be overcome in the future by altering the reaction conditions or the choice of nitrogen protecting group, and Dr Ranjan Jana is presently pursuing this goal.

Determination of Product Stereochemistry

Having synthesized numerous products using the alkene difunctionalization reaction in high enantioselectivity and generally good diastereoselectivity, we were interested in determining the relative and absolute stereochemistry of the products formed with our methodology. Fortunately, x-ray quality crystals of product **42** were obtained,

allowing for the assignment of relative stereochemistry (Figure 2.46). Mosher ester analysis was used to determine the absolute stereochemistry (Figure 2.47).[78,79] Product **93**, obtained using water as the exogenous nucleophile was used in this analysis. Following phenol protection, diastereomeric Mosher esters **103** and **104** were synthesized by coupling alcohol **102** with each enantiomer of Mosher's acid (α-methoxy-α-trifluoromethyl-phenylacetic acid). Comparison of the chemical shifts in the proton NMR spectra revealed that the protons on the tetrahydrofuran ring were shifted upfield in the (*S*)-Mosher ester **103**, relative to the same protons in the (*R*)-Mosher ester **104**. This indicates that these protons are shielded by the phenyl substituent on the ester, and these substituents are on the same face of the conformer drawn. Based on this analysis in combination with the crystal structure data, the absolute stereochemistry is assigned as (*R*,*R*). Knowledge of the relative and absolute configuration of the product is crucial in the development of a working stereochemical model, which will be addressed in Chapter 3.

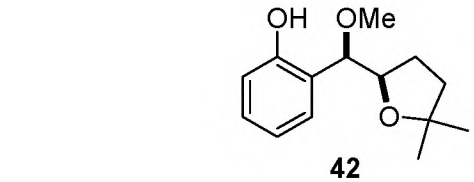

42

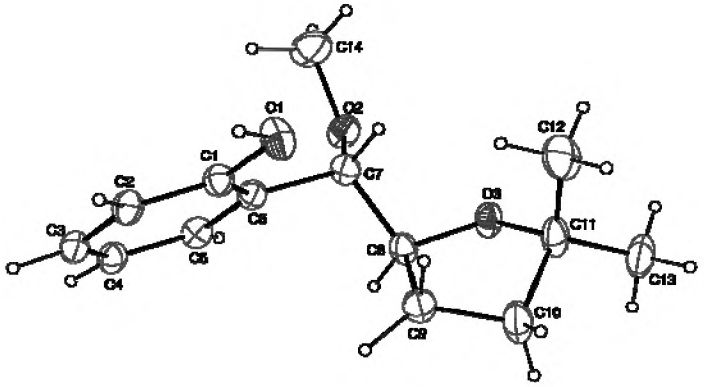

Figure 2.46. X-ray crystal structure of product **42**.

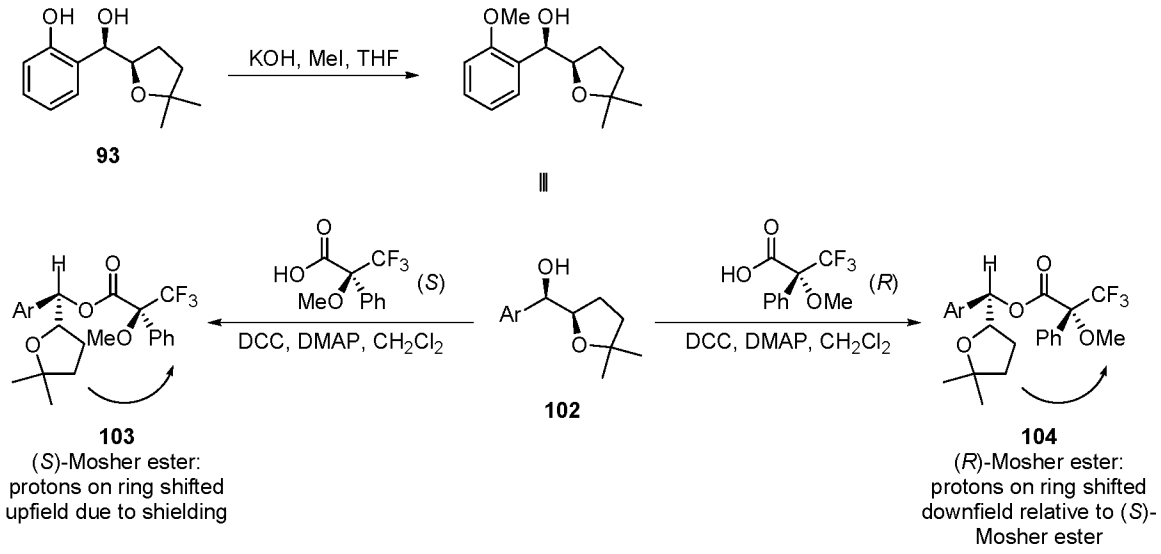

Figure 2.47. Mosher ester analyis.

Conclusion

The successful development of an enantioselective palladium-catalyzed alkene difunctionalization reaction was accomplished, using nucleophiles tethered to alkenes capable of quinone methide formation.[62] A key step in the optimization of the reaction conditions was the use of a ligated copper complex as a cocatalyst, which drastically improved reaction rate and yield, with no detrimental effect on enantioselectivity. Furthermore, conditions were developed which allow for the use of exogenous nucleophiles other than solvent. In evaluating the scope of the reaction, alcohols, water, and sodium azide were found to add successfully as exogenous nucleophile. With regard to the intramolecular nucleophile scope, alcohols were found to work significantly better than nitrogen nucleophiles, and five and six membered rings could be formed. Insight into the mechanism of the reaction, especially concerning the role of copper in the reaction, would contribute significantly to the understanding of the reaction and potentially allow for alternative conditions which allow for previously incompatible

substrates to react, especially nitrogen nucleophiles. Chapter 3 will focus on studies to increase our understanding of this reaction.

Experimental

General Considerations

Unless otherwise noted, all reactions were performed under a nitrogen atmosphere with stirring. Toluene, CH_2Cl_2, dichloroethane and THF were dried before use by passing through a column of activated alumina. Methanol was distilled from magnesium methoxide. Et_3N was distilled from CaH_2. 3Å molecular sieves were powdered and activated by flame heating under vacuum (ca. 3 min). *n*-Butanol, *n*-Butenol and etheleneglycol monomethylether were purified by distillation from $MgSO_4$. All other reagents were purchased from commercial sources and used without further purification. Yields were calculated for material judged homogeneous by thin-layer chromatography and NMR. Thin-layer chromatography was performed with EMD silica gel 60 F254 plates eluting with the solvents indicated, visualized by a 254 nm UV lamp, or stained either with potassium permanganate, *p*-anisaldehyde, phosphomolybdic acid, or ninhydrin. Flash column chromatography was performed with EcoChrom MP Silitech 32-63D 60Å silica gel, or with Brockmann I activated basic alumina (pH 9-10), slurry packed with solvents indicated in glass columns. Nuclear magnetic resonance spectra were acquired at 300, 400, or 500 MHz for ^1H, and 75, 100, or 125 MHz for ^{13}C. Chemical shifts for proton nuclear magnetic resonance (^1H NMR) spectra are reported in parts per million downfield relative to the line of $CHCl_3$ singlet at 7.26 ppm. Chemical shifts for carbon nuclear magnetic resonance (^{13}C NMR) spectra are reported in parts per million downfield relative to the center-line of the $CDCl_3$ triplet at 77.23 ppm. The

abbreviations s, d, t, dd, td, ddd, and m stand for the resonance multiplicities singlet, doublet, triplet, doublet of doublets, triplet of doublets, doublet of doublets of doublets, and multiplet, respectively. Optical rotations were obtained (Na D line) using a Perkin Elmer Model 343 Polarimeter fitted with a micro cell with a 1 dm path length; concentrations are reported in g/100 mL. IR spectra were recorded using a Nicolate FTIR instrument. GC (gas chromatography) analysis was performed using a Hewlett Packard HP 6890 Series GC system fitted with a HP-Chiral permethylated β-cyclodextrin column. HPLC (high pressure liquid chromatography) analysis was performed using a Hewlett Packard Series 1100 instrument fitted with a chiral stationary phase (as indicated). SFC (supercritical fluid chromatography) analysis was performed at 40 °C, using a Thar instrument fitted with a chiral stationary phase (as indicated). HRMS (high resolution mass spectrometry) analysis was performed using Waters LCP Premier XE. Glassware for all reactions was oven-dried at 110 °C and cooled in a dry atmosphere prior to use. Known compounds **38**,[80] ligands **18**, **35**, **36**, **43-52**,[61,63-66,81] $Pd(PPh_3)_2Cl_2$,[82] **62**,[83] **63**,[84] **68**,[85] **71**,[71] **74**,[72] **75**,[73] and **80**,[74] were prepared according to literature procedures.

Synthesis of a Model Substrate

Preparation of 40

To an oven-dried 500 mL round bottom flask equipped with a stir bar were added 23.4 g of **38** (51.0 mmol, 2.30 equiv.) and 200 mL toluene. To this was added a solution of 5.80 g KO*t*Bu (51.2 mmol, 2.33 equiv.) in 40 mL of THF dropwise via cannulation. The reaction mixture slowly turned a deep red color over 4 h. The mixture was cooled to −78 °C and 2.70 g of salicylaldehyde **39** (22.2 mmol, 1.00 equiv.), dissolved in 20 mL of

toluene were added dropwise via cannulation. The mixture was allowed to slowly warm to ambient temperature and stirred 48 h then quenched with 50 mL of saturated NH_4Cl solution. The mixture was diluted with 100 mL of Et_2O and washed with 100 mL (2 x 50 mL) of water and 60 mL of brine. The organic layer was dried over $MgSO_4$, filtered, and the solvent removed in vacuo. The crude mixture was purified by flash silica-gel column chromatography with 10%-20% EtOAc/hexanes as eluent to give 4.15 g (85% yield, average of two reactions). Isomeric ratio *Z:E* = 10:1, major isomer: R_f = 0.52 with 33% EtOAc/hexanes, colorless oil, ^{1}H-NMR (300 MHz, $CDCl_3$) δ = 7.02-7.28 (m, 2 H), 6.85-6.95 (m, 2 H), 6.38-6.48 (d, *J* = 11.2 Hz, 2 H), 5.89 (s, 1 H), 5.74-5.86 (m, 1 H), 4.08-4.16 (m, 2 H), 2.37-2.48 (m, 4 H), 1.18-1.29 (m, 3 H). ^{13}C-NMR (75 MHz, $CDCl_3$) δ = 173.3, 153.1, 134.4, 129.9, 128.8, 125.1, 123.8, 120.5, 116.1, 60.9, 33.9, 24.3, 14.3. IR: 3392, 2981, 1705, 1450, 1269, 1195, 1154, 754 cm^{-1}. HRMS $C_{13}H_{16}O_3$ $(M+Na)^+$ calcd. 243.0997, obsvd. 243.0996.

Preparation of 41

To an oven dried 500 mL round bottom flask equipped with a stir bar were added 4.10 g of **40** (18.6 mmol, 1.00 equiv.) in 180 mL THF. To this was slowly added a solution of 3.0 M MeMgBr (130 mmol, 7.00 equiv.) at 0 °C. The reaction mixture was then allowed to warm to rt and was stirred for 12 h. The reaction was quenched by the slow addition of 20 mL of 1 M HCl solution. The mixture was diluted with 50 mL of Et_2O and washed with 100 mL (2 x 50 mL) of water and 60 mL of brine. The organic extract was dried over $MgSO_4$, filtered, and the solvent was removed in vacuo. The crude mixture was purified by flash silica-gel column chromatography with 1 L of 1:1 EtOAc:hexanes as eluent to give 3.34 g of **41** in 87% yield. Isomeric ratio *Z:E* = 10:1,

major isomer: R_f = 0.32 with 33% EtOAc/hexanes, colorless solid. mp = 74-75 °C. ^{1}H-NMR (400 MHz, $CDCl_3$) δ = 7.28-7.07 (m, 2 H), 6.95-6.87 (m, 2 H), 6.40-6.37 (d, *J* = 10.9 Hz), 5.95-5.88 (m, 1 H), 5.34 (s, 1 H), 2.28-2.19 (m, 2 H), 1.67-1.57 (m, 2 H), 1.19 (s, 6 H). ^{13}C-NMR (100 MHz, $CDCl_3$) δ = 152.9, 137.0, 129.8, 128.8, 123.9, 123.4, 120.4, 115.5, 71.3, 43.3, 29.4, 24.1. IR: 3410, 3013, 2971, 1604, 1448, 1377, 1261, 1210, 1147, 1131, 904, 755 cm^{-1}. HRMS $C_{13}H_{18}O_2$ $(M+Na)^+$ calcd. 229.1204, obsvd. 229.1201.

Preparation of Catalyst Complexes

Preparation of Pd[(*S*)-quinox-*i*Pr]Cl_2

To an oven dried 100 mL round bottom flask equipped with stir bar were added 381 mg of $Pd(MeCN)_2Cl_2$ (1.47 mmol, 1.00 equiv.), 300 mg of (*S*)-quinox-*i*Pr ligand (1.47 mmol, 1.00 equiv.) and 80 mL of DCE under a nitrogen atmosphere. The reaction mixture was heated at reflux for 10 h. The reaction mixture was then allowed to cool to rt and concentrated to ca. 2 mL. To this mixture, 3 mL of CH_2Cl_2 was added, and precipitation was observed. The remaining solvent was removed in vacuo and dried overnight under vacuum to give the desired complex in quantitative yield (680 mg). $[\alpha]^{20}_D$ = –57° (c = 0.19, $CHCl_3$), ^{1}H-NMR (400 MHz, $CDCl_3$) δ = 9.59 (d, *J* = 8.7 Hz, 1 H), 8.39 (d, *J* = 8.0 Hz, 1 H), 7.83 (d, *J* = 8.4 Hz, 1 H), 7.71 (d, *J* = 8.4 Hz, 1 H), 7.56 (m, 2 H), 5.07 (t, *J* = 10.6 Hz, 1 H), 4.76-4.71 (m, 2 H), 2.89-2.74 (m, 1 H), 0.95 (d, *J* = 6.9 Hz, 3 H), 0.81 (d, *J* = 6.6 Hz, 3 H). ^{13}C-NMR (100 MHz, $CDCl_3$) δ = 169.9, 148.7, 145.9, 141.6, 132.3, 131.3, 129.8, 129.5, 127.9, 120.7, 72.1, 67.7, 29.3, 18.8, 14.5. IR: 2958, 1651, 1589, 1371, 923, 839 cm^{-1}.

Preparation of Cu[(*S*)-quinox-*i*Pr]Cl_2

To an oven dried 50 mL round bottom flask equipped with stir bar were added 45.3 mg of $CuCl_2$ (0.340 mmol, 1.00 equiv.), 81 mg of (*S*)-quinox-*i*Pr ligand (0.34 mmol, 1.0 equiv.) and 16 mL of MeOH under a nitrogen atmosphere. The reaction mixture was heated at reflux for 10 h. The reaction mixture was then allowed to cool to rt and concentrated to ca. 2 mL. Approximately 3 mL of CH_2Cl_2 were added, and precipitation was observed. The remaining solvent was removed in vacuo and dried overnight under vacuum to give complex in quantitative yield (126.3 mg). $[\alpha]^{20}_D$ = +229 (c = 0.17, $CHCl_3$), IR: 1651, 1590, 1510, 1254, 1165, 758 cm^{-1}, HRMS $C_{16}H_{24}O_5$ $(M+Na)^+$ calcd. 338.0247, obsvd. 338.0249.

Optimization of Reaction Conditions

General Procedure for Optimization

For optimization, four reactions were run simultaneously in separate 5 mL side-arm flasks attached to a four-neck cow fitted with a three way adaptor with a balloon of O_2 attached. A standard solution was prepared by the addition of 412.6 mg of the substrate **41** and 63.3 mg of the internal standard 2-methoxynaphthalene to a 2 mL volumetric flask, followed by the addition of MeOH. The flask was briefly sonicated to dissolve **41** and stirred to give a solution with [**41**] = 1.00 M and [2-methoxynaphthalene] = 0.20 M.

Each optimization reaction was performed as described in the following example: To a 5 mL side-arm round bottom flask equipped with a stir bar were added 2.6 mg $Pd(MeCN)_2Cl_2$ (0.010 mmol, 0.10 equiv.), 2.7 mg of $CuCl_2$ (0.020 mmol, 0.20 equiv.), 7.7 mg (*S*)-quinox-*i*Pr (0.032 mmol, 0.32 eqiuv), 4.0 mg of $KHCO_3$ (0.040 mmol, 0.40

equiv.), and 900 μL of MeOH, and the flask was attached to a four-neck cow (Note: for reactions using cosolvents, 800 μL of solvent and 100 μL MeOH were added). A three-way joint fitted with a balloon of O_2 was attached and the apparatus was evacuated (using house vacuum) and refilled with oxygen three times. The mixture was stirred vigorously for 20 min at rt. A 100 μL portion of the standard solution of **41** (0.100 mmol, 1 equiv.) and 2-methoxy naphthalene (0.020 mmol, 0.20 equiv.) was added dropwise to the reaction mixture. Aliquots (ca. 50 μL) of the reaction were taken periodically via syringe. Reaction samples were passed through a short silica plug eluting with 2 mL of EtOAc and analyzed by GC and referenced against a time zero sample containing the standard solution of **41** and 2-methoxynaphthalene diluted in EtOAc. GC yields were calculated based on the ratio of product to internal standard corrected for the response factor. Enantiomeric and diastereomeric ratios were determined using GC with a column equipped with a chiral stationary phase (see Table 2.8 for separation conditions).

Preparation of 53

To a 100 mL oven dried round bottom flask equipped with a stir bar were added 1.6 g **40** (7.27 mmol, 1 equiv.) followed by 40 mL THF under a nitrogen atmosphere. The reaction mixture was cooled to 0 °C. To this were added 544 mg $LiAlH_4$ portion wise (14.5 mmol, 2 equiv.). The reaction mixture was allowed to slowly warm to rt and stirred overnight. The reaction mixture was cooled to 0 °C, and quenched by the sequential addition of 544 μL of water, 544 μL 15% NaOH, and 1630 μL water. The reaction mixture was warmed to rt, $MgSO_4$ was added, and the mixture was stirred for 15 min and then filtered. The filtrate was concentrated in vacuo and the crude mixture was purified by silica gel column chromatography with 1:3 EtOAc:hexanes to give 777 mg of

53 (60% yield, average of two reactions). Isomeric ratio *Z:E* = 10:1, major isomer: R_f = 0.20 with 33% EtOAc/hexanes, white solid. mp = 45-47 °C. ^{1}H-NMR (300 MHz, $CDCl_3$) δ = 7.06-7.21 (m, 2 H), 6.83-6.94 (m, 2 H), 6.38-6.46 (d, *J* = 11.2 Hz, 1 H), 5.82-5.95 (m, 1 H), 3.59-3.68 (t, *J* = 6.4Hz, 2 H), 2.17-2.25 (m, 2 H), 1.62-1.74 (m, 2 H). ^{13}C-NMR (75 MHz, $CDCl_3$) δ = 135.9, 130.0, 128.8, 124.1, 120.4, 115.6, 62.7, 32.1, 25.5. IR: 3404, 2938, 2881, 1604, 1448, 1358, 1269, 1225, 1036, 841 cm^{-1}. HRMS $C_{11}H_{14}O_2$ $(M+Na)^+$ calcd. 201.0886, obsvd. 201.0886.

Preparation of 54

To a 25 mL round bottom flask equipped with a stirbar were added 320 mg of **40** (1.45 mmol, 1 equiv.) followed by 1 mL of MeOH, 0.5 mL of water, and 402 mg of K_2CO_3 (2.90 mmol, 2 equiv.) The flask was fitted with a condenser and heated to 64 °C for 24 h. The mixture was cooled to rt, and 20 mL of Et_20 and 10 mL of water were added. The aqueous phase was adjusted to pH 3 with the addition of 1 M HCl. The phases were separated, and the aqueous phase was extracted with 3 x 20 mL Et_2O. The organic phases were combined, washed with water and with brine, dried over Na_2SO_4, filtered and concentrated in vacuo. The mixture was purified by silica gel column chromatography with 1:1 EtOAc:hexanes to give 252 mg of **54** (84% yield, average of two reactions). Isomeric ratio *Z:E* = 6:1, major isomer: R_f = 0.60 with EtOAc, pale yellow solid. mp = 68-72 °C. ^{1}H-NMR (300 MHz, $CDCl_3$) δ = 7.18 (ddd, *J* = 7.9, 7.9, 1.7 Hz, 1 H), 7.08 (dd, *J* = 5.9, 1.8 Hz, 1 H), 6.92-6.88 (m, 2 H), 6.46 (d, *J* = 11.3 Hz, 1 H), 5.85 (dt, *J* = 11.2, 6.8 Hz, 1 H), 2.57-2.39 (m, 4 H). ^{13}C-NMR (75 MHz, $CDCl_3$) δ = 179.4, 152.7, 134.0, 129.9, 129.0, 125.2, 123.5, 120.5, 115.7, 33.5, 23.9. IR: 3015, 1700,

1449, 1199, 1149, 749 cm^{-1}. HRMS $C_{11}H_{12}O_3$ $(M+Na)^+$ calcd. 215.0684, obsvd. 215.0691.

Preparation of 61

To an oven dried 100 mL round bottom flask equipped with a stir bar were added 150 mg of **56** (0.60 mmol, 1 equiv.), which was prepared following the procedure described above for **40**, in 10 mL THF. To this was slowly added a solution of 3.0 M MeMgBr (3.6 mmol, 6 equiv.) at 0 °C. The reaction mixture was then allowed to warm to rt stirred for 12 h. The reaction was quenched by the slow addition of 20 mL of 1 M HCl solution. The mixture was diluted with 50 mL of Et_2O and washed with 100 mL (2 x 50 mL) of water and 60 mL of brine. The organic extract was dried over $MgSO_4$, filtered, and the solvent was removed in vacuo. The crude mixture was purified by flash silica-gel column chromatography with 1:1 EtOAc:hexanes as eluent to give 70 mg of **61** in 50% yield. Isomeric ratio: *Z:E* = 12:1, major isomer: R_f = 0.3 with 1:1 EtOAc:hexanes, white solid. mp = 90-94 °C. ^{1}H-NMR (300 MHz, $CDCl_3$) δ = 7.32 (dd, *J* = 7.7, 1.7 Hz, 1 H), 7.09 (ddd, *J* = 7.5, 7.5, 1.7 Hz, 1 H), 6.87 (ddd, *J* = 7.3, 7.3, 1.2 Hz, 1 H), 6.79 (dd, *J* = 8.0, 1.1 Hz, 1 H), 6.59 (d, *J* = 15.9 Hz, 1H), 6.17 (dt, *J* = 15.9, 7.0 Hz, 1 H), 5.49 (bs, 1 H), 2.26 (dd, *J* = 6.4, 6.4 Hz, 2 H), 1.56-1.33 (m, 6 H), 1.23 (s, 6 H). ^{13}C-NMR (75 MHz, $CDCl_3$) δ = 152.8, 133.2, 128.2, 127.5, 125.3, 124.6, 121.0, 116.0, 71.6, 43.7, 33.4, 29.8, 29.5, 23.9. IR: 3286, 2933, 1602, 1455, 1370, 1246, 972, 750. 3410, 3013, 2971, 1604, 1448, 1377, 1261, 1210, 1147, 1131, 904, 755 cm^{-1}. HRMS $C_{15}H_{22}O_2$ $(M+Na)^+$ calcd. 257.1517, obsvd. 257.1525.

Preparation of 64

To an oven-dried 100 mL Schlenk flask were added 2.10 g of **62** (8.00 mmol, 1 equiv.) and 40 mL of Et_3N. The solution was degassed by 2 cycles of freeze-pump-thaw. To a second oven-dried Schlenk flask were added 1.26 g of **63** (8.96 mmol, 1.12 equiv.), 20 mL of Et_3N and 40 mL of THF. The solution was degassed by 2 cycles of freeze-pump-thaw. To an oven-dried 250 mL round bottom flask equipped with stir bar were added 169 mg of $Pd(PPh_3)_2Cl_2$ (0.240 mmol, 0.0300 equiv.) and 91.4 mg of CuI (0.480 mmol, 0.0600 equiv.). The solutions of **62** and **63** were sequentially transferred via cannula into the flask containing the catalysts. The reaction mixture was then stirred at rt overnight. The reaction mixture was diluted with 50 mL of Et_2O and then 50 mL of 1 M HCl was added and the mixture was allowed to stir for 30 min. The organic layer was washed with 50 mL of 1 M HCl (2 x 25 mL) and 20 mL of brine. The organic extract was dried over $MgSO_4$, filtered, and the solvent was removed in vacuo. The crude mixture was purified by flash silica-gel column chromatography with 10% to 20% EtOAc/hexanes as eluent to give 2.03 g of **64** (92.3% yield, average of two reactions). R_f = 0.20 with 20% EtOAc/hexanes, colorless oil, ^{1}H-NMR (300 MHz, $CDCl_3$) δ = 7.44 (dd, J = 7.6, 1.7 Hz, 1 H), 7.30 (ddd, J = 8.0, 7.6, 1.7 Hz, 1 H), 7.17 (ddd, J = 7.6, 7.6, 1.4 Hz, 1 H), 7.05 (dd, J = 8.1, 1.4 Hz, 1 H), 4.11 (t, J = 6.5 Hz, 2 H), 2.47 (t, J = 6.9 Hz, 2 H), 2.33 (s, 3 H), 2.06 (s, 3 H), 1.84-1.76 (m, 2 H), 1.71-1.63 (m, 2 H). ^{13}C-NMR (75 MHz, $CDCl_3$) δ = 171.4, 169.1, 151.7, 133.3, 129.0, 126.1, 122.3, 118.0, 94.7, 76.2, 64.1, 28.0, 25.4, 21.2, 21.1, 19.4. IR: 1761, 1733, 1487, 1366, 1237, 1207, 1180, 1037, 907, 755 cm^{-1}. HRMS $C_{16}H_{18}O_4$ $(M+Na)^+$ calcd. 297.1103, obsvd. 297.1097.

Preparation of 65

To an oven dried 50 mL Schlenk flask equipped with a stir bar were added 261 mg of 5% Pd/$BaSO_4$, 150 μL of quinoline (1.27 mmol, 0.42 equiv.) and 5 mL of MeOH. A three-way joint fitted with a balloon of H_2 was attached and the flask. To a separate, oven-dried 50 mL round bottom flask were added 823 mg of **64** (3.00 mmol) and 10 mL MeOH. The solution of **64** was transferred via cannula to the Schlenk flask. An additional 5 mL of MeOH were used for rinsing. The Schlenk flask was evacuated and refilled with H_2 three times. Upon completion as determined by TLC (four days), the reaction mixture was filtered through plug of celite® using 50 mL of MeOH. The filtrate was concentrated in vacuo and dissolved in 100 mL of CH_2Cl_2, washed with 100 mL 0.2 M HCl (2 x 50 mL) and 50 mL brine, dried over Na_2SO_4, filtered, and the solvent was removed in vacuo. The crude mixture was purified by flash silica-gel column chromatography with 1:4 EtOAc:hexanes as eluent to give 576 mg of **65** as a 10:1 mixture of alkene isomers (75% yield, average of 2 reactions). R_f = 0.60 with 2:3 EtOAc:hexanes, colorless oil. Major isomer: ^{1}H-NMR (300 MHz, $CDCl_3$) δ = 7.30-7.15 (m, 3 H), 7.08-6.98 (m, 1 H), 6.30 (d, *J* = 11.5 Hz, 1H), 5.72 (ddd, *J* = 14.7, 11.5, 7.3 Hz, 1 H), 4.03 (t, *J* = 6.6 Hz, 2 H), 2.27 (s, 3 H), 2.21 (ddd, *J* = 14.7, 7.4, 1.7 Hz, 2 H), 2.06 (s, 3 H), 1.68-1.40 (m, 4 H). ^{13}C-NMR (75 MHz, $CDCl_3$) δ = 171.4, 169.4, 148.6, 134.4, 130.6, 130.5, 128.2, 125.9, 123.9, 122.4, 64.5, 28.4, 28.3, 26.2, 21.2, 21.1. IR: 1762, 1733, 1483, 1448, 1367, 1237, 1197, 1170, 1037, 1010, 912, 760 cm^{-1}. HRMS $C_{12}H_{16}O_2$ $(M+Na)^+$ calcd. 299.1254, obsvd. 299.1257.

Preparation of 66

To a 50 mL round bottom flask equipped with stir bar were added 300 mg of **65** (1.09 mmol, 1 equiv.), 300 mg of K_2CO_3 (2.18 mmol, 2.00 equiv.) and 5 mL of MeOH. The reaction mixture was allowed to stir for 10 h. Upon completion by TLC analysis, the reaction mixture was diluted with 20 mL of CH_2Cl_2 and washed with 20 mL of 1 M HCl, 20 mL of water, and 20 mL of brine, dried over Na_2SO_4, filtered, and the solvent was removed in vacuo. The crude mixture was purified by flash silica-gel column chromatography with 2:3 EtOAc:hexanes as eluent to give 188 mg of **66** as a 10:1 mixture of alkene isomers (83% yield, average of two reactions). R_f = 0.45 with 1:1 EtOAc:hexanes, pale yellow oil, major isomer: ^{1}H-NMR (300 MHz, $CDCl_3$) δ = 7.18-7.08 (m, 2 H), 6.93-6.84 (m, 2 H), 6.41 (d, J = 11.3 Hz, 1H), 5.86 (dddd, J = 11.3, 7.3, 7.3, 1.1 Hz, 1 H), 5.71 (bs, 1 H), 3.59 (t, J = 6.3 Hz, 2 H), 2.15 (ddd, J = 14.6, 7.3, 1.6 Hz, 2 H), 1.85 (bs, 1 H), 1.64-1.36 (m, 4 H). ^{13}C-NMR (75 MHz, $CDCl_3$) δ = 153.0, 136.1, 129.9, 128.7, 124.1, 123.8, 120.3, 115.4, 62.8, 32.2, 28.4, 25.7. IR: 3303, 2934, 2859, 1604, 1451, 1228, 1037, 753 cm^{-1}. HRMS $C_{12}H_{16}O_2$ $(M+Na)^+$ calcd. 215.1043, obsvd. 215.1058.

Preparation of 67[71]

A dry 100 mL round bottom flask equipped with a stir bar is charged with 220 mg of sodium hydride (60% weight in oil, 5.5 mmol, 1.1 equiv.). To this suspension, 20 mL of dry THF were added and the suspension was cooled to 0 °C in an ice bath. In a separate flask, 2.08 g of 2,2-dimethyl-1,3-propanediol (20 mmol, 4 equiv.) were dissolved in 10 mL of THF. This solution was transferred dropwise to the flask containing the sodium hydride suspension via cannula. The mixture is warmed to rt and

stirred for 3 h. A 560 μL portion of propargyl bromide (80% weight in toluene, 5.0 mmol, 1 equiv.) was added, and the flask was fitted with a condenser and heated to reflux for 24 h. The reaction mixture was cooled to rt and approximately 30 mL of water were added. The mixture is extracted with EtOAc (4 x 30 mL). The combined organic phase was washed with brine, dried over Na_2SO_4, filtered, and concentrated in vacuo. The crude mixture was purified by flash silica-gel column chromatography with 1:3 to 1:1 EtOAc:hexanes as eluent to give 589 mg of **67** (83% yield). R_f = 0.55 with 1:1 EtOAc:hexanes, colorless oil. ^{1}H-NMR (300 MHz, $CDCl_3$) δ = 4.13 (d, *J* = 2.5 Hz, 2 H), 3.43 (bs, 2 H), 3.36 (s, 2 H), 2.43 (t, *J* = 2.4 Hz, 1 H), 2.29 (bs, 1 H), 0.92 (s, 6 H). ^{13}C-NMR (75 MHz, $CDCl_3$) δ = 79.9, 78.5, 74.7, 71.2, 58.8, 36.4, 22.0. IR: 32.57, 2962, 2875, 2117, 1713, 1475, 1231, 1038 cm^{-1}. HRMS $C_8H_{14}O_2$ $(M+Na)^+$ calcd. 165.0891, obsvd. 165.0886.

Preparation of 69

To an oven-dried 100 mL Schlenk flask were added 1.16 g of **68** (3.46 mmol, 1 equiv.) and 10 mL of Et_3N and 10 mL of THF. The solution was degassed by two cycles of freeze-pump-thaw. To a second oven-dried Schlenk flask were added 552 mg of **67** (3.88 mmol, 1.12 equiv.), 10 mL of Et_3N and 10 mL of THF. The solution was degassed by two cycles of freeze-pump-thaw. To an oven-dried 100 mL round bottom flask equipped with stir bar were added 72.9 mg of $Pd(PPh_3)_2Cl_2$ (0.104 mmol, 0.0300 equiv.) and 39.6 mg of CuI (0.208 mmol, 0.0600 equiv.). The solutions of **68** and **67** were sequentially transferred via cannula into the flask containing the catalysts. The reaction mixture was then stirred at rt overnight. The reaction mixture was diluted with 30 mL of Et_2O and washed with 50 mL of 1 M HCl (2 x 25 mL) and 20 mL of brine. The organic

extract was dried over Na_2SO_4, filtered, and the solvent was removed in vacuo. The crude mixture was purified by flash silica-gel column chromatography with to 20% EtOAc/hexanes as eluent to give 632 mg of **69** (52% yield). R_f = 0.65 with 1:1 EtOAc:hexanes, colorless oil, ^{1}H-NMR (300 MHz, $CDCl_3$) δ = 7.38 (dd, *J* = 7.6, 1.7 Hz, 1 H), 7.20 (ddd, *J* = 8.2, 7.5, 1.8 Hz, 1 H), 6.90 (ddd, *J* = 7.5, 7.5, 1.2 Hz, 1 H), 6.82 (dd, *J* = 8.1, 1.1 Hz, 1 H), 4.37 (s, 2 H), 3.46 (d, *J* = 6.1 Hz, 2 H), 3.43 (s, 2 H), 2.37 (t, *J* = 6.1, 1 H), 1.03 (s, 9 H), 0.94 (s, 6 H), 0.23 (s, 6 H). ^{13}C-NMR (75 MHz, $CDCl_3$) δ = 156.9, 133.9, 130.0, 121.4, 120.0, 115.2, 88.7, 83.9, 79.0, 71.6, 59.9, 36.5, 25.9, 22.1, 18.5, -4.1. HRMS $C_{20}H_{32}O_3Si$ $(M+Na)^+$ calcd. 371.2018, obsvd. 371.2023.

Preparation of 70

To a 25 mL round bottom flask were added 630 mg of **69** (1.8 mmol, 1 equiv.) and 5 mL of THF. The reaction mixture was cooled to 0 °C in an ice bath and 1.8 mL of TBAF (1.0 M in THF, 1.8 mmol, 1 equiv.) were added. The mixture was stirred for 5 min and 10 mL of saturated NH_4Cl and 20 mL of Et_2O were added at 0 °C. The organic phase was washed with saturated NH_4Cl, water, and brine, dried over Na_2SO_4, filtered, and concentrated in vacuo. The crude mixture was purified by flash silica-gel column chromatography with to 1:3 acetone:hexanes as eluent to give 410 mg material. R_f = 0.5 with 1:1 EtOAc:hexanes, colorless oil. ^{1}H-NMR and TLC showed decomposition, thus the product was taken to the next step without further characterization.

In a 50 mL round bottom flask, the product of deprotection was dissolved in 4 mL of THF and cooled to 0 °C in an ice bath. In a separate flask, 1.0 mL of Red-Al (sodium bis(2-methoxyethoxy)aluminum hydride, 65% weight in toluene, 3.4 mmol, 2 equiv.) were dissolved in 4 mL of THF. This solution was transfered dropwise via cannula to the

cooled flask. A further 2 mL of THF was used for rinsing. The mixture was stirred at 0 °C for 1 h, then warmed to rt. To this, 20 mL of 0.5 M HCl were added slowly. Gas evolution was observed. This mixture was extracted with Et_2O (4 x 20 mL). The combined organic phase was washed with brine, dried over Na_2SO_4, filtered, and concentrated in vacuo. The crude mixture was purified by flash silica-gel column chromatography with 1:3 acetone:hexanes as eluent to give 68 mg of **70** (17% yield). R_f = 0.5 with 1:1 EtOAc:hexanes, colorless oil. ^{1}H-NMR (300 MHz, $CDCl_3$) δ = 7.69 (dd, *J* = 7.7, 1.7 Hz, 1 H), 7.12 (ddd, *J* = 8.0, 7.4, 1.8 Hz, 1 H), 6.91-6.83 (m, 2 H), 6.78 (dd, *J* = 8.1, 1.1 Hz, 1 H), 6.26 (dt, *J* = 16.1, 5.8 Hz, 1 H), 4.16 (dd, *J* = 5.8, 1.5 Hz, 2 H), 3.53 (s, 2 H), 3.37 (s, 3 Hz), 0.95 (s, 6 H). ^{13}C-NMR (75 MHz, $CDCl_3$) δ = 153.8, 129.0, 127.5, 127.4, 126.7, 123.9, 120.6, 116.1, 79.4, 72.5, 71.9, 36.3, 22.1. IR: 3279, 2960, 2871, 1654, 1603, 1457, 1255, 1092, 1034, 753 cm^{-1}. HRMS $C_{14}H_{20}O_3$ $(M+Na)^+$ calcd. 259.1310, obsvd. 259.1308.

Preparation of 72

To an oven-dried 100 mL round bottom flask were added 2.90 g of **62** (11.1 mmol, 1 equiv.), 10 mL of THF, and 10 mL of Et_3N. The solution was degassed by two cycles of freeze-pump-thaw. To a second dried round bottom flask were added 1.24 g of **71** (12.4 mmol, 1.12 equiv.), 10 mL of THF, and 10 mL of Et_3N. The solution was degassed by two cycles of freeze-pump-thaw. To an oven-dried round bottom flask equipped with stir bar were added 233 mg of $Pd(PPh_3)_2Cl_2$ (0.332 mmol, 0.0300 equiv.) and 127 mg of CuI (0.664 mmol, 0.0600 equiv.). Solutions of **62** and **71** were sequentially transferred via cannula into the flask containing the catalysts. The reaction mixture was stirred at rt for 1 h. The reaction mixture was diluted with 50 mL of CH_2Cl_2

and washed with 100 mL (2 x 50 mL) of 1 M HCl, 50 mL of saturated NH_4Cl, and 50 mL of brine. The organic phase was dried over Na_2SO_4, filtered, and the solvent was removed in vacuo. The crude mixture was purified by flash silica-gel column chromatography with 1:2 EtOAc:hexanes to 1:1 EtOAc:hexanes as eluent to give 1.85 g of **72** (71.3% yield, average of two reactions). R_f = 0.20 with 1:1 EtOAc:hexanes, colorless oil. ^{1}H-NMR (300 MHz, $CDCl_3$) δ = 7.49 (dd, J = 7.6, 1.7 Hz, 1 H), 7.36 (ddd, J = 7.6, 7.6, 1.7 Hz, 1 H), 7.20 (ddd, J = 7.6, 7.6, 1.2 Hz, 1 H), 7.09 (dd, J = 8.1, 1.2 Hz, 1 H), 4.43 (s, 2 H), 3.78 (bdd, J = 9.1, 5.2 Hz, 2 H), 3.70 (m, 2 H), 2.34 (s, 3 H), 2.07 (bs, 1 H). ^{13}C-NMR (75 MHz, $CDCl_3$) δ = 169.2, 151.8, 133.4, 130.0, 126.1, 122.5, 116.8, 90.0, 81.7, 71.3, 62.0, 59.3, 21.1. IR: 3426, 2935, 1760, 1486, 1446, 1368, 1180, 1102, 1010, 908, 756, 733 cm^{-1}. HRMS $C_{13}H_{14}O_4$ $(M+Na)^+$ calcd. 257.0784, obsvd. 257.0789.

Preparation of 73

To an oven-dried 50 mL round bottom flask were added 300 mg of **72** (1.28 mmol, 1 equiv.) and 5 mL THF. The mixture was cooled to 0 °C in an ice bath. In a separate oven-dried round bottom flask 1.6 mL of Red-Al solution (sodium bis(2-methoxyethoxy)aluminum hydride, 65% by weight in toluene, 5.3 mmol, 4.0 equiv.) were diluted with 5 mL of THF. The solution of Red-Al was transferred dropwise via cannula to the reaction mixture. The reaction mixture was stirred at 0 °C for 1 h, and then warmed to rt. To this were slowly added 20 mL of 0.5 M HCl (gas evolution observed) followed by 20 mL of CH_2Cl_2. The phases were separated, and the aqueous phase was extracted with 80 mL of CH_2Cl_2 (4 x 20 mL). The combined organic phase was washed with brine, dried over Na_2SO_4, filtered, and the solvent was removed in vacuo. The crude mixture was purified by flash silica-gel column chromatography with

2% MeOH/CH_2Cl_2 as eluent to give 201 mg of **73** (1:1 mixture of alkene isomers) (81% yield, average of two reactions). R_f = 0.40 with 10% MeOH/CH_2Cl_2, colorless oil. ^{1}H-NMR (300 MHz, $CDCl_3$) δ = 7.37 (dd, *J* = 7.6, 1.7 Hz, 1 H), 7.19 (dddd, *J* = 7.7, 7.4, 1.6, 0.7 Hz, 1 H), 7.13 (ddd, *J* = 8.0, 7.4, 1.7 Hz, 1 H), 7.05 (ddd, *J* = 8.0, 1.9, 0.7 Hz, 1 H), 6.93-6.85 (m, 4 H), 6.78 (dd, *J* = 8.0, 1.0 Hz, 1 H), 6.65 (d, *J* = 11.4 Hz, 1 H), 6.30 (dt, *J* = 16.1, 6.0 Hz, 1 H), 6.07 (dt, *J* = 11.4, 7.1 Hz, 1 H), 5.99 (bs, 1 H), 5.61 (bs, 1 H), 4.22 (dd, *J* = 6.0, 1.4 Hz, 2 H), 4.07 (dd, *J* = 7.1, 1.1 Hz, 2 H), 3.82-3.71 (m, 4 H), 3.64 (ddd, *J* = 4.3, 4.3, 1.5 Hz, 2 H), 3.57 (ddd, *J* = 3.4, 2.1, 1.5 Hz, 2 H), 2.38-2.26 (m, 2 H). ^{13}C-NMR (75 MHz, $CDCl_3$) δ = 153.4, 153.1, 130.2, 130.0, 129.4, 129.0, 128.7, 127.8, 127.7, 127.1, 124.0, 123.0, 120.9, 120.6, 116.2, 116.2, 72.2, 72.1, 71.5, 67.7, 62.1, 61.9. IR: 3301, 2932, 2867, 1656, 1603, 1455, 1357, 1251, 1093, 1054, 976, 753 cm^{-1}. HRMS $C_{11}H_{14}O_3$ $(M+Na)^+$ calcd. 217.0835, obsvd. 217.0845.

Preparation of 105

To a dry 100 mL round bottom flask were added 1.85 g aldehyde **74** (7.05 mmol, 1 equiv.), 2.99 g of **75** (14.1 mmol, 2 equiv.), and 5.4 g freshly activated 3 Å molecular sieves. Dry MeOH (15 mL) was added and the reaction mixture was stirred at rt for 1 h, and then 1.77 g of $NaBH_3CN$ (28.2 mmol, 4 equiv.) were added and the mixture was stirred at rt for 20 h. The reaction mixture was diluted with CH_2Cl_2 and washed with saturated $NaHCO_3$ and brine, dried over Na_2SO_4, filtered and concentrated in vacuo. One half of the filtrate in a 100 mL round bottom flask was dissolved in 30 mL of THF, and 2.2 mL of Et_3N (16 mmol, 4.0 equiv.) was added. In a separate flask, 2.29 g of *p*-toluenesulfonyl chloride (12.0 mmol, 3.00 equiv.) were dissolved in 10 mL THF. This solution of *p*-toluenesulfonyl chloride was transferred to the reaction mixture via cannula.

After 2 h, the mixture was diluted with CH_2Cl_2, washed with water and brine, dried over Na_2SO_4, filtered, and concentrated in vacuo. The crude mixture was purified by flash silica-gel column chromatography with 1:1 CH_2Cl_2:hexanes as eluent to give 824 mg of **105**. (36% yield) R_f = 0.3 with 1:1 CH_2Cl_2:hexanes, colorless oil. ^{1}H-NMR (300 MHz, $CDCl_3$) δ = 7.76-7.65 (m, 2 H), 7.31-7.26 (m, 3 H), 7.16-7.04 (m, 2 H), 6.91-6.85, (m, 1 H), 6.79 (d, *J* = 16.0 Hz, 1 H), 6.77 (dd, *J* = 8.1, 1.2 Hz, 1 H), 5.90 (dt, *J* = 16.0, 6.9 Hz, 1 H), 4.03 (dd, *J* = 6.9, 1.1 Hz, 2 H), 3.74 (t, *J* = 6.6 Hz, 2 H), 3.27 (t, *J* = 6.5 Hz, 2 H), 2.42 (s, 3 H), 0.99 (s, 9 Hz), 0.85 (s, 9 H), 0.19 (s, 6 H), 0.01 (s, 6 H). ^{13}C-NMR (75 MHz, $CDCl_3$) δ = 153.0, 143.3, 137.7, 129.9, 129.2, 128.9, 127.8, 127.4, 126.7, 124.3, 121.5, 119.7, 62.4, 52.2, 49.0, 26.1, 26.0, 21.7, 18.5, 18.4, -4.0, -5.2.

Preparation of 76

To a 100 mL round bottom flask containing 795 mg **105** (1.38 mmol, 1 equiv.) were added 4 mL of THF and 2.9 mL of TBAF (1.0 M solution in THF, 2.9 mmol, 2.1 equiv.). The reaction mixture was stirred at rt for 30 min, diluted with 50 mL Et_2O and washed with saturated NH_4Cl. The organic phase was dried over Na_2SO_4, filtered, and concentrated in vacuo. The crude mixture was purified by flash silica-gel column chromatography with 1:1 EtOAc:hexanes as eluent to give 454 mg of **76**. (95% yield) R_f = 0.3 with 1:1 EtOAc:hexanes, white solid. The solid was purified further by recrystalization from warm EtOAc/pentane. ^{1}H-NMR (300 MHz, $CDCl_3$) δ = 7.75-7.67 (m, 2 H), 7.34-7.30 (m, 3 H), 7.20 (dd, *J* = 7.7, 1.7 Hz, 1 H), 7.15-7.09 (m, 1 H), 6.89-6.83 (m, 1 H), 6.79-6.73 (m, 2 H), 6.05 (dt, *J* = 15.8, 6.5 Hz, 1 H), 5.91 (bs, 1 H), 3.99 (dd, *J* = 6.6, 1.4 Hz, 2 H), 3.79 (t, *J* = 5.2 Hz, 2 H), 3.29 (t, *J* = 5.3 Hz, 2 H). ^{13}C-NMR (75 MHz, $CDCl_3$) δ = 153.4, 143.9, 136.1, 130.1, 129.3, 129.2, 127.8, 127.5, 125.9,

123.6, 121.0, 116.3, 61.5, 52.6, 50.3, 21.8. IR: 3439, 1599, 1456, 1329, 1153, 753 cm^{-1}. HRMS $C_{18}H_{21}NO_4S$ $(M+Na)^+$ calcd. 370.1089, obsvd. 370.1097.

Preparation of 81

To an oven-dried 100 mL round bottom flask were added 1.05 g of **62** (4.0 mmol, 1 equiv.), 10 mL of THF, and 10 mL of Et_3N. The solution was degassed by two cycles of freeze-pump-thaw. To a second dried round bottom flask were added 1.20 g of **80** (4.48 mmol, 1.12 equiv.), 10 mL of THF, and 10 mL of Et_3N. The solution was degassed by two cycles of freeze-pump-thaw. To an oven-dried round bottom flask equipped with stir bar were added 84.2 mg of $Pd(PPh_3)_2Cl_2$ (0.120 mmol, 0.0300 equiv.) and 45.7 mg of CuI (0.240 mmol, 0.0600 equiv.). Solutions of **62** and **80** were sequentially transferred via cannula into the flask containing the catalysts. The reaction mixture was stirred at rt for 1 h. The reaction mixture was diluted with 50 mL of CH_2Cl_2 and washed with 100 mL (2 x 50 mL) of 1 M HCl, 50 mL of saturated NH_4Cl, and 50 mL of brine. The organic phase was dried over Na_2SO_4, filtered, and the solvent was removed in vacuo. The crude mixture was purified by flash silica-gel column chromatography with 1:3 acetone:hexanes to 1:2 acetone:hexanes as eluent to give 572 mg of **81** (35% yield). R_f = 0.60 with 1:1 EtOAc:hexanes, yellow oil. ^{1}H-NMR (300 MHz, $CDCl_3$) δ = 7.92-7.88 (m, 2 H), 7.39 (dd, J = 7.6, 1.7 Hz, 1 H), 7.33-7.23 (m, 3 H), 7.15 (ddd, J = 7.6, 7.6, 1.2 Hz, 1 H), 7.05 (dd, J = 8.1, 1.2 Hz, 1 H), 4.19 (t, J = 6.6 Hz, 2 H), 2.68 (t, J = 6.6 Hz, 2 H), 2.37 (s, 3 H), 2.28 (s, 3 H). ^{13}C-NMR (75 MHz, $CDCl_3$) δ = 169.6, 151.7, 150.6, 145.0, 135.5, 133.1, 129.6, 129.4, 128.3, 126.4, 126.0, 122.2, 117.2, 90.1, 64.2, 21.7, 20.9, 19.9. IR: 1753, 1445, 1347, 1211, 1185, 1160, 1088, 661, 546 cm^{-1}

Preparation of 82

To an oven dried 50 mL Schlenk flask equipped with a stir bar were added 124 mg of 5% $Pd/BaSO_4$, 71 μL of quinoline and 5 mL of MeOH. A three-way joint fitted with a balloon of H_2 was attached and the flask. To a separate, oven-dried 50 mL round bottom flask were added 570 mg of **81** (1.42 mmol) and 5 mL MeOH. The solution of **81** was transferred via cannula to the Schlenk flask. An additional 2 mL of MeOH were used for rinsing. The Schlenk flask was evacuated and refilled with H_2 three times. Upon completion as determined by TLC (approximately 3 days), the reaction mixture was filtered through plug of celite® using 50 mL of MeOH. The filtrate was concentrated in vacuo and dissolved in 100 mL of CH_2Cl_2, washed with 100 mL of 0.2 M HCl (2 x 50 mL) and 50 mL brine, dried over Na_2SO_4, filtered, and the solvent was removed in vacuo. The crude mixture was dissolved in 20 mL MeOH in a round bottom flask and 415 mg of K_2CO_3 (3.0 mmol, 2.1 equiv.) were added and the reaction mixture was stirred at rt for 12 h. The reaction mixture was concentrated to approximately 5 mL and diluted with CH_2Cl_2. This solution was washed with 0.5 M HCl, water, and brine. The organic phase was dried over Na_2SO_4, filtered, and concentrated in vacuo. This residue was purified by flash silica-gel column chromatography with 1:1:2 acetone:CH_2Cl_2:hexanes as eluent to give 103 mg of **82** as a 4:1 mixture of alkene isomers (20% yield). R_f = 0.4 with 1:1:2 acetone:CH_2Cl_2:hexanes, pale yellow oil. Major isomer (*cis*): ^{1}H-NMR (300 MHz, $CDCl_3$) δ = 7.92-7.86 (m, 2 H), 7.34-7.23 (m, 2 H), 7.18-7.02 (m, 2 H), 6.91-6.85 (m, 2 H), 6.50 (d, *J* = 11.4 Hz, 1H), 5.72 (dt, *J* = 11.2, 7.3 Hz, 1 H), 4.10 (t, *J* = 6.4 Hz, 2 H), 2.44-2.36 (m, 5 H). ^{13}C-NMR (75 MHz, $CDCl_3$) δ = 152.8, 150.8, 145.3, 135.5, 130.3, 129.8, 129.0, 128.5, 127.6, 126.9, 123.6, 120.6, 115.7, 66.1, 28.1, 21.8. IR: 3252, 1733,

1450, 1343, 1225, 1157, 1089, 814, 756, 662, 547 cm^{-1}. HRMS $C_{18}H_{19}NO_5S$ $(M+Na)^+$ calcd. 384.0882, obsvd. 384.0894.

Preparation of 84

To an oven-dried 100 mL round bottom flask were added 1.05 g of **62** (4.00 mmol, 1 equiv.), 10 mL of THF, and 20 mL of Et_3N. The solution was degassed by two cycles of freeze-pump-thaw. To a second dried round bottom flask were added 985 mg of **83** (4.48 mmol, 1.12 equiv.) and 30 mL of THF. The solution was degassed by two cycles of freeze-pump-thaw. To an oven-dried round bottom flask equipped with stir bar were added 96 mg of $Pd(PPh_3)_2Cl_2$ (0.14 mmol, 0.030 equiv.) and 45.7 mg of CuI (0.240 mmol, 0.0600 equiv.). Solutions of **62** and **83** were sequentially transferred via cannula into the flask containing the catalysts. The reaction mixture was stirred at rt for 8 h. The reaction mixture was diluted with 50 mL of CH_2Cl_2 and washed with 100 mL (3 x 50 mL) of 1 M HCl, 50 mL of saturated NH_4Cl, and 50 mL of brine. The organic phase was dried over Na_2SO_4, filtered, and the solvent was removed in vacuo. The crude mixture was purified by flash silica-gel column chromatography with 1:3 EtOAc:hexanes to 1:2 EtOAc:hexanes as eluent to give 1.28 g of **84** (92% yield). R_f = 0.60 with 1:1 EtOAc:hexanes, yellow oil. ^{1}H-NMR (300 MHz, $CDCl_3$) δ = 7.83-7.80 (m, 2 H), 7.69-7.63 (m, 2 H), 7.35 (dd, J = 7.8, 1.6 Hz, 1 H), 7.29-7.23 (m, 1 H), 7.11 (ddd, J = 7.6, 7.6, 1.3 Hz, 1 H), 7.01 (ddd, J = 8.1, 1.3, 0.4 Hz, 1 H), 3.84 (t, J = 6.9 Hz, 2 H), 2.51 (t, J = 6.9 Hz, 2 H), 2.35 (s, 3 H), 2.00 (apparent quintet, J = 7.0 Hz, 2 H). ^{13}C-NMR (75 MHz, $CDCl_3$) δ = 169.3, 168.6, 151.6, 134.1, 133.4, 132.3, 129.0, 125.9, 123.5, 122.3, 117.8, 94.0, 76.4, 37.6, 27.7, 21.1, 17.7. IR: 1763, 1709, 1396, 1187, 719 cm^{-1}. HRMS $C_{21}H_{17}NO_4$ $(M+Na)^+$ calcd. 370.1055, obsvd. 370.1061.

Preparation of 85

To an oven dried 50 mL Schlenk flask equipped with a stir bar were added 124 mg of 5% $Pd/BaSO_4$, 71 μL of quinoline and 5 mL of MeOH. A three-way joint fitted with a balloon of H_2 was attached and the flask. To a separate, oven-dried 50 mL round bottom flask were added 500 mg of **84** (1.44 mmol) and 5 mL MeOH. The solution of **84** was transferred via cannula to the Schlenk flask. An additional 2 mL of MeOH were used for rinsing. The Schlenk flask was evacuated and refilled with H_2 three times. Upon completion as determined by TLC, the reaction mixture was filtered through a plug of celite® using 50 mL of MeOH. The filtrate was concentrated in vacuo and dissolved in 100 mL of CH_2Cl_2, washed with 100 mL 0.2 M HCl (2 x 50 mL) and 50 mL brine, dried over Na_2SO_4, filtered, and the solvent was removed in vacuo. The crude mixture was dissolved in 10 mL MeOH in a round bottom flask and 100 μL of hydrazine (3.12 mmol, 2.17 equiv.) were added and the reaction mixture was stirred at rt for 12 h. The reaction mixture was concentrated in vacuo and dried under high vacuum. To this residue were added 15 mL CH_2Cl_2 and 600 μL Et_3N (4.3 mmol, 3 equiv.). The reaction mixture was cooled to 0 °C and 250 μL of methyl chloroformate were added dropwise. The reaction mixture was allowed to slowly warm to rt and stirred for 12 h. The mixture was diluted with CH_2Cl_2 and washed with saturated NH_4Cl twice, with water, and with brine. The organic phase was dried over Na_2SO_4, filtered, and concentrated in vacuo. This residue was then dissolved in 10 mL THF, 10 mL MeOH, and 10 mL water and approximately 100 mg of Na_2CO_3 were added. The mixture was stirred for approximately 24 h. A solution of 1 M HCl was added to adjust the pH to 2-3, and then the mixture was extracted with Et_2O (5 x 20 mL). The combined organic phase was washed with brine,

dried over Na_2SO_4, filtered, and concentrated in vacuo. This residue was purified by flash silica-gel column chromatography with 1:2 EtOAc:hexanes as eluent to give 112 mg of **85** (41% yield). R_f = 0.4 with 1:1 EtOAc:hexanes, pale yellow oil. ^{1}H-NMR (300 MHz, $CDCl_3$) δ = 7.16 (ddd, *J* = 7.7, 7.7, 1.7 Hz, 1 H), 7.10-7.05 (m, 1 H), 6.91-6.86 (m, 2 H), 6.43 (d, *J* = 11.3 Hz, 1 H), 5.84 (dt, *J* = 11.2, 7.3 Hz, 1 H), 5.64 (bs, 1 H), 4.66 (bs, 1 H), 3.63 (s, 3 H), 3.14 (dd, *J* = 6.6, 6.6 Hz, 2 H), 2.16 (apparent dq, *J* = 7.3, 1.7 Hz, 2 H), 1.60 (apparent quintet, *J* = 7.1 Hz, 2 H). ^{13}C-NMR (75 MHz, $CDCl_3$) δ = 153.1, 135.0, 129.9, 128.8, 127.2, 124.6, 120.4, 115.6, 52.3, 40.5, 29.7, 25.9. IR: 3330, 2932, 1692, 1530, 1450, 1263, 755 cm^{-1}. HRMS $C_{13}H_{17}NO_3$ $(M+Na)^+$ calcd. 258.1106, obsvd. 258.1116.

Palladium-Catalyzed Alkene Difunctionalization

Preparation of 42

To a 100 mL Schlenk flask equipped with a stir bar were added 5.2 mg $Pd(MeCN)_2Cl_2$ (0.020 mmol, 0.040 equiv.), 4.0 mg of CuCl (0.040 mmol, 0.080 equiv.), 16.8 mg of (*S*)-quinox-*i*Pr (0.700 mmol, 0.140 equiv.), 20.0 mg of $KHCO_3$ (0.200 mmol, 0.400 equiv.), 1 mL of MeOH (25 mmol, 50 equiv.), 2 mL of THF, and 2 mL toluene. A three-way joint fitted with a balloon of O_2 was attached and flask was evacuated and refilled with O_2 three times. The mixture was stirred for 20 min at rt under an atmosphere of O_2. To the reaction mixture, 103 mg of **41** (0.500 mmol, 1 equiv.) were added. The reaction mixture was stirred for 3 h and diluted with 10 mL of EtOAc. The reaction mixture was then washed with 10 mL 1 M NH_4Cl, 10 mL brine, dried over Na_2SO_4, filtered, and concentrated in vacuo. The crude mixture was purified by flash silica-gel column chromatography with 2% to 10% EtOAc/hexanes as eluent to give 85.7

mg of product (72% yield, average of two reactions). Diastereomeric ratio: 10:1. R_f = 0.70 with 33% EtOAc/hexanes, white solid. mp = 81-84 °C. $[\alpha]^{20}_D$ = –31.5 (c = 3.53, $CHCl_3$). Major diastereomer: ^{1}H-NMR (400 MHz, $CDCl_3$) δ = 8.12 (s, 1 H), 7.20 (ddd, *J* = 8.9, 7.2, 1.6, 1 H), 7.09 (dd, *J* = 7.6, 1.8 Hz, 1 H), 6.91-6.82 (m, 2 H), 4.42-4.32 (m, 2 H), 3.36 (s, 3 H), 1.83 (ddd, *J* = 14.4 Hz, *J* = 7.0 Hz, *J* = 1.4 Hz, 2 H), 1.72-1.49 (m, 2 H), 1.24 (s, 3 H), 1.22 (s, 3 H). ^{13}C-NMR (100 MHz, $CDCl_3$) δ = 155.8, 129.5, 129.3, 123.5, 119.9, 117.7, 85.5, 82.8, 81.1, 57.9, 38.3, 28.3, 28.2, 27.9, 27.7. IR: 3285, 2869, 2930, 1487, 1456, 1367, 1236, 1102, 1056, 754 cm^{-1}. HRMS $C_{14}H_{20}O_3$ $(M+Na)^+$ calcd. 259.1310, obsvd. 259.1308.

Preparation of 86

To a 100 mL side-arm round bottom flask equipped with a stir bar were added 5.3 mg $Pd(MeCN)_2Cl_2$ (0.020 mmol, 0.040 equiv.), 4.0 mg of CuCl (0.040 mmol, 0.080 equiv.), 16.8 mg of (*S*)-quinox-*i*Pr (0.700 mmol, 0.140 equiv.), 20 mg of $KHCO_3$ (0.20 mmol, 0.40 equiv.) and 2.6 mL of toluene. A three-way joint fitted with a balloon of O_2 was attached and flask was evacuated and refilled three times with O_2. The mixture was stirred for 20 min at rt. To the reaction mixture, a 2.3 mL of *n*-butanol (25 mmol, 50 equiv.) and 103 mg of **41** (0.500 mmol, 1.00 equiv.) were added. The reaction mixture was stirred for 12 h and diluted with 10 mL of EtOAc. The reaction mixture was then washed with 1 M NH_4Cl (10 mL) followed by brine (10 mL). The organic layer was dried over Na_2SO_4 and concentrated in vacuo. The crude mixture was purified with flash silica-gel column chromatography with 10% EtOAc/hexanes as eluent to give 87.5 mg of product (63% yield, average of two reactions). Diastereomeric ratio: 5:1, major diastereomer: R_f = 0.75 with 33% EtOAc/hexanes, colorless liquid. $[\alpha]^{20}_D$ = –8.2 (c =

1.0, $CHCl_3$), ^{1}H-NMR (500 MHz $CDCl_3$) δ = 8.31 (s, 1 H), 7.22 (dd, *J* = 1.6, 8.7 Hz, 1 H), 7.09 (dd, *J* = 1.6, 7.5 Hz, 1 H), 6.91-6.83 (m, 2 H), 4.43 (d, *J* = 4.1 Hz, 1 H), 4.3 (ddd, *J* = 7.1, 4.2 Hz, 1 H), 3.47 (ddd, *J* = 9.3, 6.7, 1.0 Hz, 1 H), 3.37 (ddd, *J* = 9.3, 6.5, 1.0 Hz, 1 H), 2.02-1.82 (m, 2 H), 1.70-1.29 (m, 6 H), 1.24 (s, 3 H), 1,21 (s, 3 H), 0.90 (t, *J* = 7.14 Hz, 3 H). ^{13}C-NMR (100 MHz $CDCl_3$) δ = 155.9, 129.2, 124.4, 119.7, 117.7, 83.3, 82.8, 81.7, 70.0, 38.4, 31.9, 28.1, 28.0, 27.9, 19.5, 14.0. IR: 3289, 2962, 2931, 1455, 1367, 1237, 1095 cm^{-1}. HRMS $C_{17}H_{26}O_3$ $(M+Na)^+$ calcd. 301.1780, obsvd. 301.1777.

Preparation of 87

Compound **87** was synthesized following the procedure described for **42** except 2.9 mL toluene and 2.1 mL of 3-butene-1-ol (25 mmol, 50 equiv.) were used. 78.6 mg (57% yield, average of two reactions). Diastereomeric ratio: 4:1, major diastereomer: R_f = 0.75 with 33% EtOAc/hexanes, colorless liquid, $[\alpha]^{20}_D$ = +11.0 (c = 0.1, $CHCl_3$), ^{1}H-NMR (500 MHz $CDCl_3$) δ = 8.28 (s, 1 H), 7.20 (td, *J* = 1.8, 7.7 Hz, 1 H), 7.04 (dd, *J* = 1.5, 7.7 Hz, 1 H), 6.90-6.83 (m, 2 H), 5.82 (ddd, *J* = 6.5, 3.3, 7.0 Hz, 1 H), 5.02-4.98 (m, 2 H), 4.44 (d, *J* =3.9, 1 H), 4.38 (ddd, *J* = 6.9, 4.1 Hz, 1 H), 3.52 (ddd, *J* = 9.2, 6.8 Hz, 1 H), 3.42 (ddd, *J* = 9.3, 6.6 Hz, 1 H), 2.38 (dd, *J* = 6.2, 8.2 Hz, 1 H), 2.09-1.82 (m, 2 H), 1.71-1.4 (m, 2 H), 1.23 (s, 3 H), 1.21 (s, 3 H). ^{13}C-NMR (125 MHz, $CDCl_3$) δ = 155.8, 135.2, 129.3, 129.3, 124.3, 119.7, 117.7, 116.8, 83.3, 82.9, 81.7, 69.3, 38.3, 34.4, 28.1, 28.0, 27.9. IR: 3284, 2971, 1733, 1652, 1558, 1487, 1054 cm^{-1}. HRMS $C_{17}H_{24}O_3$ $(M+Na)^+$ calcd. 299.1623, obsvd. 299.1615.

Preparation of 88

Compound **88** was synthesized following the procedure described for **42** except 1.5 mL of THF, 1.5 mL toluene, and 2.0 mL of 2-methoxyethanol (25 mmol, 50 equiv.) were used. 74.2 mg (53% yield, average of two reactions). Diastereomeric ratio: 9:1, major diastereomer: R_f = 0.35 with 33% EtOAc/hexanes, colorless oil, $[\alpha]^{20}_D$ = –35.0 (c = 0.15, $CHCl_3$), ^{1}H-NMR (400 MHz $CDCl_3$) δ = 8.20 (s, 1 H), 7.20 (dd, *J* = 1.8, 6.9 Hz, 1 H), 7.11 (dd, *J* = 7.7 Hz, 1 H), 6.91-6.85 (m, 2 H), 4.54 (d, *J* = 4.4 Hz, 1 H), 4,43 (ddd, *J* = 7.0, 4.3, 4.3 Hz, 1 H), 3.65-3.51 (m, 4 H), 3.33 (s, 3 H), 2.00-1.83 (m, 2 H), 1.74-1.61 (m, 1 H), 1.56-1.49 (m, 1 H), 1.24 (s, 3 H), 1.20 (s, 3 H). ^{13}C-NMR (100 MHz, $CDCl_3$) δ = 155.9, 129.5, 129.4, 124.3, 119.9, 118.0, 83.3, 82.9, 81.7, 72.1, 69.1, 59.2, 38.4, 28.1, 28.0, 28.0. IR: 3266, 2968, 2872, 1486, 1097, 753 cm^{-1}. HRMS $C_{16}H_{24}O_4$ $(M+Na)^+$ calcd. 303.1572, obsvd. 303.1566.

Preparation of 89

Compound **89** was synthesized following the procedure described for **42** except 3.3 mL toluene and 1.7 mL of 2-chloroethanol (25 mmol, 50 equiv.) were used. 86.6 mg (61% yield, average of two reactions). Diastereomeric ratio: 5:1, major diastereomer: $[\alpha]^{20}_D$ = –38.0 (c = 0.6, $CHCl_3$) R_f = 0.50 with 20% EtOAc/hexanes, colorless oil, ^{1}H-NMR (400 MHz $CDCl_3$) δ = 8.29 (s, 1 H), 7.22 (ddd, *J* = 7.5, 0.9 Hz, 1 H), 7.13-7.09 (m, 1 H), 6.93-6.85 (m, 2 H), 4.50 (d, *J* = 3.4 Hz, 1 H), 4.43 (td, *J* = 7.0, 3.5 Hz, 1 H), 3.76-3.55 (m, 4 H), 3.33 (s, 3 H), 2.01 (m, 2 H), 1.74-1.58 (m, 2 H), 1.26 (s, 3 H), 1.24 (s, 3 H). ^{13}C-NMR (100 MHz, $CDCl_3$) δ = 155.7, 129.8, 129.4, 124.2, 120.0, 118.1, 83.4, 81.9, 69.7, 43.3, 38.3, 28.1, 27.9, 27.8. IR: 3265, 2966, 1490, 1461, 1364, 1190, 1104, 1049, 754 cm^{-1}. HRMS $C_{15}H_{21}ClO_3$ $(M+Na)^+$ calcd. 307.1077, obsvd. 307.1079.

Preparation of 90

Compound **90** was synthesized following the procedure described for **42** except 0.7 mL of THF and 0.7 mL toluene (1:1) and 1.6 mL of benzylalcohol (15 mmol, 50 equiv.) were used. 47.7 mg (51% yield, average of two reactions). Diastereomeric ratio: 6:1, major diastereomer: R_f = 0.50 with 20% EtOAc/hexanes, colorless liquid, $[\alpha]^{20}_D$ = –49.5 (c = 0.39, $CHCl_3$), ^{1}H-NMR (300 MHz $CDCl_3$) δ = 8.33 (s, 1 H), 7.36-7.29 (m, 5 H), 7.22 (td, *J* = 7.7, 1.4 Hz, 1 H), 7.11 (dd, *J* = 7.5, 1.5 Hz, 1 H), 6.94 (dd, *J* = 8.0, 1.0 Hz, 1 H), 6.88 (td, *J* = 7.4, 1.1 Hz, 1 H), 4.64 (d, *J* = 12.0 Hz, 1 H), 4.54 (d, *J* = 3.9 Hz, 1 H), 4.43 (td, *J* = 7.0, 3.9 Hz, 1 H), 4.34 (d, *J* = 12.0 Hz, 1 H), 1.99-1.88 (m, 2 H), 1.66 (dt, *J* = 12.0, 7.3 Hz, 1 H), 1.59-1.51 (m, 1 H), 1.22 (s, 3 H), 1.20 (s, 3 H). ^{13}C-NMR (75 MHz, $CDCl_3$) δ = 155.9, 137.9, 129.5, 129.4, 128.5, 128.1, 127.9, 124.0, 119.9, 118.0, 83.0, 81.7, 81.6, 71.2, 38.3, 28.0, 27.9, 27.8. IR: 3285, 2970, 2870, 1717, 1615, 1506, 1455, 1180, 1097, 1027, 756 cm^{-1}. HRMS $C_{20}H_{24}O_3$ $(M+Na)^+$ calcd. 335.1623, obsvd. 335.3925.

Preparation of 91

Compound **91** was synthesized following the procedure described for **42** except 1.9 mL toluene and 1.1 mL of 2-(trimethylsilyl)ethanol (7.5 mmol, 25 equiv.) were used. 62.1 mg (64% yield, average of two reactions). Diastereomeric ratio: 5:1, major diastereomer: R_f = 0.85 with 20% EtOAc/hexanes, colorless liquid, $[\alpha]^{20}_D$ = –21 (c = 0.25, $CHCl_3$), ^{1}H-NMR (300 MHz $CDCl_3$) δ = 8.31 (s, 1 H), 7.18 (td, *J* = 7.7, 1.1 Hz, 1 H), 7.10 (dd, *J* = 7.5, 1.5 Hz, 1 H), 6.89-6.84 (m, 2 H), 4.50 (d, *J* = 4.5 Hz, 1 H), 4.37 (td, *J* = 7.1, 4.6 Hz, 1 H), 3.63-3.57 (m, 1 H), 3.50-3.45 (m, 1 H), 1.91-1.80 (m, 2 H), 1.63 (dt, *J* = 12.1, 7.5 Hz, 1 H), 1.46 (ddd, *J* = 12.1, 8.2, 6.3 Hz, 1 H), 1.21 (s, 3 H) 1.16 (s, 3

H), 1.04 (m, 1 H), 0.92 (m, 1 H), -0.02 (s, 9 H). ^{13}C-NMR (75 MHz, $CDCl_3$) δ = 155.9, 129.1, 129.0, 124.3, 119.7, 117.6, 82.6, 82.2, 81.5, 67.6, 38.3, 28.1, 27.8, 27.7, 18.5, 1.2. IR: 3304, 2966, 2894, 1586, 1486, 1384, 1248, 1096, 859, 836, 755 cm^{-1}. HRMS $C_{18}H_{30}O_3Si$ $(M+Na)^+$ calcd. 345.1862, obsvd. 345.1861.

Preparation of 92

Compound **92** was synthesized following the procedure described for **42** except 3.0 mL toluene and 2.0 mL of (−)-myrtenol (12.5 mmol, 25 equiv.) were used. 97.9 mg (55% yield, average of two reactions). Diastereomeric ratio: 9:1, major diastereomer: $[\alpha]^{20}_D = -31.3$ (c = 0.7, $CHCl_3$) R_f = 0.76 with 33% EtOAc/hexanes, colorless liquid. ^{1}H-NMR (400 MHz $CDCl_3$) δ = 8.28 (s, 1 H), 7.20-7.16 (m, 1 H), 7.08 (dd, *J* = 7.5, 1.4 Hz, 1 H), 6.89-6.83 (m, 2 H), 5.46 (dt, *J* = 2.9, 1.4 Hz, 1 H) 4.51 (d, *J* = 3.9 Hz, 1 H), 4.38 (td, *J* = 5.4, 3.2 Hz, 1 H), 3.90 (dd, *J* = 12.3, 1.7 Hz, 1H), 3.75-3.72 (m, 1 H), 2.33 (dt, *J* = 8.6, 5.6 Hz, 1 H), 2.24 (m, 2 H), 2.12 (t, *J* = 5.6 Hz, 1 H), 2.01 (m, 1 H), 1.94-1.88 (m, 2 H), 1.66-1.61 (m, 1 H) 1.54-1.50 (m, 1 H), 1.27 (s, 3 H), 1.21 (s, 3 H), 1.19 (s, 3 H) 1.07 (d, *J* = 8.6 Hz, 1 H), 0.86 (s, 3 H). ^{13}C-NMR (100 MHz, $CDCl_3$) δ = 155.7, 144.9, 129.1, 129.2, 129.0, 124.1, 120.1, 119.5, 117.5, 82.6, 81.6, 81.5, 81.5, 76.7, 72.4, 43.4, 41.0, 40.8, 38.1, 37.9, 31.5, 31.3, 31.2, 28.0, 27.7, 27.6, 26.2, 21.1, 20.9. IR: 3303, 2969, 2914, 1615, 1486, 1381, 1282, 1126, 1035, 887, 753 cm^{-1}. HRMS $C_{23}H_{32}O_3$ $(M+Na)^+$ calcd. 379.2249, obsvd. 379.2254.

Preparation of 93

To a 100 mL side-arm round bottom flask equipped with a stir bar were added 8.3 mg Pd[(*S*)-quinox-*i*Pr]Cl_2 (0.020 mmol, 0.040 equiv.), 15.0 mg of Cu[(*S*)-quinox-*i*Pr]Cl_2

(0.0400 mmol, 0.0800 equiv.), 1.2 mg of (*S*)-quinox-*i*Pr (0.0050 mmol, 0.010 equiv.), 4.4 mg of $NaHCO_3$ (0.050 mmol, 0.10 equiv.) and 4.5 mL *t*AmylOH. A three-way joint fitted with a balloon of O_2 was attached and the flask was evacuated and refilled three times with O_2. The mixture was stirred for 20 min at rt. To the reaction mixture, 450 μL of water (25 mmol, 50 equiv.) and 103 mg of **41** (0.500 mmol, 1 equiv.) were added. The reaction mixture was stirred for 24 h and diluted with 10 mL of EtOAc. The reaction mixture was then washed with 1 M NH_4Cl (10 mL) followed by brine (10 mL). The organic layer was dried over Na_2SO_4 and concentrated in vacuo. The crude mixture was purified with flash silica-gel column chromatography with EtOAc/hexanes (4% to 10%) as eluent to give 69.9 mg of product (63% yield, average of two reactions). Diastereomeric ratio: 5:1, major diastereomer: R_f = 0.60 with 33% EtOAc/hexanes, white solid. $[\alpha]^{20}_D$ = −17.0 (c = 0.1, $CHCl_3$). ^{1}H-NMR (300 MHz, $CDCl_3$) δ = 8.40 (s, 1 H), 7.20 (ddd, *J* = 8.1, 7.4, 1.7 Hz, 1 H), 7.04 (dd, *J* = 7.6, 1.7 Hz, 1 H), 6.89 (dd, *J* = 8.1, 1.1 Hz, 1 H), 6.84 (td, *J* = 7.4, 1.2 Hz, 1 H), 4.58 (d, *J* = 6.8 Hz, 1 H), 4.27 (apparent q, *J* = 6.8 Hz, 1 H), 3.31 (bs, 1 H), 1.95-1.83 (m, 2 H), 1.81-1.75 (m, 2 H), 1.33 (s, 3 H), 1.27 (s, 3 H). ^{13}C-NMR (75 MHz, $CDCl_3$) δ = 156.1, 129.7, 128.8, 124.4, 119.9, 118.0, 83.3, 81.1, 78.9, 38.5, 29.1, 28.3, 28.2. IR: 3297, 2968, 1237, 752 cm^{-1}. HRMS $C_{13}H_{18}O_3$ $(M+Na)^+$ calcd. 245.1154, obsvd. 245.1146.

Preaparation of 94

Compound **94** was synthesized following the procedure described for **93** except 3.6 mL *t*AmylOH and 1.4 mL of ethylene glycol (25 mmol, 50 equiv.) were used. 78.5 mg (59% yield, average of two reactions). Diastereomeric ratio: 10:1, major diastereomer: R_f = 0.30 with 66% EtOAc/hexanes, colorless liquid. $[\alpha]^{20}_D$ = −100 (c =

0.1, $CHCl_3$). ^{1}H-NMR (400 MHz, $CDCl_3$) δ = 8.27 (s, 1 H), 7.21 (td, *J* = 7.7, 1.2 Hz, 1 H), 7.07 (dd, *J* = 7.5, 1.6 Hz, 1 H), 6.91 (dd, *J* = 8.1, 0.9 Hz, 1 H), 6.87 (td, *J* = 7.4, 1.1 Hz, 1 H), 4.44-4.38 (m, 2 H), 3.81-3.64 (m, 3 H), 3.58 (ddd, *J* = 10.7, 5.9, 3.0 Hz, 1 H), 2.89 (bs, 1 H), 1.93-1.87 (m, 2 H), 1.75-1.65 (m, 2 H), 1.29 (s, 3 H), 1.27 (s, 3 H). ^{13}C-NMR (100 MHz, $CDCl_3$) δ = 155.9, 129.8, 129.3, 124.1, 118.1, 85.1, 83.1, 81.7, 71.5, 61.9, 38.5, 28.5, 28.3, 28.0. IR: 3263, 2967, 2869, 1454, 1041, 754 cm^{-1}. HRMS $C_{15}H_{22}O_4$ $(M+Na)^+$ calcd. 289.1416, obsvd. 289.1417.

Preparation of 95

To a 100 mL side-arm round bottom flask equipped with a stir bar were added 8.3 mg Pd[(*S*)-quinox-*i*Pr]Cl_2 (0.020 mmol, 0.040 equiv.), 15.0 mg of Cu[(*S*)-quinox-*i*Pr]Cl_2 (0.0400 mmol, 0.0800 equiv.), 1.2 mg of (*S*)-quinox-*i*Pr (0.0050 mmol, 0.010 equiv.), 4.4 mg of $NaHCO_3$ (0.050 mmol, 0.10 equiv.) and 5.0 mL *t*AmylOH. A three-way joint fitted with a balloon of O_2 was attached and flask was emptied and refilled three times with O_2. The mixture was stirred for 20 min at rt. To the reaction mixture, 65 mg of NaN_3 (1.0 mmol, 2.0 equiv.) and 103 mg of **41** (0.200 mmol, 1 equiv.) were added. The reaction mixture was stirred for 48 h at 30 °C and diluted with 10 mL of EtOAc. The reaction mixture was then washed with 1.0 M NH_4Cl (10 mL) followed by brine (10 mL). The organic layer was dried over Na_2SO_4 and concentrated in vacuo. The product was purified with flash silica-gel column chromatography with 2% to 10% EtOAc/hexanes as eluent to give 62.9 mg of product (50% yield, average of two reactions). $[\alpha]^{20}_D$ = +22.1 (c = 0.25, $CHCl_3$). ^{1}H-NMR for major diastereomer (400 MHz $CDCl_3$) δ = 8.21 (s, 1 H), 7.28-7.23 (m, 1H), 7.18-7.15 (dd, *J* = 1.5, 7.5 Hz, 1 H), 7.01-6.88 (m, 2 H), 4.70-4.65 (d, *J* = 3.2 Hz, 1 H), 4.35-4.25 (td, *J* = 3.2, 6.7 Hz, 1 H), 1.9-1.8 (m, 2 H), 1.78-1.62 (m, 2

H), 1.23 (s, 6 H). ^{13}C-NMR (125 MHz, $CDCl_3$) δ = 155.3, 130.3, 129.9, 123.3, 120.4, 118.8, 84.3, 81.5, 66.9, 38.1, 28.4, 28.0, 27.8. IR: 3264, 2971, 2100, 1456, 1251, 754 cm^{-1}. HRMS $C_{13}H_{17}N_3O_2$ $(M+Na)^+$ calcd. 270.1216, obsvd. 270.1214.

^{1}H-NMR for minor diastereomer (400 MHz $CDCl_3$) δ = 8.34 (s, 1 H), 7.28-7.23 (m, 1 H), 7.18-7.15 (dd, *J* = 1.5, 7.5 Hz, 1 H), 7.01-6.88 (m, 2 H), 4.78-4.75 (d, *J* = 3.2, 1 H), 4.44-4.38 (td, *J* = 3.2, 6.7 Hz, 1 H), 2.1-1.9 (m, 2 H), 1.78-1.62 (m, 2 H), 1.31 (s, 3 H), 1.27 (s, 3 H). ^{13}C-NMR (125 MHz, $CDCl_3$) δ = 155.4, 130.6, 130.5, 120.2, 118.8, 83.9, 81.6, 68.5, 38.1, 28.8, 28.0, 27.8. IR: 3264, 2971, 2100, 1456, 1251, 754 cm^{-1}.

Preparation of 96

Compound **96** was synthesized following the procedure described for **42**; 89.0 mg of **96** (0.500 mmol, 1 equiv.) were added**.** The reaction was stirred for 7 h. Yield = 68%, average of two reactions. Diastereomeric ratio: 10:1, major diastereomer: R_f = 0.40 with 33% EtOAc/hexanes, white solid. mp = 64-65 °C. $[\alpha]^{20}_D$ = –62.0 (c = 0.1, $CHCl_3$). ^{1}H-NMR (400 MHz, $CDCl_3$) δ = 8.09 (s, 1 H), 7.22 (dd, *J* = 1.6, 8.3 Hz, 1 H), 7.09 (dd, *J* = 7.5, 1.9 Hz, 1 H), 6.94-6.84 (m, 2 H), 4.39-4.20 (m, 2 H), 3.98-3.78 (m, 2 H), 3.39 (s, 3 H), 1.89-1.65 (m, 4 H). ^{13}C-NMR (100 MHz, $CDCl_3$) δ = 155.9, 129.7, 129.4, 123.0, 119.9, 117.6, 86.2, 81.5, 69.2, 57.9, 28.2, 26.0. IR: 3282, 2933, 2874, 1486, 1456, 1149, 1057, 753 cm^{-1}. HRMS $C_{12}H_{16}O_3$ $(M+Na)^+$ calcd. 231.0997, obsvd. 231.0990.

Preparation of 97

To a 100 mL side-arm round bottom flask equipped with a stir bar were added 5.2 mg $Pd(MeCN)_2Cl_2$ (0.020 mmol, 0.040 equiv.), 4.0 mg of CuCl (0.040 mmol, 0.080 equiv.), 16.8 mg of (*S*)-quinox-*i*Pr (0.0700 mmol, 0.140 equiv.), 20.0 mg of $KHCO_3$ (0.200 mmol, 0.400 equiv.), 1 mL of MeOH (25 mmol, 50 equiv.), 1 mL of THF, and 2

mL toluene. A three-way joint fitted with a balloon of O_2 was attached, and the flask was evacuated and refilled with O_2 three times. The mixture was stirred for 20 min at rt under an atmosphere of O_2. To the reaction mixture, 96.1 mg of **66** (0.500 mmol, 1 equiv.) in a solution in 1 mL THF were added. The reaction mixture was stirred for 24 h and diluted with 10 mL of EtOAc. The reaction mixture was then washed with 1 M NH_4Cl (10 mL) followed by brine (10 mL). The organic layer was dried over Na_2SO_4 and concentrated in vacuo. The crude mixture was purified with flash silica-gel column chromatography with 2% to 10% EtOAc/hexanes as eluent to give 55.0 mg of product (50% yield, average of two reactions). Diastereomeric ratio: 6:1, major diastereomer: R_f = 0.66 with 1:1 EtOAc:hexanes, white solid. mp = 98-103 °C. $[\alpha]^{20}_D = -14.0$ (c = 0.28, $CHCl_3$). ^{1}H-NMR (300 MHz, $CDCl_3$) δ = 7.97 (s, 1 H), 7.22 (ddd, *J* = 7.7, 7.7, 1.7 Hz, 1 H), 7.03 (dd, *J* = 7.5, 1.7 Hz, 1 H), 6.91-6.83 (m, 2 H), 4.23 (d, *J* = 5.6 Hz, 1 H), 4.16-4.05 (m, 1 H), 3.75-3.68 (m, 1 H), 3.49 (ddd, *J* = 11.5, 11.5, 2.7 Hz, 1 H), 3.38 (s, 3H), 1.85-1.75 (m, 1 H), 1.65-1.15 (m, 5 H). ^{13}C-NMR (75 MHz, $CDCl_3$) δ = 155.8, 129.9, 129.7, 122.9, 119.9, 117.6, 87.3, 80.0, 69.1, 57.9, 28.1, 25.9, 23.1. IR: 3326, 2937, 2855, 1506, 1457, 1241, 1082, 756 cm^{-1}. HRMS $C_{13}H_{18}O_3$ $(M+Na)^+$ calcd. 245.1148, obsvd. 245.1152.

Preparation of 98

To a 200 mL side-arm round bottom flask equipped with a stir bar were added 5.2 mg $Pd(MeCN)_2Cl_2$ (0.020 mmol, 0.040 equiv.), 4.0 mg of CuCl (0.040 mmol, 0.080 equiv.), 16.8 mg of (*S*)-quinox-*i*Pr (0.0700 mmol, 0.140 equiv.), 42.0 mg of $NaHCO_3$ (0.500 mmol, 1.00 equiv.), 1.0 mL of MeOH (25 mmol, 50 equiv.), 1 mL of THF, and 2 mL toluene. A three-way joint fitted with a balloon of O_2 was attached, and the flask was evacuated and refilled with O_2 three times. The mixture was stirred for 20 min at rt. To

the reaction mixture, 97.1 mg of **73** (0.500 mmol, 1 equiv.) in a solution in 1 mL THF were added. The reaction mixture was stirred for 24 h and diluted with 10 mL of CH_2Cl_2. The reaction mixture was then washed with 1 M NH_4Cl (10 mL) followed by brine (10 mL). The organic layer was dried over Na_2SO_4 and concentrated in vacuo. The crude mixture was passed through a plug of alumina with 200 mL of 1:1 EtOAc:hexanes followed by 10% MeOH/EtOAc (to separate the product from ligand, which are inseparable by silica chromatography). The portion eluted with 10% MeOH/EtOAc was concentrated in vacuo, then purified with flash silica-gel column chromatography with 1% MeOH/CH_2Cl_2 as eluent to give 39.5 mg of the product (30% yield, average of two reactions). Diastereomeric ratio: 6:1, major diastereomer: R_f = 0.60 with 10% MeOH/CH_2Cl_2, clear oil. $[\alpha]^{20}_D = -26.3$ (c = 1.88, $CHCl_3$). ^{1}H-NMR (300 MHz, $CDCl_3$) δ = 7.64 (s, 1 H), 7.23 (dd, *J* = 8.5, 1.5 Hz, 1 H), 6.98 (dd, *J* = 7.6, 1.8 Hz, 1 H), 6.93-6.83 (m, 2 H), 4.27 (d, *J* = 6.0 Hz, 1 H), 3.97 (ddd, *J* = 9.3, 6.1, 3.4 Hz, 1 H), 3.90 (bdd, *J* = 9.9, 2.1 Hz, 1 H), 3.77 (ddd, *J* = 11.2, 11.2, 2.8 Hz, 1 H), 3.69 (bdd, *J* = 9.9, 2.8 Hz, 1 H), 3.59 (ddd, *J* = 11.2, 11.2, 2.8 Hz, 1 H), 3.51-3.41 (m, 2 H), 3.39 (s, 3 H). ^{13}C-NMR (75 MHz, $CDCl_3$) δ = 155.8, 130.2, 129.2, 121.5, 120.2, 117.6, 84.3, 68.3, 67.1, 66.4, 57.9, 29.9. IR: 3363, 3054, 2859, 1489, 1457, 1265, 1242, 1123, 1083, 731, 702 cm^{-1}. HRMS $C_{12}H_{16}O_4$ $(M+Na)^+$ calcd. 247.0941, obsvd. 247.0945.

Preparation of 99

To a 100 mL side-arm round bottom flask equipped with a stir bar were added 3.4 mg Pd[(*S*)-quinox-*i*Pr]Cl_2 (0.0080 mmol, 0.040 equiv.), 6.0 mg of Cu[(*S*)-quinox-*i*Pr]Cl_2 (0.016 mmol, 0.080 equiv.), 0.5 mg of (*S*)-quinox-*i*Pr (0.002 mmol, 0.01 equiv.), 1.7 mg of $NaHCO_3$ (0.020 mmol, 0.10 equiv.) and 2.0 mL MeOH. A three-way joint fitted with

a balloon of O_2 was attached and the flask was evacuated under house vacuum and refilled with O_2 three times. The mixture was stirred for 20 min at rt. To the reaction mixture, 38.4 mg of **54** (0.200 mmol, 1 equiv.) were added. The reaction mixture was stirred for 12 h. The crude reaction mixture was passed through a plug of silica with of EtOAc. The product was purified with flash silica-gel column chromatography with 1:2 acetone:hexanes as eluent to give 34.0 mg of product (84% yield, average of two reactions). Colorless oil. $[\alpha]^{20}_D = -8$ (c = 0.11, $CHCl_3$). ^{1}H-NMR (300 MHz $CDCl_3$) δ = 7.23 (ddd, *J* = 7.4, 7.4, 1.7 Hz, 1 H), 7.05 (dd, *J* = 8.0, 1.8 Hz, 1 H), 6.91-6.85 (m, 2 H), 4.61 (dd, *J* = 7.3, 7.3, 6.3 Hz, 1 H), 4.41 (d, *J* = 6.3 Hz, 1 H), 3.46 (s, 3 H), 2.47-2.41 (m, 2 H), 2.03 (dd, *J* = 8.1 Hz, 2 H). ^{13}C-NMR (75 MHz, $CDCl_3$) δ = 177.0, 155.9, 130.3, 129.4, 120.4, 120.1, 117.4, 86.1, 81.4, 58.2, 28.5, 24.7. IR: 3356, 2929, 1754, 1458, 1347, 1190, 1112, 758 cm^{-1}. HRMS $C_{12}H_{14}O_4$ $(M+Na)^+$ calcd. 245.0790, obsvd. 245.0783.

Preparation of 100

To a 100 mL side-arm round bottom flask equipped with a stir bar were added 2.1 mg $Pd(MeCN)_2Cl_2$ (0.0080 mmol, 0.040 equiv.), 1.6 mg of CuCl (0.016 mmol, 0.080 equiv.), 6.7 mg of (*S*)-quinox-*i*Pr (0.028 mmol, 0.14 equiv.), 8.0 mg of $KHCO_3$ (0.080 mmol, 0.40 equiv.), 400 uL of MeOH (25 mmol, 50 equiv.), 1.6 mL toluene. A three-way joint fitted with a balloon of O_2 was attached, and flask was evacuated and refilled with O_2 three times. The mixture was stirred for 20 min at rt. To the reaction mixture, 69.5 mg of **76** (0.200 mmol, 1 equiv.) were added. The reaction mixture was stirred for 24 h and diluted with 10 mL of EtOAc. The reaction mixture was then washed with 1 M NH_4Cl (10 mL) followed by brine (10 mL). The organic layer was dried over Na_2SO_4

and concentrated in vacuo. The crude mixture was purified with flash silica-gel column chromatography with 0.5% to 1% MeOH/CH_2Cl_2 as eluent. Diastereomeric ratio: 5:1, major diastereomer: R_f = 0.7 with 2:1 EtOAc:hexanes, colorless oil. $[\alpha]^{20}_D$ = +24.0 (c = 0.18, $CHCl_3$). ^{1}H-NMR (300 MHz, $CDCl_3$) δ = 7.61-7.57 (s, 2 H), 7.43 (s, 1 H), 7.36-7.31 (m, 2 H), 7.27-7.21 (m, 1 H), 6.99 (dd, *J* = 7.9, 1.7 Hz, 1 H), 6.91-6.86 (m, 2 H), 4.28 (d, *J* = 4.7 Hz, 1 H), 3.99 (ddd, *J* = 11.5, 3.1, 1.7 Hz, 1 H), 3.89 (ddd, *J* = 10.1, 4.7, 2.6 Hz, 1 H), 3.69 (ddd, *J* = 11.3, 11.3, 2.7 Hz, 1 H), 3.50-3.38 (m, 2 H), 3.33 (s, 3 H), 2.51-2.39 (m, 2 H), 2.44 (s, 3 H). ^{13}C-NMR (75 MHz, $CDCl_3$) δ = 155.8, 144.3, 132.2, 130.3, 130.0, 129.5, 128.0, 121.4, 120.3, 117.7, 84.5, 66.3, 57.9, 47.2, 45.4, 29.9, 21,8. IR: 3371, 2922, 1597, 1456, 1346, 1166, 1088, 757, 549 cm^{-1}. HRMS $C_{19}H_{23}NO_5S$ $(M+Na)^+$ calcd. 400.1195, obsvd. 400.1204.

Preparation of 101

To a 100 mL side-arm round bottom flask equipped with a stir bar were added 3.4 mg Pd[(*S*)-quinox-*i*Pr]Cl_2 (0.0080 mmol, 0.040 equiv.), 6.0 mg of Cu[(*S*)-quinox-*i*Pr]Cl_2 (0.016 mmol, 0.080 equiv.), 0.5 mg of (*S*)-quinox-*i*Pr (0.002 mmol, 0.01 equiv.), 1.7 mg of $NaHCO_3$ (0.020 mmol, 0.10 equiv.) and 1.4 mL MeOH. A three-way joint fitted with a balloon of O_2 was attached and flask was evacuated under house vacuum and refilled with O_2 three times. The mixture was stirred for 30 min at rt. To the reaction mixture, 47.1 mg of **85** (0.200 mmol, 1 equiv.) in 600 μL of MeOH were added. The reaction mixture was stirred for 48 h. The crude reaction mixture was passed through a plug of silica with of EtOAc. The product was purified with flash silica-gel column chromatography with 1:3 EtOAc:hexanes as eluent to give 7.7 mg of product (15% yield). Pale yellow oil. $[\alpha]^{20}_D$ = +40 (c = 0.05, $CHCl_3$). ^{1}H-NMR (300 MHz $CDCl_3$) δ =

7.19 (ddd, J = 8.7, 6.0, 2.7 Hz, 1 H), 6.87-6.80 (m, 3 H), 4.73 (bs, 1 H), 4.31 (bs, 1 H), 3.75 (s, 3 H), 3.48 (s, 3H), 3.33 (bs, 1 H), 2.98 (bs, 1 H), 1.98-1.79 (m, 2 H), 1.70-1.51 (m, 2 H). IR: 3294, 2928, `674, 1457, 1394, 1106, 757 cm^{-1}. HRMS $C_{14}H_{19}NO_4$ $(M+Na)^+$ calcd. 288.1212, obsvd. 288.1206.

The enantiomeric ratios of the products were determined by chromatographic separation of enantiomers by GC, HPLC, or SFC with a chiral stationary phase. The conditions, retention times, and enantiomeric ratios are tabulated in Table 2.8.

Preparation of Mosher esters[79]

To an oven dried 5 mL round bottom flask equipped with a stir bar were added 38.0 mg of **93** (0.170 mmol, 1.00 equiv.) in 1.7 mL THF. To the reaction mixture, 10.0 mg of KOH (0.170 mmol, 1.00 equiv.) and 21 μL of MeI (0.34 mmol, 2.0 equiv.) were added at rt. After 2 h the solution was diluted with EtOAc and washed with water (2 x 5 mL). The organic layer was dried over Na_2SO_4 and concentrated in vacuo. The product was used without further purification.

Synthesis of 104 (*R*)-Mosher ester

To an oven dried 5 mL round bottom flask equipped with a stir bar were added 20.2 mg of **102** (0.0850 mmol, 2.00 equiv.) in 400 μL CH_2Cl_2. To the reaction mixture, 19.2 mg of DCC (0.0920 mmol, 2.20 equiv.) 1.5 mg of DMAP (0.30 equiv.) and 10 mg of (*R*)-MTPA (0.043 mmol, 1.0 equiv.) were added at rt. After 2 days, the solution was diluted with EtOAc and washed with solution of saturated NH_4Cl (2 mL) followed by water (2 x 5 mL). The organic layer was dried over Na_2SO_4 and concentrated in vacuo. The product was purified with flash silica-gel column chromatography with

Table 2.8. Separation conditions for determination of enantiopurity.

entry	Compound	Conditions	Retention time	er
1	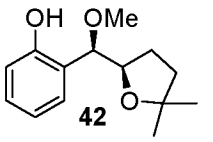 **42**	GC, β-cyclodextrin column 120 °C for 20 min, increase to 140 °C at 0.4 °C/min hold at 140 °C for 2 min, increase to 200 °C at 5 °C/min hold at 200 °C for 8 min	56.8 and 57.9 min	97.9:2.1
2	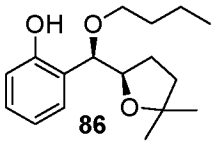 **86**	SFC, 1% Methanol, 3 mL/min Whelko chiral column	3.9 and 4.5 min	96.4:3.6[a]
3	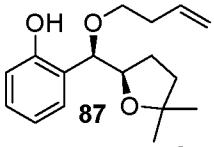 **87**	SFC, 1% Methanol, 1 mL/min Whelko chiral column	11.6 and 12.7 min	96.0:4.0[a]
4	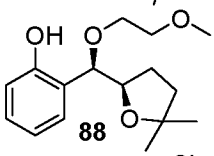 **88**	SFC, 1% Methanol, 3 mL/min 5 μm Cellucoat chiral column	4.9 and 5.7 min	97.7:2.3
5	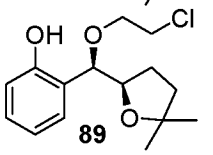 **89**	SFC, 1% Methanol, 3 mL/min Whelko chiral column	3.7 and 4.3 min	94.0:6.0[a]
6	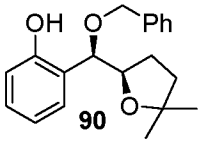 **90**	SFC, 1% Methanol, 3 mL/min Whelko chiral column	7.4 and 8.1 min	96.9:3.1[a]
7	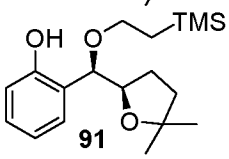 **91**	HPLC, 0.5% IPA/Hex, 1 mL/min OJ-H chiral column	29.8 and 32.6 min	99.4:0.6[b]
8	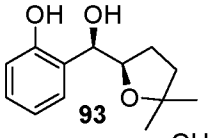 **93**	HPLC, 0.5% IPA/Hex, 1 mL/min OJ-H chiral column	29.8 and 32.6 min	98.4:1.6
9	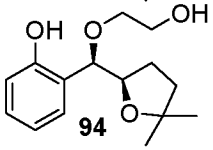 **94**	SFC, 1% MeCN, 3 mL/min Cellucoat chiral column	2.5 and 3.9 min	94.9:5.1
10	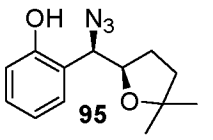 **95**	HPLC, 1% IPA:Hex, 1 mL/min OD chiral column	10.0 and 13.7 min for major 18.5 and 32.9 min for minor	91.9:8.1 91.9:8.1

(a) Product was converted to the corresponding methoxy phenol derivative using KOH and MeI.
(b) Product was converted to the free alcohol via deprotection using $BF_3{\cdot}OEt_2$.

Table 2.8. (continued)

entry	Compound	Conditions	Retention time	er
11	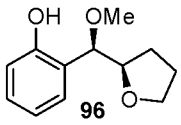 **96**	SFC, 1% Methanol, 1 mL/min AD-H chiral column	12.2 and 13.7 min	94.8:5.2
12	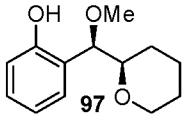 **97**	SFC, 1% Ethanol, 1.5 mL/min Whelko chiral column	12.5 and 14.1 min	94.3:5.7
13	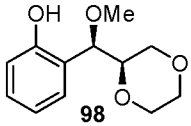 **98**	SFC, 1% Methanol, 1.5 mL/min Whelko chiral column	12.3 and 14.1 min	92.0:8.0
14	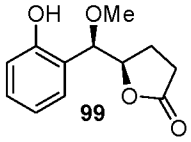 **99**	HPLC, 5% IPA:Hex, 1 mL/min OD chiral column	28.0 and 36.2 min	55.6:44.4
15	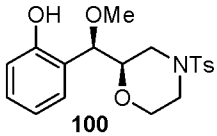 **100**	SFC, 4% Methanol, 3 mL/min OJ-H chiral column	8.9 and 13.2 min	81:19
16	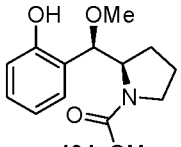 **101**	HPLC, 1% IPA:Hex, 1 mL/min OJ-H chiral column	13.9 and 17.4 min	88:12

EtOAc/hexanes as eluent to give the product in 40% yield. ^{1}H-NMR (500 MHz, $CDCl_3$) δ = 7.56 (d, 2 H), 7.40-7.31 (m, 4 H), 7.05 (dd, J = 7.6, 1.6 Hz, 1 H), 6.90-6.84 (m, 2 H), 6.32 (d, J = 8.5 Hz, 1 H), 4.32-4.28 (m, 1 H), 3.87 (s, 3 H), 3.63 (s, 3 H), 1.83-1.67 (m, 4 H), 1.30 (s, 3 H), 1.23 (s, 3 H).

Synthesis of 103 (*S*)-Mosher ester

The (*S*)-Mosher ester was prepared according to the procedure described above, using (*S*)-MTPA. ^{1}H-NMR (500 MHz, $CDCl_3$) δ = 7.56 (m, 2 H), 7.40-7.27 (m, 4 H), 6.93 (td, J = 7.5, 1.0 Hz, 1 H), 6.89 (dd, J = 8.3, 0.9 Hz, 1 H), 6.44 (d, J = 7.3 Hz, 1 H), 4.26 (ddd, J = 7.2, 6.0 Hz, 1 H), 3.86 (s, 3 H), 3.51 (s, 3 H), 1.82-1.57 (m, 4 H), 1.26 (s, 3 H), 1.14 (s, 3 H).

The differences in chemical shifts of the (*R*)- and (*S*)-Mosher esters were calculated and used to determine the absolute enantiomer (Table 2.9).

Table 2.9. Difference in chemical shifts for Mosher ester analysis.

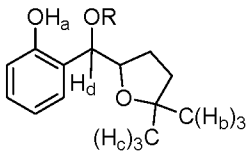

H_a	(*S*)-Mosher ester: δ = 3.869 (*R*)-Mosher ester: δ = 3.874	$\Delta\delta^{SR}$ = +0.005
H_b	(*S*)-Mosher ester: δ = 1.259 (*R*)-Mosher ester: δ = 1.306	$\Delta\delta^{SR}$ = -0.047
H_c	(*S*)-Mosher ester: δ = 1.149 (*R*)-Mosher ester: δ = 1.231	$\Delta\delta^{SR}$ = -0.082
H_d	(*S*)-Mosher ester: δ = 6.448 (*R*)-Mosher ester: δ = 6.316	$\Delta\delta^{SR}$ = +0.132

References

(1) Kolb, H. C.; VanNieuwenhze, M. S.; Sharpless, K. B. *Chem. Rev.* **1994**, *94*, 2483.

(2) Kolb, H. C.; Sharpless, K. B. *Transition Metals for Organic Synthesis* **1998**, *2*, 219.

(3) Sharpless, K. B.; Patrick, D. W.; Truesdale, L. K.; Biller, S. A. *J. Am. Chem. Soc.* **1975**, *97*, 2305.

(4) Sharpless, K. B.; Chong, A. O.; Oshima, K. *J. Org. Chem.* **1976**, *41*, 177.

(5) Herranz, E.; Biller, S. A.; Sharpless, K. B. *J. Am. Chem. Soc.* **1978**, *100*, 3596.

(6) Li, G.; Chang, H.-T.; Sharpless, K. B. *Angew. Chem., Int. Ed. Engl.* **1996**, *35*, 451.

(7) Bruncko, M.; Schlingloff, G.; Sharpless, K. B. *Angew. Chem., Int. Ed. Engl.* **1997**, *36*, 1483.

(8) Li, G.; Angert, H. H.; Sharpless, K. B. *Angew. Chem., Int. Ed. Engl.* **1997**, *35*, 2813.

(9) Rudolph, J.; Sennhenn, P. C.; Vlaar, C. P.; Sharpless, K. B. *Angew. Chem., Int. Ed. Engl.* **1997**, *35*, 2810.

(10) Reddy, K. L.; Sharpless, K. B. *J. Am. Chem. Soc.* **1998**, *120*, 1207.

(11) Demko, Z. P.; Bartsch, M.; Sharpless, K. B. *Org. Lett.* **2000**, *2*, 2221.

(12) Schlingloff, G.; Sharpless, K. B. *Asymmetric Oxidation Reactions* **2001**, 104.

(13) Donohoe, T. J.; Johnson, P. D.; Helliwell, M.; Keenan, M. *Chem. Commun.* **2001**, 2078.

(14) Donohoe, T. J.; Johnson, P. D.; Cowley, A.; Keenan, M. *J. Am. Chem. Soc.* **2002**, *124*, 12934.

(15) Donohoe, T. J.; Callens, C. K. A.; Thompson, A. L. *Org. Lett.* **2009**, *11*, 2305.

(16) Zeng, W.; Chemler, S. R. *J. Am. Chem. Soc.* **2007**, *129*, 12948.

(17) Sherman, E. S.; Chemler, S. R.; Tan, T. B.; Gerlits, O. *Org. Lett.* **2004**, *6*, 1573.

(18) Fuller, P. H.; Chemler, S. R. *Org. Lett.* **2007**, *9*, 5477.

(19) Fuller, P. H.; Kim, J.-W.; Chemler, S. R. *J. Am. Chem. Soc.* **2008**, *130*, 17638.

(20) Michaelis, D. J.; Shaffer, C. J.; Yoon, T. P. *J. Am. Chem. Soc.* **2007**, *129*, 1866.

(21) Michaelis, D. J.; Ischay, M. A.; Yoon, T. P. *J. Am. Chem. Soc.* **2008**, *130*, 6610.

(22) Benkovics, T.; Du, J.; Guzei, I. A.; Yoon, T. P. *J. Org. Chem.* **2009**, *74*, 5545.

(23) Bäckvall, J.-E. *Met.-Catal. Cross-Coupling React. (2nd Ed.)* **2004**, *2*, 479.

(24) Beccalli, E. M.; Broggini, G.; Martinelli, M.; Sottocornola, S. *Chem. Rev.* **2007**, *107*, 5318.

(25) Jensen, K. H.; Sigman, M. S. *Org. Biomol. Chem* **2008**, *6*, 4083.

(26) Bäckvall, J. E.; Nordberg, R. E. *J. Am. Chem. Soc.* **1981**, *103*, 4959.

(27) Bäckvall, J. E.; Bystroem, S. E.; Nordberg, R. E. *J. Org. Chem.* **1984**, *49*, 4619.

(28) Bäckvall, J. E.; Nystroem, J. E.; Nordberg, R. E. *J. Am. Chem. Soc.* **1985**, *107*, 3676.

(29) Bäckvall, J. E.; Gogoll, A. *Tetrahedron Lett.* **1988**, *29*, 2243.

(30) Bäckvall, J. E.; Vaagberg, J. O. *J. Org. Chem.* **1988**, *53*, 5695.

(31) Bäckvall, J. E.; Andersson, P. G. *J. Am. Chem. Soc.* **1990**, *112*, 3683.

(32) Bäckvall, J. E. *Pure Appl. Chem.* **1992**, *64*, 429.

(33) Bar, G. L. J.; Lloyd-Jones, G. C.; Booker-Milburn, K. I. *J. Am. Chem. Soc.* **2005**, *127*, 7308.

(34) Du, H.; Zhao, B.; Shi, Y. *J. Am. Chem. Soc.* **2007**, *129*, 762.

(35) Du, H.; Yuan, W.; Zhao, B.; Shi, Y. *J. Am. Chem. Soc.* **2007**, *129*, 11688.

(36) Xu, L.; Shi, Y. *J. Org. Chem.* **2008**, *73*, 749.

(37) Du, H.; Yuan, W.; Zhao, B.; Shi, Y. *J. Am. Chem. Soc.* **2007**, *129*, 7496.

(38) Du, H.; Zhao, B.; Shi, Y. *J. Am. Chem. Soc.* **2008**, *130*, 8590.

(39) Semmelhack, M. F.; Bodurow, C. *J. Am. Chem. Soc.* **1984**, *106*, 1496.

(40) Semmelhack, M. F.; Kim, C.; Zhang, N.; Bodurow, C.; Sanner, M.; Dobler, W.; Meier, M. *Pure Appl. Chem.* **1990**, *62*, 2035.

(41) Arai, M. A.; Kuraishi, M.; Arai, T.; Sasai, H. *J. Am. Chem. Soc.* **2001**, *123*, 2907.

(42) Minami, K.; Kawamura, Y.; Koga, K.; Hosokawa, T. *Org. Lett.* **2005**, *7*, 5689.

(43) Kawamura, Y.; Imai, T.; Hosokawa, T. *Synlett* **2006**, 3110.

(44) Yip, K.-T.; Yang, M.; Law, K.-L.; Zhu, N.-Y.; Yang, D. *J. Am. Chem. Soc.* **2006**, *128*, 3130.

(45) He, W.; Yip, K.-T.; Zhu, N.-Y.; Yang, D. *Org. Lett.* **2009**, *11*, 5626.

(46) Scarborough, C. C.; Stahl, S. S. *Org. Lett.* **2006**, *8*, 3251.

(47) Muniz, K. *Angew. Chem., Int. Ed.* **2009**, *48*, 9412.

(48) Alexanian, E. J.; Lee, C.; Sorensen, E. J. *J. Am. Chem. Soc.* **2005**, *127*, 7690.

(49) Streuff, J.; Hoevelmann, C. H.; Nieger, M.; Muniz, K. *J. Am. Chem. Soc.* **2005**, *127*, 14586.

(50) Muniz, K. *J. Am. Chem. Soc.* **2007**, *129*, 14542.

(51) Muniz, K.; Hoevelmann, C. H.; Streuff, J. *J. Am. Chem. Soc.* **2008**, *130*, 763.

(52) Liu, G.; Stahl, S. S. *J. Am. Chem. Soc.* **2006**, *128*, 7179.

(53) Desai, L. V.; Sanford, M. S. *Angew. Chem., Int. Ed.* **2007**, *46*, 5737.

(54) Li, Y.; Song, D.; Dong, V. M. *J. Am. Chem. Soc.* **2008**, *130*, 2962.

(55) Wang, A.; Jiang, H.; Chen, H. *J. Am. Chem. Soc.* **2009**, *131*, 3846.

(56) Sibbald, P. A.; Michael, F. E. *Org. Lett.* **2009**, *11*, 1147.

(57) Rosewall, C. F.; Sibbald, P. A.; Liskin, D. V.; Michael, F. E. *J. Am. Chem. Soc.* **2009**, *131*, 9488.

(58) Chevrin, C.; Le Bras, J.; Henin, F.; Muzart, J. *Synthesis* **2005**, 2615.

(59) Thiery, E.; Chevrin, C.; Le Bras, J.; Harakat, D.; Muzart, J. *J. Org. Chem.* **2007**, *72*, 1859.

(60) Schultz, M. J.; Sigman, M. S. *J. Am. Chem. Soc.* **2006**, *128*, 1460.

(61) Zhang, Y.; Sigman, M. S. *J. Am. Chem. Soc.* **2007**, *129*, 3076.

(62) Jensen, K. H.; Pathak, T. P.; Zhang, Y.; Sigman, M. S. *J. Am. Chem. Soc.* **2009**, *131*, 17074.

(63) Chelucci, G.; Medici, S.; Saba, A. *Tetrahedron Asymmetry* **1999**, *10*, 543.

(64) Cheng, J.; Deming, T. J. *Macromolecules* **1999**, *32*, 4745.

(65) Meyers, A. I.; Gabel, R. A. *J. Org. Chem.* **1982**, *47*, 2633.

(66) Debono, N.; Djakovitch, L.; Pinel, C. *J. Organomet. Chem.* **2006**, *691*, 741.

(67) Henry, P. M. *J. Am. Chem. Soc.* **1966**, *88*, 1595.

(68) Bäckvall, J. E.; Akermark, B.; Ljunggren, S. O. *J. Am. Chem. Soc.* **1979**, *101*, 2411.

(69) Fuerstner, A.; Davies, P. W.; Gress, T. *J. Am. Chem. Soc.* **2005**, *127*, 8244.

(70) Anslyn, E. V.; Dougherty, D. A. Catalysis. In Modern Physical Organic Chemistry, University Science Books, Sausalito, CA, 2006; pp 497.

(71) Harada, T.; Muramatsu, K.; Mizunashi, K.; Kitano, C.; Imaoka, D.; Fujiwara, T.; Kataoka, H. *J. Org. Chem.* **2008**, *73*, 249.

(72) Labrosse, J. R.; Lhoste, P.; Sinou, D. *Synth. Commun.* **2002**, *32*, 3667.

(73) Larsen, S. B.; Bang-Andersen, B.; Johansen, T. N.; Jorgensen, M. *Tetrahedron* **2008**, *64*, 2938.

(74) Tamaru, Y.; Kimura, M.; Tanaka, S.; Kure, S.; Yoshida, Z.-i. *Bull. Chem. Soc. Jpn.* **1994**, *67*, 2838.

(75) Pathak, T. P.; Gligorich, K. M.; Welm, B. E.; Sigman, M. S. *J. Am. Chem. Soc.* **2010**, *132*, 7870.

(76) Hayashi, T.; Yamasaki, K.; Mimura, M.; Uozumi, Y. *J. Am. Chem. Soc.* **2004**, *126*, 3036.

(77) Liu, G.; Stahl, S. S. *J. Am. Chem. Soc.* **2007**, *129*, 6328.

(78) Dale, J. A.; Mosher, H. S. *J. Am. Chem. Soc.* **1973**, *95*, 512.

(79) Hoye, T. R.; Jeffrey, C. S.; Shao, F. *Nat. Protoc.* **2007**, *2*, 2451.

(80) Braddock, D. C.; Cansell, G.; Hermitage, S. A. *Chem. Commun.* **2006**, 2483.

(81) Cornejo, A.; Fraile, J. M.; Garcia, J. I.; Gil, M. J.; Herrerias, C. I.; Legarreta, G.; Martinez-Merino, V.; Mayoral, J. A. *J. Mol. Catal. A: Chem.* **2003**, *196*, 101.

(82) Hahn, F. E.; von Fehren, T.; Wittenbecher, L.; Froehlich, R. *Naturforsch. B* **2004**, *59*, 541.

(83) Bianco, A.; Cavarischia, C.; Guiso, M. *Nat. Prod. Res.* **2006**, *20*, 93.

(84) Sharma, S.; Oehlschlager, A. C. *J. Org. Chem.* **1989**, *54*, 5064.

(85) Wu, M.-J.; Lee, C.-Y.; Lin, C.-F. *Angew. Chem., Int. Ed.* **2002**, *41*, 4077.

CHAPTER 3

ADVANCING MECHANISTIC UNDERSTANING OF AN ENANTIOSELECTIVE PALLADIUM-CATALYZED ALKENE DIFUNCTIONALIZATION REACTION

Introduction

Following the successful development of a highly enantioselective palladium-catalyzed alkene difunctionalization reaction wherein two distinct nucleophiles are added across an alkene in a regioselective manner (see Chapter 2),[1] questions remained about the mechanism of this reaction (Figure 3.1). These questions focused on three topics: the *o*-quinone methide intermediate, the role of copper in catalysis, and the origin of stereoselectivity. Specifically, could we provide additional evidence for the existence of the quinone methide? Is it possible to utilize this intermediate to develop new reactions? What is the lifetime of this intermediate? Concerning copper, is it possible that copper is involved in a step other than reoxidation of Pd^0 to Pd^{II}?[2] If so, how does the ligand on copper affect the outcome of the reaction? Finally, can we learn more about the enantiodetermining and diastereodetermining steps? This chapter details the mechanistic investigations undertaken in hopes of gaining a better understanding of this reaction and provides a background to put these studies in perspective.

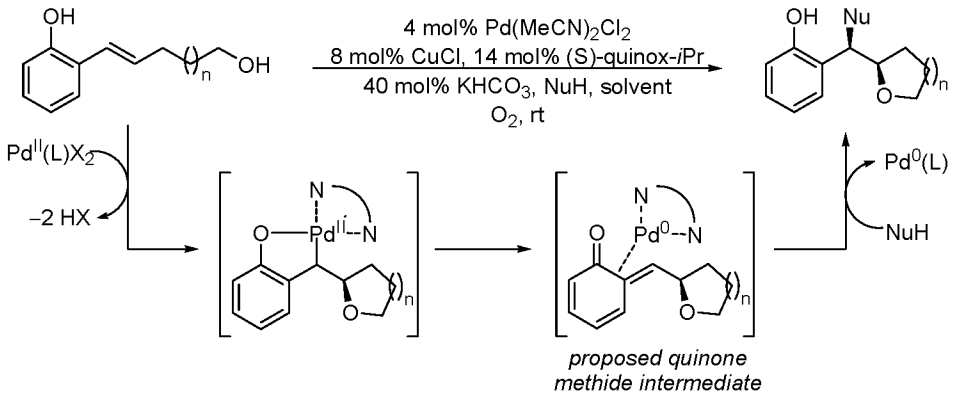

Figure 3.1. Quinone methide approach to an enantioselective palladium-catalyzed alkene difunctionalization reaction.

Quinone Methides as Reactive Intermediates

Background

Quinone methides **A** are electrophilic intermediates that have been used in the synthesis of *ortho*-functionalized phenols **1** and chroman derivatives **2** through 1,4-conjugate addition and cycloaddition reactions, respectively (Figure 3.2).[3] Given their highly reactive nature, due to the propensity to regain aromaticity, most reactions of quinone methides involve in situ generation of the intermediate, and dimerization and trimerization are common competing reactions. Formation of quinone methide intermediates has been accomplished oxidatively,[4] thermally,[5-7] photolytically,[8-10] acid promoted,[11] and via an anionic cascade method[12] (Figure 3.2).

One of the most common reactions of quinone methides is an inverse electron demand Diels-Alder reaction with an electron-rich dienophile, such as an enol ether (Figure 3.3).[3,13] This reaction has synthetic utility as it forms a chroman, a core structure found in many biologically active compounds.[14] Depending on the substitution of the two reactive partners, this transformation has the potential to set three contiguous

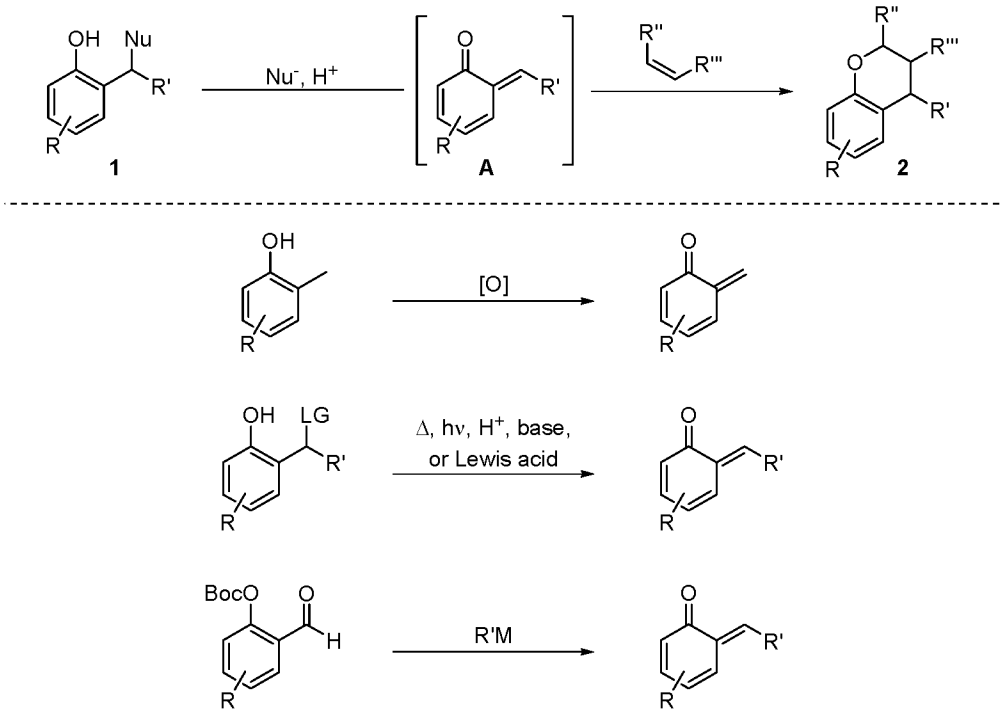

Figure 3.2. 1,4-conjugate addition and [4+2] cycloaddition reactions with quinone methide intermediates and traditional methods for their formation.

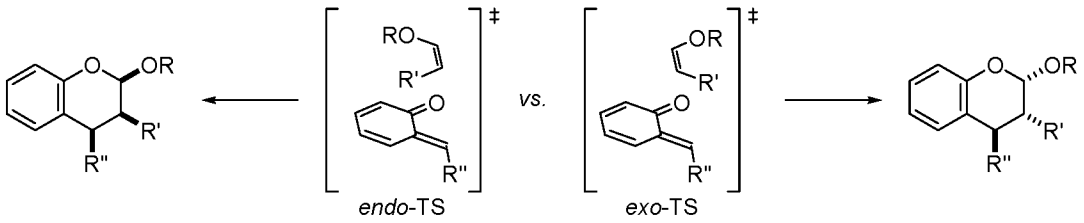

Figure 3.3. [4+2] cycloaddition transition states and resulting diastereomeric outcomes.

stereocenters. Diastereoselectivity is affected by the size of substituents on the quinone methide and dieneophile (R, R', and R'' in Figure 3.3).[13] Additionally, diastereoselectivity can depend on reaction conditions. Often the forcing conditions used to generate quinone methide intermediates, such as high temperature or strong Lewis acids, result in a decrease in *endo*/*exo* selectivity.[3]

In terms of setting the absolute stereochemistry about the chroman core, relatively few examples exist. Pettus and coworkers reported the diastereoselective [4+2] cycloaddition of *o*-quinone methides using chiral enol ethers, such as **4**, to set the absolute stereochemistry of chroman **5** (Figure 3.4).[15] Depending on the chiral substituent, high diastereoselectivity can be achieved. This approach has been implemented in the synthesis of natural products (+)-Mimosifoliol,[15] (+)-Tolterodine, and (–)-Berkelic acid.[16]

Another example of a diastereoselective [4+2] cycloaddition to set the absolute stereochemistry of the chroman is found in a report by Korthals and Wulff (Figure 3.5).[17] In this case, a protected chiral propargyl alcohol **6** is employed as a partner in a benzannulation reaction resulting in the formation of intermediate **A** in high diastereoselectivity. This chromium arene intermediate is proposed to form a chiral Cr-quinone methide intermediate **B**, which undergoes an intramolecular [4+2] cycloaddition to form highly enantiomerically enriched products containing three fused rings.

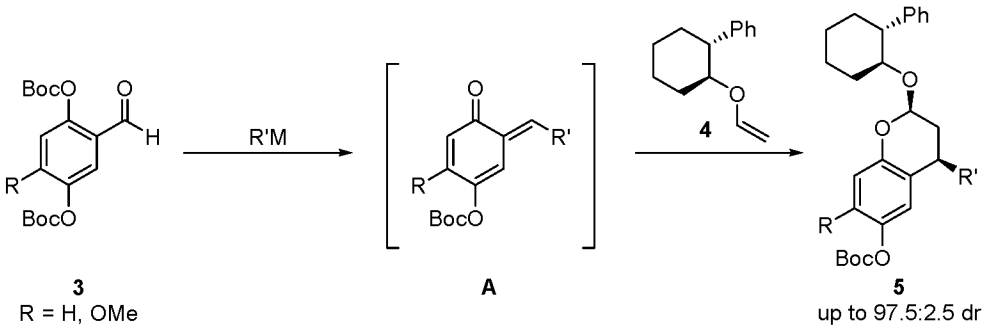

Figure 3.4. Diastereoselective [4+2] cycloaddition of quinone methides with chiral enol ethers.

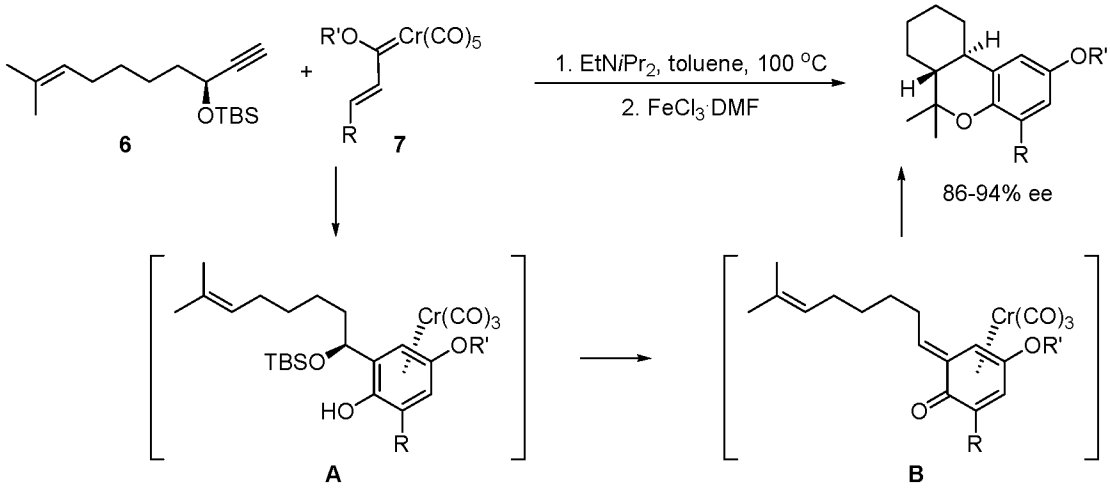

Figure 3.5. Diastereoselective [4+2] cycloaddition involving a chiral chromium complexed *o*-quinone methide intermediate.

Evidence for Palladium-Catalyzed Quinone Methide Formation

Based on the proposed mechanism, it was envisioned that a [4+2] cycloaddition would be possible with the quinone methide intermediate proposed in our alkene difunctionalization reaction. In addition to providing support for our mechanistic hypothesis, this could potentially lead to a powerful synthetic method to form chroman derivatives enantioselectively. Reaction of **8** with ethyl propenyl ether **9** under the standard palladium-catalyzed alkene-difunctionalization conditions in the absence of another exogenous nucleophile resulted in the Diels-Alder adduct **10** in 72% yield, with 86% ee and 33:5:1 dr (Figure 3.6). In addition, the analogous product **12** derived from the primary alcohol substrate **11** was obtained in 67% yield, 92% ee and 33:8:1 dr. This reaction sets four contiguous stereocenters in one step. To the best of our knowledge, this is the first example of a [4+2] cycloaddition of an *o*-quinone methide intermediate where a catalytic, rather than stoichiometric, source of chiral information is used to control the absolute stereochemistry.

The relative stereochemistry of the major diastereomer of the chroman product was assigned by a combination of ^{1}H NMR coupling constant analysis[13] and product derivation. A Jones oxidation[18] of the Diels-Alder adduct provided lactone **13**, for which a crystal structure was obtained, allowing for verification of the relative stereochemistry at the carbons α and β to the aromatic ring (Figure 3.7). The major diastereomer is consistent with an inverse electron demand Diels-Alder reaction proceeding via an *endo* transition state with an *E*-quinone methide.[3,13] The *E*-isomer of the quinone methide is assumed based on the negative steric interactions likely in the *Z*-isomer (Figure 3.7). The

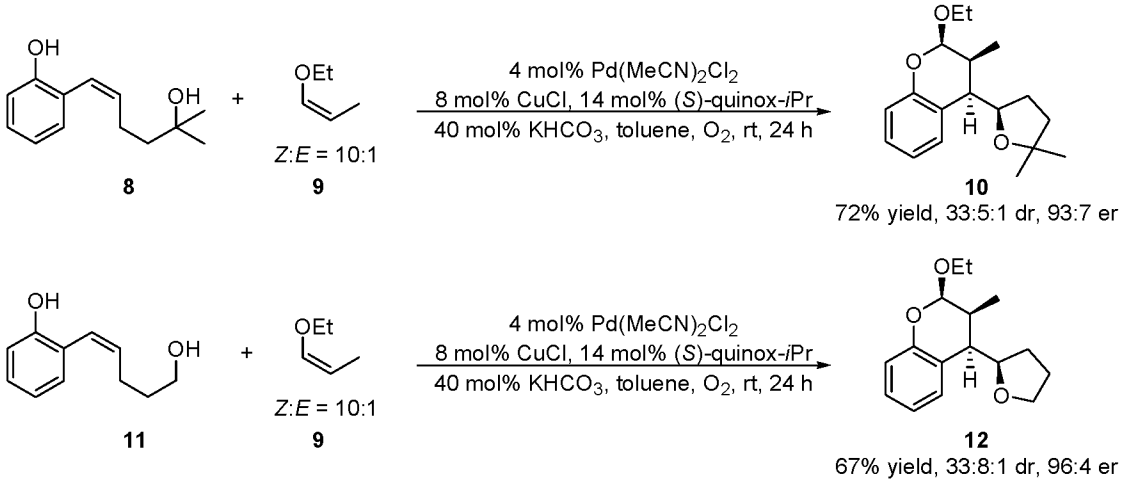

Figure 3.6. Diels-Alder reaction with a quinone methide.

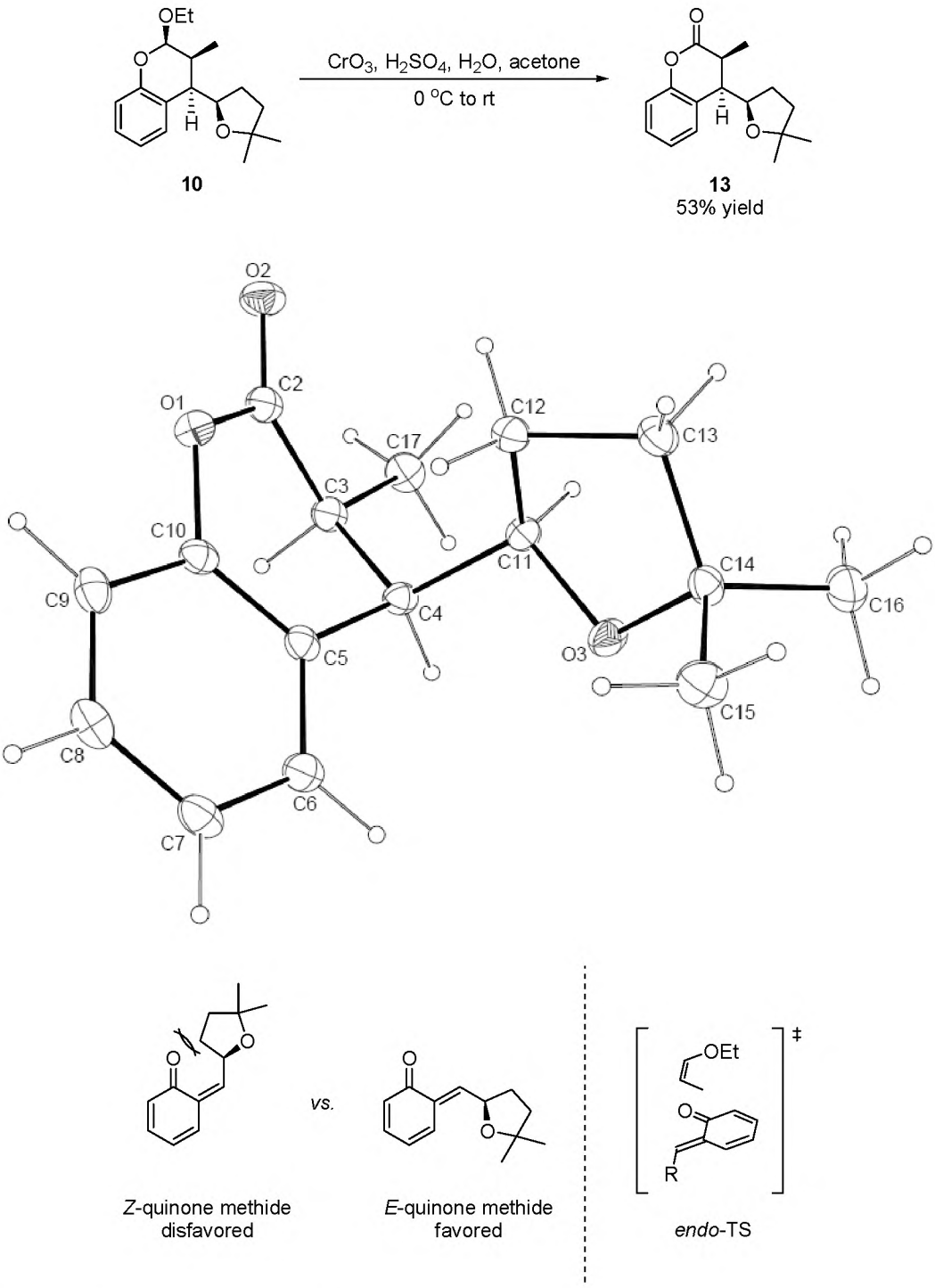

Figure 3.7. Derivatization of chroman **10** and crystal structure of lactone **13** used to inform relative stereochemistry.

relative stereochemistry between the carbons α and β to the aromatic ring (originating from the alkene) matches that observed from alkene dialkoxylation, indicating that the dienophile approaches the quinone methide from the same an face as alcohol nucleophile.[1] This facial selectivity is controlled either by the stereocenter on the tetrahydrofuran ring or potentially by the ligand on palladium (the potential for ligand effects on diastereoselectivity is addressed later in this chapter).

Attempts to obtain a pure sample of the *E*-enol ether were unsuccessful, however, when a lower *Z*:*E* ratio was used, the major diastereomer of **10** is still (*R,S,R,R*), but the ratio to the diastereomer arising from the *E*-enol ether (*S,S,R,R*) decreases (Figure 3.8). Note that the ratio of (*R,S,R,R*) to (*S,R,S,R*), which arises from the facial selectivity in approach of the enol ether to the quinone methide, is nearly constant. This provides evidence for a concerted reaction, where the *E*-isomer of enol ether reacts slower than the *Z*-isomer. Such a finding supports the existence of a quinone methide intermediate, as opposed to a stepwise mechanism involving insertion into the Pd-alkyl bond, followed by oxocarbenium formation, and attack by the phenol intermediate, as such a mechanism would not be expected to result in different diastereomers from each enol ether isomer.

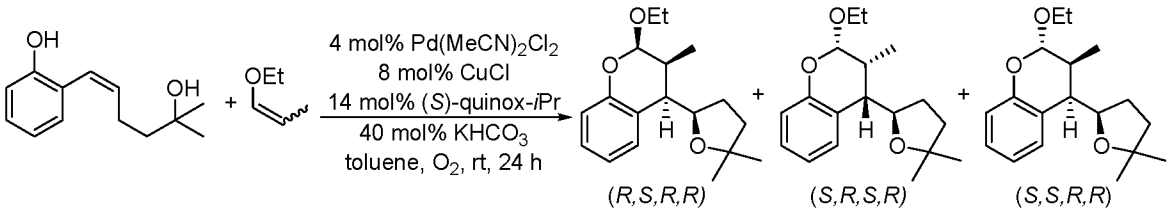

Z:*E* = 10:1	7.1	:	1	: 0.3
Z:*E* = 4.8:1	8.5	:	1	: 0.5
Z:*E* = 1.6 :1	8.7	:	1	: 1.4

Figure 3.8. Effect of enol ether isomeric ratio on diastereoselectivity.

In addition to providing mechanistic evidence, the Diels-Alder reaction also has synthetic potential. The reaction sets four contiguous stereocenters in one synthetic step with high selectivity using a catalytic amount of chiral material. Further investigation of the potential scope of this reaction is ongoing in our research group.

Copper as a Cocatalyst in Palladium Oxidase Catalysis

Background

Copper is commonly employed as a cooxidant in palladium-catalyzed reactions where O_2 is the stoichiometric oxidant, such as the Wacker oxidation (Figure 3.9).[19] In traditional mechanistic analysis of this reaction, the function of copper is interpreted only as a catalyst to regenerate Pd^{II} from Pd^0, which is formed in an independent substrate oxidation step. $Cu^{II}Cl_2$ is regenerated with hydrochloric acid and molecular oxygen.[20] However, the innocence of copper in the steps involved in substrate oxidation has been called into question. Hosokawa and coworkers have suggested that a bimetallic Pd-Cu species is an active catalyst, based on the isolation of a polymeric complex $[(PdCl_2)_2CuCl_2(DMF)_4]_n$, which catalyzes the Wacker oxidation of 1-decene.[21,22] However, demonstration that an isolated complex can be used does not necessarily indicate the identity of the active catalyst in solution. More recently, they have proposed a Pd-Cu bimetallic complex **14** as the active catalyst in an enantioselective Wacker-type cyclization (Figure 3.10).[23] In this case, isolation of the complex is not reported, and no kinetic evidence in support of the proposal is provided. Furthermore, other explanations for improved yields with copper, such as prevention of catalyst decomposition or facilitation of nucleophile delivery, were not discounted. Nevertheless, copper certainly has the potential to have a more complex function in palladium-catalyzed oxidations.

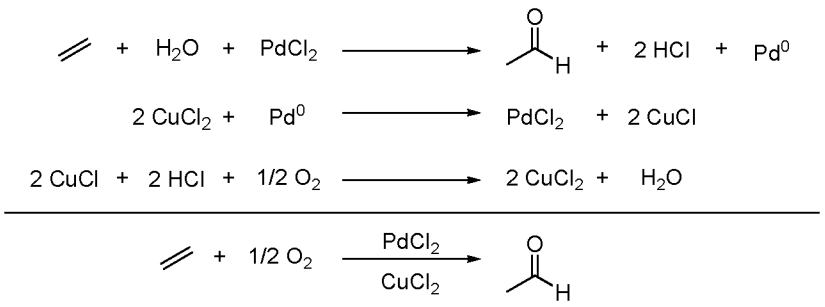

Figure 3.9. Wacker oxidation of ethylene to acetaldehyde.

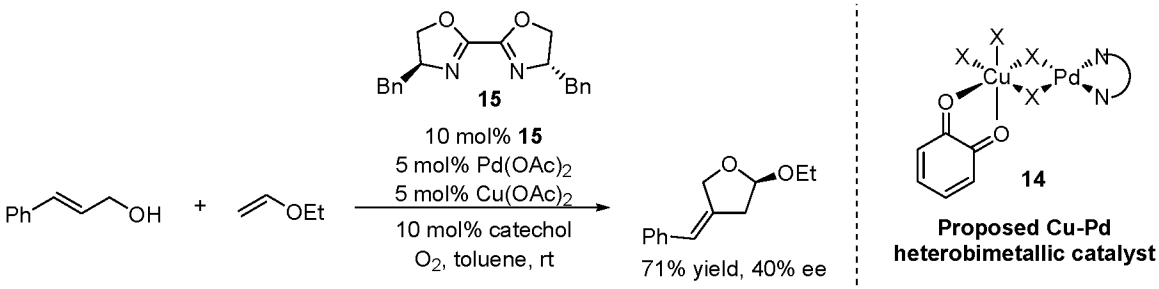

Figure 3.10. Enantioselective alkene difunctionalization reaction.

During optimization of reaction conditions for the palladium-catalyzed alkene difunctionalization reaction developed in our laboratory, copper was observed to have a significant impact on the outcome of the reaction (Figure 3.11; see Chapter 2 for details). Despite improved reactivity, the use of copper is often avoided in asymmetric palladium-catalyzed reactions, as it often has a negative effect on enantioselectivity.[24,25] We have demonstrated a reasonable solution using sufficient ligand to coordinate both metals. Nevertheless, it would be advantageous to understand why copper is beneficial.

Copper has the potential to influence a number of steps in the proposed mechanism (Figure 3.12). For example, copper could promote substrate binding through a copper-phenoxide species that is subsequently delivered to palladium, facilitate quinone methide formation, or act as a Lewis acid to promote attack of the quinone methide

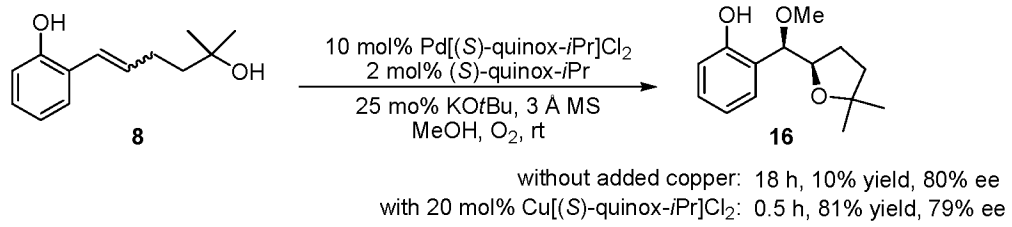

Figure 3.11. Effect of copper in a palladium-catalyzed alkene difunctionalization reaction.

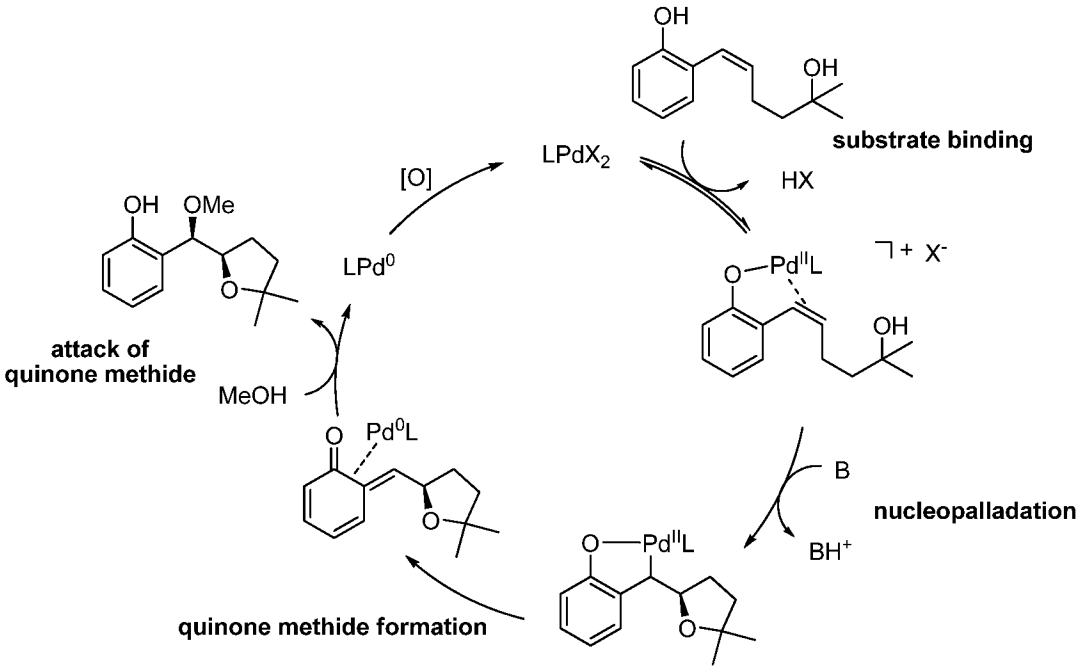

Figure 3.12. Proposed mechanism.

intermediate. A more detailed understanding of the role of copper may have implications for other reactions, as well as enlighten the development of new reactions. In an effort to better understand the potential role of copper in our reaction, as well as probe the reaction mechanism and the lifetime of the quinone methide intermediate, a kinetic investigation of the palladium-catalyzed alkene difunctionalization reaction was initiated.

Kinetic Analysis

In collaboration with Mr. Jonathan Webb, a visiting graduate student, kinetic measurements were taken using an oxygen uptake instrument[26] to monitor the rate of oxygen consumption. GC analysis was used to confirm that O_2 consumption corresponds to product yield, with 1/2 mmol O_2 consumed per mmol product formed. Initial rate measurements were used to determine the dependence on the concentration of each reaction component.

First order dependence in [palladium] was observed (Figure 3.13, A), which points to a single palladium atom involved in catalysis. Saturation in [substrate] was observed (Figure 3.13 B), indicating that at low [substrate], substrate binding affects the overall rate of the reaction, but as [substrate] approaches a certain concentration palladium becomes saturated with substrate, and at this point increasing [substrate] does not increase reaction rate. This is consistent with substrate binding prior to the rate limiting step. Nonetheless, many possibilities for the rate limiting step remain, including nucleopalladation, quinone methide formation, attack of the quinone methide, or Pd^0 oxidation.

Saturation in [Cu] was observed, indicating a step prior to the rate limiting step

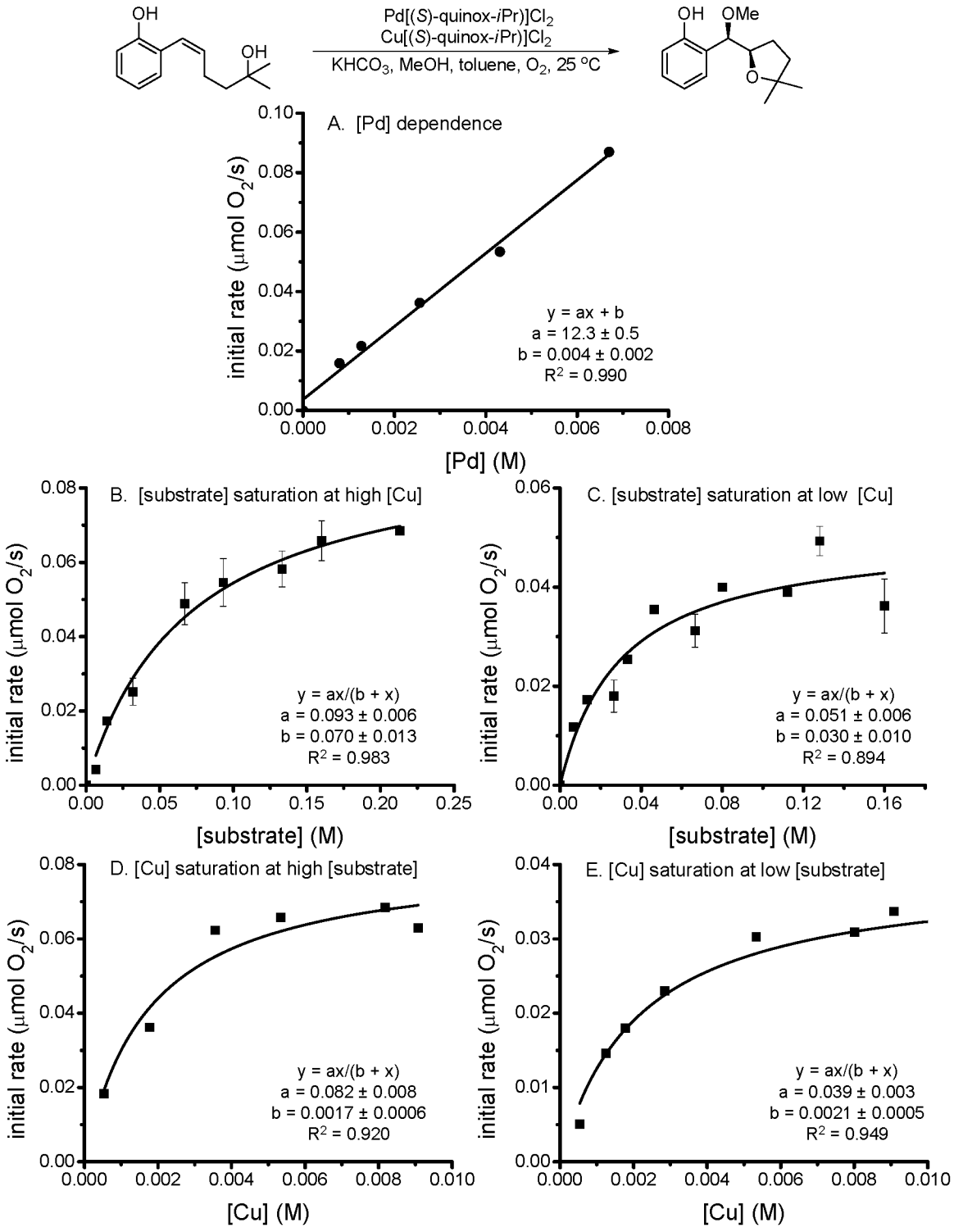

Figure 3.13. Rate dependence on [Pd], [substrate], and [Cu]. Conditions: [$KHCO_3$] = 0.026 M, 1:4 MeOH:toluene, O_2, 25 °C, A. [substrate] = 0.16 M, [Cu] = 0.0017 M, B. [Pd] = 0.0026 M, [Cu] = 0.0053 M, C. [Pd] = 0.0026 M, [Cu] = 0.0017 M, D. [Pd] = 0.0026 M, [substrate] = 0.16 M E. [Pd] = 0.0026 M, [substrate] = 0.026 M.

involves copper, evidence that copper is involved in a step other than just catalyst turnover (Figure 3.13 D). To determine if the saturation behavior in copper and substrate are independent, [substrate] and [Cu] dependence measurements were repeated at different conditions, such that [substrate] dependence was determined at both low and high [Cu] (Figure 3.13 B and C), and [Cu] dependence was determined at low and high [substrate] (Figure 3.13 D and E). It is interesting that in all four cases saturation is observed, suggesting that they are independent and thus occur in different steps. If both [copper] and [substrate] saturation occur in the same step, such as copper assisted substrate binding via the formation of a Cu-phenoxide, saturation behavior would depend on the total concentration of such a species, and thus [copper] and [substrate] saturation would not be independent.

Dependence on molecular oxygen was determined by changing the partial pressure of O_2 and N_2 at a constant total pressure. Zero order dependence in O_2 partial pressure is observed, indicating that O_2 is involved subsequent to the rate limiting step (Figure 3.14). It should be noted that a modest effect of the rate of stirring was observed, suggesting that at a certain point, the reaction becomes limited by mass transport of O_2 into the reaction solution (see experimental section for details).

The effect of base on reaction rate is complex (Figure 3.15). Initially, there appears to be a positive order in [$KHCO_3$] at low [$KHCO_3$] and inhibition at high [$KHCO_3$]. However, based on the observation that reaction yield also decreases at high [$KHCO_3$], it is possible that this is a reflection of catalyst decomposition.

Finally, dependence on [MeOH] was determined at low [$KHCO_3$], where the

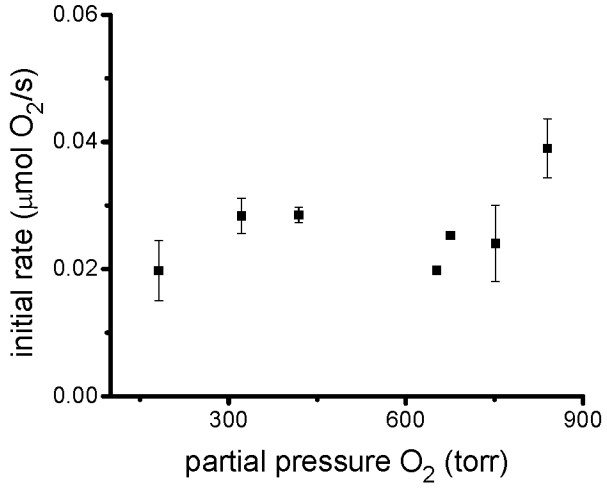

Figure 3.14. Zero order dependence on partial pressure of O_2 (with N_2). Conditions: [Pd] = 0.0026 M, [Cu] = 0.0017 M, [substrate] = 0.16 M, [$KHCO_3$] = 0.026 M, 25 °C, total pressure = 850 torr.

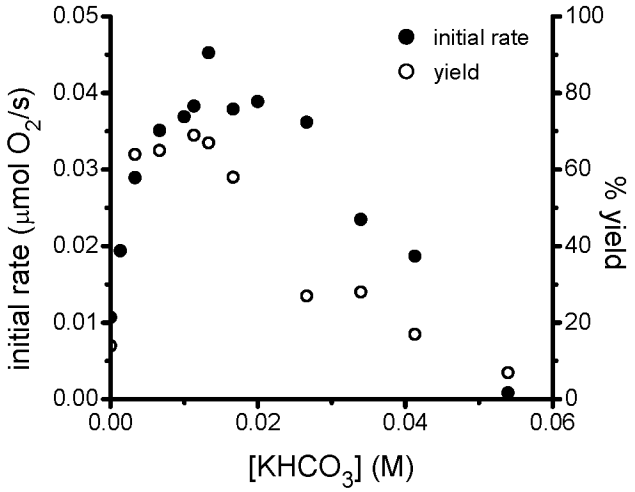

Figure 3.15. Complex order in [base]. Conditions: [Pd] = 0.0026 M, [Cu] = 0.0017 M, [substrate] = 0.16 M, 25 °C.

reaction is well behaved, and at high [substrate], where saturation is assumed. A positive order in [MeOH] is observed (Figure 3.16, A). This indicates that MeOH is involved in the rate determining step, providing strong evidence that attack of the quinone methide intermediate is the rate determining step. While the plot of ln(rate) *vs.* ln([MeOH]) has a slope less than one (Figure 3.16, B), this is likely due to the fact that this experiment was performed under conditions where the system is not saturated in [Cu], which may result in a situation where more than one step is influencing the overall rate measured.[27] While changing [MeOH] also has an effect on solution polarity, which may affect reaction rate, one would not expect to see a linear correlation from a polarity effect alone.

Dependence on [MeOH] also indicates that Pd is still bound when the quinone methide is attacked (Figure 3.17, top), as attack of a dissociated quinone methide (Figure 3.17, bottom), even if rate limiting in terms of product formation, would allow palladium to reenter the catalytic cycle, and thus should not affect rate of O_2 consumption.

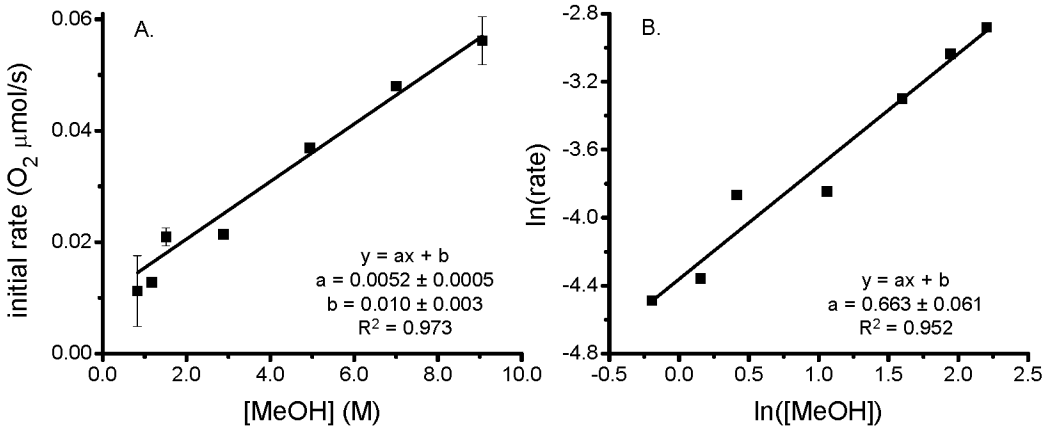

Figure 3.16. Positive dependence on [MeOH]. Conditions: [Pd] = 0.0026 M, [Cu] = 0.0017 M, [substrate] = 0.16 M, [$KHCO_3$] = 0.010 M, 25 °C.

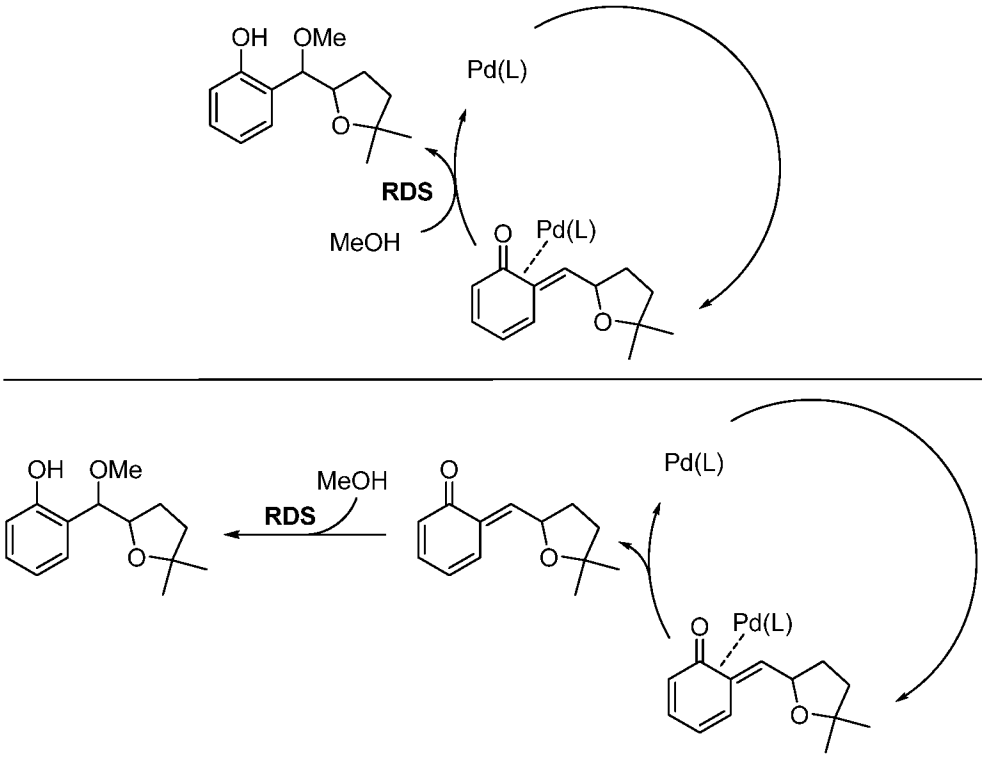

Figure 3.17. Attack of Pd-bound or free quinone methide intermediate.

Proposed Mechanisms

In order to employ the kinetic data to deepen our mechanistic understanding, we needed to account for the observed dependencies. Most significantly, our original mechanism needed to be modified to account for the observation of *independent* [Cu] and [substrate] saturation. Thus we proposed three distinct mechanisms in which copper is involved in steps besides catalyst turnover or substrate binding (Figure 3.18, A-C). The first three steps, which do not differ among the mechanisms, are the disassociation of an anionic ligand from intermediate **A** to provide an open coordination site on **B**, substrate binding to form **C**, and intramolecular nucleopalladation to reach Pd-alkyl species **D**. From the common intermediate **D**, the three proposed mechanisms differ. In mechanism

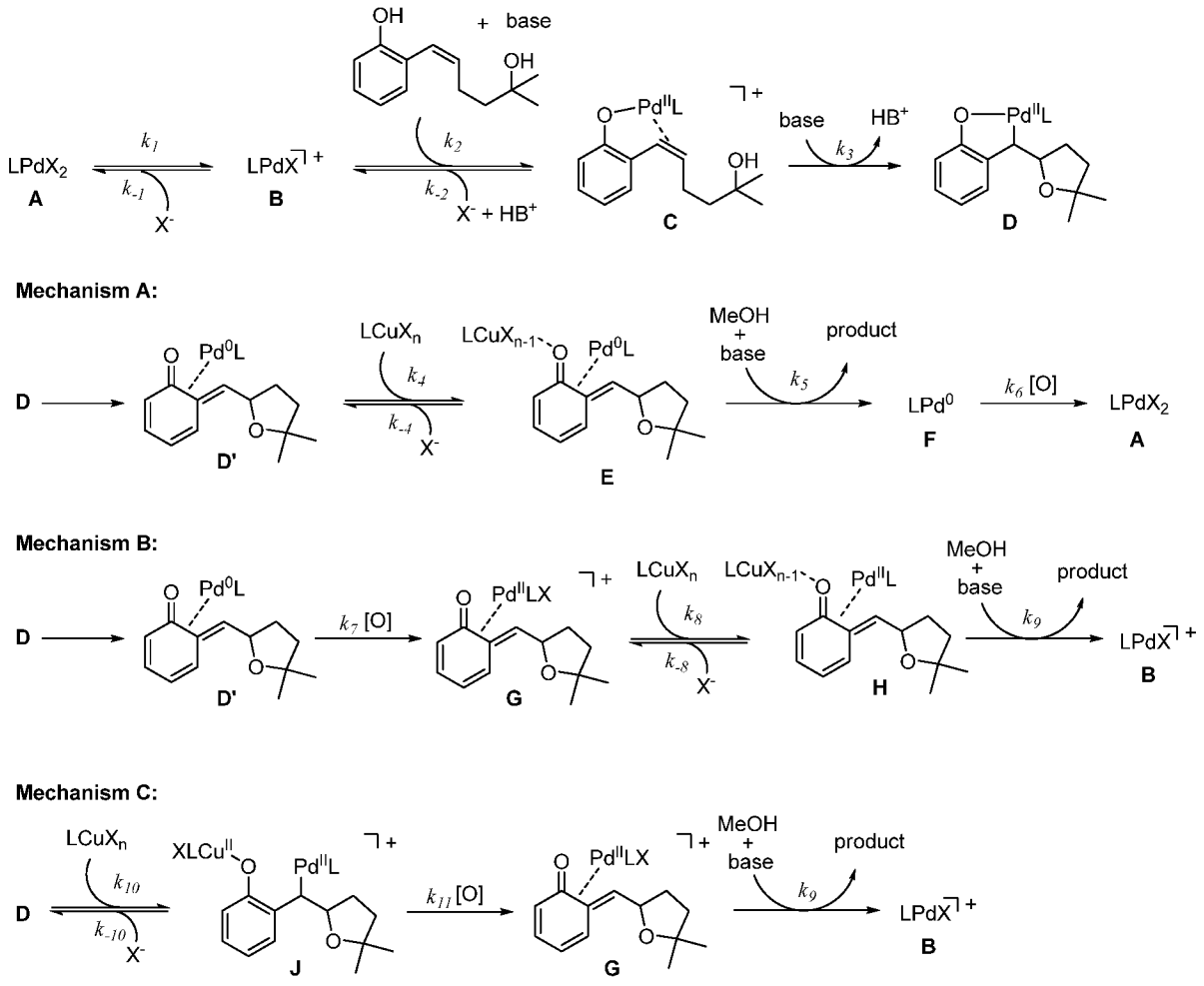

Figure 3.18 Proposed mechanisms.

A, **D** undergoes quinone methide formation with concurrent reduction of palladium. Copper is invoked as a Lewis acid to form the activated quinone methide species **E**, which undergoes nucleophilic attack by MeOH. Pd^0 is oxidized to regenerate the active catalyst, a process most likely involving Cu^{II}, although direct O_2 oxidation is possible in the absence of copper. Alternatively, mechanism B proposes oxidation of Pd^0 in intermediate **D'** to Pd^{II}-quinone methide **G** prior to copper coordination to the quinone methide, but still invokes Lewis acid activation of the quinone methide as intermediate **H**. In contrast, mechanism C accounts for the possibility of copper assisted quinone methide formation. Coordination of copper to **D** forms the hetero-bimetallic species **J**, followed by oxidation to a Pd^{II}-quinone methide intermediate **G**, likely through single electron transfer.[28] In all three mechanisms, rate limiting nucleophilic attack of the quinone methide intermediate by MeOH forms the product and releases palladium. It should be pointed out that the precise location of metals within a given intermediate cannot be deduced kinetically, and the structures merely represent a reasonable binding mode. To determine if the three mechanisms could be distinguished kinetically, a rate law was derived for each.

Rate Law Derivation

The King-Altman method[29] was used to derive rate laws for mechanisms A, B, and C above (Table 3.1, see the experimental section for a detailed discussion of the rate law derivation). Each derived rate law is rather complex. Therefore, to investigate whether each is consistent with empirical observations made under certain conditions, further simplifications were made by making assumptions specific to each set of

Table 3.1. Derived and simplified rate laws for proposed mechanisms.

Derived Rate Laws

Mechanism A

$$\frac{d[P]}{dt} = \frac{k_1k_2k_3k_4k_5k_6[Pd_T][sub][Cu][MeOH][Ox][base]^2}{\left(\begin{array}{c} k_2k_3k_4k_5k_6[sub][Cu][MeOH][Ox][base]^2 + k_{-1}k_3k_4k_5k_6[Cu][MeOH][[X^-][Ox][base] + \\ k_{-1}k_{-2}k_4k_5k_6[Cu][MeOH][X^-]^2[Ox] + k_1k_3k_4k_5k_6[Cu][MeOH][Ox][base] + \\ k_1k_{-2}k_4k_5k_6[Cu][MeOH][[X^-][Ox] + k_1k_2k_4k_5k_6[sub][Cu][MeOH][Ox][base] + \\ k_1k_2k_3k_5k_6[sub][MeOH][Ox][base]^2 + k_1k_2k_3k_{-4}k_6[sub][X^-][Ox][base] + \\ k_1k_2k_3k_4k_6[sub][Cu][Ox][base] + k_1k_2k_3k_4k_5[sub][Cu][MeOH][base]^2 \end{array}\right)}$$

Mechanism B

$$\frac{d[P]}{dt} = \frac{k_1k_2k_3k_7k_8k_9[Pd_T][sub][Cu][MeOH][Ox][base]^2}{\left(\begin{array}{c} k_{-1}k_3k_7k_8k_9[Cu][MeOH][X^-][Ox][base] + k_{-1}k_{-2}k_7k_8k_9[Cu][MeOH][X^-]^2[Ox] + \\ k_1k_3k_7k_8k_9[Cu][MeOH][Ox][base] + k_1k_{-2}k_7k_8k_9[Cu][MeOH][X^-][Ox] + \\ k_1k_2k_7k_8k_9[sub][Cu][MeOH][Ox][base]\ k_1k_2k_3k_8k_9[sub][Cu][MeOH][base]^2 + \\ k_1k_2k_3k_7k_9[sub][MeOH][Ox][base]^2 + k_1k_2k_3k_7k_{-8}[sub][X^-][Ox][base] + \\ k_1k_2k_3k_7k_8[sub][Cu][Ox][base] \end{array}\right)}$$

Mechanism C

$$\frac{d[P]}{dt} = \frac{k_1k_2k_3k_{10}k_{11}k_{12}[Pd_T][sub][Cu][MeOH][Ox][base]^2}{\left(\begin{array}{c} k_{-1}k_3k_{10}k_{11}k_{12}[Cu][MeOH][X^-][Ox][base] + k_{-1}k_{-2}k_{10}k_{11}k_{12}[Cu][MeOH][X^-]^2[Ox] + \\ k_1k_3k_{10}k_{11}k_{12}[Cu][MeOH][Ox][base] + k_1k_{-2}k_{10}k_{11}k_{12}[Cu][MeOH][X^-][Ox] + \\ k_1k_2k_{10}k_{11}k_{12}[sub][Cu][MeOH][Ox][base] + k_1k_2k_3k_{11}k_{12}[sub][MeOH][Ox][base]^2 + \\ k_1k_2k_3k_{-10}k_{12}[sub][MeOH][X^-][base]^2 + k_1k_2k_3k_{10}k_{12}[sub][Cu][MeOH][base]^2 + \\ k_1k_2k_3k_{12}k_{11}[sub][Cu][Ox][base] \end{array}\right)}$$

Simplified Rate Laws

	at high [Cu]	at high [sub]	at high [Cu] and high [sub]
A	$\frac{d[P]}{dt} = \frac{K_1k_2k_5[Pd_T][sub][MeOH][base]}{K_1k_2[sub] + k_5[MeOH]([X^-] + K_1)}$	$\frac{d[P]}{dt} = \frac{k_4k_5[Pd_T][Cu][MeOH][base]}{k_4[Cu] + k_5[MeOH][base] + k_{-4}[X^-]}$	$\frac{d[P]}{dt} = k_5[Pd_T][MeOH][base]$
B	$\frac{d[P]}{dt} = \frac{K_1k_2k_9[Pd_T][sub][MeOH][base]}{K_1k_2[sub] + k_9[MeOH]([X^-] + K_1)}$	$\frac{d[P]}{dt} = \frac{k_8k_9[Pd_T][Cu][MeOH][base]}{k_8[Cu] + k_9[MeOH][base] + k_{-8}[X^-]}$	$\frac{d[P]}{dt} = k_9[Pd_T][MeOH][base]$
C	$\frac{d[P]}{dt} = \frac{K_1k_2k_5[Pd_T][sub][MeOH][base]}{K_1k_2[sub] + k_{12}[MeOH]([X^-] + K_1)}$	$\frac{d[P]}{dt} = \frac{k_{10}k_{12}[Pd_T][Cu][MeOH][base]}{k_{12}[MeOH][base] + k_{10}[Cu]}$	$\frac{d[P]}{dt} = k_{12}[Pd_T][MeOH][base]$

conditions. In doing so, we observed that the simplified rate laws are fairly similar for all three mechanisms, and are consistent with kinetic data. Specifically, when [Cu] is high, the simplified rate law shows saturation is [substrate]. Likewise, when [substrate] is high, there is saturation in [Cu]. Finally, when both [substrate] and [Cu] are high, the rate law reflects a first order dependence on [Pd_T] and [MeOH].

None of the three proposed mechanisms can be ruled out as they are essentially indistinguishable kinetically, thus the specific role of copper remains ambiguous. We can, however, rule out a mechanism involving rate limiting Pd^0 to Pd^{II} oxidation by copper, as the rate law derived for this mechanism is inconsistent with empirically observed saturation in [Cu].

Given the reactive nature of quinone methides, rate limiting attack by MeOH may seem surprising. However, having palladium coordinated to the quinone methide may mitigate its reactivity. In fact, quinone methide-transition metal complexes have been isolated with osmium,[30,31] tungsten,[32] rhodium, and iridium.[33] Furthermore, the proposal of rate limiting attack of the quinone methide intermediate results in derived rate laws consistent with kinetic measurements. Nevertheless, we sought to further examine the rate limiting step of the reaction through substrate electronic effects.

Investigation of Substrate Electronic Effects

To probe the effect of substrate electronic perturbation on the reaction, a series of substrates with substitution at the 4-postiton were synthesized and evaluated (Figure 3.19). Initial rates were measured under conditions where saturation in [Cu] and [substrate] could be assumed in order to examine the proposed rate limiting step.

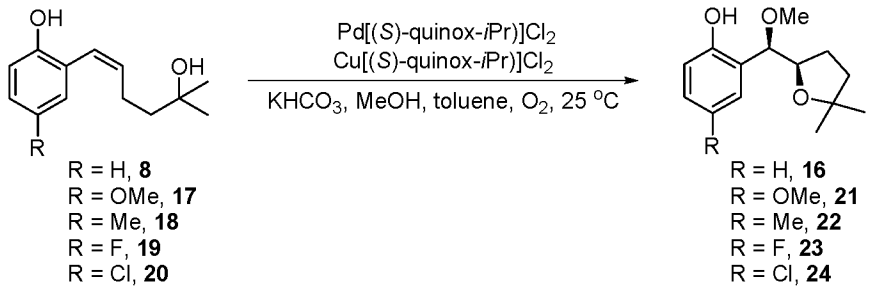

Figure 3.19. Evaluation of substrate electron effects.

Because such a substitution has the potential to influence two reactive sites, either the phenol or the alkene, Hammett plots were constructed using both σ_p and σ_m values (Figure 3.20). Neither plot shows a linear correlation, suggesting electronic perturbation does not occur at just one site.

Considering the Hammett equation (Table 3.2), a Hammett plot should result in a linear relationship only if one position has a much more significant effect than the other (i.e. if $\sigma_m >> \sigma_p$ or $\sigma_p >> \sigma_m$). This is the case when a reactant has only one reactive site on an aromatic ring. However, in this reaction, both *meta* and *para* sites are potentially involved during the reaction. The Jaffé equation simply takes the Hammett equation and divides by one of the sigma values.[34,35] This operation results in an equation which allows for a linear relationship even when two sites are perturbed. Depending on which σ-value is in the denominator, the slope of the resulting plot gives one ρ-value and the y-intercept gives the other ρ-value.

Two plots were constructed with the initial rate data measured in the alkene difunctionalization reaction: $\log(k_X/k_H)/\sigma_m$ *vs.* σ_p/σ_m and $\log(k_X/k_H)/\sigma_p$ *vs.* σ_m/σ_p (Figure 3.21). A linear relationship is observed in both cases. The y-intercept from plot A matches (within error) the slope of plot B. This is crucial as both represent ρ_p. The same is true for ρ_m, thus validating the linear free energy relationship.

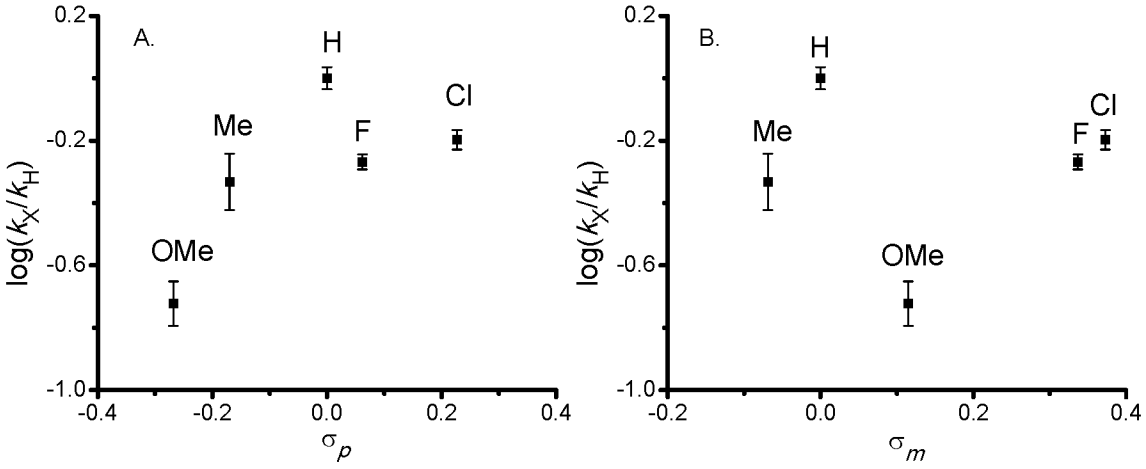

Figure 3.20. Hammett plots for substrate. A. $\log(k_X/k_H)$ vs. σ_p. B. $\log(k_X/k_H)$ vs. σ_m, Conditions: [Pd] = 0.0027 M, [Cu] = 0.0053 M, [$KHCO_3$] = 0.027 M, [substrate] = 0.17 M.

Table 3.2. Hammett and Jaffé equations.

Hammett Equation:	Jaffé Equation:
$\log\left(\frac{k_X}{k_H}\right) = \rho_m\sigma_m + \rho_p\sigma_p$	$\frac{\log\left(\frac{k_X}{k_H}\right)}{\sigma_m} = \frac{\rho_p\sigma_p}{\sigma_m} + \rho_m$ *or* $\frac{\log\left(\frac{k_X}{k_H}\right)}{\sigma_p} = \frac{\rho_m\sigma_m}{\sigma_p} + \rho_p$

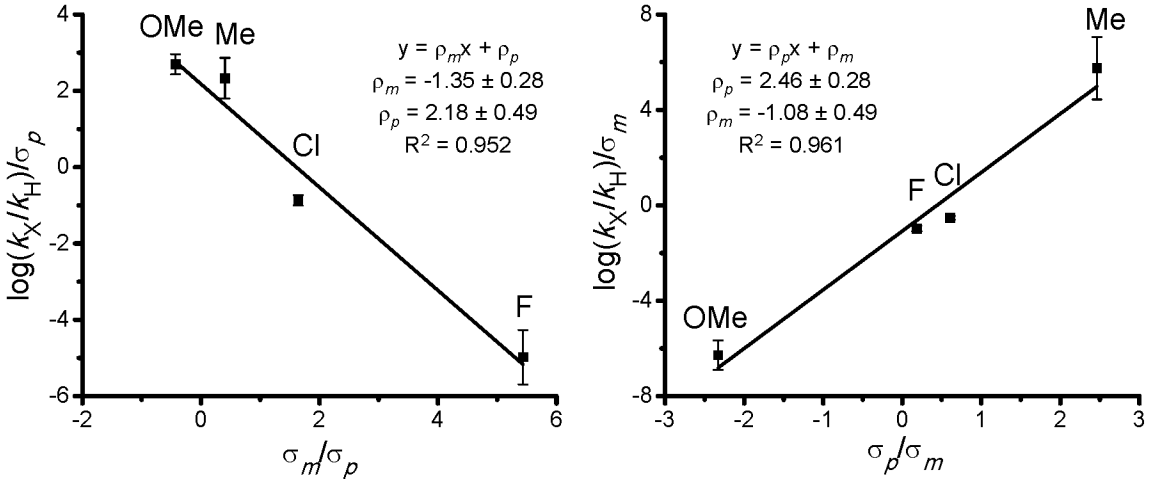

Figure 3.21. Jaffé plots for substrate. A. $\log(k_X/k_H)/\sigma_p$ vs. σ_m/σ_p. B. $\log(k_X/k_H)/\sigma_m$ vs. σ_p/σ_m. Conditions: [Pd] = 0.0027 M, [Cu] = 0.0053 M, [$KHCO_3$] = 0.027 M, [substrate] = 0.17 M.

Evaluation of the Jaffé plots reveals that $\rho_p = +2.3$ and $\rho_m = -1.2$. The resonance structure shown in Figure 3.22, which places a negative charge on the oxygen and a positive charge on the benzylic carbon, is often invoked to explain the reactivity of quinone methides. Such a species has a build up of negative charge *para* to the R-substituent and positive charge *meta* to the R-substituent. If this species is involved in the transition state of the rate limiting step, one would expect electron withdrawing groups to destabilize the positive charge at the at the *meta* positive, leading to a negative ρ_m value. Likewise, electron donating groups *para* to the oxygen would destabilize the negative charge, and result in a positive ρ_p value. Thus the observed Jaffé relationship signifies a substituent effect consistent with rate limiting quinone methide attack.

In comparing the enantiomeric ratio of products from this series of substrates, no electronic effect on enantioselectivity is observed (Table 3.3). Indicating that the electronic nature of the aromatic ring has little impact on the enantiodetermining step, nucleopalladation.

Further Mechanistic Analysis

Buoyed by the mechanistic insight gained from kinetic analysis, we were interested in exploring experiments to gain additional insight into the reaction mechanism, both in terms of the role of copper and the origin of enantioselectivity and diastereoselectivity.

In our stereochemical analysis, the initial nucleopalladation step sets the chiral center β to the aromatic ring and determines the enantiomeric excess of the product. The facial selectivity of this addition is determined by the chiral ligand on palladium (vide

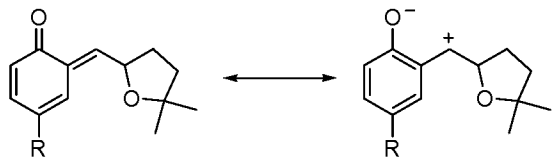

Figure 3.22. Rate limiting attack of quinone methide.

Table 3.3. Lack of effect of substrate electronics on enantioselectivity.

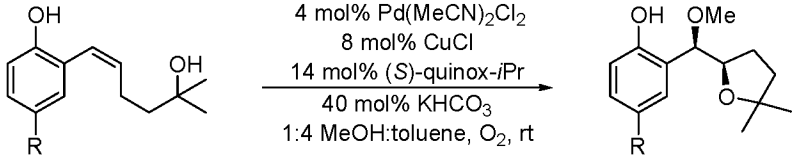

entry	R	ee (%)	er	dr
1	F	97.8	98.9:1.1	2.9:1
2	Cl	93.9	97.0:3.0	4.5:1
3	H	93.2	96.6:3.4	8.1:1
4	Me	93.8	96.9:3.1	6.8:1
5	OMe	93.1	96.5:3.5	9.9:1

infra). On the other hand, the chiral center α to the aromatic ring is set in the diastereoselective addition of MeOH to the quinone methide, and this step is believed to be influenced by the adjacent chiral center at the β-position (Figure 3.23). The ether is assumed to orient away from the quinone methide, as illustrated in the Newman projection, and the nucleophile attacks preferentially over the hydrogen substituent, leading to the observed major diastereomer. However, considering the possible coordination of either palladium or copper at this stage, the ligand on a coordinated metal has the potential to affect the outcome of this addition.

To probe this possibility, we chose to evaluate ligand effects on the diastereoselective outcome of the reaction. In order to perform such analysis, however,

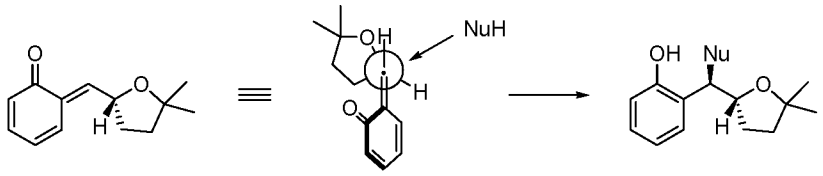

Figure 3.23. Stereochemical model for diastereoselectivity.

we needed to increase our understanding of ligand exchange. Based on the detrimental effect of unligated copper on enantioselectivity in the intermolecular alkene dialkoxylation reaction of **25** (Table 3.4),[24] we hypothesized that the ligand preferentially coordinates to copper, or that the equilibrium of equation 3.1 lies to the right. If there is sufficient ligand, both metals are coordinated.

$$\text{Pd[(}S\text{)-quinox-}i\text{Pr]X}_2 + \text{CuX}_2 \rightleftharpoons \text{PdX}_2 + \text{Cu[(}S\text{)-quinox-}i\text{Pr]X}_2 \qquad \text{(eq. 3.1)}$$

However, if we start with preformed complexes of both metals, how rapid is ligand exchange between the two metals (eq. 3.2)? To answer this question, an experiment was designed wherein the palladium and copper complexes with opposite enantiomers of the ligand are employed in the reaction. A change in diastereoselectivity, either an increase or decrease, would indicate that copper is involved in the rate limiting step and that the ligand on copper influences stereoinduction. A decrease in enantiomeric excess will indicate a loss of catalyst enantiopurity resulting from rapid ligand exchange.

$$\text{Pd[(}R\text{)-quinox-}i\text{Pr]Cl}_2 + \text{Cu[(}S\text{)-quinox-}i\text{Pr]Cl}_2 \rightleftharpoons \text{Pd[(}S\text{)-quinox-}i\text{Pr]Cl}_2 + \text{Cu[(}R\text{)-quinox-}i\text{Pr]Cl}_2 \qquad \text{(eq. 3.2)}$$

The use of Pd[(*R*)-quinox-*i*Pr]Cl_2 and Cu[(*S*)-quinox-*i*Pr]Cl_2 under the standard reaction conditions resulted in complete conversion to nearly racemic product (Figure

Table 3.4. Evidence for ligand exchange between copper and palladium.

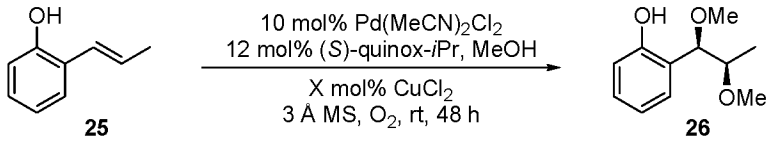

mol% $CuCl_2$	% GC yield	% ee	er
0	67	82	91:9
2.5	80	72	86:14
5	78	59	80:20
10	81	26	63:37
20	88	10	55:45

3.24, 4% ee (*S*,*S*) and 7:1 dr, as compared to 93% ee (*R*,*R*) and 7:1 dr with Pd[(*S*)-quinox-*i*Pr]Cl_2 and Cu[(*S*)-quinox-*i*Pr]Cl_2). This points to rapid ligand exchange on the timescale of this reaction, thus no insight into ligand influence on diastereoselectivity was gained.

It was hypothesized that other ligands may not exchange as rapidly. Copper complexes with 2,2'-bipyridine, phenanthroline, and bathocuproine were prepared and evaluated (Table 3.5). Catalytic systems with Cu(bipyridine)Cl_2 (entry 1) and Cu(phenanthroline)Cl_2 (entry 2) were significantly slower, with only 3% and 7% yields, respectively, at 30 min. compared to complete conversion for the all-(*S*)-quinox-*i*Pr system. Additionally, ligand exchange occurs between copper and palladium, as the enantiomeric excess of the product decreases as the reaction progresses (80% ee at 30

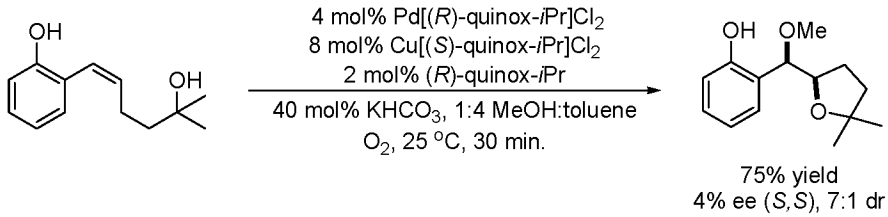

Figure 3.24. Effect of opposite enantiomers of palladium and copper complexes.

Table 3.5. Evaluation of copper complexes with achiral ligands.

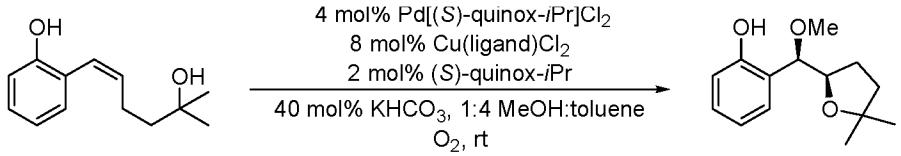

	entry	copper complex	time	% conv.	% yield	% ee	dr
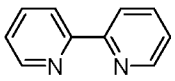 2,2'-bipyridine	1	Cu(2,2'-bipyridine)Cl_2	30 min.	31	3	80	5:1
			2 days	99	55	12	6:1
	2	Cu(phenanthroline)Cl_2	30 min.	30	7	81	7:1
			2 days	98	52	18	6:1
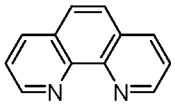 phenanthroline	3	Cu(bathocuproine)Cl_2	5 min.	27	9	91	6:1
			10 min.	53	22	91	6:1
			30 min.	86	49	92	6:1
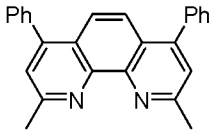 bathocuproine			2 h	100	63	91	7:1
	4	$Pd(MeCN)_2Cl_2$, $CuCl_2$ 14 mol% bathocuproine	30 min.	19	1	--	6:1
			2 h	50	5	--	5:1
			17 h	96	27	--	13:1

min. and 12% ee at completion for Cu(bipyridine)Cl_2, entry 1 and 81% ee at 30 min. and 18% ee at completion for Cu(phenanthroline)Cl_2, entry 2). Interestingly, Cu(bathocuproine)Cl_2 behaves differently (entry 3). The reaction is complete within 2 h, with good yield and only slightly diminished enantiomeric excess (91% ee), and a similar diastereomeric ratio (7:1) as observed with Cu[(*S*)-quinox-*i*Pr]Cl_2 (93% ee and 7:1 dr). In contrast to the systems using Cu(bipyridine)Cl_2 and Cu(phenanthroline)Cl_2, ee is constant over the course of the reaction with Cu(bathocuproine)Cl_2, implying that ligand exchange does not occur. However, another explanation exists: ligand exchange is rapid, and the resulting Pd(bathocuproine)X_2 catalyst is significantly less active than the Pd[(*S*)-quinox-*i*Pr]X_2 catalyst. In exploring this possibility, a control experiment was performed using bathocuproine as the ligand for both metals (entry 4). This reaction is indeed significantly slower, with only 5% yield after 2 h, and 27% yield with near complete

conversion of the substrate. Unfortunately, given the potential for ligand exchange, no evidence was gained to either indicate or rule out copper involvement in the diastereoselective step. Nevertheless, a highly enantioselective system using an achiral ligand on copper was discovered, thus reducing the necessary loading of chiral material by more than half.

Lewis Acids

Both mechanisms A and B invoke copper as a Lewis acid. To probe this possibility, other Lewis acid additives where tested in the reaction (Table 3.6). Of all of the Lewis acids tested, only $FeCl_3$ (entries 3 & 7) and $ZnCl_2$ (entry 5) demonstrated a positive effect on the product yield compared to the reaction without an added Lewis acid (entry 1). Even in these cases, however, the reaction is much slower, with completion occurring after approximately 24 h whereas the reactions employing copper are complete in approximately 30 min. (entries 2 and 6). While this does not rule out the possibility of copper acting as a Lewis acid to activate the quinone methide intermediate for attack, which would explain the positive effect with $ZnCl_2$, it suggests that it is likely serving another purpose as well. This points to Mechanism C, which invokes copper assisted quinone methide formation. Copper is known to catalyze the oxidation of catechol to quinone with molecular oxygen,[28] and a similar process could occur in this reaction. Moreover, the observation that $FeCl_3$ improves product yield, albeit at a significantly slower rate than copper, is in agreement with this analysis, as iron has also been shown to facilitate quinone formation.[36]

Table 3.6. Evaluation of Lewis acid additives.

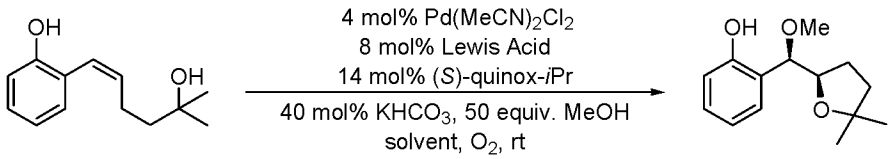

entry	Lewis acid	solvent	time	conv. (%)	yield (%)	ee (%)	er	dr
1	--	1:1 THF:tol	19 h	43	2	nd	nd	nd
2	CuCl	toluene	30 min	97	75	93	97:3	8:1
3	$FeCl_3$	toluene	17 h	99	57	81	90:10	6:1
4	$Ti(OiPr)_3Cl$	toluene	17 h	35	2	92	96:4	2:1
5	$ZnCl_2$	toluene	17 h	29	6	88	94:6	4:1
6	$CuCl_2$	1:1 THF:tol	30 min	100	81	94	97:3	11:1
7	$FeCl_3$	1:1 THF:tol	19 h	62	22	84	92:8	4.5:1
8	$ZnCl_2$	1:1 THF:tol	19 h	77	28	91	95:5	4:1
9	$AlCl_3$	1:1 THF:tol	19 h	42	6	82	91:9	4:1
10	$In(OTf)_3$	1:1 THF:tol	19 h	29	2	89	94:6	2.4:1
11	$LaCl_3$	1:1 THF:tol	19 h	87	3	nd	nd	nd
12	$YbCl_3$	1:1 THF:tol	19 h	67	1	nd	nd	nd
13	$Zn(OTf)_2$	1:1 THF:tol	48 h	68	3	85	93:7	1.7:1
14	$La(OTf)_3$	1:1 THF:tol	48 h	59	2	88	94:6	2.3:1
15	$Yb(OTf)_3$	1:1 THF:tol	48 h	64	2	83	91:9	2.3:1
16	$PtCl_2$	1:1 THF:tol	16 h	38	1	nd	nd	nd
17	$PtCl_2$	toluene	16 h	47	2	nd	nd	nd
18	$AuCl_3$	1:1 THF:tol	16 h	67	5	78	88:12	5:1
19	$AuCl_3$	toluene	16 h	79	11	95	98:2	4:1

On the Origin of Enantioselectivity

A better understanding of the origin of enantioselectivity would be beneficial in the future development of reactions based on aspects of this reaction. As mentioned previously, our stereochemical analysis invokes initial nucleopalladation at the β-position as the enantiodetermining step. Evidence for this hypothesis was provided in an experiment by Dr. Yang Zhang. When a trisubstituted alkene **27** was submitted to the intermolecular alkene dialkoxylation reaction conditions, the product **28** was obtained in

0% ee (Figure 3.25).[24] This is indicative of initial oxypalladation at the β-position. As two of the substituents are at this position are identical, the subsequent quinone methide intermediate is achiral, leading to racemic product. A mechanism involving enantioselective addition at the α-position would be expected to result in enantiomerically enriched product **28**.

When considering the development of a stereochemical model for this reaction, many variables affecting selectivity on nucleopalladation need to be taken into account. Two possible mechanisms for this step are *cis*-nucleopalladation, where both the alkene and the nucleophile are coordinated to palladium, and the alkene inserts into the Pd-Nu bond, and *trans*-nucleopalladation, where the nucleophile attacks the alkene from the face opposite palladium. Unfortunately, because the stereochemical information at the α-position is lost upon quinone methide formation, it is difficult to envision a method to directly elucidate the precise mechanistic nature of this step. Furthermore, because this step is fast, it cannot be probed kinetically. If *trans*-nucleopalladation is operative, there is the potential for the substrate to be bound to palladium in either a monodentate or

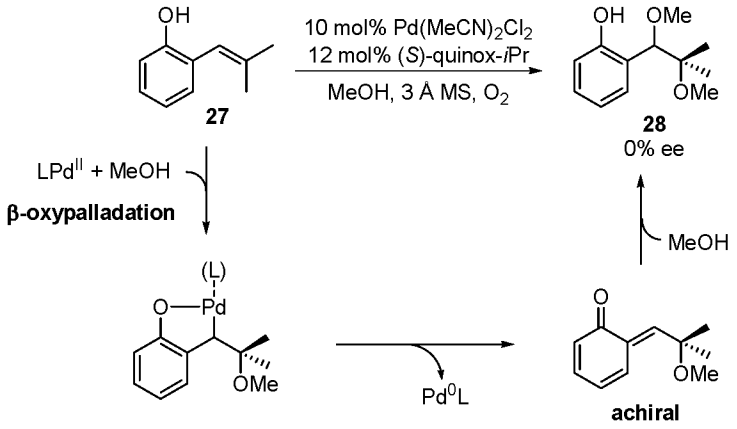

Figure 3.25. Evidence for initial oxypalladation at the β-position.

bidentate mode (through the alkene and the phenoxide). Further complicating analysis, it cannot be determined whether the *E*- or *Z*-isomer of the alkene is the reactive species, since alkene isomerization has been shown to be rapid.[37] Additionally, because the ligand is not C_2-symmetric, the two potential coordination sites are not identical. In light of these issues, we believed that the best way to probe the enantiodetermining nucleopalladation step is through a systematic examination of ligand effects.

Ligand Electronic Effects

Several pyridine oxazoline and quinoline oxazoline ligands were evaluated during the optimization of this reaction (see Chapter 2). It was observed that the reaction using (*S*)-pyrox-*t*Bu is well behaved and gives relatively high enantiomeric excess (80%). While less selective than (*S*)-quinox-*i*Pr, it was presumed that derivatives of (*S*)-pyrox-*t*Bu would be synthetically easier to access. Therefore, a series of 4-substituted pyrox-*t*Bu ligands was chosen for evaluation.

Ligands **29-33** were synthesized in two steps from commercially available picolinic acid derivatives (see experimental section for details), and tested in the Pd-catalyzed alkene difunctionalization reaction under our standard conditions. A subtle ligand electronic effect on enantioselectivity was revealed (Table 3.7). A Hammett plot was constructed by plotting log(er) *vs.* σ, resulting in a LFER with a slope of -0.26 (Figure 3.26). A negative ρ value indicates that more electron rich ligands lead to improved enantioselectivity.

A reasonable explanation to account for this effect was postulated. A palladium alkene intermediate that is more electron rich is less electrophilic, and thus at a lower

Table 3.7. Evaluation of electronic effects of pyridine oxazoline ligands.

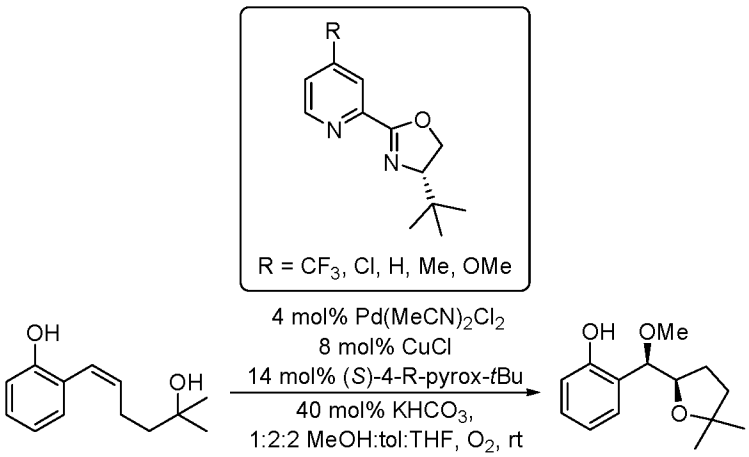

entry	R	time	% conv.	% yield	% ee	er	dr
1	CF_3	3 h	67	46	68.9	84.5:15.5	15:1
2	Cl	3 h	67	39	74.2	87.1:12.9	13:1
3	H	3 h	83	56	82.1	91.0:9.0	14:1
4	Me	3 h	79	49	81.6	90.8:9.2	13:1
5	OMe	3 h	79	49	81.7	90.9:9.1	14:1

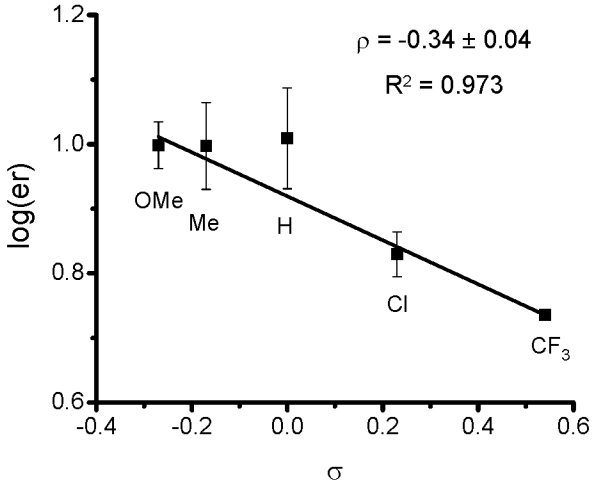

Figure 3.26. Hammett plot relating enantioselectivity to ligand electronics.

energy than the analogous system with an electron poor substituent on the ligand (Figure 3.27). This suggests that the nucleopalladation reaction is less exothermic, and thus by the Hammond postulate, goes through a later transition state. Such a transition state is more product-like, where there should be a greater difference between the activation energies to reach the two enantiomers.[38]

Given the significant number of variables associated with nucleopalladation, several aspects of the mechanism need to be assumed in order to develop a working model to explain enantioselectivity. First we assume that intramolecular nucleopalladation occurs on a Pd-substrate species which is bidentate, coordinated through the alkene and the phenoxide. Given the evidence that nucleophilic attack occurs at the anti-Markovnikov β-position, it seems necessary to invoke a reason for this normally electron-rich site to be the more electrophilic site upon coordination. Substrate binding in a bidentate fashion would require the aromatic ring to rotate out of conjugation with the alkene, and thus inhibit the phenol's ability to donate electron density to the alkene. An experiment by Dr. Mitchell Schultz supports this hypothesis. When a

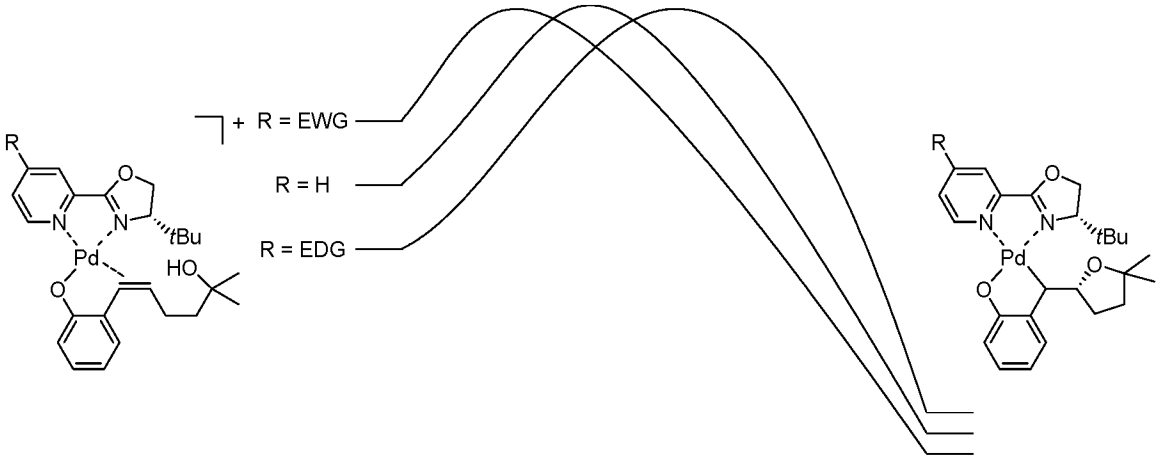

Figure 3.27. Reaction energy diagram.

methyl-protected propenyl phenol **34** is submitted to the intermolecular dialkoxylation reaction conditions, a mixture of regiomeric ketone isomers **35** and **36** is obtained, presumably from the acetal intermediates **A** and **B**, indicating that nucleopalladation is not regioselective (Figure 3.28).[37] Furthermore, the lack of a substrate electronic effect on enantioselectivity (Table 3.3) is consistent with the alkene being out of conjugation with the aromatic ring during nucleopalladation.

Assuming a bidentate substrate-Pd species undergoes nucleopalladation eliminates the *cis*-nucleopalladation pathway because all four coordination sites on palladium are occupied. This leaves eight possible binding geometries to obtain the product (two possible alkene isomers, two possible faces of each alkene, two possible sites for the alkene to coordinate). The second assumption is that, given the bulky nature of the substituent on the oxazoline, the substrate will coordinate in a manner that orients the alkyl chain toward the opposite face of the palladium-plane. This eliminates four of the eight possibilities. Two of the remaining possibilities lead to the minor enantiomer of the product. The last two possibilities are (1) the *E*-isomer bound *trans* to the oxazoline, and (2) the *Z*-isomer bound *trans* to the pyridine. In examination of physical models, the former seems to have slight steric interactions between the alkyl chain and the pyridine portion of the ligand, while the latter seems to orient the chain away from the ligand. Thus the model shown in Figure 3.29 is presented to explain the observed stereoselectivity. While thermodynamically less stable than the *E*-isomer, the *Z*-alkene may be the more reactive species, both in terms of alkene binding and ability to access conformers that lead to product formation. Furthermore, a stereochemical model which

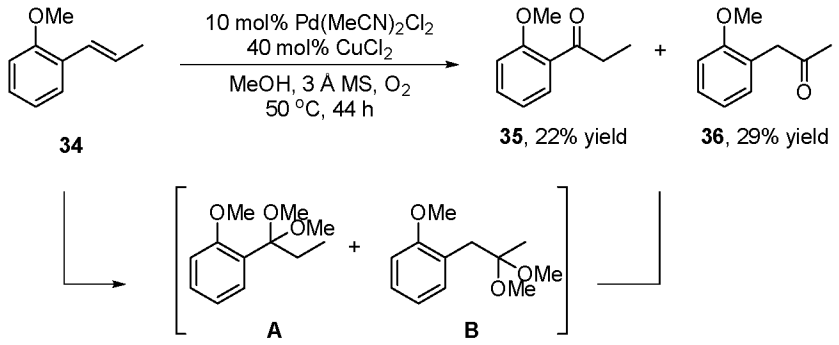

Figure 3.28. Mixture of products obtained with protected phenol.

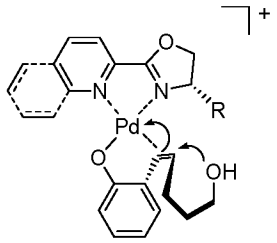

Figure 3.29. Working stereochemical model.

involves coordination of the alkene *trans* to the pyridine is consistent with the observed electronic effect of the ligand on enantioselectivity.

Conclusion

Detailed investigation of a palladium-catalyzed alkene difunctionalization reaction provided insight into the mechanistic details. This includes evidence for a quinone methide intermediate, which may provide an opportunity for new reaction development. Kinetic evidence for rate limiting attack of the quinone methide was uncovered, supported by the observation of a linear free energy relationship correlating substrate electronic nature to the rate of reaction. The Jaffé relationship is used to interpret the complex influence of an aromatic substituent when there are two potential reactive sites on the aromatic ring. Rate limiting quinone methide attack is

unprecedented given the highly reactive nature of quinone methides. This finding may explain the poor mass recovery observed under unoptimized conditions, as a buildup of the quinone methide intermediate could lead to undesired reactivity, such as dimerization and trimerization. While the precise function of copper in this reaction was not elucidated, evidence for copper involvement in more than just catalyst turnover was discovered. The kinetic data and results using other Lewis acids support copper facilitated quinone formation. Ligand exchange between copper and palladium was found to be rapid in most cases, but an enantioselective system was developed which uses an achiral copper complex in conjunction with a chiral palladium complex, thus reducing the loading of chiral material. Finally, understanding of the enantiodetermining nucleopalladation step is advanced by the observation of a linear free energy relationship between ligand electronics and enantioselectivity, where more electron rich ligands are found to lead to higher enantioselectivity.

The insight gained in this study leads the way for new reaction development. The potential to trap the quinone methide intermediate was demonstrated by an inverse electron demand Diels-Alder reaction. Mr. Tejas Pathak is currently investigating the potential scope of this reaction, as well as the use of other types of nucleophiles, such as indole derivatives.[39] Additionally, other methods to enantioselectively form quinone methide intermediates, such as through palladium-catalyzed cross coupling, are being explored. An understanding of the kinetic influence of reaction components should aid in the optimization of conditions for new reactions. Finally, insight into the factors that affect stereoselectivity in asymmetric catalysis is an ongoing goal.

Experimental

General Considerations

Unless otherwise noted, all reactions were performed under a nitrogen atmosphere with stirring. Toluene, CH_2Cl_2, and THF were dried before use by passing through a column of activated alumina. Methanol was distilled from magnesium methoxide. Triethylamine was distilled from CaH_2. All other reagents were purchased from commercial sources and used without further purification. Yields were calculated for material judged homogeneous by thin-layer chromatography and NMR. Thin-layer chromatography was performed with EMD silica gel 60 F254 plates eluting with the solvents indicated, visualized by a 254 nm UV lamp, or stained either with potassium permanganate, or phosphomolybdic acid. Flash column chromatography was performed with EcoChrom MP Silitech 32-63D 60Å silica gel, or with Brockmann I activated basic alumina (pH 9-10), slurry packed with solvents indicated in glass columns. Nuclear magnetic resonance spectra were acquired at 300, 400, or 500 MHz for ^1H, and 75, 100, or 125 MHz for ^{13}C. Chemical shifts for proton nuclear magnetic resonance (^1H NMR) spectra are reported in parts per million downfield relative to the line of $CHCl_3$ singlet at 7.26 ppm. Chemical shifts for carbon nuclear magnetic resonance (^{13}C NMR) spectra are reported in parts per million downfield relative to the center-line of the $CDCl_3$ triplet at 77.23 ppm. The abbreviations s, d, t, dd, td, ddd, q, and m stand for the resonance multiplicities singlet, doublet, triplet, doublet of doublets, triplet of doublets, doublet of doublets of doublets, quartet, and multiplet, respectively. Optical rotations were obtained (Na D line) using a Perkin Elmer Model 343 Polarimeter fitted with a micro cell with a 1 dm path length; concentrations are reported in g/100 mL. IR spectra were recorded using

a Nicolate FTIR instrument. GC (gas chromatography) analysis was performed using a Hewlett Packard HP 6890 Series GC system fitted with a HP-Chiral permethylated β-cyclodextrin column. HRMS (high resolution mass spectrometry) analysis was performed using Waters LCP Premier XE. Glassware for all reactions was oven-dried at 110 °C and cooled in a dry atmosphere prior to use.

Synthesis of Diels-Alder Adduct 10

To a 250 mL side-arm round bottom flask equipped with a stir bar were added 5.2 mg $Pd(MeCN)_2Cl_2$ (0.020 mmol, 0.040 equiv.), 4.0 mg of CuCl (0.040 mmol, 0.080 equiv.), 16.8 mg of (*S*)-quinox-*i*Pr (0.070 mmol, 0.140 equiv.), 20.0 mg of $KHCO_3$ (0.200 mmol, 0.40 equiv.), and 2.2 mL toluene. A three-way joint fitted with a balloon of O_2 was attached, and the flask was evacuated and refilled with O_2 three times. The mixture was stirred for 20 min at rt. To the reaction mixture, 103 mg of **8** (0.500 mmol, 1 equiv.) as a solution in 2.8 mL of ethyl propenyl ether **9** (25 mmol, 50 equiv., *Z*:*E* = 10:1) were added (*Note*: ethyl propenyl ether was purchased as a 3:1 mixture of isomers and enriched through multiple fractional distillations). The reaction flask was evacuated and refilled with O_2 twice more. The reaction mixture was stirred for 24 h and passed through a plug of silica with 50 mL EtOAc and concentrated in vacuo, then purified with flash alumina column chromatography with hexanes followed by 1% EtOAc/hexanes to 2% EtOAc/hexanes as eluent to give 104.1 mg of the product (72% yield). Diastereomeric ratio: 33:5:1, major diastereomer: R_f = 0.60 with 1:4 EtOAc:hexanes, clear oil. $[\alpha]^{20}_D$ = –30.8 (c = 1.73, $CHCl_3$), ^{1}H-NMR (300 MHz, $CDCl_3$) δ = 7.31-7.28 (m, 1 H), 7.13 (ddd, *J* = 7.7 Hz, *J* = 7.7 Hz, *J* = 1.7 Hz, 1 H), 6.87-6.81 (m, 2 H), 5.04 (d, *J* = 2.6 Hz, 1 H), 4.34 (ddd, *J* = 6.8 Hz, *J* = 6.8 Hz, *J* = 4.6 Hz, 1 H), 3.98 (dq, *J* = 9.5 Hz,

J = 7.1 Hz, 1 H), 3.60 (dq, J = 9.5 Hz, J = 7.1 Hz, 1 H), 3.09 (dd, J = 5.0 Hz, J = 5.0 Hz, 1 H), 2.42 (qdd, J = 7.1 Hz, J = 5.5 Hz, J = 2.5 Hz, 1 H), 2.18-2.07 (m, 1 H), 1.71-1.50 (m, 3 H), 1.31 (s, 3 H), 1.23 (t, J = 7.1 Hz, 3 H), 1.20 (s, 3 H), 1.07 (d, J = 7.1 Hz, 3 H). ^{13}C-NMR (75 MHz, $CDCl_3$) δ = 153.2, 129.4, 127.8, 123.1, 120.3, 116.6, 101.6, 79.7, 77.8, 64.6, 43.4, 39.0, 33.8, 30.7, 29.0, 27.3, 15.3, 10.6. IR: 2969, 2879, 1581, 1487, 1454, 1376, 1365, 1222, 1149, 1093, 1040, 978, 932, 752 cm^{-1}. HRMS $C_{18}H_{26}O_3$ $(M+Na)^+$ calcd. 313.1780, obsvd. 313.1775. er = 93.3:6.7, GC analysis: β-cyclodextrin column at 122 °C for 270 min; retention times:246.2 min and 252.3 min.

The relative stereochemistry was assigned by a combination of coupling constants, as compared to reported Diels Alder adducts with ethyl propenyl ether and a related quinone methide,[13] and x-ray crystal structure analysis of the lactone derivative **13** (see Appendix B). Figure 3.30 shows the coupling constants for the major (*R,S,R,R*) and minor (*S,S,R,R*) diastereomers compared to the corresponding Diels-Alder adducts **49-52**. The coupling constants of the major diastereomer are similar to those for **49** and **50**, obtained by Pochini and coworkers when the *Z*-enol ether was used. Likewise, the coupling constants of the minor diastereomer are similar to those for **51** and **52**, obtained when the *E*-enol ether was used.

Synthesis of Diels-Alder Adduct 12

To a 250 mL side-arm round bottom flask equipped with a stir bar were added 5.2 mg $Pd(MeCN)_2Cl_2$ (0.020 mmol, 0.040 equiv.), 4.0 mg of CuCl (0.040 mmol, 0.080 equiv.), 16.8 mg of (*S*)-^{i}PrQuinox (0.070 mmol, 0.140 equiv.), 20.0 mg of $KHCO_3$ (0.200 mmol, 0.40 equiv.), and 2.2 mL toluene. A three-way joint fitted with a balloon of O_2

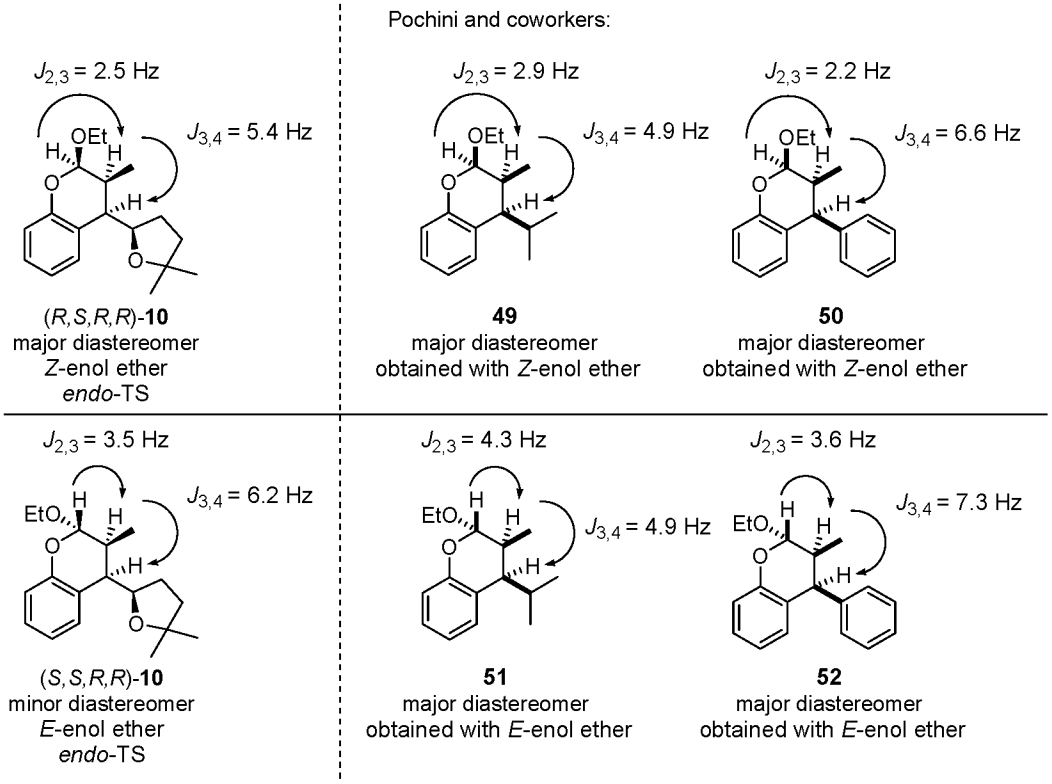

Figure 3.30. Comparison of coupling constants of **10** to known compounds **49-52** characterized by Pochini and coworkers.

was attached, and the flask was evacuated and refilled with O_2 three times. The mixture was stirred for 20 min at rt under an atmosphere of O_2. To the reaction mixture, 89.1 mg of **11** (0.500 mmol, 1 equiv.) as a solution in 2.8 mL of ethyl propenyl ether **9** (25 mmol, 50 equiv., *Z*:*E* = 10:1) were added. The reaction flask was evacuated and refilled with O_2 twice more. The reaction mixture was stirred for 24 h and passed through a plug of silica with 50 mL EtOAc and concentrated in vacuo, then purified with flash alumina column chromatography with 1% EtOAc/hexanes to 2% EtOAc/hexanes as eluent to give 88.2 mg of the product (67% yield). Diastereomeric ratio: 33:8:1, major diastereomer: R_f = 0.70 with 1:3 EtOAc:hexanes, clear oil. $[\alpha]^{20}_D$ = –36.1 (c = 0.58, $CHCl_3$), ^{1}H-NMR (300 MHz, $CDCl_3$) δ = 7.26-7.22 (m, 1 H), 7.13 (ddd, *J* = 7.7 Hz, *J* = 7.7 Hz, *J* = 1.7 Hz, 1 H),

6.88-6.81 (m, 2 H), 5.07 (d, J = 2.5 Hz, 1 H), 4.22 (ddd, J = 7.1 Hz, J = 7.1 Hz, J = 5.5 Hz, 1 H), 3.98 (dq, J = 9.6 Hz, J = 7.1 Hz, 1 H), 3.90 (ddd, J = 7.3 Hz, J = 5.3 Hz, J = 5.3 Hz, 1 H), 3.65 (dd, J = 7.3 Hz, J = 7.1 Hz, 1 H), 3.61 (dq, J = 9.6 Hz, J = 7.1 Hz, 1 H), 3.15 (dd, J = 5.3 Hz, J = 5.3 Hz, 1 H), 2.43 (qdd, J = 7.0 Hz, J = 5.5 Hz, J = 2.5 Hz, 1 H), 2.13-2.03 (m, 1 H), 1.94-1.71 (m, 2 H), 1.65-1.53 (m, 1 H), 1.24 (t, J = 7.1 Hz, 3 H), 1.06 (d, J = 7.0 Hz, 3 H). ^{13}C-NMR (75 MHz, $CDCl_3$) δ = 153.3, 129.1, 127.9, 122.7, 120.5, 116.7, 101.7, 79.1, 67.4, 64.7, 43.4, 33.7, 30.4, 26.7, 15.3, 10.1. IR: 2977, 2875, 1581, 1487, 1454, 1375, 1352, 1237, 1222, 1159, 1064, 1041, 981, 931, 754 cm^{-1}. HRMS $C_{16}H_{22}O_3$ $(M+Na)^+$ calcd. 285.1467, obsvd. 285.1472. er = 95.9:4.1, GC analysis: β-cyclodextrin column at 122 °C for 330 min; retention times:276.5 min and 286.6 min.

Synthesis of Lactone 13[18]

The Jones Reagent was prepared by addition of 2.5 mL of conc. H_2SO_4 to 2.5 g of CrO_3. The solution was cooled to 0 °C and 7.5 mL of cold H_2O were added slowly with rapid stirring. In a 100 mL round bottom flask, 132 mg of **10** were dissolved in 5 mL of acetone under an atmosphere of nitrogen. The reaction flask was cooled to 0 °C and 800 μL of Jones Reagent (2.0 mmol, 4.0 equiv.) were added dropwise. The reaction mixture was slowly warmed to rt and stirred for 3 h. The reaction was quenched by the dropwise addition of *iso*-propanol until the reaction mixture turned from orange to green. Approximately 10 mL of brine were added, and the mixture was extracted with EtOAc (3 x 10 mL). The combined organic phase was washed with brine, dried over Na_2SO_4, filtered, and concentrated in vacuo, then purified by flash silica-gel column chromatography with 4% EtOAc/hexanes to 10% EtOAc/hexanes as eluent to give 69 mg of product (53% yield). R_f = 0.40 with 1:4 EtOAc:hexanes, colorless solid, mp = 79-86

°C. $[\alpha]^{20}_D$ = +43.5 (c = 0.45, $CHCl_3$), ^{1}H-NMR (300 MHz, $CDCl_3$) δ = 7.30-7.24 (m, 2 H), 7.08 (ddd, *J* = 7.5 Hz, *J* = 7.5 Hz, *J* = 1.3 Hz, 1 H), 7.04 (dd, *J* = 8.4 Hz, *J* = 1.5 Hz, 1 H), 4.22 (ddd, *J* = 9.4 Hz, *J* = 5.5 Hz, *J* = 4.9 Hz, 1 H), 3.27 (dd, *J* = 6.4 Hz, *J* = 5.0 Hz, 1 H), 3.04 (dq, *J* = 6.9 Hz, *J* = 6.9 Hz, 1 H), 1.80-1.71 (m, 1 H), 1.68-1.59 (m, 1 H), 1.49 (dd, *J* = 7.8 Hz, *J* = 3.0 Hz, 1 H), 1.41 (d, *J* = 7.0 Hz, 3 H), 1.44-1.34 (m, 1 H), 1.22 (s, 3 H), 0.89 (s, 3 H). ^{13}C-NMR (75 MHz, $CDCl_3$) δ = 171.9, 152.0, 130.9, 128.8, 124.1, 123.9, 116.6, 80.6, 77.4, 44.4, 38.7, 37.1, 28.7, 28.6, 27.8, 12.8. IR; 2968, 2871, 1767, 1487, 1457, 1379, 1215, 1142, 1083, 1056, 757 cm^{-1}. HRMS $C_{16}H_{20}O_3$ $(M+Na)^+$ calcd. 283.1310, obsvd. 283.1315. X-ray quality single crystals were obtained by recrystallization from cold pentane.

Preparation of Pd[(*S*)-quinox-*i*Pr]Cl_2

To an oven dried 100 mL round bottom flask were weighed 270 mg of $Pd(MeCN)_2Cl_2$ (1.04 mmol, 1 equiv.) and 255 mg (*S*)-quinox-*i*Pr (1.06 mmol, 1.02 equiv.) and the flask was purged with N_2. The solids were dissolved in CH_2Cl_2 (50 mL) and stirred overnight at rt. The solvent was removed in vacuo and the residue was dissolved in a minimum amount of CH_2Cl_2 and precipitated with Et_2O. The solids were recovered by filtration, washed with copious amounts of Et_2O, and dried under high vacuum overnight to provide 410 mg of a red-brown powder (95% yield). See Chapter 2 experimental for spectral data.

Preparation of Cu[(*S*)-quinox-*i*Pr]Cl_2

To an oven dried 100 mL round bottom flask were weighed 170 mg $CuCl_2$ (1.26 mmol, 1 equiv.) and 310 mg (*S*)-quinox-*i*Pr (1.29 mmol, 1.02 equiv.) and the flask was purged with N_2. The solids were dissolved in MeOH (50 mL) and stirred overnight at rt.

The solvent was removed in vacuo and the residue was dissolved in a minimum amount of MeOH and precipitated with Et_2O. The solids were recovered by filtration, washed with copious amounts of Et_2O, and dried under high vacuum overnight to provide 450 mg of a pale brown powder (95% yield). See Chapter 2 experimental for spectral data.

Standard Kinetic Protocol

All reactions were analyzed in situ using an instrument designed to measure O_2-uptake over the course of the reaction. At each concentration of MeOH and substrate a background curve was acquired and subtracted from corresponding curves obtained from catalytic reactions. The O_2-uptake was recorded on an instrument fitted with a pressure transducer; the pressure changes were recorded in torr and mmol O_2 and exported to an Excel™ spreadsheet. The instrumental set-up was similar to one previously reported[26] and was capable of monitoring six individual reactions simultaneously. Initial rates were measured up to 5-10% conversion based on O_2 consumption and fit using a linear regression (slope = k_{obs}) reported in μmol O_2/s. After the reaction was complete the tube was sampled for supplementary analysis by GC and/or chiral GC to confirm product formation. Note that standard solutions of the metal catalysts could not be prepared at the desired concentrations due to low solubility, thus Pd[(*S*)-quinox-*i*Pr]Cl_2 and Cu[(*S*)-quinox-*i*Pr]Cl_2 complexes were used for all kinetic experiments for greater accuracy in weighing.

Each experiment was conducted in a similar manner following the example procedure: to each oven dried glass 25.4 mm O.D. pressure tube were weighed Pd[(*S*)-quinox-*i*Pr]Cl_2 (1.6 mg, 0.0040 mmol), Cu[(*S*)-quinox-*i*Pr]Cl_2 (3.0 mg, 0.0080 mmol), and $KHCO_3$ (4.0 mg, 0.040 mmol), followed by the addition of a stir bar and 1.25 mL of

a freshly prepared solution of 4:1 toluene:MeOH. Each tube was then attached to the O_2-uptake instrument and evacuated by a Welch Vacuum pump (VWR 55009-288) to 2-3 torr and refilled with O_2 to 850 torr: this evacuation/refill procedure was repeated four times. The tubes were immersed in an oil bath at 25 °C and stirred at 700 rpm. The reactions were allowed to equilibrate for 30 min by monitoring the internal pressure of each tube. Substrate (165 mg, 0.800 mmol) and tetradecane (30 mg, 0.15 mmol), which was added as an internal standard, were weighed into a 2 mL volumetric flask and filled to the mark with 4:1 toluene:MeOH. The substrate solution (250 μL) was added via syringe to each tube after the pressure stabilized. O_2-uptake curves were generated by sampling the internal pressure at a rate of one point/s; each point was an average of 1000 pressure measurements, taken over 30 min to 3 h, depending on the conditions.

[Palladium] Dependence

Dependence on [palladium] was determined following the example procedure above, with the following modifications: 0.4 mg to 4.0 mg of Pd[(*S*)-quinox-*i*Pr]Cl_2 (0.001 mmol to 0.0010 mmol) were used. For determination of [Pd] dependence at high [substrate] and low [Cu] (Figure 3.13 A), 1.0 mg Cu[(*S*)-quinox-*i*Pr]Cl_2, (0.0027 mmol) were used. A 0.960 M standard solution of substrate was prepared by adding 396 mg substrate (1.92 mmol) and 80 mg tetradecane (0.40 mmol) to a 2 mL volumetric flask and adding 4:1 toluene:MeOH to the mark. A 250 μL portion of this solution was added to each tube via syringe for a final reaction volume of 1.5 mL. Data for [Palladium] dependence are tabulated in Table 3.8.

Table 3.8. Initial rate data for [Pd] dependence.
Data for Figure 3.13 A.

[Pd[(*S*)-quinox-*i*Pr]Cl_2], M	initial rate (μmol O_2/s)
0.0008	0.016
0.0013	0.022
0.0026	0.036
0.0043	0.053
0.0067	0.087

[Substrate] Dependence

Dependence on [substrate] was determined following the example procedure above, with the following modifications: for determination of [substrate] dependence at high [Cu] (Figure 3.13 B) 3.0 mg Cu[(*S*)-quinox-*i*Pr]Cl_2 (0.0080 mmol) were used; for determination of [substrate] dependence at low [Cu] (Figure 3.13 C), 1.0 mg Cu[(*S*)-quinox-*i*Pr]Cl_2, (0.0027 mmol) were used. To each of the reaction tubes, 1.25 mL to 1.48 mL of 4:1 toluene:MeOH were initially added, such that the final volume, upon addition of the standard solution of substrate, would be 1.5 mL. Two different standard solutions of substrate were used, depending on the initial [substrate] for a given reaction: a 0.400 M solution was prepared by adding 165 mg substrate (0.800 mmol) and 30 mg tetradecane (0.15 mmol) to a 2 mL volumetric flask and adding 4:1 toluene:MeOH to the mark; a 0.960 M solution was prepared by adding 396 mg substrate (1.92 mmol) and 80 mg tetradecane (0.40 mmol) to a 2 mL volumetric flask and adding 4:1 toluene:MeOH to the mark. A portion (250 μL to 25 μL) of one of these solutions was added to each tube via syringe for a final reaction volume of 1.5 mL. Data for [substrate] dependence are tabulated in Tables 3.9 and 3.10.

Table 3.9. Initial rate data for [substrate] dependence at high [Cu]. Data for Figure 3.13 B.

[substrate], M	initial rate (μmol O_2/s)
0	0
0.0067	0.0043
0.014	0.017
0.032	0.025
0.067	0.049
0.093	0.055
0.13	0.058
0.16	0.066
0.21	0.069

Table 3.10. Initial rate data for [substrate] dependence at low [Cu]. Data for Figure 3.13 C.

[substrate], M	initial rate (μmol O_2/s)
0	0
0.0067	0.012
0.013	0.017
0.027	0.018
0.033	0.025
0.046	0.036
0.067	0.031
0.080	0.040
0.11	0.039
0.13	0.049
0.16	0.036

[Copper] Dependence

Dependence on [copper] was determined following the example procedure above, with the following modifications: 0.3 mg to 6.0 mg Cu[(*S*)-quinox-*i*Pr]Cl_2 (0.0008-0.016 mmol) were used. A 1.25 mL portion of 4:1 toluene:MeOH was initially added to the reaction tubes. Two different standard solutions of substrate were used: for determination of [Cu] dependence at low [substrate], a 0.400 M solution was prepared by adding 165 mg substrate (0.800 mmol) and 30 mg tetradecane (0.15 mmol) to a 2 mL volumetric flask and adding 4:1 toluene:MeOH to the mark; for determination of [Cu] at high [substrate], a 0.960 M solution was prepared by adding 396 mg substrate (1.92 mmol) and 80 mg tetradecane (0.40 mmol) to a 2 mL volumetric flask and adding 4:1 toluene:MeOH to the mark. A 250 μL portion of one of these solutions was added to each tube via syringe for a final reaction volume of 1.5 mL. Data for [copper] dependence are tabulated in Table 3.11 and 3.12.

Table 3.11. Initial rate data for [Cu] dependence at high [substrate]. Data for Figure 3.13 D.

[Cu[(*S*)-quinox-*i*Pr]Cl_2], M	initial rate (μmol O_2/s)
0.0005	0.018
0.0018	0.036
0.0036	0.062
0.0055	0.066
0.0082	0.069
0.0097	0.063
0.011	0.055

Table 3.12. Initial rate data for [Cu] dependence at low [substrate]. Data for Figure 3.13 E.

[Cu[(*S*)-quinox-*i*Pr]Cl_2], M	initial rate (μmol O_2/s)
0.0005	0.0051
0.0012	0.015
0.0018	0.018
0.0028	0.023
0.0053	0.030
0.0080	0.031
0.0097	0.034
0.011	0.029

Dependence on O_2 Partial Pressure

Dependence on O_2 partial pressure was determined following the example procedure above, with the following modifications: reactions were performed under mixed O_2 and N_2 atmospheres, created by purging the gas reservoir of the O_2-uptake instrument for 10 min with either N_2 or O_2 then refilled such that the desired atmospheric composition would be obtained (20–100% O_2). For each reaction, 1.6 mg Pd[(*S*)-quinox-*i*Pr]Cl_2 (0.0040 mmol), 1.0 mg Cu[(*S*)-quinox-*i*Pr]Cl_2 (0.0027 mmol), and 4.0 mg $KHCO_3$ (0.040 mol), and 250 μL of a 0.96 M solution of substrate were used. Data for O_2 partial pressure dependence are tabulated in Table 3.13.

Table 3.13. Initial rate data for O_2 partial pressure. Data for Figure 3.14.

partial pressure O_2	percent O_2	initial rate (μmol O_2/s)	error
850	100	0.039	0.0047
750	90	0.024	0.0060
650	85	0.020	
675	80	0.025	
420	50	0.029	0.0012
320	40	0.028	0.0028
180	20	0.020	0.0047

Stir Rate Dependence

The effect of stir rate was examined following the example procedure above, with the following modifications: the stir rate was controlled by a digital stir plate set at the specified rate. At high [Cu] (Figure 3.30), 3.0 mg Cu[(*S*)-quinox-*i*Pr]Cl_2 (0.0080 mmol) were used and the system was filled with O_2 to 1550 torr, and 250 μL of a 0.960 M solution of substrate (0.240 mmol) were added to each reaction. At low [Cu] (Figure 3.31), 1.0 mg Cu[(*S*)-quinox-*i*Pr]Cl_2 (0.0027 mmol) were used and the system was filled with O_2 to 850 torr, and 250 μL of a 0.960 M solution of substrate (0.240 mmol) were added to each reaction. Data for stir rate dependence are tabulated in Tables 3.14 and 3.15 and illustrated in Figures 3.31 and 3.32.

Table 3.14. Initial rate data for stir rate dependence at 1500 torr. Data for Figure 3.31.

stir rate, rpm	initial rate (μmol O_2/s)
300	0.055
500	0.051
600	0.067
700	0.063
850	0.077
1000	0.086

Table 3.15. Initial rate data for stir rate dependence at 850 torr. Data for Figure 3.32.

stir rate, rpm	initial rate (μmol O_2/s)
300	0.025
500	0.025
600	0.021
700	0.027
850	0.021

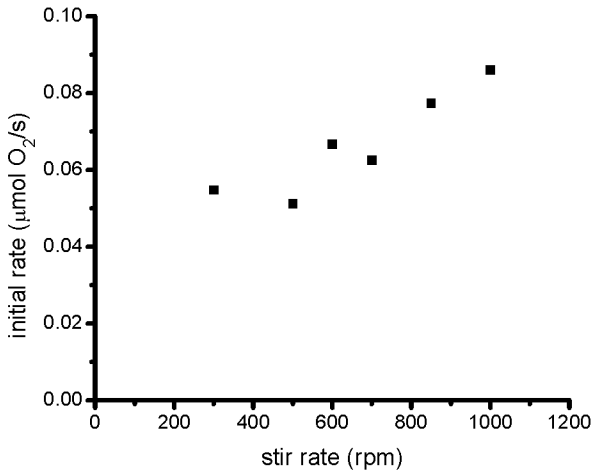

Figure 3.31. Stir rate dependence. Conditions: 1500 torr, [substrate] = 0.16 M, [Pd] = 0.0025 M, [Cu] = 0.0055 M, [$KHCO_3$] = 0.025 M.

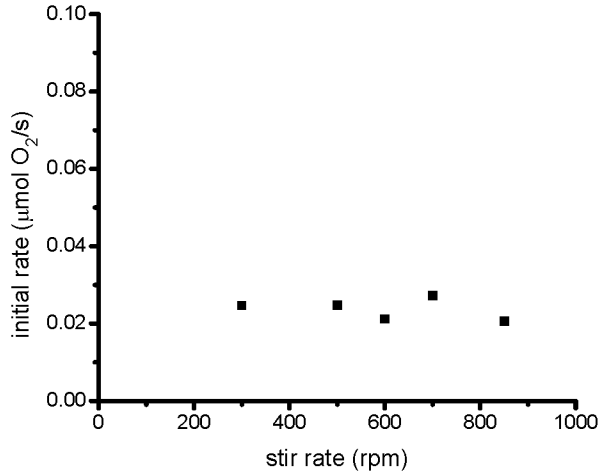

Figure 3.32. Stir rate dependence. Conditions: 850 torr, [substrate] = 0.16 M, [Pd] = 0.0025 M, [Cu] = 0.0016 M, [$KHCO_3$] = 0.025 M.

[$KHCO_3$] Dependence

Dependence on [$KHCO_3$] was determined following the example procedure above, with the following modifications: 0 mg to 12.0 mg $KHCO_3$ (0-0.120 mmol) and 1.0 mg Cu[(*S*)-quinox-*i*Pr]Cl_2 (0.0027 mmol) were used, and 250 μL of a 0.960 M solution of substrate (0.240 mmol) were added to each reaction. Data for [$KHCO_3$] dependence are tabulated in Table 3.16.

[MeOH] Dependence

Dependence on [MeOH] was determined following the example procedure above, with the following modifications: 1.5 mg $KHCO_3$ (0.015 mmol) and 1.0 mg Cu[(*S*)-quinox-*i*Pr]Cl_2 (0.0027 mmol) were used. To each tube were added one of several different freshly prepared solutions of toluene:MeOH (1.25 mL, 0% to 40% MeOH), and 250 μL of a 0.960 M solution of substrate (0.240 mmol) in 4:1 toluene:MeOH were added to each reaction. Data for [MeOH] dependence are tabulated in Table 3.17.

Rate Law Derivation

The rate laws for mechanisms A, B, and C were derived using the King-Altman method. Mechanism A along with the corresponding open forms and the rate law derivation is depicted in Figure 3.33.[29] A simplified depiction of mechanism B along with the open forms and the rate law derivation is depicted in Figure 3.34. A simplified depiction of mechanism C along with the open forms and the rate law derivation is depicted in Figure 3.35.

Table 3.16. Initial rate and yield data for [$KHCO_3$] dependence. Data for Figure 3.15

[$KHCO_3$], M	initial rate (μmol O_2/s)	GC yield (%)
0	0.011	14
0.0013	0.019	
0.0033	0.029	64
0.0067	0.035	65
0.010	0.037	
0.011	0.038	69
0.013	0.045	67
0.017	0.038	58
0.020	0.039	
0.027	0.036	27
0.034	0.024	28
0.041	0.019	17
0.054	0.009	7

Table 3.17. Initial rate data for [MeOH] dependence. Data for Figure 3.16.

[MeOH], M	initial rate (μmol O_2/s)	er
0.82	0.011	24
1.17	0.013	23
1.51	0.021	22
2.88	0.021	19
4.94	0.037	17
7.00	0.048	13
9.06	0.056	12

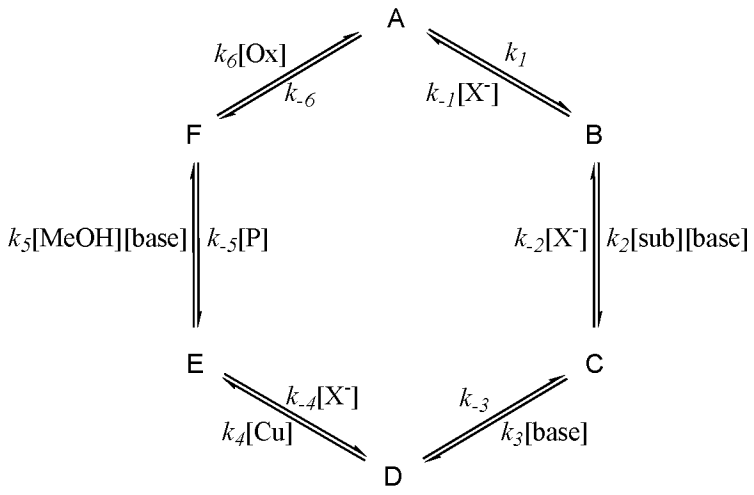

Open forms:

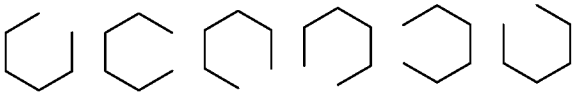

Assume $k_{-3} = k_{-5} = k_{-6} = 0$ i.e. assume that steps 3, 5, and 6 are irreversible

[A] = $k_2k_3k_4k_5k_6$[sub][Cu][MeOH][Ox][base]^3 + $k_{-1}k_3k_4k_5k_6$[Cu][MeOH][X$^-$][Ox][base]^2 + $k_{-1}k_{-2}k_4k_5k_6$[Cu][MeOH][X$^-$]^2[base][Ox]

[B] = $k_1k_3k_4k_5k_6$[Cu][MeOH][Ox][base]^2 + $k_1k_{-2}k_4k_5k_6$[Cu][MeOH][X$^-$][Ox][base]

[C] = $k_1k_2k_4k_5k_6$[sub][Cu][MeOH][Ox][base]^2

[D] = $k_1k_2k_3k_5k_6$[sub][MeOH][Ox][base]^3 + $k_1k_2k_3k_{-4}k_6$[sub][X$^-$][Ox][base]^2

[E] = $k_1k_2k_3k_4k_6$[sub][Cu][Ox][base]^2

[F] = $k_1k_2k_3k_4k_5$[sub][Cu][MeOH][base]^3

Figure 3.33. Rate law derivation for mechanism A.

The total concentration of palladium is equal to sum of each palladium intermediate.

$$[Pd_T] = [\mathbf{A}] + [\mathbf{B}] + [\mathbf{C}] + [\mathbf{D}] + [\mathbf{E}] + [\mathbf{F}]$$

$$\frac{[Pd_T]}{[\mathbf{A}] + [\mathbf{B}] + [\mathbf{C}] + [\mathbf{D}] + [\mathbf{E}] + [\mathbf{F}]} = 1$$

Assuming step 5 is rate limiting

$$\frac{d[P]}{dt} = k_5[\mathbf{E}][MeOH][base] = \frac{k_5[\mathbf{E}][MeOH][base][Pd_T]}{[\mathbf{A}] + [\mathbf{B}] + [\mathbf{C}] + [\mathbf{D}] + [\mathbf{E}] + [\mathbf{F}]}$$

$$\frac{d[P]}{dt} = \frac{k_1k_2k_3k_4k_5k_6[Pd_T][sub][Cu][MeOH][Ox][base]^3}{\left(\begin{array}{c} k_2k_3k_4k_5k_6[sub][Cu][MeOH][Ox][base]^3 + k_{-1}k_3k_4k_5k_6[Cu][MeOH][[X^-][Ox][base]^2 + \\ k_{-1}k_{-2}k_4k_5k_6[Cu][MeOH][[X^-]^2[base][Ox] + k_1k_3k_4k_5k_6[Cu][MeOH][Ox][base]^2 + \\ k_1k_{-2}k_4k_5k_6[Cu][MeOH][[X^-][Ox][base] + k_1k_2k_4k_5k_6[sub][Cu][MeOH][Ox][base]^2 + \\ k_1k_2k_3k_5k_6[sub][MeOH][Ox][base]^3 + k_1k_2k_3k_{-4}k_6[sub][X^-][Ox][base]^2 + \\ k_1k_2k_3k_4k_6[sub][Cu][Ox][base]^2 + k_1k_2k_3k_4k_5[sub][Cu][MeOH][base]^3 \end{array}\right)}$$

$$\frac{d[P]}{dt} = \frac{k_1k_2k_3k_4k_5k_6[Pd_T][sub][Cu][MeOH][Ox][base]^2}{\left(\begin{array}{c} k_2k_3k_4k_5k_6[sub][Cu][MeOH][Ox][base]^2 + k_{-1}k_3k_4k_5k_6[Cu][MeOH][[X^-][Ox][base] + \\ k_{-1}k_{-2}k_4k_5k_6[Cu][MeOH][[X^-]^2[Ox] + k_1k_3k_4k_5k_6[Cu][MeOH][Ox][base] + \\ k_1k_{-2}k_4k_5k_6[Cu][MeOH][[X^-][Ox] + k_1k_2k_4k_5k_6[sub][Cu][MeOH][Ox][base] + \\ k_1k_2k_3k_5k_6[sub][MeOH][Ox][base]^2 + k_1k_2k_3k_{-4}k_6[sub][X^-][Ox][base] + \\ k_1k_2k_3k_4k_6[sub][Cu][Ox][base] + k_1k_2k_3k_4k_5[sub][Cu][MeOH][base]^2 \end{array}\right)}$$

assume $[Pd_T]$ - [**F**] >> [**F**] or that k_6 is fast

$$\left(\begin{array}{c} k_2k_3k_4k_5k_6[sub][Cu][MeOH][Ox][base]^2 + \\ k_{-1}k_3k_4k_5k_6[Cu][MeOH][X^-][Ox][base] + \\ k_{-1}k_{-2}k_4k_5k_6[Cu][MeOH][X^-]^2[Ox] + \\ k_1k_3k_4k_5k_6[Cu][MeOH][Ox][base] + \\ k_1k_{-2}k_4k_5k_6[Cu][MeOH][[X^-][Ox] + \\ k_1k_2k_4k_5k_6[sub][Cu][MeOH][Ox][base] + \\ k_1k_2k_3k_5k_6[sub][MeOH][Ox][base]^2 + \\ k_1k_2k_3k_{-4}k_6[sub][X^-][Ox][base] + \\ k_1k_2k_3k_4k_6[sub][Cu][Ox][base] \end{array}\right) >> k_1k_2k_3k_4k_5[sub][Cu][MeOH][base]^2$$

$$\frac{d[P]}{dt} = \frac{k_1k_2k_3k_4k_5[Pd_T][sub][Cu][MeOH][base]^2}{\left(\begin{array}{c} k_2k_3k_4k_5[sub][Cu][MeOH][base]^2 + k_{-1}k_3k_4k_5[Cu][MeOH][[X^-][base] + \\ k_{-1}k_{-2}k_4k_5[Cu][MeOH][X^-]^2 + k_1k_3k_4k_5[Cu][MeOH][base] + \\ k_1k_{-2}k_4k_5[Cu][MeOH][[X^-] + k_1k_2k_4k_5[sub][Cu][MeOH][base] + \\ k_1k_2k_3k_5[sub][MeOH][base]^2 + k_1k_2k_3k_{-4}[sub][X^-][base] + k_1k_2k_3k_4[sub][Cu][base] \end{array}\right)}$$

Figure 3.33 (continued).

assume $k_3 >> k_5$

$$k_3[\text{base}]\begin{pmatrix} k_2k_4k_5[\text{sub}][\text{Cu}][\text{MeOH}][\text{base}] + \\ k_{-1}k_4k_5[\text{Cu}][\text{MeOH}][\text{X}^-] + \\ k_1k_4k_5[\text{Cu}][\text{MeOH}] \\ +k_1k_2k_5[\text{sub}][\text{MeOH}][\text{base}] + \\ k_1k_2k_{-4}[\text{sub}][\text{X}^-] + k_1k_2k_4[\text{sub}][\text{Cu}] \end{pmatrix} >> \begin{pmatrix} k_{-1}k_{-2}k_4k_5[\text{Cu}][\text{MeOH}][\text{X}^-]^2 + \\ k_1k_{-2}k_4k_5[\text{Cu}][\text{MeOH}][[\text{X}^-] + \\ k_1k_2k_4k_5[\text{sub}][\text{Cu}][\text{MeOH}][\text{base}] \end{pmatrix}$$

$$\frac{\text{d[P]}}{\text{dt}} = \frac{k_1k_2k_4k_5[\text{Pd}_\text{T}][\text{sub}][\text{Cu}][\text{MeOH}][\text{base}]}{\begin{pmatrix} k_2k_4k_5[\text{sub}][\text{Cu}][\text{MeOH}][\text{base}] + k_{-1}k_4k_5[\text{Cu}][\text{MeOH}][\text{X}^-] + \\ k_1k_4k_5[\text{Cu}][\text{MeOH}] + k_1k_2k_5[\text{sub}][\text{MeOH}][\text{base}] + \\ k_1k_2k_{-4}[\text{sub}][\text{X}^-] + k_1k_2k_4[\text{sub}][\text{Cu}] \end{pmatrix}}$$

When [Cu] is high

$$k_2k_4[\text{sub}][\text{Cu}]\left(k_5[\text{MeOH}][\text{base}] + k_1\right) + k_4k_5[\text{Cu}][\text{MeOH}]\left(k_{-1}[\text{X}^-] + k_1\right) >> k_1k_2[\text{sub}]\left(k_5[\text{MeOH}][\text{base}] + k_{-4}[\text{X}^-]\right)$$

$$\frac{\text{d[P]}}{\text{dt}} = \frac{k_1k_2k_4k_5[\text{Pd}_\text{T}][\text{sub}][\text{Cu}][\text{MeOH}][\text{base}]}{k_2k_4[\text{sub}][\text{Cu}]\left(k_5[\text{MeOH}][\text{base}] + k_1\right) + k_4k_5[\text{Cu}][\text{MeOH}]\left(k_{-1}[\text{X}^-] + k_1\right)}$$

$$\frac{\text{d[P]}}{\text{dt}} = \frac{k_1k_2k_5[\text{Pd}_\text{T}][\text{sub}][\text{MeOH}][\text{base}]}{k_2[\text{sub}]\left(k_5[\text{MeOH}][\text{base}] + k_1\right) + k_5[\text{MeOH}]\left(k_{-1}[\text{X}^-] + k_1\right)}$$

assume $k_5[\text{MeOH}][\text{base}] << k_1$

$$\frac{\text{d[P]}}{\text{dt}} = \frac{K_1k_2k_5[\text{Pd}_\text{T}][\text{sub}][\text{MeOH}][\text{base}]}{K_1k_2[\text{sub}] + k_5[\text{MeOH}]\left([\text{X}^-] + K_1\right)}$$

When [sub] is high

$$k_2k_4[\text{sub}][\text{Cu}]\left(k_5[\text{MeOH}][\text{base}] + k_1\right) + k_1k_2[\text{sub}]\left(k_5[\text{MeOH}][\text{base}] + k_{-4}[\text{X}^-]\right) >> k_4k_5[\text{Cu}][\text{MeOH}]\left(k_{-1}[\text{X}^-] + k_1\right)$$

$$\frac{\text{d[P]}}{\text{dt}} = \frac{k_1k_4k_5[\text{Pd}_\text{T}][\text{Cu}][\text{MeOH}][\text{base}]}{k_4[\text{Cu}]\left(k_5[\text{MeOH}][\text{base}] + k_1\right) + k_1\left(k_5[\text{MeOH}][\text{base}] + k_{-4}[\text{X}^-]\right)}$$

assume $k_5[\text{MeOH}][\text{base}] << k_1$

$$\frac{\text{d[P]}}{\text{dt}} = \frac{k_4k_5[\text{Pd}_\text{T}][\text{Cu}][\text{MeOH}][\text{base}]}{k_4[\text{Cu}] + k_5[\text{MeOH}][\text{base}] + k_{-4}[\text{X}^-]}$$

Figure 3.33 (continued).

When [sub] and [Cu] are high

$$k_2k_4[\text{sub}][\text{Cu}]\left(k_5[\text{MeOH}][\text{base}] + k_1\right) >> k_4k_5[\text{Cu}][\text{MeOH}]\left(k_{-1}[\text{X}^-] + k_1\right) + k_1k_2[\text{sub}]\left(k_5[\text{MeOH}][\text{base}] + k_{-4}[\text{X}^-]\right)$$

$$\frac{d[P]}{dt} = \frac{k_1k_2k_4k_5[Pd_T][\text{sub}][\text{Cu}][\text{MeOH}][\text{base}]}{k_2k_4[\text{sub}][\text{Cu}]\left(k_5[\text{MeOH}][\text{base}] + k_1\right)} = \frac{k_1k_5[Pd_T][\text{MeOH}][\text{base}]}{\left(k_5[\text{MeOH}][\text{base}] + k_1\right)}$$

Since k_5 is slow and first order dependence on [MeOH] is observed, assume $k_5[\text{MeOH}][\text{base}] << k_1$

$$\frac{d[P]}{dt} = k_5[Pd_T][\text{MeOH}][\text{base}]$$

Figure 3.33 (continued).

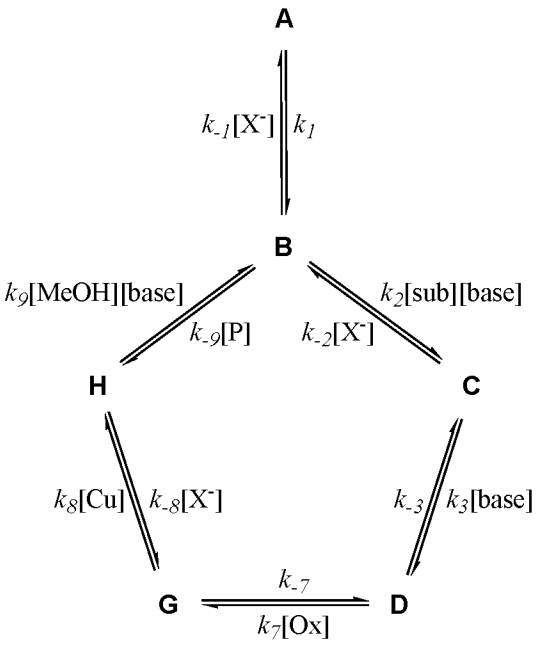

Open forms:

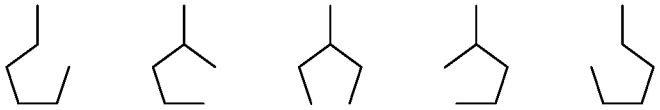

assume $k_{-3} = k_{-7} = k_{-9} = 0$ i.e. assume that steps 3, 7, and 9 are irreversible

[A] = $k_{-1}k_3k_7k_8k_9$[Cu][MeOH][X$^-$][Ox][base]^2 + $k_{-1}k_{-2}k_7k_8k_9$[Cu][MeOH][X$^-$]^2[Ox][base]

[B] = $k_1k_3k_7k_8k_9$[Cu][MeOH][Ox][base]^2 + $k_1k_{-2}k_7k_8k_9$[Cu][MeOH][X$^-$][Ox][base]

[C] = $k_1k_2k_7k_8k_9$[sub][Cu][MeOH][Ox][base]^2

[D] = $k_1k_2k_3k_8k_9$[sub][Cu][MeOH][base]^3

[G] = $k_1k_2k_3k_7k_9$[sub][MeOH][Ox][base]^3 + $k_1k_2k_3k_7k_{-8}$[sub][X$^-$][Ox][base]^2

[H] = $k_1k_2k_3k_7k_8$[sub][Cu][Ox][base]^2

Figure 3.34. Rate law derivation for mechanism B.

The total concentration of palladium is equal to sum of each palladium intermediate.

$$[Pd_T] = [\mathbf{A}] + [\mathbf{B}] + [\mathbf{C}] + [\mathbf{D}] + [\mathbf{G}] + [\mathbf{H}]$$

$$\frac{[Pd_T]}{[\mathbf{A}] + [\mathbf{B}] + [\mathbf{C}] + [\mathbf{D}] + [\mathbf{G}] + [\mathbf{H}]} = 1$$

Assuming step 9 is rate limiting

$$\frac{d[P]}{dt} = k_9[\mathbf{H}][MeOH][base] = \frac{k_9[\mathbf{H}][MeOH][base][Pd_T]}{[\mathbf{A}] + [\mathbf{B}] + [\mathbf{C}] + [\mathbf{D}] + [\mathbf{G}] + [\mathbf{H}]}$$

$$\frac{d[P]}{dt} = \frac{k_1k_2k_3k_7k_8k_9[Pd_T][sub][Cu][MeOH][Ox][base]^3}{\left(\begin{array}{c} k_{-1}k_3k_7k_8k_9[Cu][MeOH][X^-][Ox][base]^2 + k_{-1}k_{-2}k_7k_8k_9[Cu][MeOH][X^-]^2[Ox][base] + \\ k_1k_3k_7k_8k_9[Cu][MeOH][Ox][base]^2 + k_1k_{-2}k_7k_8k_9[Cu][MeOH][X^-][Ox][base] + \\ k_1k_2k_7k_8k_9[sub][Cu][MeOH][Ox][base]^2\ k_1k_2k_3k_8k_9[sub][Cu][MeOH][base]^3 + \\ k_1k_2k_3k_7k_9[sub][MeOH][Ox][base]^3 + \ k_1k_2k_3k_7k_{-8}[sub][X^-][Ox][base]^2 + \\ k_1k_2k_3k_7k_8[sub][Cu][Ox][base]^2 \end{array}\right)}$$

$$\frac{d[P]}{dt} = \frac{k_1k_2k_3k_7k_8k_9[Pd_T][sub][Cu][MeOH][Ox][base]^2}{\left(\begin{array}{c} k_{-1}k_3k_7k_8k_9[Cu][MeOH][X^-][Ox][base] + k_{-1}k_{-2}k_7k_8k_9[Cu][MeOH][X^-]^2[Ox] + \\ k_1k_3k_7k_8k_9[Cu][MeOH][Ox][base] + k_1k_{-2}k_7k_8k_9[Cu][MeOH][X^-][Ox] + \\ k_1k_2k_7k_8k_9[sub][Cu][MeOH][Ox][base] + k_1k_2k_3k_8k_9[sub][Cu][MeOH][base]^2 + \\ k_1k_2k_3k_7k_9[sub][MeOH][Ox][base]^2 + k_1k_2k_3k_7k_{-8}[sub][X^-][Ox][base] + \\ k_1k_2k_3k_7k_8[sub][Cu][Ox][base] \end{array}\right)}$$

assume $[Pd_T]$ - [**G**] >> [**G**] or that k_7 is fast

$$\left(\begin{array}{c} k_{-1}k_3k_7k_8k_9[Cu][MeOH][X^-][Ox][base] + \\ k_{-1}k_{-2}k_7k_8k_9[Cu][MeOH][X^-]^2[Ox] + \\ k_1k_3k_7k_8k_9[Cu][MeOH][Ox][base] + \\ k_1k_{-2}k_7k_8k_9[Cu][MeOH][X^-][Ox] + \\ k_1k_2k_7k_8k_9[sub][Cu][MeOH][Ox][base] + \\ k_1k_2k_3k_7k_9[sub][MeOH][Ox][base]^2 + \\ k_1k_2k_3k_7k_{-8}[sub][X^-][Ox][base] + \\ k_1k_2k_3k_7k_8[sub][Cu][Ox][base] \end{array}\right) >> k_1k_2k_3k_8k_9[sub][Cu][MeOH][base]^2$$

$$\frac{d[P]}{dt} = \frac{k_1k_2k_3k_8k_9[Pd_T][sub][Cu][MeOH][base]^2}{\left(\begin{array}{c} k_{-1}k_3k_8k_9[Cu][MeOH][X^-][base] + k_{-1}k_{-2}k_8k_9[Cu][MeOH][X^-]^2 + \\ k_1k_3k_8k_9[Cu][MeOH][base] + k_1k_{-2}k_8k_9[Cu][MeOH][X^-] + \\ k_1k_2k_8k_9[sub][Cu][MeOH][base] + k_1k_2k_3k_9[sub][MeOH][base]^2 + \\ k_1k_2k_3k_{-8}[sub][X^-][base] + k_1k_2k_3k_8[sub][Cu][base] \end{array}\right)}$$

Figure 3.34 (continued).

assume k_3 fast, i.e. $k_3 >> k_9$

$$k_3[\text{base}]\begin{pmatrix} k_{-1}k_8k_9[\text{Cu}][\text{MeOH}][\text{X}^-] + \\ k_1k_8k_9[\text{Cu}][\text{MeOH}] + \\ k_1k_2k_9[\text{sub}][\text{MeOH}][\text{base}] + \\ k_1k_2k_{-8}[\text{sub}][\text{X}^-] + k_1k_2k_8[\text{sub}][\text{Cu}] \end{pmatrix} >> \begin{pmatrix} k_{-1}k_{-2}k_8k_9[\text{Cu}][\text{MeOH}][\text{X}^-]^2 + \\ k_1k_{-2}k_8k_9[\text{Cu}][\text{MeOH}][\text{X}^-] + \\ k_1k_2k_8k_9[\text{sub}][\text{Cu}][\text{MeOH}][\text{base}] \end{pmatrix}$$

$$\frac{\text{d[P]}}{\text{dt}} = \frac{k_1k_2k_8k_9[\text{Pd}_\text{T}][\text{sub}][\text{Cu}][\text{MeOH}][\text{base}]}{\begin{pmatrix} k_{-1}k_8k_9[\text{Cu}][\text{MeOH}][\text{X}^-] + k_1k_8k_9[\text{Cu}][\text{MeOH}] + \\ k_1k_2k_9[\text{sub}][\text{MeOH}][\text{base}] + k_1k_2k_{-8}[\text{sub}][\text{X}^-] + \\ k_1k_2k_8[\text{sub}][\text{Cu}] \end{pmatrix}}$$

When [Cu] is high

$$k_1k_2k_8[\text{sub}][\text{Cu}] + k_8k_9[\text{Cu}][\text{MeOH}]\left(k_{-1}[\text{X}^-] + k_1\right) >> k_1k_2[\text{sub}]\left(k_9[\text{MeOH}][\text{base}] + k_{-8}[\text{X}^-]\right)$$

$$\frac{\text{d[P]}}{\text{dt}} = \frac{k_1k_2k_8k_9[\text{Pd}_\text{T}][\text{sub}][\text{Cu}][\text{MeOH}][\text{base}]}{k_1k_2k_8[\text{sub}][\text{Cu}] + k_8k_9[\text{Cu}][\text{MeOH}]\left(k_{-1}[\text{X}^-] + k_1\right)}$$

$$\frac{\text{d[P]}}{\text{dt}} = \frac{k_1k_2k_9[\text{Pd}_\text{T}][\text{sub}][\text{MeOH}][\text{base}]}{k_1k_2[\text{sub}] + k_9[\text{MeOH}]\left(k_{-1}[\text{X}^-] + k_1\right)}$$

When [sub] is high

$$k_8k_9[\text{Cu}][\text{MeOH}]\left(k_{-1}[\text{X}^-] + k_1\right) << k_1k_2k_8[\text{sub}][\text{Cu}] + k_1k_2[\text{sub}]\left(k_9[\text{MeOH}][\text{base}] + k_{-8}[\text{X}^-]\right)$$

$$\frac{\text{d[P]}}{\text{dt}} = \frac{k_1k_2k_8k_9[\text{Pd}_\text{T}][\text{sub}][\text{Cu}][\text{MeOH}][\text{base}]}{k_1k_2k_8[\text{sub}][\text{Cu}] + k_1k_2[\text{sub}]\left(k_9[\text{MeOH}][\text{base}] + k_{-8}[\text{X}^-]\right)}$$

$$\frac{\text{d[P]}}{\text{dt}} = \frac{k_8k_9[\text{Pd}_\text{T}][\text{Cu}][\text{MeOH}][\text{base}]}{k_8[\text{Cu}] + k_9[\text{MeOH}][\text{base}] + k_{-8}[\text{X}^-]}$$

At high [sub], high [Cu]

$$k_1k_2k_8[\text{sub}][\text{Cu}] >> k_8k_9[\text{Cu}][\text{MeOH}]\left(k_{-1}[\text{X}^-] + k_1\right) + k_1k_2[\text{sub}]\left(k_9[\text{MeOH}][\text{base}] + k_{-8}[\text{X}^-]\right)$$

$$\frac{\text{d[P]}}{\text{dt}} = \frac{k_1k_2k_8k_9[\text{Pd}_\text{T}][\text{sub}][\text{Cu}][\text{MeOH}][\text{base}]}{k_1k_2k_8[\text{sub}][\text{Cu}]}$$

$$\frac{\text{d[P]}}{\text{dt}} = k_9[\text{Pd}_\text{T}][\text{MeOH}][\text{base}]$$

Figure 3.34 (continued).

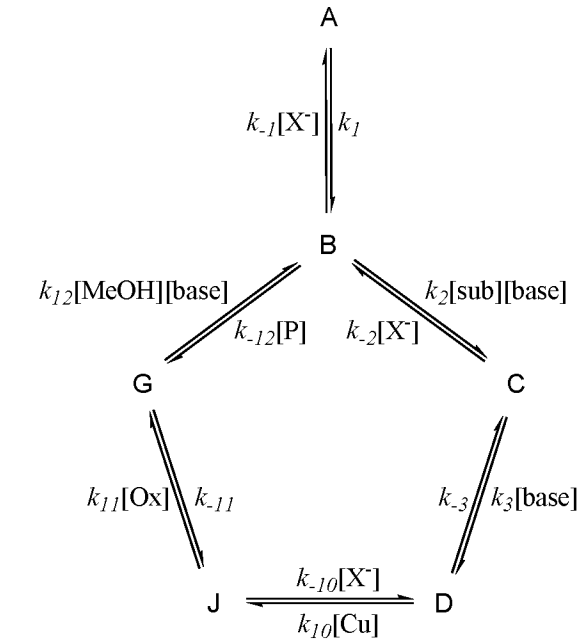

Open forms:

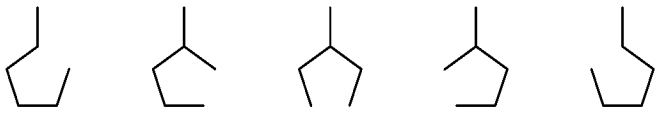

assume $k_{-3} = k_{-11} = k_{-12} = 0$ i.e. that steps 3, 11, and 12 are irreversible

[A] = $k_{-1}k_3k_{10}k_{11}k_{12}$[Cu][MeOH][X$^-$][Ox][base]^2 + $k_{-1}k_{-2}k_{10}k_{11}k_{12}$[Cu][MeOH][X$^-$]^2[Ox][base]

[B] = $k_1k_3k_{10}k_{11}k_{12}$[Cu][MeOH][Ox][base]^2 + $k_1k_{-2}k_{10}k_{11}k_{12}$[Cu][MeOH][X$^-$][Ox][base]

[C] = $k_1k_2k_{10}k_{11}k_{12}$[sub][Cu][MeOH][Ox][base]^2

[D] = $k_1k_2k_3k_{10}k_{11}k_{12}$[sub][MeOH][Ox][base]^3 + $k_1k_2k_3k_{-10}k_{12}$[sub][MeOH][X$^-$][base]^3

[J] = $k_1k_2k_3k_{10}k_{12}$[sub][Cu][MeOH][base]^3

[G] = $k_1k_2k_3k_{10}k_{11}$[sub][Cu][Ox][base]^2

Figure 3.35. Rate law derivation for mechanism C.

The total concentration of palladium is equal to sum of each palladium intermediate.

$$[Pd_T] = [\mathbf{A}] + [\mathbf{B}] + [\mathbf{C}] + [\mathbf{D}] + [\mathbf{J}] + [\mathbf{G}]$$

$$\frac{[Pd_T]}{[\mathbf{A}] + [\mathbf{B}] + [\mathbf{C}] + [\mathbf{D}] + [\mathbf{J}] + [\mathbf{G}]} = 1$$

Assuming step 9 is rate limiting

$$\frac{d[P]}{dt} = k_{12}[\mathbf{G}][MeOH][base] = \frac{k_{12}[\mathbf{G}][MeOH][base][Pd_T]}{[\mathbf{A}] + [\mathbf{B}] + [\mathbf{C}] + [\mathbf{D}] + [\mathbf{J}] + [\mathbf{G}]}$$

$$\frac{d[P]}{dt} = \frac{k_1k_2k_3k_{10}k_{11}k_{12}[Pd_T][sub][Cu][MeOH][Ox][base]^3}{\left(\begin{array}{c} k_{-1}k_3k_{10}k_{11}k_{12}[Cu][MeOH][X^-][Ox][base]^2 + k_{-1}k_{-2}k_{10}k_{11}k_{12}[Cu][MeOH][X^-]^2[Ox][base] \\ + k_1k_3k_{10}k_{11}k_{12}[Cu][MeOH][Ox][base]^2 + k_1k_{-2}k_{10}k_{11}k_{12}[Cu][MeOH][X^-][Ox][base] + \\ k_1k_2k_{10}k_{11}k_{12}[sub][Cu][MeOH][Ox][base]^2 + k_1k_2k_3k_{11}k_{12}[sub][MeOH][Ox][base]^3 + \\ k_1k_2k_3k_{-10}k_{12}[sub][MeOH][X^-][base]^3 + k_1k_2k_3k_{10}k_{12}[sub][Cu][MeOH][base]^3 + \\ k_1k_2k_3k_{10}k_{11}[sub][Cu][Ox][base]^2 \end{array}\right)}$$

$$\frac{d[P]}{dt} = \frac{k_1k_2k_3k_{10}k_{11}k_{12}[Pd_T][sub][Cu][MeOH][Ox][base]^2}{\left(\begin{array}{c} k_{-1}k_3k_{10}k_{11}k_{12}[Cu][MeOH][X^-][Ox][base] + k_{-1}k_{-2}k_{10}k_{11}k_{12}[Cu][MeOH][X^-]^2[Ox] + \\ k_1k_3k_{10}k_{11}k_{12}[Cu][MeOH][Ox][base] + k_1k_{-2}k_{10}k_{11}k_{12}[Cu][MeOH][X^-][Ox] + \\ k_1k_2k_{10}k_{11}k_{12}[sub][Cu][MeOH][Ox][base] + k_1k_2k_3k_{11}k_{12}[sub][MeOH][Ox][base]^2 + \\ k_1k_2k_3k_{-10}k_{12}[sub][MeOH][X^-][base]^2 + k_1k_2k_3k_{10}k_{12}[sub][Cu][MeOH][base]^2 + \\ k_1k_2k_3k_{10}k_{11}[sub][Cu][Ox][base] \end{array}\right)}$$

assume [J] << $[Pd_T]$ - [J] i.e. that k_{11} is fast, or

$$\left(\begin{array}{c} k_{-1}k_3k_{10}k_{11}k_{12}[Cu][MeOH][X^-][Ox][base] + \\ k_{-1}k_{-2}k_{10}k_{11}k_{12}[Cu][MeOH][X^-]^2[Ox] + \\ k_1k_3k_{10}k_{11}k_{12}[Cu][MeOH][Ox][base] + \\ k_1k_{-2}k_{10}k_{11}k_{12}[Cu][MeOH][X^-][Ox] + \\ k_1k_2k_{10}k_{11}k_{12}[sub][Cu][MeOH][Ox][base] + \\ k_1k_2k_3k_{11}k_{12}[sub][MeOH][Ox][base]^2 + \\ k_1k_2k_3k_{10}k_{11}[sub][Cu][Ox][base] \end{array}\right) >> \left(\begin{array}{c} k_1k_2k_3k_{-10}k_{12}[sub][MeOH][X^-][base]^2 + \\ k_1k_2k_3k_{10}k_{12}[sub][Cu][MeOH][base]^2 \end{array}\right)$$

Figure 3.35 (continued).

$$\frac{d[P]}{dt} = \frac{k_1k_2k_3k_{10}k_{12}[Pd_T][sub][Cu][MeOH][base]^2}{\left(\begin{array}{c} k_{-1}k_3k_{10}k_{12}[Cu][MeOH][X^-][base] + k_{-1}k_{-2}k_{10}k_{12}[Cu][MeOH][X^-]^2 + \\ k_1k_3k_{10}k_{12}[Cu][MeOH][base] + k_1k_{-2}k_{10}k_{12}[Cu][MeOH][X^-] + \\ k_1k_2k_{10}k_{12}[sub][Cu][MeOH][base] + k_1k_2k_3k_{12}[sub][MeOH][base]^2 + \\ k_1k_2k_3k_{10}[sub][Cu][base] \end{array}\right)}$$

assume $k_3 >> k_{12}$ or that

$$\left(\begin{array}{c} k_{-1}k_3k_{10}k_{12}[Cu][MeOH][X^-][base] + \\ k_1k_3k_{10}k_{12}[Cu][MeOH][base] + \\ k_1k_2k_3k_{12}[sub][MeOH][base]^2 + \\ k_1k_2k_3k_{10}[sub][Cu][base] \end{array}\right) >> \left(\begin{array}{c} k_{-1}k_{-2}k_{10}k_{12}[Cu][MeOH][X^-]^2 + \\ k_1k_{-2}k_{10}k_{12}[Cu][MeOH][X^-] + \\ k_1k_2k_{10}k_{12}[sub][Cu][MeOH][base] \end{array}\right)$$

$$\frac{d[P]}{dt} = \frac{k_1k_2k_3k_{10}k_{12}[Pd_T][sub][Cu][MeOH][base]^2}{\left(\begin{array}{c} k_{-1}k_3k_{10}k_{12}[Cu][MeOH][X^-][base] + k_1k_3k_{10}k_{12}[Cu][MeOH][base] + \\ k_1k_2k_3k_{12}[sub][MeOH][base]^2 + k_1k_2k_3k_{10}[sub][Cu][base] \end{array}\right)}$$

$$\frac{d[P]}{dt} = \frac{k_1k_2k_{10}k_{12}[Pd_T][sub][Cu][MeOH][base]}{\left(\begin{array}{c} k_{-1}k_{10}k_{12}[Cu][MeOH][X^-] + k_1k_{10}k_{12}[Cu][MeOH] + \\ k_1k_2k_{12}[sub][MeOH][base] + k_1k_2k_{10}[sub][Cu] \end{array}\right)}$$

at high [Cu]

$k_{-1}k_{10}k_{12}[Cu][MeOH][X^-] + k_1k_{10}k_{12}[Cu][MeOH] + k_1k_2k_{10}[sub][Cu] >> k_1k_2k_{12}[sub][MeOH][base]$

$$\frac{d[P]}{dt} = \frac{k_1k_2k_{10}k_{12}[Pd_T][sub][Cu][MeOH][base]}{\left(\begin{array}{c} k_{-1}k_{10}k_{12}[Cu][MeOH][X^-] + k_1k_{10}k_{12}[Cu][MeOH] \\ + \ k_1k_2k_{10}[sub][Cu] \end{array}\right)}$$

$$\frac{d[P]}{dt} = \frac{k_1k_2k_{12}[Pd_T][sub][MeOH][base]}{\left(k_{-1}k_{12}[MeOH][X^-] + k_1k_{12}[MeOH] + \ k_1k_2[sub]\right)}$$

$$\frac{d[P]}{dt} = \frac{K_1k_2k_{12}[Pd_T][sub][MeOH][base]}{K_1k_2[sub] + k_{12}[MeOH]\left([X^-] + K_1\right)}$$

Figure 3.35 (continued).

at high [sub]

$$\frac{d[P]}{dt} = \frac{k_1k_2k_{10}k_{12}[Pd_T][sub][Cu][MeOH][base]}{\left(\begin{array}{c} k_{-1}k_{10}k_{12}[Cu][MeOH][X^-] + k_1k_{10}k_{12}[Cu][MeOH] + \\ k_1k_2k_{12}[sub][MeOH][base] + k_1k_2k_{10}[sub][Cu] \end{array}\right)}$$

$k_{-1}k_{10}k_{12}[Cu][MeOH][X^-] + k_1k_{10}k_{12}[Cu][MeOH] << k_1k_2k_{12}[sub][MeOH][base] + k_1k_2k_{10}[sub][Cu]$

$$\frac{d[P]}{dt} = \frac{k_1k_2k_{10}k_{12}[Pd_T][sub][Cu][MeOH][base]}{k_1k_2k_{12}[sub][MeOH][base] + k_1k_2k_{10}[sub][Cu]}$$

$$\frac{d[P]}{dt} = \frac{k_{10}k_{12}[Pd_T][Cu][MeOH][base]}{k_{12}[MeOH][base] + k_{10}[Cu]}$$

at high [sub] high [Cu]

$$\frac{d[P]}{dt} = k_{12}[Pd_T][MeOH][base]$$

Figure 3.35 (continued).

Synthesis of substrates 8, 17-20:

Substrates **8**, **17-20** were synthesized by Wittig olefination followed by Grignard addition, as summarized in Figure 3.36.

Preparation of ester 39 (R = H)

To an oven-dried 500 mL round bottom flask equipped with a stir bar were added 23.4 g of **37**[40] (51.0 mmol, 2.30 equiv.) and 200 mL toluene. To this was added a solution of 5.80 g KO*t*Bu (51.2 mmol, 2.33 equiv.) in 40 mL of THF dropwise via cannula. The reaction mixture slowly turned a deep red color over 4 h. The mixture was cooled to –78 °C and 2.70 g of salicylaldehyde **38** (22.2 mmol, 1.00 equiv.), dissolved in 20 mL of toluene, were added dropwise via cannula. The mixture was allowed to slowly warm to rt and stirred 48 h then quenched with 50 mL of saturated NH_4Cl solution. The mixture was diluted with 100 mL of diethyl ether and washed with 100 mL (2 x 50 mL) of water and 60 mL of brine. The organic layer was dried over $MgSO_4$, filtered, and the solvent removed in vacuo. The crude mixture was purified by flash silica-gel column chromatography with 10%-20% EtOAc/hexanes as eluent to give 4.15 g of **39** (85% yield, average of two reactions). Isomeric ratio: *Z*:*E* ~10:1, major isomer: R_f = 0.52 with 33% EtOAc/hexanes, colorless oil, ^{1}H-NMR (300 MHz, $CDCl_3$) δ = 7.02-7.28 (m, 2 H), 6.85-6.95 (m, 2 H), 6.38-6.48 (d, *J* = 11.2 Hz, 2 H), 5.89 (s, 1 H), 5.74-5.86 (m, 1 H),

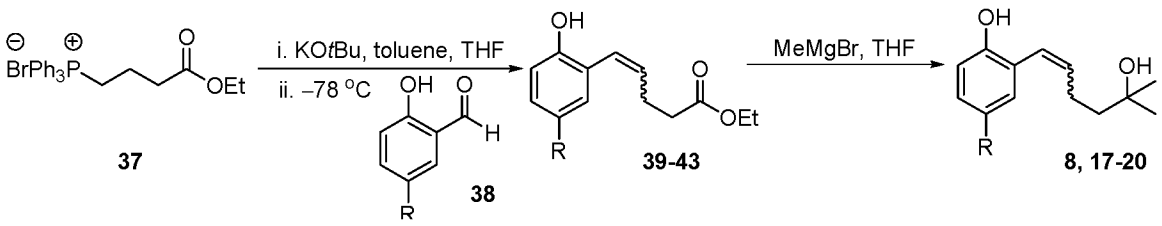

Figure 3.36. Synthesis of substrates **8**, **17-20**.

4.08-4.16 (m, 2 H), 2.37-2.48 (m, 4 H), 1.18-1.29 (m, 3 H). ^{13}C-NMR (75 MHz, $CDCl_3$) δ = 173.3, 153.1, 134.4, 129.9, 128.8, 125.1, 123.8, 120.5, 116.1, 60.9, 33.9, 24.3, 14.3. IR: 3392, 2981, 1705, 1450, 1269, 1195, 1154, 754 cm^{-1}. HRMS $C_{13}H_{16}O_3$ $(M+Na)^+$ calcd. 243.0997, obsvd. 243.0996.

Preparation of ester 40 (R = OMe)

Compound **40** was prepared according to the procedure described above for **39**. 95% yield. Isomeric ratio: *Z:E* ~10:1, major isomer: R_f = 0.30 with 20% EtOAc/hexanes, colorless oil, ^{1}H-NMR (400 MHz, $CDCl_3$) δ = 7.02 (d, *J* = 8.2 Hz, 1 H), 6.60 (s, 1 H), 6.46-6.39 (m, 3 H), 5.66 (dt, *J* = 11.8 Hz, *J* = 6.2 Hz, 1 H), 4.11 (q, *J* = 7.2 Hz, 2 H), 3.73 (s, 3 H), 2.40-2.48 (m, 4 H), 1.22 (t, *J* = 7.2 Hz, 3 H). ^{13}C-NMR (75 MHz, $CDCl_3$) δ = 174.6, 154.3, 147.0, 134.3, 130.6, 124.9, 124.2, 116.8, 114.3, 60.9, 55.4, 34.1, 24.3, 14.3. IR: 3408, 2980, 1729, 1492, 1197, 1145, 808 cm^{-1}. HRMS $C_{14}H_{18}O_4$ $(M+Na)^+$ calcd. 273.1103, obsvd. 273.1111.

Preparation of ester 41 (R = Me)

Compound **41** was prepared according to the procedure described above for **39**. 92% yield. Isomeric ratio: *Z:E* ~10:1, major isomer: R_f = 0.42 with 33% EtOAc/hexanes, colorless oil, ^{1}H-NMR (400 MHz, $CDCl_3$) δ = 6.98 (d, *J* = 8.2 Hz, 1 H), 6.93 (s, 1 H), 6.83 (dd, *J* = 8.2 Hz, *J* = 0.8 Hz, 1 H), 6.47 (d, J = 11.2 Hz, 1 H), 5.84-5.77 (m, 1 H), 4.17 (q, J = 8.3 Hz, 2 H), 2.49-2.47 (m, 4 H), 2.30 (s, 3 H), 1.27 (t, J = 8.3 Hz, 3 H). ^{13}C-NMR (75 MHz, $CDCl_3$) δ = 173.7, 150.8, 133.4, 130.2, 129.3, 125.4, 123.5, 115.7, 60.8, 33.9, 28.2, 24.2, 20.7, 14.3. IR: 3411, 2981, 1711, 1494, 1178, 906, 787, 726 cm^{-1}. HRMS $C_{14}H_{18}O_3$ $(M+Na)^+$ calcd. 257.1154, obsvd. 257.1165.

Preparation of ester 42 (R = F)

Compound **42** was prepared according to the procedure described above for **39**. 84% yield. Isomeric ratio: *Z:E* ~10:1, major isomer: R_f = 0.32 with 20% EtOAc/hexanes, colorless oil, ^{1}H-NMR (400 MHz, $CDCl_3$) δ = 6.85-6.77 (m, 2 H), 6.37 (dd, *J* = 11.1 Hz, *J* = 6.4 Hz, 1 H), 6.01 (d, *J* = 39.4 Hz, 1 H), 5.84-5.77 (m, 1 H), 4.13 (q, *J* = 7.2 Hz, 2 H), 2.47-2.36 (m, 4 H), 1.23 (t, *J* = 7.1 Hz, 3 H). ^{13}C-NMR (75 MHz, $CDCl_3$) δ = 173.1, 157.9, 149.1, 134.9 (d), 124.4 (d), 116.8 (q), 115.8 (q), 115.2 (q), 61.0, 34.7, 24.2, 14.3. IR: 3392, 2980, 1702, 1478, 1269, 1195, 1148, 814 cm^{-1}. HRMS $C_{13}H_{15}O_3F$ $(M+Ag)^+$ calcd. 345.0056, obsvd. 345.0081.

Preparation of ester 43 (R = Cl)

Compound **43** was prepared according to the procedure described above for **39**. 90% yield. Isomeric ratio: *Z:E* ~10:1, major isomer: R_f = 0.32 with 20% EtOAc/hexanes, colorless oil, ^{1}H-NMR (400 MHz, $CDCl_3$) δ = 7.09 (dd, *J* = 8.6 Hz, *J* = 2.6 Hz, 1 H), 7.04 (d, *J* = 2.6 Hz, 1 H), 6.82 (d, *J* = 8.6 Hz, 1 H), 6.34 (d, *J* = 11.3 Hz, 1 H), 6.29 (s, 1 H), 5.79 (dt, *J* = 11.3 Hz, *J* = 6.9 Hz, 1 H), 4.13 (q, *J* = 7.2 Hz, 2 H), 2.47-2.37 (m, 4 H), 1.23 (t, *J* = 7.2 Hz, 3 H). ^{13}C-NMR (75 MHz, $CDCl_3$) δ = 173.8, 151.7, 134.9, 129.4, 128.6, 125.3, 124.9, 124.2, 117.3, 61.1, 33.6, 24.2, 14.3. IR: 3392, 2980, 1702, 1478, 1269, 1195, 1148, 814 cm^{-1}. HRMS $C_{13}H_{15}O_3Cl$ $(M+Na)^+$ calcd. 277.0607, obsvd. 277.0618.

Preparation of substrate 8 (R = H)

To an oven dried 500 mL round bottom flask equipped with a stir bar were added 4.10 g of **39** (18.6 mmol, 1.00 equiv.) in 180 mL THF. To this was slowly added a solution of 3.0 M MeMgBr (130 mmol, 7.00 equiv.) at 0 °C. The reaction mixture was

then allowed to warm to rt and was stirred for 12 h. The reaction was quenched by the slow addition of 20 mL of 1 M HCl solution. The mixture was diluted with 50 mL of diethyl ether and washed with 100 mL (2 x 50 mL) of water and 60 mL of brine. The organic extract was dried over $MgSO_4$, filtered, and the solvent was removed in vacuo. The crude mixture was purified by flash silica-gel column chromatography with 1 L of 50% EtOAc/hexanes as eluent to give 3.34 g of **8** (87% yield). Isomeric ratio *Z*:*E* > 20:1, major isomer: R_f = 0.32 with 33% EtOAc/hexanes, colorless solid. mp = 74-75 °C. ^{1}H-NMR (400 MHz, $CDCl_3$) δ = 7.28-7.07 (m, 2 H), 6.95-6.87 (m, 2 H), 6.40-6.37 (d, *J* = 10.9 Hz, 1 H), 5.95-5.88 (m, 1 H), 5.34 (s, 1 H), 2.28-2.19 (m, 2 H), 1.67-1.57 (m, 2 H), 1.19 (s, 6 H). ^{13}C-NMR (100 MHz, $CDCl_3$) δ = 152.9, 137.0, 129.8, 128.8, 123.9, 123.4, 120.4, 115.5, 71.3, 43.3, 29.4, 24.1. IR: 3410, 3013, 2971, 1604, 1448, 1377, 1261, 1210, 1147, 1131, 904, 755 cm^{-1}. HRMS $C_{13}H_{18}O_2$ $(M+Na)^+$ calcd. 229.1204, obsvd. 229.1201.

Preparation of substrate 17 (R = OMe)

Compound **17** was prepared according to the procedure described above for **8**. 82% yield. Isomeric ratio: *Z*:*E* > 20:1, major isomer: R_f = 0.30 with 33% EtOAc/hexanes, colorless solid. ^{1}H-NMR (400 MHz, $CDCl_3$) δ = 6.83 (d, *J* = 8.7 Hz, 2 H), 6.74 (dd, *J* = 8.7 Hz, *J* = 3.0 Hz, 1 H), 6.66 (d, *J* = 2.9 Hz, 1 H), 6.35 (d, *J* = 11.2 Hz, 1 H), 5.91 (dt, *J* =11.2 Hz, *J* = 7.4 Hz, 1 H), 5.01 (bs, 1 H), 3.77 (s, 3 H), 2.27-2.18 (m, 2 H), 1.64-1.58 (m, 2 H), 1.19 (s, 6 H). ^{13}C-NMR (100 MHz, $CDCl_3$) δ = 159.8, 154.3, 135.9, 131.1, 123.6, 116.2, 106.5, 101.3, 71.3, 55.9, 43.2, 29.5, 24.2. IR: 3410, 3013, 2971, 1604, 1448, 1377, 1261, 1210, 1147, 1131, 904, 784 cm^{-1}. HRMS $C_{14}H_{20}O_3$ $(M+Na)^+$ calcd. 259.1310, obsvd. 259.1320.

Preparation of substrate 18 (R = Me)

Compound **18** was prepared according to the procedure described above for **8.** 97% yield. Isomeric ratio: *Z:E* > 20:1, major isomer: R_f = 0.20 with 20% EtOAc/hexanes, colorless solid. MP = 130-132 °C. ^{1}H-NMR (400 MHz, $CDCl_3$) δ = 6.98-6.95 (m, 1 H), 6.90 (s, 1 H), 6.79 (d, *J* = 8.2 Hz, 1 H), 6.35 (d, *J* = 11.2 Hz, 1 H), 5.89 (dt, *J* = 11.2 Hz, *J* = 7.4 Hz, 1 H), 5.2 (bs, 1 H), 2.27 (s, 3 H), 2.24-2.18 (m, 2 H), 1.67-1.57 (m, 2 H), 1.19 (s, 6 H). ^{13}C-NMR (100 MHz, $CDCl_3$) δ = 150.7, 136.6, 130.1, 129.5, 129.3, 123.6, 115.3, 71.3, 43.3, 29.4, 24.1, 20.7. IR: 3405, 3085, 2966, 1503, 1421, 1371, 1274, 1202, 1151, 1122, 807, 713 cm^{-1}. HRMS $C_{14}H_{20}O_2$ $(M+Na)^+$ calcd. 243.1361, obsvd. 243.1369.

Preparation of -substrate 19 (R = F)

Compound **19** was prepared according to the procedure described above for **8.** 72% yield. Isomeric ratio: *Z:E* = 10:1, major isomer: R_f = 0.30 with 20% EtOAc/hexanes, colorless solid. ^{1}H-NMR (400 MHz, $CDCl_3$) δ = 6.85-6.79 (m, 3 H), 6.31 (d, *J* = 11.2 Hz, 1 H), 5.91 (dt, *J* = 11.2 Hz, *J* = 7.4 Hz, 1 H), 2.24-2.18 (m, 2 H), 1.61-1.58 (m, 2 H), 1.19 (s, 6 H). ^{13}C-NMR (75 MHz, $CDCl_3$) δ = 156.8 (d, *J* = 237.9 Hz), 149.0 (d, *J* = 2.2 Hz), 137.7, 125.1 (d, *J* = 7.7 Hz), 122.7 (d, *J* = 1.1 Hz), 116.4 (d, *J* = 8.2 Hz), 115.9 (d, *J* = 22.5 Hz), 115.1 (d, *J* = 23.1 Hz), 71.5, 43.0, 29.5, 24.1. IR: 3261, 2970, 1652, 1485, 1434, 1183, 876, 769 cm^{-1}. HRMS $C_{13}H_{17}O_2F$ $(M+Ag)^+$ calcd. 331.0264, obsvd. 331.0280.

Preparation of substrate 20 (R = Cl)

Compound **20** was prepared according to the procedure described above for **8.** 85% yield. Isomeric ratio: *Z:E* > 20:1, major isomer: R_f = 0.20 with 20%

EtOAc/hexanes, colorless solid. mp = 102-103 °C. ^{1}H-NMR (400 MHz, $CDCl_3$) δ = 7.01 (dd, *J* = 8.6 Hz, *J* = 2.6 Hz, 1 H), 7.06 (d, *J* = 2.6 Hz, 1 H), 6.81 (d, *J* = 8.6 Hz, 1 H), 6.28 (d, *J* = 11.2 Hz, 1 H), 5.94-5.89 (m, 1 H), 2.21-2.16 (m, 2 H), 1.61-1.58 (m, 2 H), 1.19 (s, 6 H). ^{13}C-NMR (100 MHz, $CDCl_3$) δ = 151.7, 137.7, 129.4, 128.5, 125.6, 124.9, 122.5, 116.3, 71.6, 42.9, 29.4, 24.1. IR: 3455, 2964, 1604, 1468, 1375, 1254, 1210, 1136, 926, 775 cm^{-1}. HRMS $C_{13}H_{15}O_2Cl$ $(M+Na)^+$ calcd. 263.0815, obsvd. 263.0801.

Evalutation of Substituted Substrates

Each reaction (Table 3.3) was performed as described in the following example: to a 50 mL Schlenk flask equipped with a stir bar were added 3.1 mg $Pd(MeCN)_2Cl_2$ (0.012 mmol, 0.040 equiv.), 2.4 mg of CuCl (0.024 mmol, 0.080 equiv.), 10.1 mg (*S*)-quinox-*i*Pr (0.042 mmol, 0.14 eqiuv), 12.0 mg of $KHCO_3$ (0.120 mmol, 0.40 equiv.), 2.4 mL of 4:1 toluene:MeOH. A three-way joint fitted with a balloon of O_2 was attached and the apparatus was evacuated (using house vacuum) and refilled with oxygen three times. The mixture was stirred vigorously for 30 min at rt. A 600 μL portion of a solution of **8** (0.30 mmol, 1 equiv.) in 4:1 toluene:MeOH was added to the reaction mixture. The reaction mixture was stirred at rt overnight, passed through a silica plug eluting with 40 mL of EtOAc and concentrated in vacuo. This residue was purified by flash column chromatography with 5% EtOAc/hexanes as eluent.

Product 16 (R=H)

Melting point = 81-84 °C. $[\alpha]^{20}_D$ = –31.5° (c = 3.53, $CHCl_3$). Major diastereomer: ^{1}H-NMR (300 MHz, $CDCl_3$) δ = 8.12 (s, 1 H), 7.20 (ddd, *J* = 8.9, *J* = 7.2, *J* = 1.6, 1 H), 7.09 (dd, *J* = 7.6 Hz, *J* = 1.8 Hz, 1 H), 6.91-6.82 (m, 2 H), 4.42-4.32 (m, 2 H), 3.36 (s, 3 H), 1.83 (ddd, *J* = 14.4 Hz, *J* = 7.0 Hz, *J* = 1.4 Hz, 2 H), 1.72-1.49 (m, 2 H),

1.24 (s, 3 H), 1.22 (s, 3 H). ^{13}C-NMR (75 MHz, $CDCl_3$) δ = 155.8, 129.5, 129.3, 123.5, 119.9, 117.7, 85.5, 82.8, 81.1, 57.9, 38.3, 28.3, 28.2, 27.9, 27.7. IR: 3285, 2869, 2930, 1487, 1456, 1367, 1236, 1102, 1056, 754 cm^{-1}. HRMS $C_{14}H_{20}O_3$ $(M+Na)^+$ calcd. 259.1310, obsvd. 259.1308. er = 96.6:3.4, GC analysis: β-cyclodextrin column at 100 °C for 20 min, increased to 130 °C at 0.4 °C/min, held at 130 °C for 2 min, increased to 200 °C at 20 °C/min; retention times: 60.4 min and 61.9 min.

Product 21 (R = OMe)

$[\alpha]^{20}_D$ = –17° (c = 0.08, $CHCl_3$). Major diastereomer: ^{1}H-NMR (300 MHz, $CDCl_3$) δ = 7.70 (s, 1 H), 6.84 (d, *J* = 8.8 Hz, 1 H), 6.76 (dd, *J* = 8.8 Hz, *J* = 2.9 Hz, 1 H), 6.69 (d, *J* = 2.9 Hz, 1 H), 4.42-4.36 (m, 2 H), 3.77 (s, 3 H), 3.37 (s, 3 H), 1.88-1.79 (m, 2 H), 1.69-1.44 (m, 2 H), 1.23 (s, 3 H), 1.18 (s, 3 H). ^{13}C-NMR (75 MHz, $CDCl_3$) δ = 153.3, 149.5, 124.7, 118.4, 114.4, 114.2, 84.4, 82.8, 81.1, 58.0, 55.9, 38.3, 28.2, 27.9, 27.7. IR: 3306, 2869, 2933, 1494, 1462, 1200, 1110, 1043, 815 cm^{-1}. HRMS $C_{15}H_{22}O_4$ $(M+Na)^+$ calcd. 289.1416, obsvd. 289.1425. er = 96.5:3.5, GC analysis: β-cyclodextrin column at 120 °C for 20 min, increased to 140 °C at 0.4 °C/min, held at 140 °C for 2 min, increased to 200 °C at 10 °C/min; retention times: 37.9 min and 39.4 min.

Product 22 (R = Me)

$[\alpha]^{20}_D$ = –2° (c = 0.19, $CHCl_3$). Major diastereomer: ^{1}H-NMR (300 MHz, $CDCl_3$) δ = 7.90 (s, 1 H), 7.00 (dd, *J* = 8.0 Hz, *J* = 2.2 Hz, 1 H), 6.88 (d, *J* = 2.0 Hz, 1 H), 6.81-6.77 (m, 1 H), 4.37 (ddd, *J* = 7.0 Hz, *J* = 7.0 Hz, *J* = 5.3 Hz, 1 H), 4.28 (d, *J* = 5.1 Hz, 1 H), 3.36 (s, 3 H), 3.43 (s, 3 H), 1.81 (apparent q, *J* = 7.1 Hz, 2 H), 1.70-1.53 (m, 2 H), 1.24 (s, 3 H), 1.22 (s, 3 H). ^{13}C-NMR (75 MHz, $CDCl_3$) δ = 153.5, 130.0, 129.7, 129.0, 123.1, 117.5, 85.9, 82.7, 81.0, 57.9, 38.3, 28.4, 28.2, 28.0, 20.8. IR: 3317, 2970,

2929, 1500, 1367, 1257, 1235, 1109, 1060, 819 cm^{-1}. HRMS $C_{15}H_{22}O_3$ $(M+Na)^+$ calcd. 273.1467 obsvd. 273.1474. er = 96.9:3.1, GC analysis: β-cyclodextrin column at 120 °C for 20 min, increased to 140 °C at 0.4 °C/min, held at 140 °C for 2 min, increased to 200 °C at 10 °C/min; retention times: 37.8 min and 39.4 min.

Product 23 (R = F)

Melting point = 91-93 °C. $[\alpha]^{20}_D$ = –11.8° (c = 0.72, $CHCl_3$). Major diastereomer: ^{1}H-NMR (300 MHz, $CDCl_3$) δ = 7.95 (s, 1 H), 6.92-6.81 (m, 4 H), 4.42-4.37 (m, 2 H), 3.36 (s, 3 H), 1.93-1.56 (m, 4 H), 1.29 (s, 3 H), 1.61 (s, 3 H). ^{13}C-NMR (75 MHz, $CDCl_3$) δ = 156.9 (d, *J* = 237.7 Hz), 151.6, 125.5 (d, *J* = 6.0 Hz), 118.9 (d, *J* = 8.1 Hz), 115.7 (d, *J* = 23.2 Hz), 115.0 (d, *J* = 23.7 Hz), 83.2, 83.0, 81.1, 58.1, 38.2, 28.0, 27.8, 27.4. IR: 3282, 2971, 1488, 1238, 1109, 819 cm^{-1}. HRMS $C_{14}H_{19}FO_3$ $(M+Na)^+$ calcd. 277.1216, obsvd. 277.1222. er = 98.9:1.1, GC analysis: β-cyclodextrin column at 100 °C for 20 min, increased to 130 °C at 0.4 °C/min, held at 130 °C for 2 min, increased to 200 °C at 20 °C/min; retention times: 60.0 min and 63.0 min.

Product 24 (R = Cl)

Melting point = 95-111 °C. $[\alpha]^{20}_D$ = –38° (c = 0.12, $CHCl_3$). Major diastereomer: ^{1}H-NMR (300 MHz, $CDCl_3$) δ = 8.19 (s, 1 H), 7.16 (dd, *J* = 8.6, *J* = 2.6, 1 H), 7.10 (d, *J* = 2.6 Hz, 1 H), 6.84 (d, *J* = 8.6 Hz, 1 H), 4.41-4.33 (m, 2 H), 3.56 (s, 3 H), 1.95-1.76 (m, 2 H), 1.71-1.48 (m, 2 H), 1.23 (s, 3 H), 1.19 (s, 3 H). ^{13}C-NMR (75 MHz, $CDCl_3$) δ = 154.5, 129.3, 128.6, 125.7, 124.9, 119.3, 84.0, 83.1, 81.1, 58.1, 38.2, 28.1, 27.8, 27.7. IR: 3251, 2970, 1484, 1368, 1246, 1111, 1057, 820, 650 cm^{-1}. HRMS $C_{14}H_{19}O_3Cl$ $(M+Na)^+$ calcd. 293.0920, obsvd. 293.0927. er = 97.0:3.0, GC analysis: β-cyclodextrin

column at 120 °C for 20 min, increased to 140 °C at 0.4 °C/min, held at 140 °C for 2 min, increased to 200 °C at 10 °C/min; retention times: 55.2 min and 57.4 min.

Determination of Substrate Electronic Effects on Rate

The electronic effect on rate was examined following the example procedure above, with the following modifications: Solutions of substrate **8**, **17-20** (1.92 mmol in 2.00 mL) and tetradecane (80 mg, 0.40 mmol) were prepared. A 250 μL portion of the substrate solution was added to each of the above tubes via syringe for a final reaction volume of 1.5 mL. Each substrate was run in duplicate. Data for substrate electronic effects are tabulated in Tables 3.18, 3.19, and 3.20.

Table 3.18. Substituent constants for Hammett and Jaffé plots.

R	σ_m	σ_p	σ_m/σ_p	σ_p/σ_m
4-H	0	0	-	-
4-Cl	0.373	0.227	1.64	0.608
4-Me	-0.069	-0.170	0.405	2.46
4-OMe	0.115	-0.268	-0.429	-2.33
4-F	0.337	0.062	5.44	0.184

Table 3.19. k_{obs} data for Hammett plots. Data for Figure 3.20.

R	k_{obs} (μmol O_2/s)	STD DEV	$\log(k_X/k_H)$	STD DEV
4-H	0.066	0.0054	0	-
4-Cl	0.041	0.0029	-0.198	0.031
4-Me	0.027	0.0055	-0.332	0.090
4-OMe	0.012	0.0020	-0.723	0.071
4-F	0.032	0.0033	-0.268	0.024

Table 3.20. Data for Jaffé plots. Data for Figure 3.21.

R	$\log(k_X/k_H)/\sigma_p$	STD DEV	$\log(k_X/k_H)/\sigma_m$	STD DEV
4-H	-	-	-	-
4-Cl	-0.87	0.14	-0.530	0.083
4-Me	2.33	0.53	5.75	1.3
4-OMe	2.67	0.27	-6.28	0.62
4-F	-4.98	0.71	-0.976	0.11

Procedure for Evaluation of Other Cocatalysts

Complexes of Cu(1,2-bipyridine)Cl_2,[41] Cu(1,10-phenanthroline)Cl_2,[42] and Cu(bathocuproine)Cl_2,[43] were prepared according to literature procedures. For the evaluation of other cocatalysts, four reactions were run simultaneously in separate 5 mL side-arm flasks attached to a four-neck cow fitted with a three way adaptor with a balloon of O_2 attached. A standard solution was prepared by the addition of 412.6 mg of the substrate **8** and 63.3 mg of the internal standard 2-methoxynaphthalene to a 2 mL volumetric flask, followed by the addition of MeOH. The flask was briefly sonicated to dissolve **8** and stirred to give a solution with [**8**] = 1.00 M and [2-methoxynaphthalene] = 0.20 M.

Each reaction was performed as described in the following example: to a 5 mL side-arm round bottom flask equipped with a stir bar were added 1.7 mg Pd[(*R*)-quinox-*i*Pr]Cl_2 (0.0040 mmol, 0.040 equiv.), 3.0 mg of Cu[(*S*)-quinox-*i*Pr]Cl_2 (0.0080 mmol, 0.080 equiv.), 0.5 mg (*S*)-quinox-*i*Pr (0.002 mmol, 0.02 eqiuv), 4.0 mg of $KHCO_3$ (0.040 mmol, 0.40 equiv.), 800 μL of toluene and 100 μL MeOH. A three-way joint fitted with a balloon of O_2 was attached and the apparatus was evacuated (using house vacuum) and refilled with oxygen three times. The mixture was stirred vigorously for 30 min at rt. A 100 μL portion of the standard solution of **8** (0.10 mmol, 1 equiv.) and 2-methoxy

naphthalene (0.020 mmol, 0.20 equiv.) was added dropwise to the reaction mixture. Aliquots (ca. 50 μL) of the reaction were taken periodically via syringe. Reaction samples were passed through a short silica plug eluting with 2 mL of EtOAc and analyzed by GC and referenced against a time zero sample containing the standard solution of **8** and 2-methoxynaphthalene diluted in EtOAc. GC yields were calculated based on the ratio of product to internal standard corrected for the response factor. Enantiomeric and diastereomeric ratios were determined using GC with a column equipped with a chiral stationary phase. GC analysis: β-cyclodextrin column at 100 °C for 20 min, increased to 130 °C at 0.4 °C/min, held at 130 °C for 2 min, increased to 200 °C at 20 °C/min; retention times: 60.4 min, 61.9 min, 63.7 min, and 64.8 min.

For Table 3.5, the procedure described above was followed, using 1.7 mg Pd[(*S*)-quinox-*i*Pr]Cl_2 (0.0040 mmol, 0.040 equiv.), 0.5 mg (*S*)-quinox-*i*Pr (0.002 mmol, 0.02 eqiuv), 4.0 mg of $KHCO_3$ (0.040 mmol, 0.40 equiv.), and 2.3 mg of Cu(1,2-bipyridine)Cl_2 or 2.5 mg Cu(1,10-phenanthroline)Cl_2 or 4.0 mg Cu(bathocuproine)Cl_2 (0.0080 mmol, 0.080 equiv.).

For Table 3.6, the procedure described above was followed, using 1.0 mg $Pd(MeCN)_2Cl_2$ (0.0040 mmol, 0.040 equiv.), 3.4 mg (*S*)-quinox-*i*Pr (0.014 mmol, 0.14 eqiuv), 4.0 mg of $KHCO_3$ (0.040 mmol, 0.40 equiv.), and 0.008 mmol of the indicated Lewis acid additive.

Synthesis of (*S*)-pyrox-*t*Bu Ligands

(*S*)-pyrox-*t*Bu (**31**) was prepared according to literature procedure.[44] Ligands **29**, **30**, and **32** were prepared as shown in Figure 3.37. A full description of this procedure, along with characterization data are provided for each.

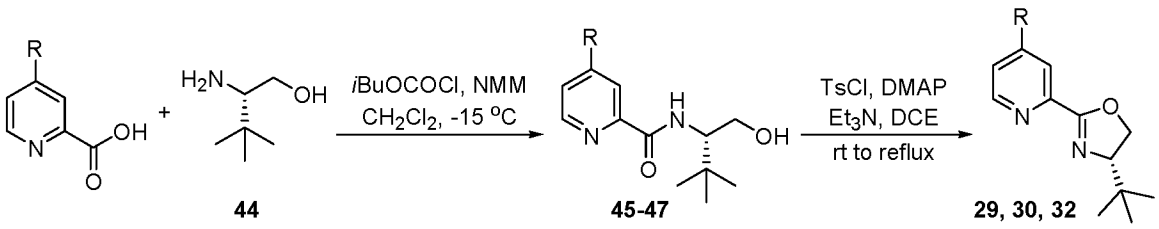

Figure 3.37. Synthesis of ligands **29**, **30**, and **32.**

Preparation of peptide 45 (R = CF_3)[45]

To a dry 100 mL round bottom flask were added 283.5 mg 4-trifluoromethylpicolinic acid (1.49mmol, 1 equiv.), 10 mL CH_2Cl_2, and 247 μL *N*-methylmorpholine (2.22 mmol, 1.50 equiv.). The reaction mixture was cooled to 0 °C in an ice bath, 226 μL of *iso*-butyl chloroformate (1.71 mmol, 1.15 equiv.) were added dropwise, and the reaction mixture was stirred for 30 min at 0 °C. In a separate flask, 191 mg of (*S*)-*tert*-leucinol **44** (1.63 mmol, 1.10 equiv.) were dissolved in 5 mL of CH_2Cl_2, and 198 μL of *N*-methylmorpholine (1.78 mmol, 1.20 equiv.) were added. This solution was transferred dropwise via cannula to the reaction flask at 0 °C. The mixture was allowed to warm to rt and stirred for 3 h. The mixture was diluted with CH_2Cl_2 and washed with saturated NH_4Cl, and brine. The organic phase was dried over Na_2SO_4, filtered, and concentrated in vacuo. The crude mixture was purified with flash silica-gel column chromatography with 1:2 EtOAc:hexanes as eluent to provide 420 mg of the amide product (98% yield). R_f = 0.6 with 2:1 EtOAc:hexanes, colorless oil. $[\alpha]^{20}_D = -10$ (c = 0.15, $CHCl_3$), ^{1}H-NMR (300 MHz, $CDCl_3$) δ = 8.74 (d, *J* = 4.9 Hz, 1 H), 8.39 (ddd, *J* = 0.7 Hz, *J* = 0.7 Hz, *J* = 0.7 Hz, 1 H), 8.22 (bd, *J* = 9.0 Hz, 1 H), 7.64 (ddd, *J* = 4.9 Hz, *J* = 0.7 Hz, *J* = 0.7 Hz, 1 H), 4.07-3.86 (m, 2 H), 3.73-3.65 (m, 1 H), 2.71 (bs, 1 H), 1.03 (s, 9 H). ^{13}C-NMR (75 MHz, $CDCl_3$) δ = 164.1, 151.3, 149.4, 140.1 (q, *J* = 34.6 Hz), 122.7 (q, *J* = 273.6 Hz), 122.0 (q, *J* = 3.3 Hz), 118.6 (q, *J* = 3.3 Hz), 63.3, 60.5,

34.0, 27.1. IR: 3380, 2963, 1671, 1530, 1329, 1140, 667 cm^{-1}. HRMS $C_{13}H_{17}N_2O_2F_3$ $(M+Na)^+$ calcd. 313.1140, obsvd. 313.1148.

Preparation of (*S*)-4-CF_3-pyrox-*t*Bu 29[46]

To a dry 100 mL round bottom flask were added 290 mg peptide **45** (1.00 mmol, 1 equiv.), 25 mg of DMAP (0.20 mmol, 0.20 equiv.), 10 mL of dichloroethane, and 560 μL triethylamine. In a separate flask, 195 mg of *p*-toluenesulfonyl chloride (1.02 mmol, 1.02 equiv.) were dissolved in 5 mL of dichloroethane. The solution of *p*-toluenesulfonyl chloride was transferred dropwise via cannula to the reaction mixture. An additional 5 mL dichloroethane were used for rinsing. The reaction mixture was stirred at rt until **45** was consumed, as determined by TLC analysis, and then heated to reflux for 12 h. The reaction mixture was diluted with CH_2Cl_2 and washed with saturated $NaHCO_3$ and brine. The organic phase was dried over Na_2SO_4, filtered, and concentrated in vacuo. The crude mixture was purified with flash silica column chromatography with 1:2 EtOAc:hexanes as eluent to provide 214 mg of the product (79% yield). R_f = 0.4 with 1:1 EtOAc:hexanes (silica TLC), R_f = 0.5 with 1:1 acetone:hexanes (alumina TLC), white solid. mp = 56-59 °C, $[\alpha]^{20}_D$ = –62.6 (c = 0.33, $CHCl_3$), ^{1}H-NMR (300 MHz, $CDCl_3$) δ = 8.89 (d, *J* = 4.9 Hz, 1 H), 8.31 (d, *J* = 0.9 Hz, 1 H), 7.61 (ddd, *J* = 4.9 Hz, *J* = 0.9 Hz, 1 H), 4.49 (dd, *J* = 10.3 Hz, *J* = 8.8 Hz, 1 H), 4.35 (dd, *J* = 8.6 Hz, *J* = 8.6 Hz, 1 H), 4.16 (dd, *J* = 10.3 Hz, *J* = 8.4 Hz, 1 H), 0.99 (s, 9 H). ^{13}C-NMR (75 MHz, $CDCl_3$) δ = 161.7, 150.9, 148.5, 139.3 (q, *J* = 34.6 Hz), 122.7 (q, *J* = 273.6 Hz), 121.1 (q, *J* = 3.3 Hz), 120.0 (q, *J* = 3.3 Hz), 77.4, 69.8, 34.2, 26.1. IR: 2956, 2906, 2871, 1646, 1324, 1252, 1138, 1082, 666 cm^{-1}. HRMS $C_{13}H_{15}N_2OF_3$ $(M+Na)^+$ calcd. 295.1034, obsvd. 295.1040.

Preparation of peptide 46 (R = Cl)[45]

To a dry 100 mL round bottom flask were added 473 mg 4-chloropicolinic acid (3.00 mmol, 1 equiv.), 15 mL CH_2Cl_2, and 500 μL *N*-methylmorpholine (4.50 mmol, 1.50 equiv.). The reaction mixture was cooled to 0 °C in an ice bath, and 480 μL of *iso*-butyl chloroformate (3.60 mmol, 1.20 equiv.) were added dropwise, and the reaction mixture was stirred for 30 min at 0 °C. In a separate flask, 386 mg of (*S*)-*tert*-leucinol **44** (3.30 mmol, 1.10 equiv.) were dissolved in 5 mL of CH_2Cl_2, and 430 μL of *N*-methylmorpholine (3.90 mmol, 1.30 equiv.) were added. This solution was transferred dropwise via cannula to the reaction flask at 0 °C. The mixture was allowed to warm to rt and stirred for 3 h. The mixture was diluted with CH_2Cl_2 and washed with 1 M HCl, water, and brine. The organic phase was dried over Na_2SO_4, filtered, and concentrated in vacuo. The crude mixture was purified with flash silica-gel column chromatography with 1:2 EtOAc:hexanes to 1:1 EtOAc:hexanes as eluent to provide 696 mg of the amide product (90% yield). R_f = 0.45 with 2:1 EtOAc:hexanes, colorless oil. $[\alpha]^{20}_D$ = –9.5 (c = 0.39, $CHCl_3$), ^{1}H-NMR (300 MHz, $CDCl_3$) δ = 8.43 (dd, *J* = 5.3 Hz, *J* = 0.6 Hz, 1 H), 8.16 (dd, *J* = 2.2 Hz, *J* = 0.6 Hz, 1 H), 7.41 (dd, *J* = 5.3 Hz, *J* = 2.2 Hz, 1 H), 4.00-3.91 (m, 2 H), 3.70-3.61 (m, 1H), 2.43 (bs, 1 H), 1.01 (s, 9 H). ^{13}C-NMR (75 MHz, $CDCl_3$) δ = 164.3, 151.3, 149.2, 146.0, 126.5, 123.1, 63.1, 60.4, 34.0, 27.1. IR: 3375, 2961, 1667, 1526, 1462, 1233, 1053, 736 cm^{-1}. HRMS $C_{12}H_{17}ClN_2O_2$ $(M+Na)^+$ calcd. 279.0876, obsvd. 279.0883.

Preparation of (*S*)-4-Cl-pyrox-*t*Bu 30[46]

To a dry 100 mL round bottom flask were added 450 mg peptide **46** (1.75 mmol, 1 equiv.), 10 mg of DMAP (0.08 mmol, 0,05 equiv.), 20 mL of dichloroethane, and 980

μL triethylamine. In a separate flask, 468 mg of *p*-toluenesulfonyl chloride (2.45 mmol, 1.40 equiv.) were dissolved in 8 mL of dichloroethane. The solution of *p*-toluenesulfonyl chloride was transferred dropwise via cannula to the reaction mixture. An additional 8 mL dichloroethane were used for rinsing. The reaction mixture was stirred at rt until **46** was consumed, as determined by TLC analysis, and then heated to reflux for 12 h. The reaction mixture was diluted with CH_2Cl_2 and washed with saturated $NaHCO_3$ and brine. The organic phase was dried over Na_2SO_4, filtered, and concentrated in vacuo. The crude mixture was purified with flash silica-gel column chromatography with 1:2 EtOAc:hexanes to 1:1 EtOAc:hexanes as eluent to provide 229 mg of the product (55% yield). R_f = 0.3 with 1:2 EtOAc:hexanes, white solid. mp = 61-64 °C $[\alpha]^{20}_D$ = –61.6 (c = 0.36, $CHCl_3$), ^{1}H-NMR (300 MHz, $CDCl_3$) δ = 8.58 (d, *J* = 5.3 Hz, 1 H), 8.08 (dd, *J* = 2.2 Hz, 1 H), 7.37 (dd, *J* = 5.3 Hz, *J* = 2.0 Hz, 1 H), 4.44 (dd, *J* = 10.3 Hz, *J* = 8.8 Hz, 1 H), 4.29 (dd, *J* = 8.5 Hz, *J* = 8.5 Hz, 1 H), 4.11 (dd, *J* = 10.3 Hz, *J* = 8.4 Hz, 1 H), 0.95 (s, 9 H). ^{13}C-NMR (75 MHz, $CDCl_3$) δ = 161.7, 150.7, 148.4, 144.9, 125.8, 124.5, 76.8, 69.7, 34.1, 26.1. IR: 2955, 2904, 2869, 1645, 1574, 1555, 1415, 1351, 1257, 966, 769 cm^{-1}. HRMS $C_{12}H_{15}ClN_2O$ $(M+Na)^+$ calcd. 261.0771, obsvd. 261.0781.

Preparation of peptide 47 (R = Me)[45]

To a dry 100 mL round bottom flask were added 320 mg 4-methylpicolinic acid (2.33 mmol, 1 equiv.), 15 mL CH_2Cl_2, and 388 μL *N*-methylmorpholine (3.49 mmol, 1.50 equiv.). The reaction mixture was cooled to 0 °C in an ice bath, 370 μL of *iso*-butyl chloroformate (2.79 mmol, 1.20 equiv.) were added dropwise, and the reaction mixture was stirred for 30 min at 0 °C. In a separate flask, 300 mg of (*S*)-*tert*-leucinol **44** (2.56 mmol, 1.10 equiv.) were dissolved in 5 mL of CH_2Cl_2, and 336 μL of *N*-

methylmorpholine (3.03 mmol, 1.30 equiv.) were added. This solution was transferred dropwise via cannula to the reaction flask at 0 °C. The mixture was allowed to warm to rt and stirred for 3 h. The mixture was diluted with CH_2Cl_2 and washed with saturated NH_4Cl, and brine. The organic phase was dried over Na_2SO_4, filtered, and concentrated in vacuo. The crude mixture was purified with flash silica-gel column chromatography with 1:3 EtOAc:hexanes to 1:1 EtOAc:hexanes as eluent to provide 487 mg of the amide product (88% yield). $R_f = 0.3$ with 2:1 EtOAc:hexanes, colorless oil. $[\alpha]^{20}_D = -17$ (c = 0.13, $CHCl_3$), ^{1}H-NMR (300 MHz, $CDCl_3$) δ = 8.38 (dd, J = 4.9 Hz, J = 0.6 Hz, 1 H), 8.30 (bd, J = 8.2 Hz, 1 H), 7.98 (ddd, J = 0.7 Hz, J = 0.7 Hz, J = 0.7 Hz, 1 H), 7.21 (ddd, J = 4.9 Hz, J = 0.7 Hz, J = 0.7 Hz, 1 H), 4.02-3.86 (m, 2 H), 3.67 (dd, J = 10.6 Hz, J = 8.4 Hz, 1 H), 2.94 (bs, 1 H), 2.40 (s, 3 H), 1.03 (s, 9 H). ^{13}C-NMR (75 MHz, $CDCl_3$) δ = 166.0, 149.6, 149.1, 148.1, 127.2, 123.4, 63.7, 60.6, 33.9, 27.2, 21.3. IR: 3373, 2960, 1664, 1525, 1473, 1205 cm^{-1}. HRMS $C_{13}H_{21}N_2O_2$ $(M+H)^+$ calcd. 237.1603, obsvd. 237.1611.

Preparation of (*S*)-4-Me-pyrox-*t*Bu 32[46]

To a dry 100 mL round bottom flask were added 274 mg peptide **47** (1.16 mmol, 1 equiv.), 28.3 mg of DMAP (0.23 mmol, 0.20 equiv.), 15 mL of dichloroethane, and 650 μL triethylamine. In a separate flask, 243 mg of *p*-toluenesulfonyl chloride (1.28 mmol, 1.10 equiv.) were dissolved in 5 mL of dichloroethane. The solution of *p*-toluenesulfonyl chloride was transferred dropwise via cannula to the reaction mixture. An additional 5 mL dichloroethane were used for rinsing. The reaction mixture was stirred at rt until **47** was consumed, as determined by TLC analysis, and then heated to reflux for 12 h. The reaction mixture was diluted with CH_2Cl_2 and washed with saturated $NaHCO_3$ and brine.

The organic phase was dried over Na_2SO_4, filtered, and concentrated in vacuo. The crude mixture was purified with flash alumina column chromatography with 1:4 acetone:hexanes as eluent to provide 191 mg of the product (75% yield). R_f = 0.2 with 1:2 EtOAc:hexanes (silica TLC), R_f = 0.5 with 1:1 acetone:hexanes (alumina TLC), clear oil. $[\alpha]^{20}_D$ = –78° (c = 0.24, $CHCl_3$), ^{1}H-NMR (300 MHz, $CDCl_3$) δ = 8.54 (d, *J* = 4.9 Hz, 1 H), 7.92 (d, *J* = 0.7 Hz, 1 H), 7.19 (ddd, *J* = 4.9 Hz, *J* = 0.7 Hz, *J* = 0.7 Hz, 1 H), 4.43 (dd, *J* = 10.3 Hz, *J* = 8.8 Hz, 1 H), 4.29 (dd, *J* = 8.5 Hz, *J* = 8.5 Hz, 1 H), 4.10 (dd, *J* = 10.3 Hz, *J* = 8.2 Hz, 1 H), 2.39 (s, 3 H), 0.96 (s, 9 H). ^{13}C-NMR (75 MHz, $CDCl_3$) δ = 162.9, 149.6, 148.1, 146.9, 126.6, 125.0, 69.4, 34.1, 26.1, 24.9, 21.1. IR 2953, 2903, 2868, 1644, 1604, 1476, 1196, 969.6, 841.5 cm^{-1}. HRMS $C_{13}H_{18}N_2O$ $(M+Na)^+$ calcd. 241.1317, obsvd. 241.1323.

Ligand **33** was prepared as illustrated in Figure 3.38. A full description of this procedure, and characterization data for intermediate **48** and ligand **33**, are provided below.

Preparation of peptide 48 (R = OMe)

To a dry 50 mL round bottom flask were added 100 mg 4-methoxypicolinic acid (0.653 mmol, 1 equiv.), 76.5 mg (*S*)-*tert*-leucinol **44** (0.653 mmol, 1 equiv.), 100 mg of HOBt hydrate (0.653 mmol, 1 equiv.), and 6 mL DMF. The reaction mixture was cooled to 0 °C in an ice bath. In a separate flask, 132 mg of EDCI·HCl were dissolved in 3 mL of DMF and 300 μL triethylamine (2.15 mmol, 3.3 equiv.). The solution of EDCI was added to the reaction mixture via syringe. An additional 2 mL (2 x 1 mL) of DMF were

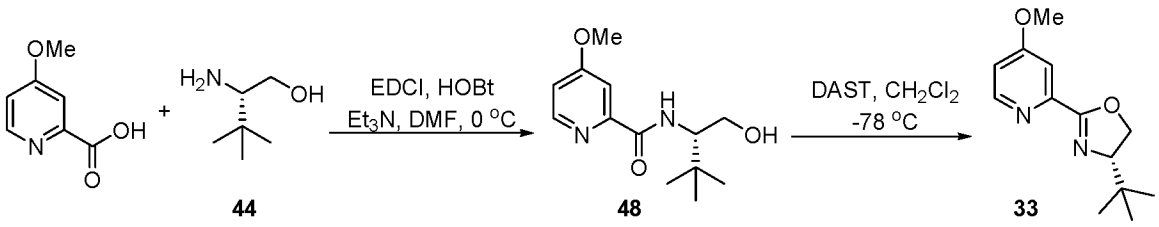

Figure 3.38. Synthesis of ligand **33**.

used for rinsing. The reaction mixture was stirred at 0 °C for 30 min then warmed to rt. The reaction mixture was diluted with EtOAc and washed thrice with water, saturated $NHCO_3$, and brine. The organic phase was dried over Na_2SO_4, filtered, and concentrated in vacuo. The crude mixture was purified with flash silica-gel column chromatography with 1:5 to 1:2 acetone:hexanes as eluent to provide 81.2 mg of the amide product (49% yield). R_f = 0.6 with 1:1 acetone:hexanes, colorless oil. $[\alpha]^{20}_D$ = –9.0 (c = 0.13, $CHCl_3$), ^{1}H-NMR (300 MHz, $CDCl_3$) δ = 8.35 (dd, *J* = 5.7 Hz, *J* = 0.6 Hz, 1 H), 8.24 (bs, 1H), 7.74 (d, *J* = 2.2 Hz, 1 H), 6.93 (dd, *J* = 5.7 Hz, *J* = 2.6, 1 H), 4.02-3.95 (m, 2 H), 3.91 (s, 3 H), 3.69 (dd, *J* = 9.5 Hz, *J* = 9.5 Hz, 1 H), 2.60 (bs, 1 H), 1.04 (s, 9 H). ^{13}C-NMR (75 MHz, $CDCl_3$) δ = 167.15, 165.6, 151.9, 149.4, 113.2, 107.7, 64.5, 60.6, 55.7, 34.0, 27.2. IR: 3366, 2960, 1659, 1596, 1520, 1305, 1031, 839 cm^{-1}. HRMS $C_{13}H_{20}N_2O_3$ $(M+Na)^+$ calcd. 275.1372, obsvd. 275.1374.

Preparation of (*S*)-4-OMe-pyrox-*t*Bu 33[47]

To a dry 50 mL round bottom flask were added 74 mg of peptide **48** (0.293 mmol, 1 equiv.) and 4 mL of CH_2Cl_2. The reaction mixture was cooled to –78 °C and 54 μL of DAST (0.41 mmol, 1.4 equiv.) were added dropwise. The reaction mixture was stirred at -78 °C for 1 h and 81 mg of K_2CO_3 (0.59 mmol, 2.0 equiv.) were added all at once. The mixture was warmed to rt, diluted with CH_2Cl_2, and washed with saturated $NaHCO_3$ and

brine. The organic phase was dried over Na_2SO_4, filtered, and concentrated in vacuo. The crude mixture was purified with flash alumina column chromatography with 1:2 to 1:1 EtOAc:hexanes as eluent to provide 62 mg of the product (91% yield). R_f = 0.4 with 1:1 acetone:hexanes (silica TLC), R_f = 0.35 with 1:1 EtOAc:hexanes (alumina TLC), colorless oil. $[\alpha]^{20}_D$ = –51 (c = 0.25, $CHCl_3$), ^{1}H-NMR (300 MHz, $CDCl_3$) δ = 8.47 (d, *J* = 5.7 Hz, 1 H), 7.58 (d, *J* = 2.6 Hz, 1 H), 6.87 (dd, *J* = 5.7 Hz, *J* = 2.6 Hz, 1 H), 4.42 (dd, *J* = 10.3 Hz, *J* = 8.6 Hz, 1 H), 4.28 (dd, *J* = 8.6 Hz, *J* = 8.6 Hz, 1 H), 4.09 (dd, *J* = 10.3 Hz, *J* = 8.4 Hz, 1 H), 3.89 (s, 3 H), 0.95 (s, 9 H). ^{13}C-NMR (75 MHz, $CDCl_3$) δ = 166.2, 162.7, 151.0, 148.7, 112.3, 109.6, 76.6, 69.4, 55.6, 34.1, 26.1. IR: 2954, 2904, 2869, 1646, 1592, 1569, 1476, 1313, 1081, 1033, 970, 847 cm^{-1}. HRMS $C_{13}H_{19}N_2O_2$ $(M+H)^+$ calcd. 235.1447, obsvd. 235.1451.

Evalutaion of pyrox-*t*Bu ligands:

For the evaluation of ligands (Table 3.7), four reactions were run simultaneously in separate 5 mL side-arm flasks attached to a four-neck cow fitted with a three way adaptor with a balloon of O_2 attached. A standard solution was prepared by the addition of 412.6 mg of the substrate **8** and 63.3 mg of the internal standard 2-methoxynaphthalene to a 2 mL volumetric flask, followed by the addition of MeOH. The flask was briefly sonicated to dissolve **8** and stirred to give a solution with [**8**] = 1.00 M and [2-methoxynaphthalene] = 0.20 M.

Each reaction was performed as described in the following example: to a 5 mL side-arm round bottom flask equipped with a stir bar were added 1.0 mg $Pd(MeCN)_2Cl_2$ (0.0040 mmol, 0.040 equiv.), 0.8 mg of CuCl (0.008 mmol, 0.08 equiv.), (*S*)-4-R-pyrox-*t*Bu **29-33** (0.014 mmol, 0.14 eqiuv), 4.0 mg of $KHCO_3$ (0.040 mmol, 0.40 equiv.), 400

μL of toluene, 400 μL of THF, and 100 μL MeOH. A three-way joint fitted with a balloon of O_2 was attached and the apparatus was evacuated (using house vacuum) and refilled with oxygen three times. The mixture was stirred vigorously for 30 min at rt. A 100 μL portion of the standard solution of **8** (0.100 mmol, 1 equiv.) and 2-methoxy naphthalene (0.020 mmol, 0.20 equiv.) was added dropwise to the reaction mixture. Aliquots (ca. 50 μL) of the reaction were taken periodically via syringe. Reaction samples were passed through a short silica plug eluting with 2 mL of EtOAc and analyzed by GC and referenced against a time zero sample containing the standard solution of **8** and 2-methoxynaphthalene diluted in EtOAc. GC yields were calculated based on the ratio of product to internal standard corrected for the response factor. Enantiomeric and diastereomeric ratios were determined using GC with a column equipped with a chiral stationary phase. GC analysis: β-cyclodextrin column at 100 °C for 20 min, increased to 130 °C at 0.4 °C/min, held at 130 °C for 2 min, increased to 200 °C at 20 °C/min; retention times: 60.4 min, 61.9 min, 63.7 min, and 64.8 min.

References

(1) Jensen, K. H.; Pathak, T. P.; Zhang, Y.; Sigman, M. S. *J. Am. Chem. Soc.* **2009**, *131*, 17074.

(2) Tsuji, J. Oxidative Reactions with Pd(II) Compounds. In Palladium Reagents and Catalysts: New Perspectives for the 21st Century, John Wiley & Sons: New York, 2004; pp27.

(3) Van De Water, R. W.; Pettus, T. R. R. *Tetrahedron* **2002**, *58*, 5367.

(4) Bolon, D. A. *J. Org. Chem.* **1970**, *35*, 715.

(5) Sprengling, G. R. *J. Am. Chem. Soc.* **1952**, *74*, 2937.

(6) Schmidt, R. R.; Beitzke, B. *Synthesis* **1982**, 750.

(7) Dorrestijn, E.; Kranenburg, M.; Ciriano, M. V.; Mulder, P. *J. Org. Chem.* **1999**, *64*, 3012.

(8) Padwa, A.; Lee, G. A. *J. Am. Chem. Soc.* **1973**, *95*, 6147.

(9) Huang, C. G.; Beveridge, K. A.; Wan, P. *J. Am. Chem. Soc.* **1991**, *113*, 7676.

(10) Chiang, Y.; Kresge, A. J.; Zhu, Y. *J. Am. Chem. Soc.* **2000**, *122*, 9854.

(11) Inoue, T.; Inoue, S.; Sato, K. *Chem. Lett.* **1990**, 55.

(12) Van De Water, R. W.; Magdziak, D. J.; Chau, J. N.; Pettus, T. R. R. *J. Am. Chem. Soc.* **2000**, *122*, 6502.

(13) Arduini, A.; Bosi, A.; Pochini, A.; Ungaro, R. *Tetrahedron* **1985**, *41*, 3095.

(14) Shen, H. C. *Tetrahedron* **2009**, *65*, 3931.

(15) Selenski, C.; Pettus, T. R. R. *J. Org. Chem.* **2004**, *69*, 9196.

(16) Huang, Y.; Pettus, T. R. R. *Synlett* **2008**, 1353.

(17) Korthals, K. A.; Wulff, W. D. *J. Am. Chem. Soc.* **2008**, *130*, 2898.

(18) Crimmins, M. T.; Jung, D. K.; Gray, J. L. *J. Am. Chem. Soc.* **1993**, *115*, 3146.

(19) Takacs, J. M.; Jiang, X.-t. *Curr. Org. Chem.* **2003**, *7*, 369.

(20) Tsuji, J. Oxidative Reactions with Pd(II) Compounds. In Palladium Reagents and Catalysts: New Perspectives for the 21st Century, John Wiley & Sons: New York, 2004; pp27

(21) Hosokawa, T.; Nomura, T.; Murahashi, S.-I. *J. Organomet. Chem.* **1998**, *551*, 387.

(22) Hosokawa, T.; Takano, M.; Murahashi, S.-I. *J. Am. Chem. Soc.* **1996**, *118*, 3990.

(23) Kawamura, Y.; Kawano, Y.; Matsuda, T.; Ishitobi, Y.; Hosokawa, T. *J. Org. Chem.* **2009**, *74*, 3048.

(24) Zhang, Y.; Sigman, M. S. *J. Am. Chem. Soc.* **2007**, *129*, 3076.

(25) Trend, R. M.; Ramtohul, Y. K.; Stoltz, B. M. *J. Am. Chem. Soc.* **2005**, *127*, 17778.

(26) Steinhoff, B. A.; Stahl, S. S. *J. Am. Chem. Soc.* **2006**, *128*, 4348.

(27) Increasing [MeOH] at high [substrate], high [Cu] results in a system that becomes limited by the rate of mass transport of molecular oxygen.

(28) Balla, J.; Kiss, T.; Jameson, R. F. *Inorg. Chem.* **1992**, *31*, 58.

(29) King, E. L.; Altman, C. *J. Phys. Chem.* **1956**, *60*, 1375.

(30) Kopach, M. E.; Harman, W. D. *J. Am. Chem. Soc.* **1994**, *116*, 6581.

(31) Stokes, S. M., Jr.; Ding, F.; Smith, P. L.; Keane, J. M.; Kopach, M. E.; Jervis, R.; Sabat, M.; Harman, W. D. *Organometallics* **2003**, *22*, 4170.

(32) Todd, M. A.; Grachan, M. L.; Sabat, M.; Myers, W. H.; Harman, W. D. *Organometallics* **2006**, *25*, 3948.

(33) Lev, D. A.; Grotjahn, D. B.; Amouri, H. *Organometallics* **2005**, *24*, 4232.

(34) Jaffe, H. H. *J. Am. Chem. Soc.* **1954**, *76*, 4261.

(35) Edwards, D. R.; Neverov, A. A.; Brown, R. S. *J. Am. Chem. Soc.* **2009**, *131*, 368.

(36) Smith, L. I.; Davis, H. R., Jr.; Sogn, A. W. *J. Am. Chem. Soc.* **1950**, *72*, 3651.

(37) Schultz, M. J.; Sigman, M. S. *J. Am. Chem. Soc.* **2006**, *128*, 1460.

(38) Palucki, M.; Finney, N. S.; Pospisil, P. J.; Gueler, M. L.; Ishida, T.; Jacobsen, E. N. *J. Am. Chem. Soc.* **1998**, *120*, 948.

(39) Pathak, T. P.; Gligorich, K. M.; Welm, B. E.; Sigman, M. S. *J. Am. Chem. Soc.* **2010**, *132*, 7870.

(40) Braddock, D. C.; Cansell, G.; Hermitage, S. A. *Chem. Commun.* **2006**, 2483.

(41) Canhota, F. P.; Salomao, G. C.; Carvalho, N. M. F.; Antunes, O. A. C. *Catal. Commun.* **2007**, *9*, 182.

(42) Detoni, C.; Carvalho, N. M. F.; Aranda, D. A. G.; Louis, B.; Antunes, O. A. C. *Appl. Catal., A* **2009**, *365*, 281.

(43) Podhajsky, S. M.; Sigman, M. S. *Organometallics* **2007**, *26*, 5680.

(44) Cheng, J.; Deming, T. J. *Macromolecules* **1999**, *32*, 4745.

(45) Anderson, G. W.; Zimmerman, J. E.; Callahan, F. M. *J. Am. Chem. Soc.* **1967**, *89*, 5012.

(46) Evans, D. A.; Peterson, G. S.; Johnson, J. S.; Barnes, D. M.; Campos, K. R.; Woerpel, K. A. *J. Org. Chem.* **1998**, *63*, 4541.

(47) Wipf, P.; Fritch, P. C. *J. Am. Chem. Soc.* **1996**, *118*, 12358.

APPENDIX A

NMR SPECTRA

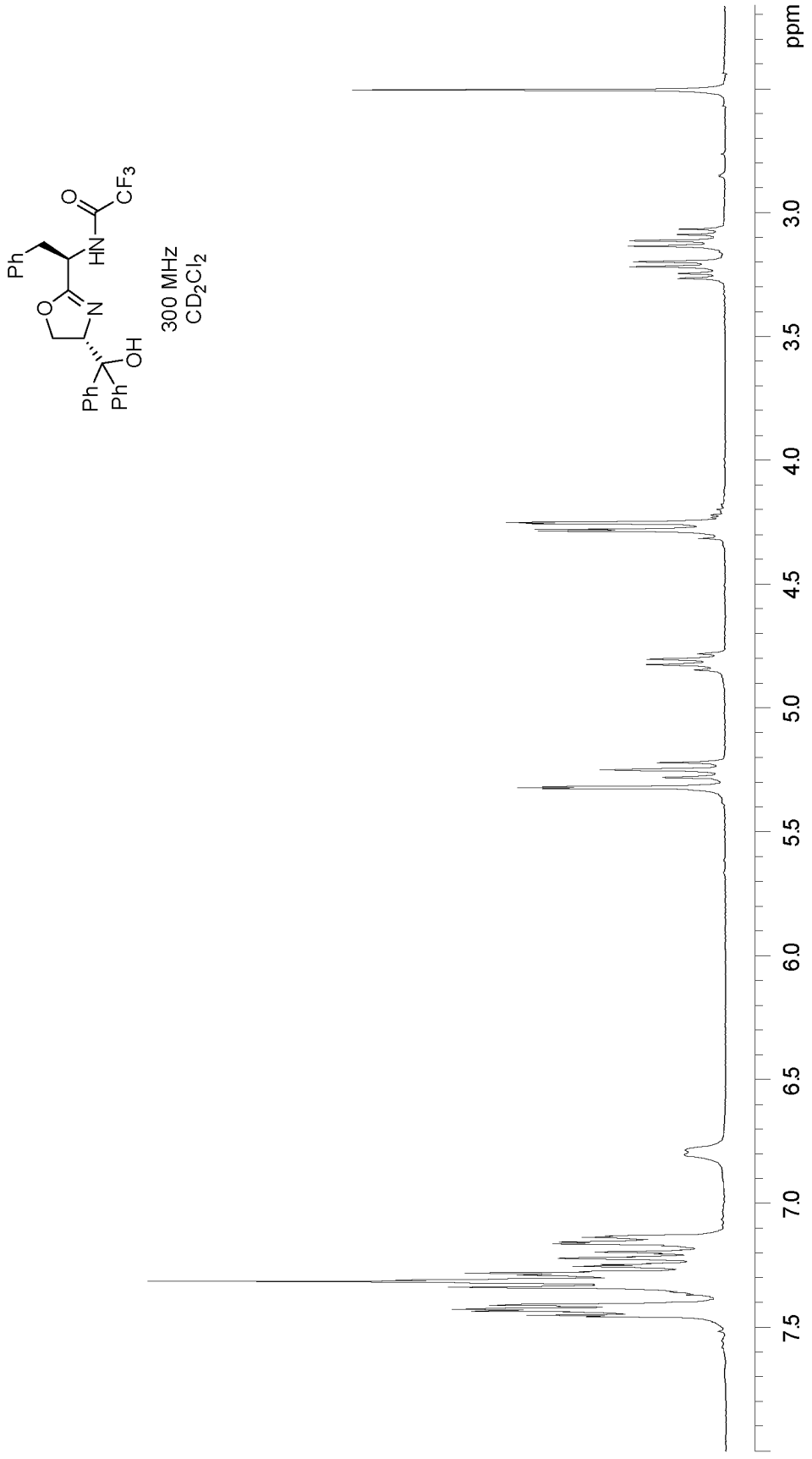
Ph
HN
O
CF3
O
N
Ph
Ph
OH
300 MHz
CD2Cl2
ppm
7.5
7.0
6.5
6.0
5.5
5.0
4.5
4.0
3.5
3.0

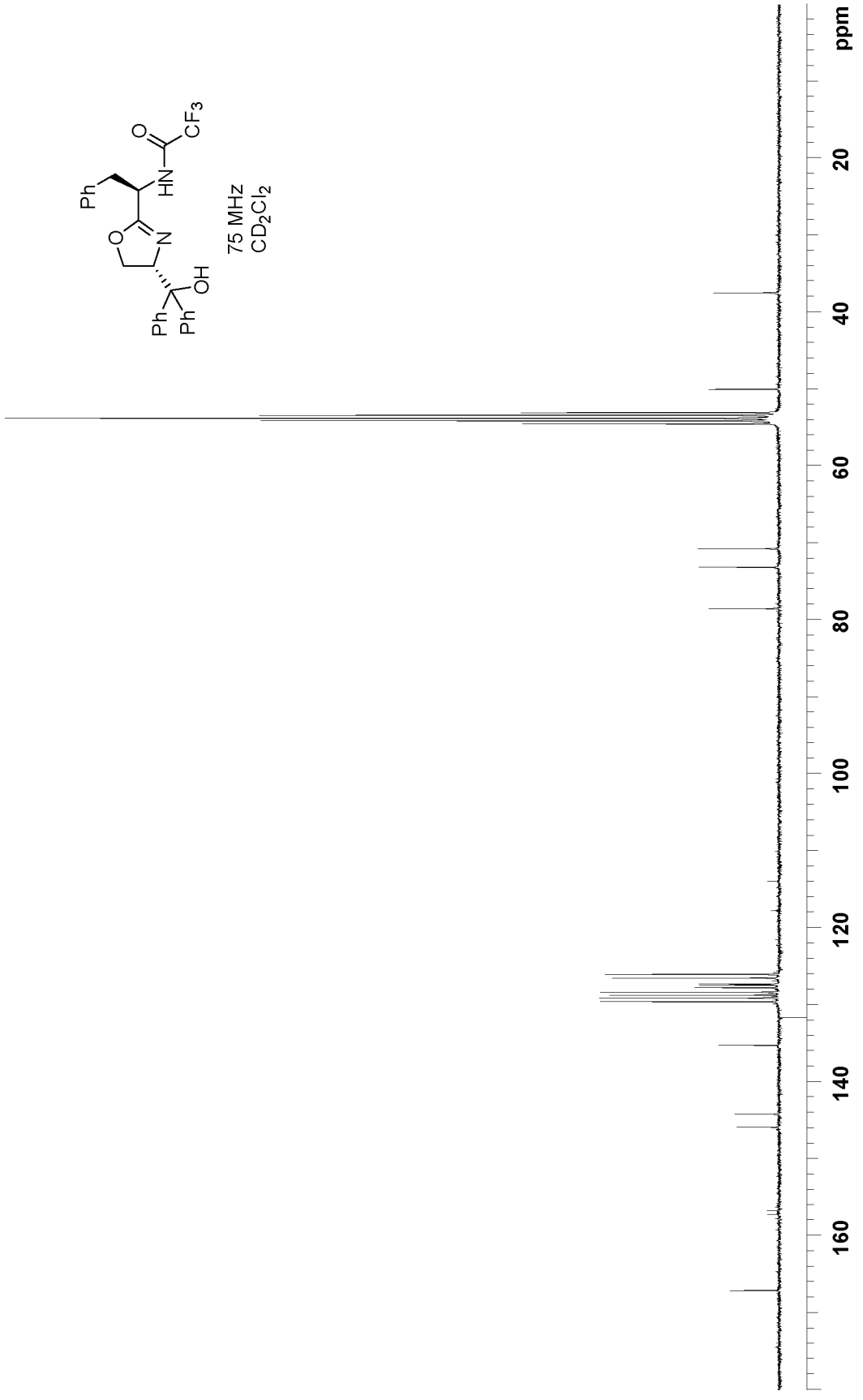
75 MHz
CD_2Cl_2
ppm
160
140
120
100
80
60
40
20

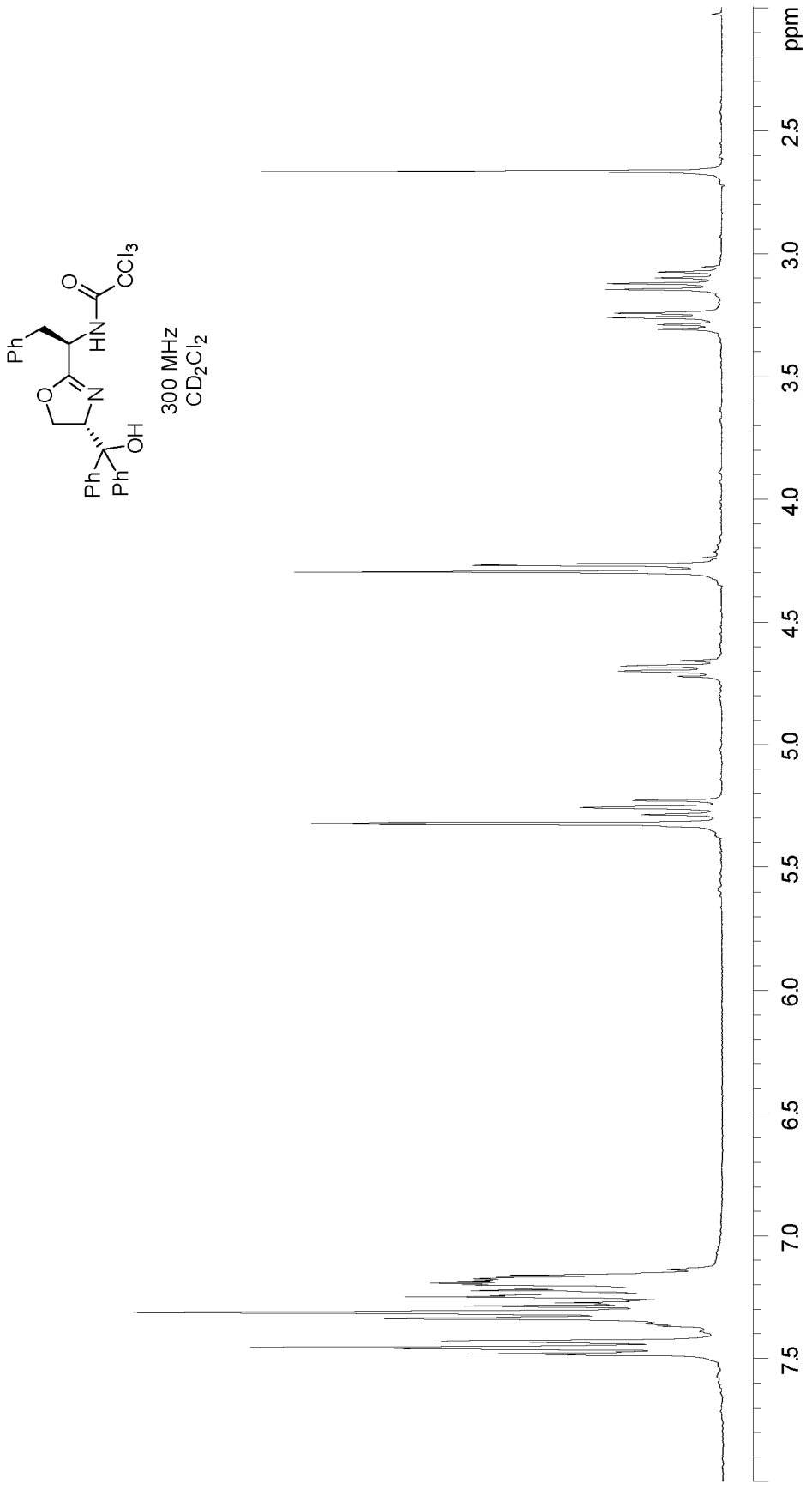
Ph
HN
O
CCl3
N
O
Ph
Ph
OH
300 MHz
CD2Cl2
ppm
2.5
3.0
3.5
4.0
4.5
5.0
5.5
6.0
6.5
7.0
7.5

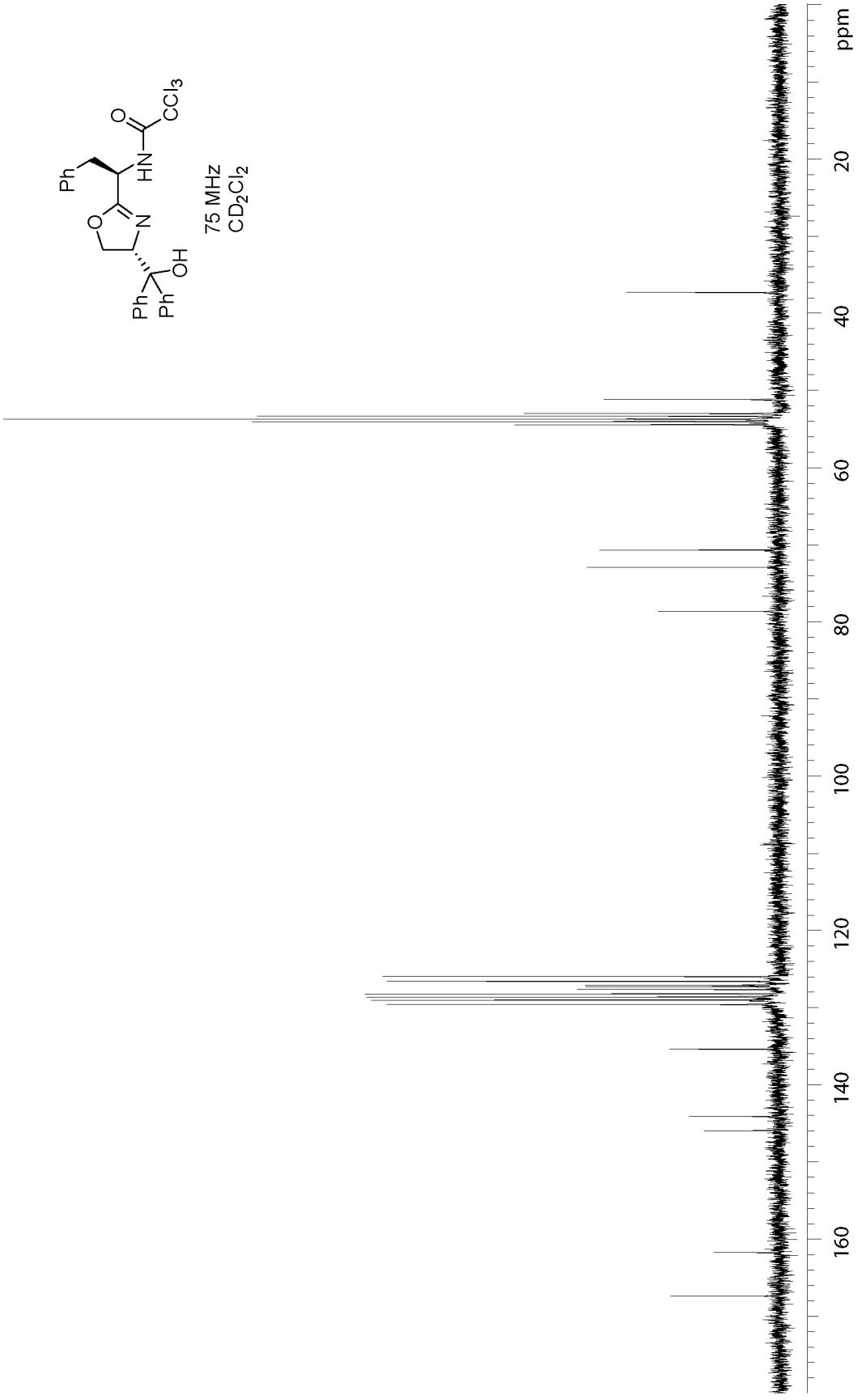
75 MHz
CD_2Cl_2
ppm
20
40
60
80
100
120
140
160

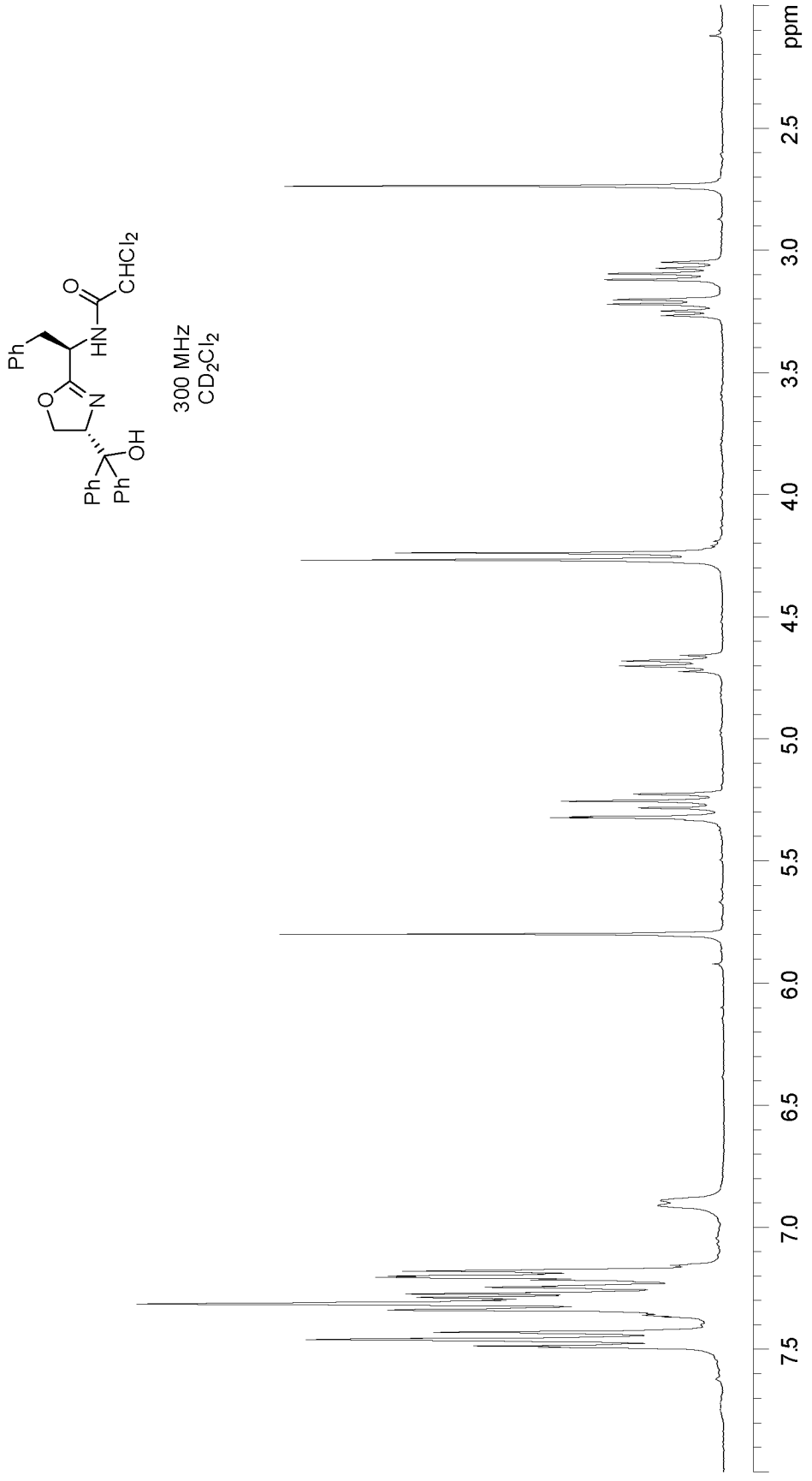
Ph
HN
O
CHCl2
O
N
Ph
Ph
OH
300 MHz
CD2Cl2
7.5
7.0
6.5
6.0
5.5
5.0
4.5
4.0
3.5
3.0
2.5
ppm

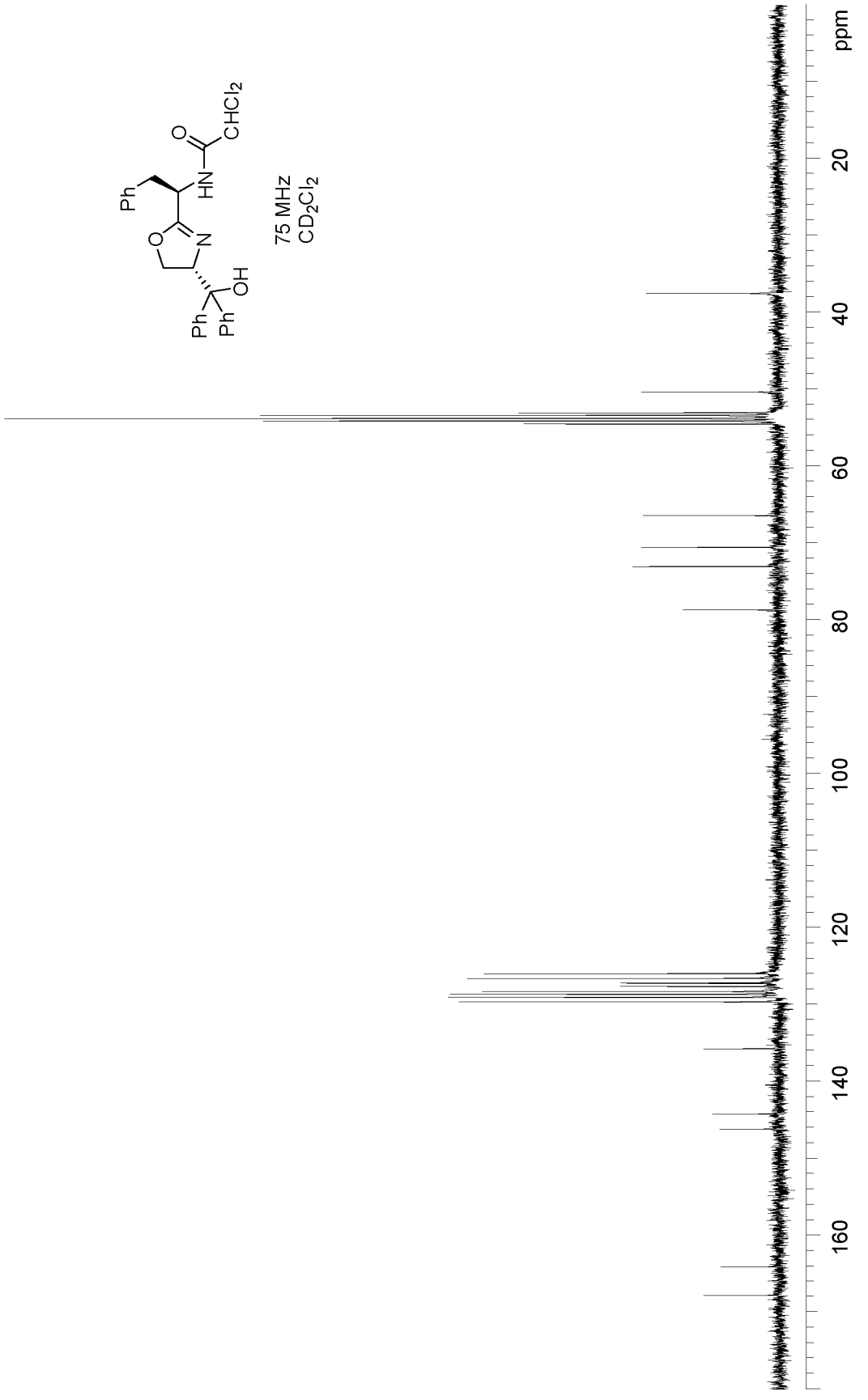
75 MHz
CD_2Cl_2
Ph
HN
O
$CHCl_2$
O
N
Ph
Ph
OH
ppm
20
40
60
80
100
120
140
160

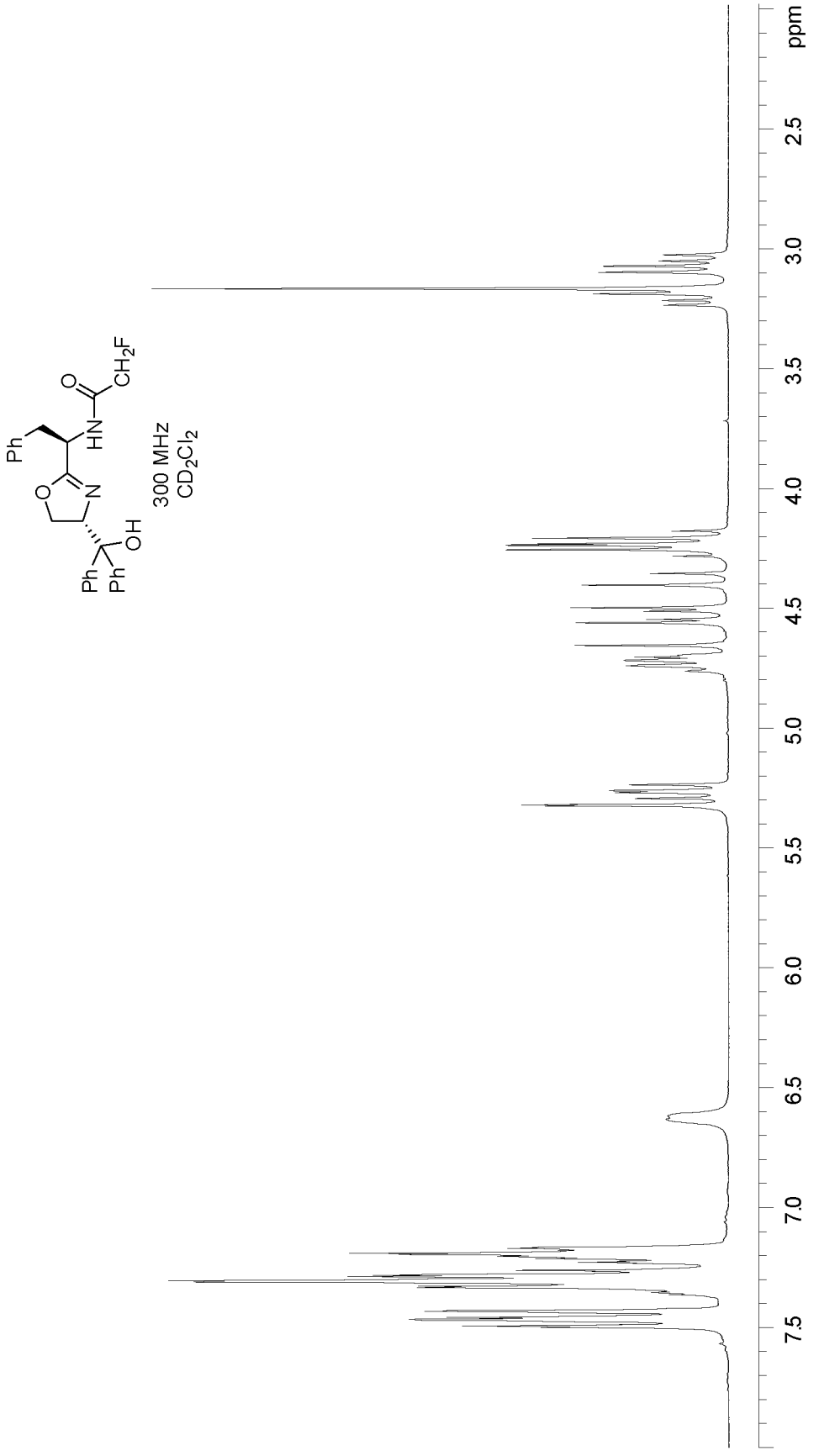
Ph
HN
O
CH2F
O
N
Ph
Ph
OH
300 MHz
CD2Cl2
ppm
7.5
7.0
6.5
6.0
5.5
5.0
4.5
4.0
3.5
3.0
2.5

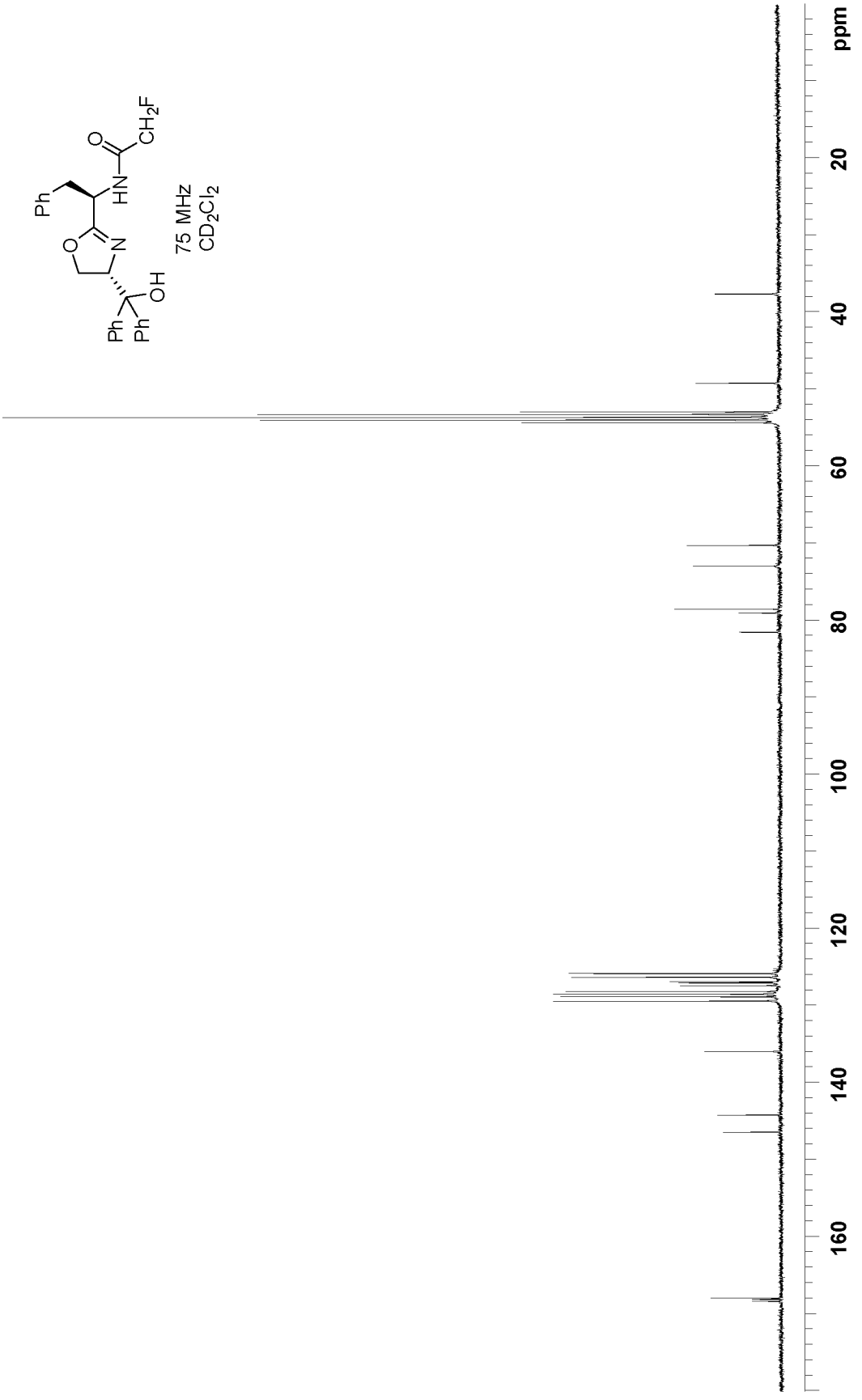
Ph
HN
O
CH2F
O
N
OH
Ph
Ph
75 MHz
CD2Cl2
ppm
20
40
60
80
100
120
140
160

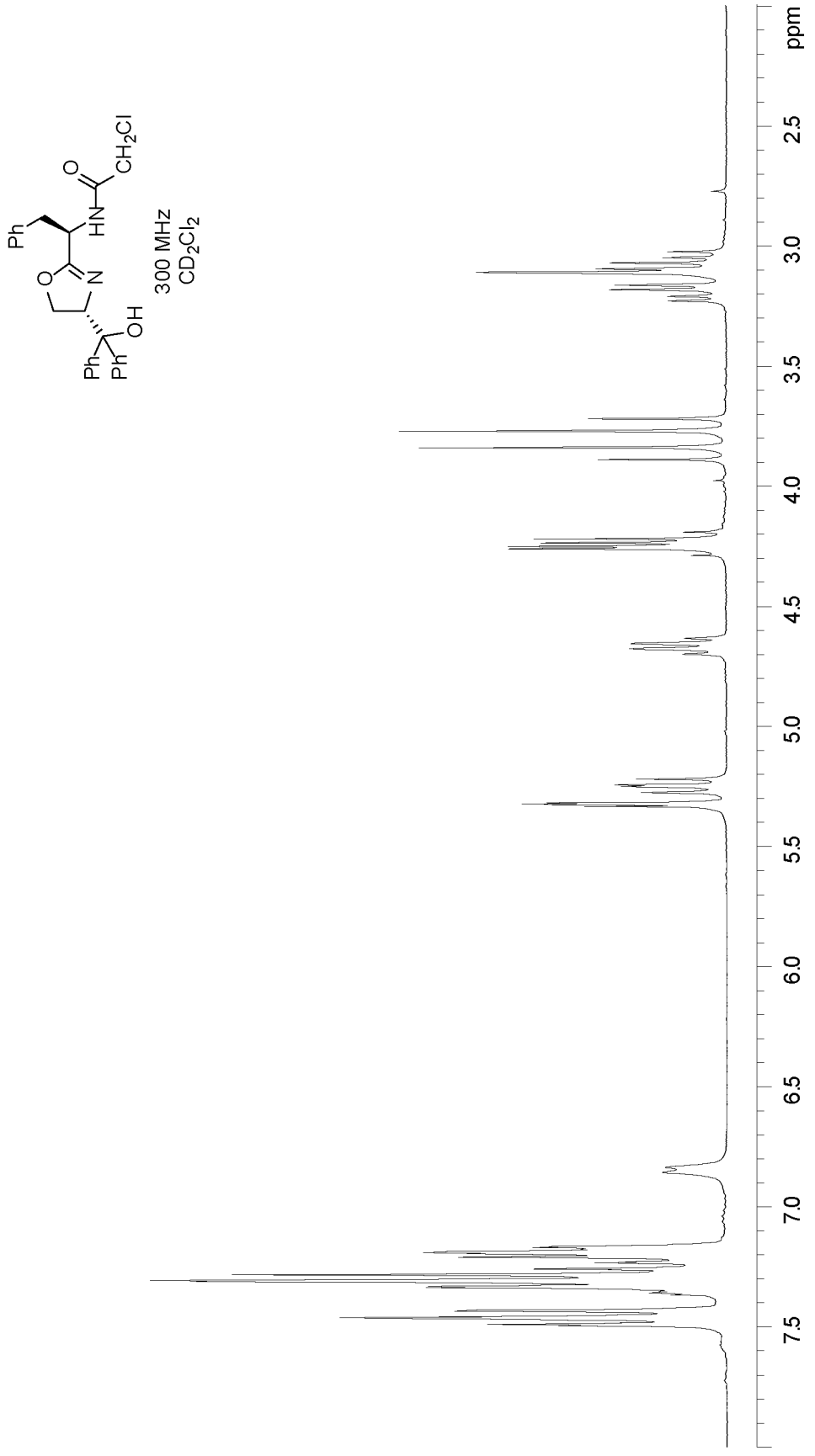
Ph
HN
O
CH2Cl
O
N
OH
Ph
Ph
300 MHz
CD2Cl2
ppm
7.5
7.0
6.5
6.0
5.5
5.0
4.5
4.0
3.5
3.0
2.5

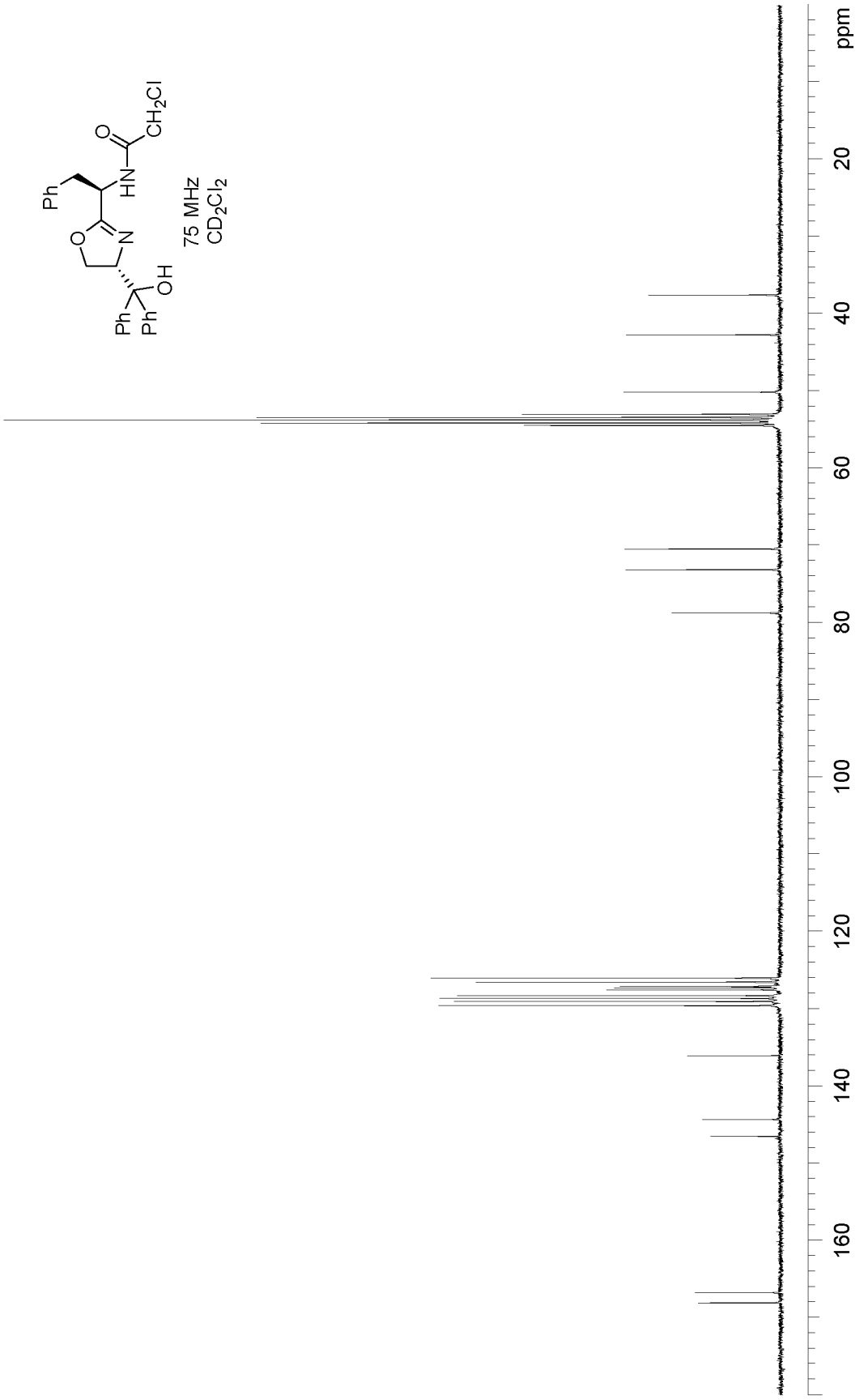
Ph
HN
O
CH2Cl
O
N
Ph
Ph
OH
75 MHz
CD2Cl2
ppm
20
40
60
80
100
120
140
160

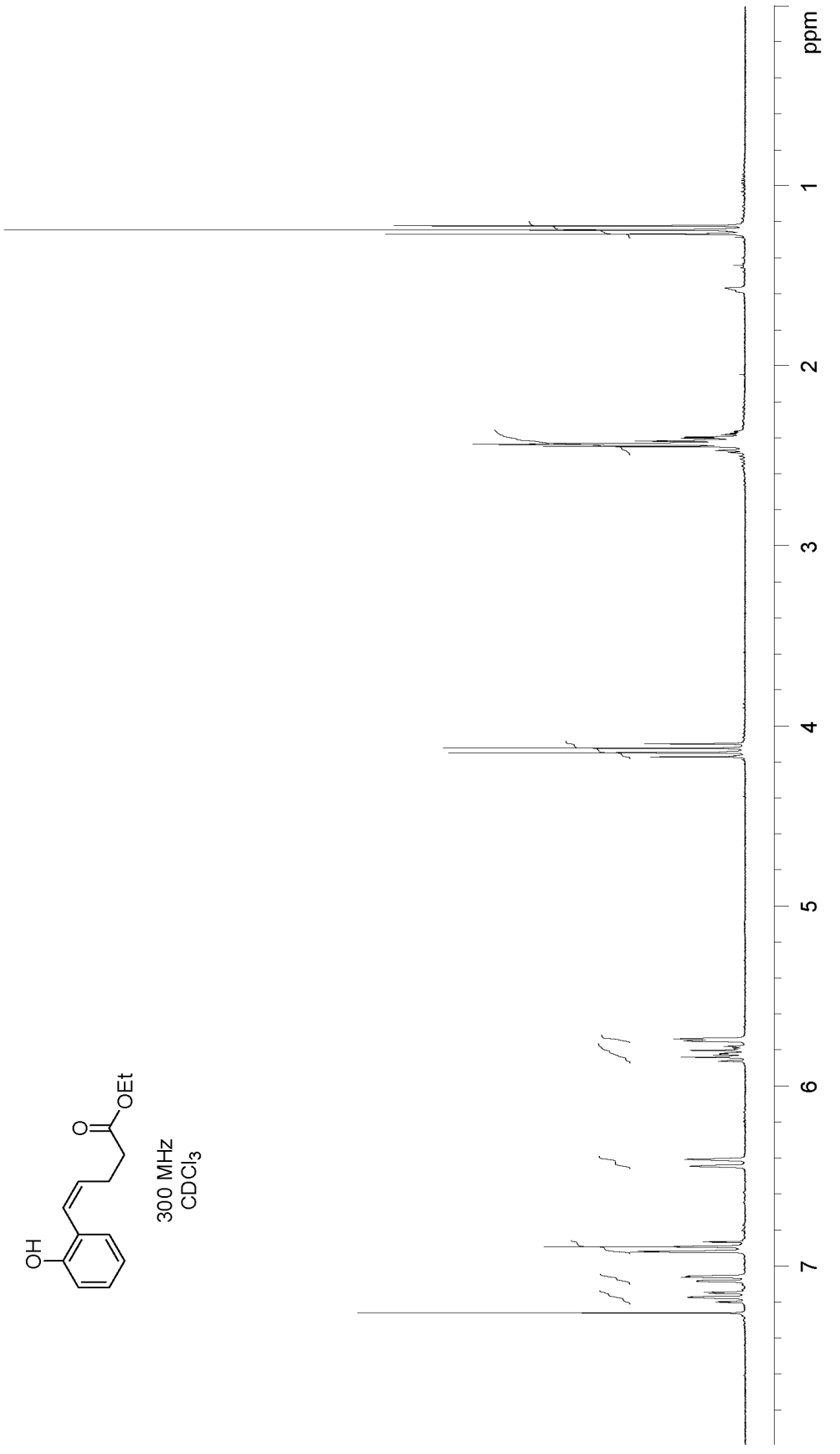
OH
O
OEt
300 MHz
CDCl3
ppm
1
2
3
4
5
6
7

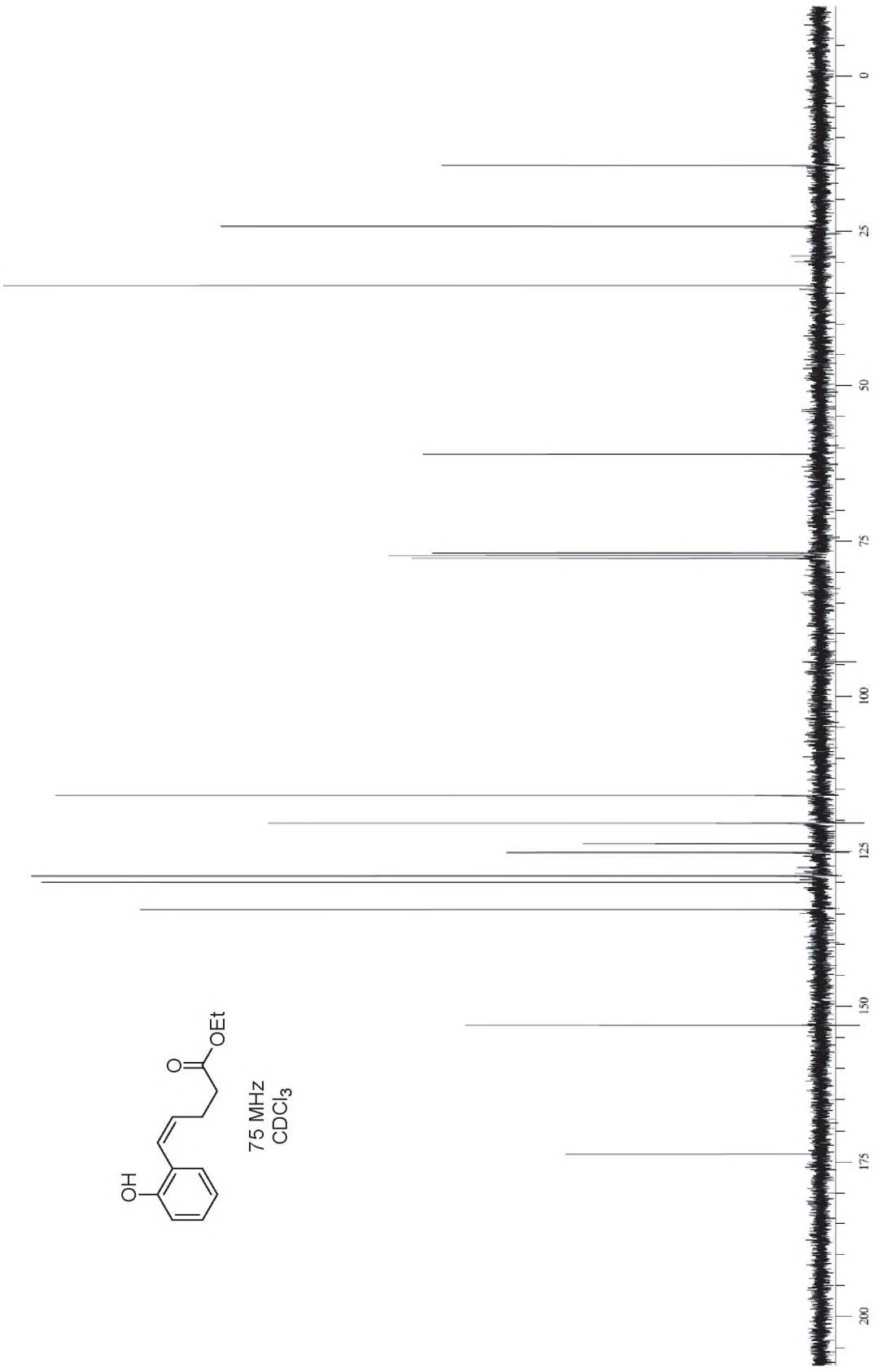
OEt
O
OH
75 MHz
CDCl3
0
25
50
75
100
125
150
175
200

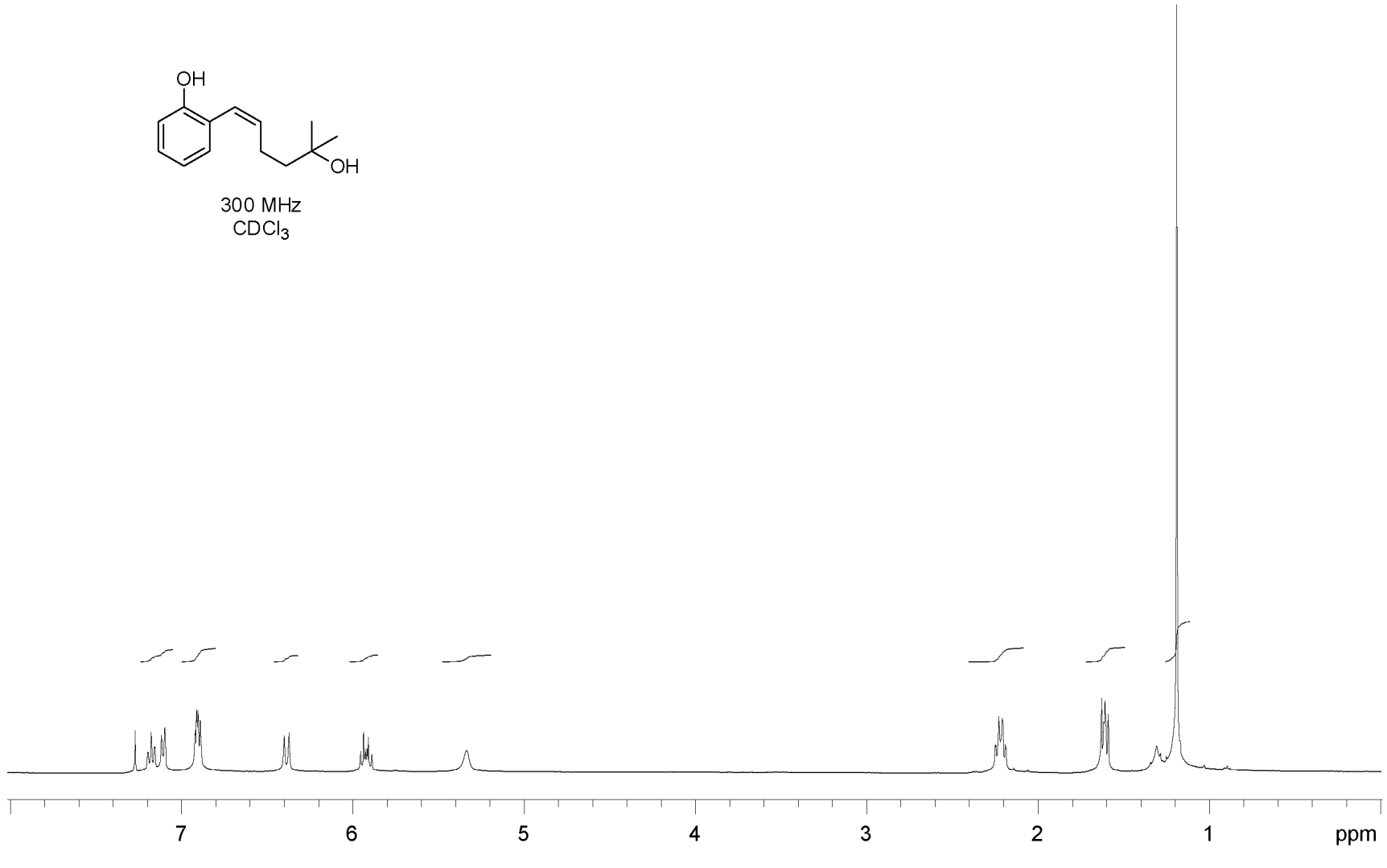
OH
OH
300 MHz
CDCl3
7
6
5
4
3
2
1
ppm

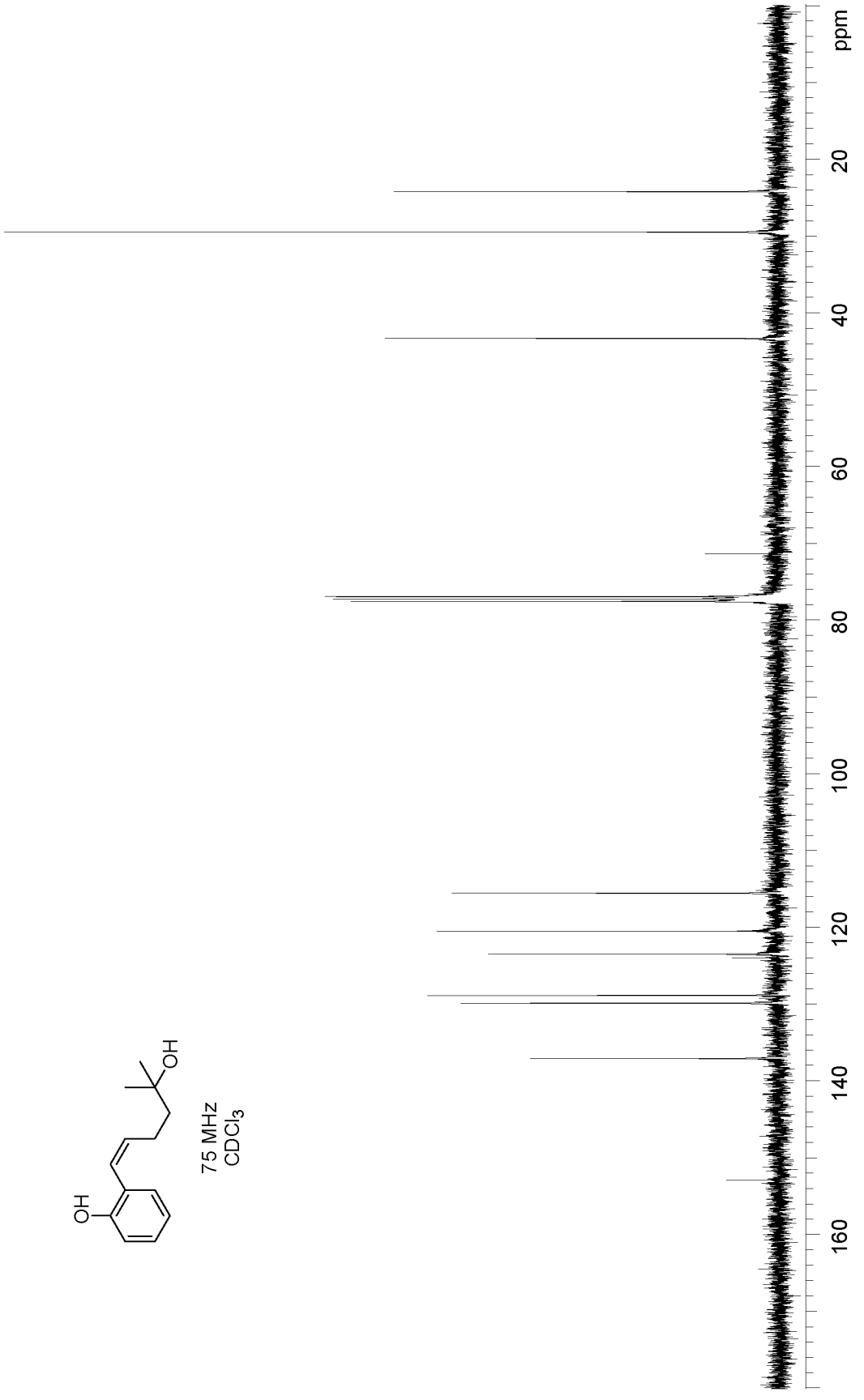
OH
OH
75 MHz
CDCl3
ppm
20
40
60
80
100
120
140
160

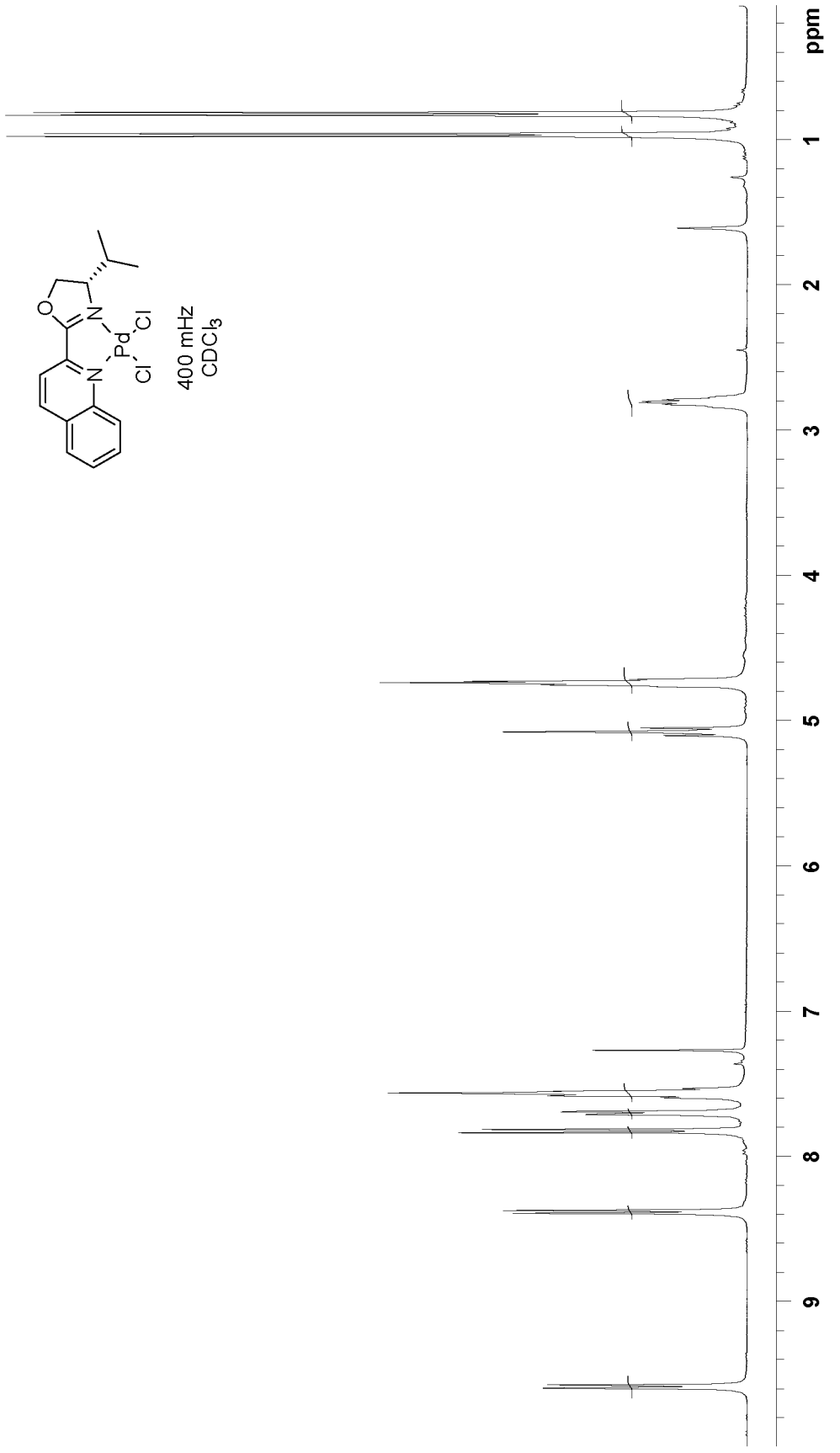
400 mHz
CDCl3
ppm
1
2
3
4
5
6
7
8
9

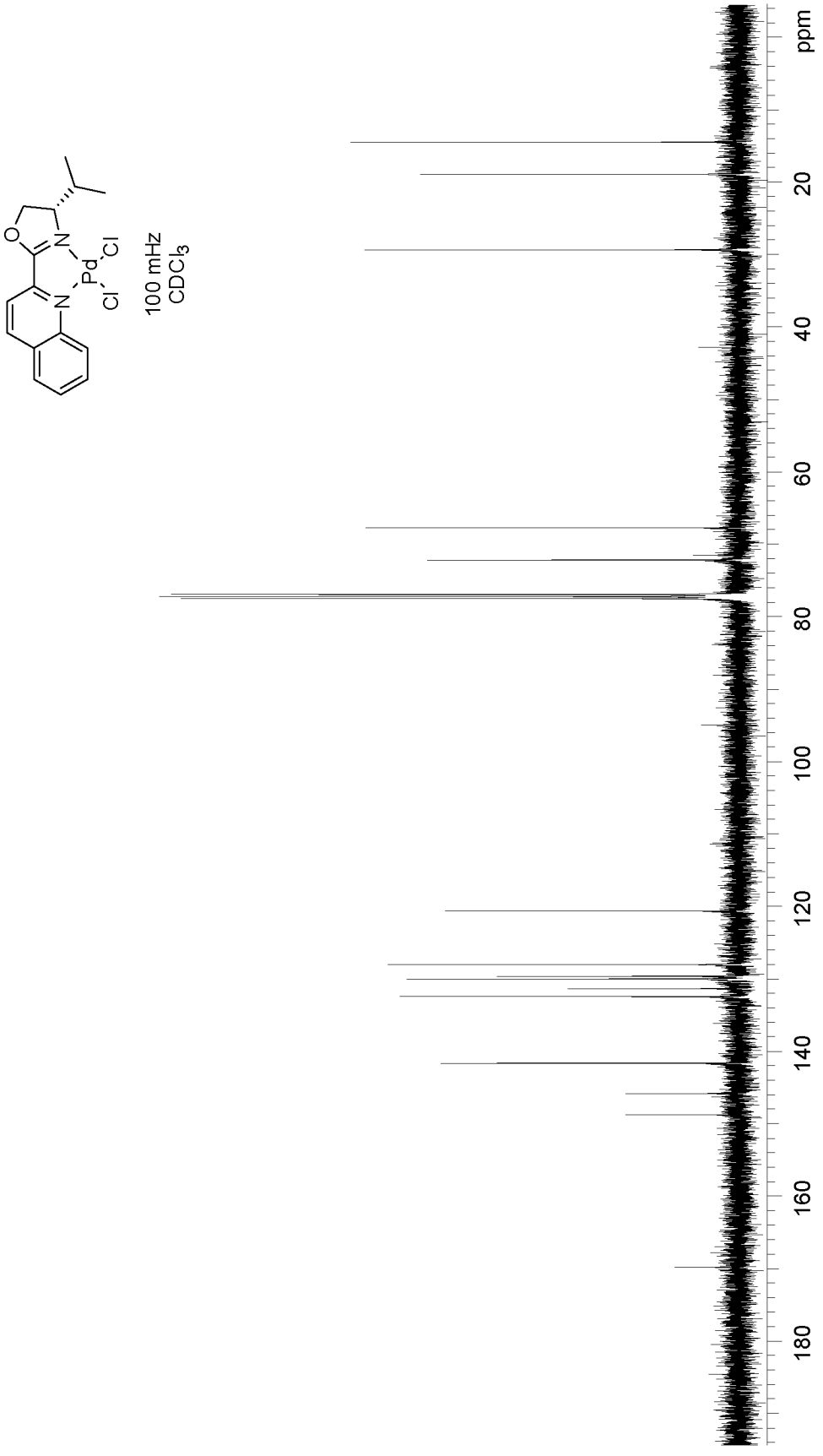
100 mHz
CDCl3
Pd
Cl
Cl
O
N
N
ppm
20
40
60
80
100
120
140
160
180

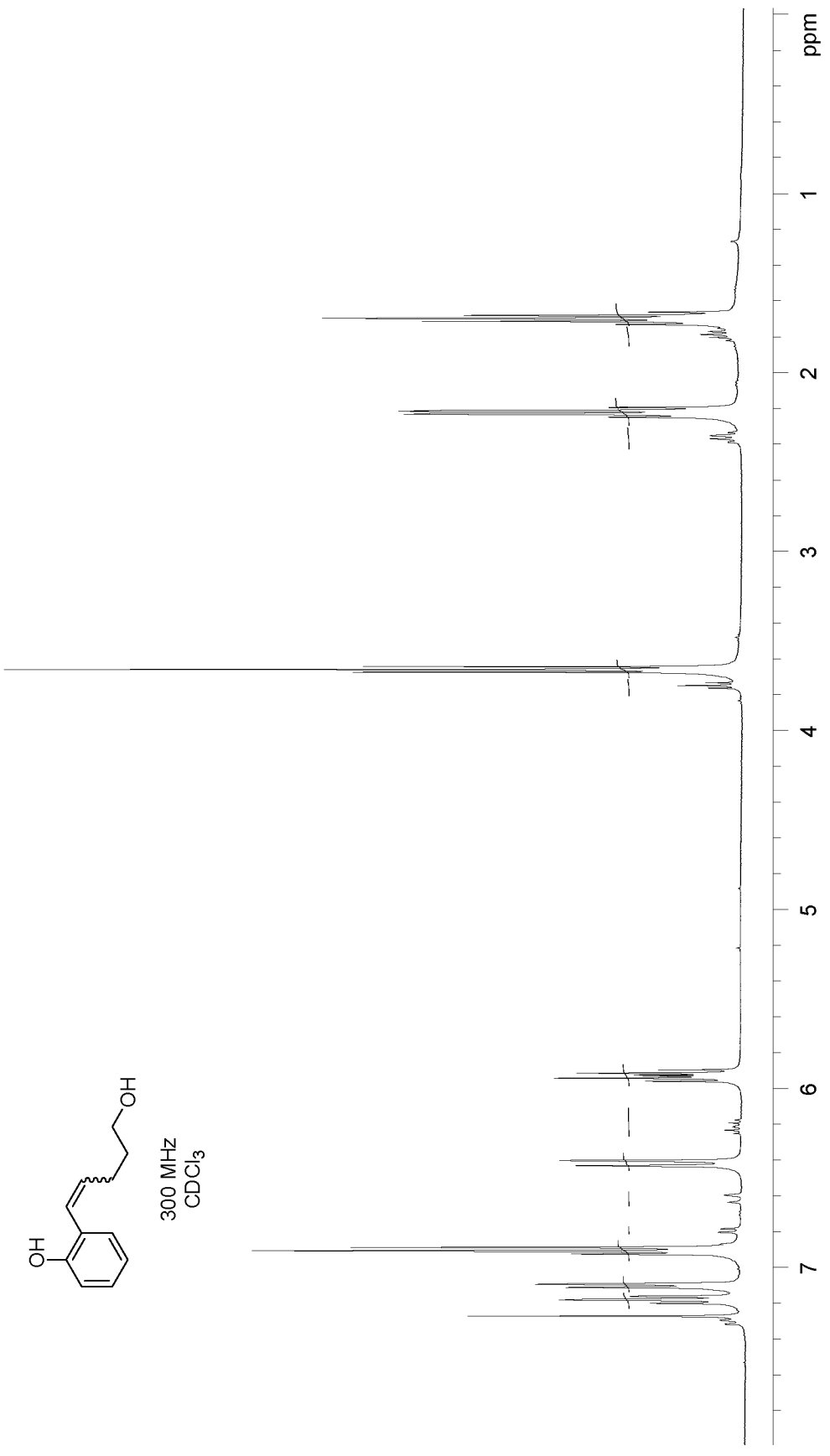
OH
OH
300 MHz
CDCl3
ppm
1
2
3
4
5
6
7

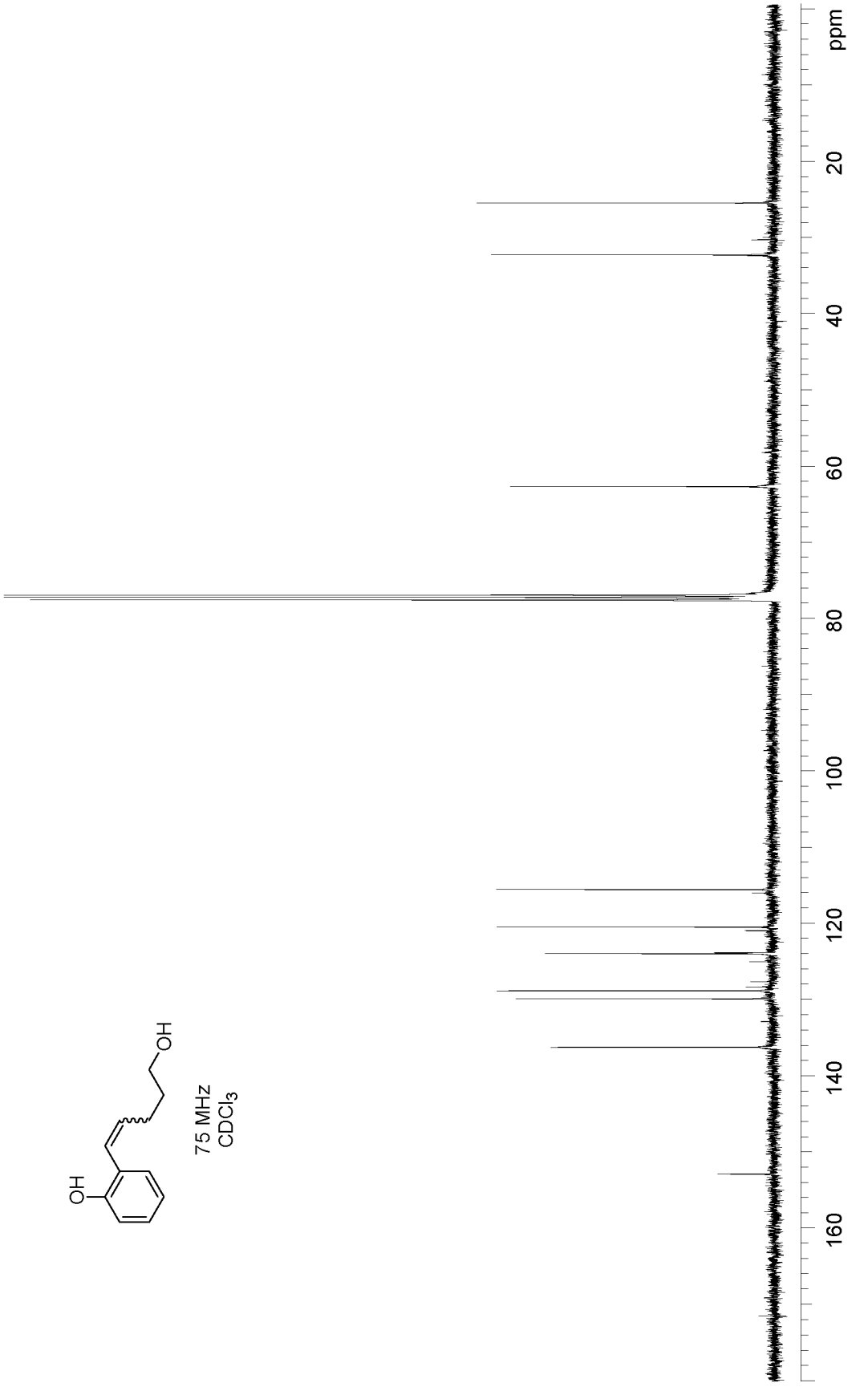
OH
OH
75 MHz
CDCl3
ppm
20
40
60
80
100
120
140
160

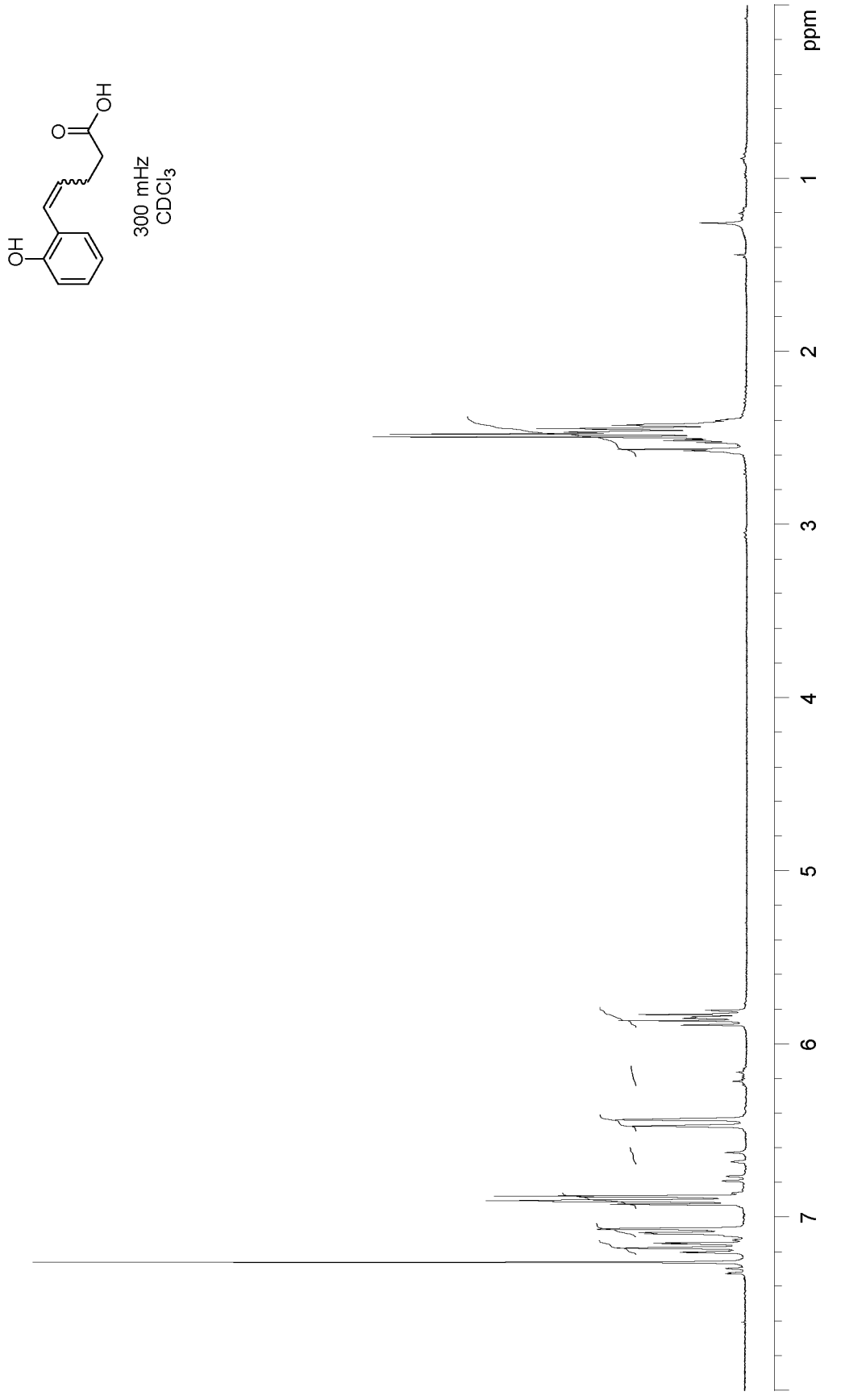
OH
O
OH
300 mHz
CDCl3
ppm
1
2
3
4
5
6
7

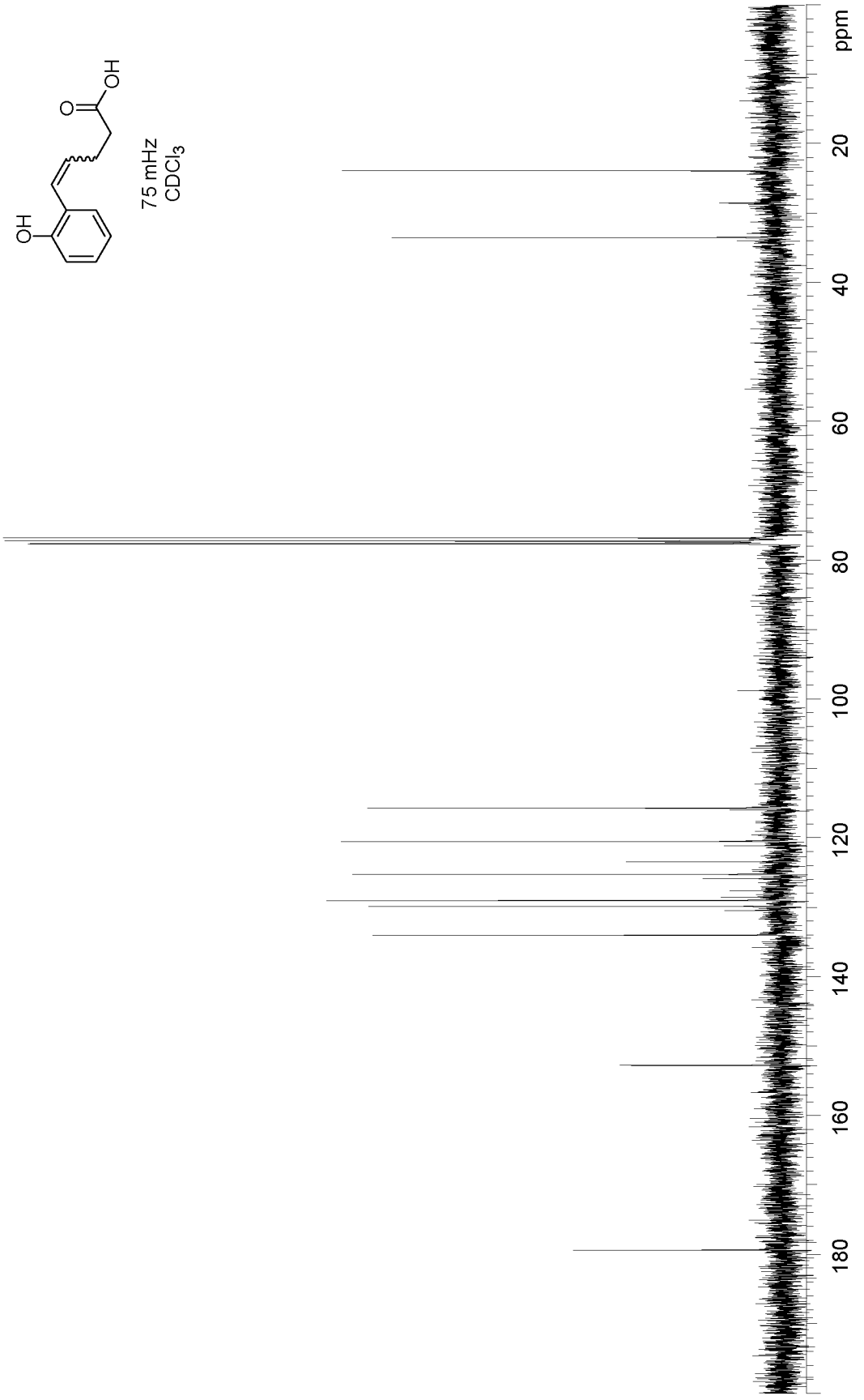
OH
O
OH
75 mHz
CDCl3
ppm
20
40
60
80
100
120
140
160
180

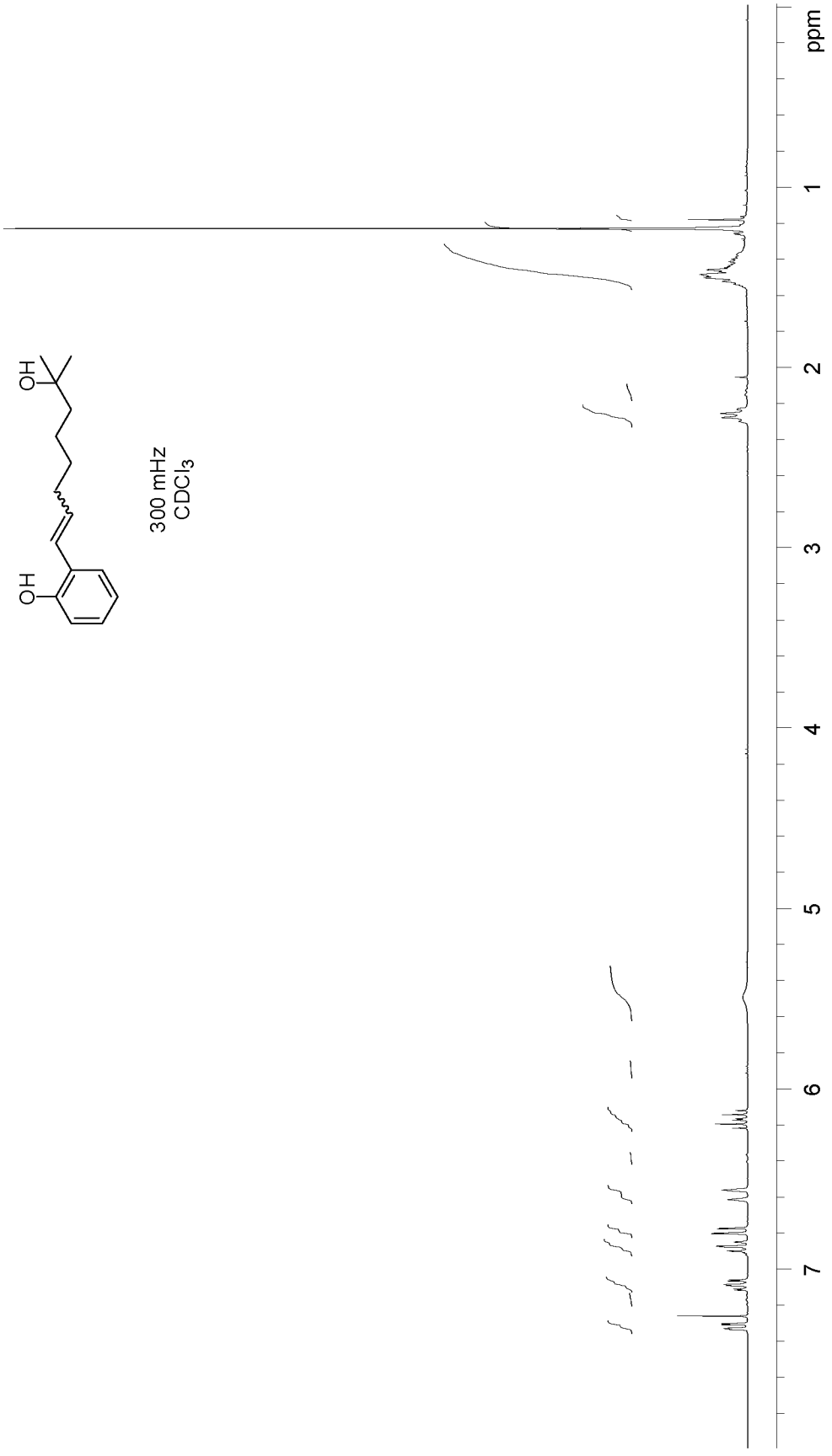
OH
OH
300 mHz
CDCl3
ppm
1
2
3
4
5
6
7

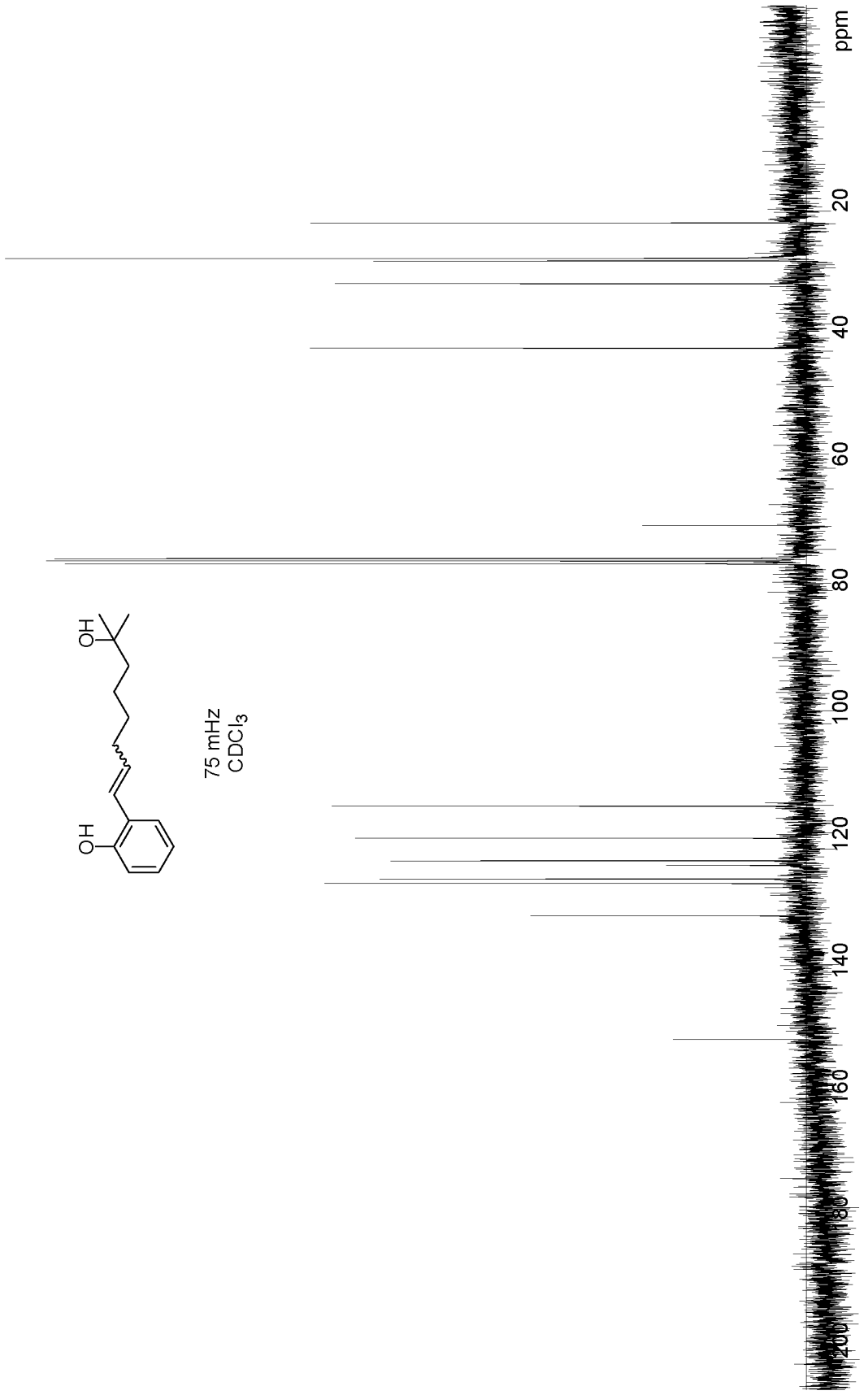
OH
OH
75 mHz
$CDCl_3$
ppm
20
40
60
80
100
120
140
160
180
200

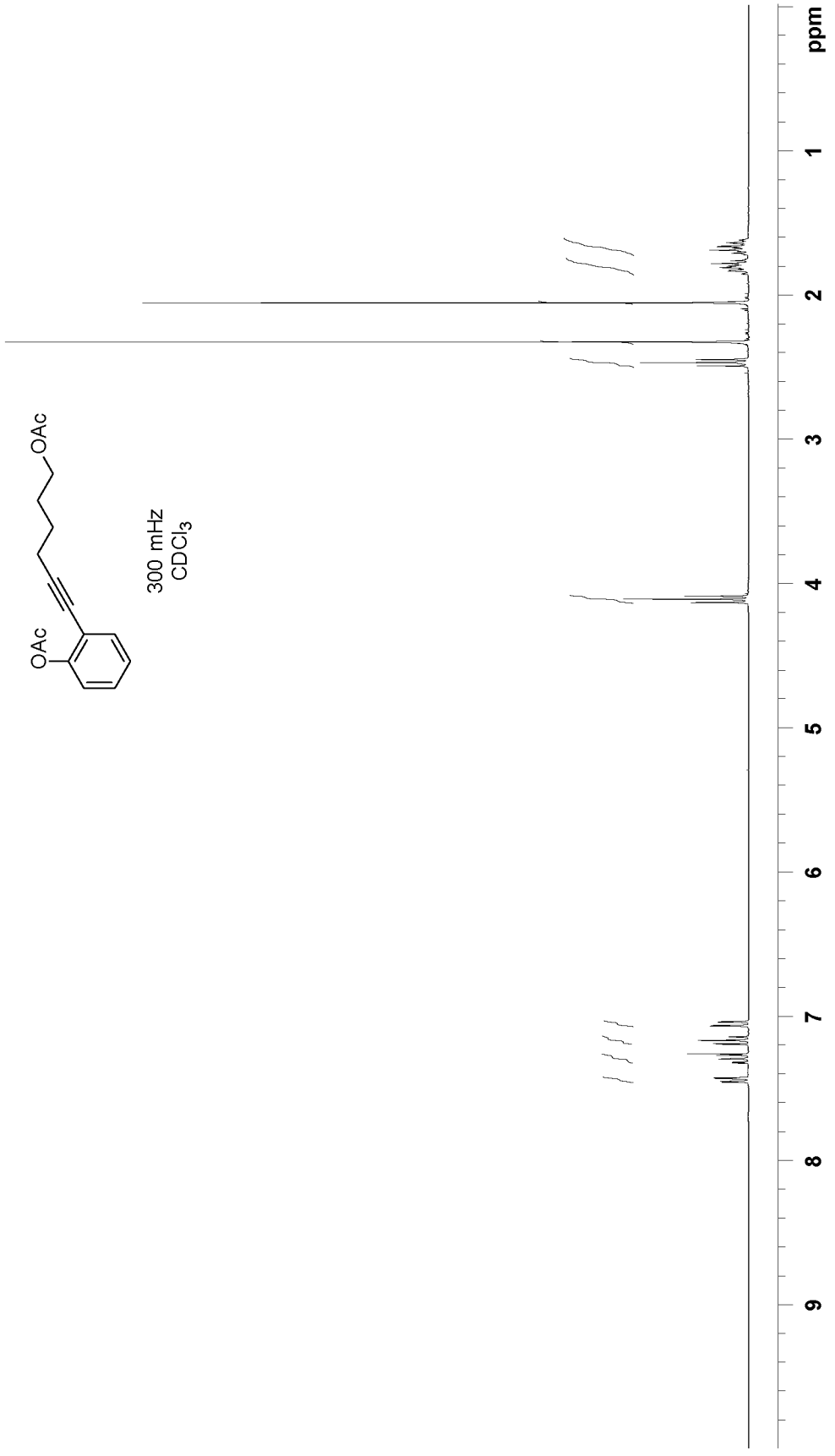
OAc
OAc
300 mHz
$CDCl_3$
ppm
1
2
3
4
5
6
7
8
9

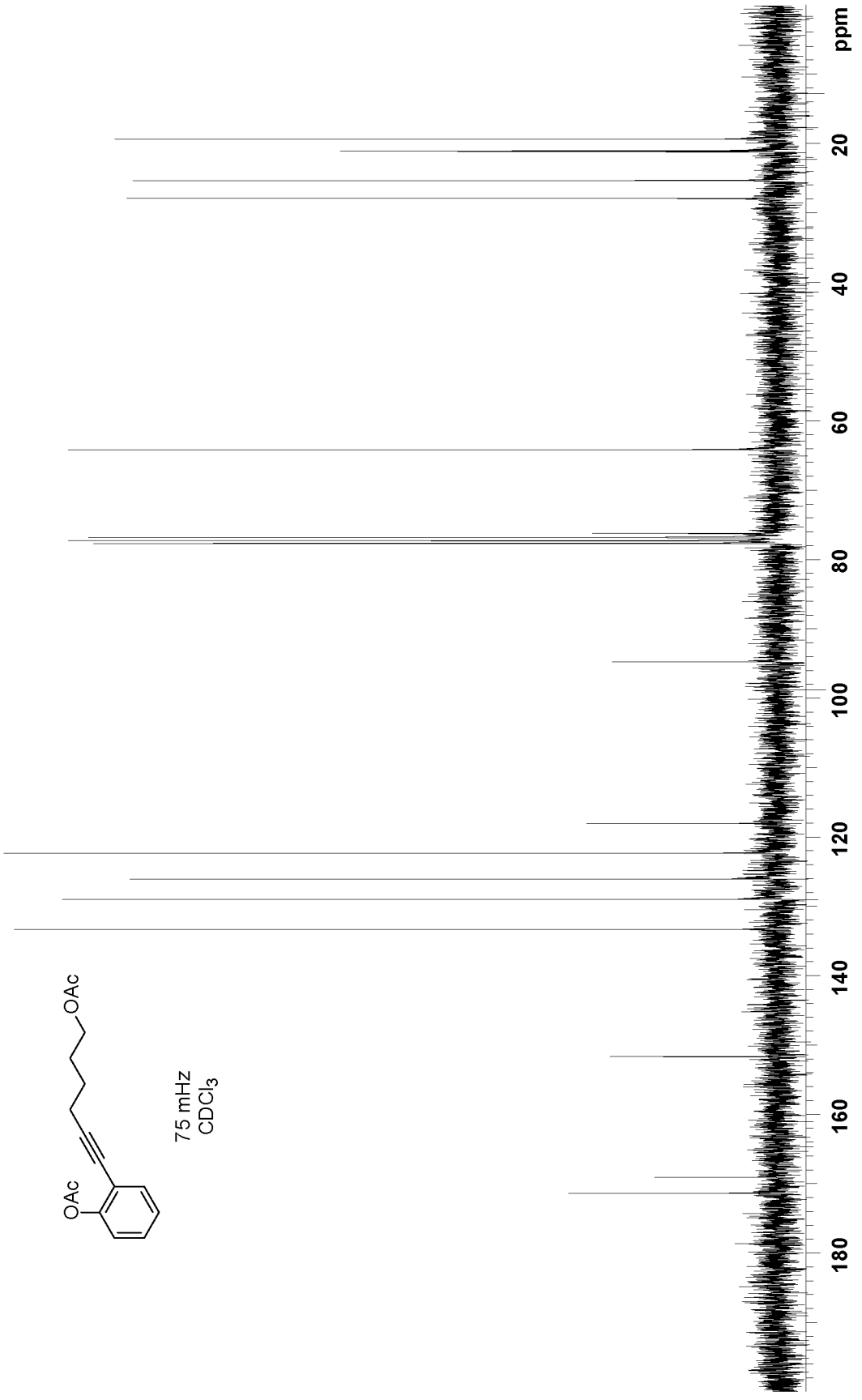
OAc
OAc
75 mHz
$CDCl_3$
ppm
20
40
60
80
100
120
140
160
180

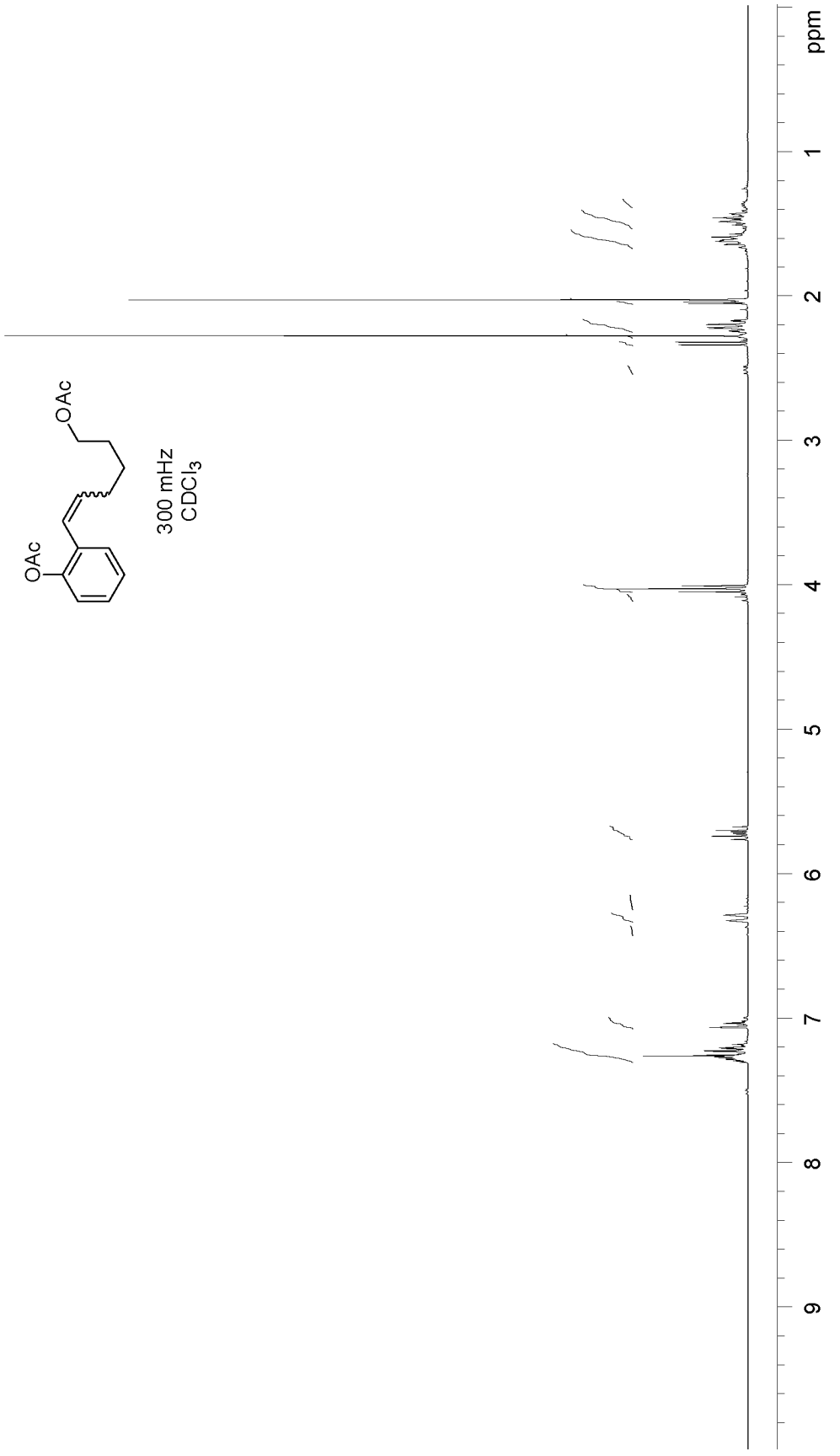
OAc
OAc
300 mHz
CDCl3
ppm
1
2
3
4
5
6
7
8
9

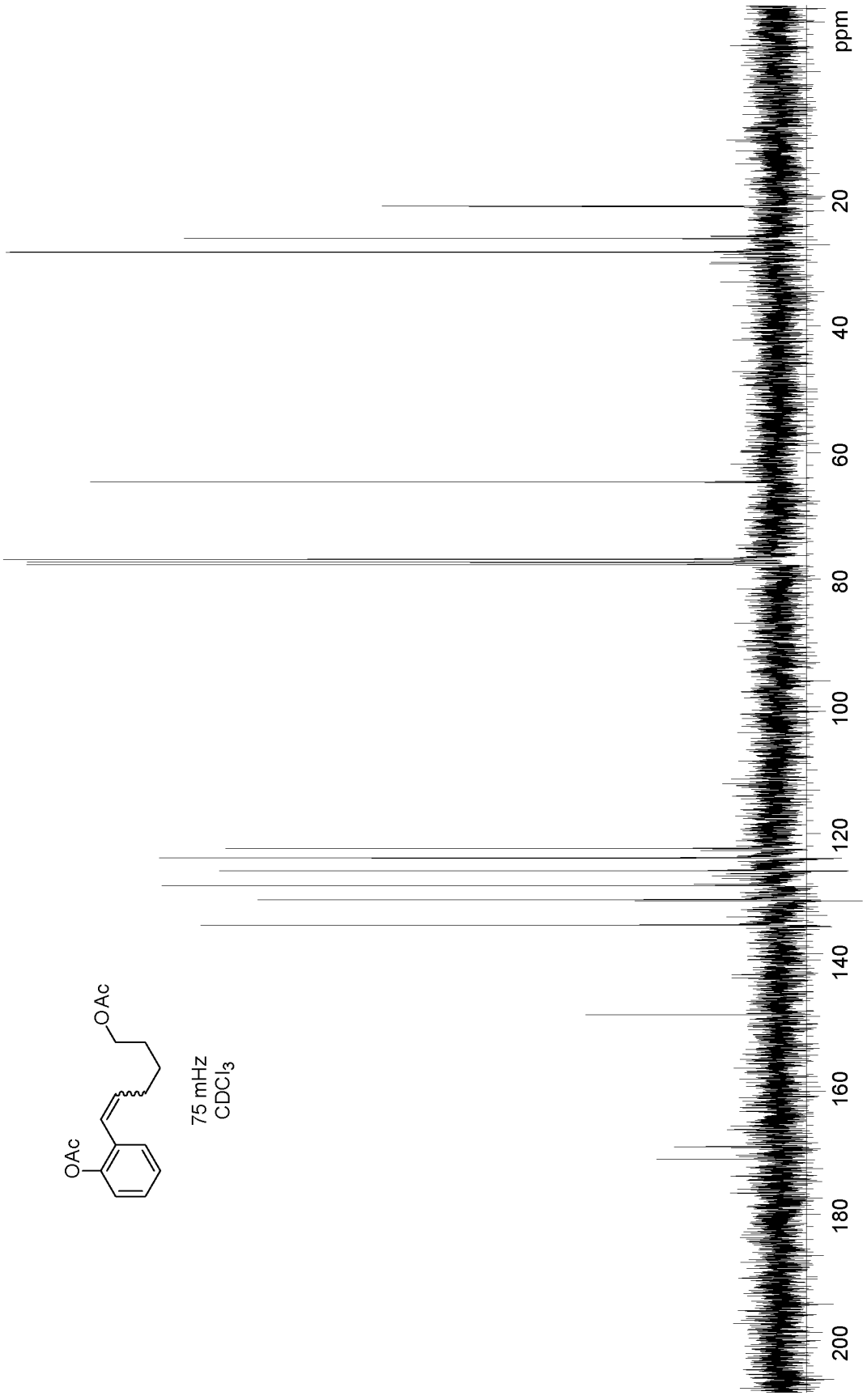
OAc
OAc
75 mHz
$CDCl_3$
ppm
20
40
60
80
100
120
140
160
180
200

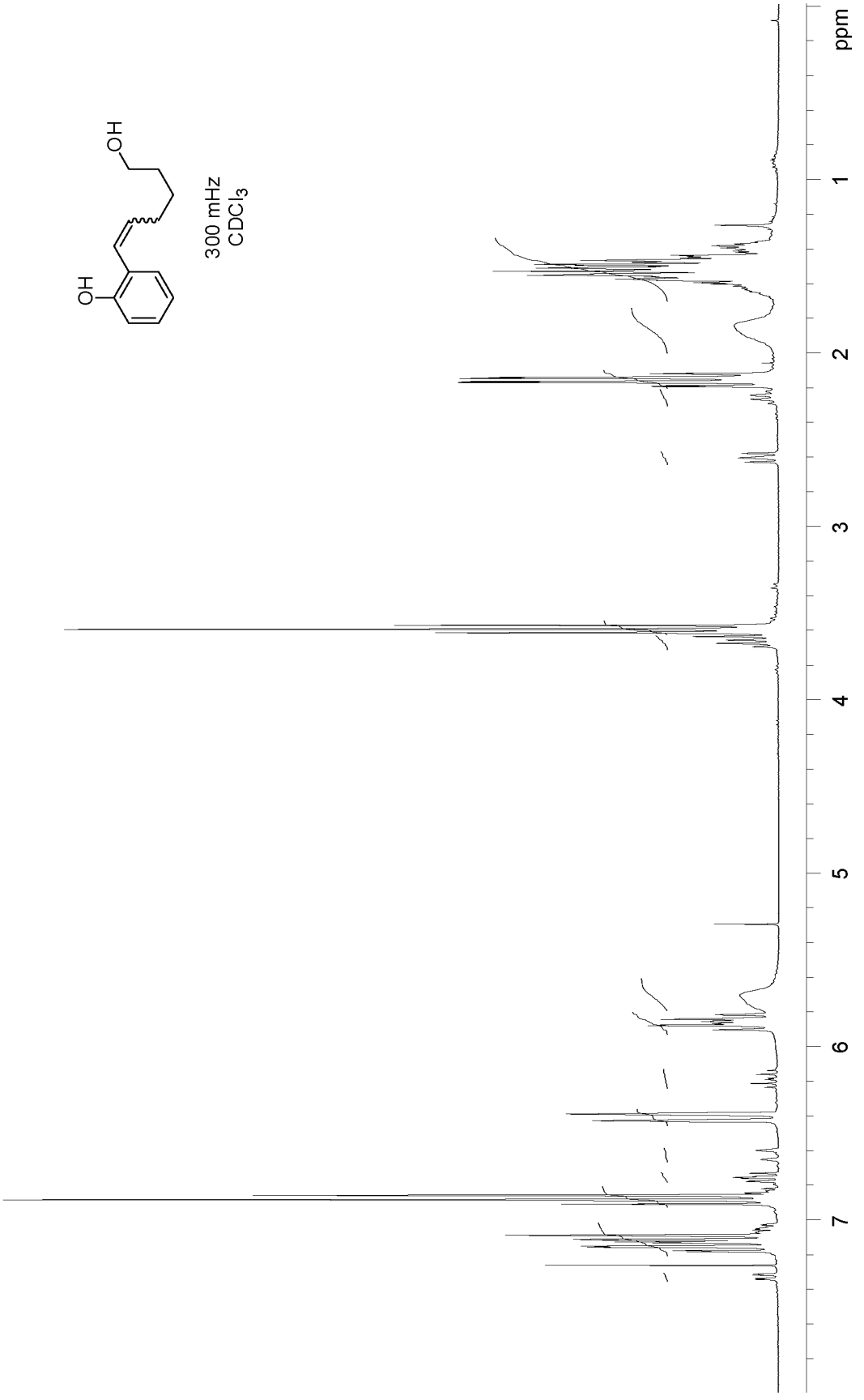
OH
OH
300 mHz
CDCl3
ppm
1
2
3
4
5
6
7

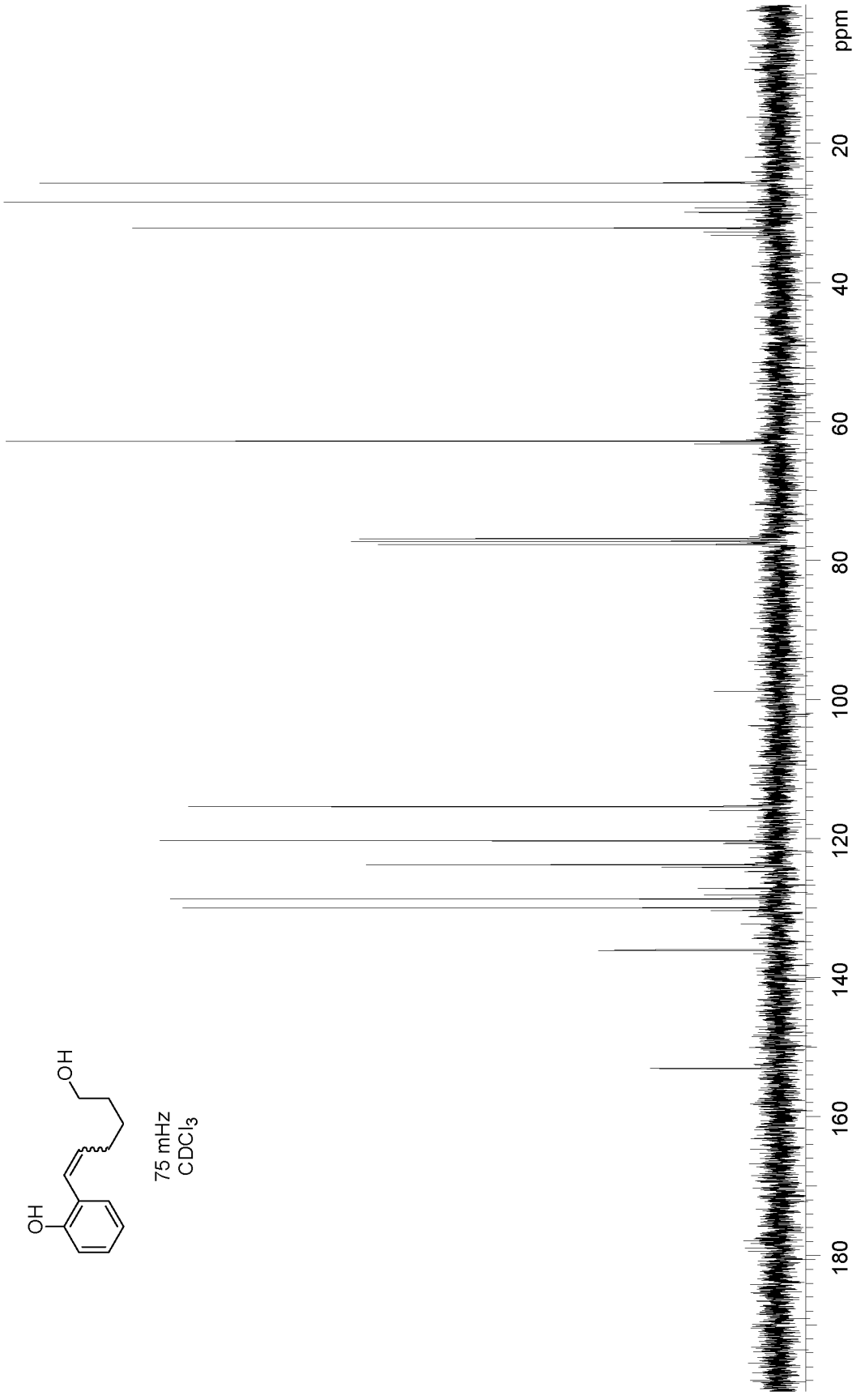
OH
OH
75 mHz
$CDCl_3$
ppm
20
40
60
80
100
120
140
160
180

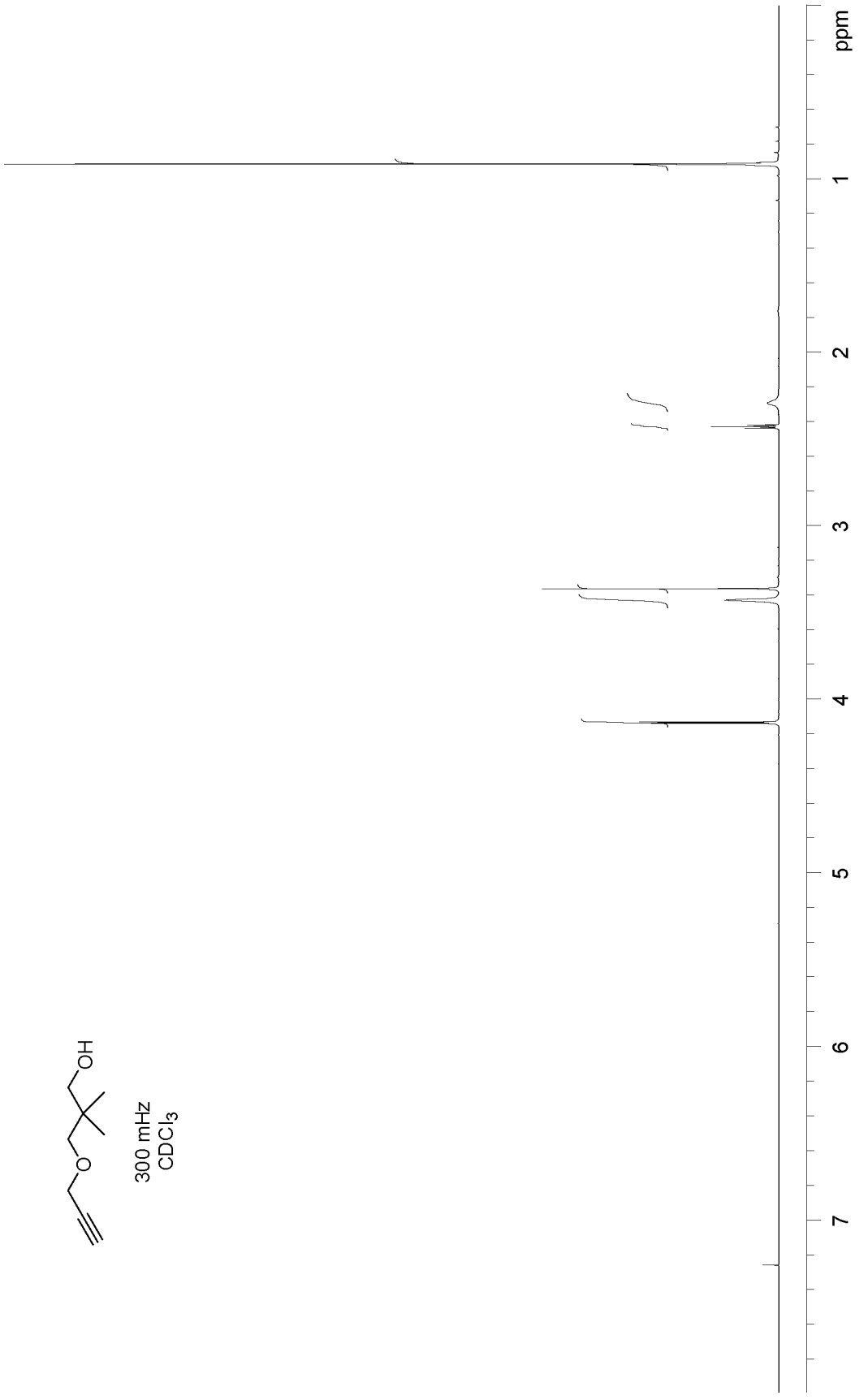
OH
O
300 mHz
CDCl3
ppm
1
2
3
4
5
6
7

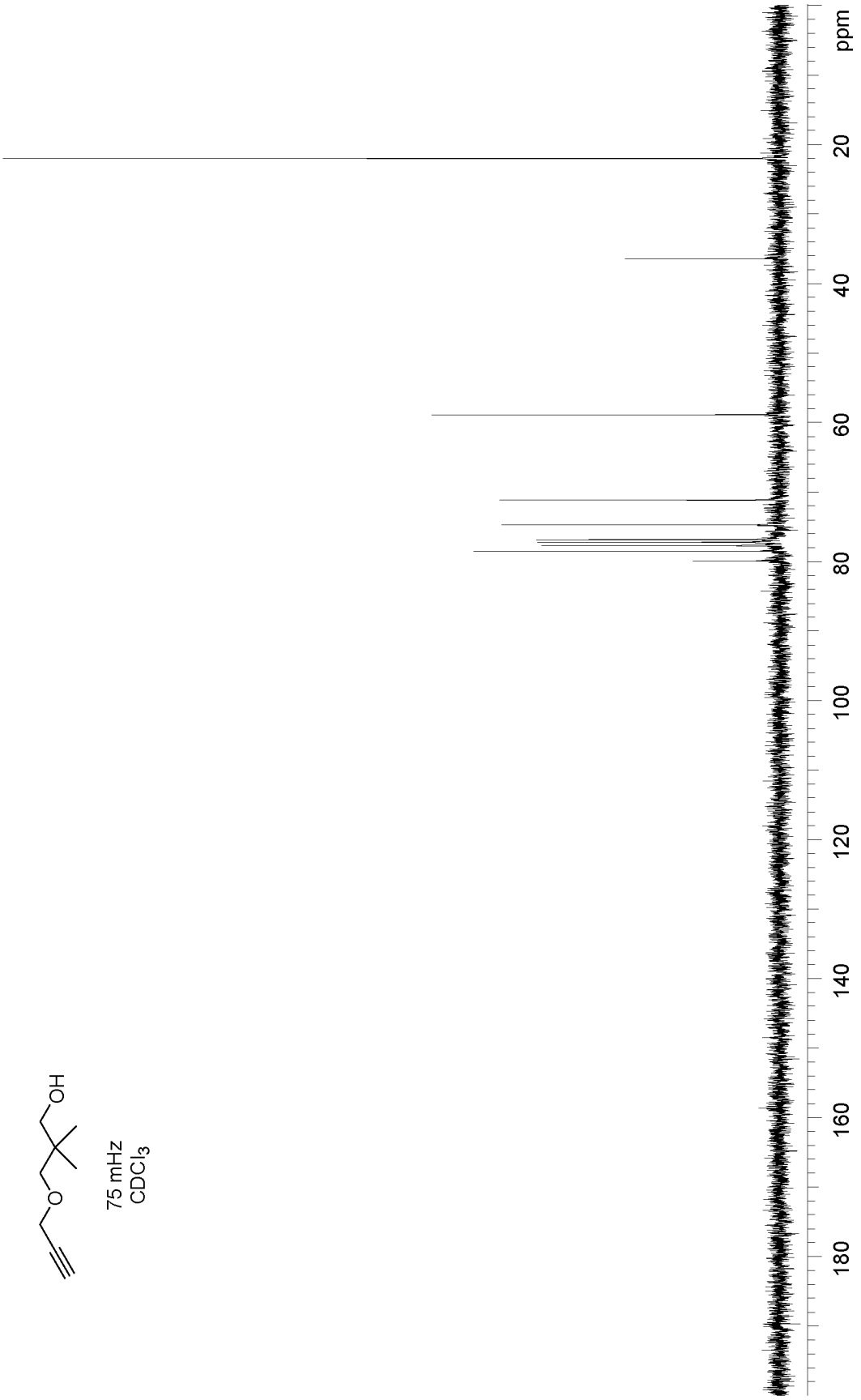
OH
O
75 mHz
$CDCl_3$
ppm
20
40
60
80
100
120
140
160
180

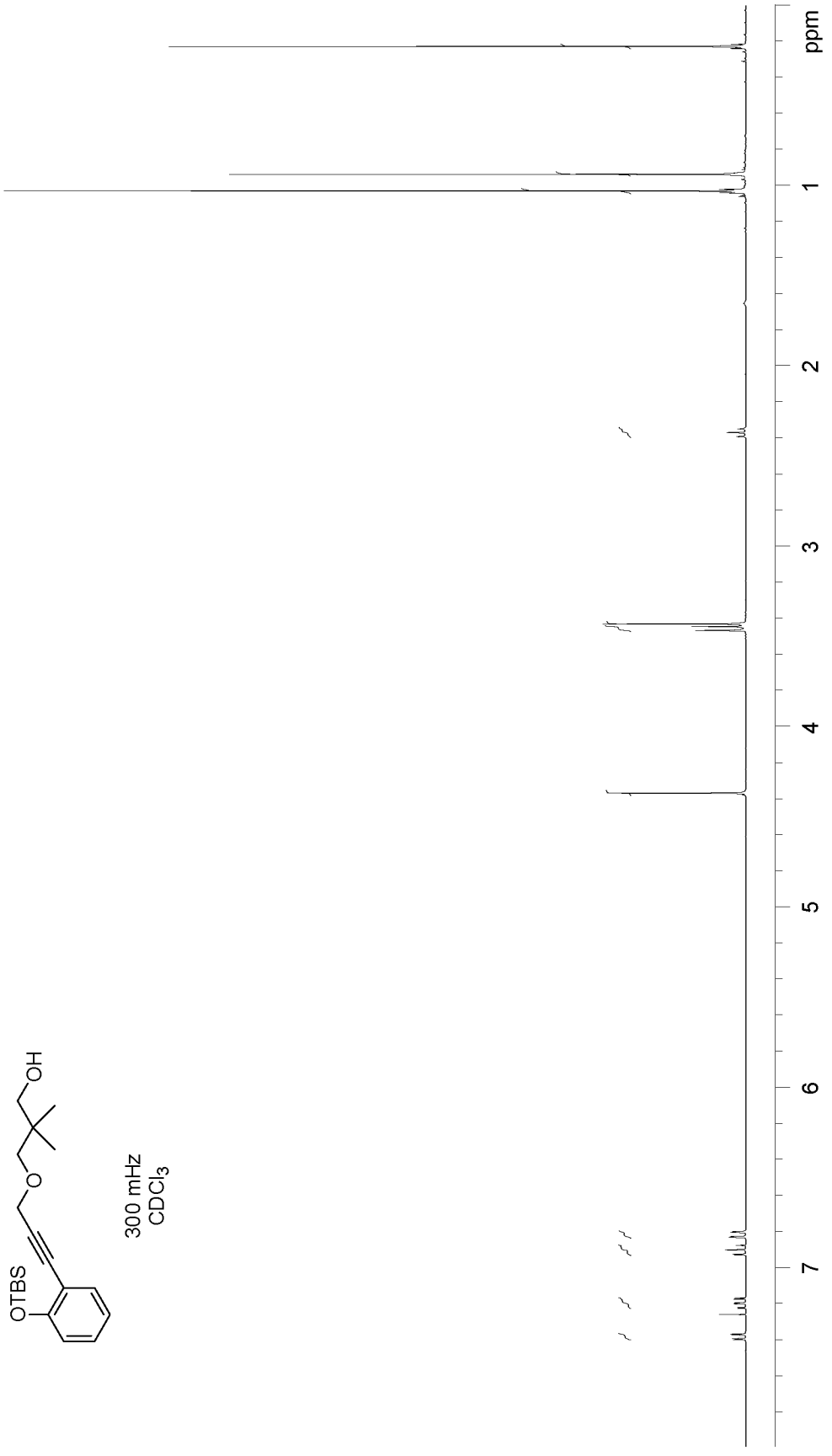
OTBS
O
OH
300 mHz
CDCl3
ppm
1
2
3
4
5
6
7

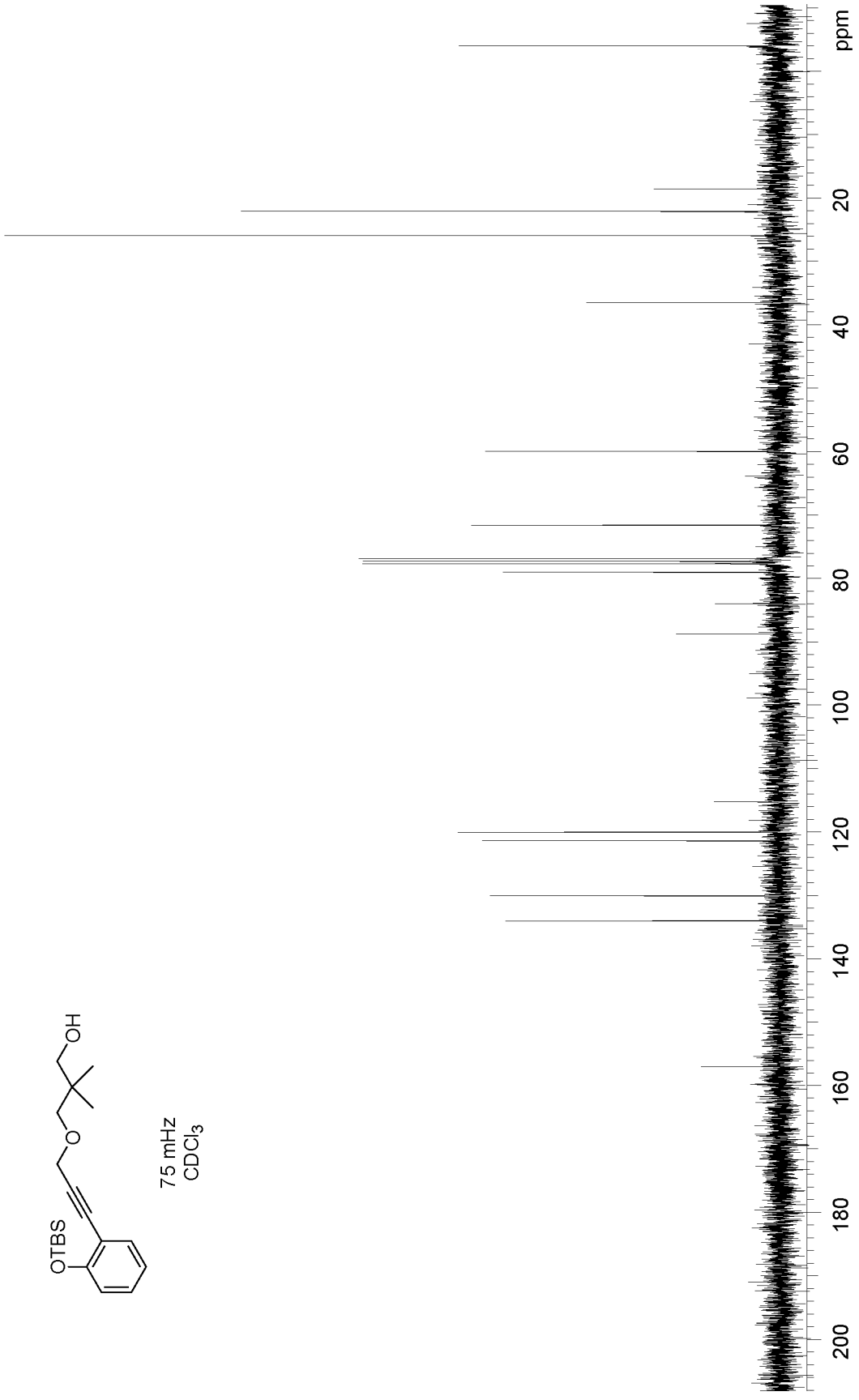
OH
O
OTBS
75 mHz
$CDCl_3$
ppm
20
40
60
80
100
120
140
160
180
200

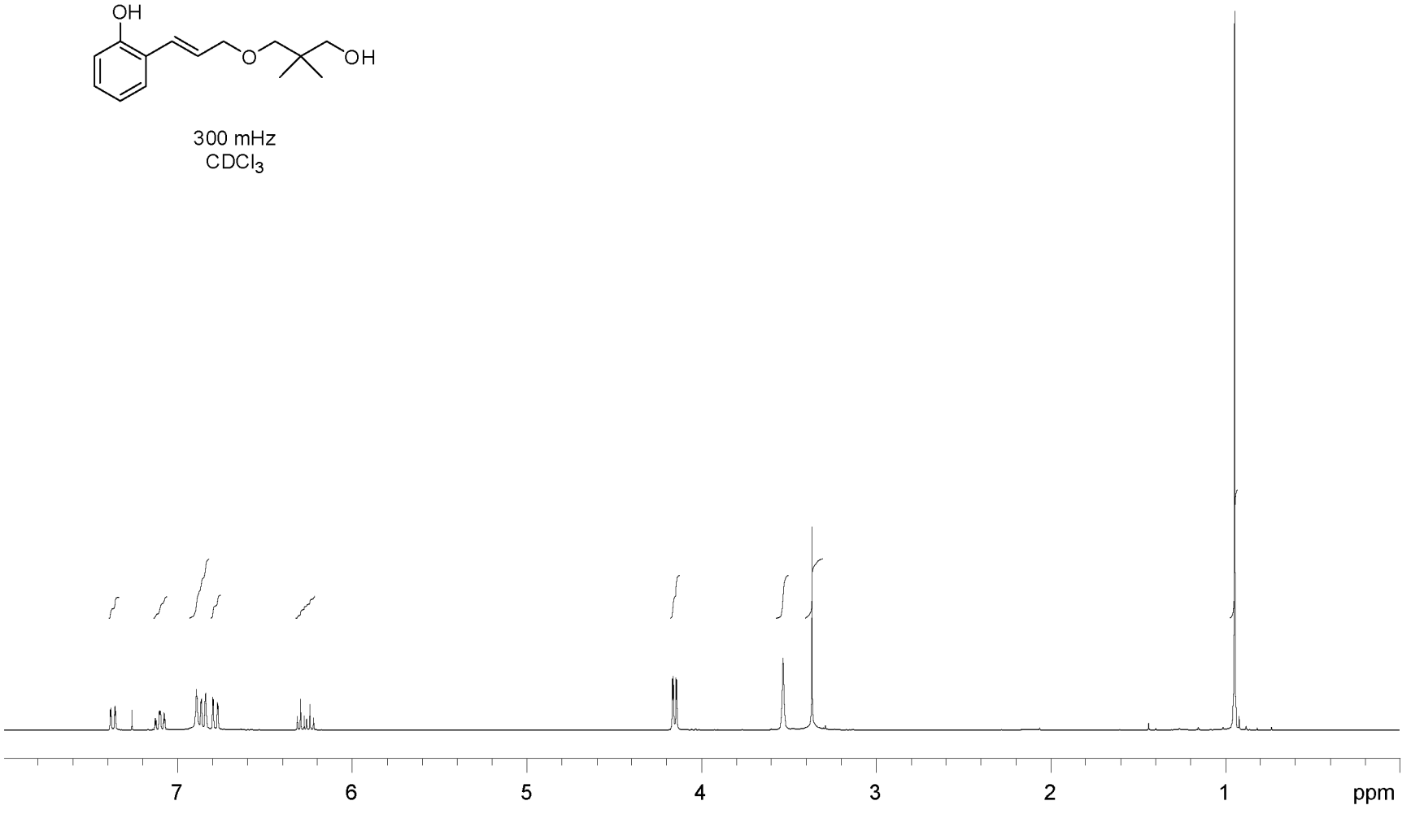
OH
O
OH
300 mHz
CDCl3
7
6
5
4
3
2
1
ppm

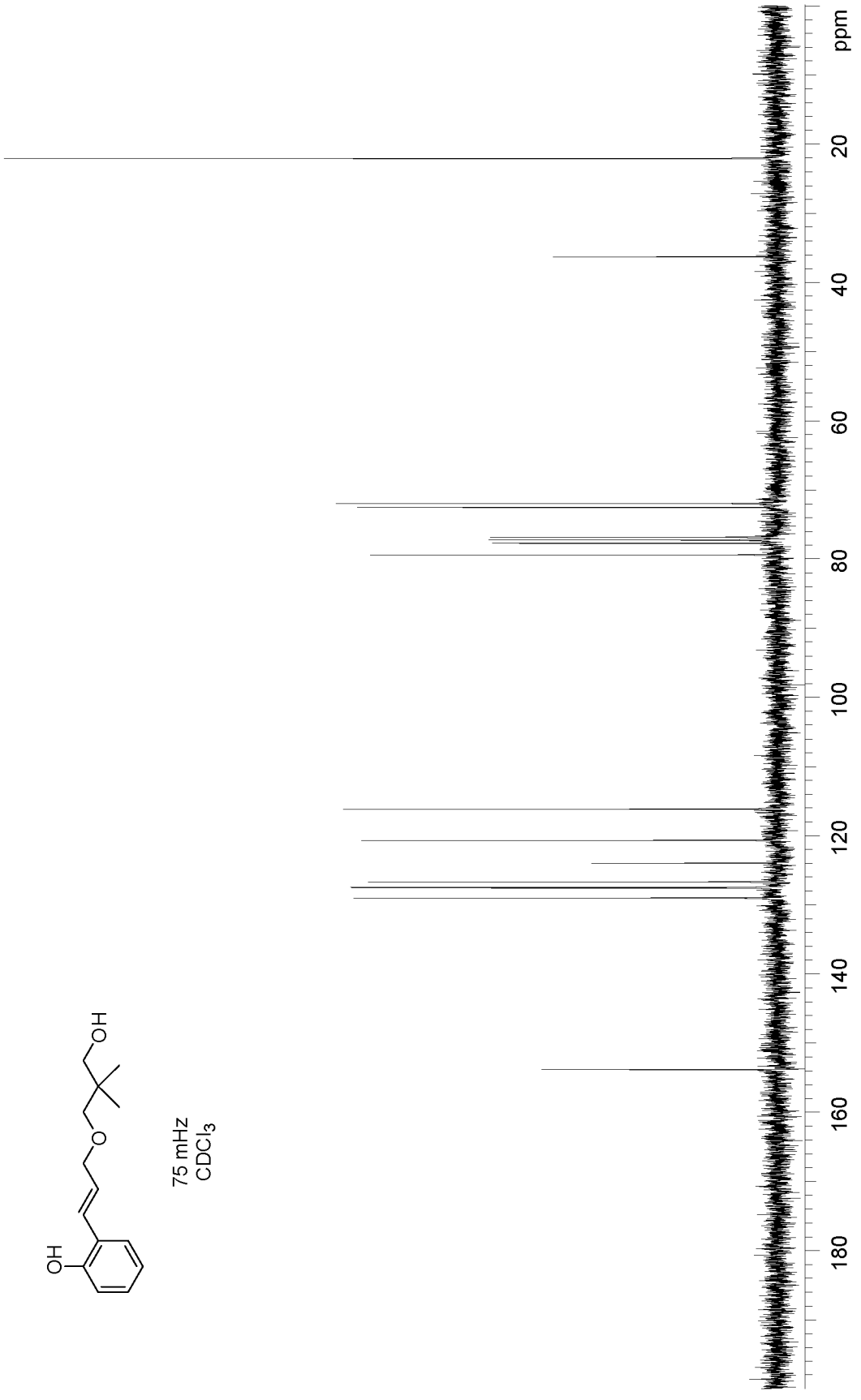
OH
O
OH
75 mHz
CDCl3
ppm
20
40
60
80
100
120
140
160
180

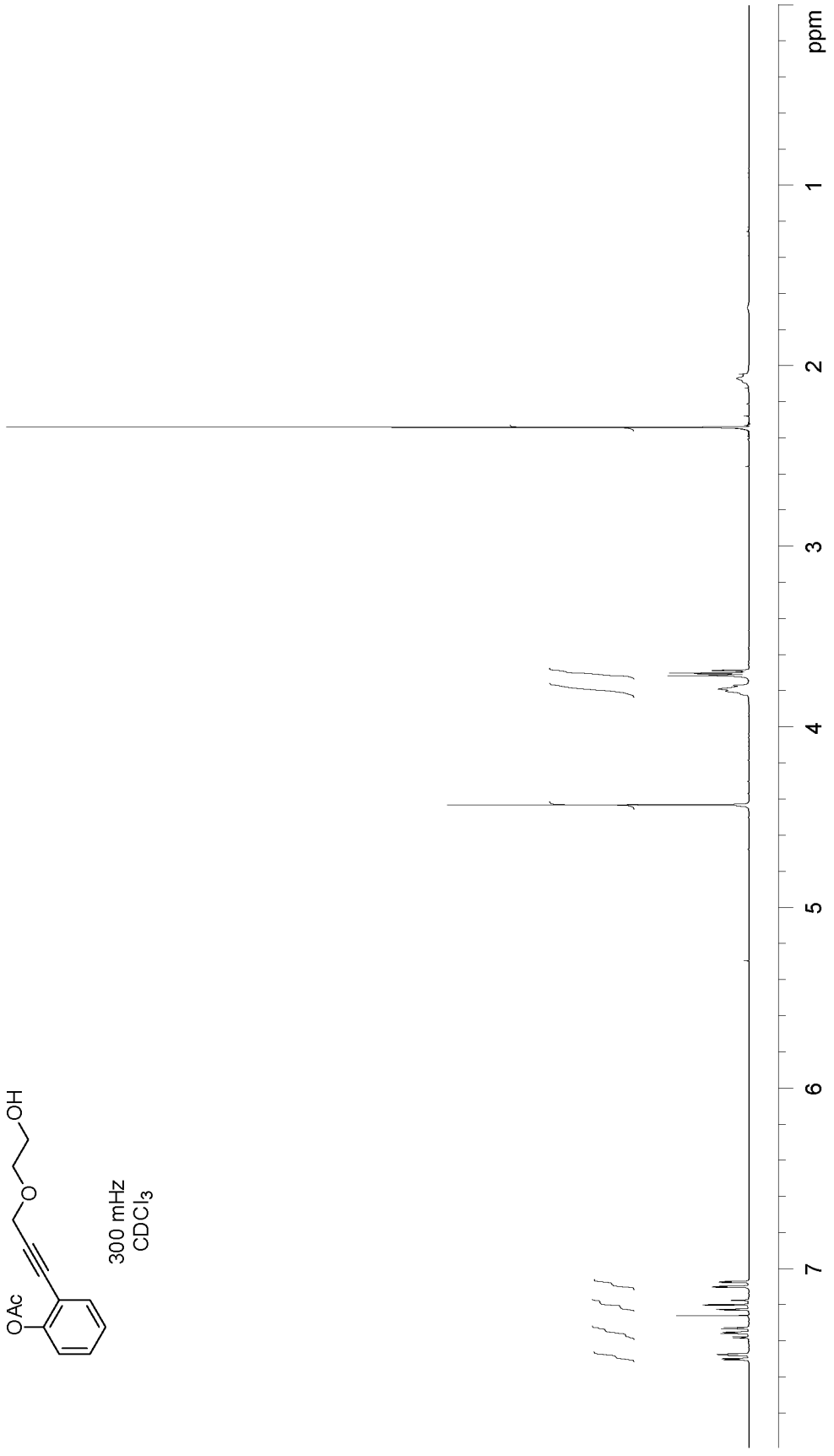
OAc
OH
O
300 mHz
$CDCl_3$
ppm
1
2
3
4
5
6
7

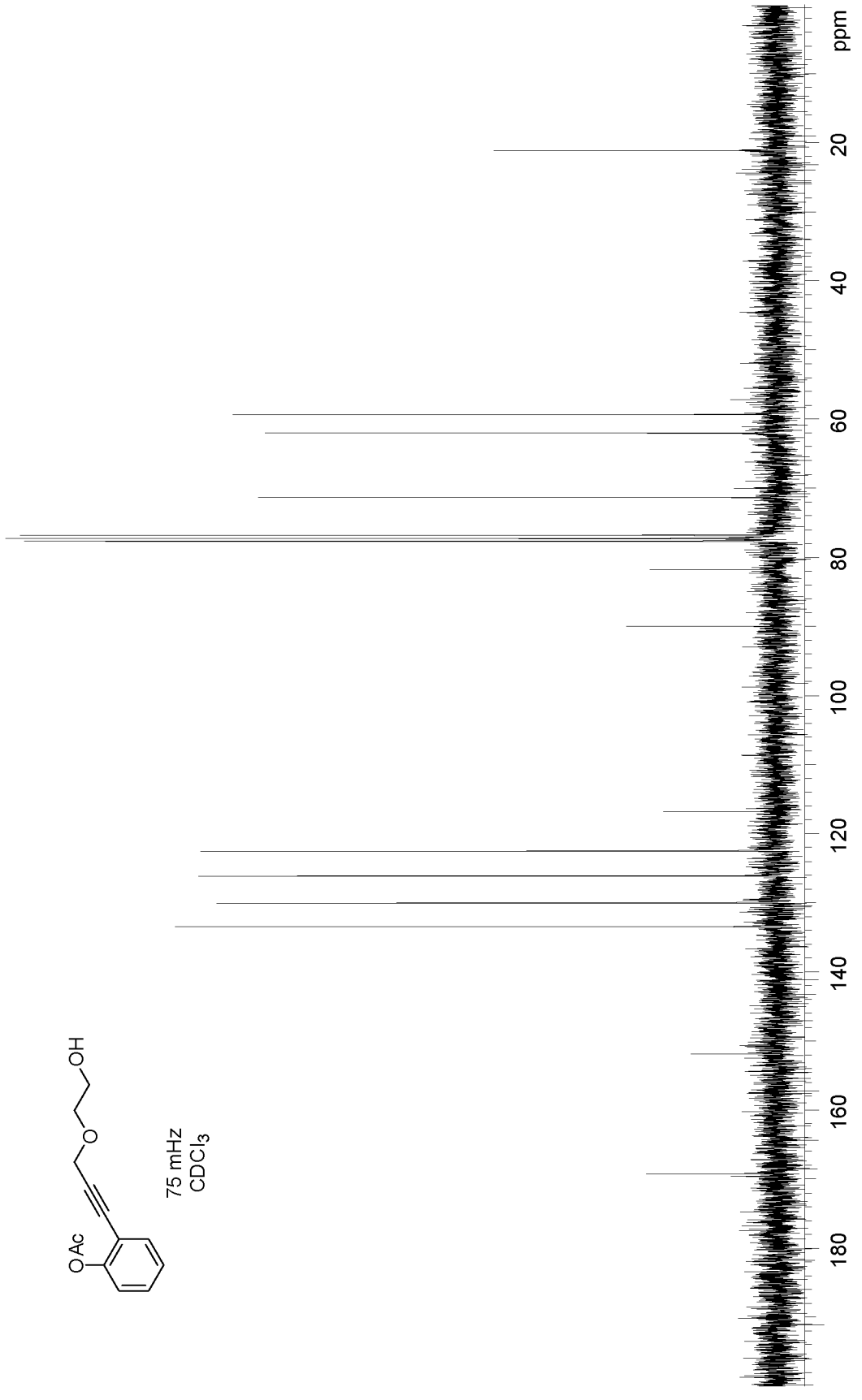
OAc
O
OH
75 mHz
$CDCl_3$
ppm
20
40
60
80
100
120
140
160
180

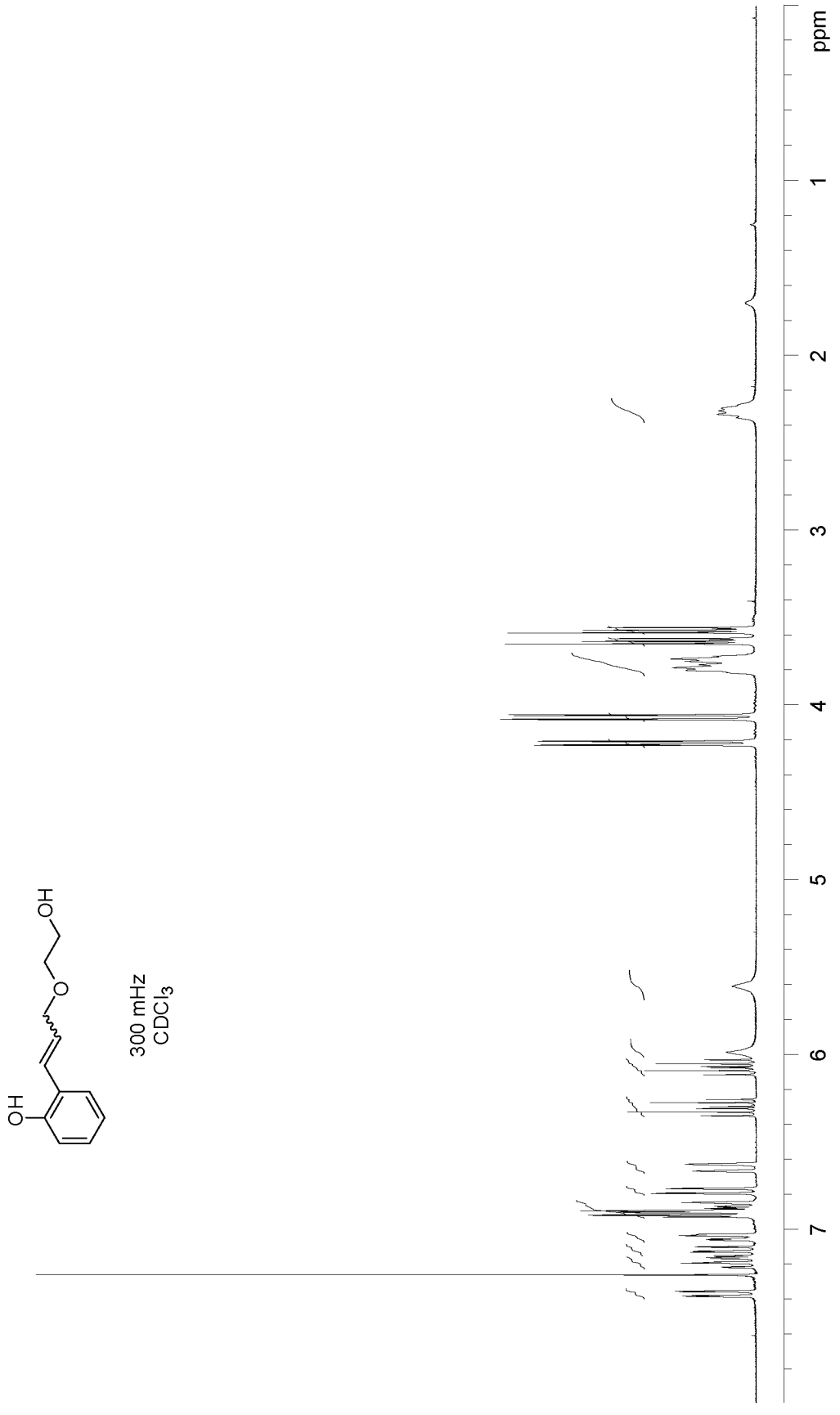
OH
O
OH
300 mHz
CDCl3
ppm
1
2
3
4
5
6
7

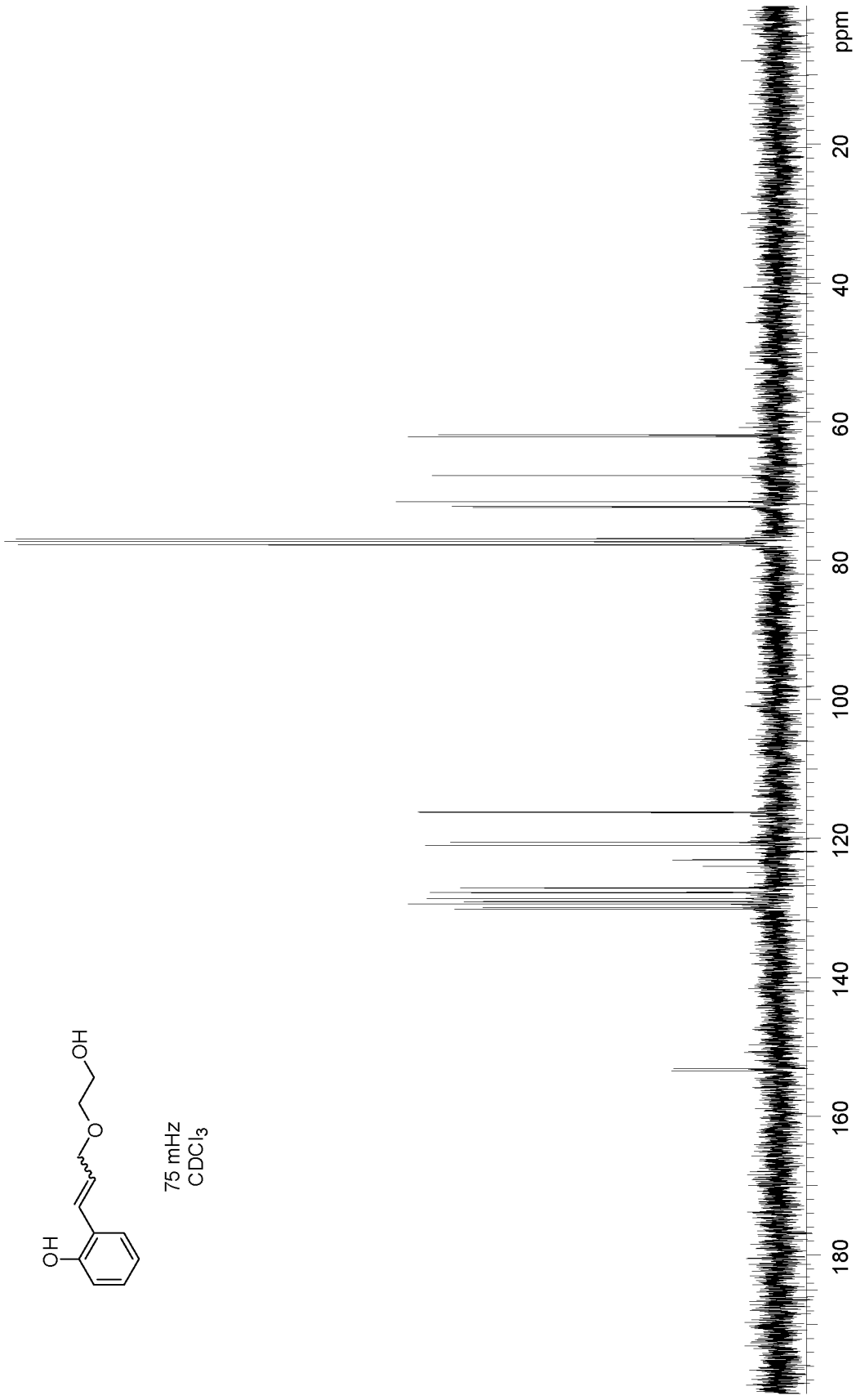
OH
O
OH
75 mHz
$CDCl_3$
ppm
20
40
60
80
100
120
140
160
180

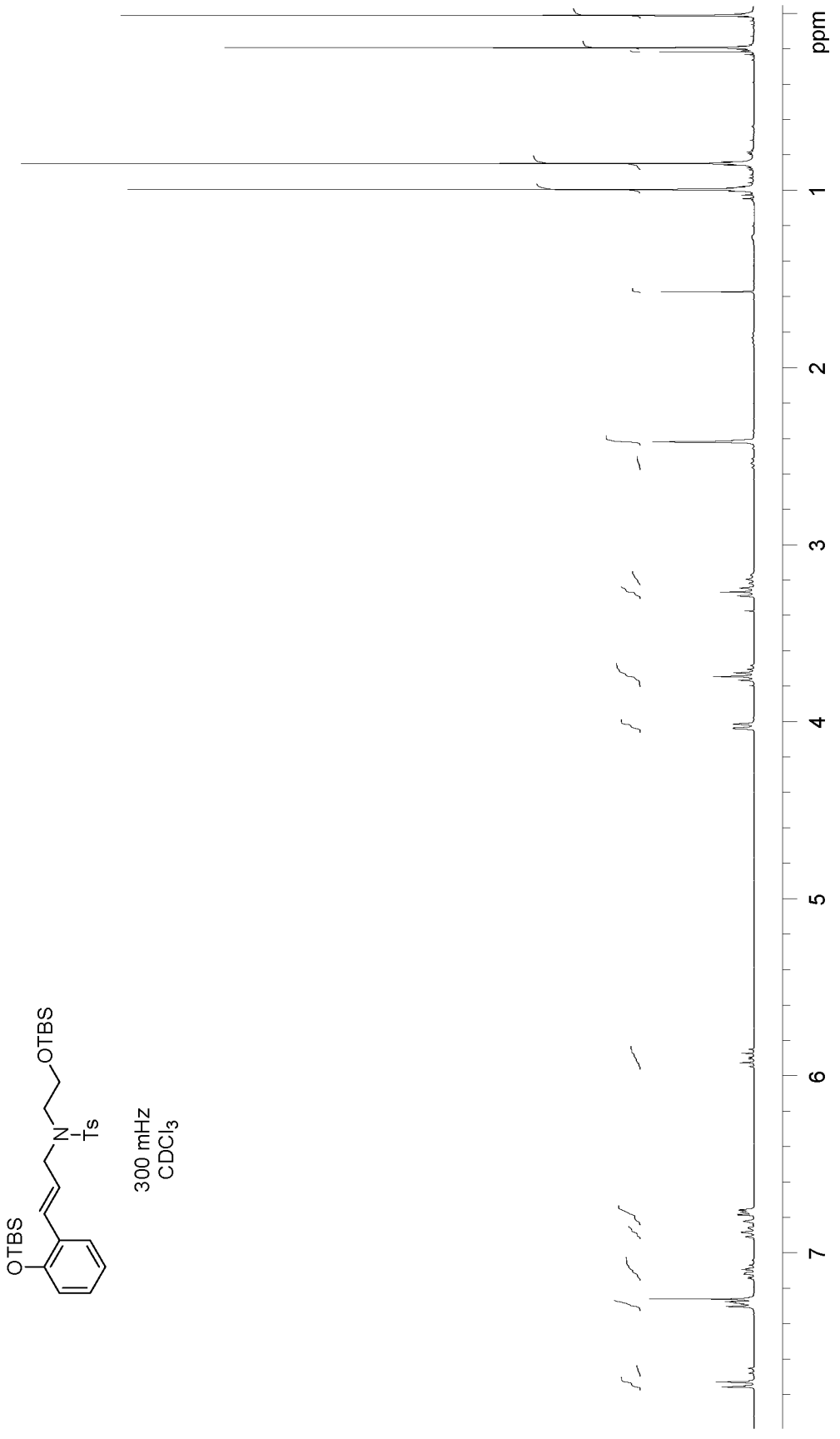
OTBS
OTBS
N
Ts
300 mHz
CDCl3
ppm
1
2
3
4
5
6
7

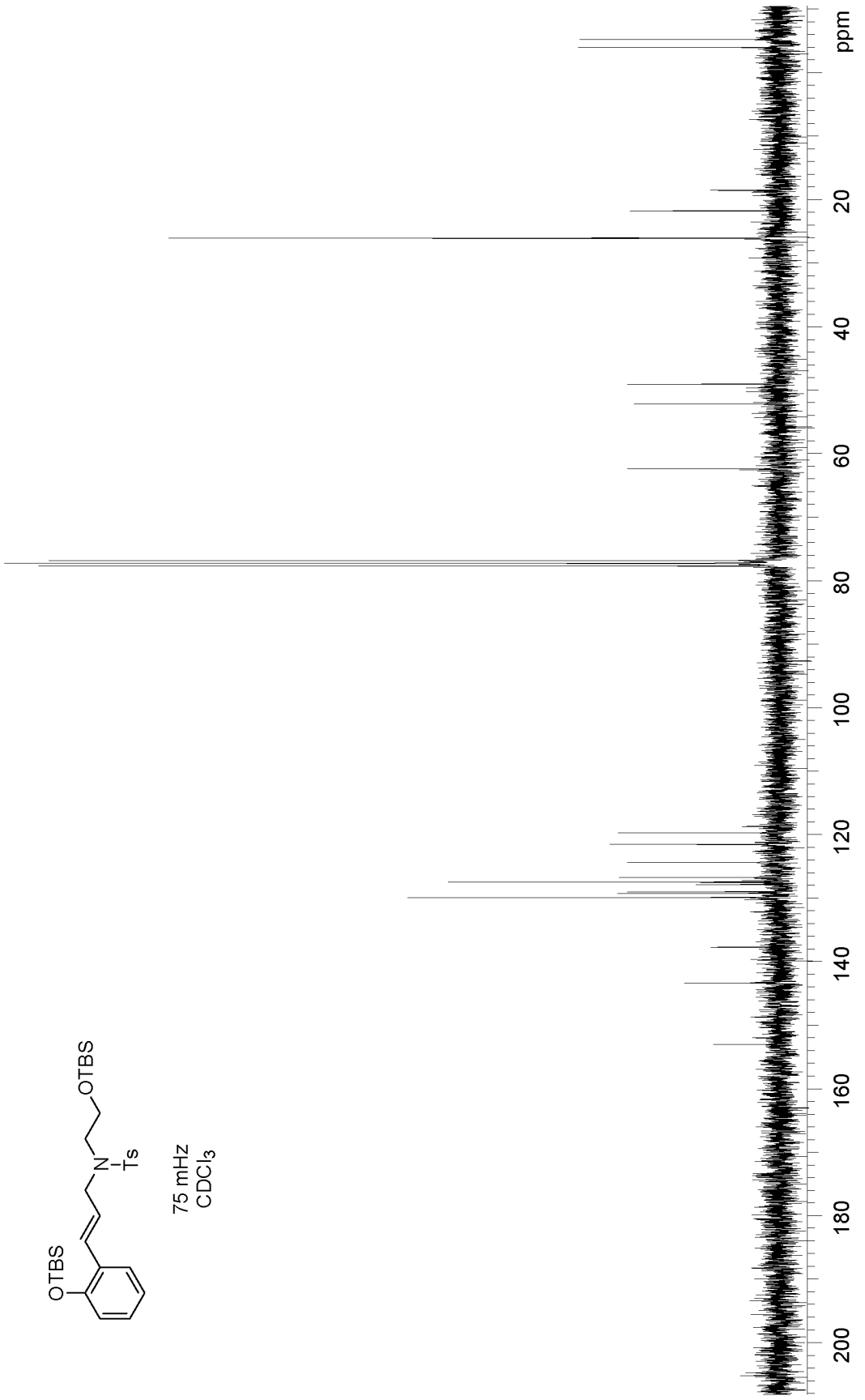
OTBS
OTBS
N
Ts
75 mHz
CDCl3
ppm
200
180
160
140
120
100
80
60
40
20

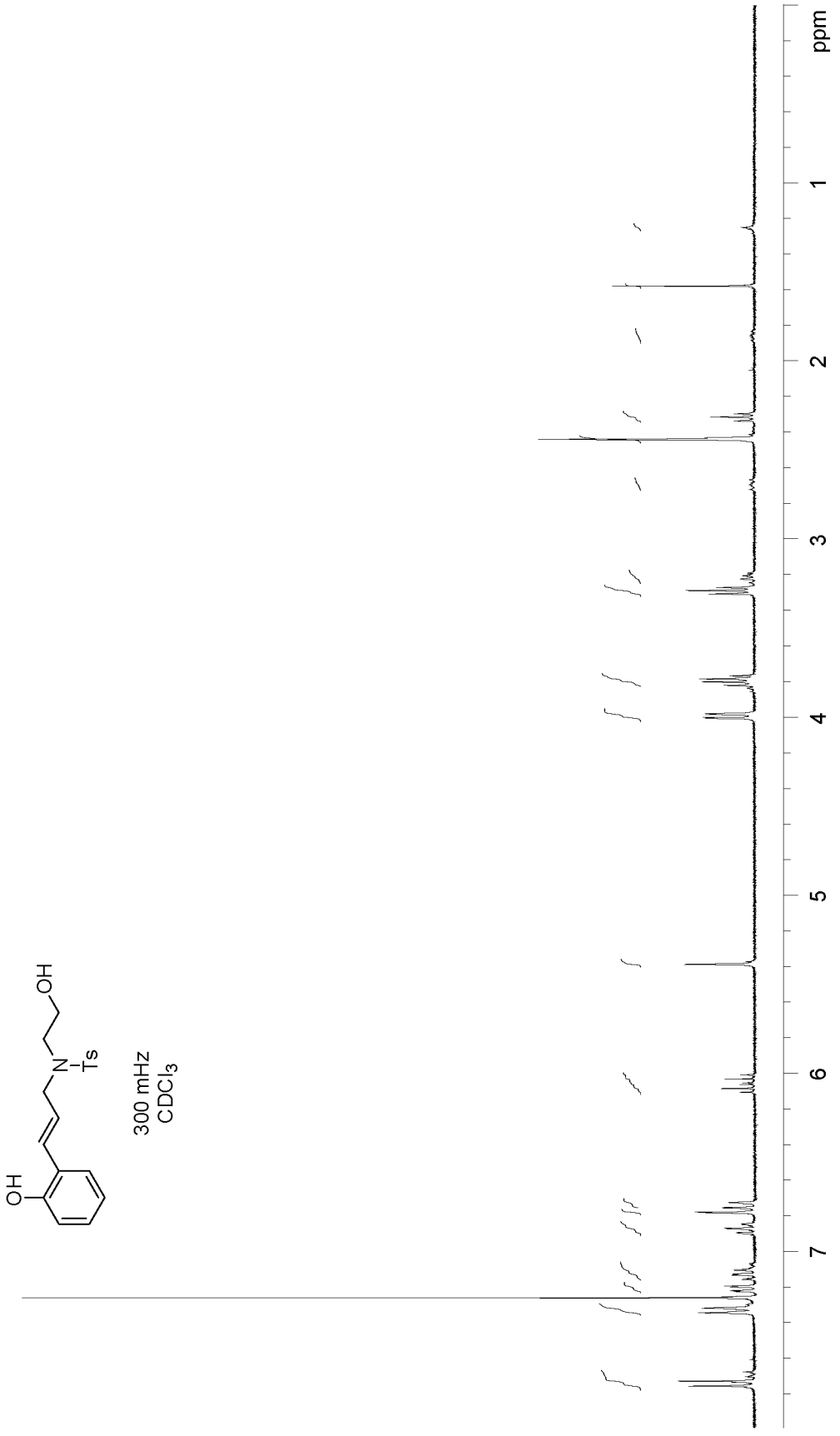
OH
N
Ts
OH
300 mHz
CDCl3
ppm
1
2
3
4
5
6
7

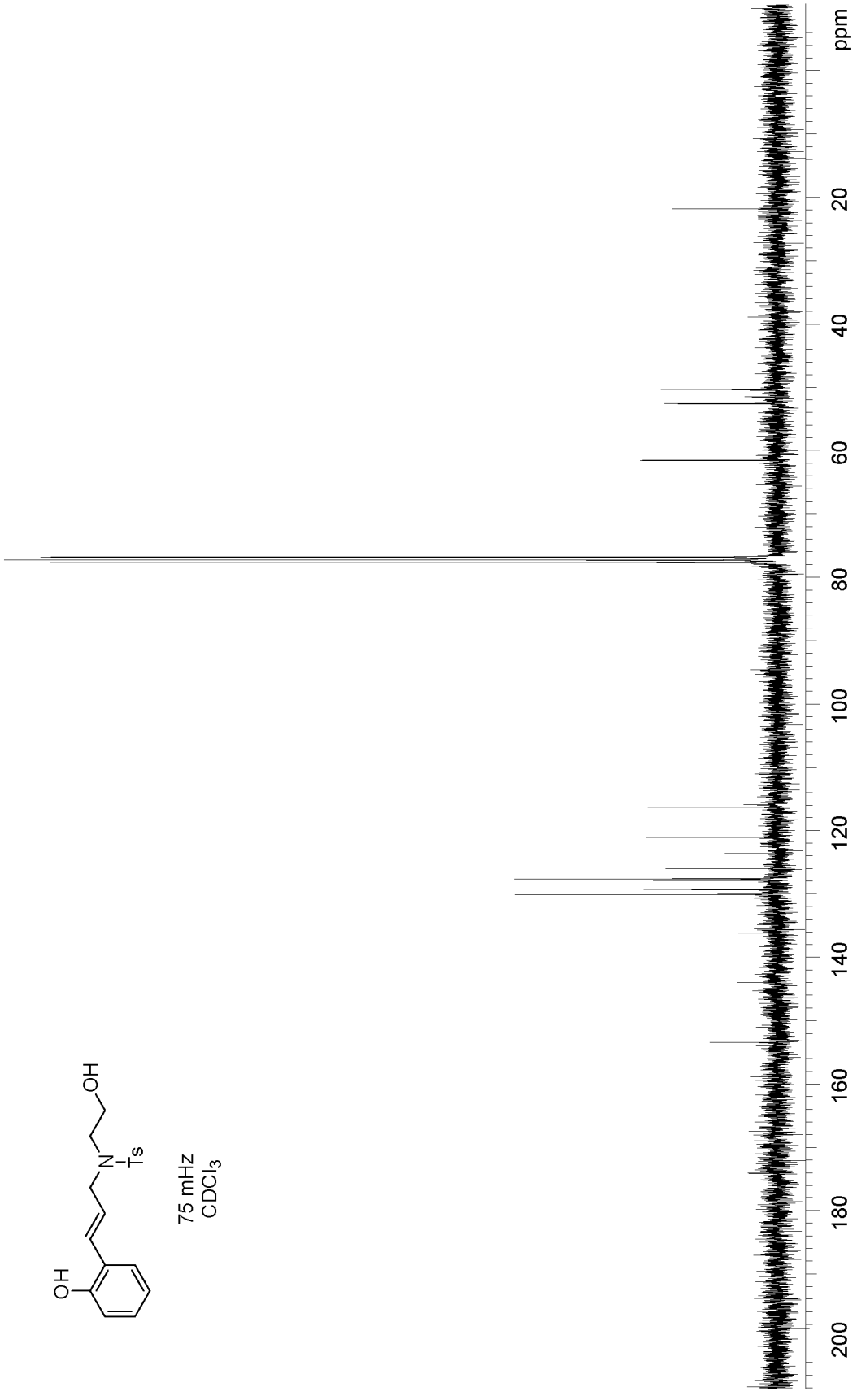
OH
N
Ts
OH
75 mHz
$CDCl_3$
ppm
200
180
160
140
120
100
80
60
40
20

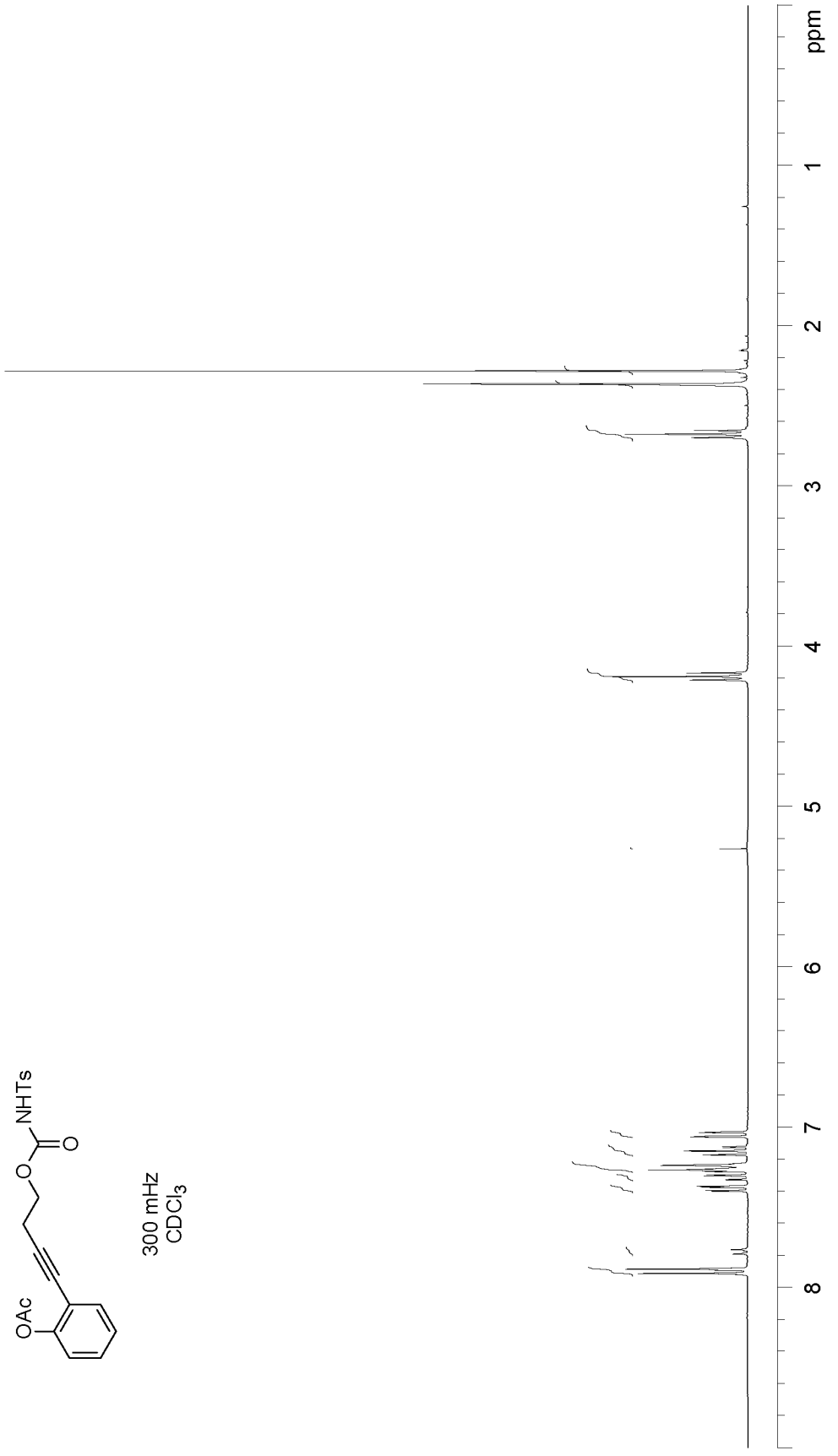
OAc
NHTs
O
O
300 mHz
CDCl3
ppm
1
2
3
4
5
6
7
8

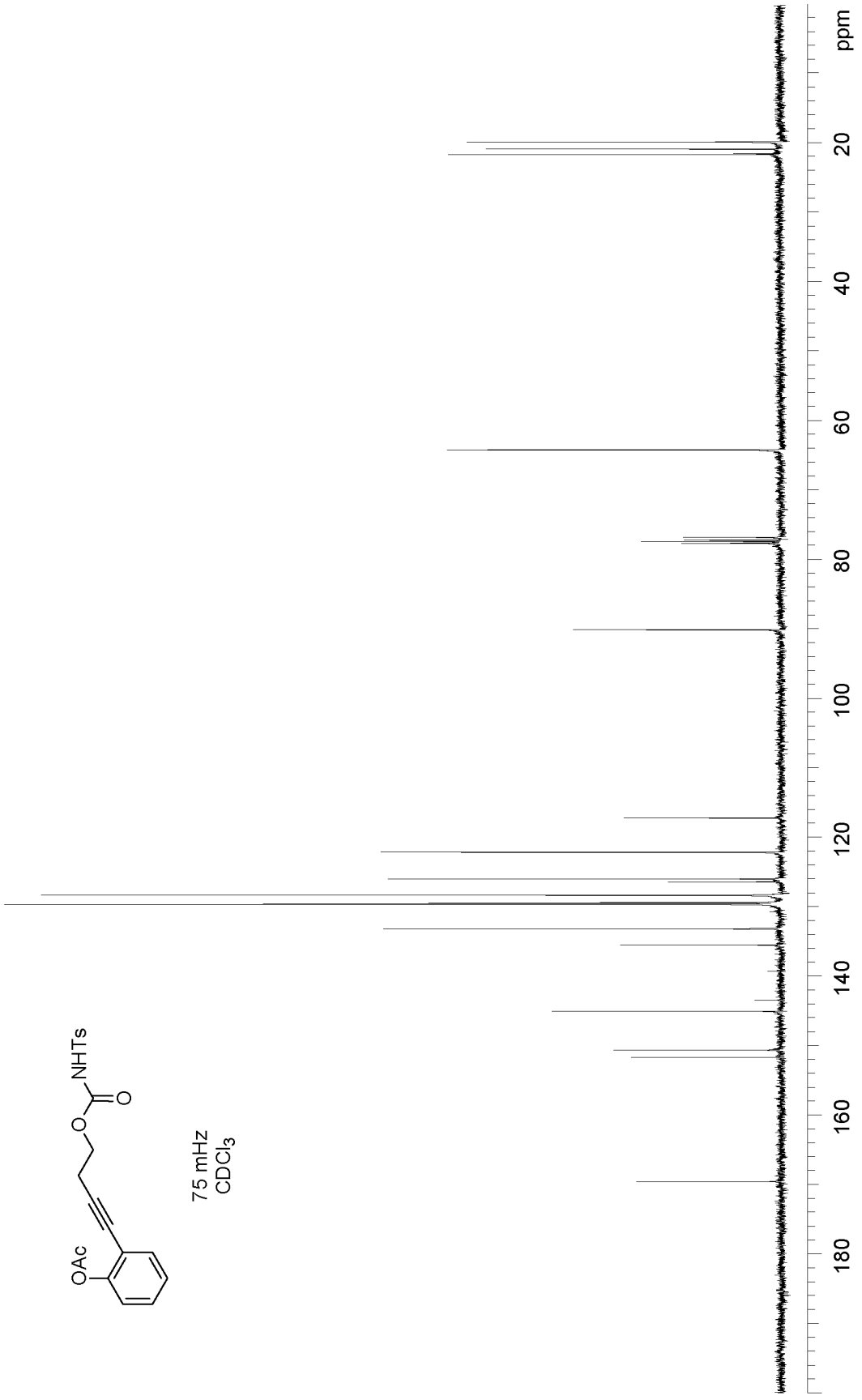
OAc
NHTs
O
O
75 mHz
$CDCl_3$
ppm
20
40
60
80
100
120
140
160
180

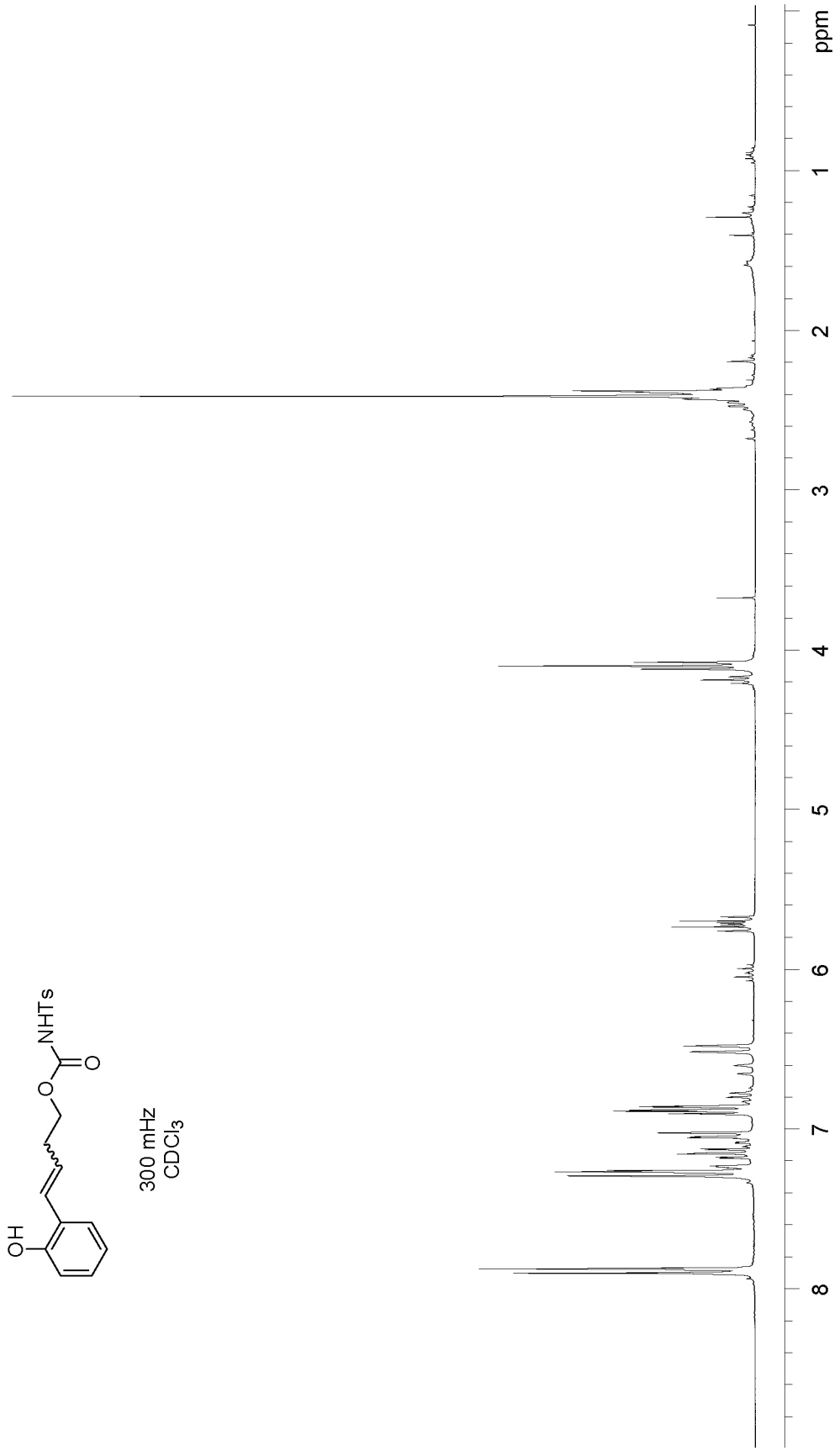
NHTs
O
O
OH
300 mHz
CDCl3
ppm
1
2
3
4
5
6
7
8

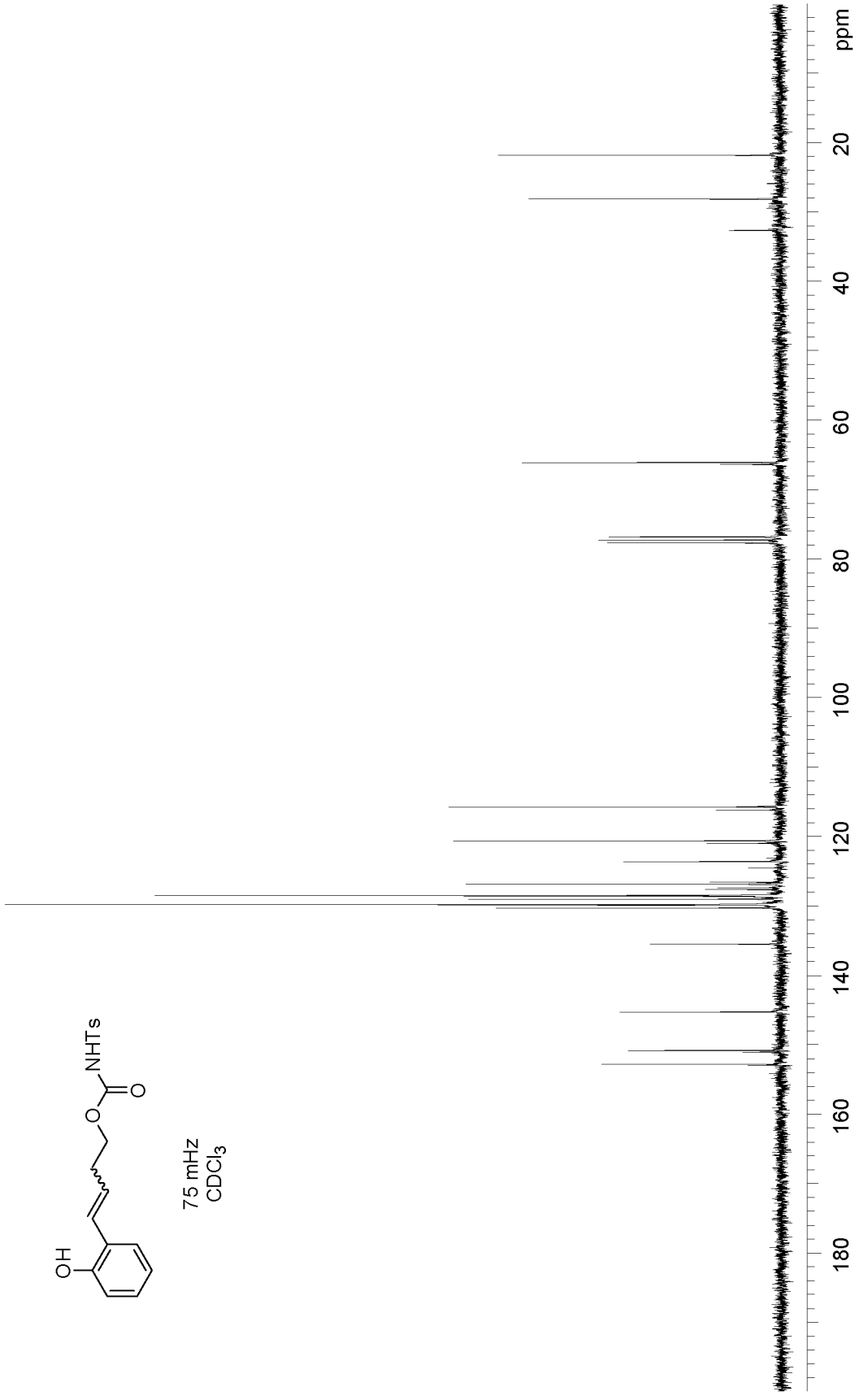
OH
NHTs
O
O
75 mHz
CDCl3
ppm
20
40
60
80
100
120
140
160
180

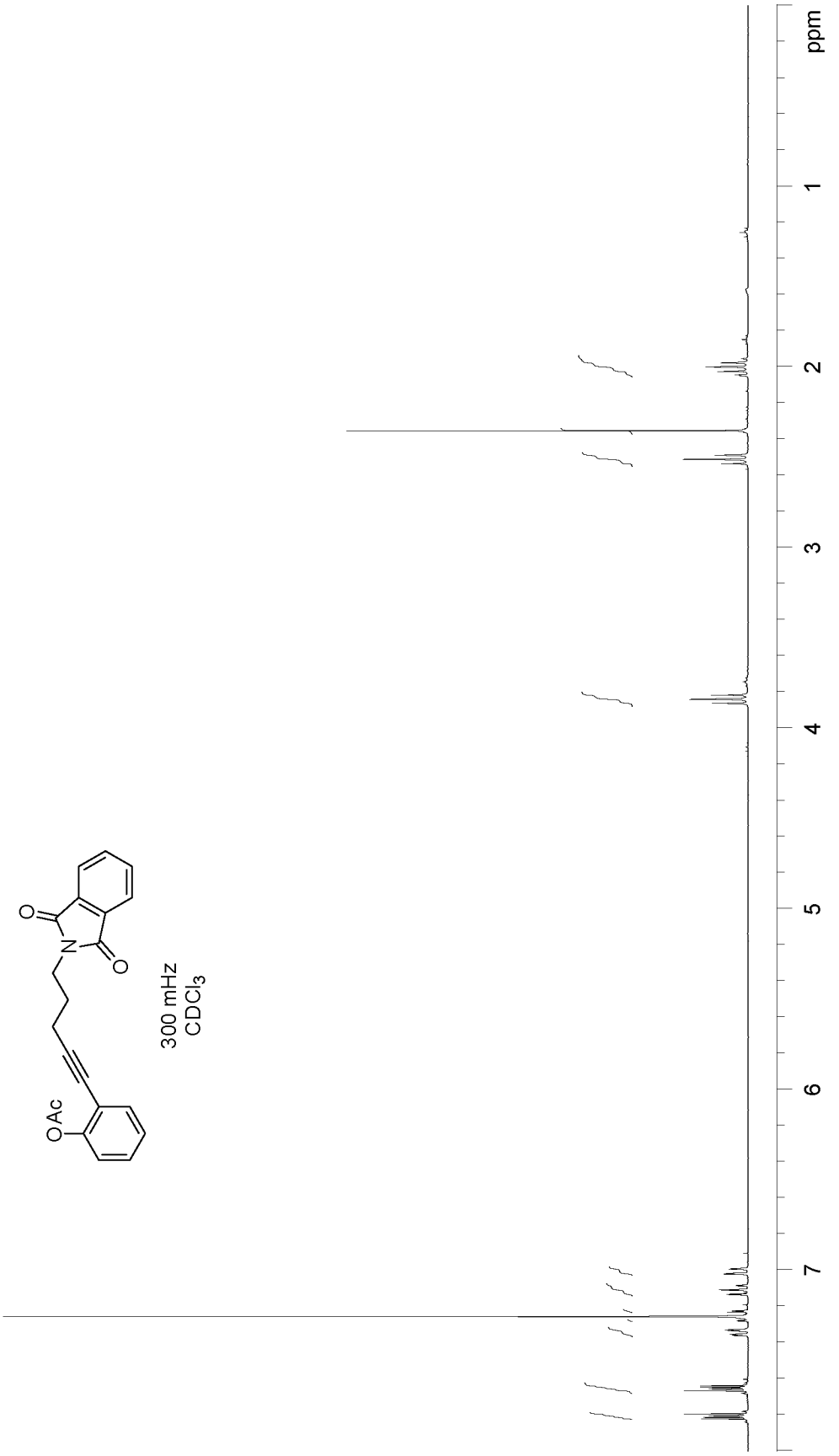
OAc
300 mHz
$CDCl_3$
ppm
1
2
3
4
5
6
7

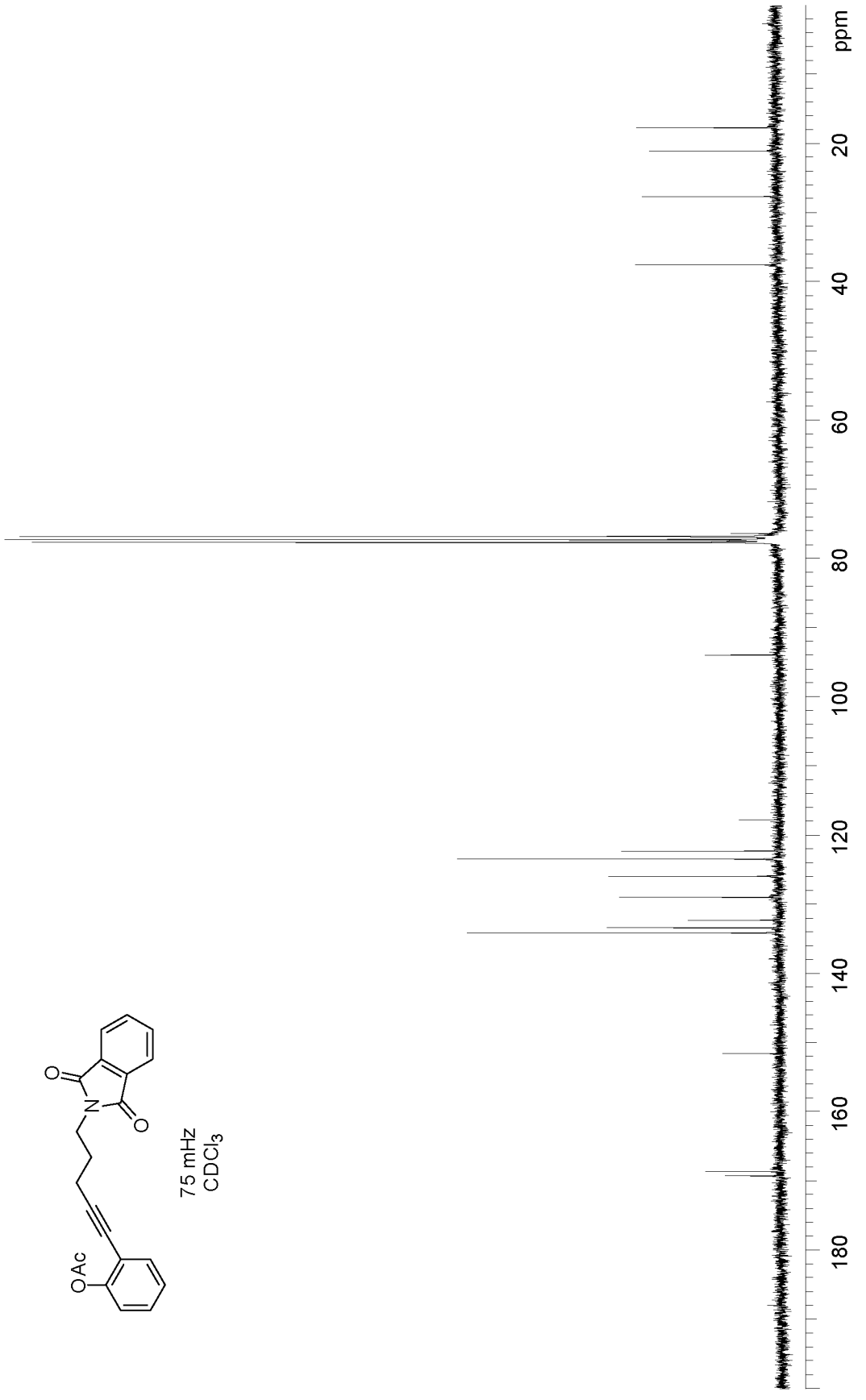
ppm
20
40
60
80
100
120
140
160
180
75 mHz
$CDCl_3$
O
N
O
O
OAc

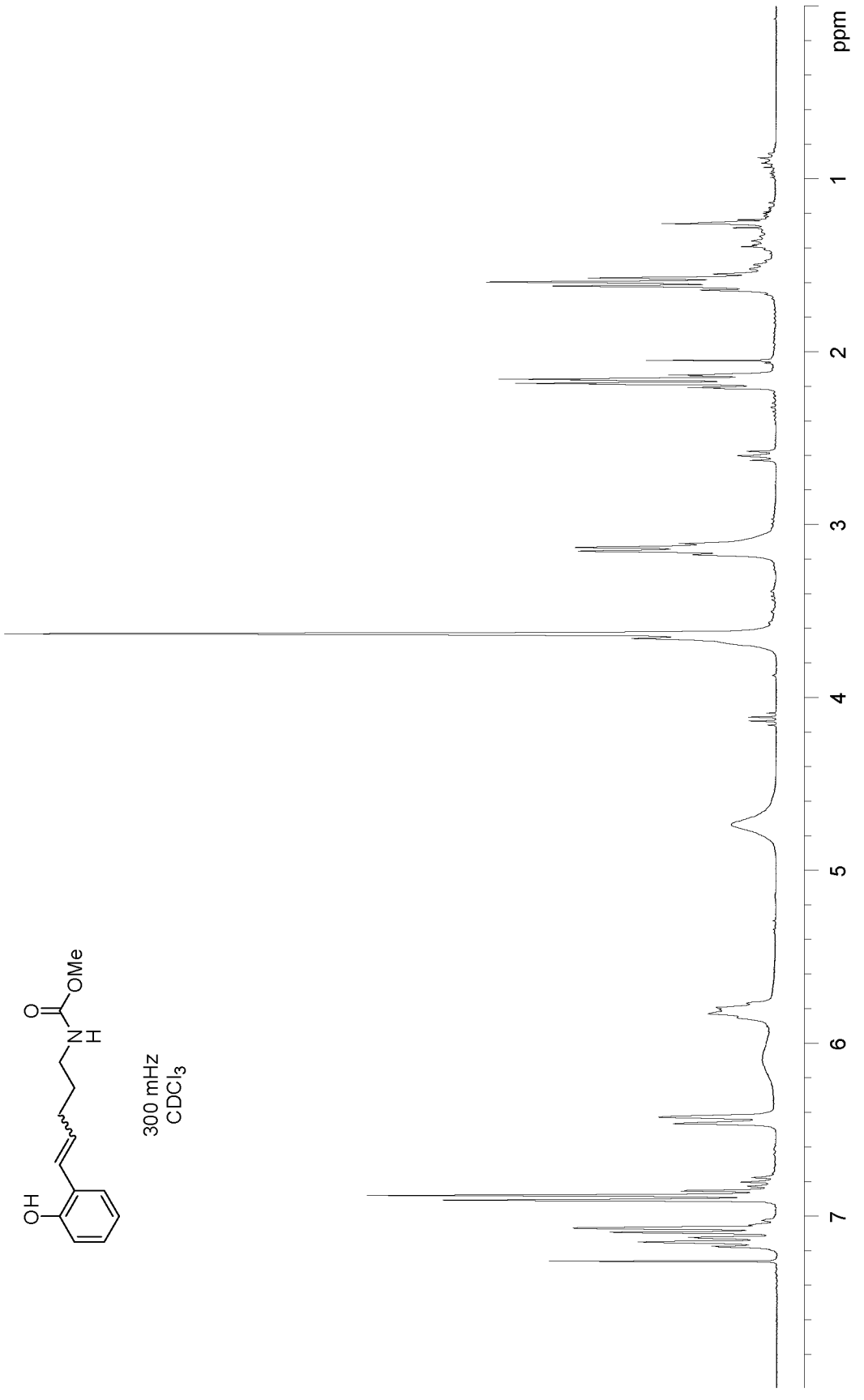
OMe
O
N
H
OH
300 mHz
CDCl3
ppm
1
2
3
4
5
6
7

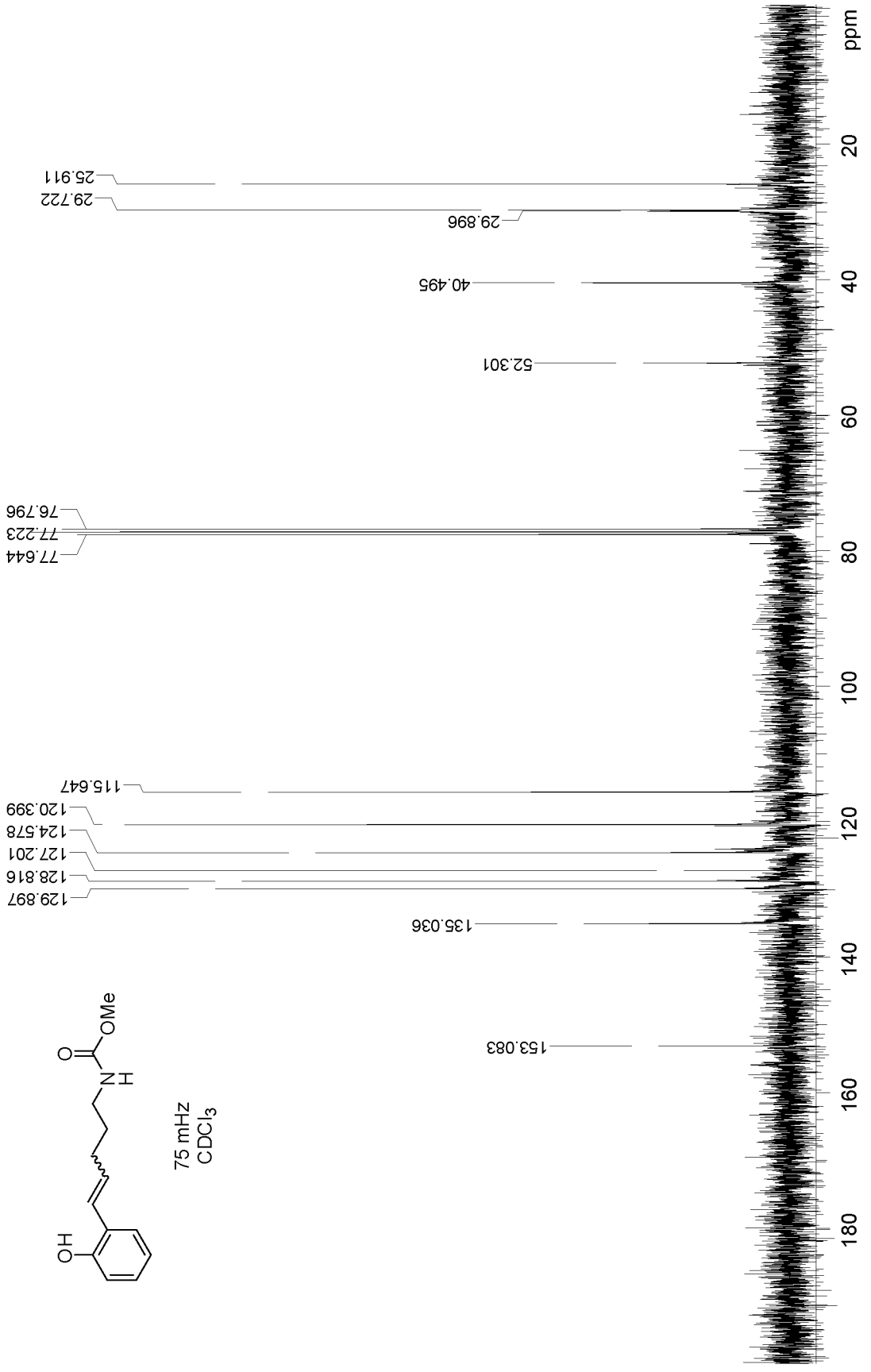
153.083
135.036
129.897
128.816
127.201
124.578
120.399
115.647
77.644
77.223
76.796
52.301
40.495
29.896
29.722
25.911
ppm
20
40
60
80
100
120
140
160
180
75 mHz
CDCl3
OH
N
H
O
OMe

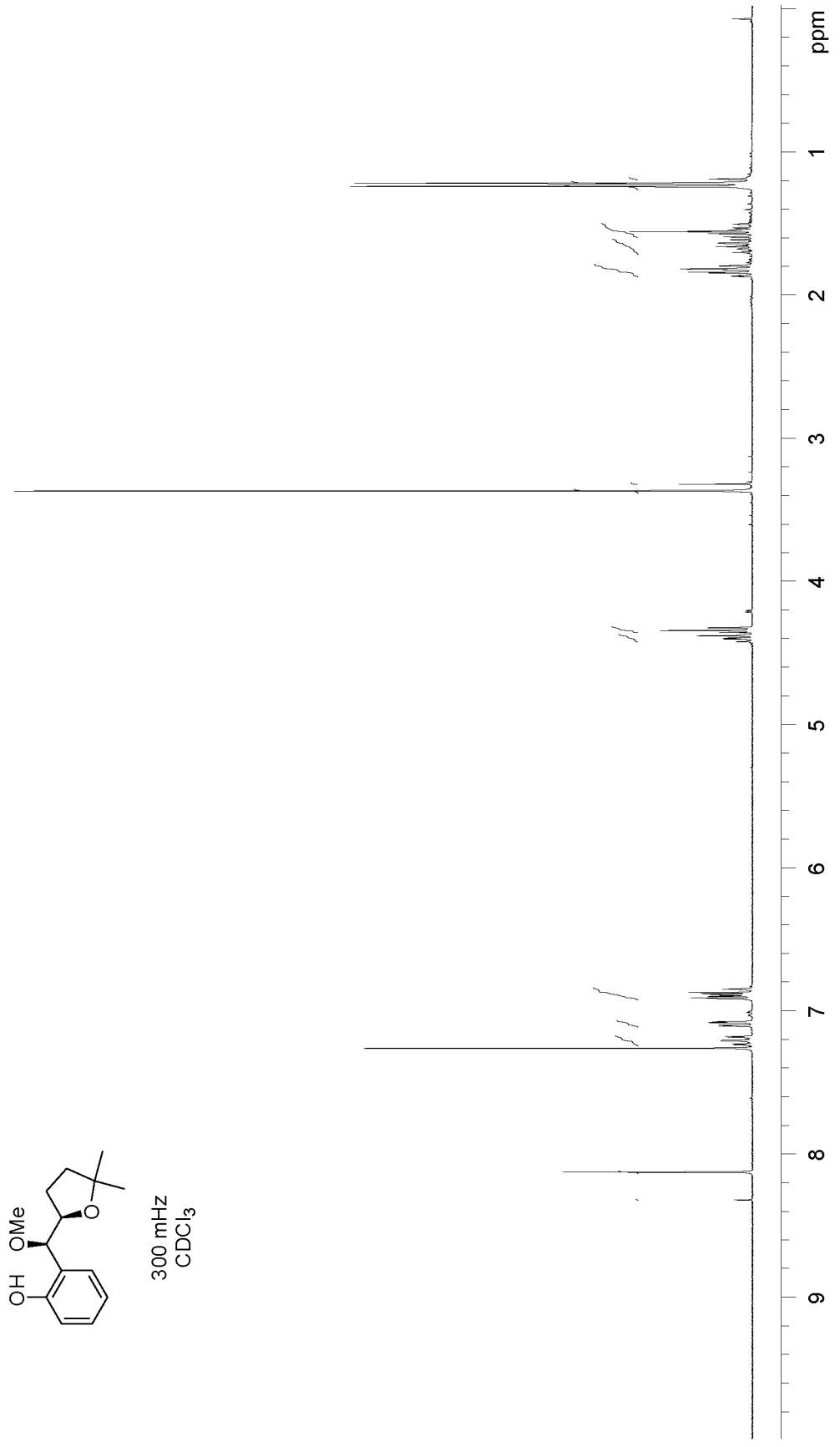
OH
OMe
O
300 mHz
CDCl3
ppm
1
2
3
4
5
6
7
8
9

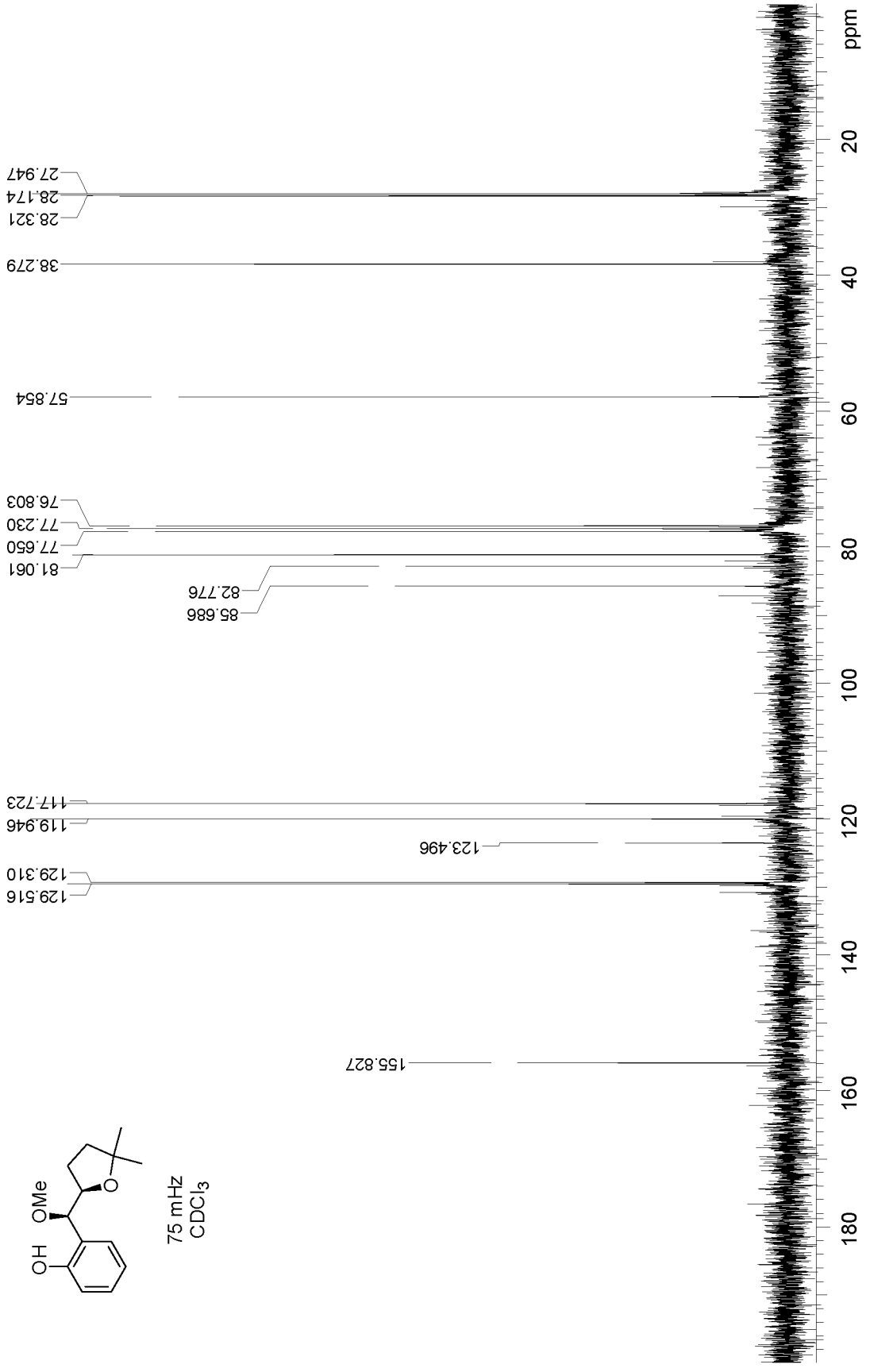
155.827
123.496
129.516
129.310
119.946
117.723
85.686
82.776
81.061
77.650
77.230
76.803
57.854
38.279
28.321
28.174
27.947
ppm
20
40
60
80
100
120
140
160
180
OMe
OH
O
75 mHz
CDCl3

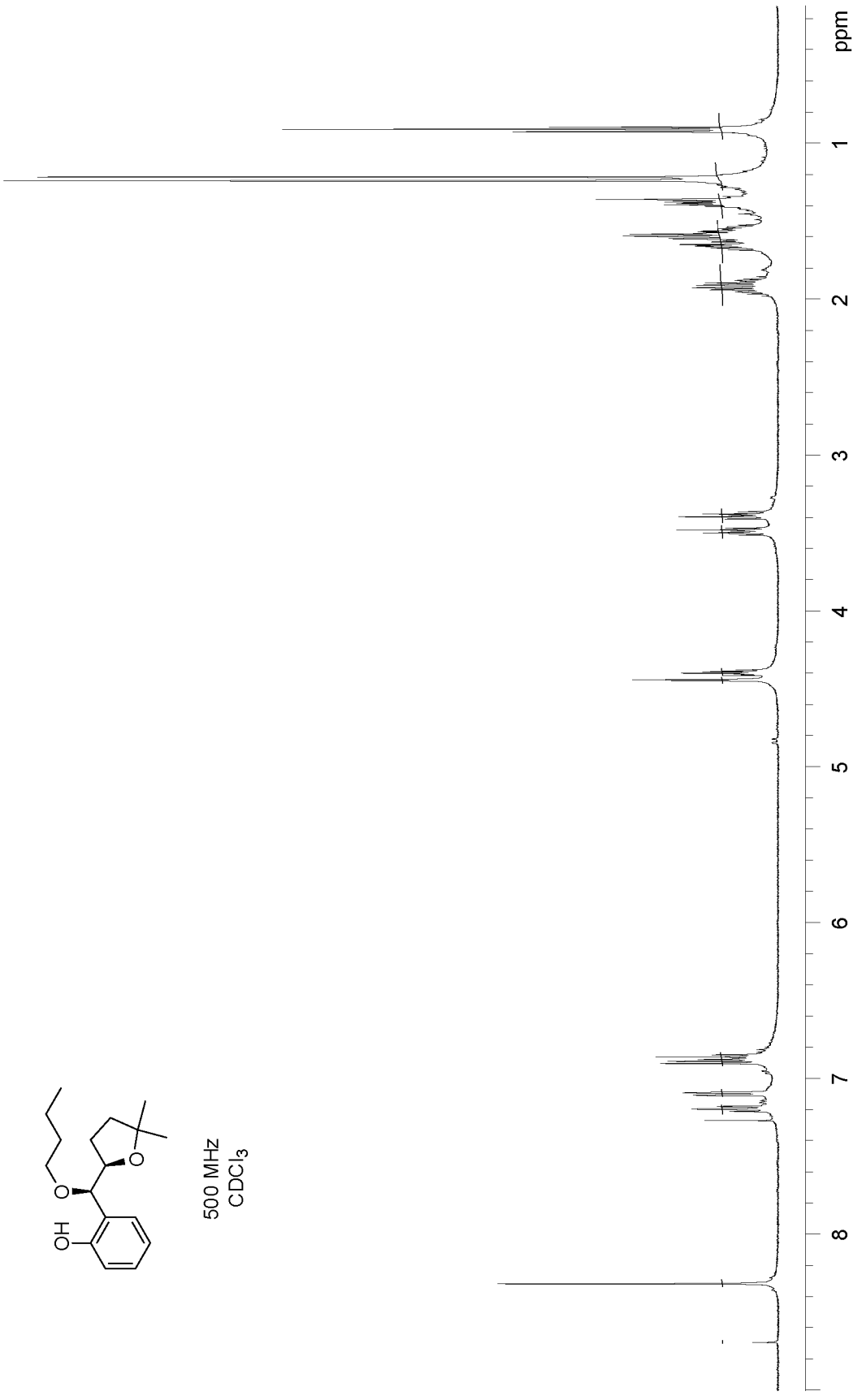
ppm
1
2
3
4
5
6
7
8
500 MHz
CDCl3
OH
O
O

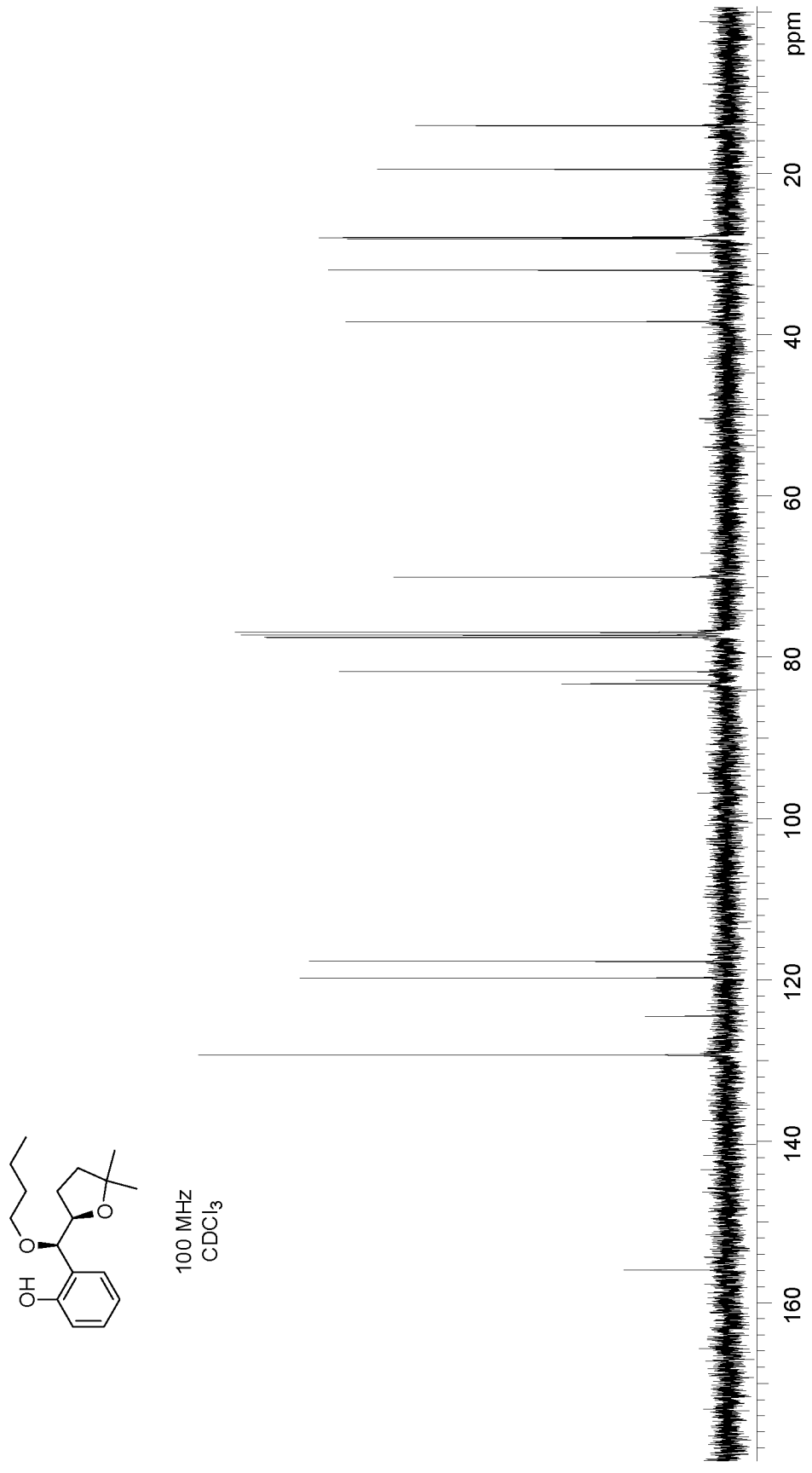
100 MHz
$CDCl_3$
ppm
20
40
60
80
100
120
140
160
OH
O
O

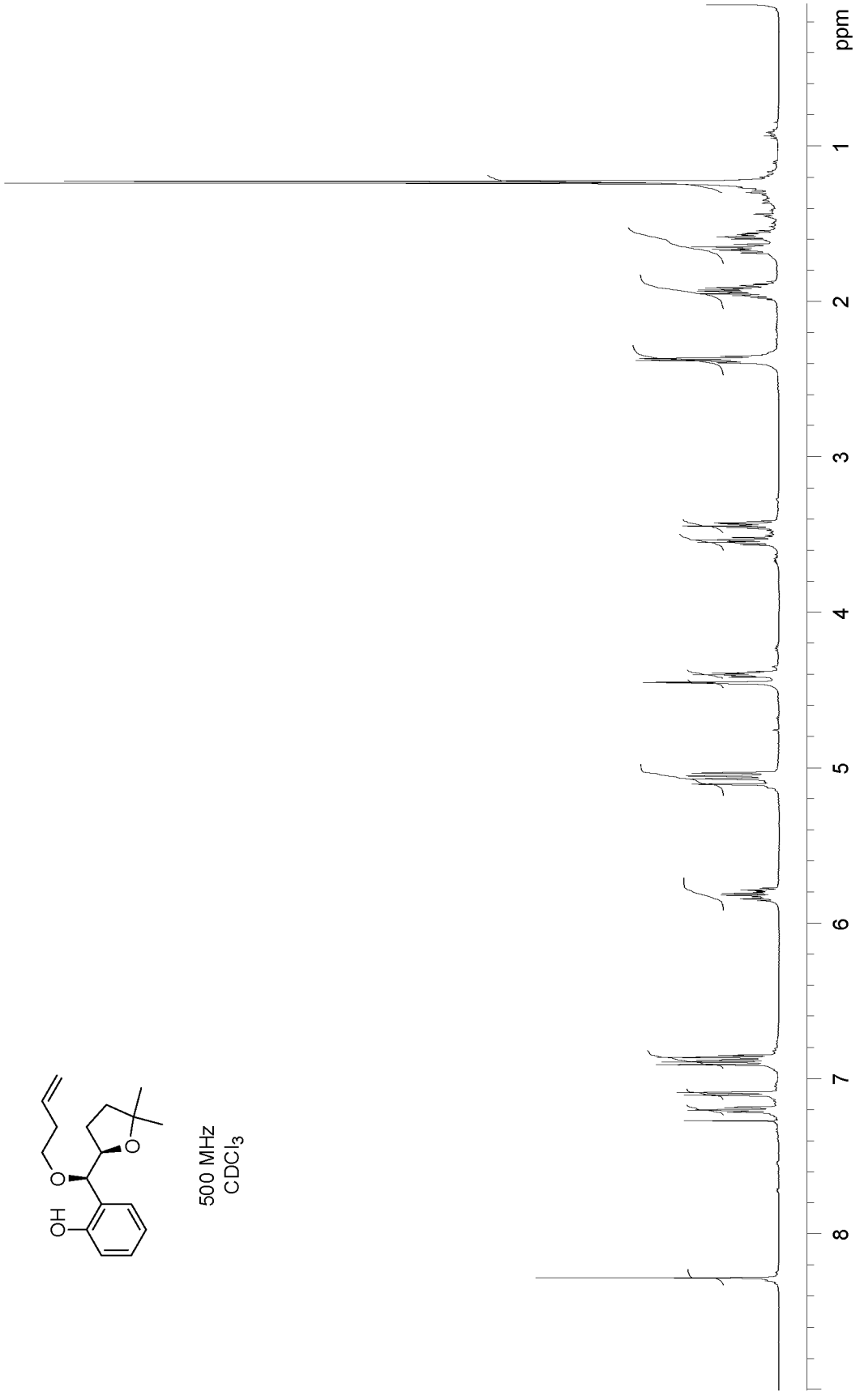
ppm
1
2
3
4
5
6
7
8
500 MHz
CDCl3
OH
O
O

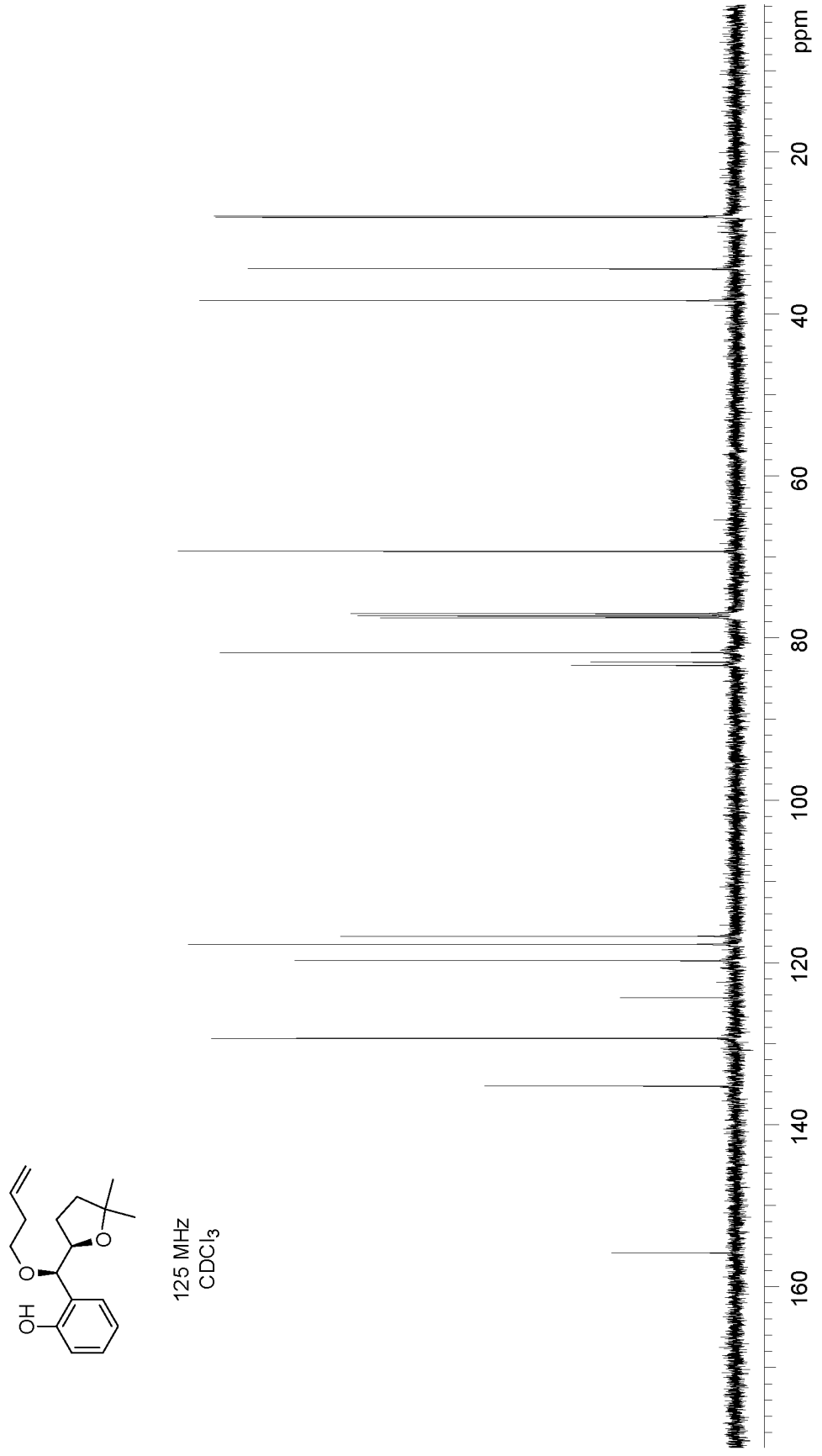
125 MHz
$CDCl_3$
ppm
20
40
60
80
100
120
140
160
OH
O
O

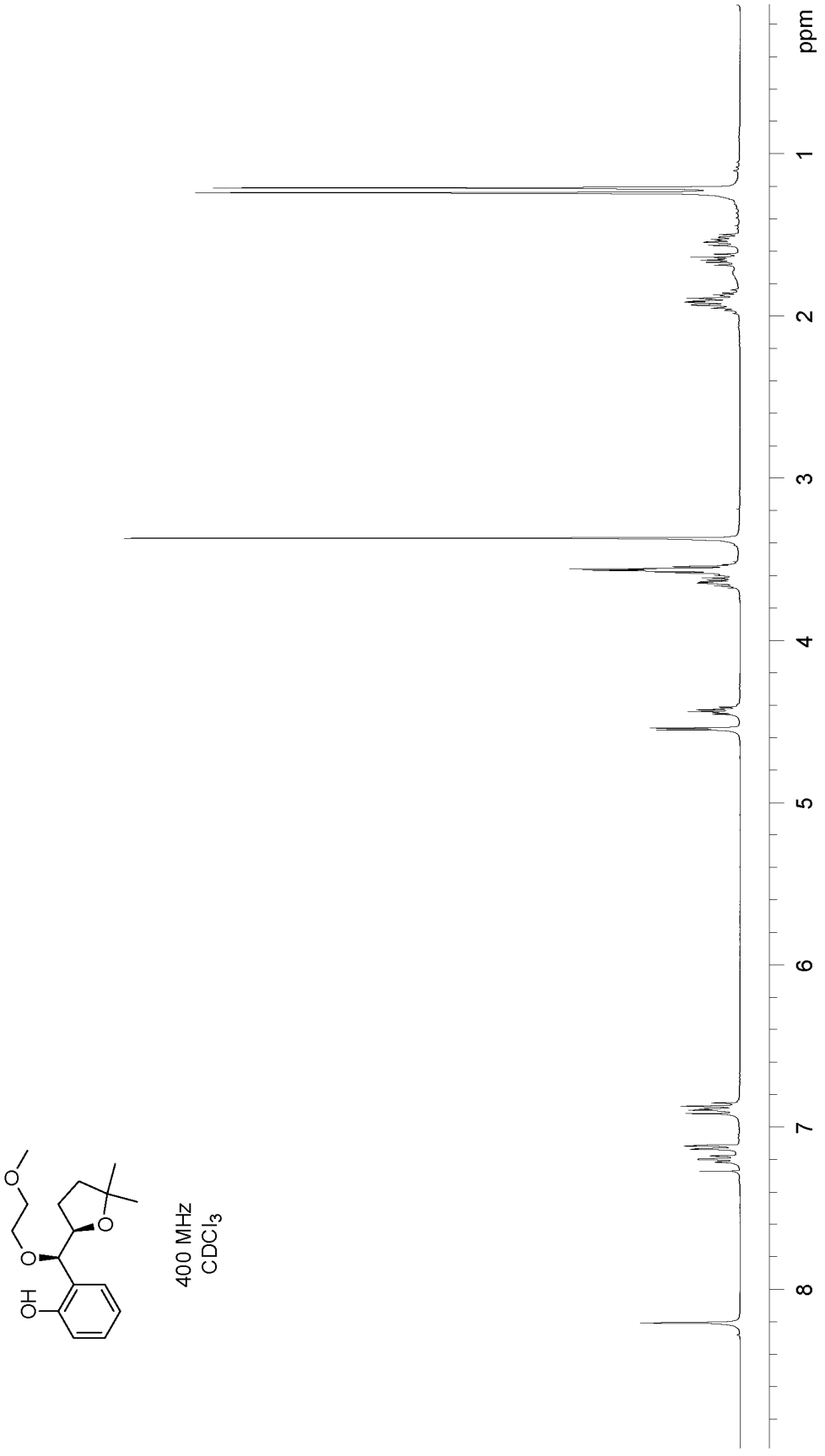
400 MHz
CDCl3
OH
O
O
O
ppm
1
2
3
4
5
6
7
8

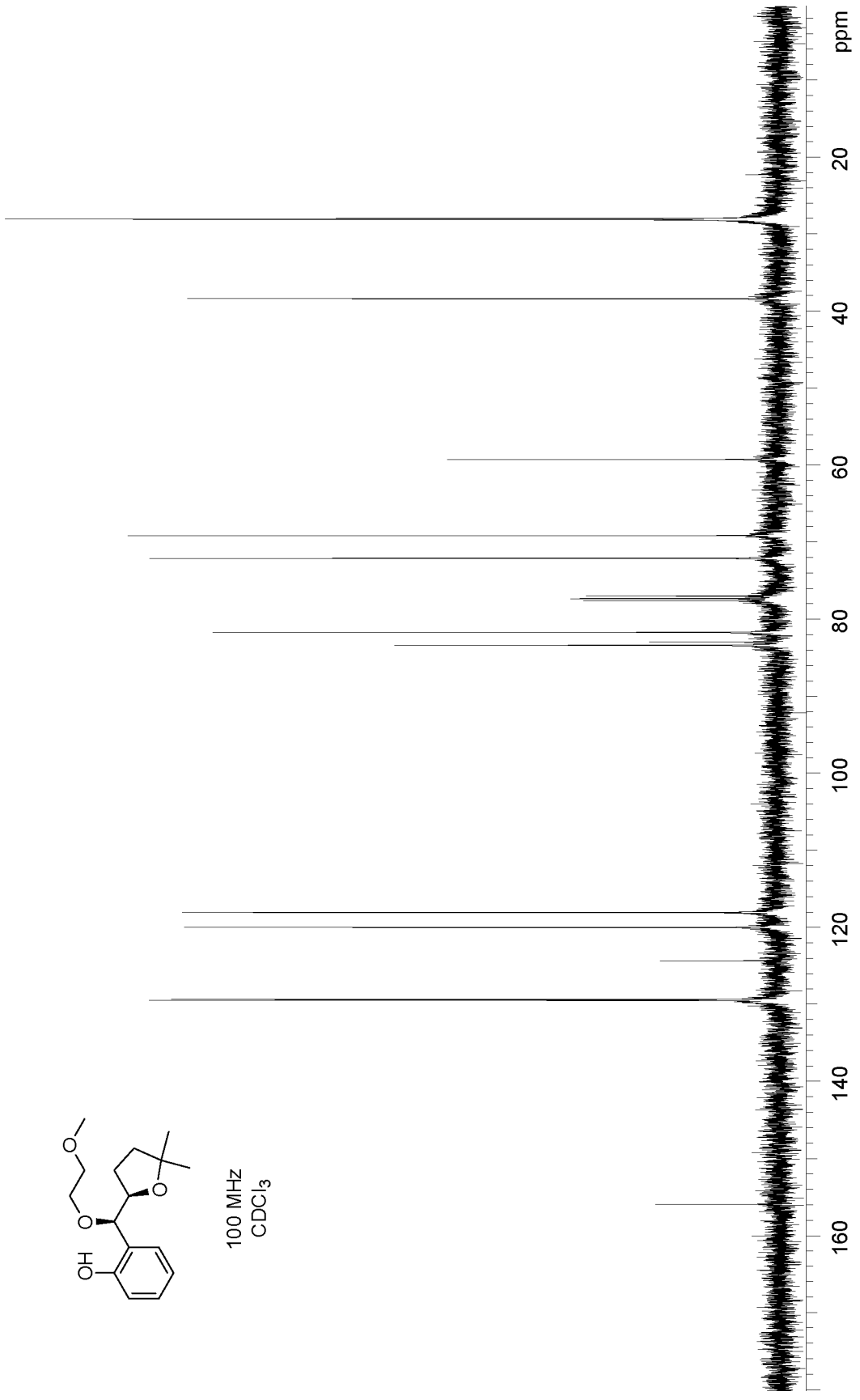
ppm
20
40
60
80
100
120
140
160
100 MHz
CDCl3
OH
O
O
O

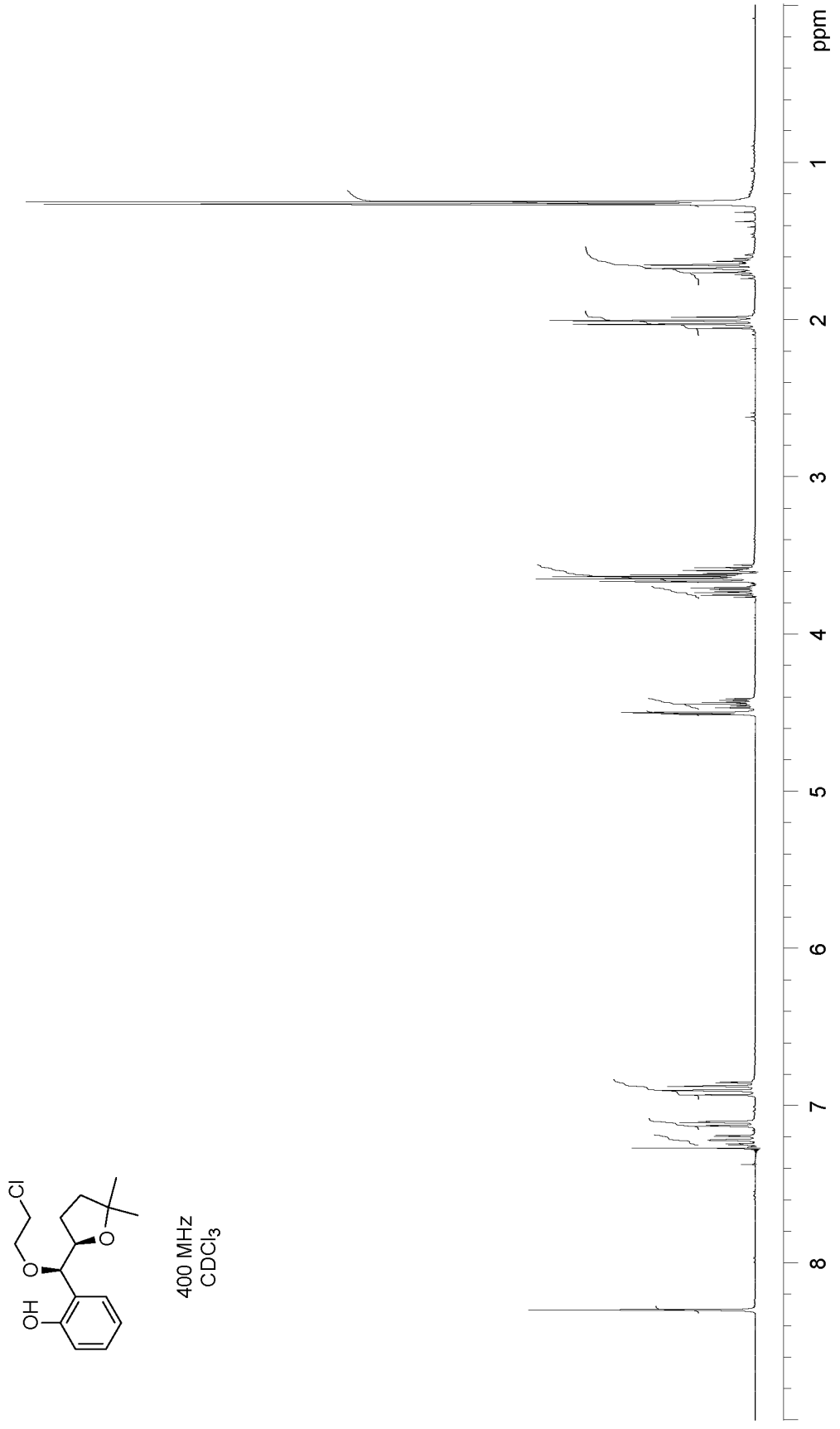
Cl
O
O
OH
400 MHz
CDCl3
ppm
1
2
3
4
5
6
7
8

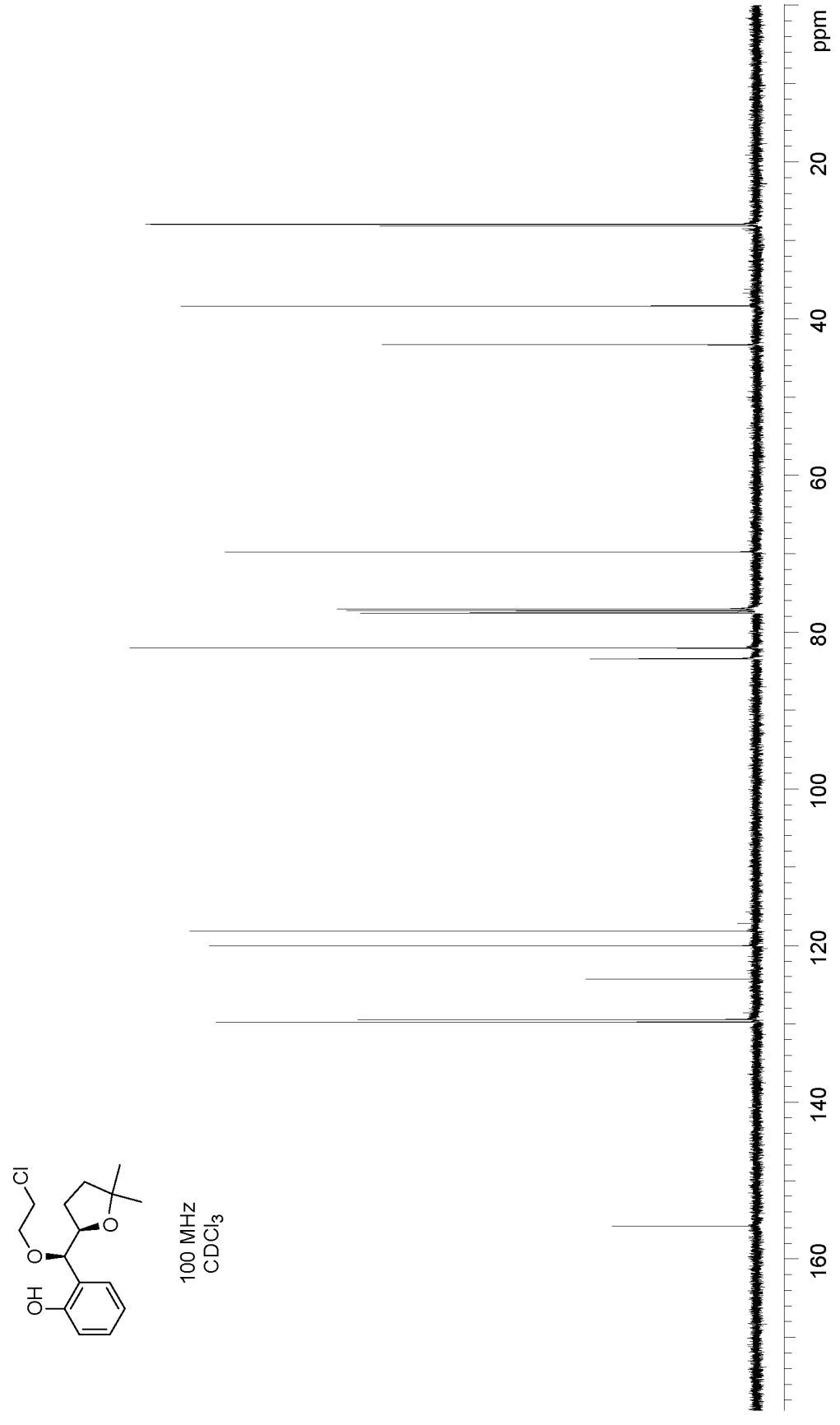
ppm
20
40
60
80
100
120
140
160
100 MHz
CDCl3
Cl
O
O
OH

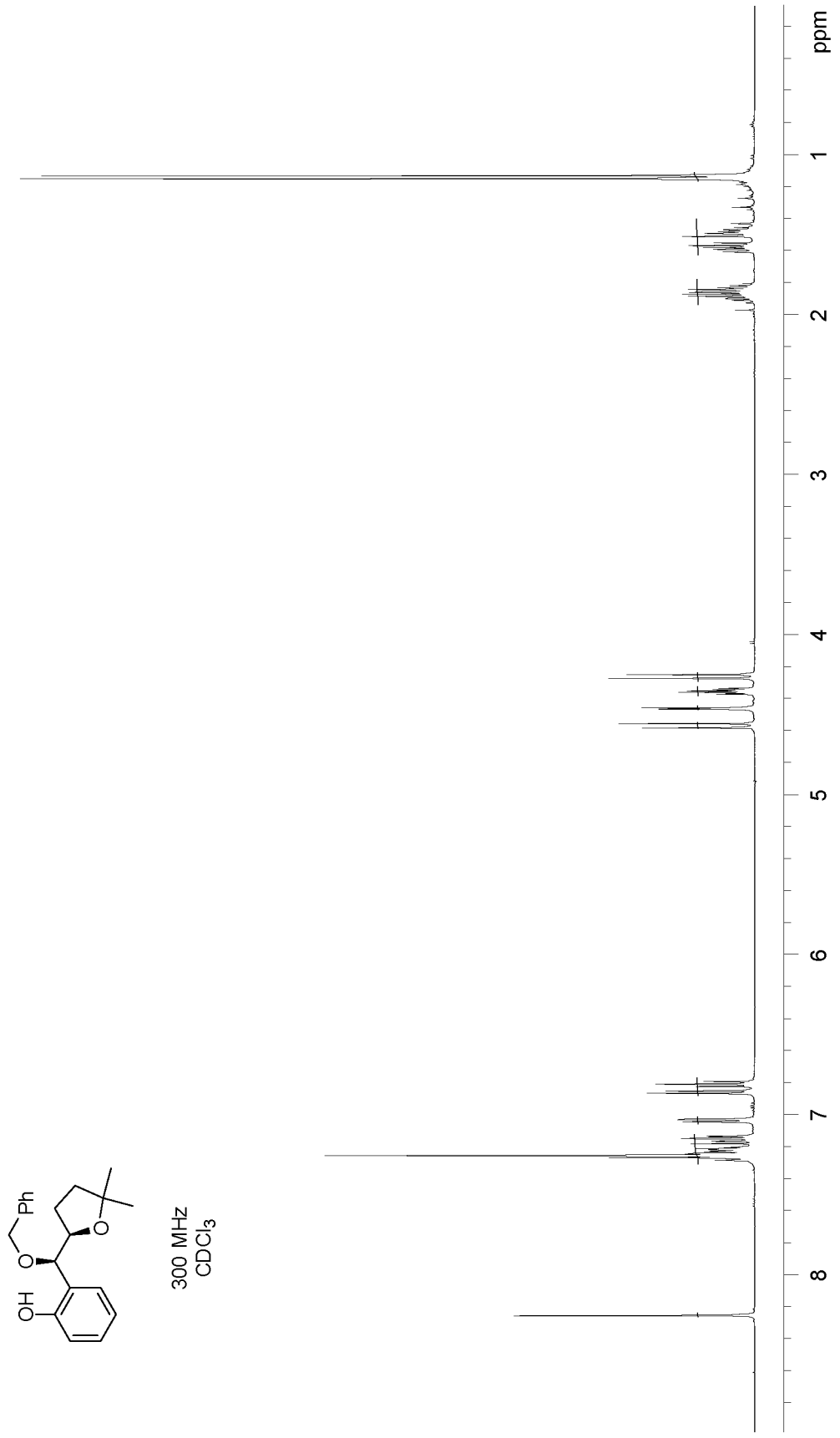
OH
O
Ph
O
300 MHz
CDCl3
ppm
1
2
3
4
5
6
7
8

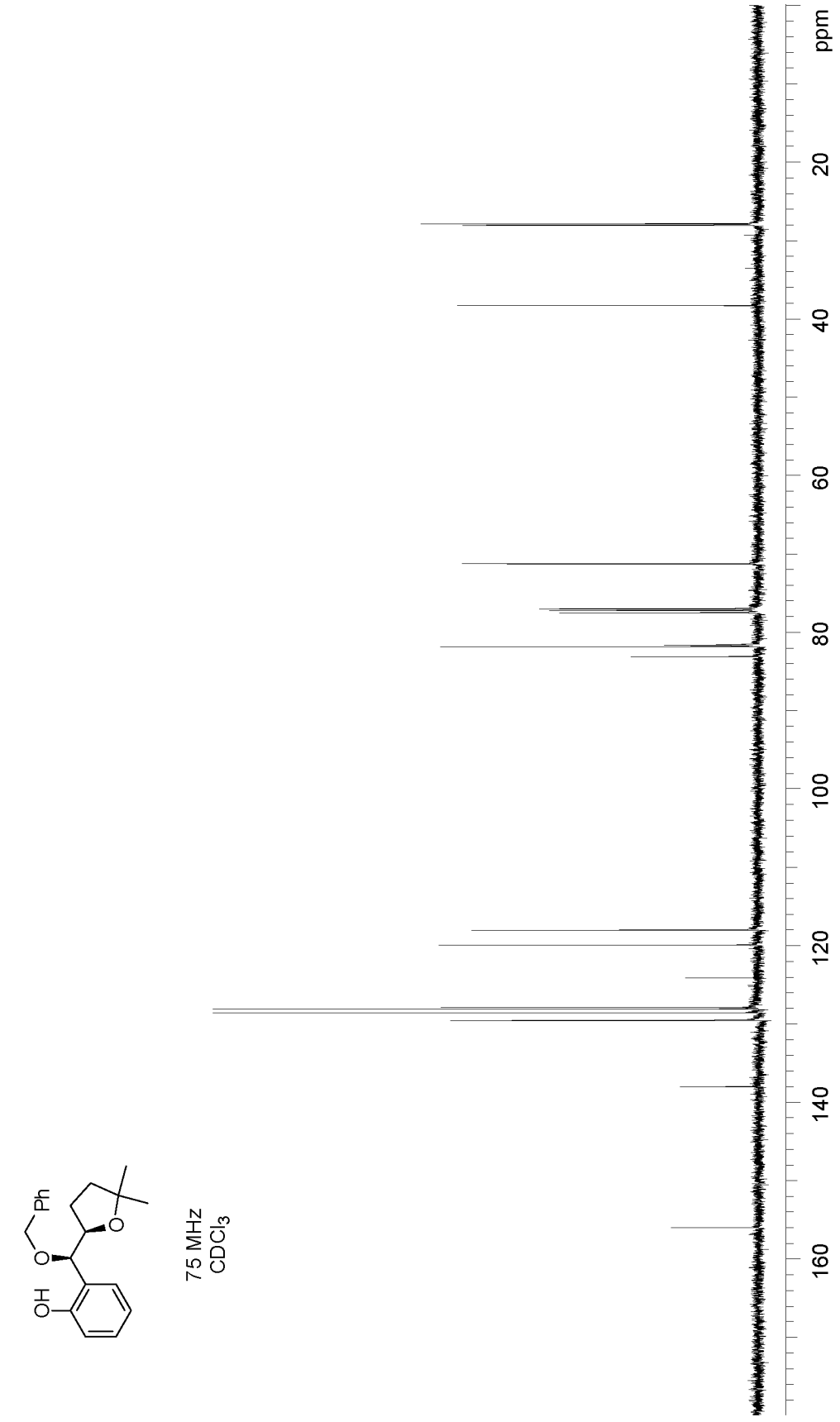
OH
O
Ph
O
75 MHz
$CDCl_3$
ppm
20
40
60
80
100
120
140
160

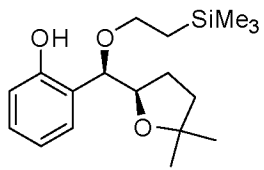

300 MHz
$CDCl_3$

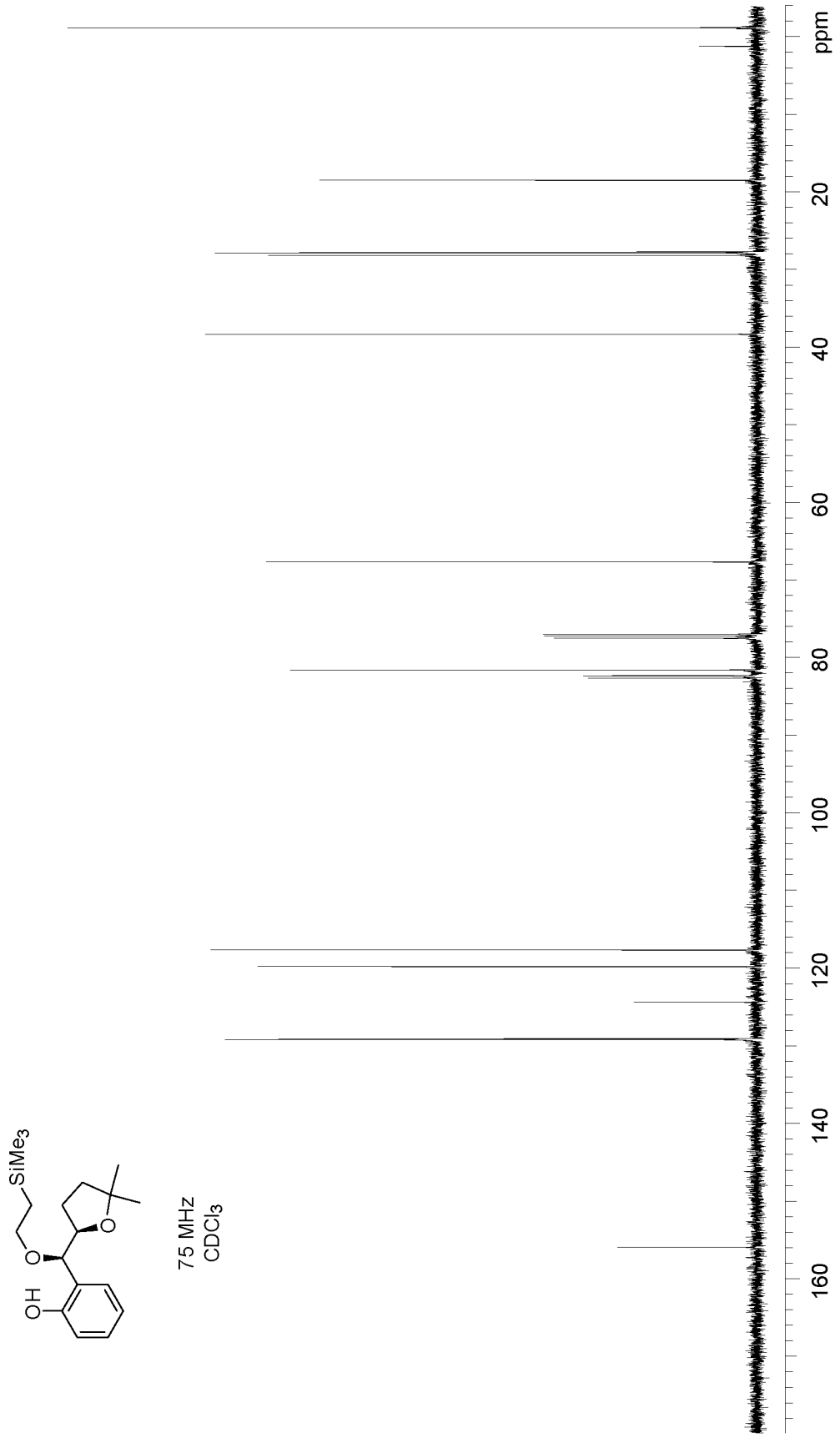
SiMe3
O
O
OH
75 MHz
CDCl3
ppm
20
40
60
80
100
120
140
160

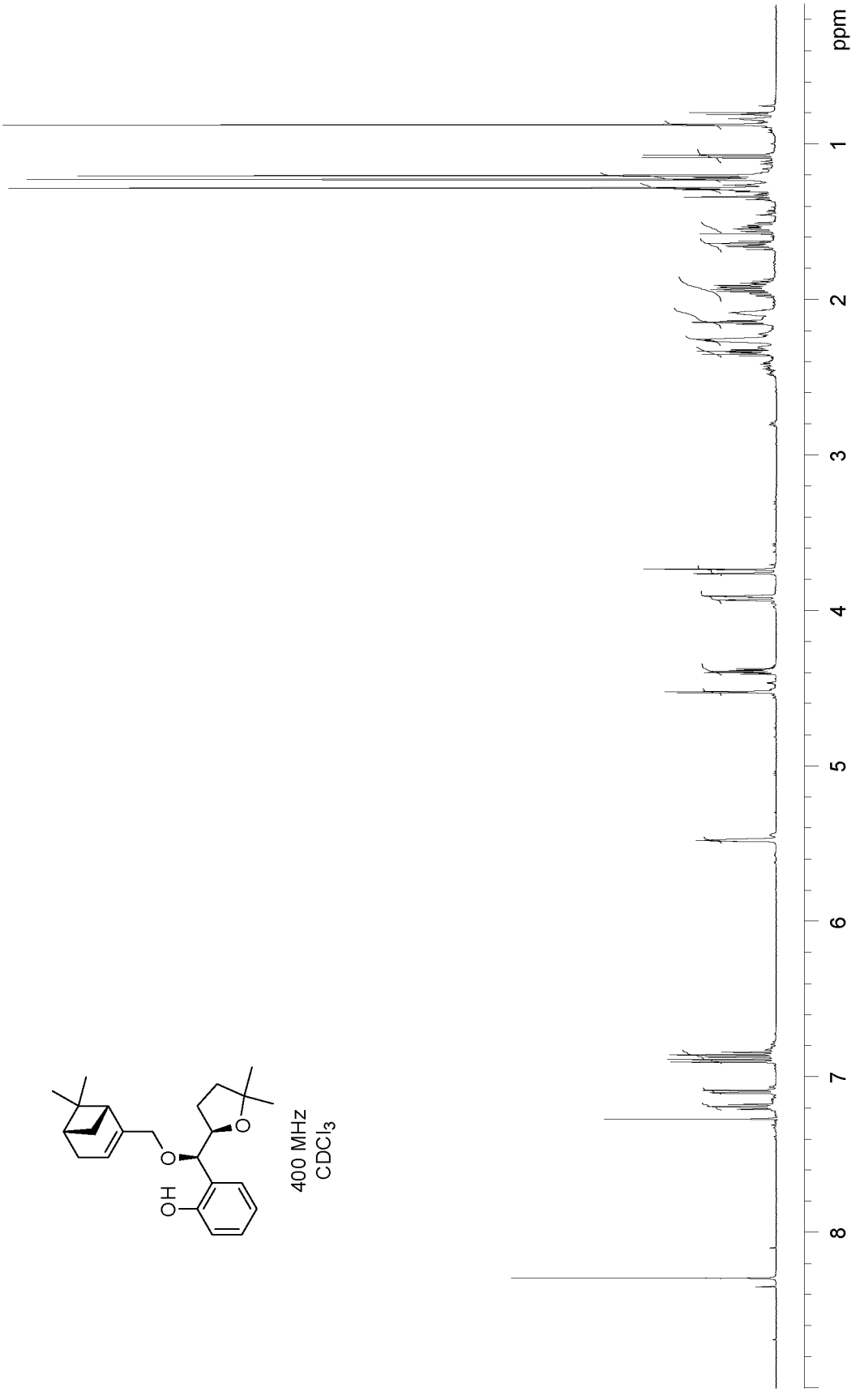
ppm
1
2
3
4
5
6
7
8
400 MHz
CDCl3
OH
O
O

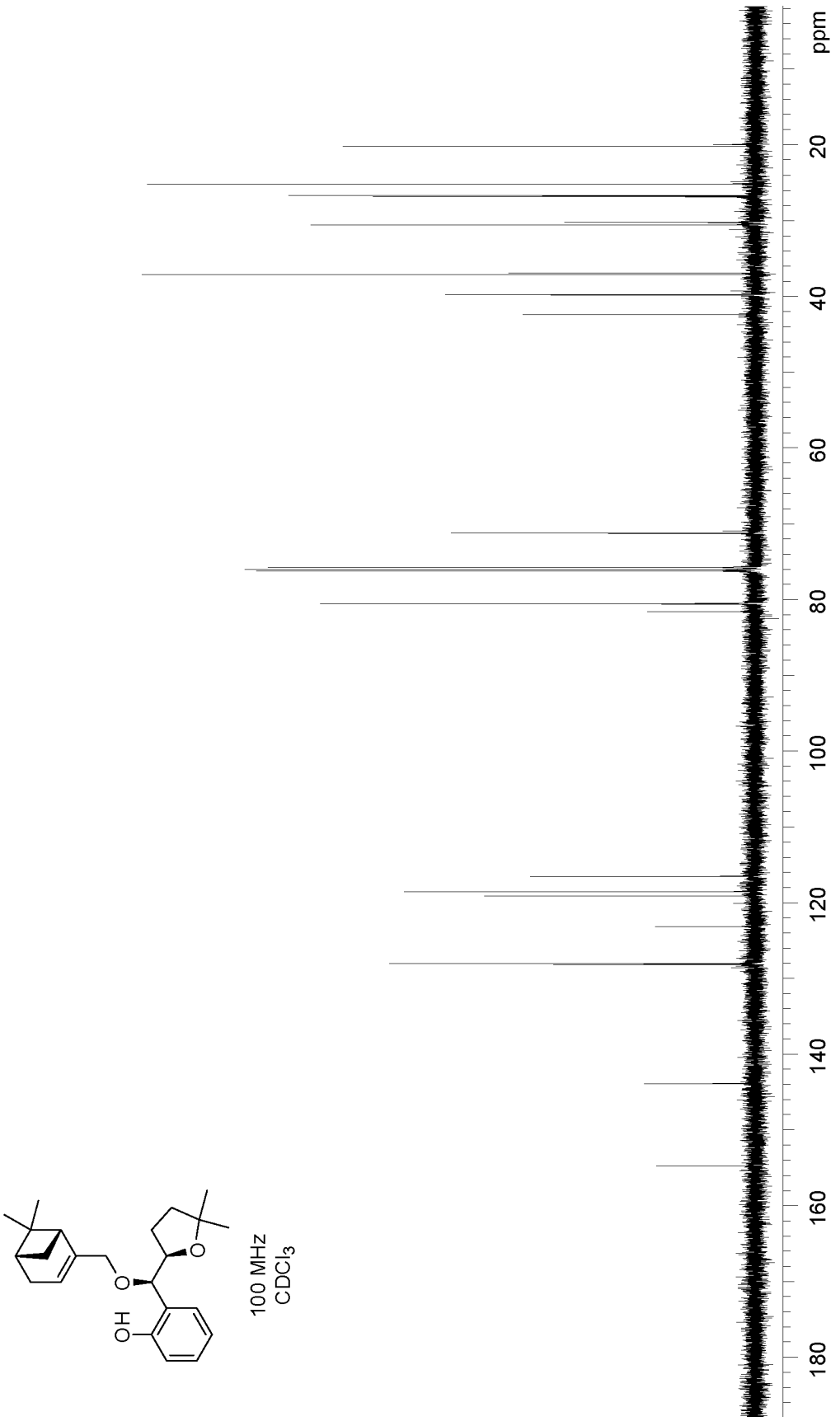
100 MHz
CDCl3
OH
O
O
ppm
20
40
60
80
100
120
140
160
180

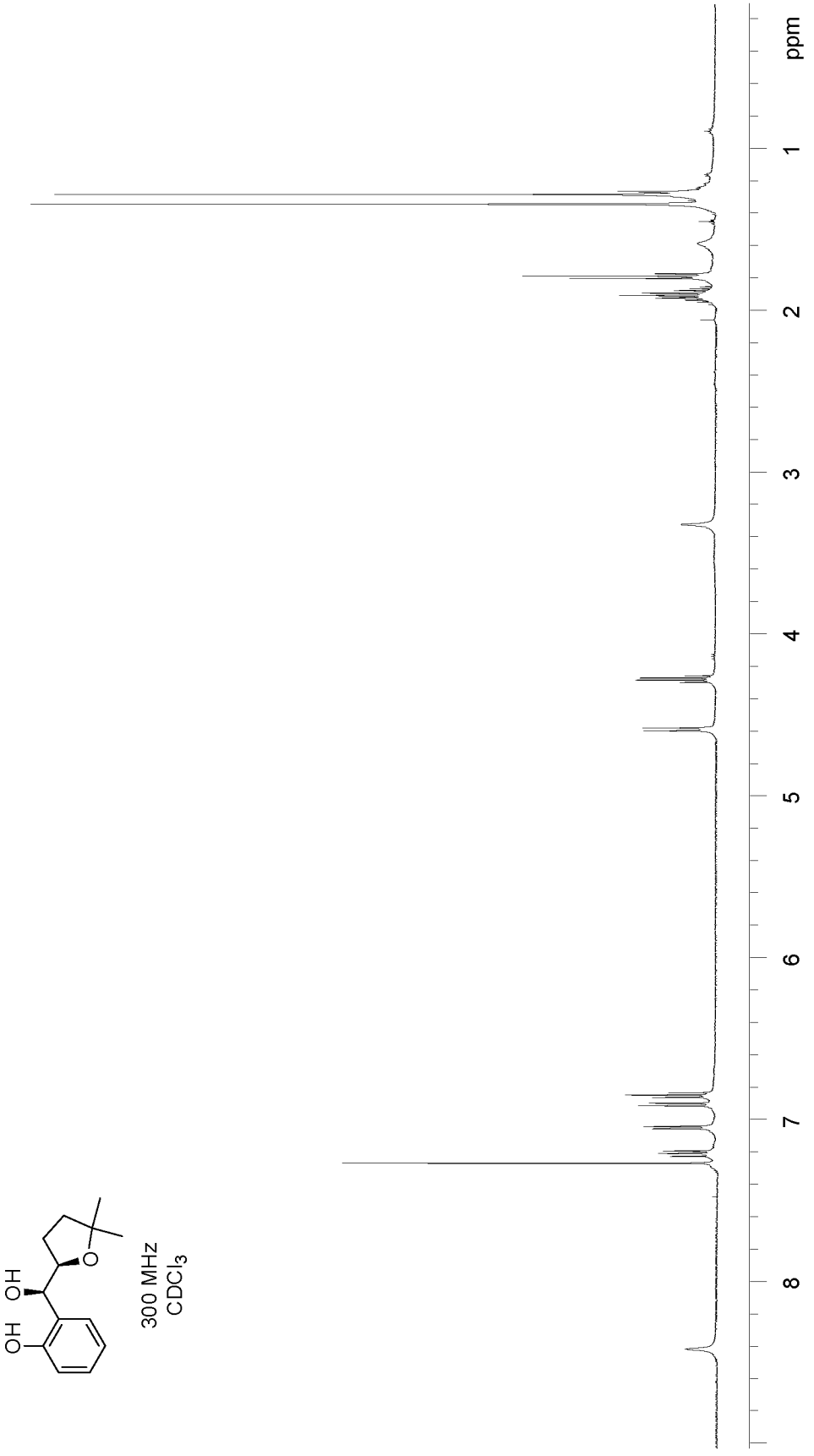
OH
OH
O
300 MHz
CDCl3
ppm
1
2
3
4
5
6
7
8

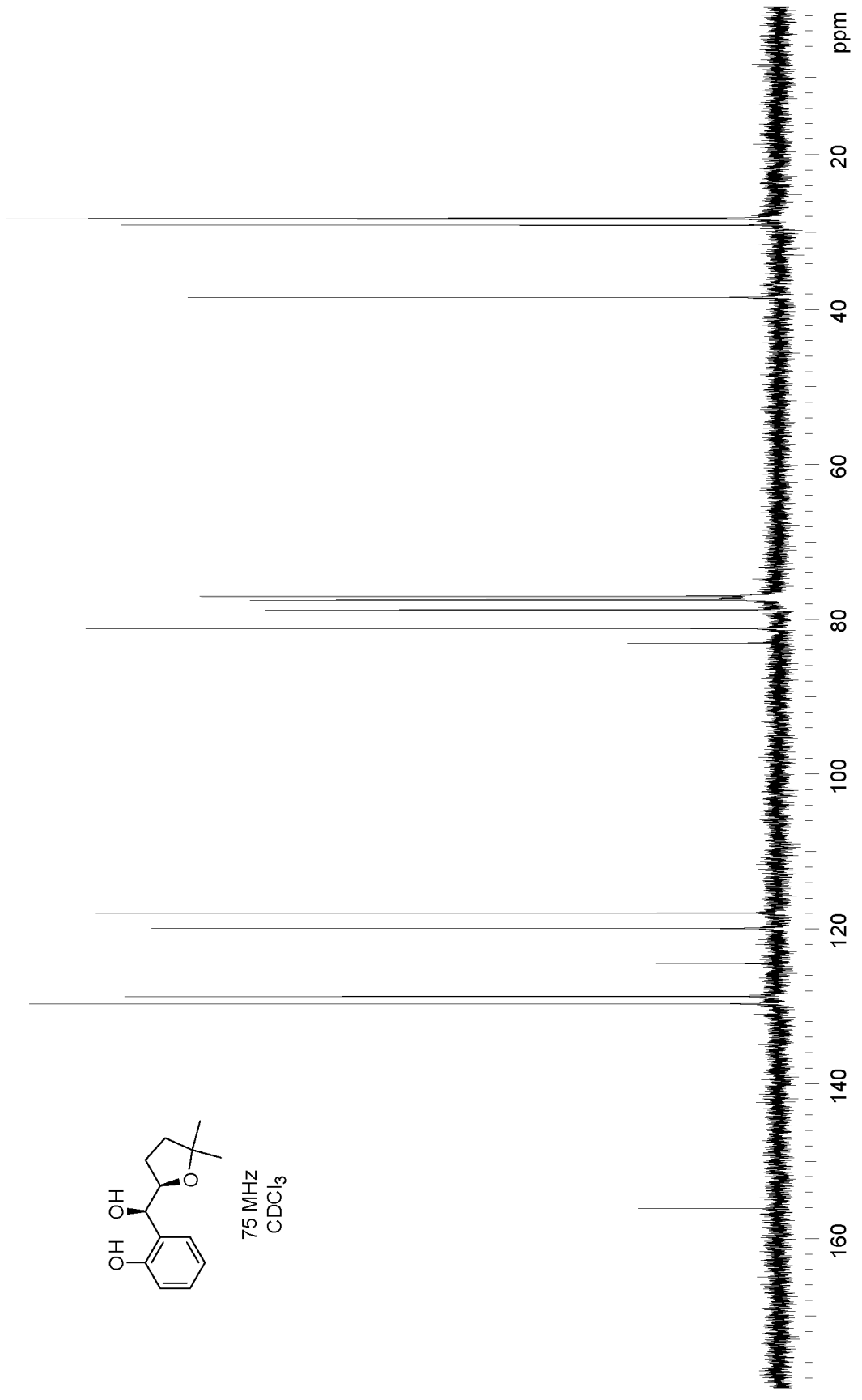
ppm
20
40
60
80
100
120
140
160
OH
OH
O
75 MHz
CDCl3

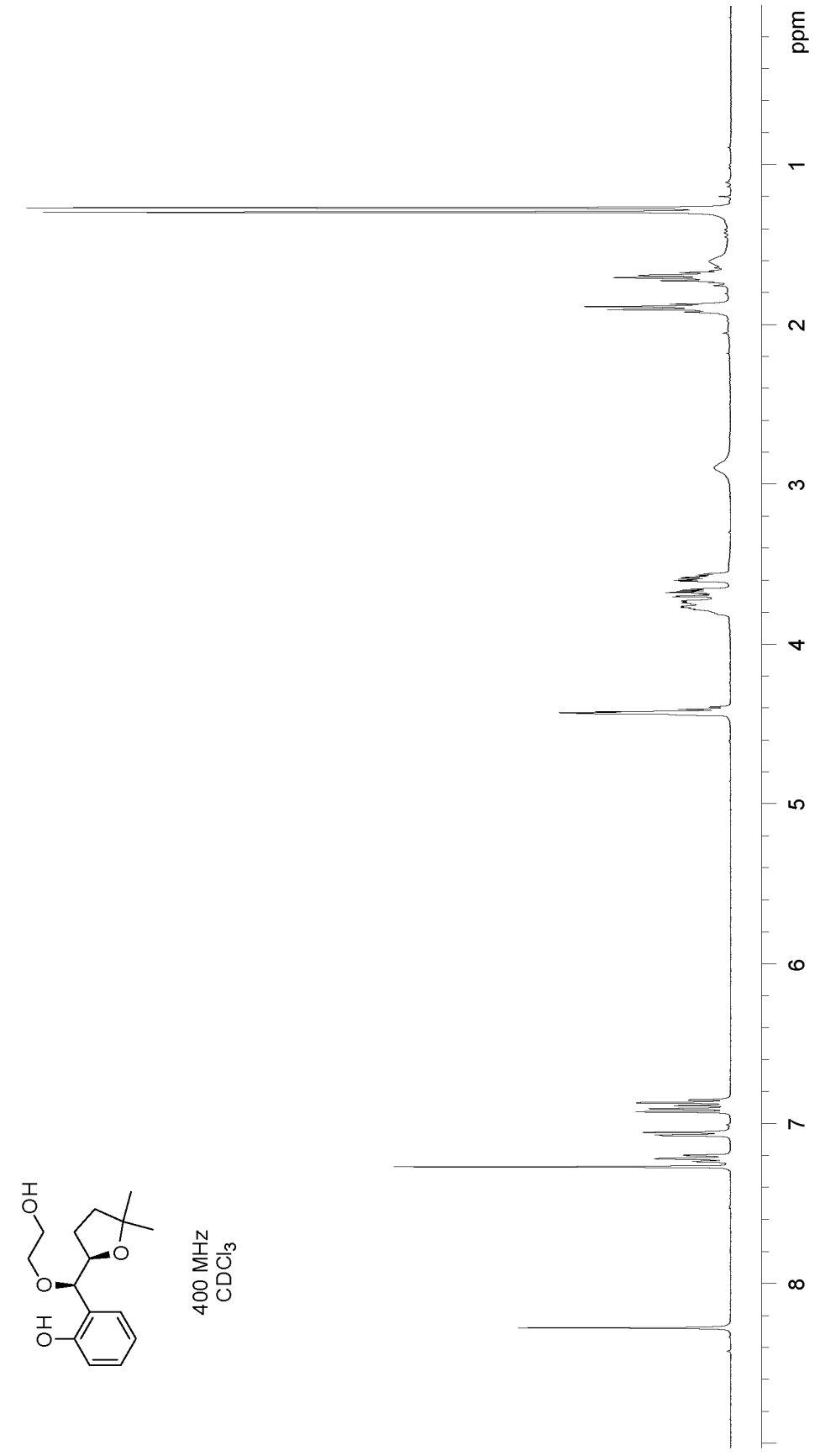
OH
O
O
OH
400 MHz
CDCl3
ppm
1
2
3
4
5
6
7
8

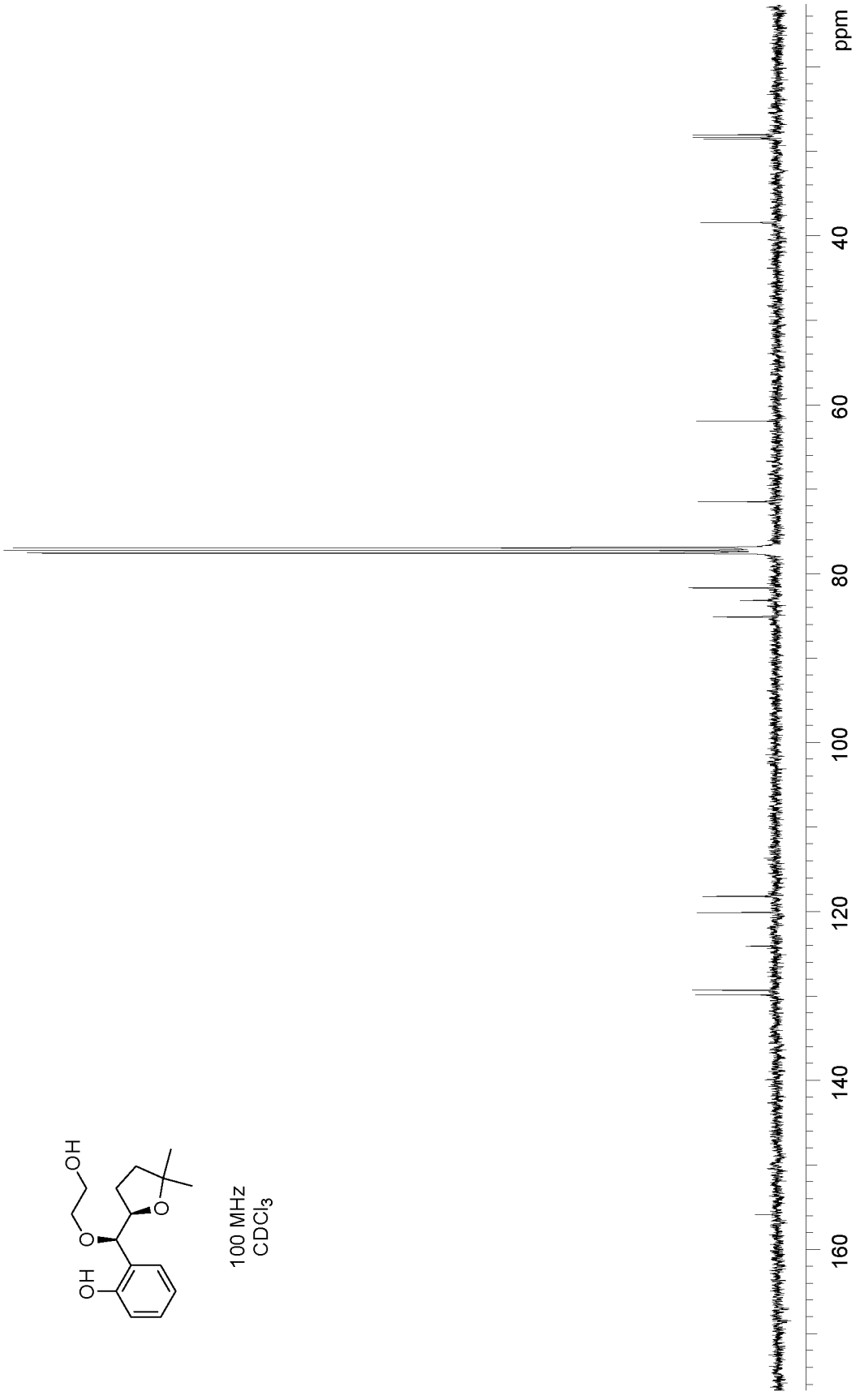
ppm
40
60
80
100
120
140
160
100 MHz
CDCl3
OH
O
O
OH

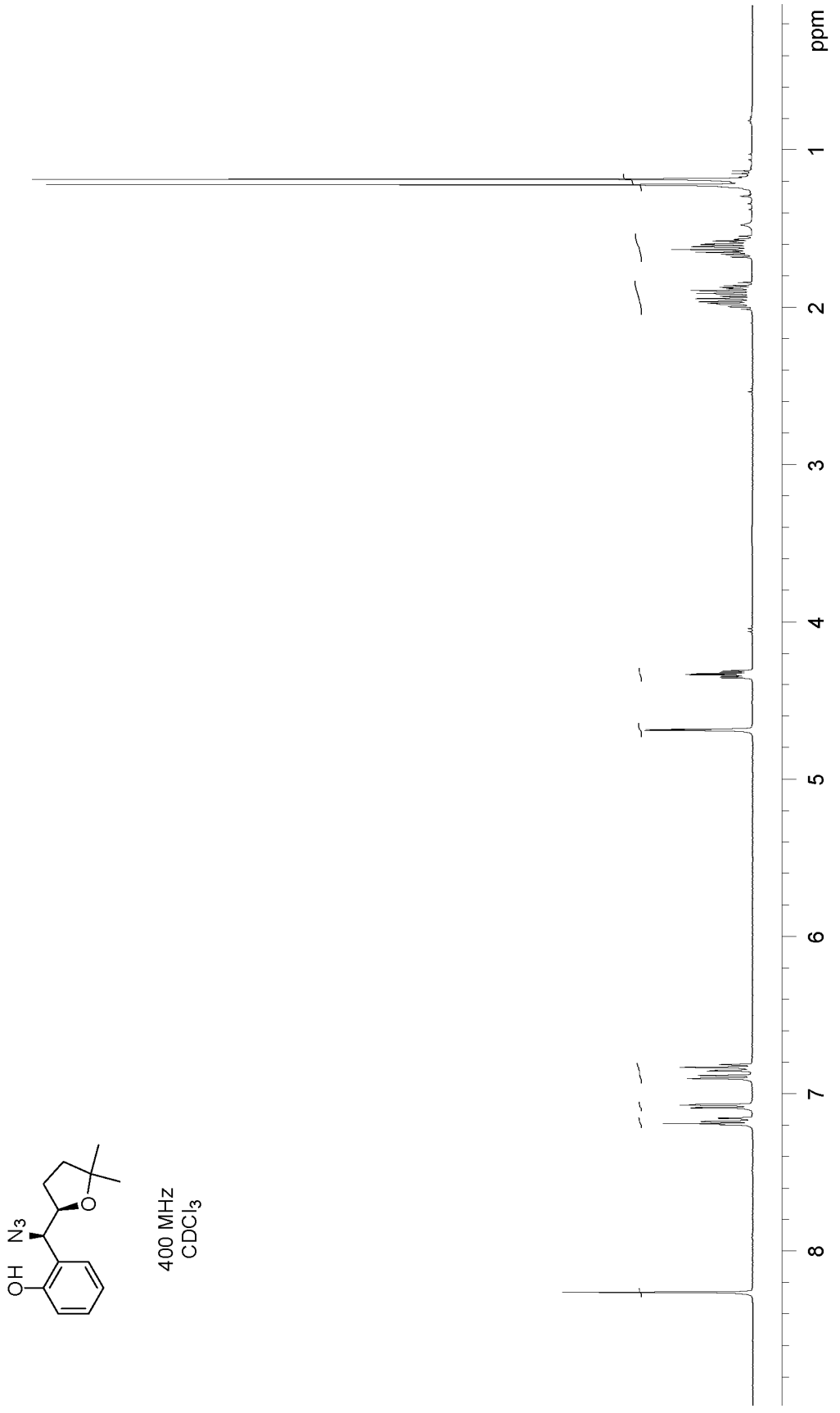
OH
N3
O
400 MHz
CDCl3
ppm
1
2
3
4
5
6
7
8

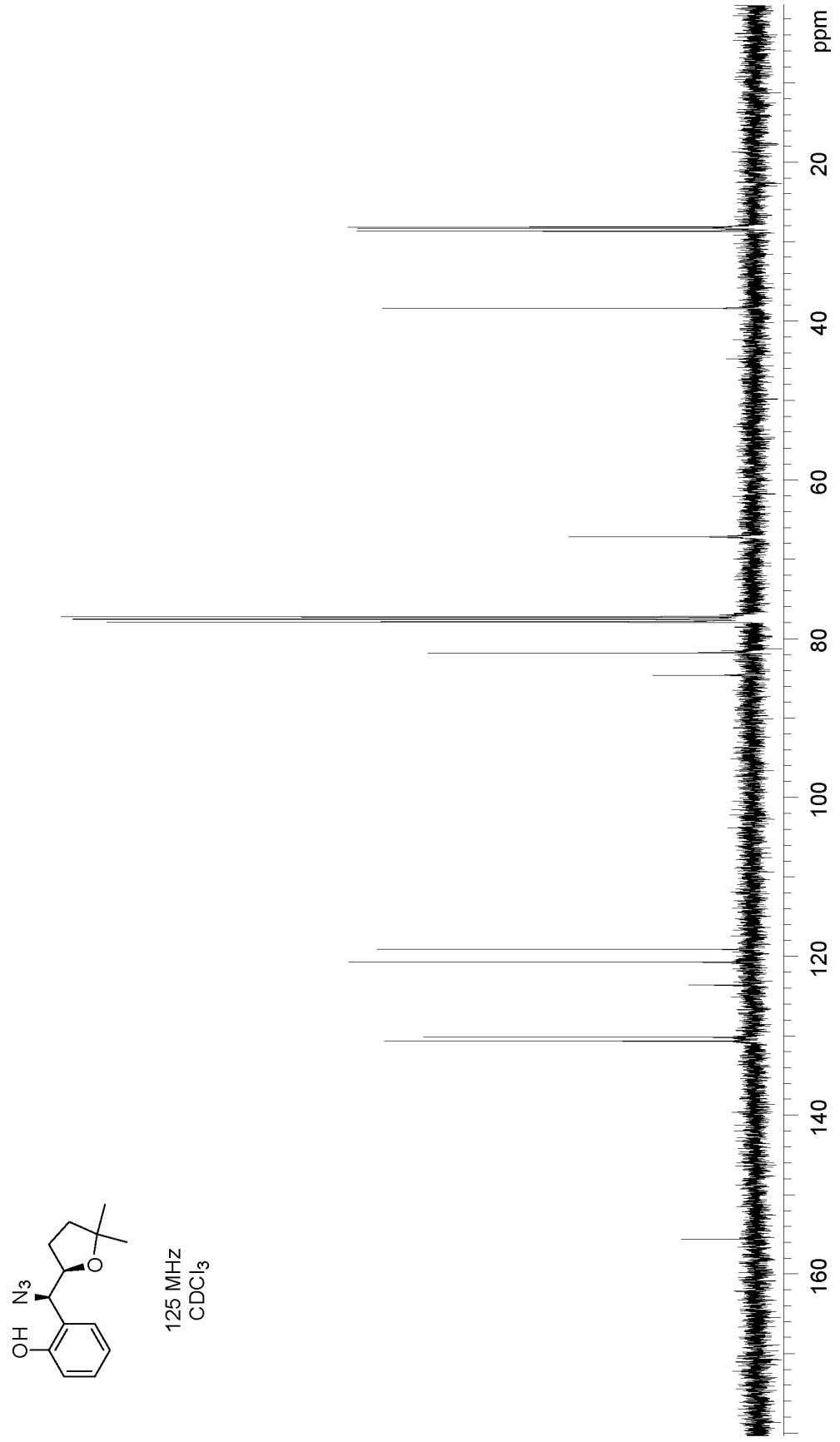
OH
N3
O
125 MHz
CDCl3
ppm
20
40
60
80
100
120
140
160

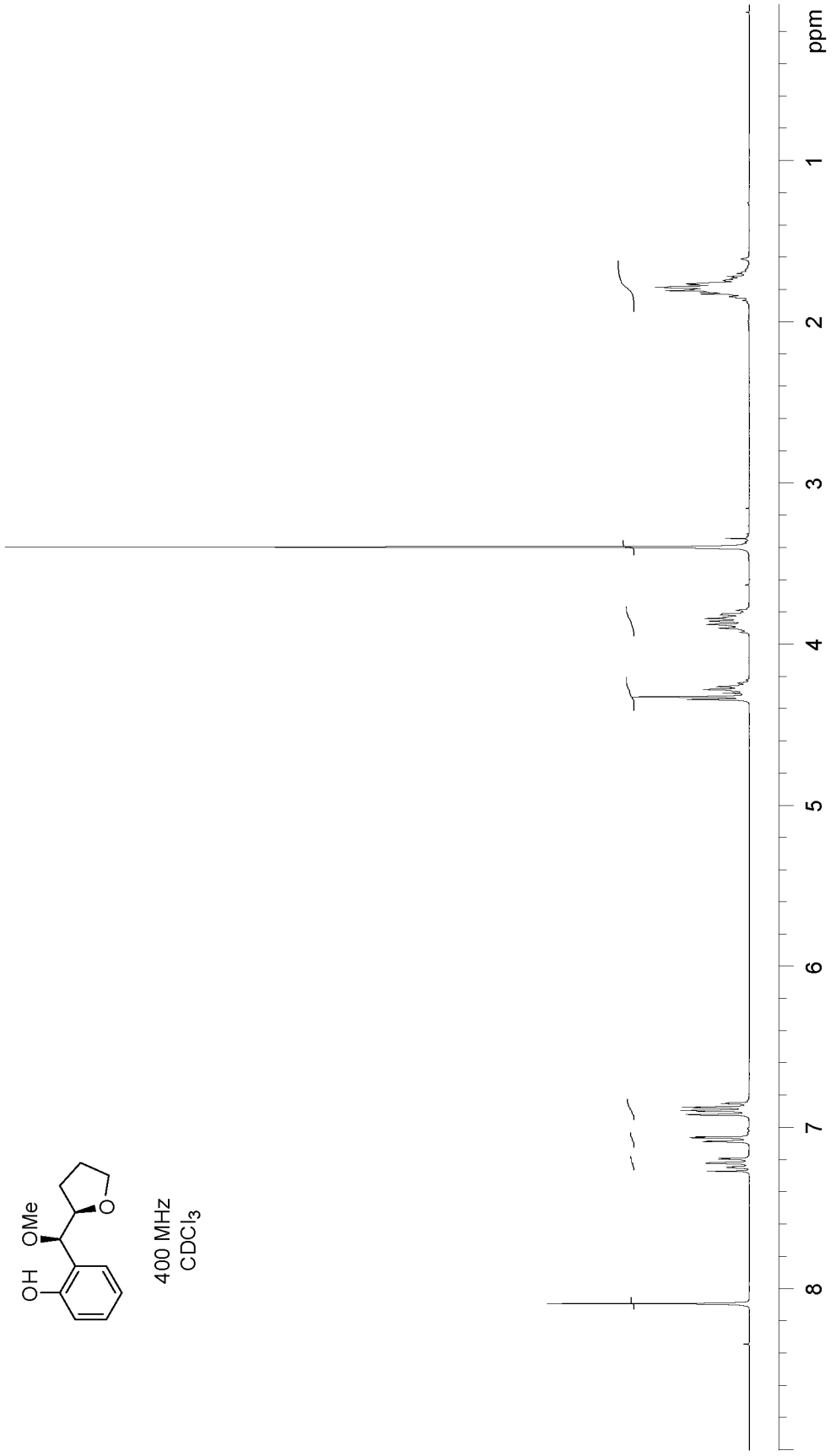
OH
OMe
O
400 MHz
CDCl3
ppm
1
2
3
4
5
6
7
8

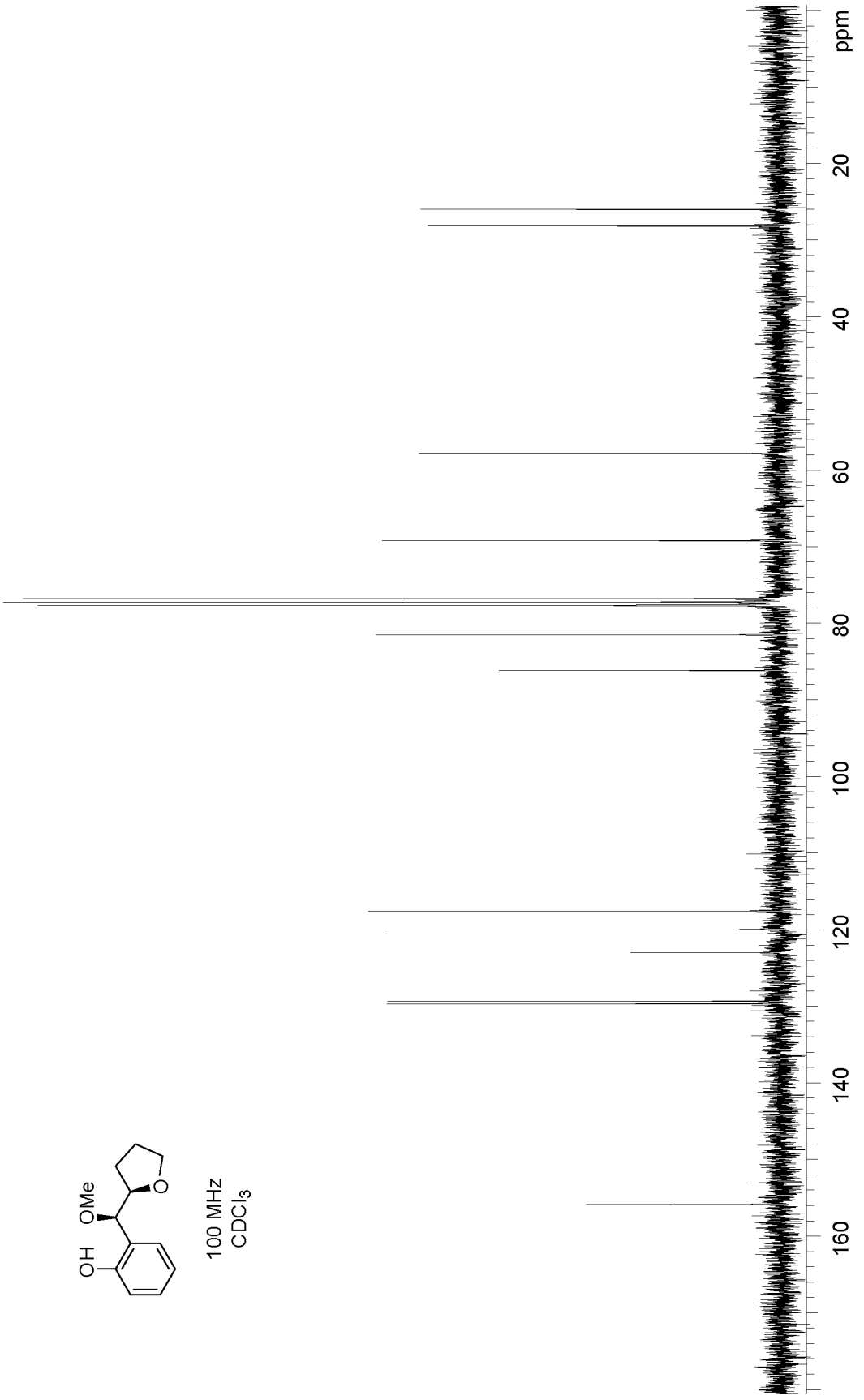
ppm
20
40
60
80
100
120
140
160
100 MHz
CDCl3
OH
OMe
O

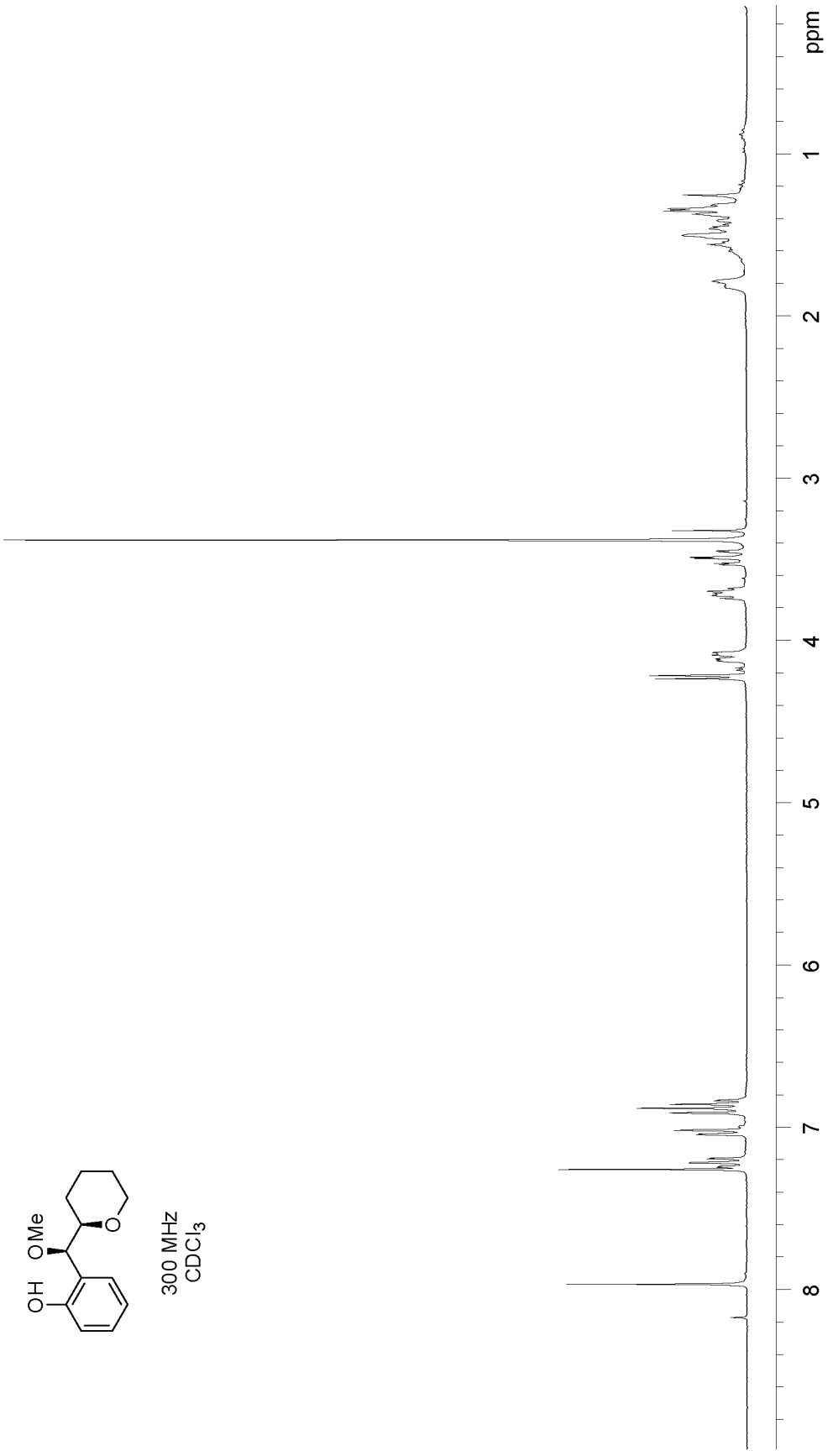
OH
OMe
O
300 MHz
CDCl3
ppm
1
2
3
4
5
6
7
8

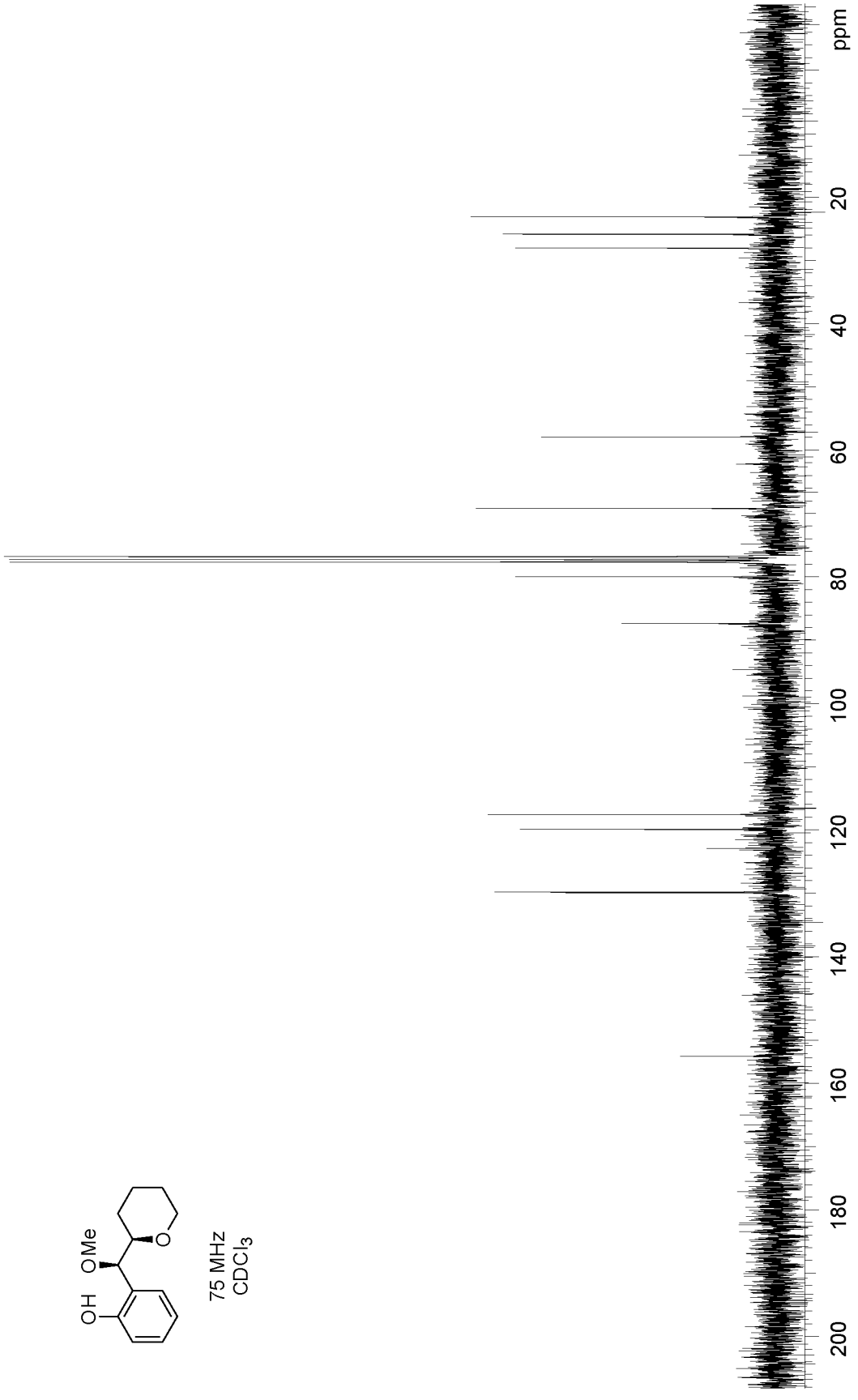
OH
OMe
O
75 MHz
$CDCl_3$
ppm
20
40
60
80
100
120
140
160
180
200

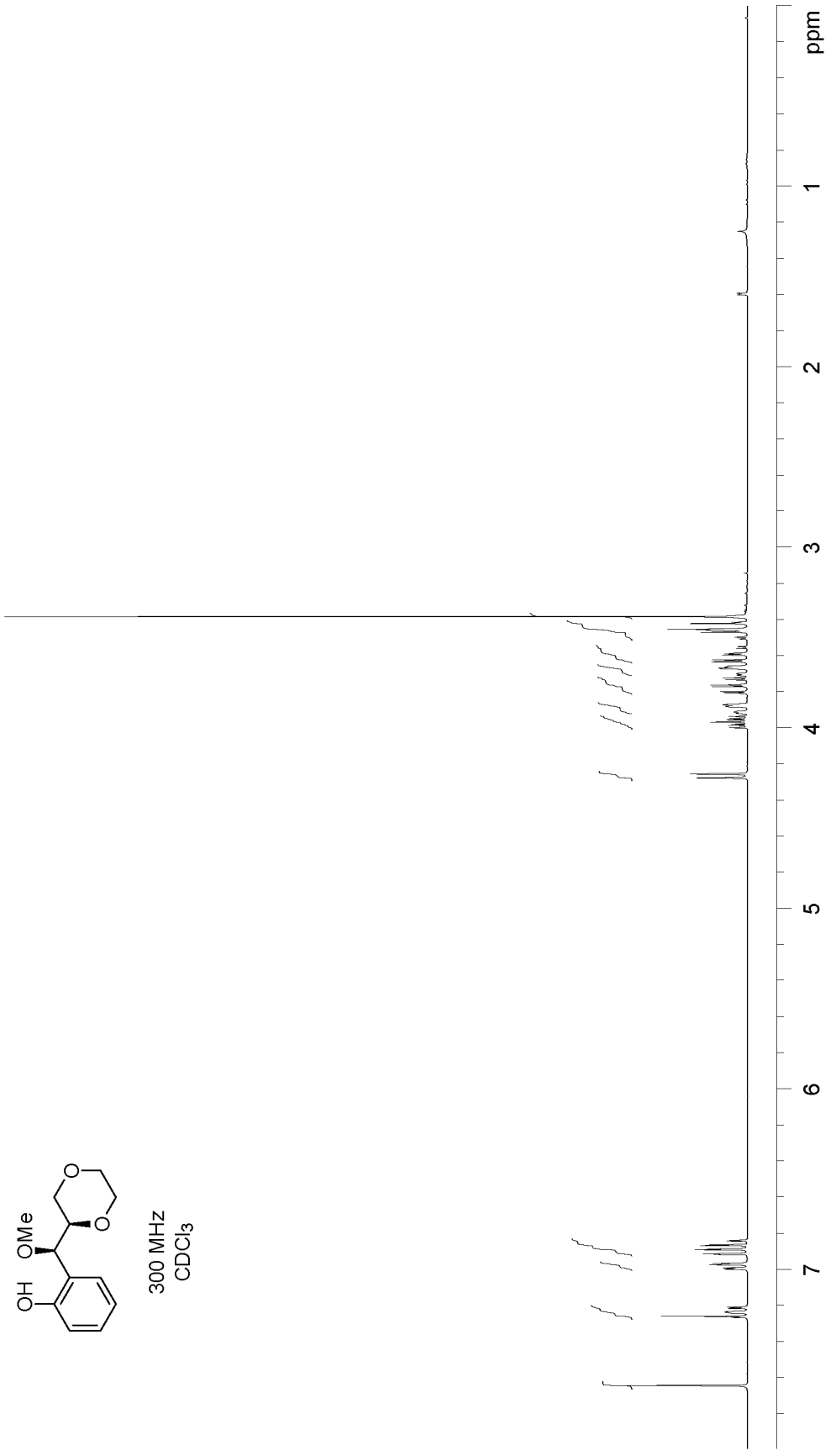
OH
OMe
O
O
300 MHz
CDCl3
ppm
1
2
3
4
5
6
7

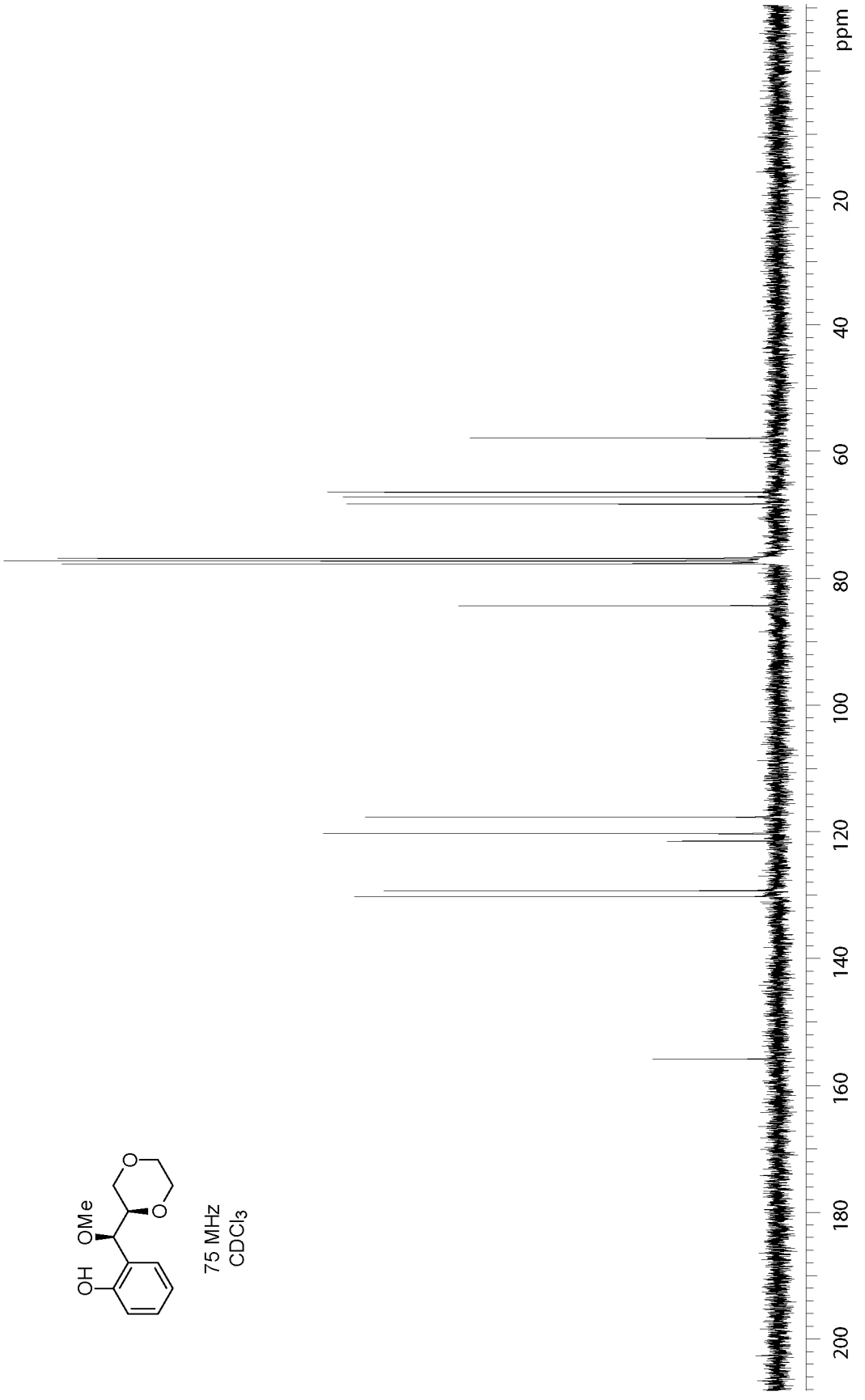
OH
OMe
O
O
75 MHz
CDCl3
ppm
20
40
60
80
100
120
140
160
180
200

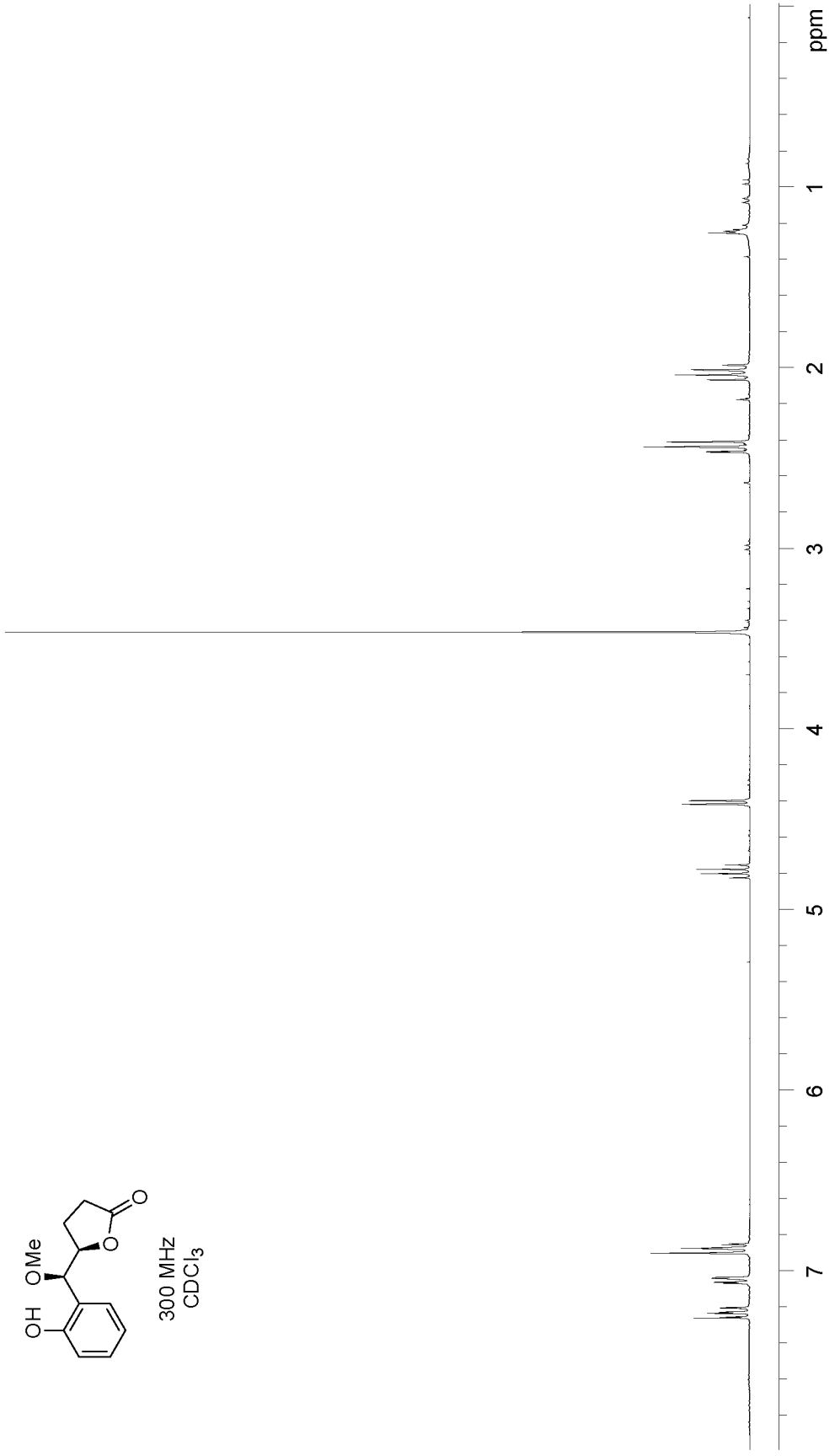
OH
OMe
O
O
300 MHz
$CDCl_3$
ppm
1
2
3
4
5
6
7

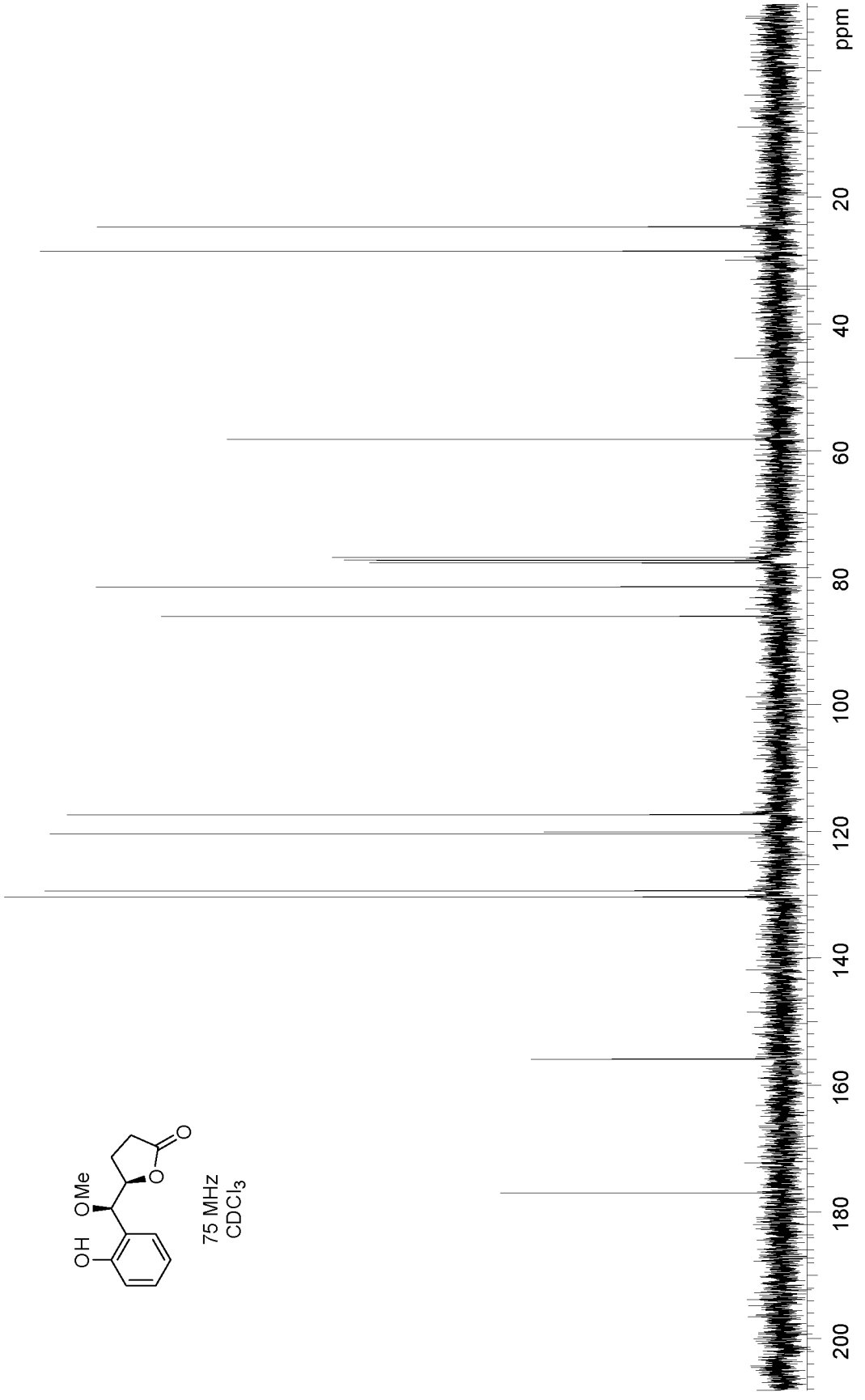
ppm
20
40
60
80
100
120
140
160
180
200
OH
OMe
O
O
O
75 MHz
CDCl3

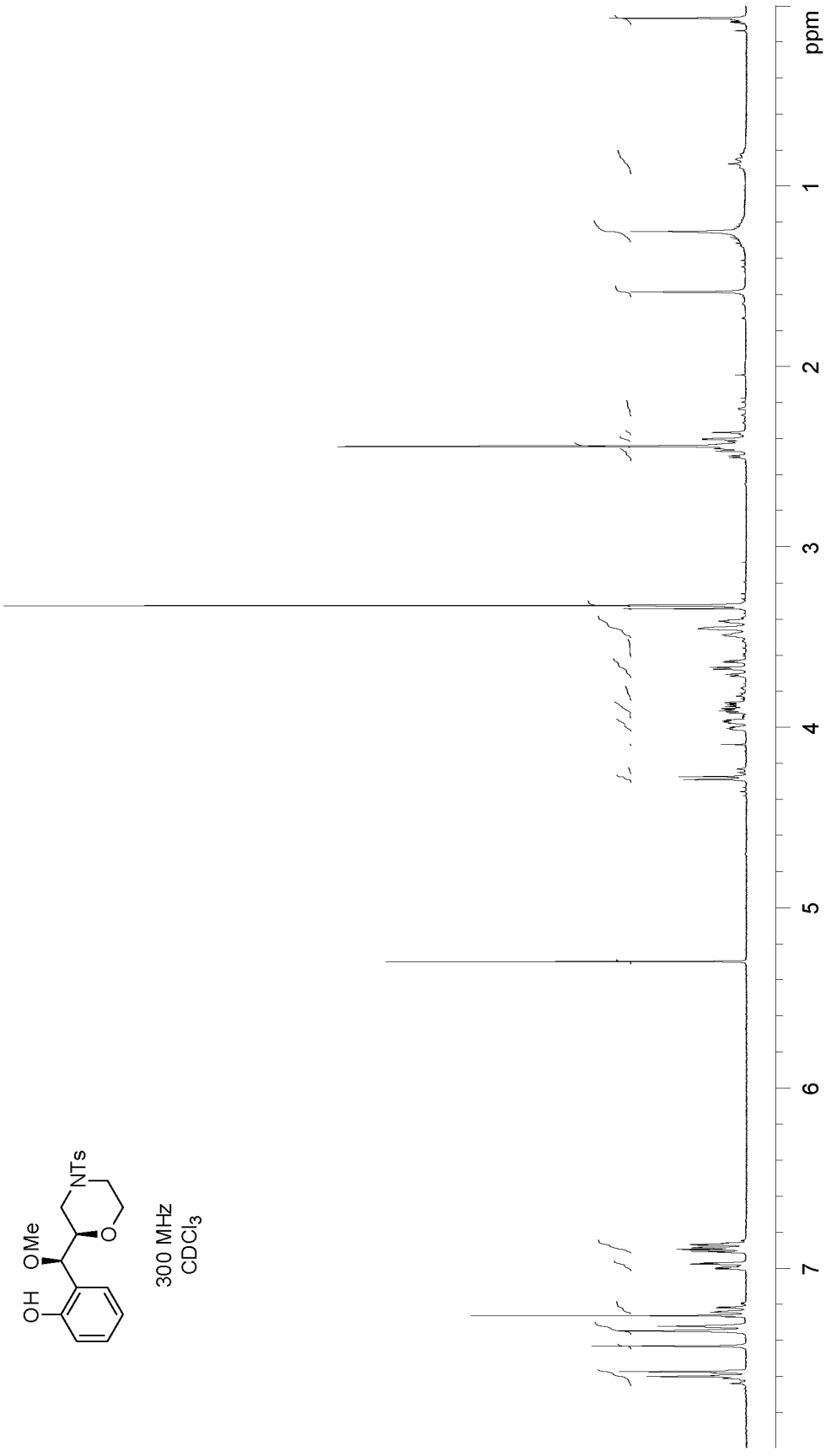
NTs
O
OMe
OH
300 MHz
$CDCl_3$
ppm
1
2
3
4
5
6
7

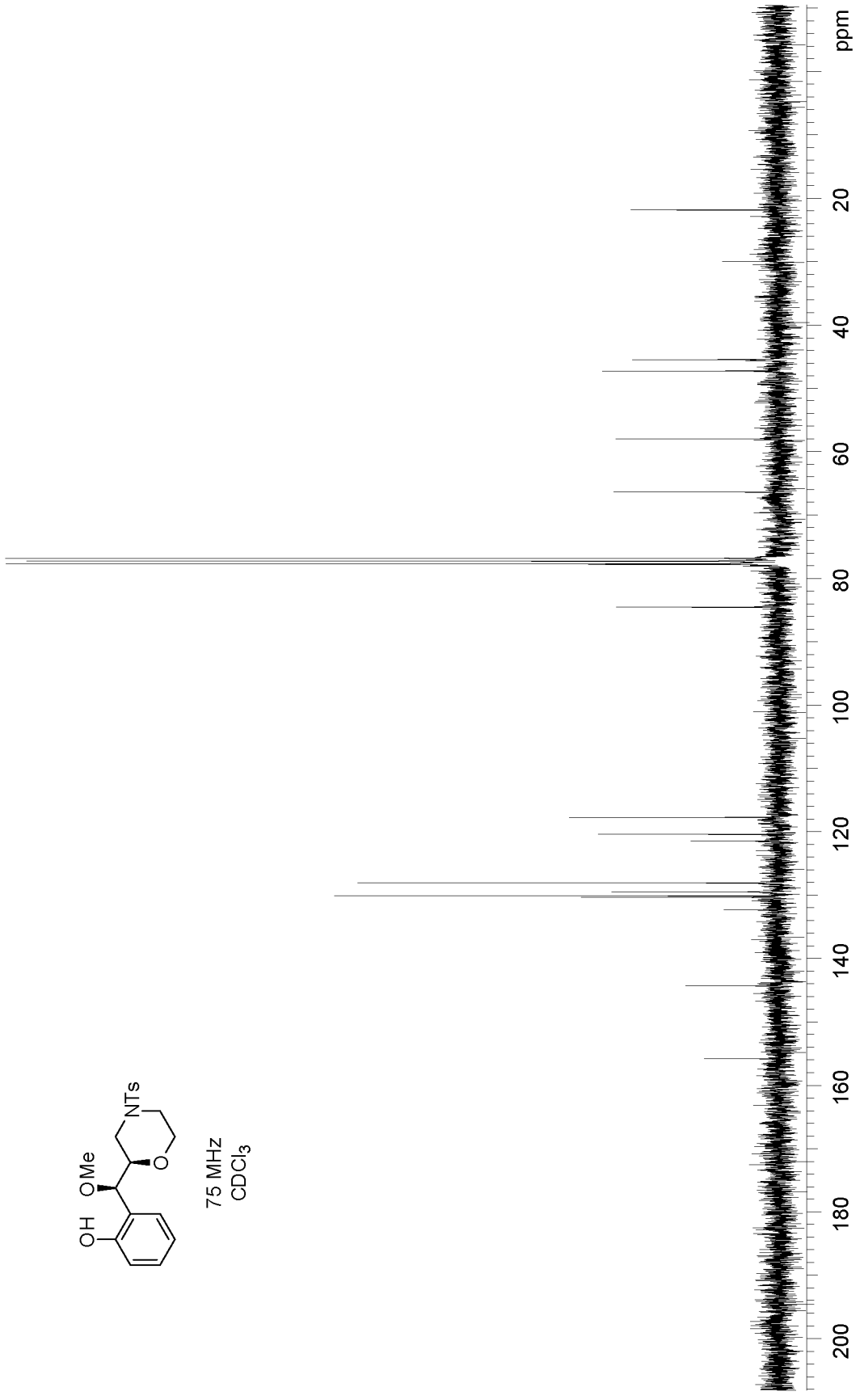
NTs
O
OMe
OH
75 MHz
$CDCl_3$
ppm
200
180
160
140
120
100
80
60
40
20

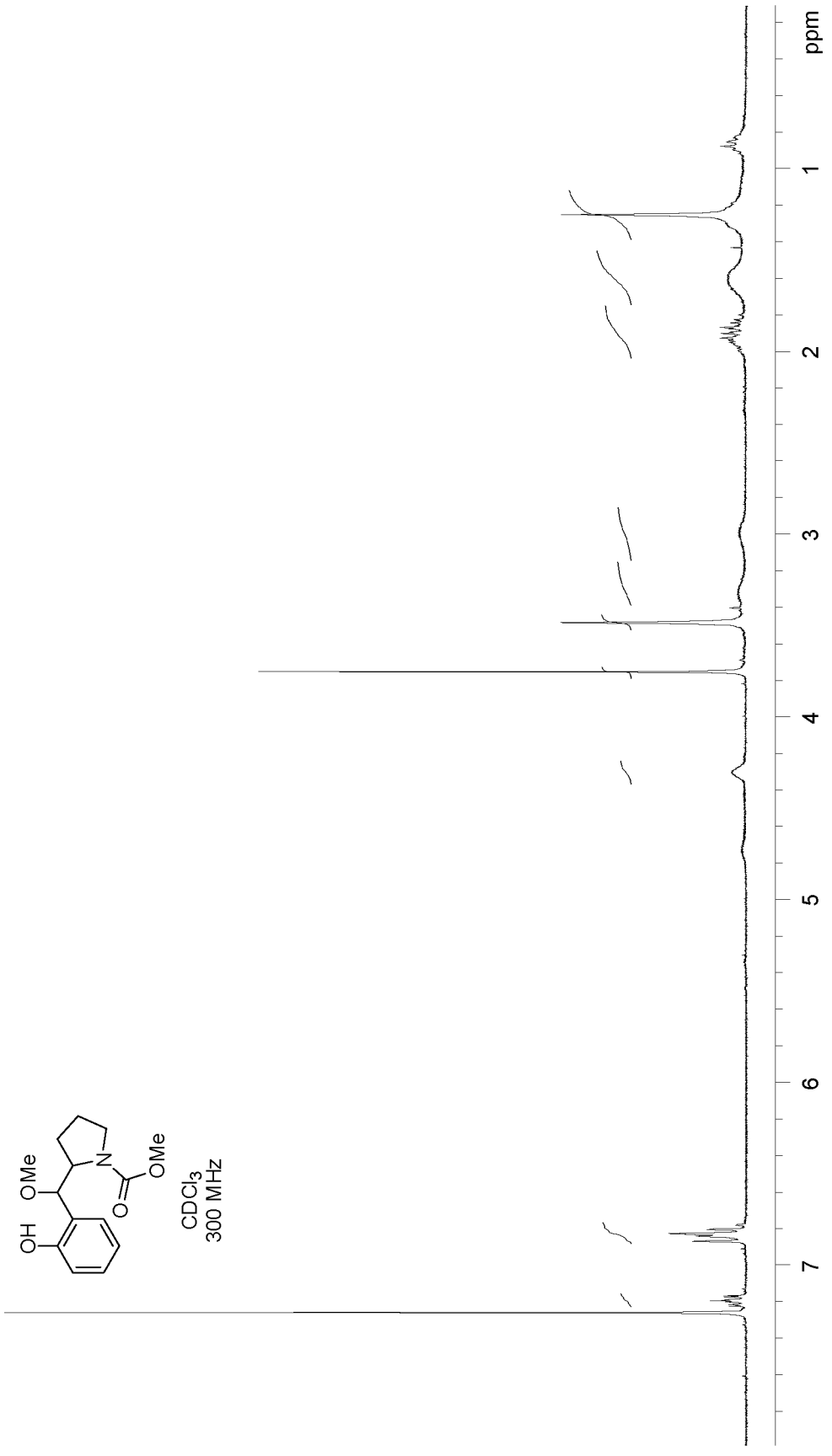
OMe
OMe
OH
O
N
CDCl3
300 MHz
ppm
1
2
3
4
5
6
7

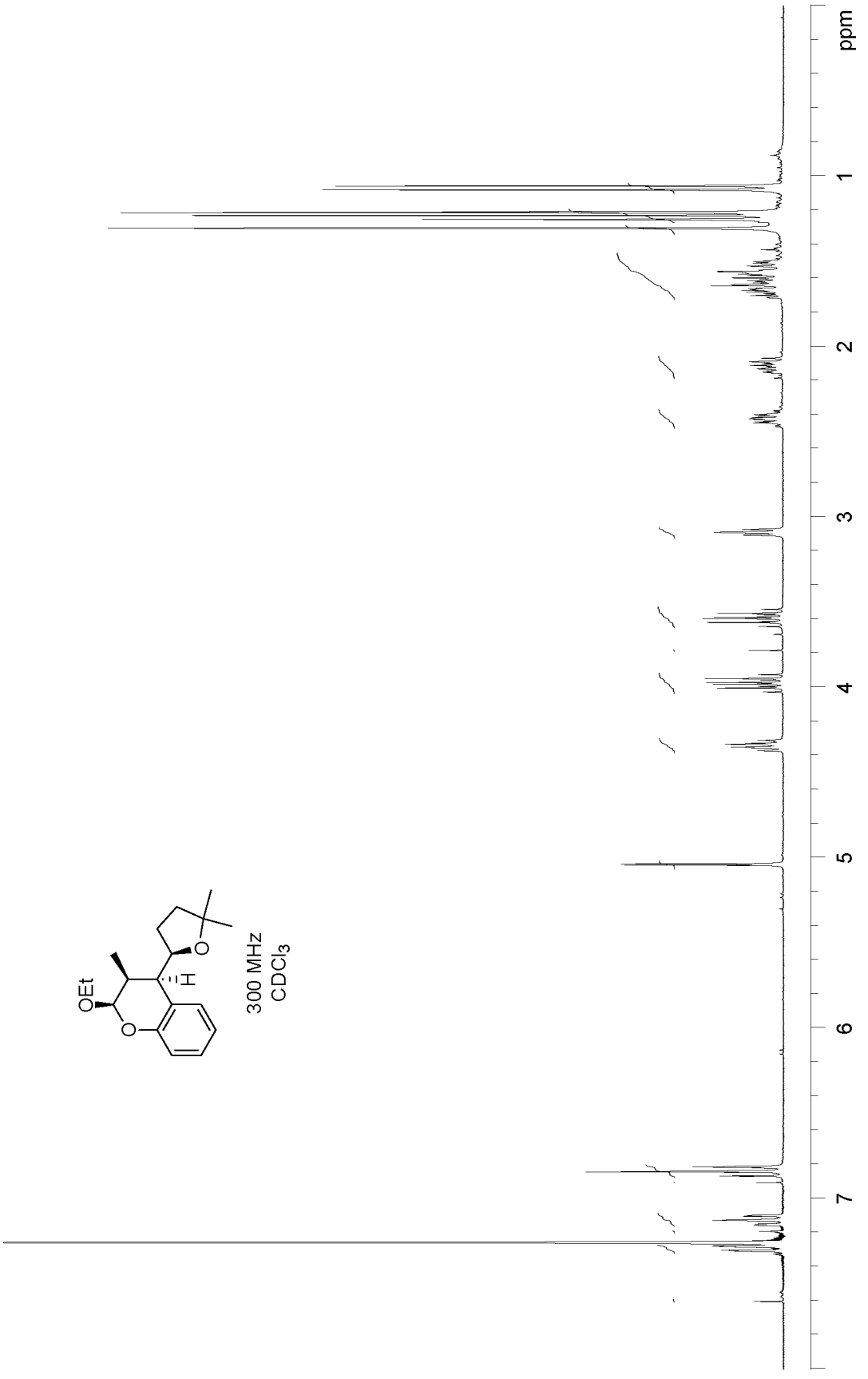
OEt
O
H
O
300 MHz
CDCl3
ppm
1
2
3
4
5
6
7

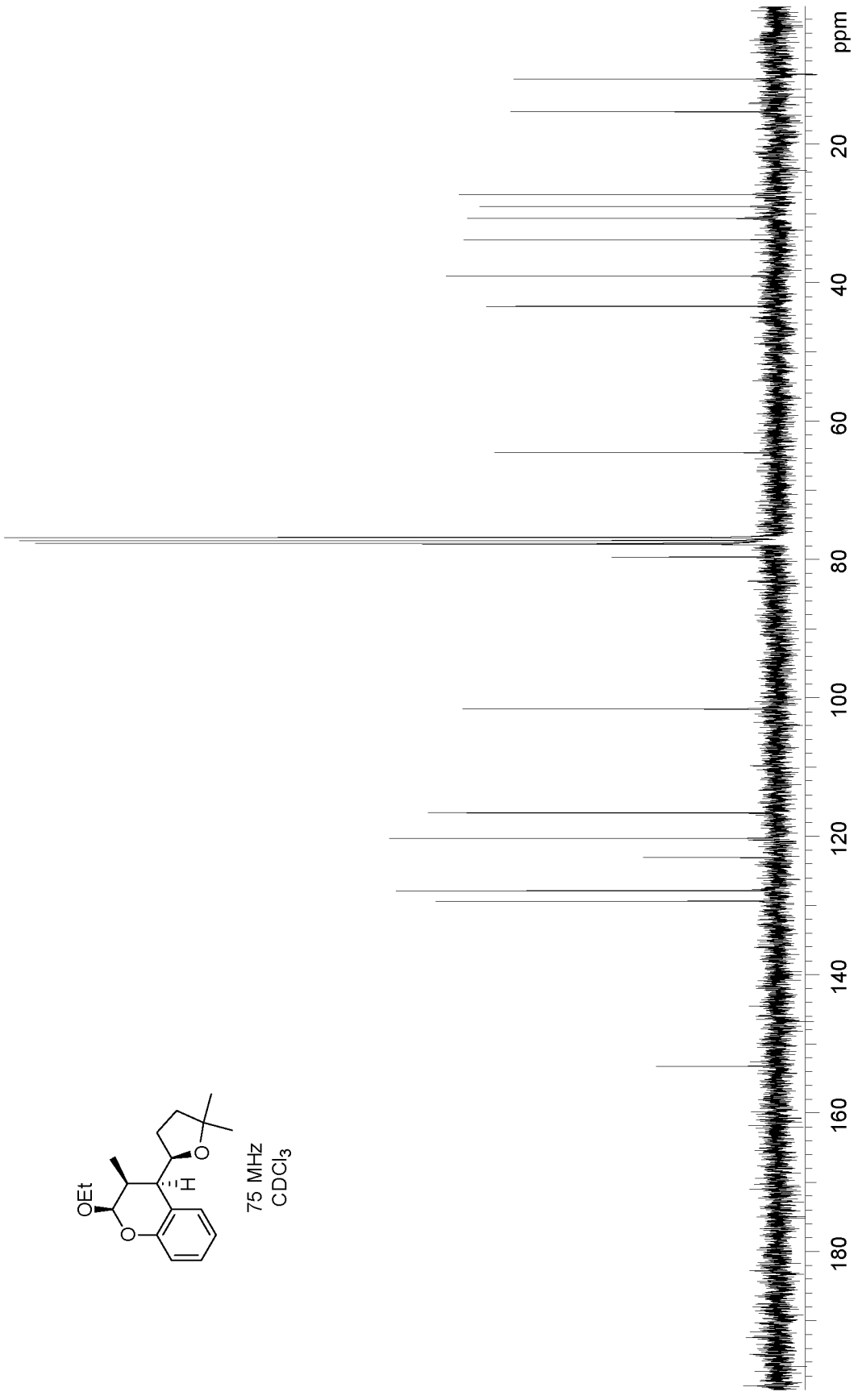
OEt
H
O
O
75 MHz
CDCl3
ppm
20
40
60
80
100
120
140
160
180

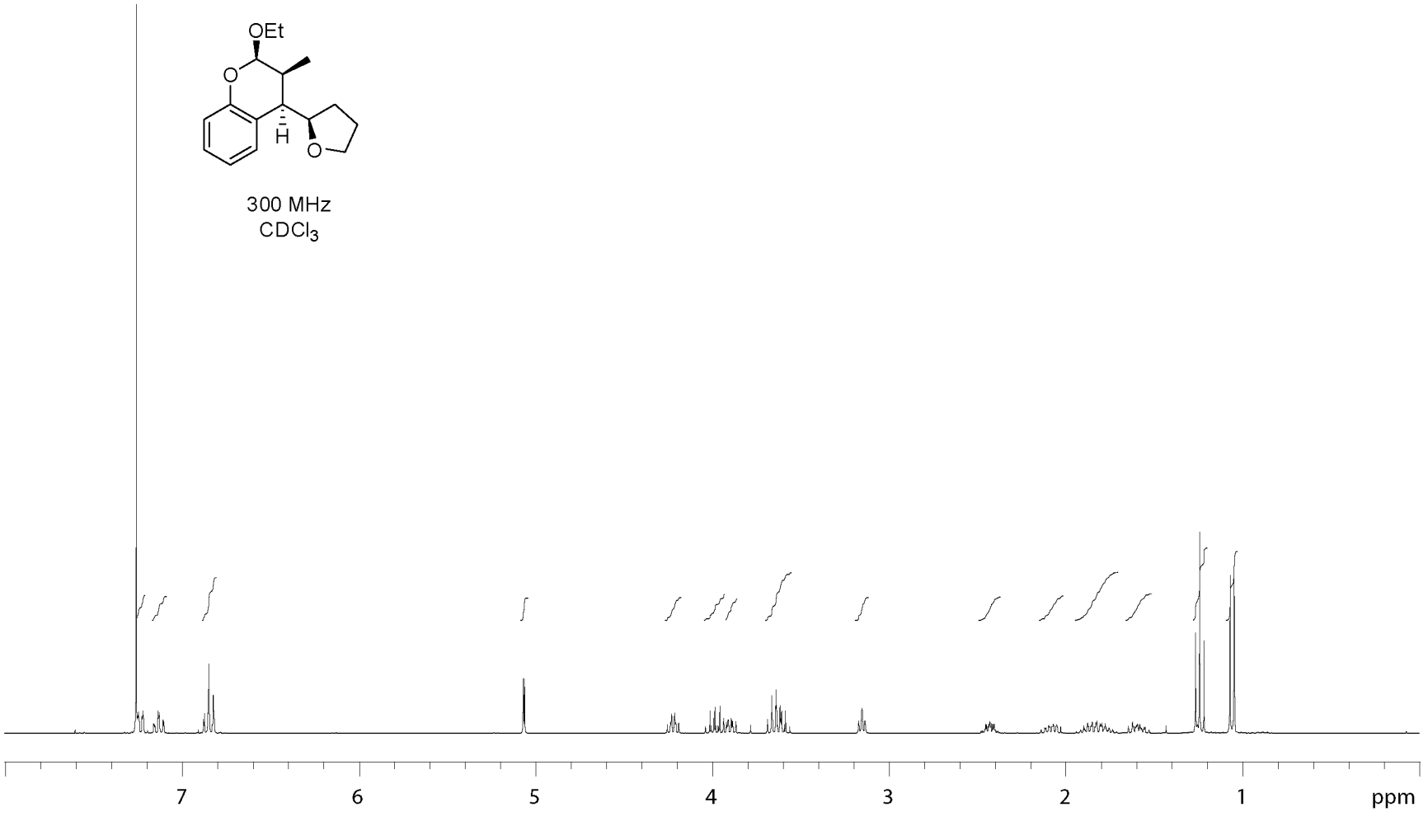
OEt
O
H
O
300 MHz
CDCl3
7
6
5
4
3
2
1
ppm

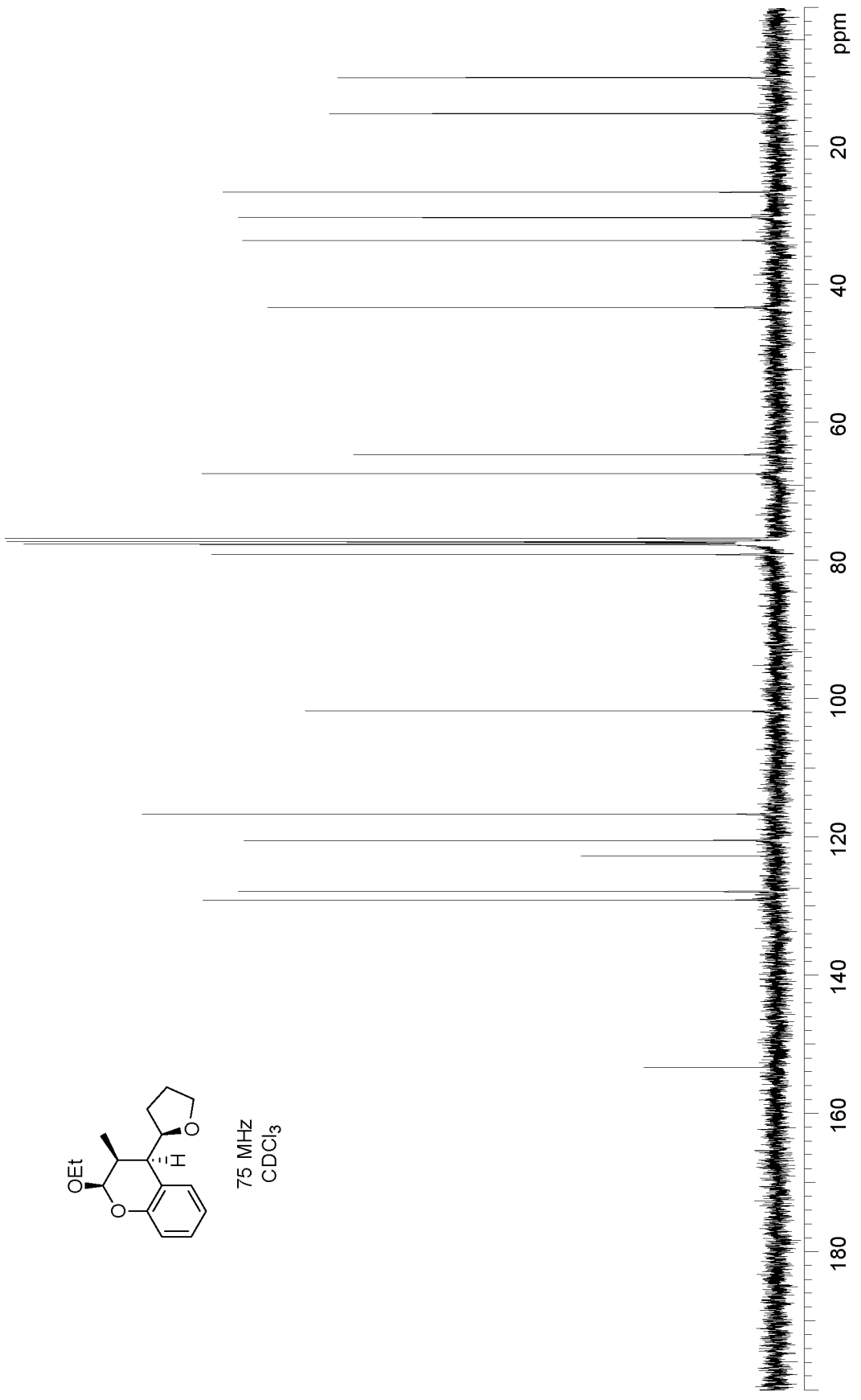
OEt
O
H
O
75 MHz
CDCl3
ppm
20
40
60
80
100
120
140
160
180

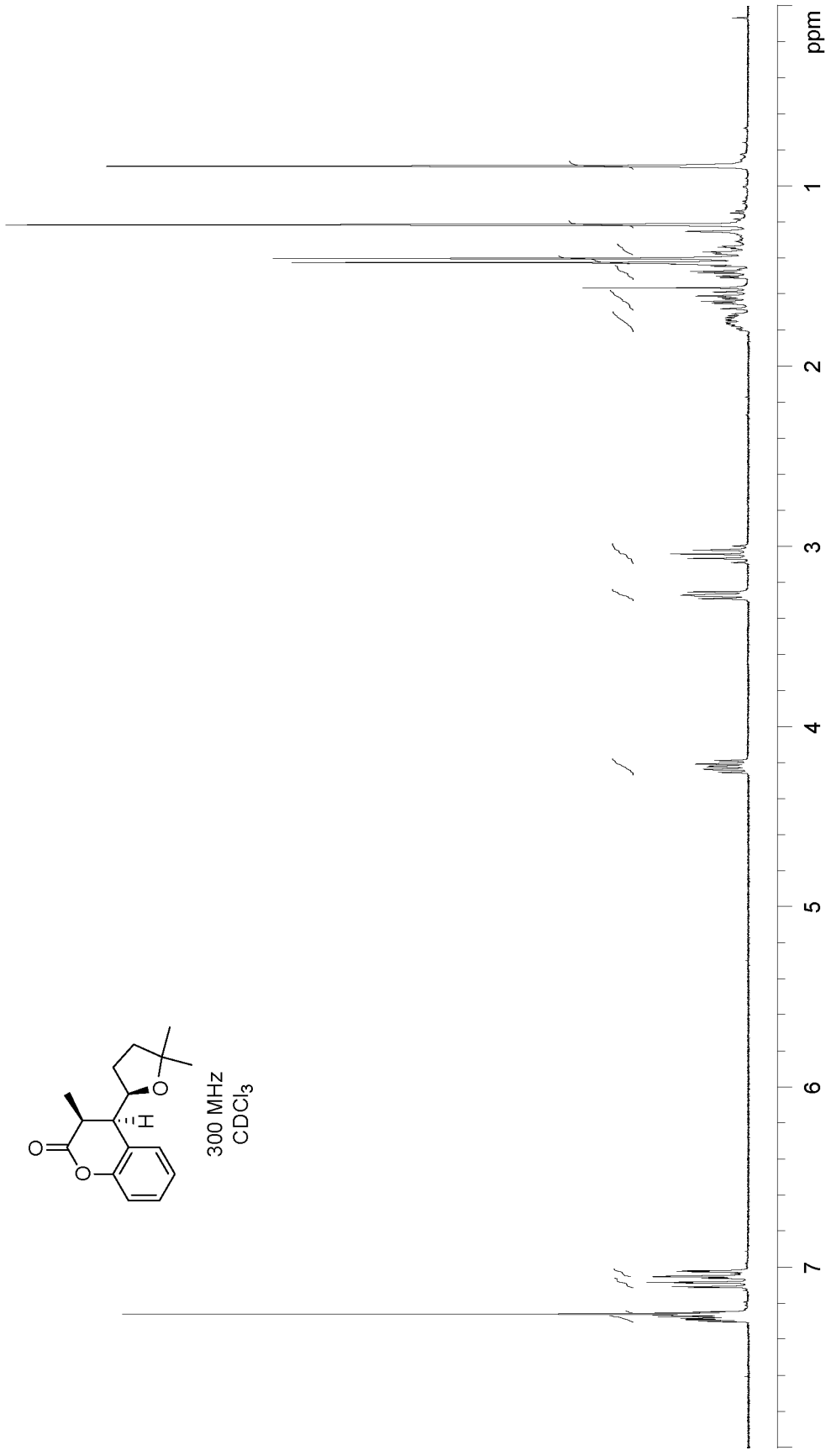
ppm
1
2
3
4
5
6
7
300 MHz
CDCl3
O
O
O
H

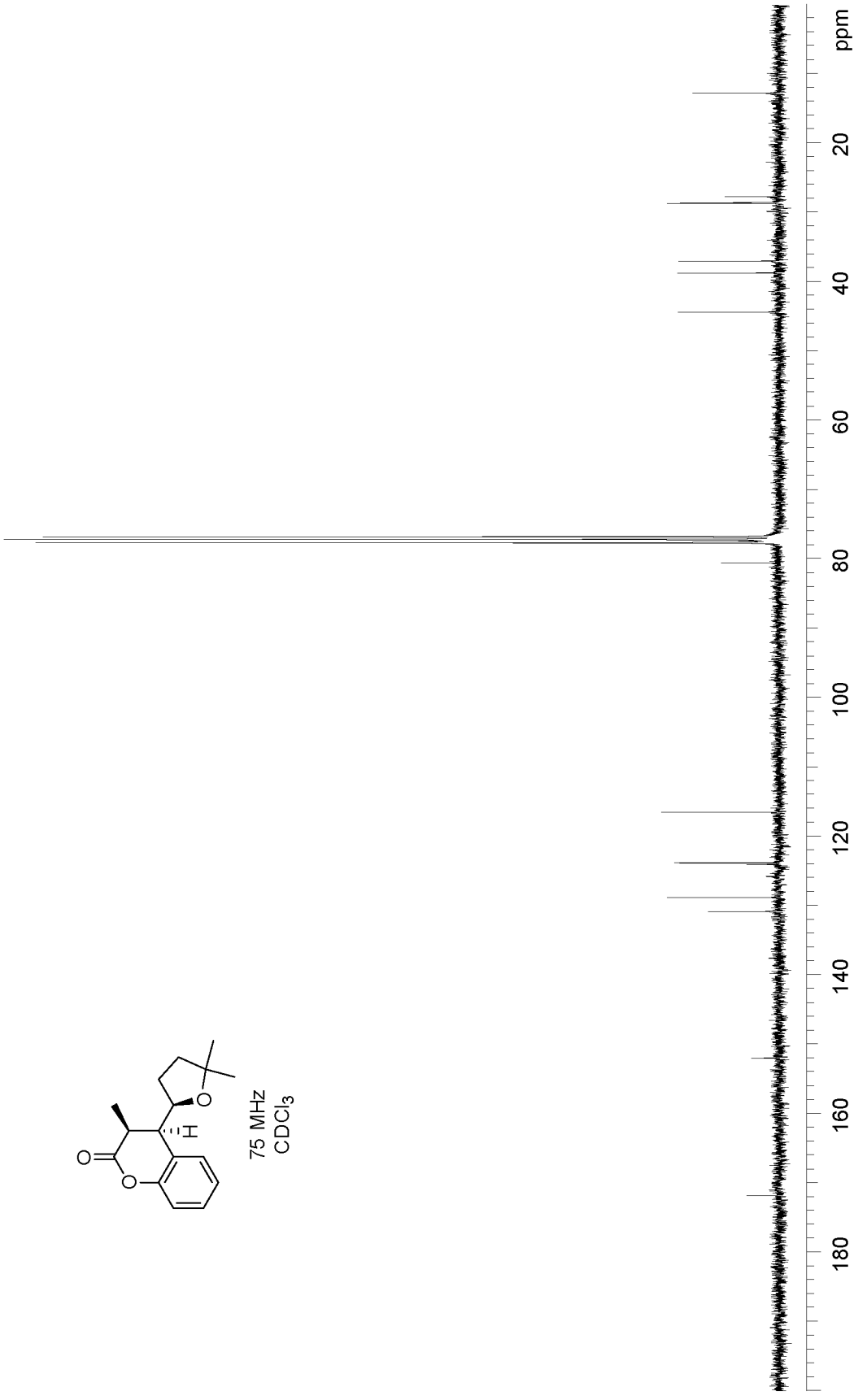
ppm
20
40
60
80
100
120
140
160
180
75 MHz
CDCl3
O
O
O
H

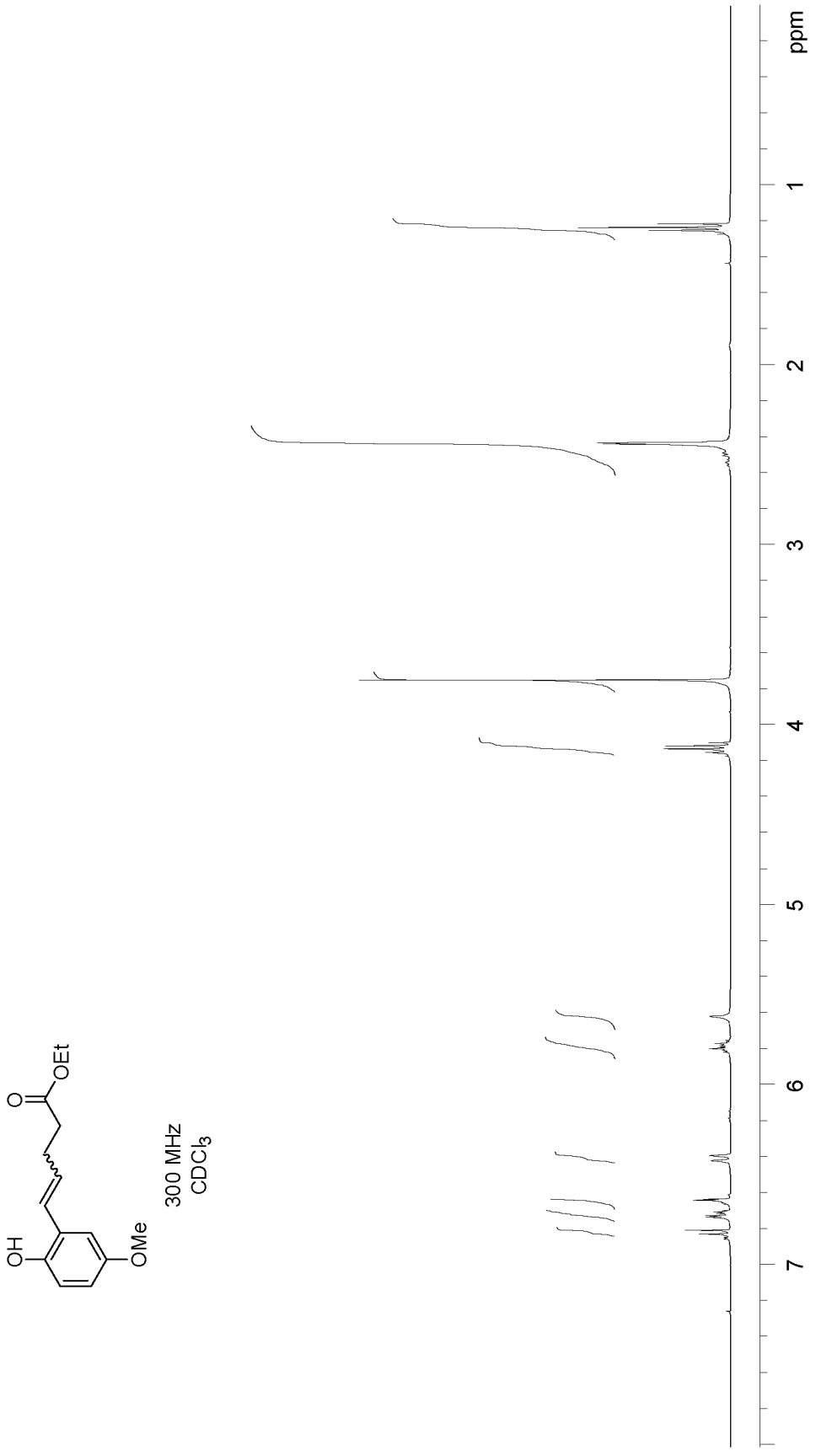
OEt
O
OH
OMe
300 MHz
CDCl3
ppm
1
2
3
4
5
6
7

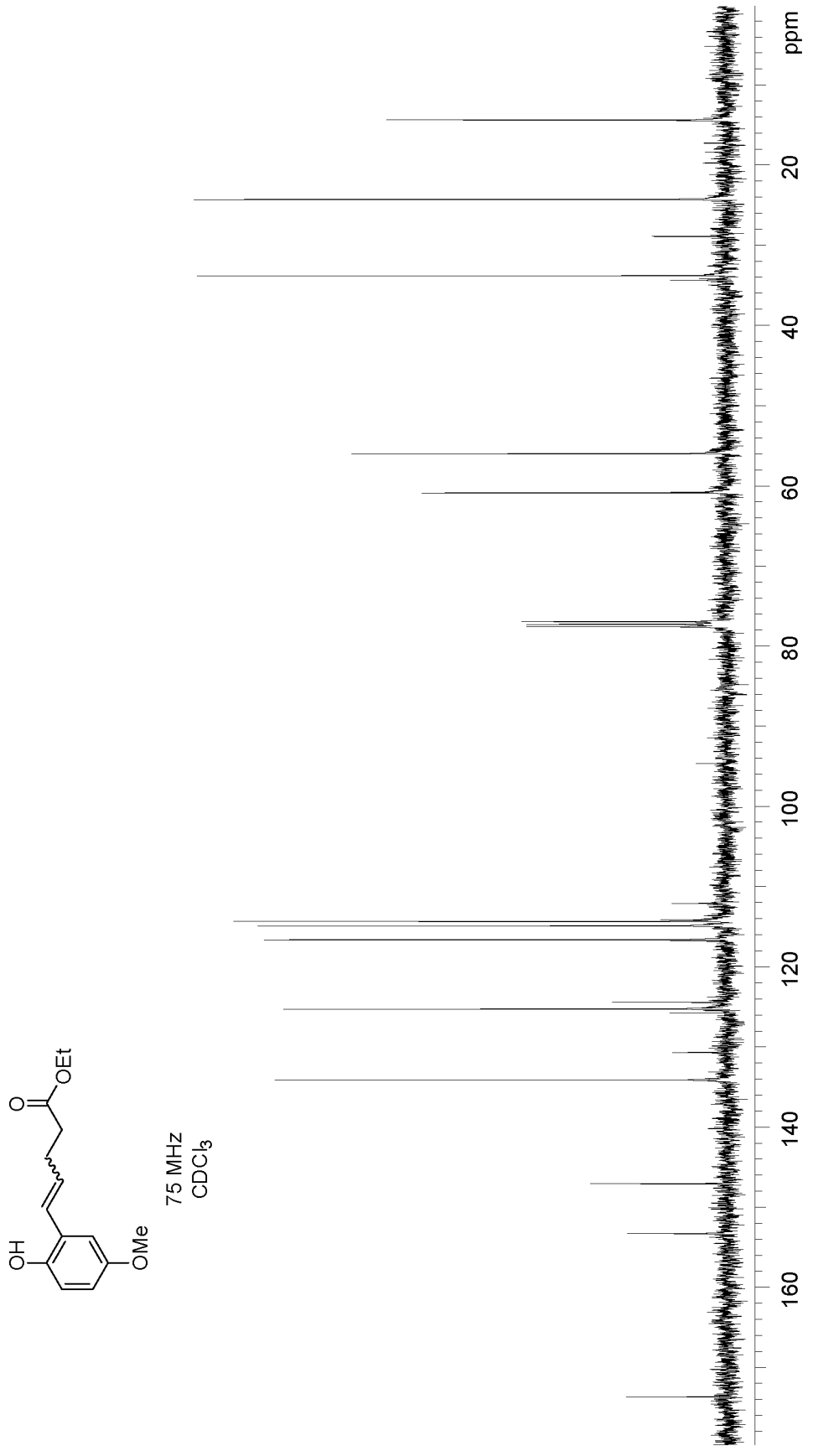
OEt
O
OH
OMe
75 MHz
CDCl3
ppm
20
40
60
80
100
120
140
160

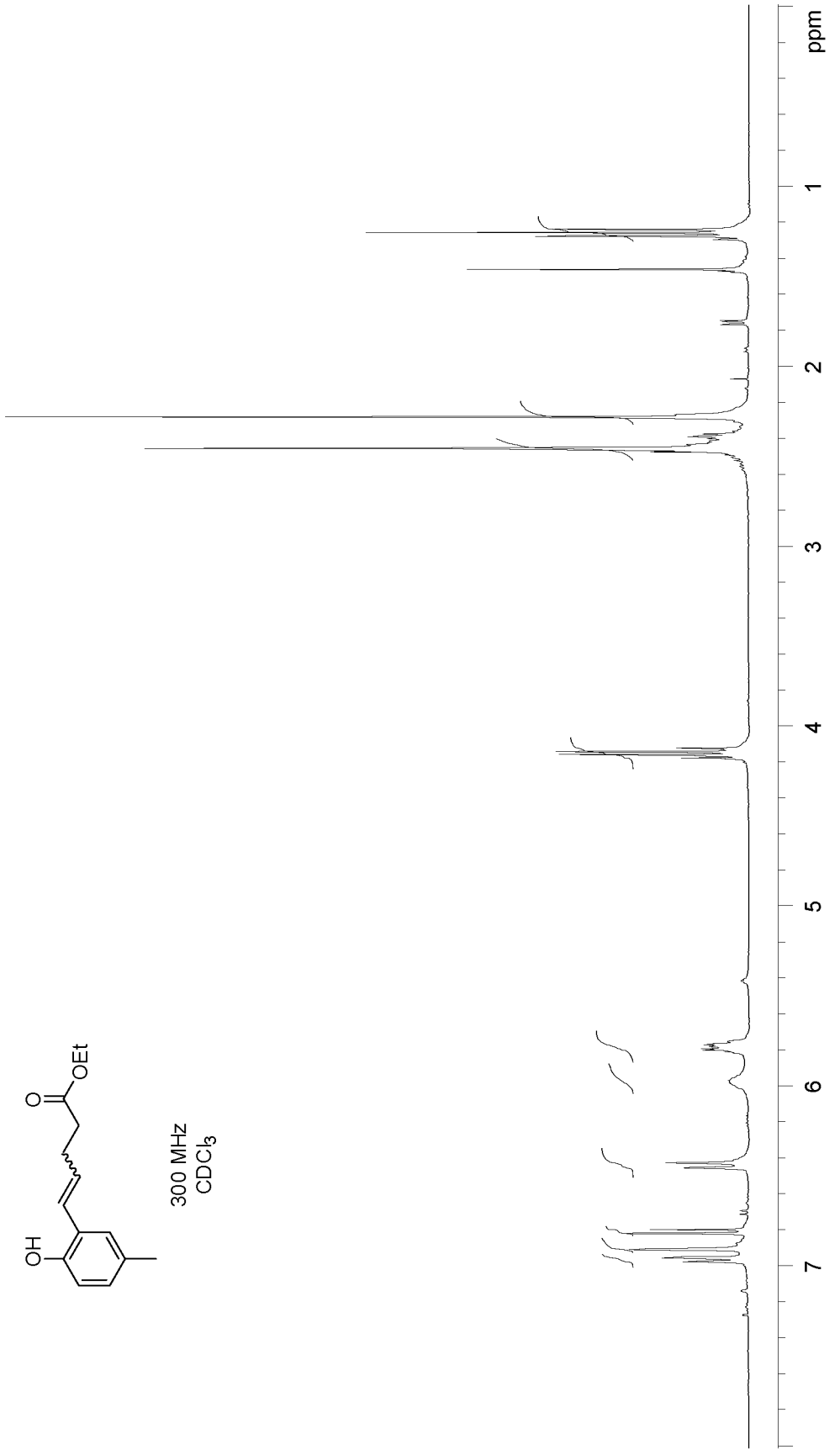
OEt
O
OH
300 MHz
CDCl3
ppm
1
2
3
4
5
6
7

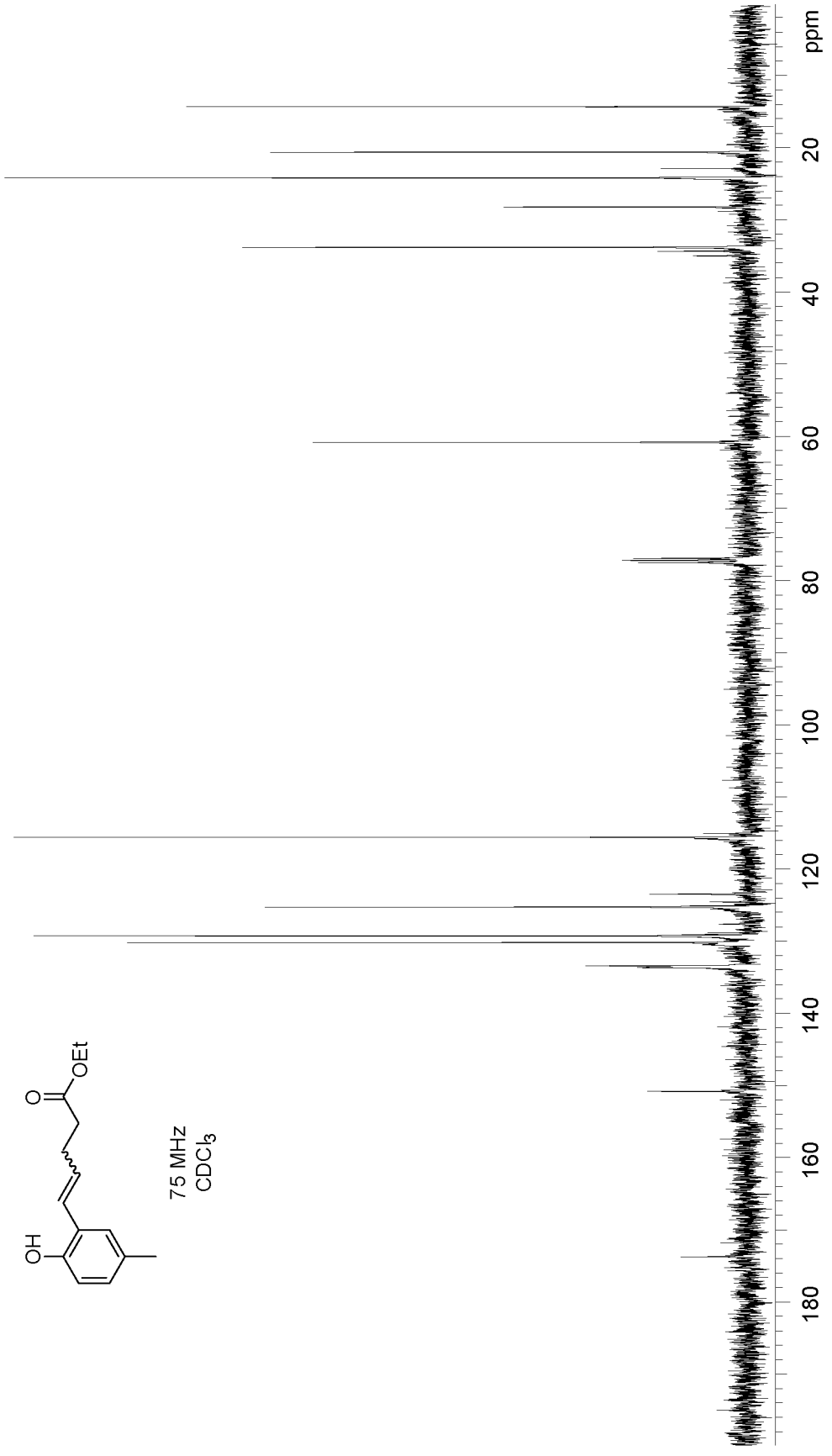
ppm
20
40
60
80
100
120
140
160
180
75 MHz
$CDCl_3$
O
OEt
OH

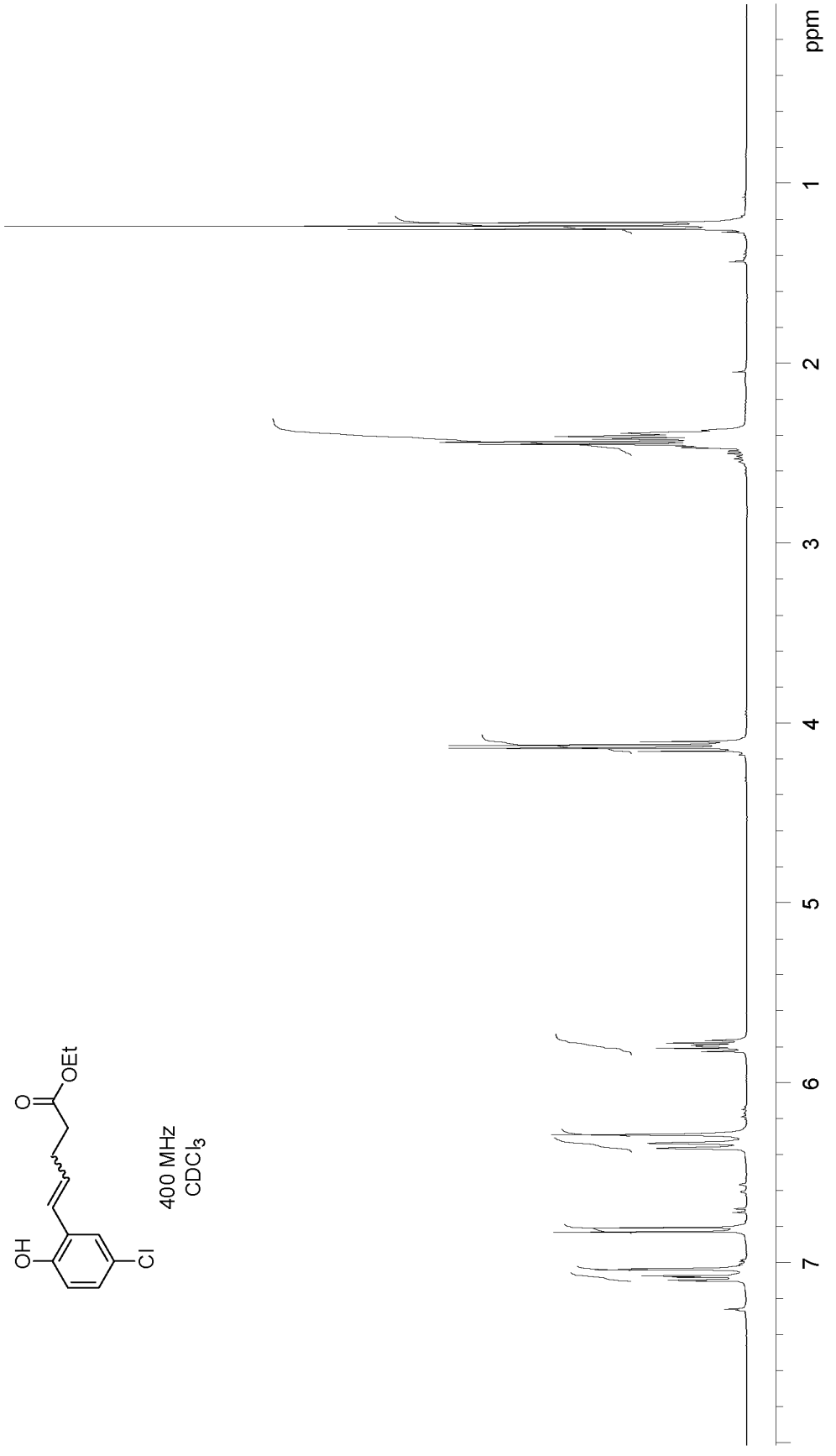
OEt
O
OH
Cl
400 MHz
CDCl3
ppm
1
2
3
4
5
6
7

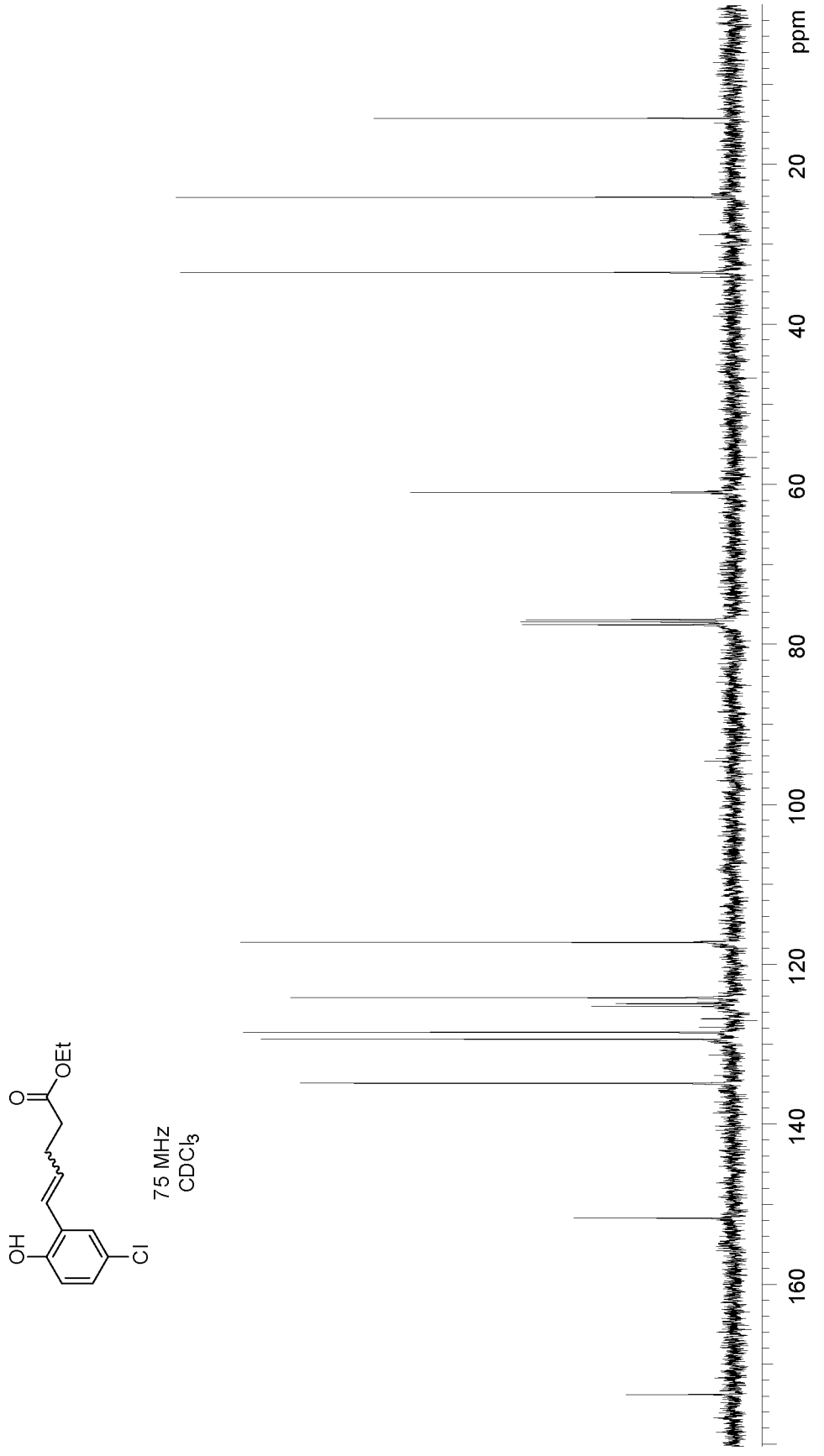
OEt
O
OH
Cl
75 MHz
CDCl3
ppm
20
40
60
80
100
120
140
160

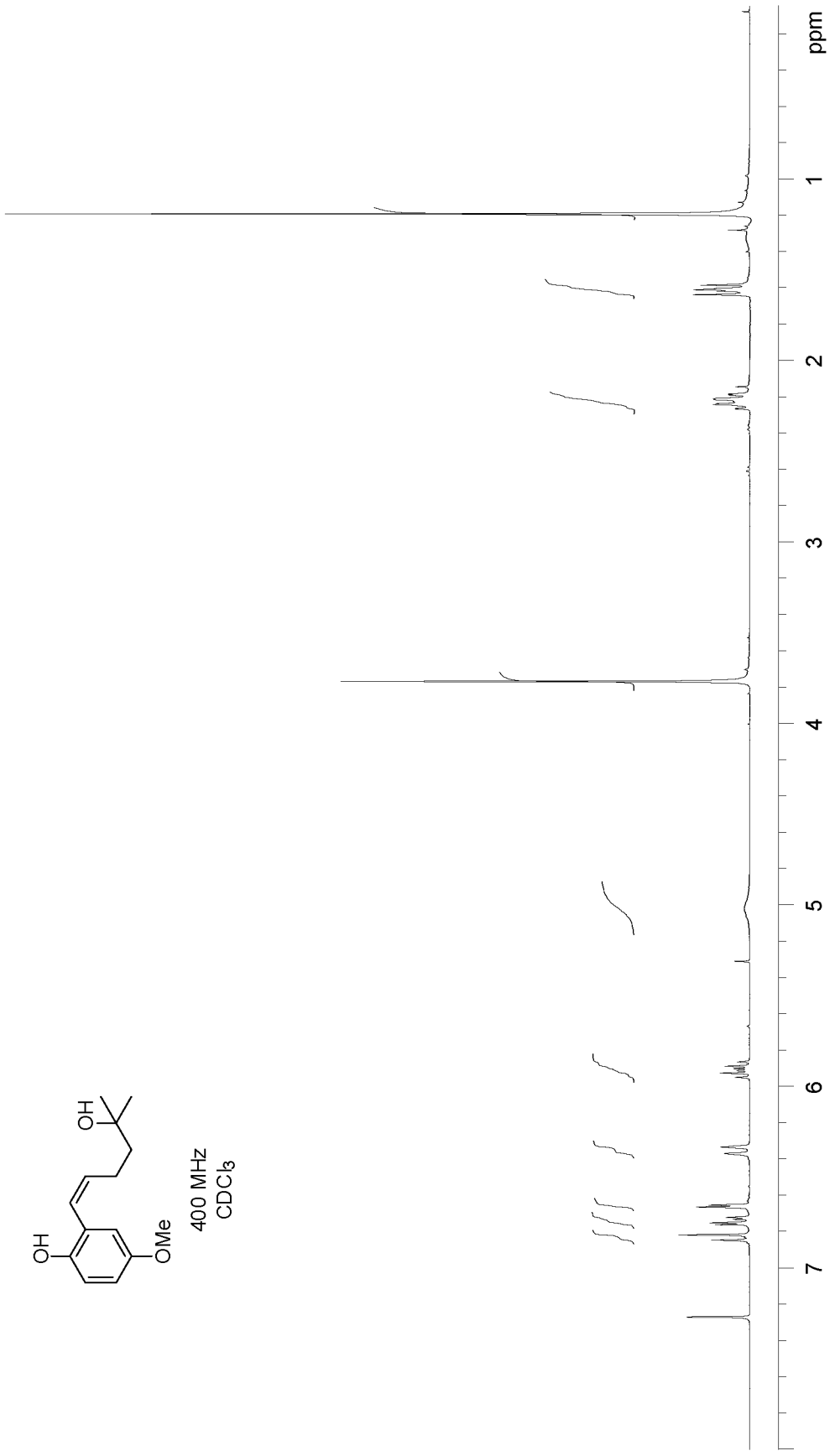
OH
OH
OMe
400 MHz
CDCl3
ppm
1
2
3
4
5
6
7

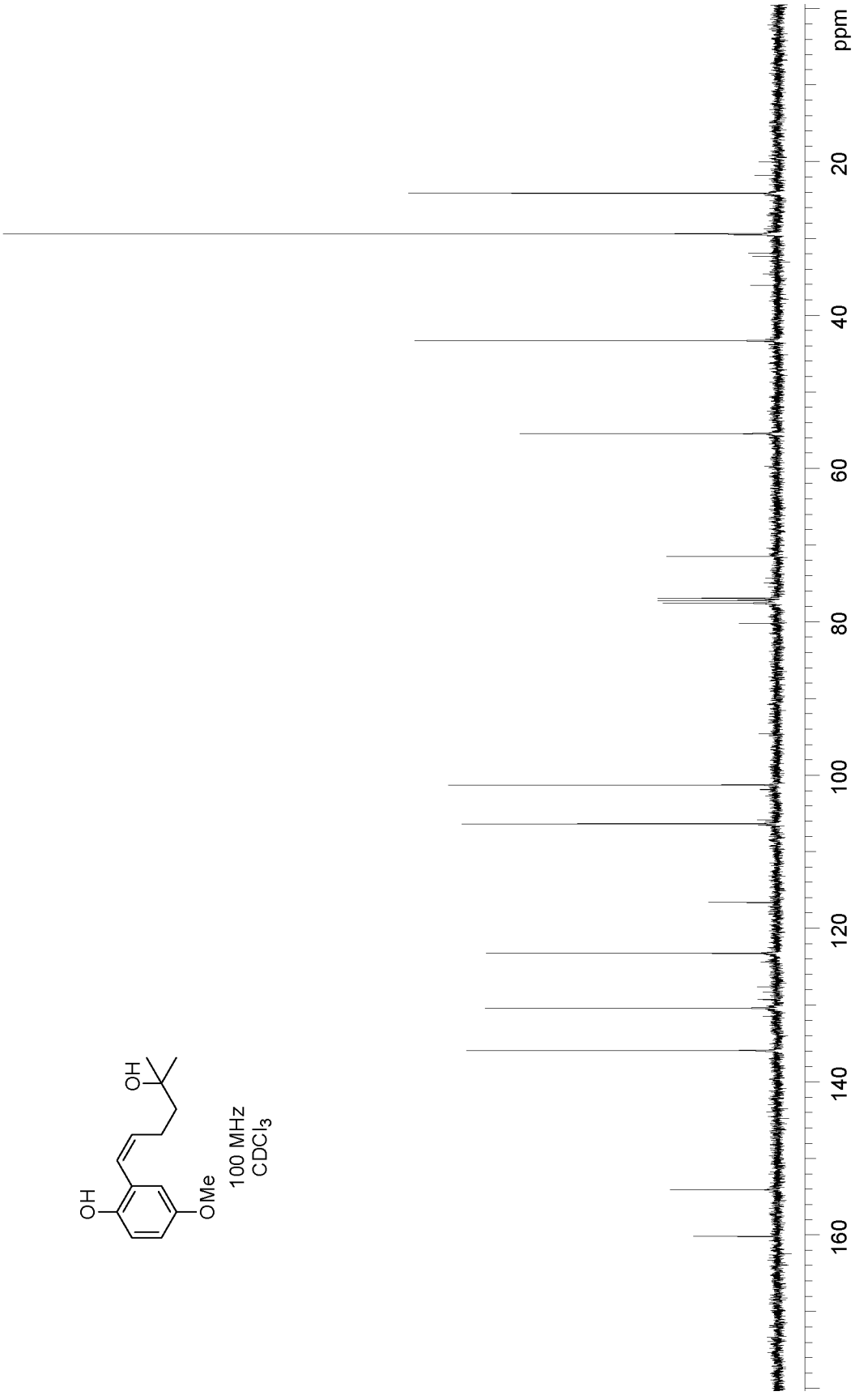
OH
OH
OMe
100 MHz
CDCl3
ppm
20
40
60
80
100
120
140
160

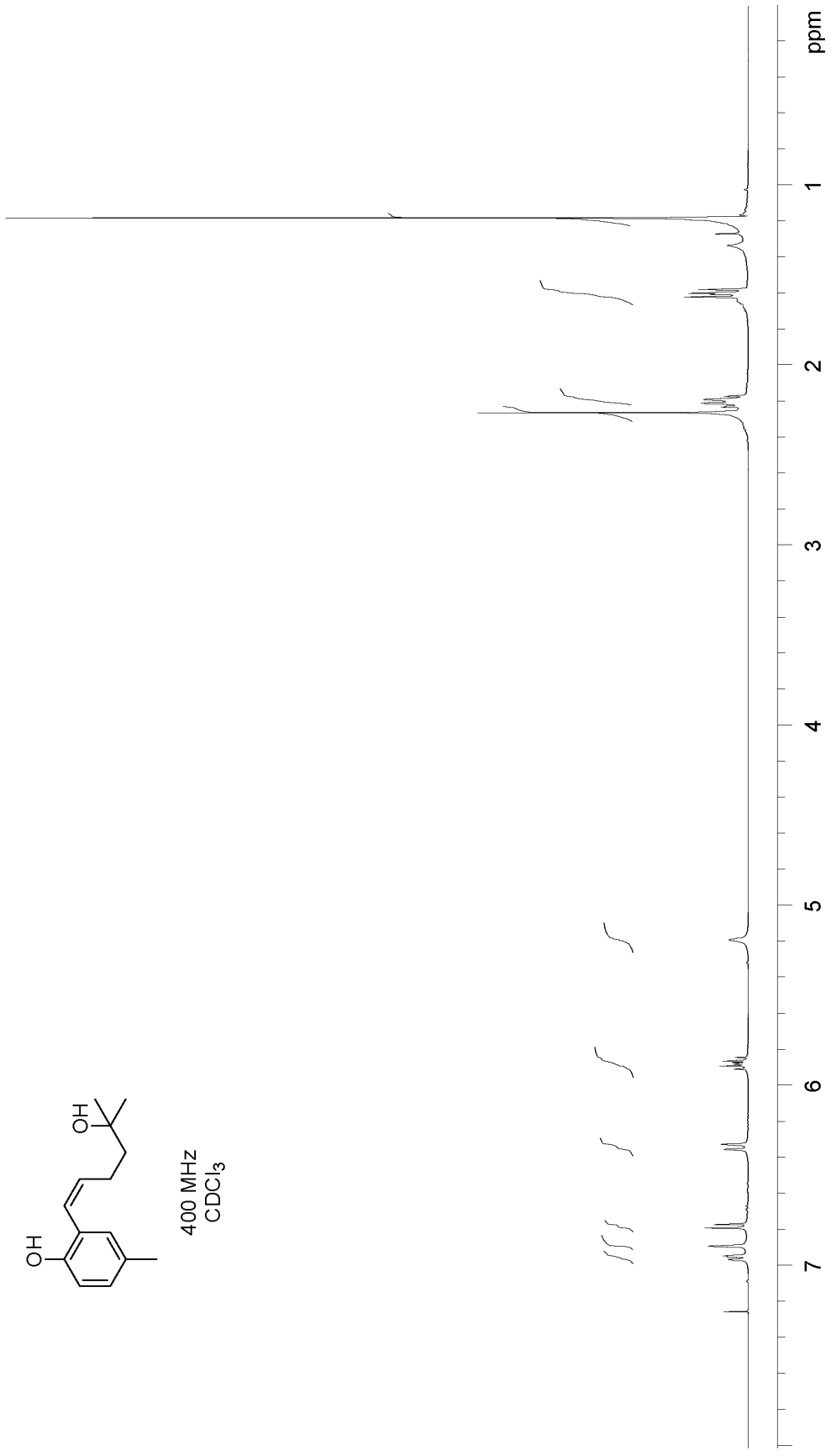
OH
OH
400 MHz
CDCl3
ppm
1
2
3
4
5
6
7

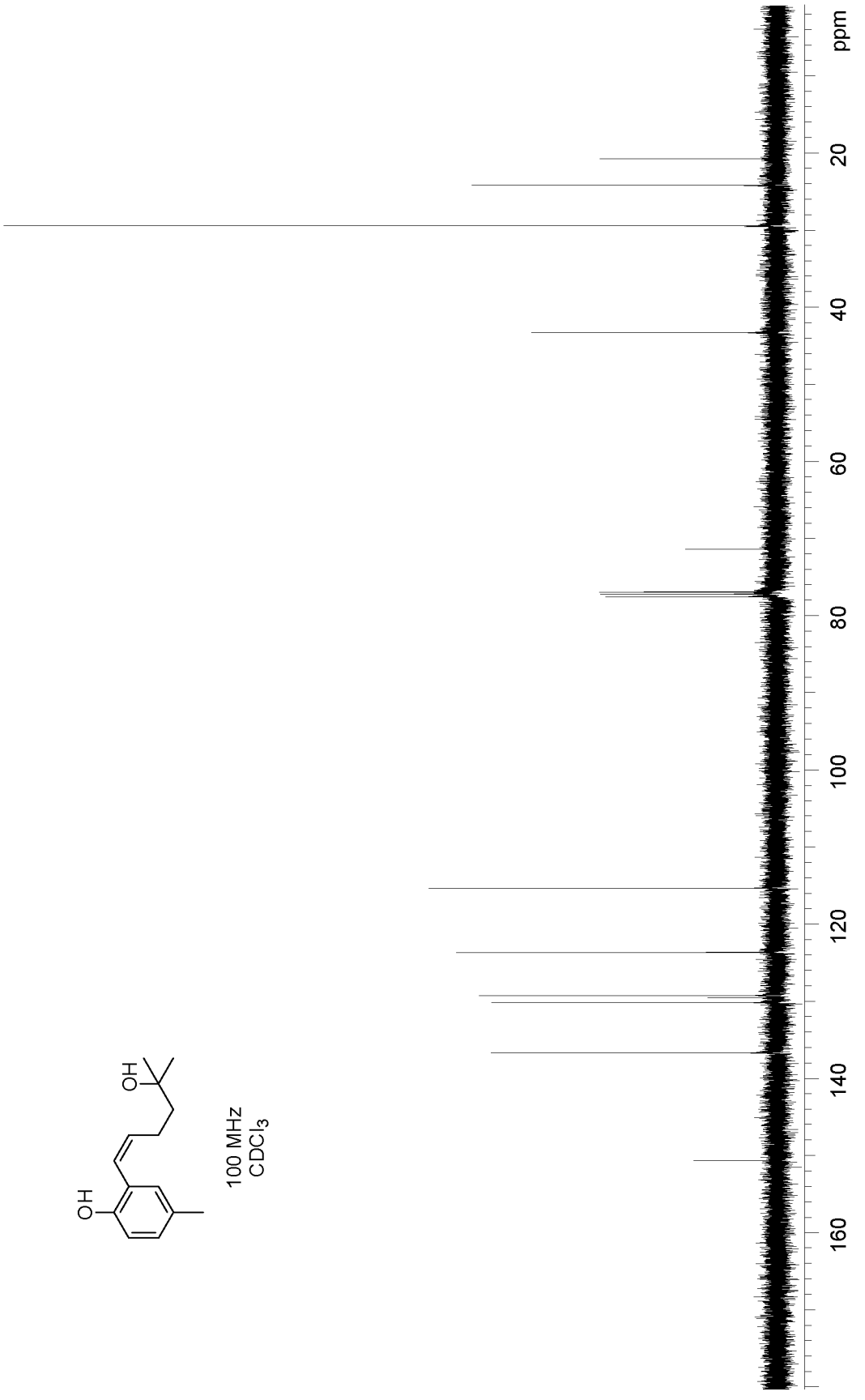
OH
OH
100 MHz
CDCl3
ppm
20
40
60
80
100
120
140
160

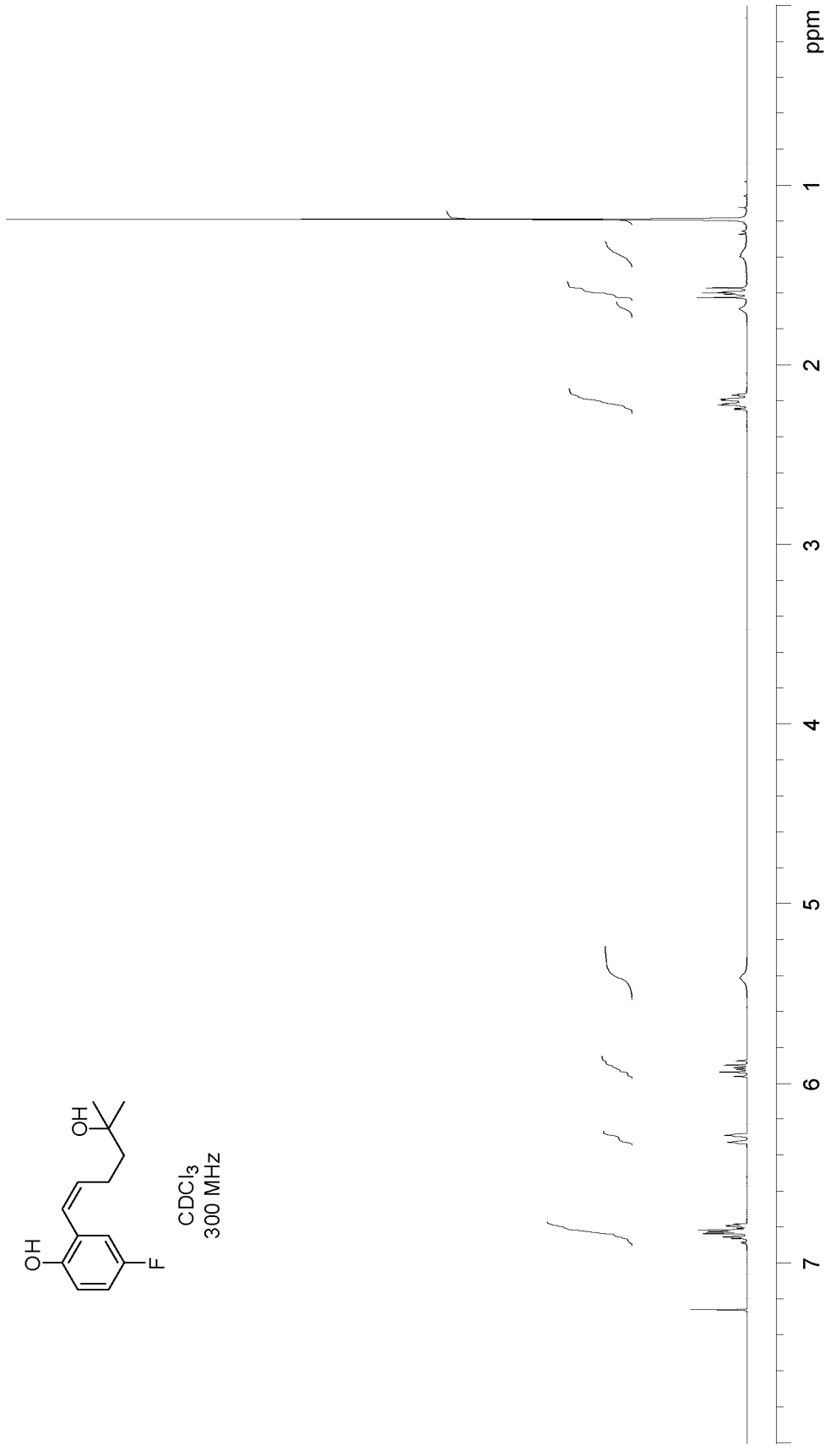
OH
OH
F
$CDCl_3$
300 MHz
ppm
1
2
3
4
5
6
7

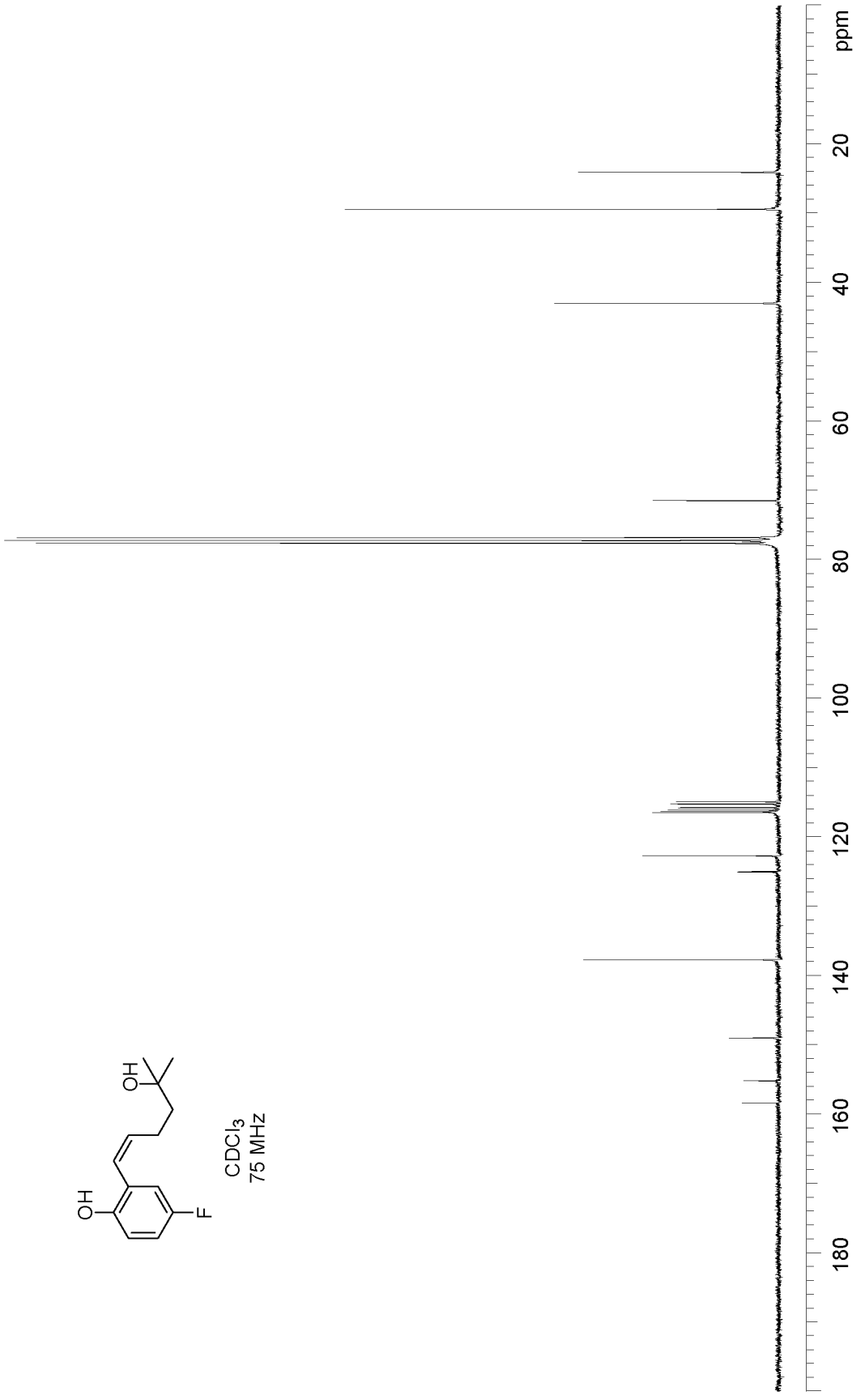
OH
OH
F
CDCl3
75 MHz
ppm
20
40
60
80
100
120
140
160
180

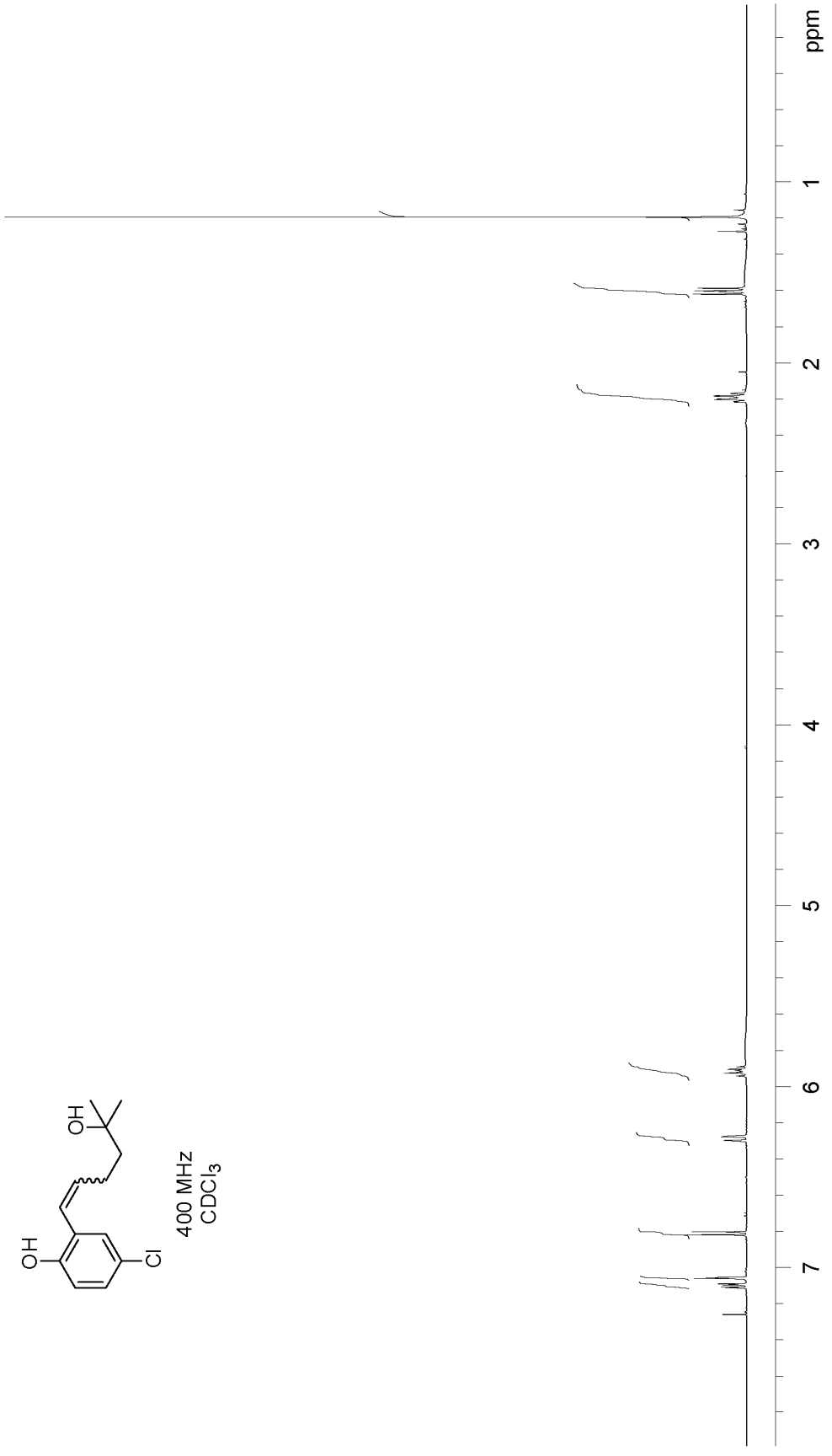
OH
OH
Cl
400 MHz
CDCl3
ppm
1
2
3
4
5
6
7

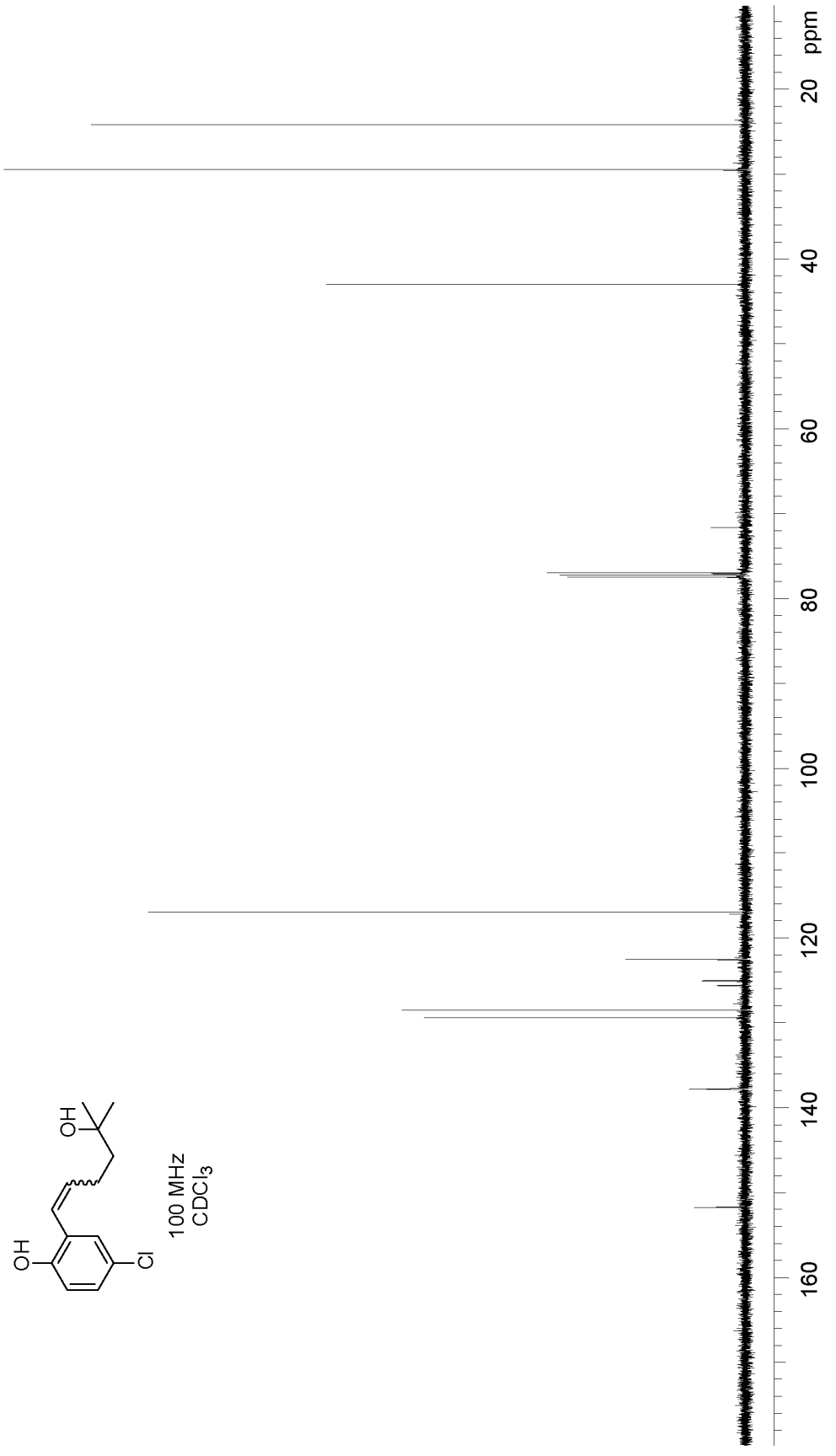
OH
OH
Cl
100 MHz
$CDCl_3$
ppm
20
40
60
80
100
120
140
160

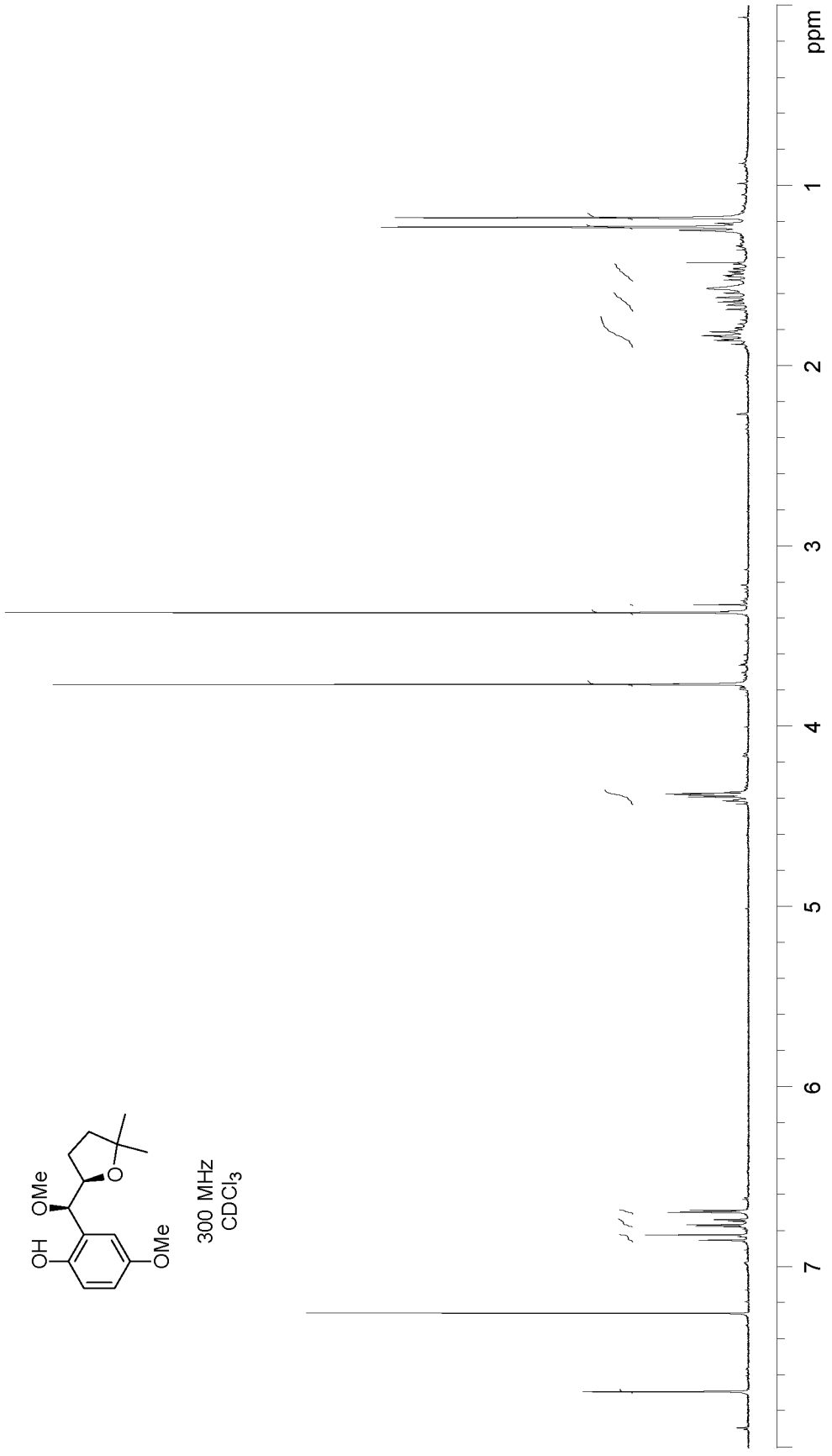
OH
OMe
O
OMe
300 MHz
CDCl3
ppm
1
2
3
4
5
6
7

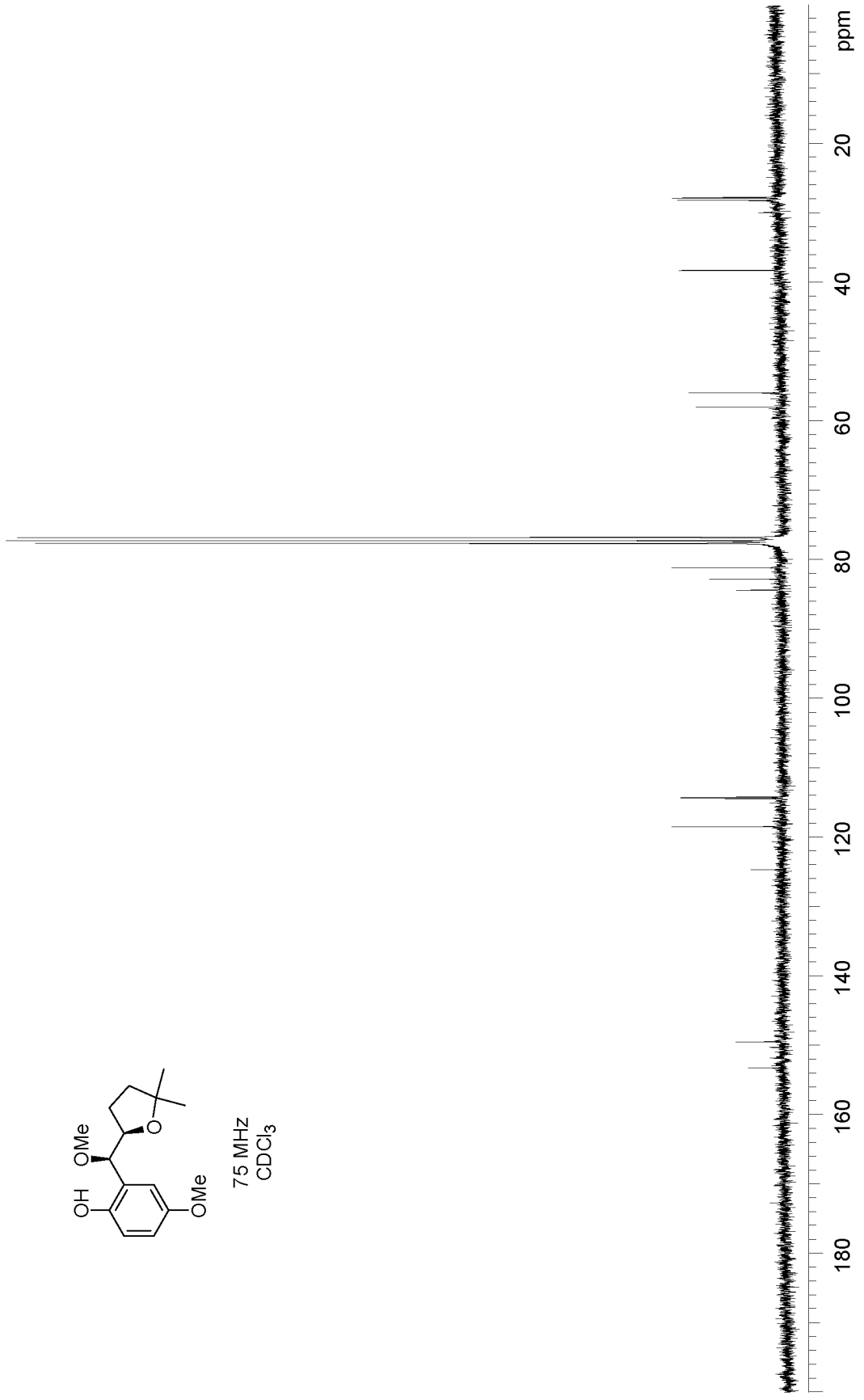
OH
OMe
OMe
O
75 MHz
$CDCl_3$
ppm
20
40
60
80
100
120
140
160
180

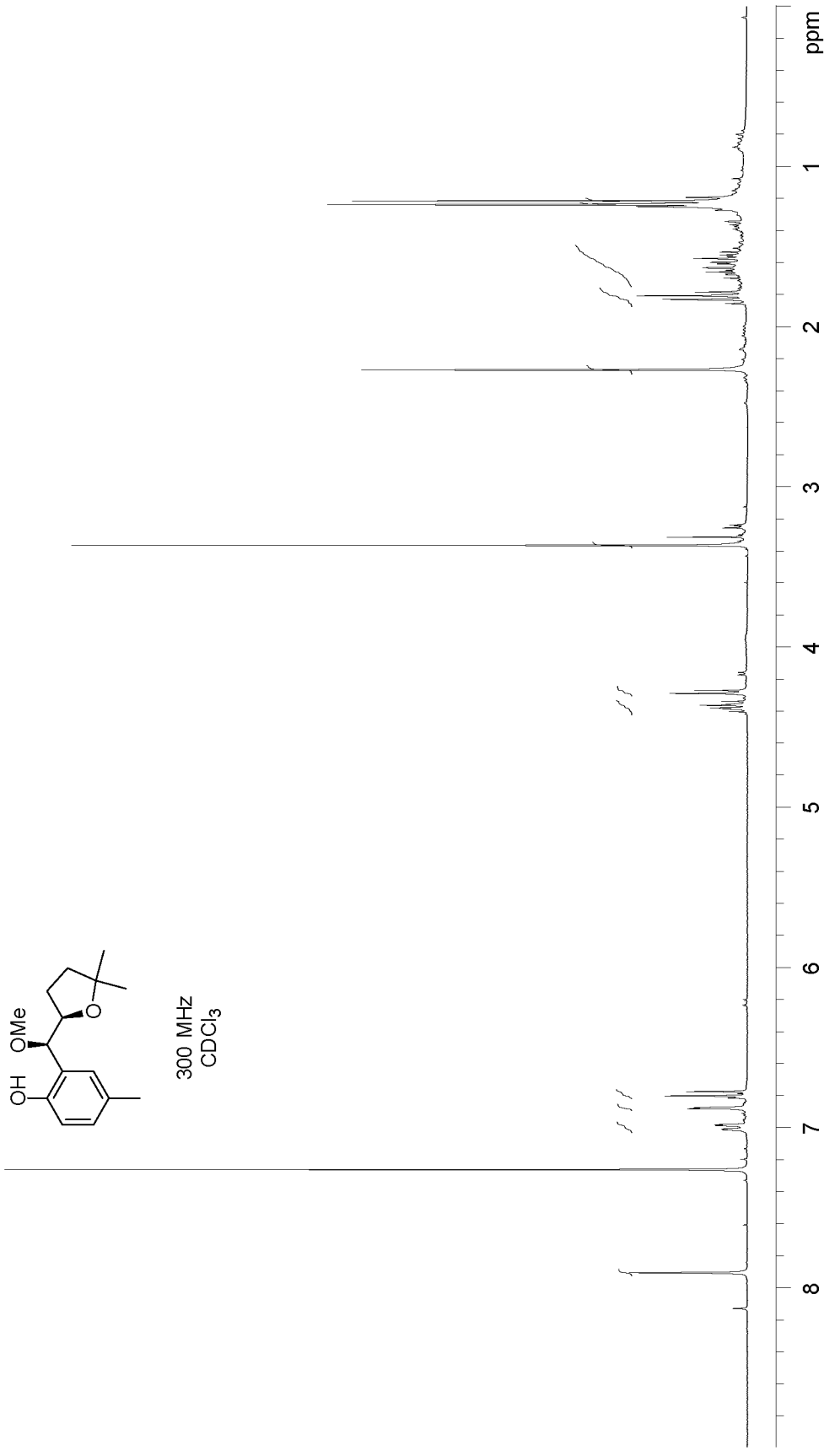
OH
OMe
O
300 MHz
CDCl3
8
7
6
5
4
3
2
1
ppm

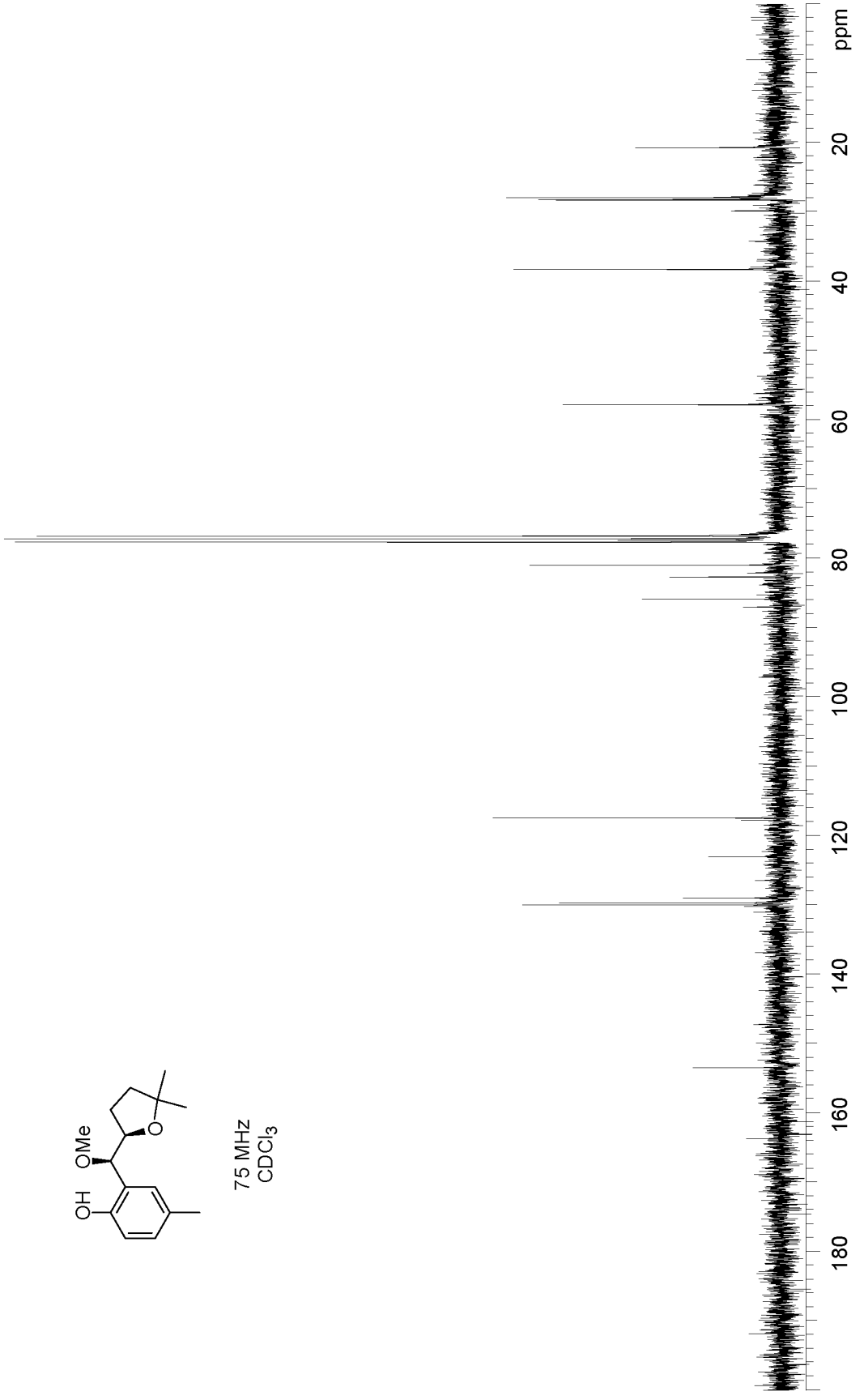
OH
OMe
O
75 MHz
$CDCl_3$
ppm
20
40
60
80
100
120
140
160
180

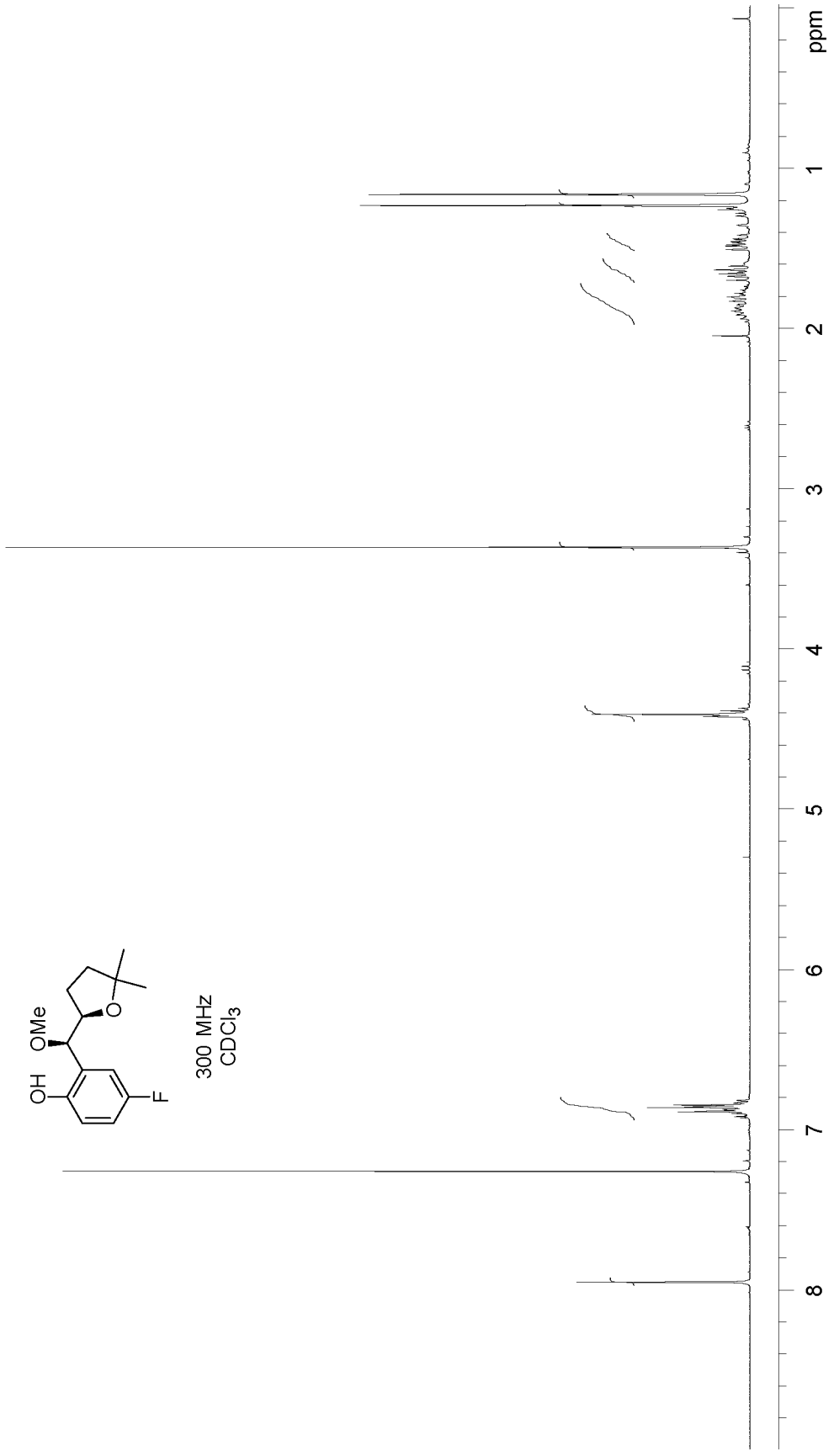
OH
OMe
O
F
300 MHz
CDCl3
ppm
1
2
3
4
5
6
7
8

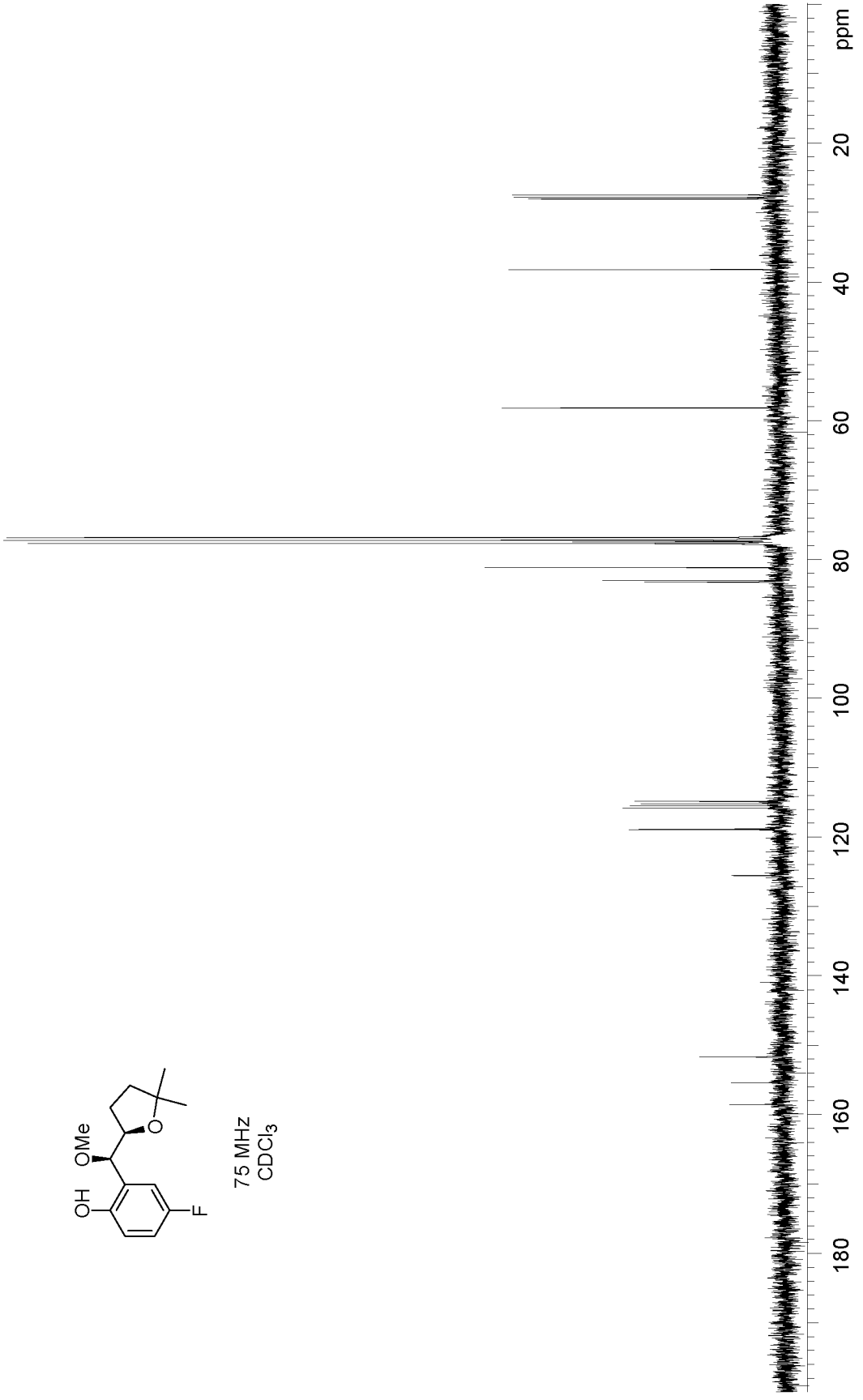
ppm
20
40
60
80
100
120
140
160
180
75 MHz
$CDCl_3$
OH
OMe
O
F

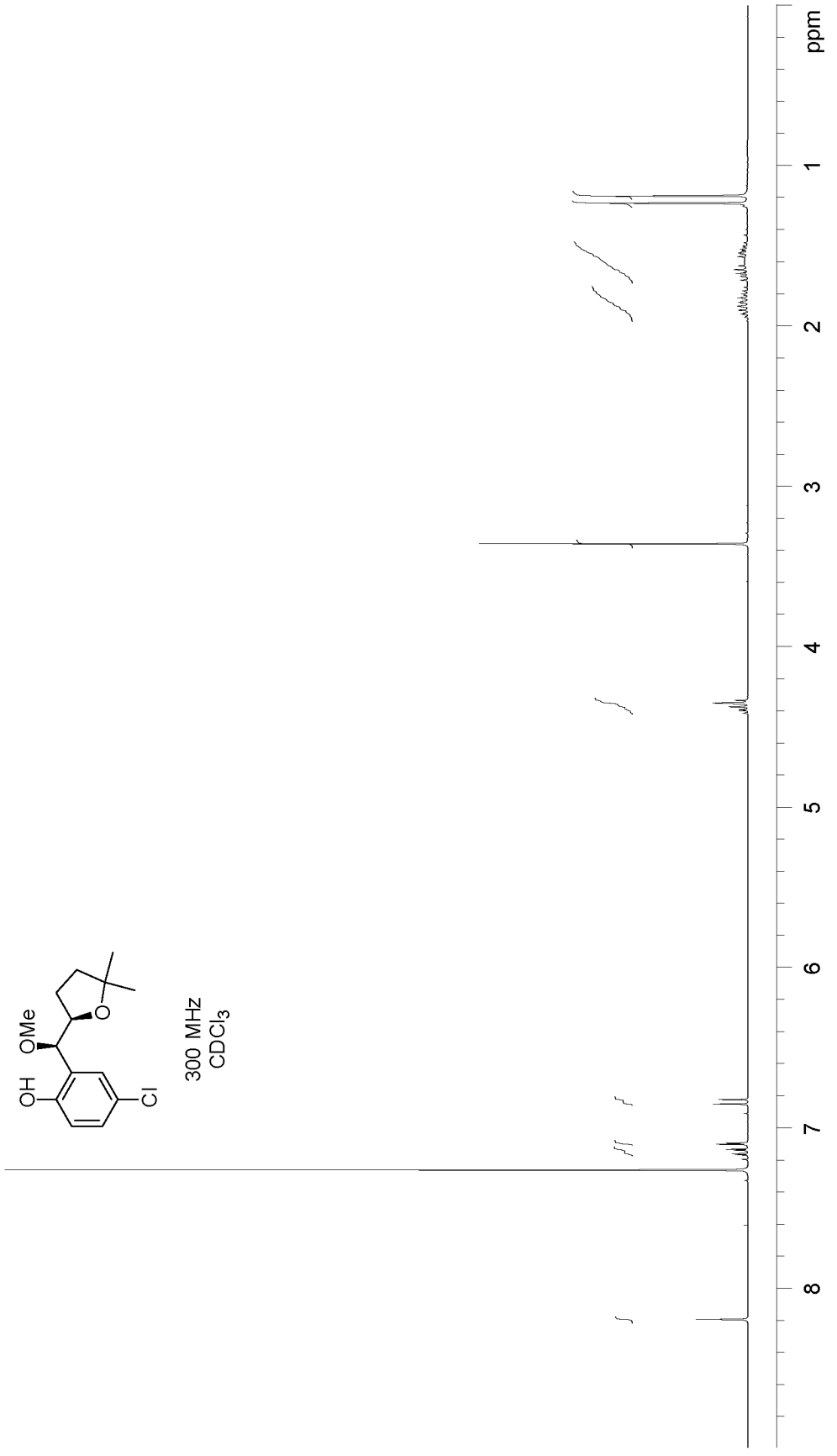
OH
OMe
O
Cl
300 MHz
CDCl3
ppm
1
2
3
4
5
6
7
8

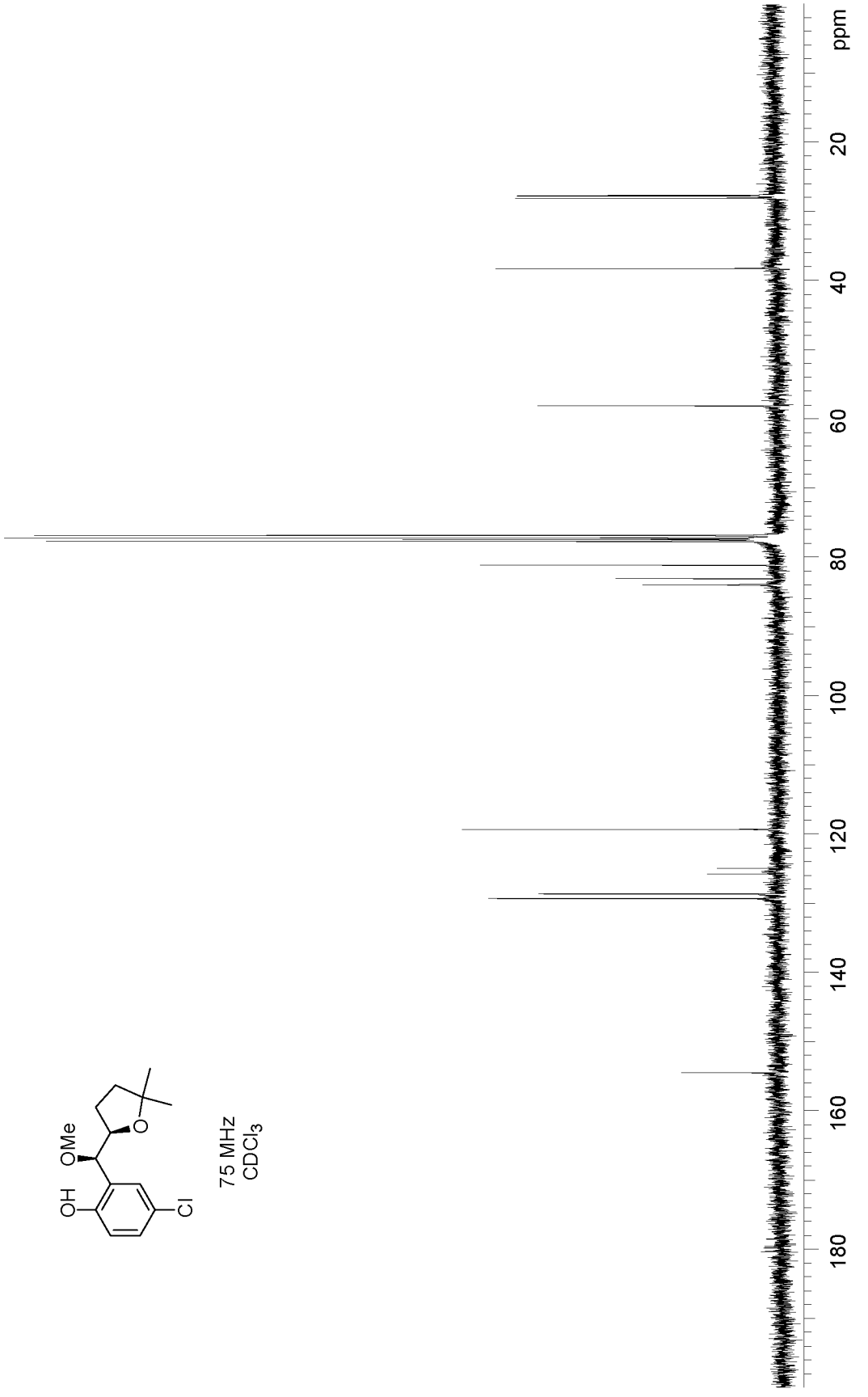
OH
OMe
O
Cl
75 MHz
CDCl3
ppm
20
40
60
80
100
120
140
160
180

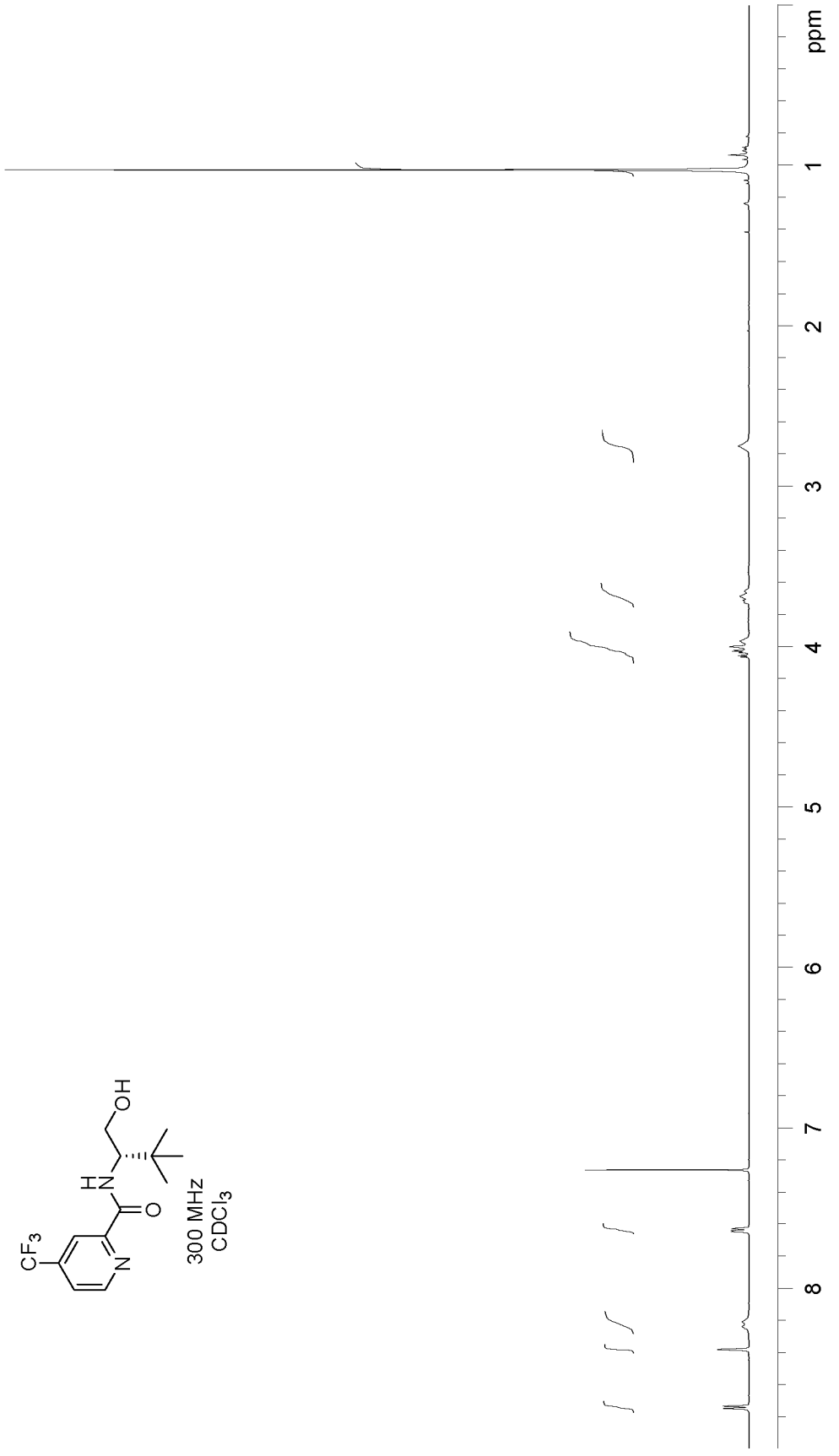
OH
H
N
O
CF3
N
300 MHz
CDCl3
ppm
1
2
3
4
5
6
7
8

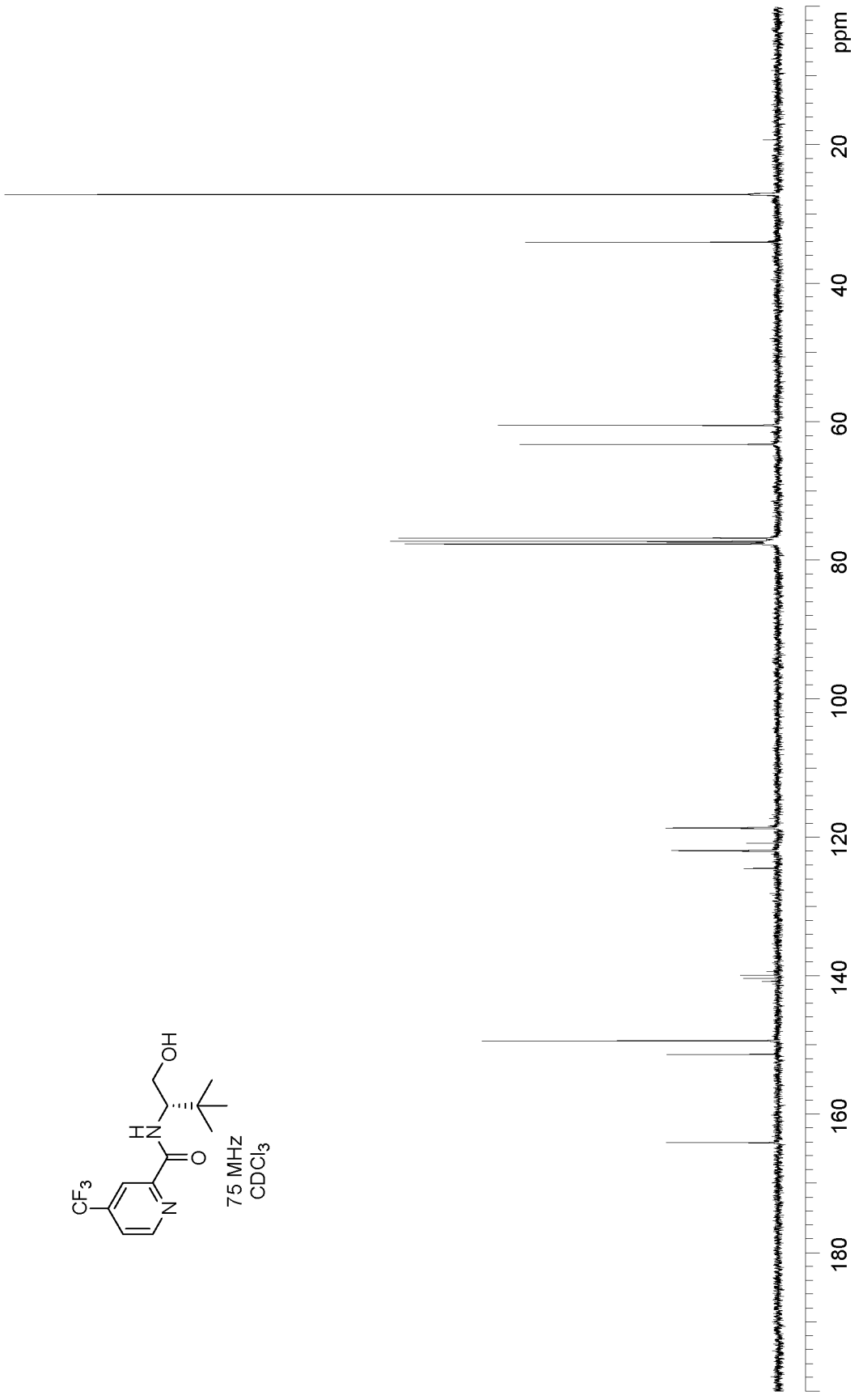
ppm
20
40
60
80
100
120
140
160
180
OH
H
N
O
N
CF3
75 MHz
CDCl3

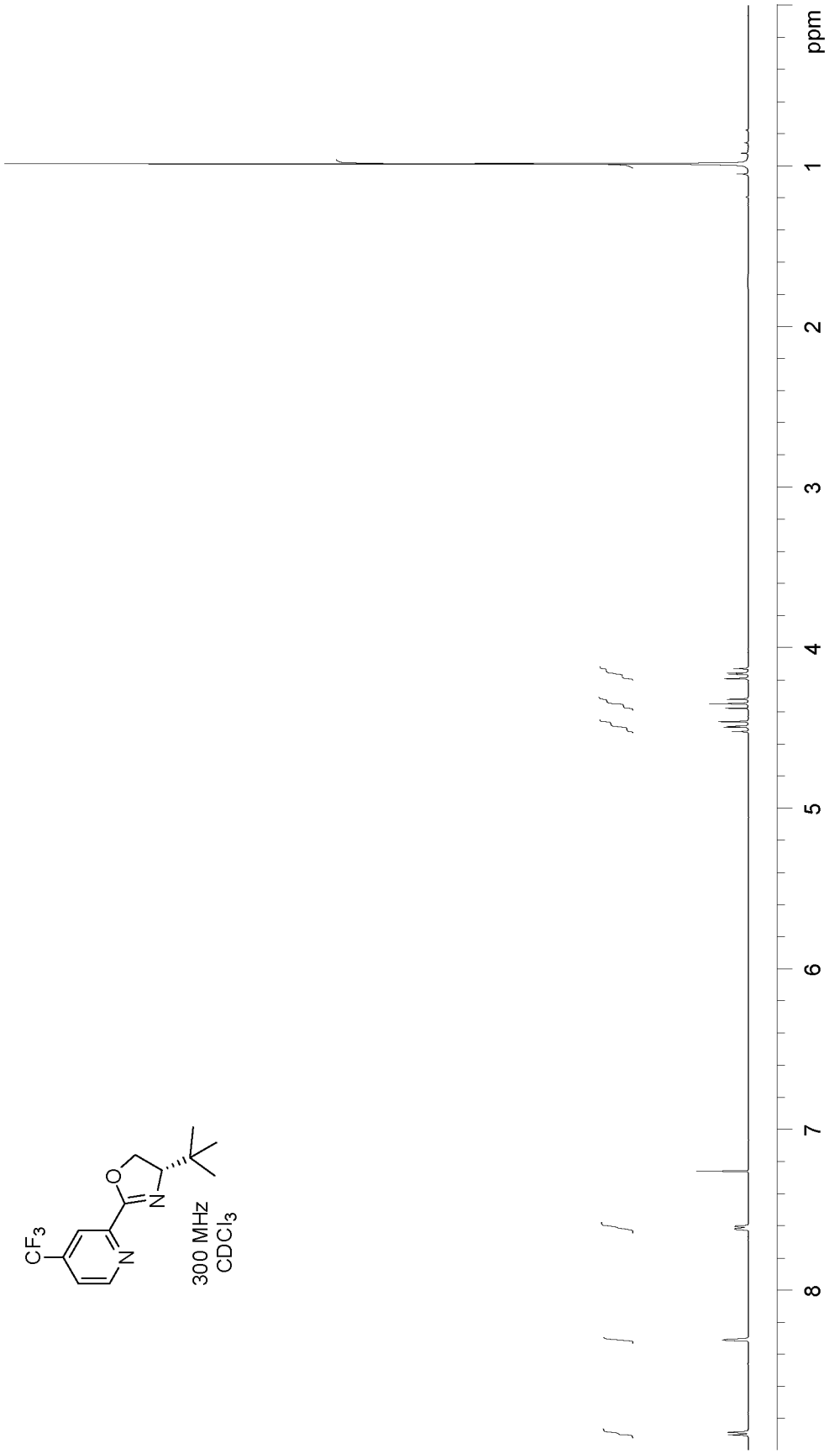
CF3
N
O
N
300 MHz
CDCl3
ppm
1
2
3
4
5
6
7
8

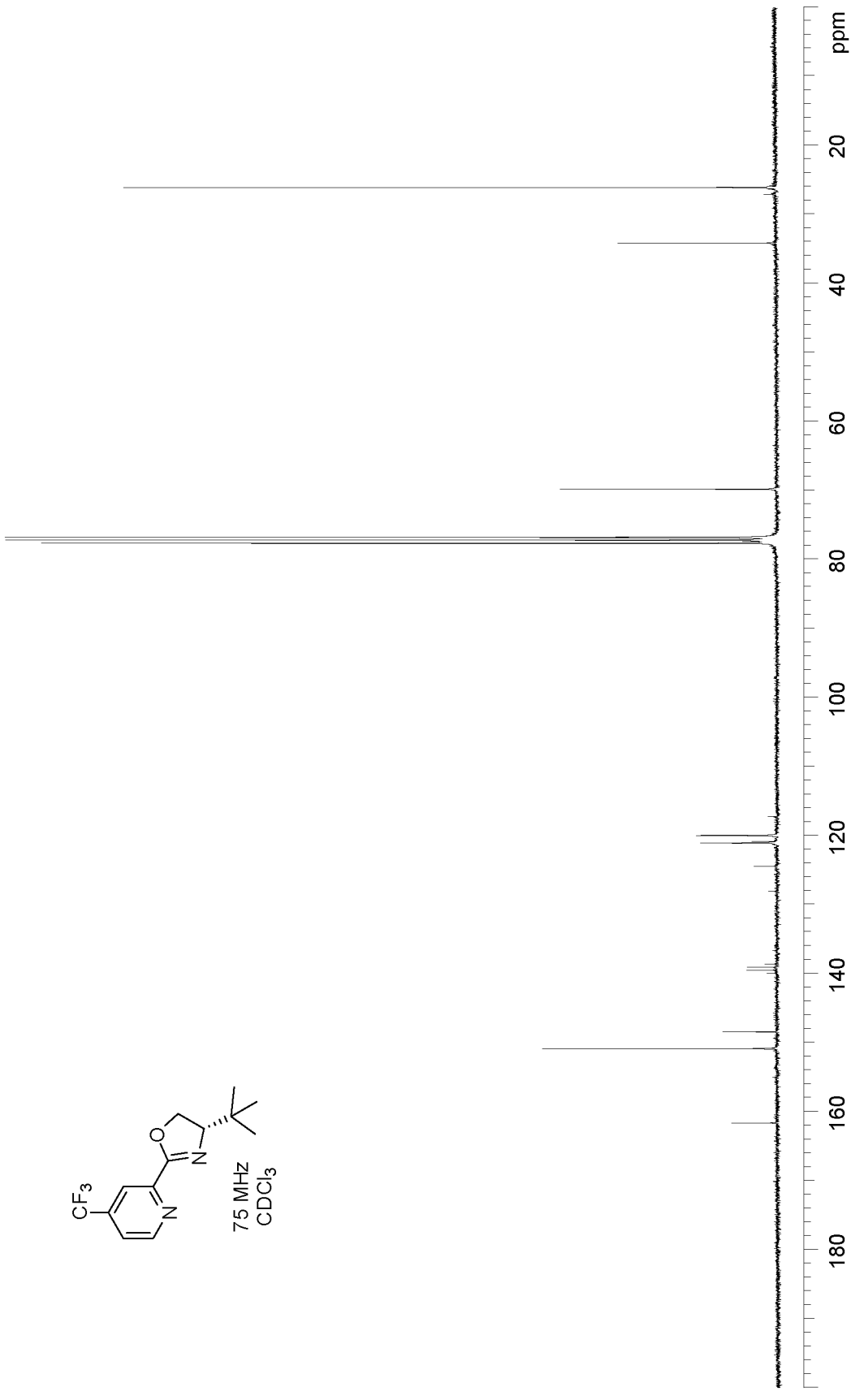
ppm
20
40
60
80
100
120
140
160
180
75 MHz
CDCl3
CF3
N
O
N

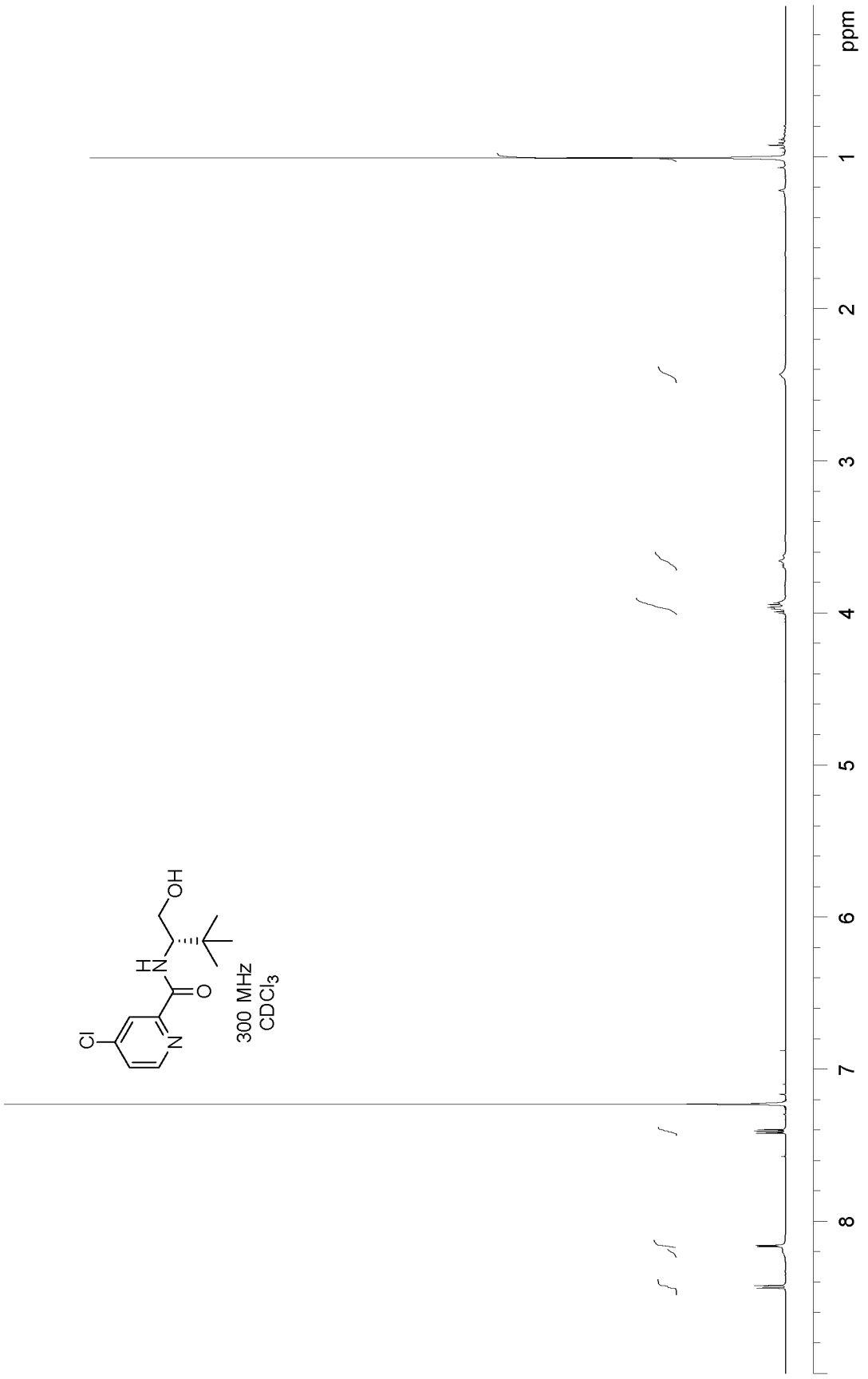
ppm
1
2
3
4
5
6
7
8
300 MHz
CDCl3
Cl
N
O
H
N
OH

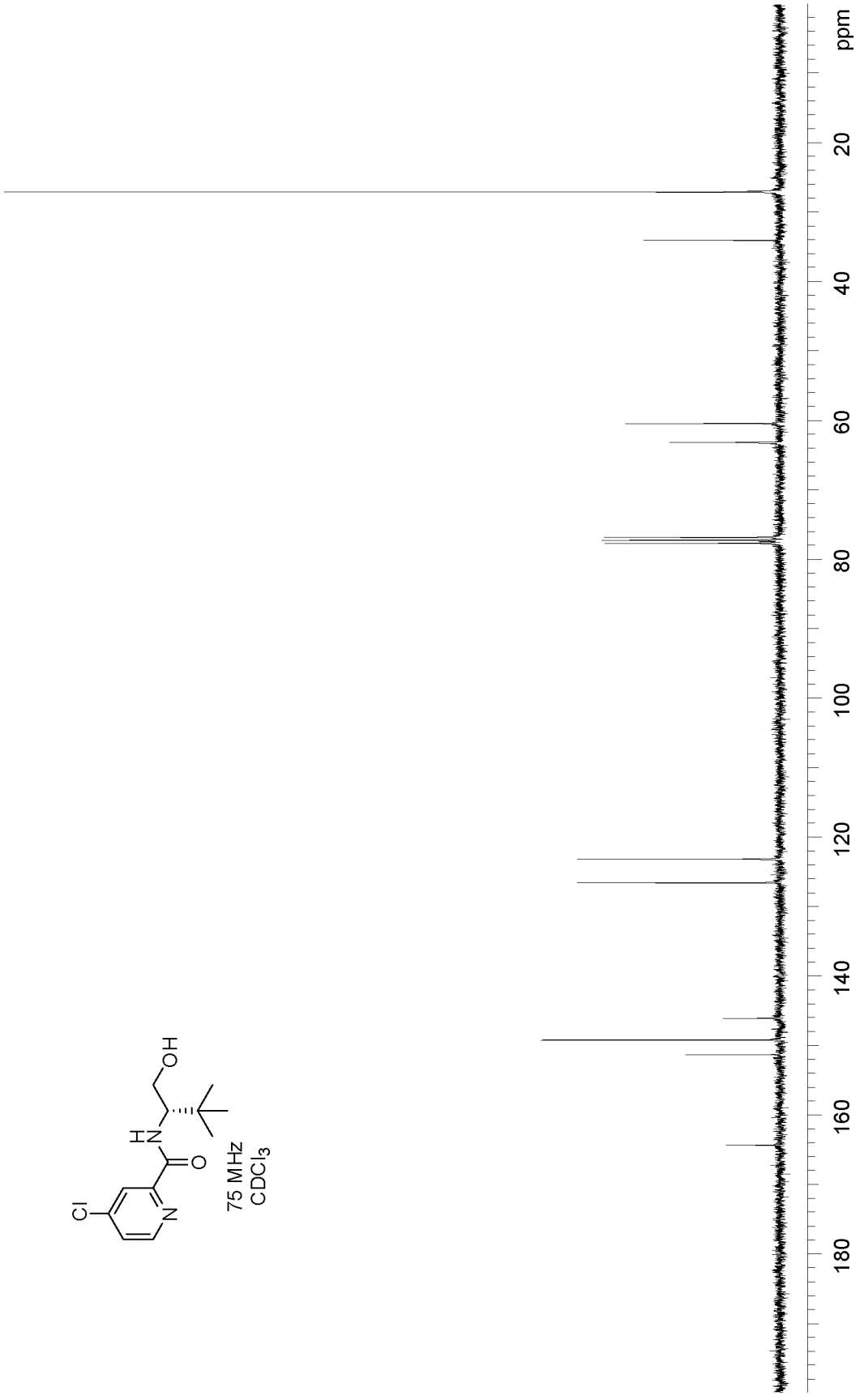
ppm
20
40
60
80
100
120
140
160
180
OH
H
N
O
N
Cl
75 MHz
CDCl3

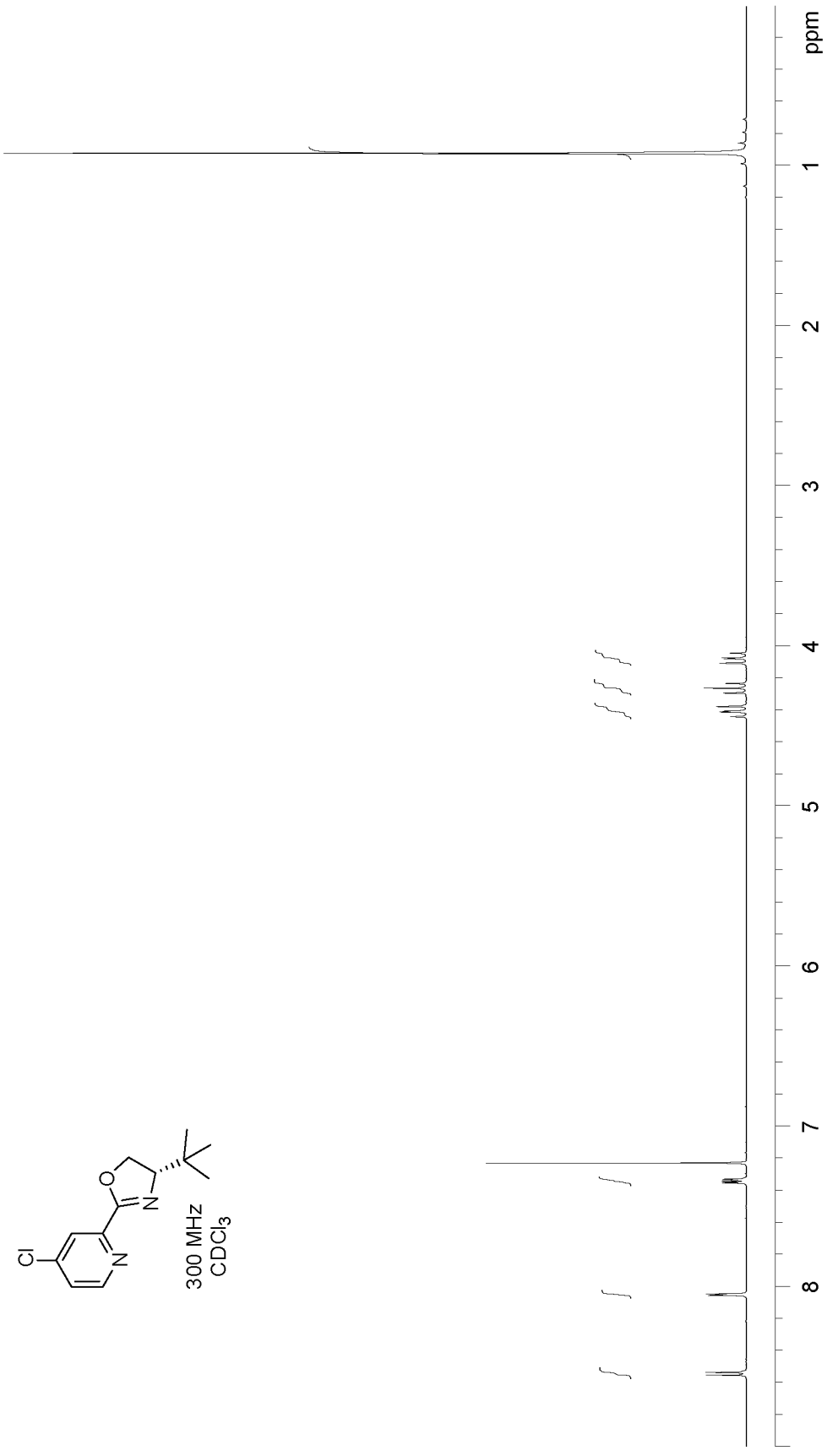
ppm
1
2
3
4
5
6
7
8
300 MHz
$CDCl_3$
Cl
N
O
N

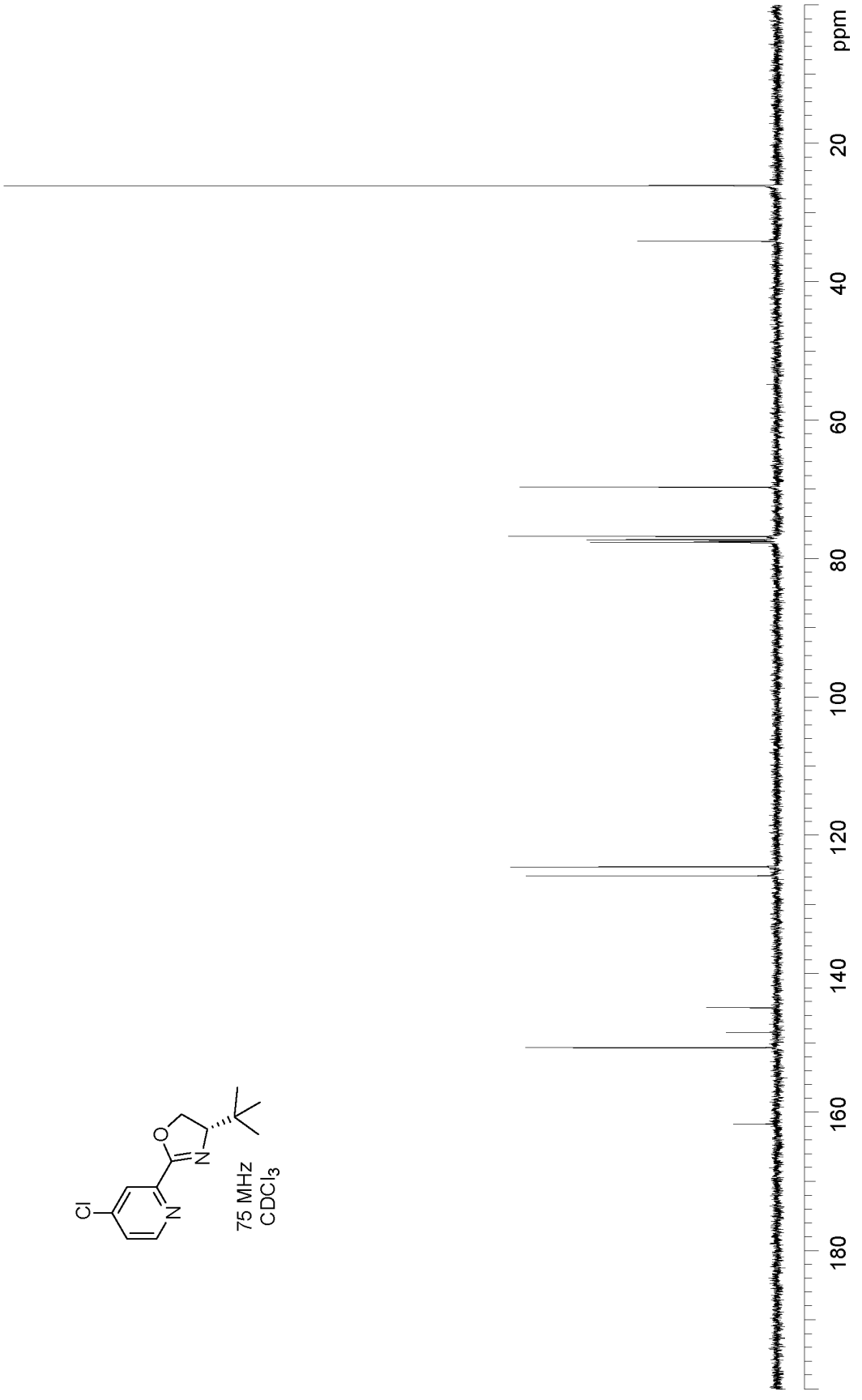
ppm
20
40
60
80
100
120
140
160
180
75 MHz
$CDCl_3$
Cl
N
O
N

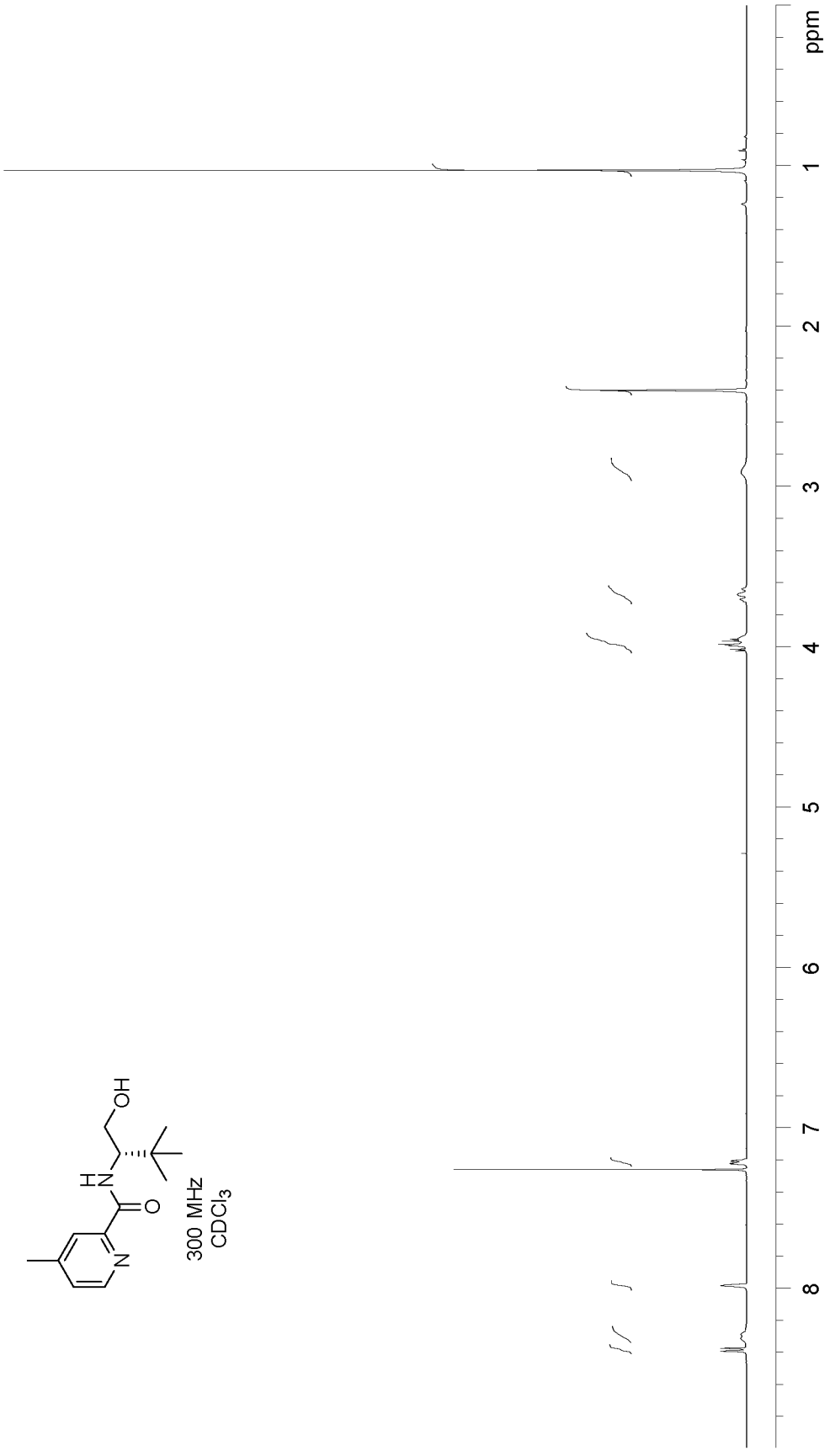
OH
HN
O
N
300 MHz
CDCl3
ppm
1
2
3
4
5
6
7
8

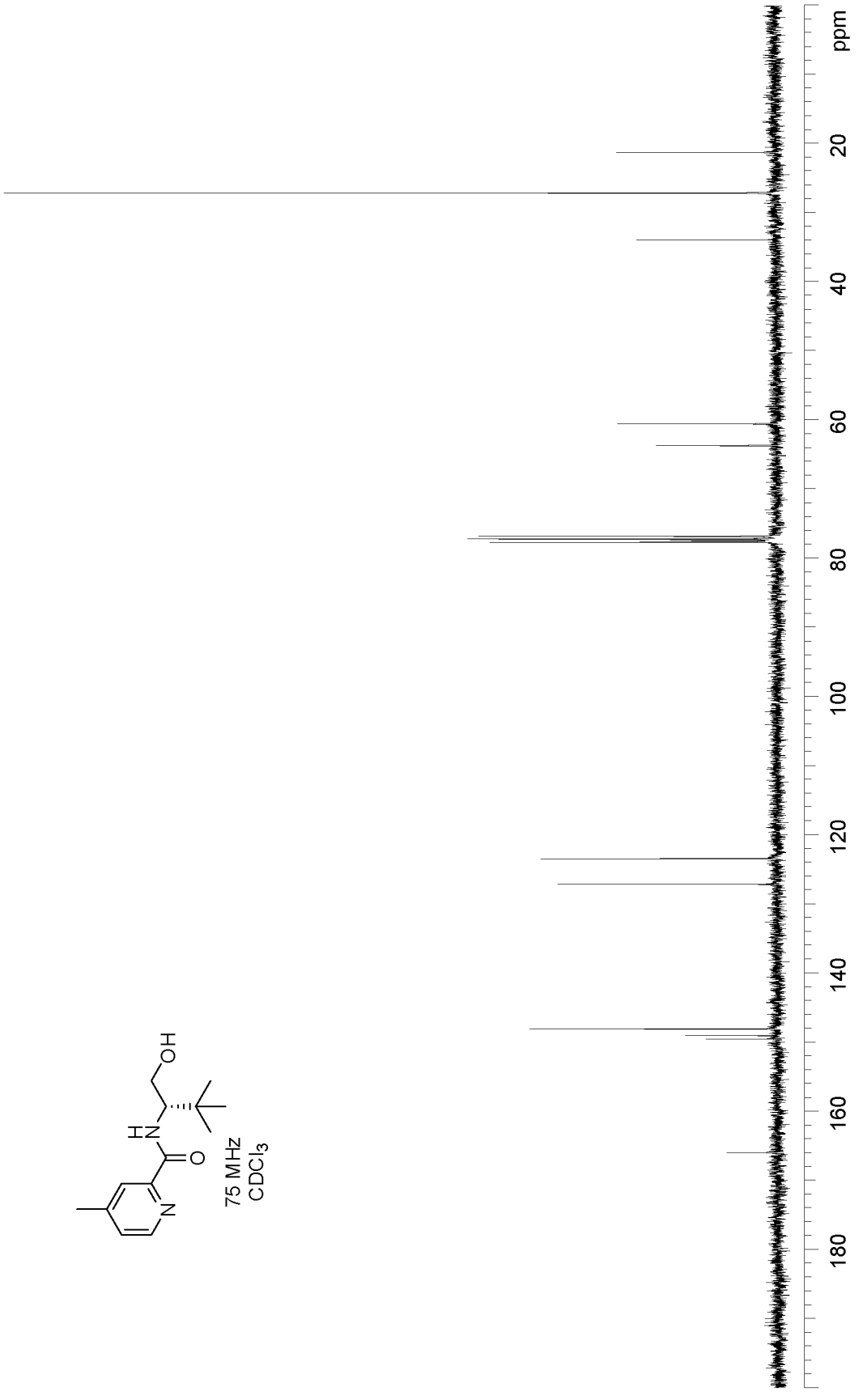
ppm
20
40
60
80
100
120
140
160
180
OH
HN
O
N
75 MHz
CDCl3

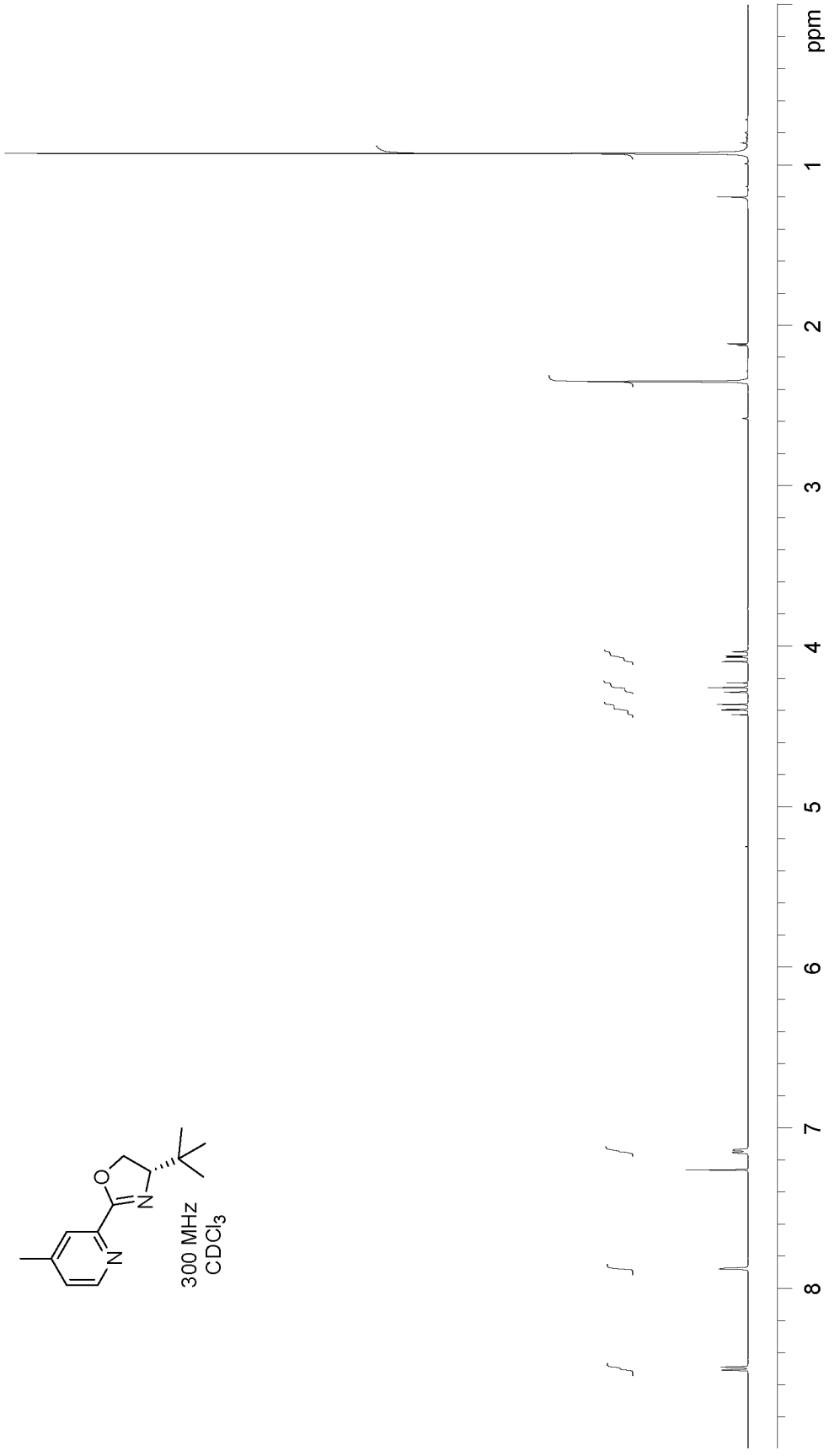
ppm
1
2
3
4
5
6
7
8
300 MHz
CDCl3
O
N
N

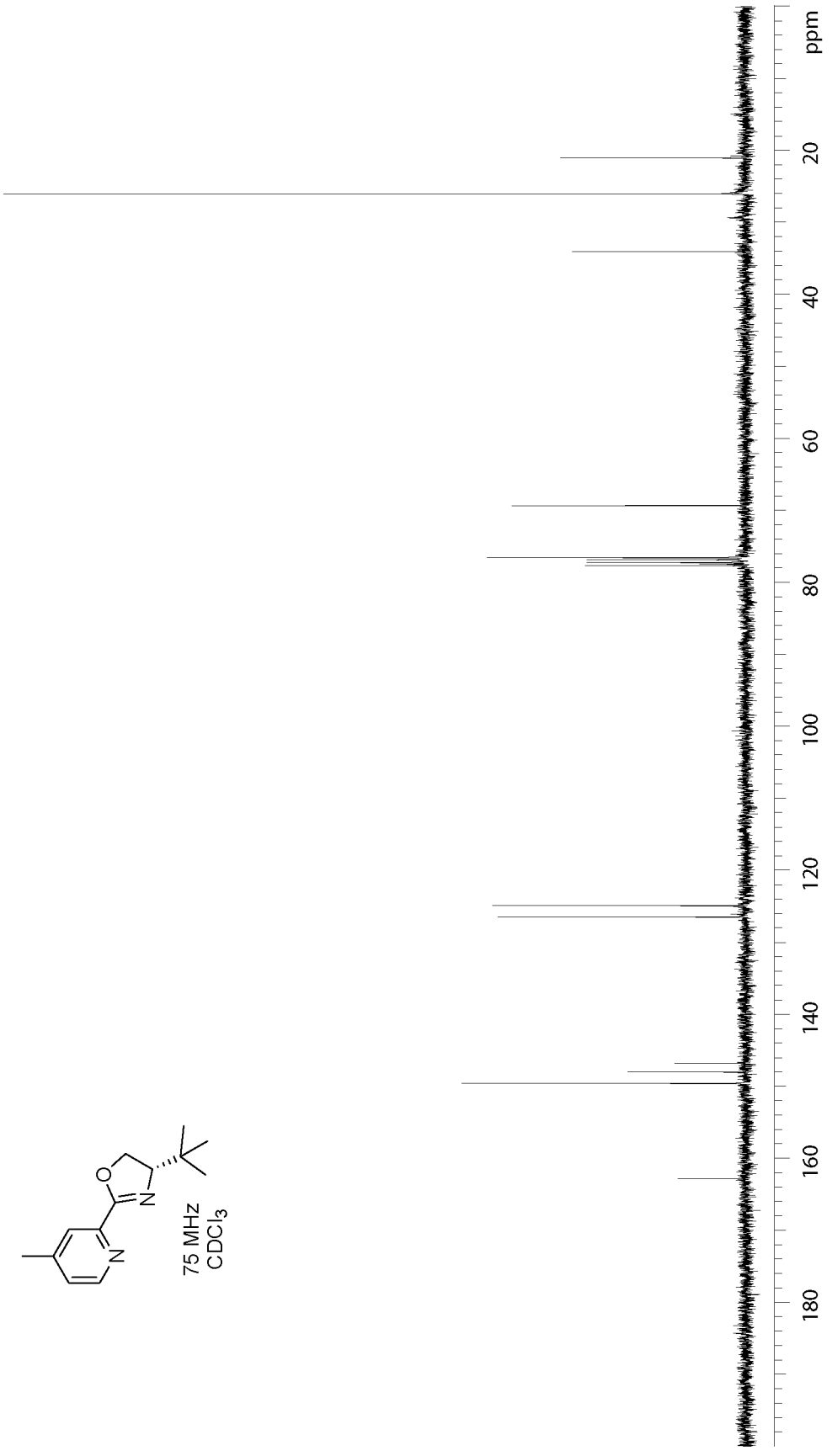
ppm
20
40
60
80
100
120
140
160
180
75 MHz
$CDCl_3$
O
N
N

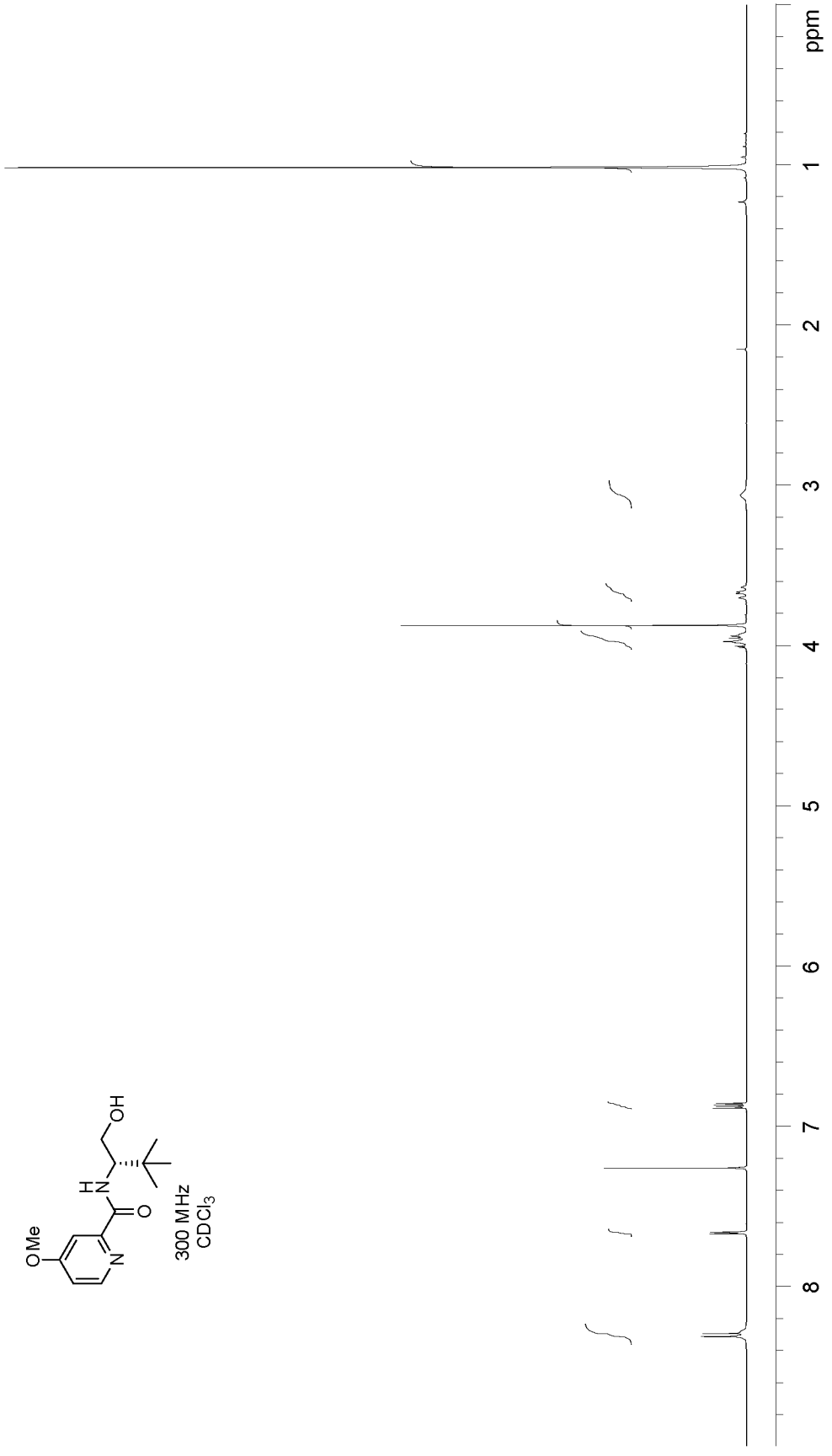
OMe
N
H
N
O
OH
300 MHz
CDCl3
ppm
1
2
3
4
5
6
7
8

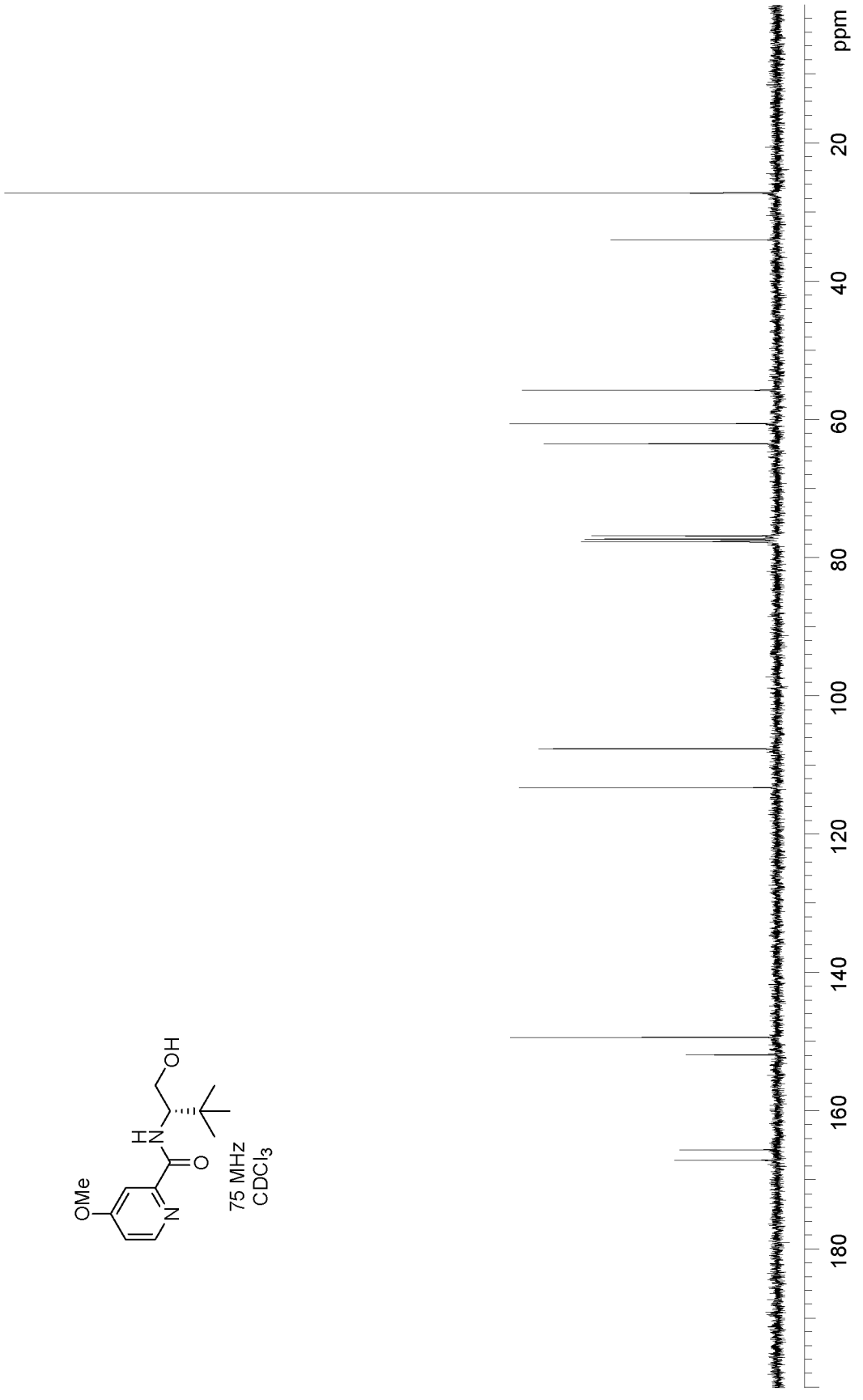
OMe
N
O
H
N
OH
75 MHz
CDCl3
ppm
20
40
60
80
100
120
140
160
180

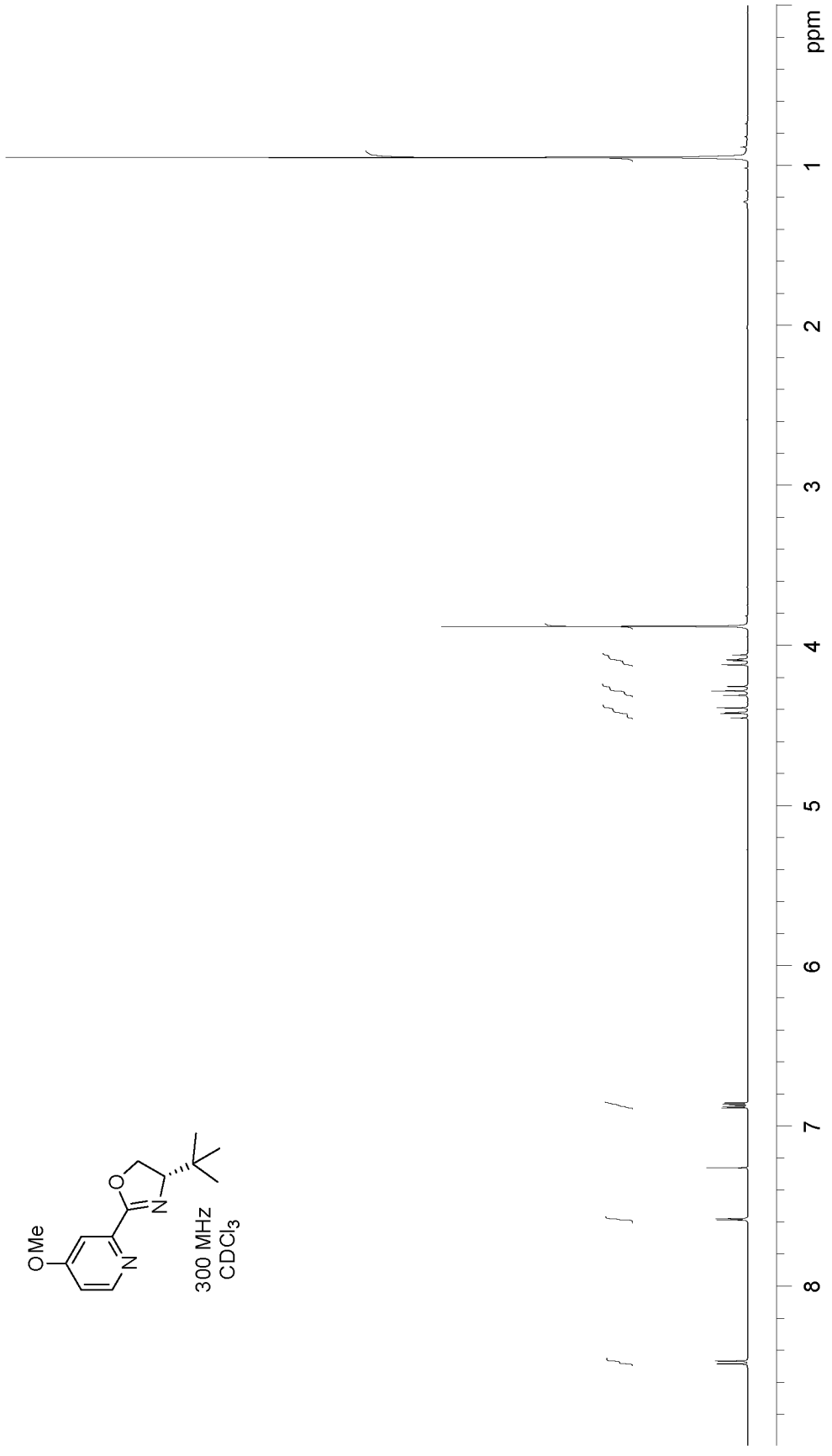
OMe
N
O
N
300 MHz
$CDCl_3$
ppm
1
2
3
4
5
6
7
8

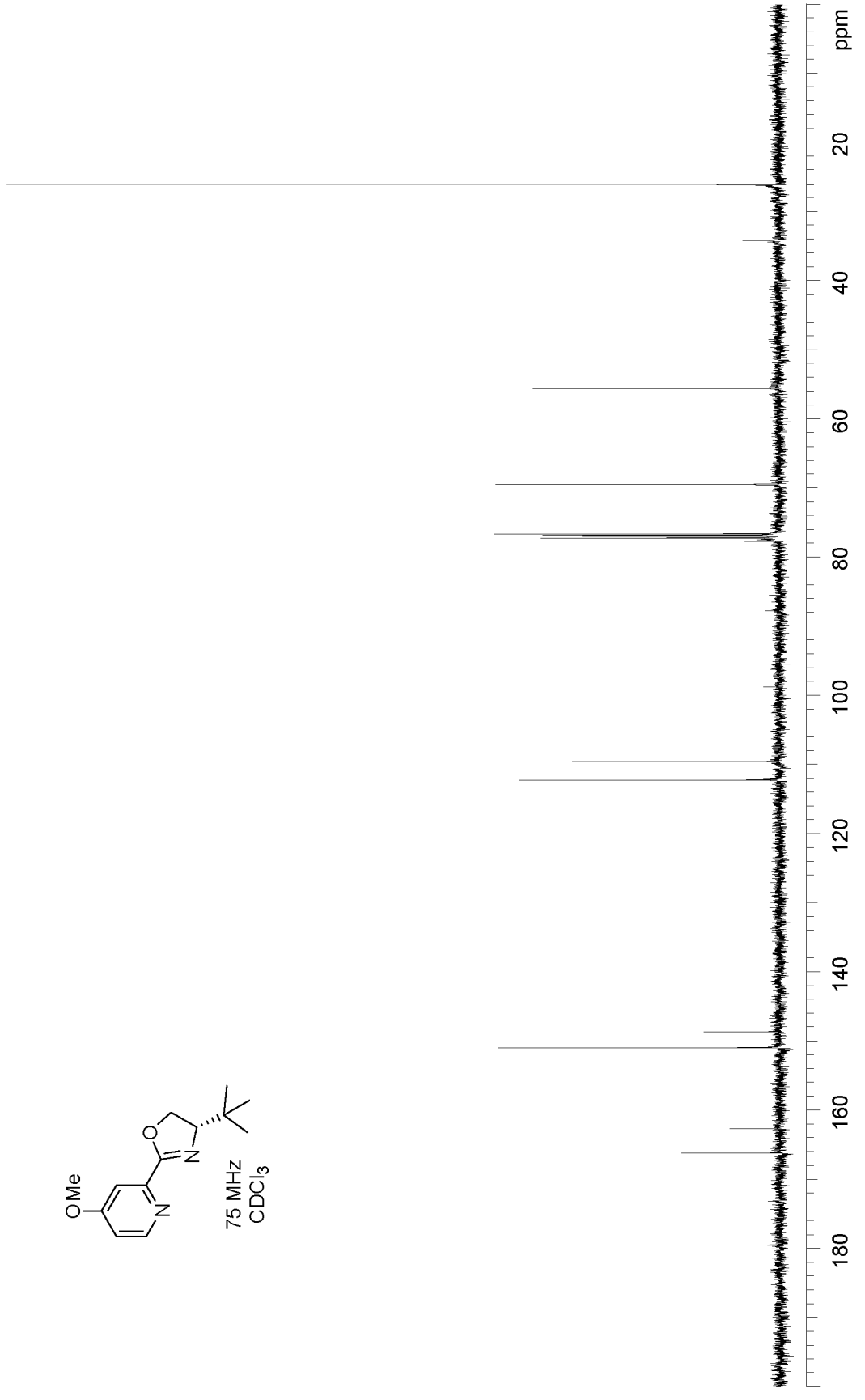
ppm
20
40
60
80
100
120
140
160
180
OMe
N
O
N
75 MHz
$CDCl_3$

APPENDIX B

X-RAY CRYSTAL STRUCTURE ANANLYSIS

X-Ray crystal structure data for dialkoxylation product 42 (Chapter 2)

Experimental

A colorless prism shaped crystal 0.35 x 0.33 x 0.20 mm in size was mounted on a glass fiber with traces of viscous oil and then transferred to a Nonius KappaCCD diffractometer equipped with Mo Kα radiation (λ= 0.71073 Å). Ten frames of data were collected at 105(1)K with an oscillation range of *1* deg/frame and an exposure time of 20 sec/frame. Indexing and unit cell refinement based on all observed reflection from those ten frames, indicated a hexagonal ***P*** lattice. A total of 3395 reflections (Θ_{max} = 27.45°) were indexed, integrated and corrected for Lorentz, polarization and absorption effects using DENZO-SMN and SCALEPAC. Postrefinement of the unit cell gave *a* = 16.7018(5) Å, b = 16.7018(5) Å, c = 9.6419(2) Å, and V = 2329.27(11) $Å^3$. Axial photographs and systematic absences were consistent with the compound having crystallized in the hexagonal space group $P6_2$. The structure was solved by a combination of direct methods and heavy atom using SIR 97. All of the nonhydrogen atoms were refined with anisotropic displacement coefficients. Hydrogen atoms were either located, refined isotropically or assigned isotropic displacement coefficients U(H) = 1.2U(C) or 1.5U(Cmethyl), and their coordinates were allowed to ride on their respective carbons using SHELXL97. The five-member ring carbon atoms (C10, C11)

exhibit orientation disorder 50:50. There are also disordered hexanes solvent molecules in the lattice. The weighting scheme employed was $w = 1/[\sigma^2(F_o^2) + (0.0992P)^2 + 1.0242P]$ where $P = (F_o^2 + 2F_c^2)/3$. The refinement converged to R1 = 0.0635, wR2 = 0.1640, and S = 1.036 for 2676 reflections with $1 > 2\sigma(I)$, and R1 = 0.0861, wR2 = 0.1819, and S = 1.036 for 3395 unique reflections and 257 parameters. The maximum Δ/σ in the final cycle of the least-squares was 0, and the residual peaks on the final difference-Fourier map ranged from -0.196 to 0.393 e/Å^3. Scattering factors were taken from the International Tables for Crystallography, Volume C. Data for crystal structure analysis are tabulated in Tables A1-A7.

Table A1. Crystal data and structure refinement for mss032.

Identification code	mss032
Empirical formula	C15.50 H23.50 O3
Formula weight	257.84
Temperature	105(1) K
Wavelength	0.71069 Å
Crystal system	Hexagonal
Space group	$P6_2$
Unit cell dimensions	a = 16.7018(5) Å 〈= 90°.
	b = 16.7018(5) Å ®= 90°.
	c = 9.6419(2) Å © = 120°.
Volume	2329.27(11) $Å^3$
Z	6
Density (calculated)	1.103 Mg/m^3
Absorption coefficient	0.075 mm^{-1}
F(000)	843
Crystal size	0.35 x 0.33 x 0.20 mm^3
Theta range for data collection	2.54 to 27.45°.
Index ranges	-21<=h<=21, -18<=k<=18, -10<=l<=12
Reflections collected	3395
Independent reflections	3395 [R(int) = 0.0000]
Completeness to theta = 27.45°	99.7 %
Absorption correction	Multi-scan
Max. and min. transmission	0.9852 and 0.9743
Refinement method	Full-matrix least-squares on F^2
Data / restraints / parameters	3395 / 4 / 257
Goodness-of-fit on F^2	1.029
Final R indices [I>2sigma(I)]	R1 = 0.0635, wR2 = 0.1640
R indices (all data)	R1 = 0.0861, wR2 = 0.1819
Absolute structure parameter	0.1(18)
Extinction coefficient	0.018(5)
Largest diff. peak and hole	0.393 and -0.196 $e.Å^{-3}$

Table A2. Atomic coordinates (x 10^4) and equivalent isotropic displacement parameters (Å^{2}x 10^3) for mss032. U(eq) is defined as one third of the trace of the orthogonalized U^{ij} tensor.

	x	y	z	U(eq)
O(1)	3818(2)	1488(1)	-421(3)	48(1)
O(2)	3603(2)	3777(2)	3(2)	45(1)
O(3)	3815(2)	3556(2)	2783(2)	42(1)
C(1)	4476(2)	2268(2)	-1069(3)	35(1)
C(2)	5068(2)	2238(2)	-2068(3)	37(1)
C(3)	5726(2)	3040(2)	-2714(3)	37(1)
C(4)	5794(2)	3883(2)	-2361(3)	37(1)
C(5)	5213(2)	3909(2)	-1359(3)	36(1)
C(6)	4550(2)	3112(2)	-700(3)	34(1)
C(7)	3929(2)	3162(2)	411(3)	35(1)
C(8)	4447(2)	3552(2)	1756(3)	35(1)
C(9)	4842(2)	2994(2)	2412(3)	43(1)
C(10)	4577(8)	2857(9)	3884(10)	57(3)
C(11)	3645(6)	2830(7)	3865(8)	47(2)
C(12)	2862(6)	1955(6)	3442(10)	66(3)
C(13)	3481(9)	3168(11)	5216(10)	69(3)
C(10')	4954(7)	3399(8)	3907(9)	53(2)
C(11')	4102(6)	3501(6)	4147(7)	47(2)
C(12')	4348(6)	4403(6)	4877(8)	69(2)
C(13')	3337(9)	2687(8)	4838(14)	72(3)
C(14)	2924(3)	3409(4)	-1044(5)	68(1)
C(15)	1666(4)	845(4)	2063(8)	53(2)
C(16)	1338(4)	743(5)	480(7)	51(2)
C(17)	1546(17)	434(14)	-1036(15)	49(5)
C(18)	1573(7)	951(6)	-2456(9)	43(2)

Table A3. Bond lengths [Å] for mss032.

O(1)-C(1)	1.365(4)
O(2)-C(14)	1.410(4)
O(2)-C(7)	1.436(3)
O(3)-C(11')	1.419(7)
O(3)-C(8)	1.450(3)
O(3)-C(11)	1.515(7)
C(1)-C(6)	1.398(4)
C(1)-C(2)	1.399(4)
C(2)-C(3)	1.385(4)
C(3)-C(4)	1.398(4)
C(4)-C(5)	1.385(4)
C(5)-C(6)	1.390(4)
C(6)-C(7)	1.522(4)
C(7)-C(8)	1.514(4)
C(8)-C(9)	1.522(4)
C(9)-C(10)	1.471(10)
C(9)-C(10')	1.563(9)
C(10)-C(11)	1.535(12)
C(11)-C(12)	1.449(14)
C(11)-C(13)	1.498(14)
C(10')-C(11')	1.533(10)
C(11')-C(13')	1.478(14)
C(11')-C(12')	1.522(11)
C(15)-C(16)	1.602(10)
C(16)-C(17)	1.645(15)
C(17)-C(18)	1.607(15)

Table A4. Bond angles [°] for mss032.

C(14)-O(2)-C(7)	113.3(3)
C(11')-O(3)-C(8)	111.2(3)
C(11')-O(3)-C(11)	40.8(4)
C(8)-O(3)-C(11)	108.2(3)
O(1)-C(1)-C(6)	117.9(2)
O(1)-C(1)-C(2)	121.8(2)
C(6)-C(1)-C(2)	120.3(3)
C(3)-C(2)-C(1)	120.5(3)
C(2)-C(3)-C(4)	119.4(3)
C(5)-C(4)-C(3)	119.8(3)
C(4)-C(5)-C(6)	121.6(3)
C(5)-C(6)-C(1)	118.4(3)
C(5)-C(6)-C(7)	120.5(2)
C(1)-C(6)-C(7)	121.1(2)
O(2)-C(7)-C(8)	105.5(2)
O(2)-C(7)-C(6)	111.1(2)
C(8)-C(7)-C(6)	111.6(2)
O(3)-C(8)-C(7)	109.0(2)
O(3)-C(8)-C(9)	105.0(2)
C(7)-C(8)-C(9)	115.0(2)
C(10)-C(9)-C(8)	107.9(5)
C(10)-C(9)-C(10')	30.5(4)
C(8)-C(9)-C(10')	96.5(4)
C(9)-C(10)-C(11)	102.4(7)
C(12)-C(11)-C(13)	112.5(9)
C(12)-C(11)-O(3)	109.0(6)
C(13)-C(11)-O(3)	107.1(8)
C(12)-C(11)-C(10)	115.0(8)
C(13)-C(11)-C(10)	110.7(8)
O(3)-C(11)-C(10)	101.7(6)
C(11')-C(10')-C(9)	105.7(6)

Table A4. (continued).

O(3)-C(11')-C(13')	108.2(8)
O(3)-C(11')-C(12')	107.3(5)
C(13')-C(11')-C(12')	112.5(8)
O(3)-C(11')-C(10')	103.3(5)
C(13')-C(11')-C(10')	112.9(7)
C(12')-C(11')-C(10')	111.9(7)
C(16)-C(15)-C(17)#1	86.0(6)
C(15)-C(16)-C(17)	140.0(9)
C(18)-C(17)-C(16)	122.8(12)
C(18)-C(17)-C(15)#2	109.9(11)
C(16)-C(17)-C(15)#2	110.7(10)

Table A5. Anisotropic displacement parameters ($Å^2 x\ 10^3$)for mss032. The anisotropic displacement factor exponent takes the form: $-2\pi^2[\ h^2 a^{*2} U^{11} + ... + 2\ h\ k\ a^*\ b^*\ U^{12}\ ]$

	U^{11}	U^{22}	U^{33}	U^{23}	U^{13}	U^{12}
O(1)	52(1)	30(1)	56(1)	2(1)	17(1)	17(1)
O(2)	52(1)	59(1)	40(1)	-5(1)	-5(1)	41(1)
O(3)	50(1)	56(1)	32(1)	3(1)	7(1)	37(1)
C(1)	37(2)	33(1)	35(2)	-2(1)	1(1)	17(1)
C(2)	44(2)	34(2)	35(2)	-4(1)	1(1)	21(1)
C(3)	39(2)	45(2)	31(1)	-4(1)	0(1)	23(1)
C(4)	41(2)	40(2)	30(1)	4(1)	0(1)	22(1)
C(5)	43(2)	33(1)	37(2)	-1(1)	-2(1)	24(1)
C(6)	36(1)	38(2)	33(2)	-1(1)	-2(1)	22(1)
C(7)	38(2)	36(2)	37(2)	0(1)	1(1)	24(1)
C(8)	37(2)	40(2)	36(1)	4(1)	6(1)	26(1)
C(9)	46(2)	51(2)	42(2)	7(1)	2(1)	30(2)
C(10)	64(6)	85(7)	43(4)	22(6)	18(4)	51(6)
C(11)	60(5)	61(6)	34(4)	21(4)	16(3)	41(4)
C(12)	67(5)	55(5)	63(5)	28(4)	14(4)	22(4)
C(13)	77(7)	107(10)	32(5)	17(5)	13(4)	53(8)
C(10')	67(6)	85(6)	35(3)	0(4)	-1(4)	58(5)
C(11')	67(4)	59(5)	37(3)	10(3)	6(3)	48(4)
C(12')	97(6)	85(6)	50(4)	-22(4)	-20(4)	66(5)
C(13')	88(7)	75(7)	75(8)	22(6)	11(6)	57(7)
C(14)	66(2)	101(3)	64(2)	-20(2)	-19(2)	61(2)
C(15)	42(3)	23(3)	91(5)	-5(3)	27(3)	15(2)
C(16)	34(3)	42(3)	62(4)	-23(3)	8(3)	8(3)
C(18)	56(5)	36(4)	39(5)	-13(3)	8(4)	23(4)

Table A6. Hydrogen coordinates (x 10^4) and isotropic displacement parameters (Å^{2}x 10^3) for mss032.

	x	y	z	U(eq)
H(10A)	5036	3375	4459	69
H(10B)	4509	2269	4237	69
H(12A)	2979	1791	2518	98
H(12B)	2305	2010	3415	98
H(12C)	2774	1474	4106	98
H(13A)	4031	3754	5466	103
H(13B)	3355	2709	5941	103
H(13C)	2949	3262	5125	103
H(10C)	4979	2975	4600	64
H(10D)	5527	4006	3978	64
H(12D)	4835	4923	4356	103
H(12E)	4568	4397	5816	103
H(12F)	3799	4472	4927	103
H(13D)	3202	2126	4329	108
H(13E)	2785	2751	4853	108
H(13F)	3517	2645	5791	108
H(14A)	2729	3858	-1276	103
H(14B)	2389	2836	-712	103
H(14C)	3180	3278	-1871	103
H(15A)	2345	1188	2191	63
H(15B)	1373	258	2592	63
H(16A)	1432	1366	280	61
H(16B)	660	341	564	61
H(17A)	2191	546	-943	59
H(18A)	1719	665	-3230	65
H(18B)	2048	1605	-2390	65
H(18C)	969	898	-2615	65

Table A6. (continued).

	x	y	z	U(eq)
H(1)	3870(30)	940(30)	-840(60)	83(15)
H(2)	5040(30)	1680(30)	-2330(50)	55(10)
H(3)	6140(20)	2990(20)	-3360(40)	33(8)
H(4)	6260(30)	4450(30)	-2920(50)	70(12)
H(5)	5230(20)	4460(20)	-1130(30)	30(7)
H(7)	3380(20)	2540(20)	670(40)	41(9)
H(8)	4990(20)	4260(20)	1540(30)	30(7)
H(9A)	5470(20)	3110(20)	1950(30)	36
H(9B)	4360(20)	2290(20)	2220(40)	36

Table A7. Torsion angles [°] for mss032.

O(1)-C(1)-C(2)-C(3)	179.7(3)
C(6)-C(1)-C(2)-C(3)	-0.7(4)
C(1)-C(2)-C(3)-C(4)	-0.2(4)
C(2)-C(3)-C(4)-C(5)	0.9(4)
C(3)-C(4)-C(5)-C(6)	-0.8(4)
C(4)-C(5)-C(6)-C(1)	0.0(4)
C(4)-C(5)-C(6)-C(7)	179.2(3)
O(1)-C(1)-C(6)-C(5)	-179.6(3)
C(2)-C(1)-C(6)-C(5)	0.7(4)
O(1)-C(1)-C(6)-C(7)	1.2(4)
C(2)-C(1)-C(6)-C(7)	-178.5(3)
C(14)-O(2)-C(7)-C(8)	-165.8(3)
C(14)-O(2)-C(7)-C(6)	73.2(3)
C(5)-C(6)-C(7)-O(2)	43.1(3)
C(1)-C(6)-C(7)-O(2)	-137.7(3)
C(5)-C(6)-C(7)-C(8)	-74.3(3)
C(1)-C(6)-C(7)-C(8)	104.9(3)
C(11')-O(3)-C(8)-C(7)	153.3(4)
C(11)-O(3)-C(8)-C(7)	109.9(5)
C(11')-O(3)-C(8)-C(9)	29.7(5)
C(11)-O(3)-C(8)-C(9)	-13.7(5)
O(2)-C(7)-C(8)-O(3)	61.1(3)
C(6)-C(7)-C(8)-O(3)	-178.2(2)
O(2)-C(7)-C(8)-C(9)	178.6(2)
C(6)-C(7)-C(8)-C(9)	-60.7(3)
O(3)-C(8)-C(9)-C(10)	-11.4(6)
C(7)-C(8)-C(9)-C(10)	-131.1(6)
O(3)-C(8)-C(9)-C(10')	-40.4(5)
C(7)-C(8)-C(9)-C(10')	-160.1(5)
C(8)-C(9)-C(10)-C(11)	31.0(9)

Table A7. (continued).

C(10')-C(9)-C(10)-C(11)	102.6(13)
C(11')-O(3)-C(11)-C(12)	168.7(9)
C(8)-O(3)-C(11)-C(12)	-89.6(6)
C(11')-O(3)-C(11)-C(13)	46.8(8)
C(8)-O(3)-C(11)-C(13)	148.5(7)
C(11')-O(3)-C(11)-C(10)	-69.3(8)
C(8)-O(3)-C(11)-C(10)	32.4(7)
C(9)-C(10)-C(11)-C(12)	79.8(9)
C(9)-C(10)-C(11)-C(13)	-151.4(10)
C(9)-C(10)-C(11)-O(3)	-37.9(9)
C(10)-C(9)-C(10')-C(11')	-75.9(12)
C(8)-C(9)-C(10')-C(11')	38.7(7)
C(8)-O(3)-C(11')-C(13')	-123.3(6)
C(11)-O(3)-C(11')-C(13')	-29.8(7)
C(8)-O(3)-C(11')-C(12')	115.0(5)
C(11)-O(3)-C(11')-C(12')	-151.4(9)
C(8)-O(3)-C(11')-C(10')	-3.4(7)
C(11)-O(3)-C(11')-C(10')	90.2(7)
C(9)-C(10')-C(11')-O(3)	-23.3(8)
C(9)-C(10')-C(11')-C(13')	93.3(10)
C(9)-C(10')-C(11')-C(12')	-138.4(7)
C(17)#1-C(15)-C(16)-C(17)	164.1(17)
C(15)-C(16)-C(17)-C(18)	-141.6(12)
C(15)-C(16)-C(17)-C(15)#2	85.8(17)

Symmetry transformations used to generate equivalent atoms:

#1 x-y,x,z+1/3 #2 y,-x+y,z-1/3

X-Ray crystal structure data for 10 (Chapter 3)

Experimental

A colorless prism shaped crystal 0.33 x 0.33 x 0.30 mm in size was mounted on a glass fiber with traces of viscous oil and then transferred to a Nonius KappaCCD diffractometer equipped with Mo Kα radiation (λ = 0.71073 Å). Ten frames of data were collected at 150(1) K with an oscillation range of *1* deg/frame and an exposure time of 20 sec/frame. Indexing and unit cell refinement based on all observed reflection from those ten frames, indicated a monoclinic ***C*** lattice. A total of 11462 reflections (Θ_{max} = 27.5°) were indexed, integrated and corrected for Lorentz, polarization and absorption effects using DENZO-SMN and SCALEPAC. Postrefinement of the unit cell gave *a* = 21.3641(6) Å, b = 10.9638(4) Å, c = 23.4509(5) Å, β =90.8210(17), and V = 5492.4(3) Å^3. Axial photographs and systematic absences were consistent with the compound having crystallized in the monoclinic space group ***C*** 2/*c*. The structure was solved by a combination of direct methods and heavy atom using SIR 97. All of the nonhydrogen atoms were refined with anisotropic displacement coefficients. Hydrogen atoms were located and refined isotropically using SHELXL97. The weighting scheme employed was $w = 1/[\sigma^2(F_o^2) + (0.0576P)^2 + 1.7804P]$ where $P = (F_o^2 + 2F_c^2)/3$. The refinement converged to R1 = 0.0473, wR2 = 0.1037, and S = 1.0150 for 4096 reflections with 1> 2σ(I), and R1 = 0.0902, wR2 = 0.1225, and S = 1.0150 for 6287 unique reflections and 503 parameters. The maximum Δ/σ in the final cycle of the least-squares was 0, and the residual peaks on the final difference-Fourier map ranged from -0.234 to 0.187 e/Å^3. Scattering factors were taken from the International Tables for Crystallography, Volume C. Data for crystal structure analysis are tabulated in Tables A8-A13.

Table A8. Crystal data and structure refinement for mss034.

Identification code	mss034
Empirical formula	C16 H20 O3
Formula weight	260.32
Temperature	150(1) K
Wavelength	0.71073 Å
Crystal system	Monoclinic
Space group	*C* 2/*c*
Unit cell dimensions	a = 21.3641(6) Å α= 90°.
	b = 10.9638(4) Å β= 90.8210(17)°.
	c = 23.4509(5) Å γ = 90°.
Volume	5492.4(3) $Å^3$
Z	16
Density (calculated)	1.259 Mg/m^3
Absorption coefficient	0.086 mm^{-1}
F(000)	2240
Crystal size	0.33 x 0.33 x 0.30 mm^3
Theta range for data collection	1.91 to 27.50°.
Index ranges	-27<=h<=27, -14<=k<=14, -30<=l<=30
Reflections collected	11462
Independent reflections	6287 [R(int) = 0.0366]
Completeness to theta = 27.50°	99.3 %
Absorption correction	Multi-scan
Max. and min. transmission	0.9748 and 0.9723
Refinement method	Full-matrix least-squares on F^2
Data / restraints / parameters	6287 / 0 / 503
Goodness-of-fit on F^2	1.015
Final R indices [I>2sigma(I)]	R1 = 0.0473, wR2 = 0.1037
R indices (all data)	R1 = 0.0902, wR2 = 0.1225
Largest diff. peak and hole	0.187 and -0.234 $e.Å^{-3}$

Table A9. Atomic coordinates (x 10^4) and equivalent isotropic displacement parameters (Å^{2}x 10^3) for mss034. U(eq) is defined as one third of the trace of the orthogonalized U^{ij} tensor.

	x	y	z	U(eq)
C(2)	152(1)	1308(2)	1829(1)	26(1)
C(2A)	2639(1)	-1115(2)	1928(1)	26(1)
C(3)	711(1)	477(2)	1798(1)	25(1)
C(3A)	3172(1)	-1996(1)	1875(1)	23(1)
C(4)	1168(1)	931(1)	1342(1)	22(1)
C(4A)	3629(1)	-1579(1)	1408(1)	22(1)
C(5)	1331(1)	2231(1)	1486(1)	23(1)
C(5A)	3825(1)	-295(1)	1546(1)	22(1)
C(6)	1918(1)	2740(2)	1398(1)	28(1)
C(6A)	4416(1)	174(2)	1430(1)	27(1)
C(7)	2041(1)	3947(2)	1543(1)	31(1)
C(7A)	4574(1)	1361(2)	1584(1)	33(1)
C(8)	1577(1)	4660(2)	1781(1)	31(1)
C(8A)	4143(1)	2099(2)	1854(1)	34(1)
C(9)	990(1)	4170(2)	1879(1)	29(1)
C(9A)	3550(1)	1658(2)	1970(1)	30(1)
C(10)	879(1)	2966(1)	1731(1)	24(1)
C(10A)	3403(1)	476(1)	1813(1)	24(1)
C(11)	917(1)	779(2)	726(1)	22(1)
C(11A)	3370(1)	-1719(1)	796(1)	23(1)
C(12)	463(1)	1726(2)	491(1)	26(1)
C(12A)	2936(1)	-737(2)	562(1)	26(1)
C(13)	552(1)	1581(2)	-151(1)	28(1)
C(13A)	3027(1)	-873(2)	-81(1)	29(1)
C(14)	1242(1)	1212(1)	-211(1)	24(1)
C(14A)	3709(1)	-1287(1)	-138(1)	25(1)
C(15)	1660(1)	2265(2)	-376(1)	35(1)

Table A9. (continued)

	x	y	z	U(eq)
C(15A)	4150(1)	-258(2)	-291(1)	37(1)
C(16)	1322(1)	143(2)	-614(1)	36(1)
C(16A)	3776(1)	-2345(2)	-552(1)	38(1)
C(17)	517(1)	-853(2)	1742(1)	32(1)
C(17A)	2948(1)	-3307(2)	1823(1)	32(1)
O(1)	269(1)	2537(1)	1818(1)	28(1)
O(1A)	2787(1)	101(1)	1918(1)	27(1)
O(2)	-385(1)	995(1)	1871(1)	34(1)
O(2A)	2096(1)	-1373(1)	1991(1)	38(1)
O(3)	1444(1)	844(1)	358(1)	28(1)
O(3A)	3899(1)	-1701(1)	427(1)	29(1)

Table A10. Bond lengths [Å] and angles [°] for mss034.

C(2)-O(2)	1.2016(18)
C(2)-O(1)	1.371(2)
C(2)-C(3)	1.506(2)
C(2A)-O(2A)	1.2032(18)
C(2A)-O(1A)	1.3705(19)
C(2A)-C(3A)	1.501(2)
C(3)-C(17)	1.521(2)
C(3)-C(4)	1.5406(19)
C(3)-H(3)	0.993(15)
C(3A)-C(17A)	1.520(2)
C(3A)-C(4A)	1.547(2)
C(3A)-H(3A)	1.007(16)
C(4)-C(5)	1.504(2)
C(4)-C(11)	1.541(2)
C(4)-H(4)	1.003(16)
C(4A)-C(5A)	1.502(2)
C(4A)-C(11A)	1.538(2)
C(4A)-H(4A)	0.985(15)
C(5)-C(10)	1.388(2)
C(5)-C(6)	1.392(2)
C(5A)-C(10A)	1.392(2)
C(5A)-C(6A)	1.394(2)
C(6)-C(7)	1.390(2)
C(6)-H(6)	0.991(17)
C(6A)-C(7A)	1.391(2)
C(6A)-H(6A)	1.013(17)
C(7)-C(8)	1.387(2)
C(7)-H(7)	0.978(17)
C(7A)-C(8A)	1.386(2)
C(7A)-H(7A)	0.981(18)
C(8)-C(9)	1.385(2)
C(8)-H(8)	0.992(19)

Table A10. (continued).

C(8A)-C(9A)	1.386(2)
C(8A)-H(8A)	1.002(19)
C(9)-C(10)	1.385(2)
C(9)-H(9)	0.983(17)
C(9A)-C(10A)	1.383(2)
C(9A)-H(9A)	0.953(17)
C(10)-O(1)	1.4020(18)
C(10A)-O(1A)	1.4046(18)
C(11)-O(3)	1.4304(16)
C(11)-C(12)	1.519(2)
C(11)-H(11)	1.041(16)
C(11A)-O(3A)	1.4323(17)
C(11A)-C(12A)	1.519(2)
C(11A)-H(11A)	1.029(16)
C(12)-C(13)	1.527(2)
C(12)-H(12A)	1.032(18)
C(12)-H(12B)	0.968(17)
C(12A)-C(13A)	1.529(2)
C(12A)-H(12C)	1.008(17)
C(12A)-H(12D)	0.984(16)
C(13)-C(14)	1.538(2)
C(13)-H(13A)	0.994(18)
C(13)-H(13B)	1.003(17)
C(13A)-C(14A)	1.533(2)
C(13A)-H(13C)	0.987(19)
C(13A)-H(13D)	1.004(18)
C(14)-O(3)	1.4535(17)
C(14)-C(15)	1.513(2)
C(14)-C(16)	1.518(2)
C(14A)-O(3A)	1.4516(17)

Table A10. (continued).

C(14A)-C(15A)	1.516(2)
C(14A)-C(16A)	1.521(2)
C(15)-H(15A)	1.00(2)
C(15)-H(15B)	0.992(19)
C(15)-H(15C)	0.99(2)
C(15A)-H(15D)	1.01(2)
C(15A)-H(15E)	0.99(2)
C(15A)-H(15F)	1.01(2)
C(16)-H(16A)	1.02(2)
C(16)-H(16B)	1.00(2)
C(16)-H(16C)	1.022(19)
C(16A)-H(16D)	1.00(2)
C(16A)-H(16E)	1.042(19)
C(16A)-H(16F)	0.99(2)
C(17)-H(17A)	1.006(18)
C(17)-H(17B)	0.972(17)
C(17)-H(17C)	1.021(19)
C(17A)-H(17D)	0.990(18)
C(17A)-H(17E)	1.013(17)
C(17A)-H(17F)	1.037(19)
O(2)-C(2)-O(1)	117.23(14)
O(2)-C(2)-C(3)	126.16(15)
O(1)-C(2)-C(3)	116.60(13)
O(2A)-C(2A)-O(1A)	116.97(14)
O(2A)-C(2A)-C(3A)	126.36(15)
O(1A)-C(2A)-C(3A)	116.65(13)
C(2)-C(3)-C(17)	111.66(14)
C(2)-C(3)-C(4)	110.46(12)
C(17)-C(3)-C(4)	115.18(13)
C(2)-C(3)-H(3)	105.2(9)
C(17)-C(3)-H(3)	107.9(9)

Table A10. (continued).

C(4)-C(3)-H(3)	105.7(8)
C(2A)-C(3A)-C(17A)	112.15(14)
C(2A)-C(3A)-C(4A)	110.90(12)
C(17A)-C(3A)-C(4A)	115.13(13)
C(2A)-C(3A)-H(3A)	105.3(9)
C(17A)-C(3A)-H(3A)	107.8(9)
C(4A)-C(3A)-H(3A)	104.8(9)
C(5)-C(4)-C(3)	107.28(12)
C(5)-C(4)-C(11)	112.93(12)
C(3)-C(4)-C(11)	113.55(12)
C(5)-C(4)-H(4)	110.4(9)
C(3)-C(4)-H(4)	106.6(8)
C(11)-C(4)-H(4)	105.9(9)
C(5A)-C(4A)-C(11A)	112.98(12)
C(5A)-C(4A)-C(3A)	107.53(12)
C(11A)-C(4A)-C(3A)	114.12(12)
C(5A)-C(4A)-H(4A)	108.0(9)
C(11A)-C(4A)-H(4A)	106.7(8)
C(3A)-C(4A)-H(4A)	107.3(8)
C(10)-C(5)-C(6)	117.54(15)
C(10)-C(5)-C(4)	118.88(13)
C(6)-C(5)-C(4)	123.57(14)
C(10A)-C(5A)-C(6A)	117.30(15)
C(10A)-C(5A)-C(4A)	119.06(13)
C(6A)-C(5A)-C(4A)	123.64(14)
C(7)-C(6)-C(5)	120.91(16)
C(7)-C(6)-H(6)	119.9(10)
C(5)-C(6)-H(6)	119.2(10)
C(7A)-C(6A)-C(5A)	120.81(16)
C(7A)-C(6A)-H(6A)	121.0(10)
C(5A)-C(6A)-H(6A)	118.1(10)

Table A10. (continued).

C(8)-C(7)-C(6)	120.06(16)
C(8)-C(7)-H(7)	119.5(10)
C(6)-C(7)-H(7)	120.5(10)
C(8A)-C(7A)-C(6A)	120.25(16)
C(8A)-C(7A)-H(7A)	121.7(11)
C(6A)-C(7A)-H(7A)	118.0(11)
C(9)-C(8)-C(7)	120.13(16)
C(9)-C(8)-H(8)	119.6(10)
C(7)-C(8)-H(8)	120.2(10)
C(7A)-C(8A)-C(9A)	120.13(16)
C(7A)-C(8A)-H(8A)	118.6(10)
C(9A)-C(8A)-H(8A)	121.2(10)
C(10)-C(9)-C(8)	118.75(16)
C(10)-C(9)-H(9)	118.3(10)
C(8)-C(9)-H(9)	122.9(10)
C(10A)-C(9A)-C(8A)	118.62(16)
C(10A)-C(9A)-H(9A)	118.9(10)
C(8A)-C(9A)-H(9A)	122.5(10)
C(9)-C(10)-C(5)	122.61(15)
C(9)-C(10)-O(1)	116.10(14)
C(5)-C(10)-O(1)	121.22(14)
C(9A)-C(10A)-C(5A)	122.89(15)
C(9A)-C(10A)-O(1A)	115.99(14)
C(5A)-C(10A)-O(1A)	121.08(14)
O(3)-C(11)-C(12)	104.46(12)
O(3)-C(11)-C(4)	107.07(12)
C(12)-C(11)-C(4)	118.57(13)
O(3)-C(11)-H(11)	107.4(8)
C(12)-C(11)-H(11)	108.5(9)
C(4)-C(11)-H(11)	110.2(8)
O(3A)-C(11A)-C(12A)	104.71(12)

Table A10. (continued).

O(3A)-C(11A)-C(4A)	106.65(12)
C(12A)-C(11A)-C(4A)	118.44(13)
O(3A)-C(11A)-H(11A)	107.7(8)
C(12A)-C(11A)-H(11A)	108.8(9)
C(4A)-C(11A)-H(11A)	109.9(8)
C(11)-C(12)-C(13)	101.56(12)
C(11)-C(12)-H(12A)	111.5(9)
C(13)-C(12)-H(12A)	109.5(9)
C(11)-C(12)-H(12B)	113.3(10)
C(13)-C(12)-H(12B)	112.5(10)
H(12A)-C(12)-H(12B)	108.3(14)
C(11A)-C(12A)-C(13A)	101.62(13)
C(11A)-C(12A)-H(12C)	109.5(9)
C(13A)-C(12A)-H(12C)	110.4(9)
C(11A)-C(12A)-H(12D)	112.6(10)
C(13A)-C(12A)-H(12D)	113.7(9)
H(12C)-C(12A)-H(12D)	108.8(14)
C(12)-C(13)-C(14)	104.45(12)
C(12)-C(13)-H(13A)	113.1(10)
C(14)-C(13)-H(13A)	113.1(10)
C(12)-C(13)-H(13B)	110.2(9)
C(14)-C(13)-H(13B)	109.3(9)
H(13A)-C(13)-H(13B)	106.7(13)
C(12A)-C(13A)-C(14A)	104.45(12)
C(12A)-C(13A)-H(13C)	111.8(11)
C(14A)-C(13A)-H(13C)	113.5(10)
C(12A)-C(13A)-H(13D)	109.4(10)
C(14A)-C(13A)-H(13D)	110.4(10)
H(13C)-C(13A)-H(13D)	107.3(14)
O(3)-C(14)-C(15)	106.18(13)
O(3)-C(14)-C(16)	108.84(13)

Table A10. (continued).

C(15)-C(14)-C(16)	110.93(14)
O(3)-C(14)-C(13)	105.17(11)
C(15)-C(14)-C(13)	113.16(14)
C(16)-C(14)-C(13)	112.13(13)
O(3A)-C(14A)-C(15A)	106.42(13)
O(3A)-C(14A)-C(16A)	108.46(13)
C(15A)-C(14A)-C(16A)	110.55(14)
O(3A)-C(14A)-C(13A)	105.43(11)
C(15A)-C(14A)-C(13A)	113.25(15)
C(16A)-C(14A)-C(13A)	112.33(14)
C(14)-C(15)-H(15A)	110.4(11)
C(14)-C(15)-H(15B)	110.4(11)
H(15A)-C(15)-H(15B)	106.8(15)
C(14)-C(15)-H(15C)	108.6(11)
H(15A)-C(15)-H(15C)	110.7(16)
H(15B)-C(15)-H(15C)	109.9(15)
C(14A)-C(15A)-H(15D)	111.9(11)
C(14A)-C(15A)-H(15E)	108.7(12)
H(15D)-C(15A)-H(15E)	108.1(15)
C(14A)-C(15A)-H(15F)	111.5(11)
H(15D)-C(15A)-H(15F)	108.6(16)
H(15E)-C(15A)-H(15F)	107.9(15)
C(14)-C(16)-H(16A)	110.0(12)
C(14)-C(16)-H(16B)	110.5(11)
H(16A)-C(16)-H(16B)	107.0(16)
C(14)-C(16)-H(16C)	109.1(10)
H(16A)-C(16)-H(16C)	110.5(15)
H(16B)-C(16)-H(16C)	109.7(15)
C(14A)-C(16A)-H(16D)	110.5(11)
C(14A)-C(16A)-H(16E)	109.7(10)
H(16D)-C(16A)-H(16E)	110.6(15)

Table A10. (continued).

C(14A)-C(16A)-H(16F)	111.0(12)
H(16D)-C(16A)-H(16F)	108.2(16)
H(16E)-C(16A)-H(16F)	106.9(15)
C(3)-C(17)-H(17A)	108.7(10)
C(3)-C(17)-H(17B)	111.9(10)
H(17A)-C(17)-H(17B)	106.7(14)
C(3)-C(17)-H(17C)	110.0(11)
H(17A)-C(17)-H(17C)	110.5(14)
H(17B)-C(17)-H(17C)	109.1(14)
C(3A)-C(17A)-H(17D)	110.7(11)
C(3A)-C(17A)-H(17E)	110.7(10)
H(17D)-C(17A)-H(17E)	108.5(14)
C(3A)-C(17A)-H(17F)	109.4(10)
H(17D)-C(17A)-H(17F)	107.4(14)
H(17E)-C(17A)-H(17F)	110.1(14)
C(2)-O(1)-C(10)	120.22(12)
C(2A)-O(1A)-C(10A)	120.36(12)
C(11)-O(3)-C(14)	110.01(11)
C(11A)-O(3A)-C(14A)	110.10(11)

Table A11. Anisotropic displacement parameters ($Å^2 x\ 10^3$)for mss034.
The anisotropic displacement factor exponent takes the form:
$-2\pi^2[\ h^2 a^{*2} U^{11} + ... + 2\ h\ k\ a^*\ b^*\ U^{12}\ ]$

	U^{11}	U^{22}	U^{33}	U^{23}	U^{13}	U^{12}
C(2)	25(1)	36(1)	18(1)	3(1)	1(1)	-3(1)
C(2A)	27(1)	29(1)	23(1)	3(1)	1(1)	-3(1)
C(3)	24(1)	30(1)	20(1)	3(1)	1(1)	-2(1)
C(3A)	26(1)	22(1)	23(1)	2(1)	-1(1)	-2(1)
C(4)	20(1)	24(1)	21(1)	2(1)	1(1)	-1(1)
C(4A)	21(1)	21(1)	23(1)	2(1)	0(1)	0(1)
C(5)	24(1)	26(1)	18(1)	1(1)	-2(1)	-2(1)
C(5A)	23(1)	23(1)	20(1)	1(1)	-2(1)	-1(1)
C(6)	27(1)	34(1)	23(1)	3(1)	0(1)	-4(1)
C(6A)	25(1)	29(1)	28(1)	1(1)	-2(1)	-2(1)
C(7)	32(1)	34(1)	27(1)	2(1)	-3(1)	-12(1)
C(7A)	29(1)	34(1)	35(1)	2(1)	-4(1)	-10(1)
C(8)	41(1)	26(1)	25(1)	1(1)	-7(1)	-6(1)
C(8A)	42(1)	26(1)	34(1)	-1(1)	-5(1)	-9(1)
C(9)	36(1)	28(1)	22(1)	-2(1)	-5(1)	3(1)
C(9A)	40(1)	25(1)	25(1)	-2(1)	0(1)	2(1)
C(10)	23(1)	29(1)	20(1)	3(1)	-3(1)	-2(1)
C(10A)	24(1)	27(1)	21(1)	3(1)	-1(1)	-2(1)
C(11)	21(1)	25(1)	21(1)	0(1)	2(1)	-2(1)
C(11A)	23(1)	22(1)	24(1)	-1(1)	1(1)	-3(1)
C(12)	22(1)	32(1)	24(1)	0(1)	-1(1)	1(1)
C(12A)	23(1)	31(1)	26(1)	-1(1)	-3(1)	0(1)
C(13)	27(1)	33(1)	24(1)	1(1)	-4(1)	-1(1)
C(13A)	31(1)	31(1)	25(1)	1(1)	-5(1)	0(1)
C(14)	28(1)	26(1)	18(1)	1(1)	-1(1)	-2(1)
C(14A)	28(1)	29(1)	20(1)	0(1)	-3(1)	-1(1)
C(15)	35(1)	36(1)	34(1)	6(1)	1(1)	-6(1)

Table A11. (continued).

	U^{11}	U^{22}	U^{33}	U^{23}	U^{13}	U^{12}
C(15A)	35(1)	38(1)	37(1)	5(1)	-1(1)	-8(1)
C(16)	38(1)	38(1)	34(1)	-9(1)	-3(1)	5(1)
C(16A)	44(1)	39(1)	32(1)	-9(1)	-3(1)	2(1)
C(17)	34(1)	31(1)	30(1)	4(1)	2(1)	-7(1)
C(17A)	36(1)	25(1)	34(1)	2(1)	3(1)	-7(1)
O(1)	23(1)	31(1)	30(1)	-1(1)	2(1)	2(1)
O(1A)	26(1)	25(1)	31(1)	1(1)	4(1)	0(1)
O(2)	23(1)	48(1)	32(1)	6(1)	2(1)	-4(1)
O(2A)	25(1)	40(1)	49(1)	9(1)	4(1)	-3(1)
O(3)	24(1)	41(1)	20(1)	4(1)	2(1)	5(1)
O(3A)	26(1)	40(1)	21(1)	3(1)	2(1)	7(1)

Table A12. Hydrogen coordinates (x 10^4) and isotropic displacement parameters (Å^{2}x 10^3) for mss034.

	x	y	z	U(eq)
H(3)	935(7)	577(14)	2169(6)	21(4)
H(3A)	3418(7)	-1921(15)	2242(7)	28(4)
H(4)	1549(7)	401(15)	1371(6)	25(4)
H(4A)	4002(7)	-2103(14)	1437(6)	18(4)
H(6)	2247(8)	2239(16)	1218(7)	36(5)
H(6A)	4732(8)	-385(16)	1246(7)	32(4)
H(7)	2456(8)	4297(15)	1482(6)	29(4)
H(7A)	5001(8)	1641(17)	1508(7)	39(5)
H(8)	1659(8)	5529(17)	1873(7)	39(5)
H(8A)	4267(8)	2955(18)	1954(7)	45(5)
H(9)	650(8)	4636(16)	2055(7)	33(5)
H(9A)	3242(8)	2138(16)	2156(7)	33(5)
H(11)	717(7)	-80(15)	674(6)	25(4)
H(11A)	3155(7)	-2553(15)	751(6)	24(4)
H(12A)	591(8)	2597(16)	613(7)	33(4)
H(12B)	35(8)	1590(16)	603(7)	33(5)
H(12C)	3085(8)	88(16)	695(7)	31(4)
H(12D)	2500(8)	-851(16)	681(7)	34(5)
H(13A)	441(8)	2328(17)	-370(7)	36(5)
H(13B)	277(7)	909(15)	-302(7)	30(4)
H(13C)	2932(8)	-109(18)	-286(8)	44(5)
H(13D)	2735(8)	-1515(16)	-233(7)	39(5)
H(15A)	1620(8)	2947(18)	-97(8)	46(5)
H(15B)	2105(9)	2008(17)	-367(7)	44(5)
H(15C)	1540(8)	2536(18)	-764(8)	49(5)
H(15D)	4132(8)	432(19)	-7(8)	51(6)
H(15E)	4584(10)	-579(18)	-291(8)	50(6)
H(15F)	4053(9)	77(19)	-683(9)	59(6)

Table A12. (continued).

	x	y	z	U(eq)
H(16A)	1157(9)	369(19)	-1012(9)	60(6)
H(16B)	1073(9)	-570(20)	-484(8)	55(6)
H(16C)	1785(9)	-85(17)	-629(8)	44(5)
H(16D)	3512(9)	-3051(19)	-431(8)	54(6)
H(16E)	4245(9)	-2600(17)	-574(7)	45(5)
H(16F)	3643(9)	-2102(18)	-944(9)	55(6)
H(17A)	283(8)	-1094(16)	2094(8)	46(5)
H(17B)	235(8)	-984(15)	1420(7)	31(5)
H(17C)	904(9)	-1389(17)	1696(8)	48(5)
H(17D)	2740(8)	-3570(17)	2177(8)	44(5)
H(17E)	2641(8)	-3397(16)	1493(7)	35(5)
H(17F)	3330(9)	-3876(17)	1765(8)	45(5)

Table A13. Torsion angles [°] for mss034.

O(2)-C(2)-C(3)-C(17)	7.9(2)
O(1)-C(2)-C(3)-C(17)	-173.22(12)
O(2)-C(2)-C(3)-C(4)	137.43(15)
O(1)-C(2)-C(3)-C(4)	-43.67(17)
O(2A)-C(2A)-C(3A)-C(17A)	8.1(2)
O(1A)-C(2A)-C(3A)-C(17A)	-173.45(13)
O(2A)-C(2A)-C(3A)-C(4A)	138.41(16)
O(1A)-C(2A)-C(3A)-C(4A)	-43.19(17)
C(2)-C(3)-C(4)-C(5)	55.48(16)
C(17)-C(3)-C(4)-C(5)	-176.89(13)
C(2)-C(3)-C(4)-C(11)	-70.01(17)
C(17)-C(3)-C(4)-C(11)	57.62(18)
C(2A)-C(3A)-C(4A)-C(5A)	54.41(16)
C(17A)-C(3A)-C(4A)-C(5A)	-176.91(13)
C(2A)-C(3A)-C(4A)-C(11A)	-71.74(16)
C(17A)-C(3A)-C(4A)-C(11A)	56.93(18)
C(3)-C(4)-C(5)-C(10)	-33.88(17)
C(11)-C(4)-C(5)-C(10)	91.99(15)
C(3)-C(4)-C(5)-C(6)	144.80(14)
C(11)-C(4)-C(5)-C(6)	-89.33(17)
C(11A)-C(4A)-C(5A)-C(10A)	94.51(16)
C(3A)-C(4A)-C(5A)-C(10A)	-32.32(18)
C(11A)-C(4A)-C(5A)-C(6A)	-86.46(18)
C(3A)-C(4A)-C(5A)-C(6A)	146.71(14)
C(10)-C(5)-C(6)-C(7)	-0.9(2)
C(4)-C(5)-C(6)-C(7)	-179.61(14)
C(10A)-C(5A)-C(6A)-C(7A)	0.9(2)
C(4A)-C(5A)-C(6A)-C(7A)	-178.16(14)
C(5)-C(6)-C(7)-C(8)	0.1(2)
C(5A)-C(6A)-C(7A)-C(8A)	-0.2(2)
C(6)-C(7)-C(8)-C(9)	0.6(2)

Table A13. (continued).

C(6A)-C(7A)-C(8A)-C(9A)	-0.3(3)
C(7)-C(8)-C(9)-C(10)	-0.5(2)
C(7A)-C(8A)-C(9A)-C(10A)	0.2(2)
C(8)-C(9)-C(10)-C(5)	-0.3(2)
C(8)-C(9)-C(10)-O(1)	-177.39(13)
C(6)-C(5)-C(10)-C(9)	1.0(2)
C(4)-C(5)-C(10)-C(9)	179.78(13)
C(6)-C(5)-C(10)-O(1)	177.94(12)
C(4)-C(5)-C(10)-O(1)	-3.3(2)
C(8A)-C(9A)-C(10A)-C(5A)	0.6(2)
C(8A)-C(9A)-C(10A)-O(1A)	-177.14(13)
C(6A)-C(5A)-C(10A)-C(9A)	-1.1(2)
C(4A)-C(5A)-C(10A)-C(9A)	178.03(14)
C(6A)-C(5A)-C(10A)-O(1A)	176.51(13)
C(4A)-C(5A)-C(10A)-O(1A)	-4.4(2)
C(5)-C(4)-C(11)-O(3)	76.40(15)
C(3)-C(4)-C(11)-O(3)	-161.17(13)
C(5)-C(4)-C(11)-C(12)	-41.29(18)
C(3)-C(4)-C(11)-C(12)	81.14(17)
C(5A)-C(4A)-C(11A)-O(3A)	75.94(15)
C(3A)-C(4A)-C(11A)-O(3A)	-160.81(12)
C(5A)-C(4A)-C(11A)-C(12A)	-41.67(18)
C(3A)-C(4A)-C(11A)-C(12A)	81.57(17)
O(3)-C(11)-C(12)-C(13)	37.86(15)
C(4)-C(11)-C(12)-C(13)	156.92(13)
O(3A)-C(11A)-C(12A)-C(13A)	36.86(15)
C(4A)-C(11A)-C(12A)-C(13A)	155.49(13)
C(11)-C(12)-C(13)-C(14)	-32.05(16)
C(11A)-C(12A)-C(13A)-C(14A)	-31.97(16)
C(12)-C(13)-C(14)-O(3)	15.36(16)
C(12)-C(13)-C(14)-C(15)	-100.11(15)

Table A13. (continued).

C(12)-C(13)-C(14)-C(16)	133.48(14)
C(12A)-C(13A)-C(14A)-O(3A)	16.18(17)
C(12A)-C(13A)-C(14A)-C(15A)	-99.77(16)
C(12A)-C(13A)-C(14A)-C(16A)	134.12(15)
O(2)-C(2)-O(1)-C(10)	-175.66(12)
C(3)-C(2)-O(1)-C(10)	5.34(18)
C(9)-C(10)-O(1)-C(2)	-162.93(13)
C(5)-C(10)-O(1)-C(2)	19.96(19)
O(2A)-C(2A)-O(1A)-C(10A)	-176.20(13)
C(3A)-C(2A)-O(1A)-C(10A)	5.24(19)
C(9A)-C(10A)-O(1A)-C(2A)	-161.87(13)
C(5A)-C(10A)-O(1A)-C(2A)	20.4(2)
C(12)-C(11)-O(3)-C(14)	-29.86(16)
C(4)-C(11)-O(3)-C(14)	-156.43(12)
C(15)-C(14)-O(3)-C(11)	129.14(14)
C(16)-C(14)-O(3)-C(11)	-111.39(14)
C(13)-C(14)-O(3)-C(11)	8.94(16)
C(12A)-C(11A)-O(3A)-C(14A)	-28.29(16)
C(4A)-C(11A)-O(3A)-C(14A)	-154.63(12)
C(15A)-C(14A)-O(3A)-C(11A)	127.96(14)
C(16A)-C(14A)-O(3A)-C(11A)	-113.09(15)
C(13A)-C(14A)-O(3A)-C(11A)	7.42(16)